frontiers | Research Topics

Recent advancements in the research models of infectious diseases

Edited by
Sam Ebenezer, Christy Rosaline Sundarraj, Azger Dusthackeer, Shakila Harshavardhan and Krupakar Parthasarathy

Published in
Frontiers in Cellular and Infection Microbiology

ISSN 1664-8714
ISBN 978-2-8325-7163-7
DOI 10.3389/978-2-8325-7163-7

Generative AI statement
Any alternative text (Alt text) provided alongside figures in the articles in this ebook has been generated by Frontiers with the support of artificial intelligence and reasonable efforts have been made to ensure accuracy, including review by the authors wherever possible. If you identify any issues, please contact us.

About Frontiers

Frontiers is more than just an open access publisher of scholarly articles: it is a pioneering approach to the world of academia, radically improving the way scholarly research is managed. The grand vision of Frontiers is a world where all people have an equal opportunity to seek, share and generate knowledge. Frontiers provides immediate and permanent online open access to all its publications, but this alone is not enough to realize our grand goals.

Frontiers journal series

The Frontiers journal series is a multi-tier and interdisciplinary set of open-access, online journals, promising a paradigm shift from the current review, selection and dissemination processes in academic publishing. All Frontiers journals are driven by researchers for researchers; therefore, they constitute a service to the scholarly community. At the same time, the *Frontiers journal series* operates on a revolutionary invention, the tiered publishing system, initially addressing specific communities of scholars, and gradually climbing up to broader public understanding, thus serving the interests of the lay society, too.

Dedication to quality

Each Frontiers article is a landmark of the highest quality, thanks to genuinely collaborative interactions between authors and review editors, who include some of the world's best academicians. Research must be certified by peers before entering a stream of knowledge that may eventually reach the public - and shape society; therefore, Frontiers only applies the most rigorous and unbiased reviews. Frontiers revolutionizes research publishing by freely delivering the most outstanding research, evaluated with no bias from both the academic and social point of view. By applying the most advanced information technologies, Frontiers is catapulting scholarly publishing into a new generation.

What are Frontiers Research Topics?

Frontiers Research Topics are very popular trademarks of the *Frontiers journals series*: they are collections of at least ten articles, all centered on a particular subject. With their unique mix of varied contributions from Original Research to Review Articles, Frontiers Research Topics unify the most influential researchers, the latest key findings and historical advances in a hot research area.

Find out more on how to host your own Frontiers Research Topic or contribute to one as an author by contacting the Frontiers editorial office: frontiersin.org/about/contact

Recent advancements in the research models of infectious diseases

Topic editors

Sam Ebenezer — Centre for Drug Discovery and Development, Sathyabama Institute of Science and Technology, India

Christy Rosaline Sundarraj — Achira Labs Pvt. Ltd, India

Azger Dusthackeer — National Institute of Research in Tuberculosis (ICMR), India

Shakila Harshavardhan — Madurai Kamaraj University, India

Krupakar Parthasarathy — Centre for Drug Discovery and Development, Sathyabama Institute of Science and Technology, India

Citation

Ebenezer, S., Sundarraj, C. R., Dusthackeer, A., Harshavardhan, S., Parthasarathy, K., eds. (2025). *Recent advancements in the research models of infectious diseases*. Lausanne: Frontiers Media SA. doi: 10.3389/978-2-8325-7163-7

Table of contents

frontiers | Frontiers in Cellular and Infection Microbiology

TYPE Editorial
PUBLISHED 07 November 2025
DOI 10.3389/fcimb.2025.1731600

OPEN ACCESS

EDITED AND REVIEWED BY
Nahed Ismail,
University of Illinois Chicago, United States

*CORRESPONDENCE
Sam Ebenezer Rajadas
samebenezer.r.cddd@sathyabama.ac.in

RECEIVED 24 October 2025
ACCEPTED 30 October 2025
PUBLISHED 07 November 2025

CITATION
Rajadas SE, Nirmal CR, Dusthackeer A, Harshavardhan S and Parthasarathy K (2025) Editorial: Recent advancements in the research models of infectious diseases. *Front. Cell. Infect. Microbiol.* 15:1731600. doi: 10.3389/fcimb.2025.1731600

Editorial: Recent advancements in the research models of infectious diseases

Sam Ebenezer Rajadas[1]*, Christy Rosaline Nirmal[2], Azger Dusthackeer[3], Shakila Harshavardhan[4] and Krupakar Parthasarathy[1]

[1]Centre for Drug Discovery and Development, Sathyabama Institute of Science and Technology, Chennai, India, [2]Achira Labs Pvt., Ltd., Bengaluru, India, [3]ICMR-National Institute for Research in Tuberculosis, Chennai, India, [4]Department of Molecular Microbiology, School of Biotechnology, Madurai Kamaraj University, Madurai, India

KEYWORDS

disease models, infectious diseases, research models, artificial intelligence in diagnosis, integrative disease modeling

Editorial on the Research Topic
Recent advancements in the research models of infectious diseases

Life on Earth is so pleasant till diseases and disorders strike. For long we believed that diseases were acts of God. It is no surprise that this was the time when people strongly supported the theory of spontaneous regeneration. The tables were turned upside down by two forefathers of microbiology, Louis Pasteur and Robert Koch. They were the first to experimentally use animal models, such as mice, rabbits, and chickens, especially in controlled settings, and exposed the pathogenicity of microbes and the experimental transmissibility of diseases. This led to the formulation of Koch's Postulates in 1884 (Dewan and Harvill, 2024). Yet, the dynamic emergence of new pathogens and antimicrobial resistance necessitates continuous advancement in the study of infection biology, as it imposes a significant burden on global health and socioeconomic stability. Central to this endeavor is the development of robust, reproducible, and physiologically relevant models that exactly display host–pathogen interactions despite its complexity. Conventional models, including *in vitro* cell cultures, *in vivo* infection systems, and compartmental epidemiological frameworks, have long provided critical mechanistic insights. However, these approaches often fail to fully capture the spatial, temporal, and immunological characteristics (Swearengen, 2018). In recent years, an exciting wave of innovation has emerged, driven by advances in systems biology, high-throughput analytics, genetic engineering, and artificial intelligence, enlightening our understanding of the contagiousness, disease progression, and host immunological defense. This Research Topic, *Recent Advancements in the Research Models of Infectious Diseases*, was conceived to showcase current innovations that are transforming our understanding of infectious processes and to highlight the interplay between experimental systems, computational modeling, and translational applications with clinical relevance.

The articles in this Research Topic highlight a diverse range of infectious disease models. This includes mathematical and computational frameworks that are increasingly being leveraged to predict clinical outcomes, as demonstrated through studies that forecast

mortality in COVID-19 patients (Xu et al.), and pneumonia-associated bloodstream infections (Zhou et al.) and even facilitating differential diagnosis (Peng et al.). These works highlight a growing recognition that predictive models, when anchored in patient-specific variables have significant potential to refine clinical decision-making and enhance the precision of infectious disease care.

At the experimental level, animal and novel nontraditional models are extending our capacity to study infection beyond conventional systems. Henriques et al. revisit the use of murine models to explore asymptomatic dengue infection, addressing both their utility and inherent limitations. Their review emphasizes the importance of refining animal models to better mirror subclinical infections that are often overlooked in spite of being epidemiologically significant (Henriques et al.). Complementing this perspective, another study explores fecal shedding patterns in SARS-CoV-2-infected rhesus macaques, providing valuable insight into viral persistence and host immune dynamics—an area with direct implications for understanding viral transmission routes and long-term pathogenesis (Böszörményi et al.).

Advances in diagnostics and biomarker-driven modeling was also featured prominently in this Research Topic. Li et al. present a stratified urine lipoarabinomannan assay for tuberculosis diagnosis, establishing a compelling link between host lymphocyte counts and pathogen-derived antigen detection. This study demonstrates how insights into the host–pathogen interface can enhance diagnostic sensitivity, particularly in immunocompromised populations where conventional methods often underperform (Li et al.). Expanding the modeling framework to an ecological scale, Zhao et al. used a MaxEnt-based approach to predict high-risk zones for avian influenza A (H7N9) infection, integrating environmental and epidemiological data to understand surveillance and preparedness strategies (Yang et al.). Additionally, the Research Topic underscores the emerging role of genomic insights, particularly those enabled by CRISPR-Cas systems, in simulating disease processes and driving novel therapeutic innovations (Al-Ouqaili et al.).

Multi-omics integration is becoming indispensable for unraveling the multilayered complexity of host responses. By merging transcriptomic, immunomic, and metabolomic data, researchers can construct network models that reveal hidden regulatory nodes and dynamic feedback loops during infection. Parallel to this, organoid and organ-on-chip systems are offering physiologically relevant microenvironments that bridge the gap between cell culture and whole-animal models (Barrila et al., 2018). These microphysiological systems enable detailed interrogation of tissue-specific infection processes while allowing manipulation of the mechanical, chemical, and immune microgradients that shape disease outcomes (Schmidiger and Portevin; Nangpal et al.).

Equally transformative are developments in computational and hybrid modeling. Artificial intelligence and machine-learning approaches, particularly, those constrained by biological or physical priors are accelerating our ability to simulate infection dynamics, predict drug responses, and identify emergent properties within complex datasets (Theodosiou and Read, 2023). Reaction diffusion and spatially explicit models are enriching our understanding of how infections propagate across tissues or populations, while phylodynamic frameworks integrating genomic and temporal data are reconstructing the invisible transmission networks that underlie epidemics (Waddel et al., 2025; Zhang and Wang, 2025). As these approaches evolve, the synergy between data-driven and mechanistic modeling will become highly significant to both fundamental and translational infection research.

Despite these advancements, challenges persist in integrating the immunological and multi-omics clinical datasets, which are prone to variability, missingness, and overfitting. The opacity of some artificial intelligent models and their algorithms can hinder clinical trust and mechanistic interpretation, thus warrants extensive validation along with ethical and biosafety considerations.

Conclusion

Infectious disease modeling is no longer confined to isolated experimental or computational silos; it is now a multidisciplinary enterprise that thrives at the intersection of biology, data science, engineering, and clinical medicine. The most impactful studies are those that embrace repeated cycles of modeling, prediction, validation, and refinement, closing the gap between theory and experiment. As we move forward, integrating these approaches is essential to accelerate discovery, enhance preparedness for unprecedented infectious threats, improve diagnostics, therapeutics, and prevention strategies. We extend our sincere appreciation to all authors, reviewers, and editorial staff whose efforts made this Research Topic possible.

Author contributions

SR: Conceptualization, Writing – original draft, Writing – review & editing. CN: Writing – review & editing. AD: Conceptualization, Writing – review & editing. SH: Writing – review & editing. KP: Writing – review & editing.

Conflict of interest

Author CN was employed by Achira Labs Pvt., Ltd.

The remaining authors declare that the research was conducted in the absence of any commercial or financial relationships that could be construed as a potential conflict of interest.

Generative AI statement

The author(s) declare that Generative AI was used in the creation of this manuscript. The Editorial was originally written by the corresponding author and reviewed by all the authors.

However, AI-based tools such as ChatGPT were used solely for language refinement and grammatical correction, without contributing to the intellectual or scientific content.

Any alternative text (alt text) provided alongside figures in this article has been generated by Frontiers with the support of artificial intelligence and reasonable efforts have been made to ensure accuracy, including review by the authors wherever possible. If you identify any issues, please contact us.

Publisher's note

References

Barrila, J., Crabbé, A., Yang, J., Franco, K., Nydam, S. D., Forsyth, R. J., et al. (2018). Modeling host-pathogen interactions in the context of the microenvironment: three-dimensional cell culture comes of age. *Infect. Immun.* 86, 1-26. doi: 10.1128/IAI.00282-18

Dewan, K. K., and Harvill, E. T. (2024). Koch's curse: How models of extreme pathology bias studies of host–pathogen interactions. *PloS Pathog.* 20, e1011997. doi: 10.1371/journal.ppat.1011997

Swearengen, J. R. (2018). Choosing the right animal model for infectious disease research. *Anim. Model. Exp. Med.* 1, 100–108. doi: 10.1002/ame2.12020

Theodosiou, A. A., and Read, R. C. (2023). Artificial intelligence, machine learning and deep learning: Potential resources for the infection clinician. *J. Infection* 87, 287–294. doi: 10.1016/j.jinf.2023.07.006

Waddel, H., Koelle, K., and Lau, M. S. Y. (2025). ScITree: Scalable Bayesian inference of transmission tree from epidemiological and genomic data. *PloS Comput. Biol.* 21, e1012657. doi: 10.1371/journal.pcbi.1012657

Zhang, L., and Wang, Z.-C. (2025). Spatial propagation phenomena for diffusive SIS epidemic models. *J. Differ Equ* 423, 240–285. doi: 10.1016/j.jde.2024.12.039

frontiers | Frontiers in Cellular and Infection Microbiology

TYPE Brief Research Report
PUBLISHED 18 December 2024
DOI 10.3389/fcimb.2024.1505720

OPEN ACCESS

EDITED BY
Sam Ebenezer,
Sathyabama Institute of Science and Technology, India

REVIEWED BY
Thibaut Naninck,
Commissariat à l'Energie Atomique et aux Energies Alternatives (CEA), France
Ivo Sirakov,
Medical University Sofia, Bulgaria

*CORRESPONDENCE
Ernst J. Verschoor
verschoor@bprc.nl

†PRESENT ADDRESS
Babs E. Verstrepen,
Department of Viroscience, Erasmus University Medical Center, Rotterdam, Netherlands

RECEIVED 03 October 2024
ACCEPTED 29 November 2024
PUBLISHED 18 December 2024

CITATION
Böszörményi KP, Stammes MA, Fagrouch Z, Acar F, Niphuis H, Kayere GK, Meijer L, Snijder EJ, van der Hoek L, Berkhout B, Bogers WM, van den Brand JMA, Kondova I, Verstrepen BE and Verschoor EJ (2024) Prolonged fecal shedding of replication-competent virus, lasting immune activation, and intestinal inflammation in a rhesus macaque after experimental SARS-CoV-2 infection. *Front. Cell. Infect. Microbiol.* 14:1505720. doi: 10.3389/fcimb.2024.1505720

Prolonged fecal shedding of replication-competent virus, lasting immune activation, and intestinal inflammation in a rhesus macaque after experimental SARS-CoV-2 infection

Kinga P. Böszörményi[1], Marieke A. Stammes[1], Zahra Fagrouch[1], Fidel Acar[1], Henk Niphuis[1], Gwendoline Kiemenyi Kayere[1], Lisette Meijer[1], Eric J. Snijder[2], Lia van der Hoek[3], Ben Berkhout[3], Willy M. Bogers[1], Judith M. A. van den Brand[4], Ivanela Kondova[1], Babs E. Verstrepen[1†] and Ernst J. Verschoor[1*]

[1]Department of Virology, Biomedical Primate Research Centre (BPRC), Rijswijk, Netherlands, [2]Molecular Virology Laboratory, Leiden University Center of Infectious Diseases, Leiden University Medical Center, Leiden, Netherlands, [3]Laboratory of Experimental Virology, Department of Medical Microbiology and Infection Prevention, Amsterdam UMC, University of Amsterdam, Amsterdam, Netherlands, [4]Division of Pathology, Faculty of Veterinary Medicine, Utrecht University, Utrecht, Netherlands

Infection of an adult rhesus macaque with SARS-CoV-2 led to viral RNAemia in nose, throat, and lungs. The animal also presented extended fecal shedding of viral genomic and subgenomic messenger RNA and replication-competent virus for more than 3 weeks after infection. Positron emission tomography revealed increased intestinal glucose metabolism which was histologically related to inflammation of the ileum. These findings highlight the potential of the virus to cause gastrointestinal infections in macaques like this is also regularly observed in COVID-19 patients and substantiates the probability of virus transmission via the fecal-oral route. This study further adds the importance of nonhuman primates as a valuable animal model to study SARS-CoV-2 infection in humans.

KEYWORDS

SARS-CoV-2, COVID-19, rhesus macaque, virus shedding, PET-CT, intestinal inflammation

1 Introduction

The disease caused by SARS-CoV-2, COVID-19, was initially regarded as a respiratory syndrome. However, it soon became clear that SARS-CoV-2 can also cause symptoms affecting various organ systems (Zhu et al., 2023) While the respiratory tract serves as the primary site of infection, the virus can also trigger gastrointestinal (GI) complications in a significant proportion of patients (Wu et al., 2020; Durairajan et al., 2023). Viral RNA can be detected in feces of infected individuals for a considerable time, often exceeding the detected RNA levels in the respiratory tract (Zhu et al., 2023).High-level expression of ACE2 receptor molecules in the GI tract could explain its susceptibility to SARS-CoV-2 infection (Ribeiro et al., 2023). Alternatively, SARS-CoV-2 may use ACE2-independent entry of cells via the GRP78 cell-surface protein as proposed for the related MERS-CoV, and for other viruses (Chu et al., 2018; Ibrahim et al., 2020; Han et al., 2023). Despite the detection of viral RNA in rectal swabs, the isolation of live virus from these samples has proven cumbersome and reports are scarce (Wolfel et al., 2020; Cerrada-Romero et al., 2022; Ribeiro et al., 2023). Presently, the involvement of SARS-CoV-2 in the pathology of the GI tract is not fully understood and requires further research, particularly in the light of the potential for fecal-oral transmission of SARS-CoV-2.

Nonhuman primates (NHPs), like macaques, are an important animal model for COVID-19 pathogenesis research. Macaques express receptor proteins that are similar to their human counterparts (Melin et al., 2020; Sirakov et al., 2020), are susceptible to infection, and macaques exhibit COVID-19 symptoms and pathology much alike observed in human patients (Caldera-Crespo et al., 2021; Saturday and van Doremalen, 2023). After infection, SARS-CoV-2 induces mild-to-moderate disease in NHPs (Böszörményi et al., 2021; Stammes et al., 2022; Saturday and van Doremalen, 2023), and viral RNA can be detected shortly after experimental infection in the nasal and tracheal area, and in the lungs. However, in macaques, viral RNA is detected sporadically in feces and viral RNA levels tend to be relatively low compared to those measured in the respiratory tract.

We previously reported inflammation of the lungs and brain of rhesus macaques in the post-acute phase of infection (Böszörményi et al., 2021; Philippens et al., 2022). Here, we describe the case of a rhesus macaque with a SARS-CoV-2 infection that coincided with inflammation of the small intestine, accompanied by a prolonged period of fecal shedding of replication-competent SARS-CoV-2.

2 Materials and methods

2.1 Ethics statement

The study was carried out at the Biomedical Primate Research Centre (BPRC). The BPRC is accredited by the American Association for Accreditation of Laboratory Animal Care (AAALAC) International and is compliant with the European directive 2010/63/EU as well as the "Standard for Humane Care and Use of Laboratory Animals by Foreign Institutions" (National Institutes of Health, ID A5539-01). The study protocol was reviewed and approved by the "Centrale Commissie Dierproeven" (license no. AVD5020020209404) according to Dutch law, article 10a of the "Wet op de Dierproeven" and BPRC's Animal Welfare Body.

All animal handlings were performed within the Department of Animal Science (ASD) and in accordance with Dutch law. ASD is regularly inspected by the responsible national authority (Nederlandse Voedsel- en Warenautoriteit, NVWA), and the AWB.

2.2 Study design

A 10-year-old, healthy, female rhesus macaque (*Macaca mulatta*) with a bodyweight of 6.6 kgs was inoculated with $1x10^5$ $TCID_{50}$ of the SARS-CoV-2/human/NLD/Leiden-0008/2020 strain (GenBank accession number: MT705206.1), which is an early 2020 isolate containing the D614G mutation in the virus' spike protein. The virus had been propagated twice on Vero E6 cells and titrated on Vero E6 cells in a 96-well format in triplicates. Plates were fixed on day 3 with 10% formalin, stained with crystal violet, and the $TCID_{50}$/mL were determined using the Spearman-Kärber method. On day 0, all animal was exposed to a dose of 1×10^5 $TCID_{50}$ of SARS-CoV-2, diluted in 5 ml phosphate-buffered saline (1x PBS). The virus was inoculated via a combination of the intratracheal route, just below the vocal cords, (4.5 ml) and intranasal route (0.25 ml in each nostril) (Böszörményi et al., 2021). The macaque was monitored for six weeks after infection (Figure 1). Body temperature was measured and nasal, tracheal, anal swabs, and blood samples were collected daily for the first 10 days, and subsequently every 3-4 days. Broncho-alveolar lavage (BAL) was performed on days 7 and 9 post-infection (pi.). Hematology and blood biochemistry parameters were measured at days 0, 1, 13 and 42.

During the post-infection follow-up period, computed tomography (CT) data were acquired at multiple timepoints pi. Positron emission tomography (PET)-CTs were performed at days 3, 13, 20, 27, 34 and 41 pi. using [^{18}F]FDG as tracer as described previously (Böszörményi et al., 2021; Philippens et al., 2022). For all experimental interventions (intratracheal and intranasal infection, swab collections, blood samplings, and imaging procedures), the animal was fasted overnight and sedated with ketamine (10 mg/kg, ketamine hydrochloride, Ketamin 10%; Alfasan Nederland BV, Woerden, the Netherlands) combined with medetomidine hydrochloride, 0.05 mg/kg (Sedastart; AST Farma B.V., Oudewater, the Netherlands) to induce sedation and muscle relaxation, both applied intramuscularly (IM).

Euthanasia was performed at day 44 pi. by using a method listed in Annex IV of the European Directive 2010/63/EU. The animal was first sedated using 12 mg/kg Ketamin combined with 0.05 mg/kg Medetomidine, followed by intravenous administration of 70 mg/kg pentobarbital (Covetrus, Cuijk, the Netherlands). Then, full necropsy was performed, and tissue samples were preserved for (immuno)histological analysis.

2.3 Detection of viral RNA in swabs, blood, and tissues

Nasal, tracheal, anal swab samples were taken at regular time-point, and at the same time, blood samples were collected for PCR

10.3389/fcimb.2024.1505720

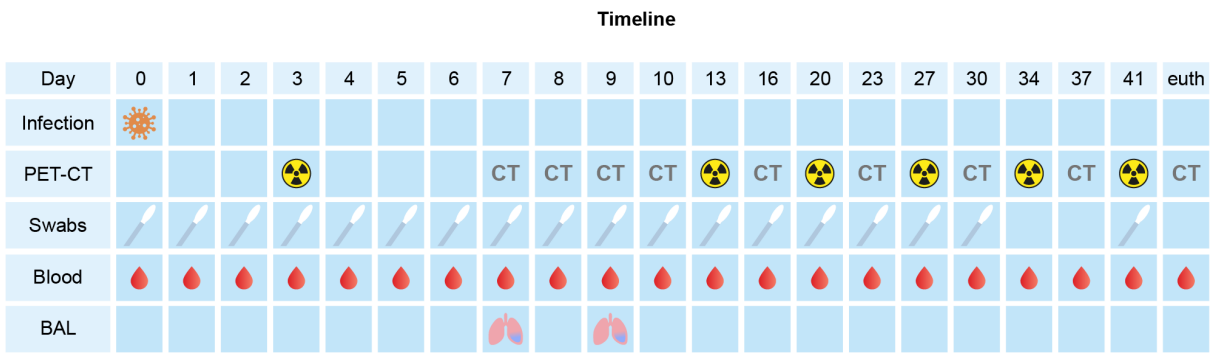

FIGURE 1
Schematic overview and timeline of the experimental procedures within the study. At the timepoints only CT was performed, it is marked with "CT". The radioactivity symbol indicates timepoint of PET-CT.

analysis. At the end of the study, the animal was euthanized, and tissue samples were collected for viral RNA detection. RNA isolation from swabs and tissue samples was done using QIAamp Viral RNA Mini kit (Qiagen Benelux BV, Venlo, The Netherlands) following the manufacturer's instructions. Detection of SARS-CoV-2 viral RNA (vRNA) and subgenomic messenger RNA (sgmRNA) was performed following published protocols (Corman et al., 2020; Wolfel et al., 2020). Detection of sgmRNA was used as a proxy of replicating virus (Dagotto et al., 2021). Both assays had a lower limit of quantification of 20 viral RNA copies per reaction and was determined using RNA standard curves that were generated by *in vitro* transcription of the target regions from synthetic DNA.

2.4 Virus isolation from fecal samples and NGS analysis

Anal swabs were assayed for the presence of replication-competent virus in Vero-E6 cells (ATCC# CRL-1586). Fecal swabs were put in 1 mL MEM, supplemented with 0.5% bovine serum albumin (BSA), fungizone (2,5 µg/mL), penicillin (100 U/mL), and streptomycin (100µµg/mL) and directly transported to the BSL3 lab, vortexed, and supernatant was clarified by centrifugation at 2800 x *g* for 5 min. Next, 250 µl of the sample was inoculated on Vero E6 cells and incubated at 37˚C in the presence of 5% CO_2 for 6 days. Cell cultures were screened daily for signs of infection by light microscope and at the same time a sample was taken for PCR analysis. RNA was isolated from the harvested cell culture supernatant and used for NGS analysis using Illumina sequencing as described previously (Ogando et al., 2020).

2.5 Imaging

Positron Emission Tomography Computed Tomography (PET-CT) data was acquired, using a MultiScan Large Field of View Extreme Resolution Research Imager (LFER) 150 PET-CT (Mediso Medical Imaging Systems Ltd., Budapest, Hungary). After sedation, the animal was positioned head-first supine (HFS) with the arms up. After the scan, upon return to its home cage, atipamezole hydrochloride (Sedastop, AST Farma B.V., Oudewater, The Netherlands, 5 mg/mL, 0.25 mg/kg) was administrated IM to antagonize medetomidine.

2.5.1 CT

CTs were acquired using a semicircular single FOV scan method, with an exposure of 90 ms and 1:4 binning using 75 kVp, 980 µA CT tube strength. CTs were reconstructed with a voxel size of 500 and 1000 µm. CT image analyses was performed using Vivoquant version 4.5 (InVicro, Boston, USA) (Stammes et al., 2021).

2.5.2 PET-CT

The PET-CTs were acquired under mechanical ventilation in combination with a forced breathing pattern. For anesthetic maintenance, a minimum alveolar concentration of isoflurane (iso-MAC) of around 0,80%-1.00% was used. A 15-minute static PET scan was acquired of brain, thorax and abdomen starting 30 minutes post injection a bolus injection of 102,71 MBq (range 97,21-107,97 MBq) ^{18}F-fluorodeoxyglucose ([^{18}F]FDG).

Afterwards the emission data was iteratively reconstructed (OSEM3D, 8 iterations and 9 subsets) into a single frame PET image normalized and corrected for attenuation, scatter, and random coincidences using the reference CT and corrected for radioactive decay. The analysis was performed in VivoQuant 4.5 (Invicro, Boston, USA). Based on repeatability parameters for correct interpretation of the results, a standardized uptake value (SUV) was used for robustness (Stammes et al., 2021).

2.6 Histopathology and immunohistochemistry

Tissue samples were collected at euthanasia on day 44 pi. (Supplementary Table 1) and preserved for histopathology by immersion in 10% neutral-buffered formalin for 72 to 96 h. Specimens for microscopic examination were processed and

embedded in paraffin, and sections of 4 µm were stained with hematoxylin and eosin (H&E).

For antigen retrieval, slides were incubated in citrate buffer (pH 6 at 97˚C) for 20 min. Endogenous peroxidase activity was inhibited using Dako Peroxidase Blocking Solution for 5 minutes. Next, after a washing step, the slides were incubated for 15 min with normal goat serum and incubated for 1 hour with the primary antibodies (SARS-CoV/SARS-CoV-2 Nucleoprotein antibody, 40143-T62 Bio-Connect; 1:10 000 diluted). After washing, the slides were incubated for 30 min with the secondary antibody (BrightVision Poly-HRP-Anti Ms-Rb IgG, one component, VWRKDPVO110HRP; undiluted). After a washing step, the chromogen (Vector NovaRed) was added for 8 min to visualize the antigen–antibody binding. Hematoxylin-eosin (H&E) staining was used for general morphology. After immunohistochemical staining, the sections were dehydrated with Alcohol-Xylene and mounted with Pertex® mounting medium (VWR International B.V., Amsterdam, The Netherlands).

3 Results

Following inoculation, no changes in body temperature, hematology and blood biochemistry were measured. SARS-CoV-2 replication was monitored by RT-qPCR (Figure 2A). Viral RNA was detected in nose and throat but was undetectable in all blood samples. RNAemia started at day 1 pi. and in both compartments a peak in RNA load was visible around day 2 and a second peak on day 7 and day 8 in the throat and nose, respectively. Then, RNA levels rapidly dropped below the limit of detection within 10 days pi. in the throat and 13 days pi. in the nose. BAL samples were positive at both collection timepoints on days 7 and 9 pi. (7,54 x 10^4 copies/mL and 2,27 x 10^4 copies/mL, respectively). Interestingly, viral RNA was also detected in anal swabs from day 1 pi. and remained consistently present until day 27 pi. This pattern contrasts with the vRNA detection in nose and throat samples which fell below the detection limit on day 13 (nose) and day 10 (throat), resembling the temporal dynamics observed in human patients (Zhu et al., 2023). Detection of subgenomic messenger RNA was used as a qualified proxy for monitoring virus replication (Dagotto et al., 2021). SgmRNA was identified in nasal and tracheal swabs from day 1 and remained detectable until days 8-10 pi., while showing the same bi-phasic pattern as the vRNA loads. Additionally, sgmRNA was present in the BAL sample collected on day 7 pi. (3,74 x 10^4 copies/mL), but not in the BAL fluid collected at day 9 pi., indicating that virus replication in the upper and lower respiratory tract of the macaque started early after infection and continued for a limited time frame.

In anal swabs, vRNA was detected over a period of 30 days, starting at day 1 pi., and detection of sgmRNA started at day 6 pi. and lasted until day 23 pi. This observation suggests that SARS-CoV-2 replicated in the gastro-intestinal (GI) tract for a substantial period. Furthermore, virus replication was substantiated by the successful recovery of infectious SARS-CoV-2 from the anal swab sample collected at day 9 pi. (Figure 2B). This was the timepoint with the highest number of sgmRNA copies detected (1.24 x 10^5 copies/mL). Virus isolation from sgmRNA-positive anal swab samples collected at other time-points was unsuccessful.

Initially, (PET-)CTs were focused on the upper part of the body, excluding the abdominal region. Here, CT revealed mild pathological changes of the lower respiratory tract with abnormalities in the lungs, predominantly ground glass opacities, and an increased uptake of [^{18}F]FDG in the mediastinal lymph nodes was detected on the longitudinal chest PET-CTs of the macaque (data not shown). However, the recurring detection of sgmRNA in anal swabs led us to expand our PET-CT investigations to the abdomen, starting on day 13 pi. An increased uptake of [^{18}F]FDG was observed, beside the mediastinal lymph nodes, in the ileal

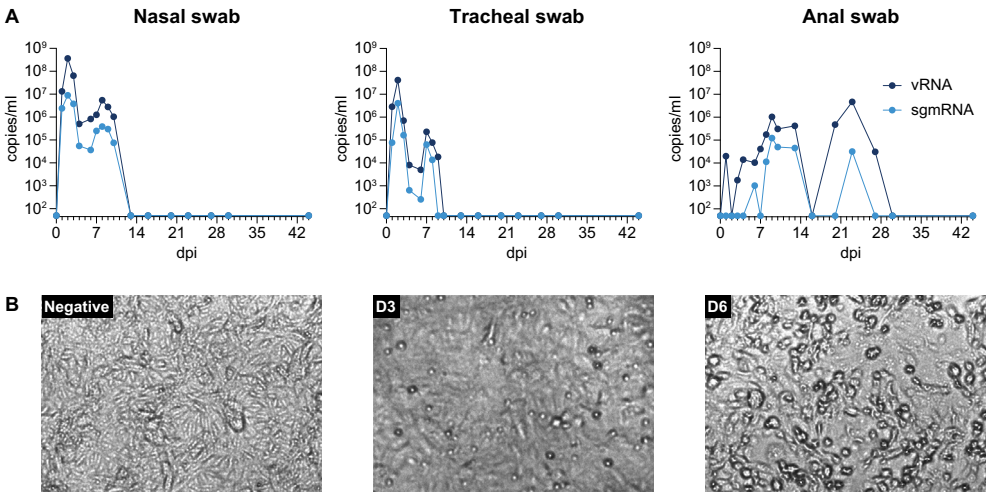

FIGURE 2
(A) SARS-CoV-2 viral RNA and sgmRNA loads in nasal, tracheal, and anal swabs taken throughout the study. **(B)** Virus re-isolation from anal swab collected at day 9 pi. Anal swab was put in 1 mL MEM, supplemented with 0.5% bovine serum albumin (BSA), fungizone (2,5 g/mL), penicillin (100 U/mL), and streptomycin (100µg/mL), vortexed, and supernatant was clarified by centrifugation at 2800 x *g* for 5 min. Next, 250 µl was inoculated onto Vero E6 cells and incubated for 6 days. From left to right: uninfected cells, Vero cells after 3 days and 6 days culturing, respectively.

part of intestinal tract. As no pre-infection scan was performed, this increase was based on comparison with scans obtained from other healthy animals. Although [^{18}F]FDG is not specific for SARS-CoV-2 and is used more for detecting general metabolic activation, the data, along with the long-term detection of sgmRNA in anal swabs, strongly suggest SARS-CoV-2 infection in the intestinal tissues and associated immune activation. In Figure 3, the longitudinal development of the metabolic activity of the ileum is presented. The [^{18}F]FDG tracer uptake increased from day 13 to 27 pi., and afterwards intensity decreased but remained detectable towards the end of the study. When analyzing the data, this observation was confirmed by the standard uptake values (SUVs). The SUVpeak (max value in 1 mm^3 spherical volume) reached its highest level on day 13 pi (SUVpeak 7.26), although this peak was observed in only a small portion of the sample. The average value in the region of interest (SUVmean), however, continued to increase until day 20 pi. (SUVmean was 1.21 at day 13 compared to 2.79 at day 20), after which it began to decrease but remained above the initially detected levels (SUVmean of 1.53 at day 41).

SARS-CoV-2 re-isolation was only successful from the anal swab sample collected at day 9. The isolated virus was subjected to NGS analysis, and its genome was compared to the original viral inoculum. Sequence analysis did not reveal specific mutations that could be linked to the enhanced or prolonged virus replication seen in the GI tract of the animal. Two non-silent mutations were identified in the spike (S) protein gene, encoding S151R and D215V substitutions, but each occurred with low frequencies of 8% and 11%, respectively. The importance of these mutations remains currently unclear.

Several tissue samples, collected at euthanasia on day 44 pi. (Supplementary Table 1), tested positive for vRNA in two independent PCR assays: mesenteric LN (2/2; 1.7 x 10^5 and 2.4 x 10^5 copies/gram), bronchial LN (2/2; 1.1 x 10^4 and 1.3 x 10^4 copies/gram), and the ileum (2/2; 1.5 x 10^4 and 1.2 x 10^4 copies/gram). Despite being positive for vRNA, these tissues tested negative in the sgmRNA assay suggesting a resolved, but widely disseminated SARS-CoV-2 infection. This was confirmed by histological analysis. Histology revealed marked lymphoid follicular hyperplasia of the mesenteric lymph nodes, severe multifocal lymphoplasmacytic gastritis, and moderate lymphoplasmacytic enteritis with marked lymphoid hyperplasia in the ileum. Immunohistochemistry was performed on the same set of tissue samples (Figure 4). Viral antigen was visualized in the mesenteric lymph node, with few numbers of cells staining positive for the viral nucleocapsid (N) protein. Similarly, occasional positive stained cells were seen in the stomach. However, in the ileal tissue sample no convincing staining of cells was observed. Thus, IHC did not provide definitive evidence of an actual infection of the ileum, but it cannot be excluded that the viral load in this tissue sample was below the detection threshold of the assay by the time the animal was sacrificed.

4 Discussion

Although nonhuman primates are widely used in SARS-CoV-2 vaccine research since the start of the COVID-19 pandemic, our knowledge of the pathology induced by SARS-CoV-2 in NHPs is relatively limited. This precludes a thorough comparison with the observed pathological consequences in human patients and therefore hinders a full appreciation of NHPs as a useful and unique animal model for COVID-19 research.

For that reason, while employing NHPs for vaccine evaluation studies, we also investigated striking clinical and pathological manifestations that were encountered in individual macaques after infection with SARS-CoV-2. We previously reported ongoing virus replication and pathogenesis in NHPs and described inflammation and aggregation of α-synuclein in brain of infected macaques (Böszörményi et al., 2021; Philippens et al., 2022).

In this report we describe prolonged SARS-CoV-2 replication in the GI tract of a rhesus macaque and the isolation of replication-competent virus from an anal swab. These findings were

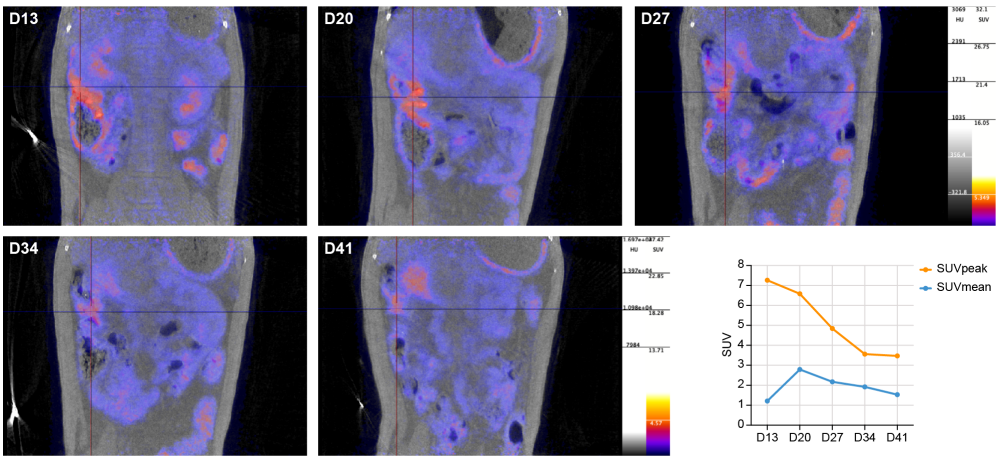

FIGURE 3
Longitudinal development of metabolic activity by increased [^{18}F]FDG uptake in the ileum from day 13 to day 41 post infection. The ileum is marked by the crosshair. The graph (bottom, right) shows the calculated SUVs throughout the study.

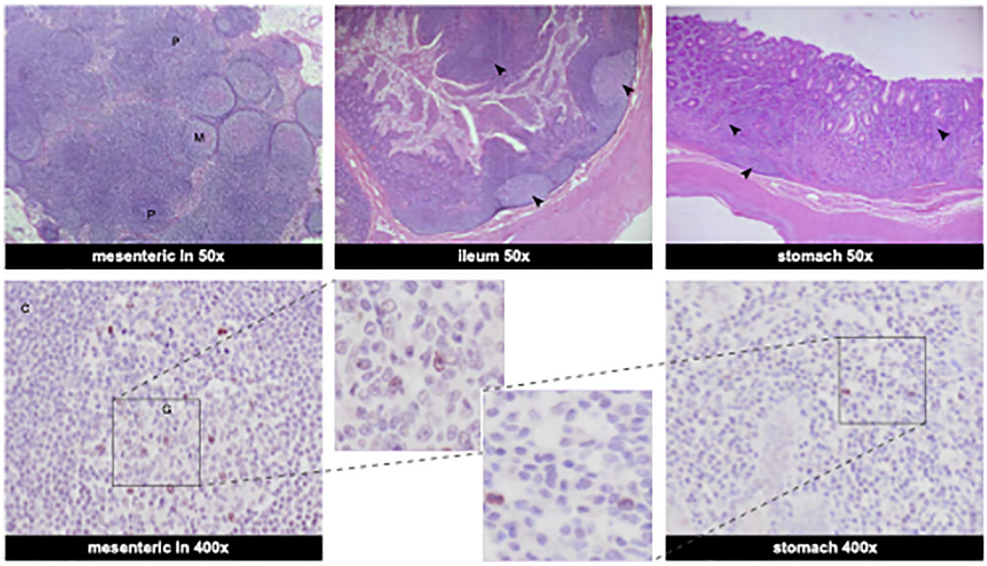

FIGURE 4
Histological findings in the gastrointestinal organs and viral antigen determined by immunohistochemistry. Top row shows HE stainings at 50x magnification. Bottom row shows SARS-CoV-2 nucleocapsid IHC staining. *Mesenteric lymph nodes:* Numerous large lymphoid follicles are present in the paracortex (P) and medulla (M) of the mesenteric lymph node (HE stainings, 50x). Few cells are positive in the germinal center (G) of the mesenteric lymph node with clear staining of the nucleus (C: cortex) (IHC staining SARS-CoV-2 Nucleocapsid protein, 400x). *Ileum*: The ileum exhibits moderate multifocal lymphoplasmacytic infiltrates in the mucosa and the Peyer's patches are associated with defined lymphoid follicles with large germinal centers and abundant lymphoid hyperplasia (marked with arrows) (ileum, HE stainings, 50x). *Stomach:* Gastric mucosa is multifocally infiltrated by numerous lymphoplasmacytic infiltrates (marked with arrows) (stomach, HE staining, 50x). Occasional large mononuclear cells are positive in the gastric mucosa (stomach, IHC, 400x). Bottom row, middle: enlarged sections of IHC staining of SARS-CoV-2 nucleocapsid-positive cells from mesenteric lymph nodes and stomach.

complemented by an active inflammation of the ileum, as was visualized by [^{18}F]FDG PET-CT. Notably, this persisted till the end of the study, well after RNA shedding in feces had become undetectable. Inflammation of the ileum was further validated by histological examination, but, despite the presence of viral RNA, evidence for viral antigen in the ileum could not be found by immunohistochemistry.

The detection of vRNA in mesenteric and bronchial lymph nodes, suggestive of a resolved virus infection, was paralleled by the detection of morphological abnormalities and provided further evidence of the wide-spread distribution of the virus (Böszörményi et al., 2021; Philippens et al., 2022).

Finding of SARS-CoV-2 RNA in fecal samples from NHP appears less common than in human patients. Viral RNA is found in the GI tract of up to 59% of COVID-19 patients, but such high numbers are seldomly reported in NHPs (Ng and Tilg, 2020; Guo et al., 2021). A single study describes vRNA detection in feces of 4/4 macaques after SARS-CoV-2 and the re-solation of virus from a fecal sample of one animal, but this study used an intragastric infection route (Jiao et al., 2021). Others, using the intratracheal/intranasal infection route, like in this report, described a single individual macaque with vRNA and sgmRNA detectable in feces but without virus culture (Beddingfield et al., 2022). NHP may not exhibit GI disease symptoms caused by SARS-CoV-2 as frequently as observed in human patients, but these figures may be influenced by the overrepresentation of publications focusing on (hospitalized) patients with severe COVID-19. The detection of replication-competent virus or sgmRNA was only successful in critically ill patients, like immunocompromised or immunosuppressed people and in pediatric patients with an immature immune system (Li et al., 2022; Mamishi et al., 2023).

This case report, described in the rhesus macaque model for COVID-19, draws attention to the possible role of silent human carriers in the spread of SARS-CoV-2 during the COVID-19 pandemic. Here, without displaying clinically apparent COVID-19-related respiratory or GI symptoms, the animal actively shed infectious virus in feces which strengthens the concerns about fecal-oral transmission of SARS-CoV-2 in the human population (Xiao et al., 2020; Boyton and Altmann, 2021).

This report adds further value to the use of animal models in studying SARS-CoV-2 infection. The macaque, a recognized NHP model for numerous human viral diseases, provides valuable insights into the biology of SARS-CoV-2 and its potential to cause long-term pathogenic sequelae in different organs, after SARS-CoV-2 infection has been resolved.

Data availability statement

The raw data supporting the conclusions of this article will be made available by the authors, without undue reservation.

Ethics statement

The animal study was approved by BPRC Animal Welfare Body (IVD@bprc.nl). The study was conducted in accordance with the local legislation and institutional requirements.

Author contributions

KB: Conceptualization, Formal analysis, Project administration, Supervision, Writing – original draft, Writing – review & editing, Investigation. MS: Formal Analysis, Methodology, Writing – original draft, Writing – review & editing, Investigation. ZF: Investigation, Methodology, Writing – review & editing. FA: Investigation, Methodology, Writing – review & editing. HN: Investigation, Methodology, Writing – review & editing. GK: Investigation, Methodology, Writing – review & editing. LM: Investigation, Methodology, Writing – review & editing. ES: Resources, Writing – review & editing, Investigation. LH: Writing – review & editing. BB: Writing – review & editing. WB: Funding acquisition, Writing – review & editing. JB: Investigation, Methodology, Writing – original draft. IK: Investigation, Methodology, Writing – review & editing. BV: Project administration, Writing – review & editing. EV: Conceptualization, Funding acquisition, Project administration, Resources, Supervision, Writing – original draft, Writing – review & editing.

Funding

The author(s) declare financial support was received for the research, authorship, and/or publication of this article. This study was supported by funding from the Biomedical Primate Research Centre.

Acknowledgments

We want to thank Francisca van Hassel for assistance with the editing of figures and the Animal Science Department of BPRC, the veterinarians and animal caretakers for all the experimental support. We would also like to thank Tim Dalebout, Natacha Ogando, and Igor Sidorov of LUMC for NGS sequencing and technical assistance.

Conflict of interest

The authors declare that the research was conducted in the absence of any commercial or financial relationships that could be construed as a potential conflict of interest.

Generative AI statement

The author(s) declare that no Generative AI was used in the creation of this manuscript.

Publisher's note

Supplementary material

The Supplementary Material for this article can be found online at: https://www.frontiersin.org/articles/10.3389/fcimb.2024.1505720/full#supplementary-material

References

Beddingfield, B. J., Rowe, L. A., Russell-Lodrigue, K. E., Doyle-Meyers, L. A., Golden, N., Spencer, S., et al. (2022). Breakthrough gastrointestinal COVID-19 and intrahost evolution consequent to combination monoclonal antibody prophylaxis. *J. Infect. Dis.* 226, 1588–1592. doi: 10.1093/infdis/jiac134

Böszörményi, K. P., Stammes, M. A., Fagrouch, Z. C., Kiemenyi-Kayere, G., Niphuis, H., Mortier, D., et al. (2021). The post-acute phase of SARS-coV-2 infection in two macaque species is associated with signs of ongoing virus replication and pathology in pulmonary and extrapulmonary tissues. *Viruses* 13 (8), 1673. doi: 10.3390/v13081673

Boyton, R. J., and Altmann, D. M. (2021). The immunology of asymptomatic SARS-CoV-2 infection: what are the key questions? *Nat. Rev. Immunol.* 21, 762–768. doi: 10.1038/s41577-021-00631-x

Caldera-Crespo, L. A., Paidas, M. J., Roy, S., Schulman, C. I., Kenyon, N. S., Daunert, S., et al. (2021). Experimental models of COVID-19. *Front. Cell Infect. Microbiol.* 11, 792584. doi: 10.3389/fcimb.2021.792584

Cerrada-Romero, C., Berastegui-Cabrera, J., Camacho-Martinez, P., Goikoetxea-Aguirre, J., Perez-Palacios, P., Santibanez, S., et al. (2022). Excretion and viability of SARS-CoV-2 in feces and its association with the clinical outcome of COVID-19. *Sci. Rep.* 12, 7397. doi: 10.1038/s41598-022-11439-7

Chu, H., Chan, C. M., Zhang, X., Wang, Y., Yuan, S., Zhou, J., et al. (2018). Middle East respiratory syndrome coronavirus and bat coronavirus HKU9 both can utilize GRP78 for attachment onto host cells. *J. Biol. Chem.* 293, 11709–11726. doi: 10.1074/jbc.RA118.001897

Corman, V. M., Landt, O., Kaiser, M., Molenkamp, R., Meijer, A., Chu, D. K., et al. (2020). Detection of 2019 novel coronavirus (2019-nCoV) by real-time RT-PCR. *Euro Surveill* 25 (3), 2000045. doi: 10.2807/1560-7917.ES.2020.25.3.2000045

Dagotto, G., Mercado, N. B., Martinez, D. R., Hou, Y. J., Nkolola, J. P., Carnahan, R. H., et al. (2021). Comparison of subgenomic and total RNA in SARS-coV-2 challenged rhesus macaques. *J. Virol.* 95 (8), e02370-20. doi: 10.1128/JVI.02370-20

Durairajan, S. S. K., Singh, A. K., Saravanan, U. B., Namachivayam, M., Radhakrishnan, M., Huang, J. D., et al. (2023). Gastrointestinal manifestations of SARS-coV-2: transmission, pathogenesis, immunomodulation, microflora dysbiosis, and clinical implications. *Viruses* 15 (6), 1231. doi: 10.3390/v15061231

Guo, M., Tao, W., Flavell, R. A., and Zhu, S. (2021). Potential intestinal infection and faecal-oral transmission of SARS-CoV-2. *Nat. Rev. Gastroenterol. Hepatol.* 18, 269–283. doi: 10.1038/s41575-021-00416-6

Han, B., Lv, Y., Moser, D., Zhou, X., Woehrle, T., Han, L., et al. (2023). ACE2-independent SARS-CoV-2 virus entry through cell surface GRP78 on monocytes - evidence from a translational clinical and experimental approach. *EBioMedicine.* 98, 104869. doi: 10.1016/j.ebiom.2023.104869

Ibrahim, I. M., Abdelmalek, D. H., Elshahat, M. E., and Elfiky, A. A. (2020). COVID-19 spike-host cell receptor GRP78 binding site prediction. *J. Infect.* 80, 554–562. doi: 10.1016/j.jinf.2020.02.026

Jiao, L., Li, H., Xu, J., Yang, M., Ma, C., Li, J., et al. (2021). The gastrointestinal tract is an alternative route for SARS-coV-2 infection in a nonhuman primate model. *Gastroenterology*. 160, 1647–1661. doi: 10.1053/j.gastro.2020.12.001

Li, W. T., Zhang, Y., Liu, M., Liu, Y. Q., and Ma, X. (2022). Prolonged viral shedding in feces of children with COVID-19: a systematic review and synthesis of data. *Eur. J. Pediatr.* 181, 4011–4017. doi: 10.1007/s00431-022-04622-5

Mamishi, S., Jalali, F., Benvari, S., Pourakbari, B., Abdolsalehi, M. R., Sadeghi, R. H., et al. (2023). SARS-CoV-2 fecal shedding pattern in pediatric patients with acute COVID-19 or COVID-19-associated multisystem inflammatory syndrome. *Clin. Exp. Pediatr.* 66, 366–368. doi: 10.3345/cep.2023.00297

Melin, A. D., Janiak, M. C., Marrone, F. 3rd, Arora, P. S., and Higham, J. P. (2020). Comparative ACE2 variation and primate COVID-19 risk. *Commun. Biol.* 3, 641. doi: 10.1038/s42003-020-01370-w

Ng, S. C., and Tilg, H. (2020). COVID-19 and the gastrointestinal tract: more than meets the eye. *Gut.* 69, 973–974. doi: 10.1136/gutjnl-2020-321195

Ogando, N. S., Dalebout, T. J., Zevenhoven-Dobbe, J. C., Limpens, R., van der Meer, Y., Caly, L., et al. (2020). SARS-coronavirus-2 replication in Vero E6 cells: replication kinetics, rapid adaptation and cytopathology. *J. Gen. Virol.* 101, 925–940. doi: 10.1099/jgv.0.001453

Philippens, IHCHM, Böszörményi, K. P., Wubben, J. A. M., Fagrouch, Z. C., van Driel, N., Mayenburg, A. Q., et al. (2022). Brain Inflammation and Intracellular alpha-Synuclein Aggregates in Macaques after SARS-CoV-2 Infection. *Viruses* 14 (4), 776. doi: 10.3390/v14040776

Ribeiro, I. P., Nascimento, L. G. D., Tort, L. F. L., Pereira, E. C., Menezes, L. S. R., Malta, F. C., et al. (2023). Infectious SARS-coV-2 particles from rectal swab samples from COVID-19 patients in Brazil. *Viruses* 15 (5), 1152. doi: 10.3390/v15051152

Saturday, T., and van Doremalen, N. (2023). Pathogenesis of severe acute respiratory syndrome coronavirus-2 in nonhuman primates. *Curr. Opin. Virol.* 63, 101375. doi: 10.1016/j.coviro.2023.101375

Sirakov, I., Bakalov, D., Popova, R., and Mitov, I. (2020). Analysis of host cell receptor GRP78 for potential natural reservoirs of SARS-coV-2. *J. Epidemiol. Glob Health* 10, 198–200. doi: 10.2991/jegh.k.200806.001

Stammes, M. A., Bakker, J., Vervenne, R. A. W., Zijlmans, D. G. M., van Geest, L., Vierboom, M. P. M., et al. (2021). Recommendations for standardizing thorax PET-CT in non-human primates by recent experience from macaque studies. *Anim. (Basel)* 11 (1), 204. doi: 10.3390/ani11010204

Stammes, M. A., Lee, J. H., Meijer, L., Naninck, T., Doyle-Meyers, L. A., White, A. G., et al. (2022). Medical imaging of pulmonary disease in SARS-CoV-2-exposed non-human primates. *Trends Mol. Med.* 28, 123–142. doi: 10.1016/j.molmed.2021.12.001

Wolfel, R., Corman, V. M., Guggemos, W., Seilmaier, M., Zange, S., Muller, M. A., et al. (2020). Virological assessment of hospitalized patients with COVID-2019. *Nature.* 581, 465–469. doi: 10.1038/s41586-020-2196-x

Wu, Y., Guo, C., Tang, L., Hong, Z., Zhou, J., Dong, X., et al. (2020). Prolonged presence of SARS-CoV-2 viral RNA in faecal samples. *Lancet Gastroenterol. Hepatol.* 5, 434–435. doi: 10.1016/S2468-1253(20)30083-2

Xiao, F., Tang, M., Zheng, X., Liu, Y., Li, X., and Shan, H. (2020). Evidence for gastrointestinal infection of SARS-cov-2. *Gastroenterology*. 158, 1831–3 e3. doi: 10.1053/j.gastro.2020.02.055

Zhu, Y., Sharma, L., and Chang, D. (2023). Pathophysiology and clinical management of coronavirus disease (COVID-19): a mini-review. *Front. Immunol.* 14, 1116131. doi: 10.3389/fimmu.2023.1116131

frontiers | Frontiers in Cellular and Infection Microbiology

TYPE Original Research
PUBLISHED 03 January 2025
DOI 10.3389/fcimb.2024.1496991

OPEN ACCESS

EDITED BY
Sam Ebenezer,
Sathyabama Institute of Science and Technology, India

REVIEWED BY
Eduardo Becerril,
National Institute of Respiratory Diseases-Mexico (INER), Mexico
Konda Mani Saravanan,
Bharath Institute of Higher Education and Research, India

*CORRESPONDENCE
Wen Dong
kongxinlab@163.com

RECEIVED 16 September 2024
ACCEPTED 29 November 2024
PUBLISHED 03 January 2025

CITATION
Yang Z, Ren ZD, Wang J and Dong W (2025) Based on the MaxEnt model the analysis of influencing factors and simulation of potential risk areas of human infection with avian influenza A (H7N9) in China.
Front. Cell. Infect. Microbiol. 14:1496991.
doi: 10.3389/fcimb.2024.1496991

Based on the MaxEnt model the analysis of influencing factors and simulation of potential risk areas of human infection with avian influenza A (H7N9) in China

Zhao Yang[1,2], Zhong Da Ren[3,4], Jie Wang[5] and Wen Dong[1,2]*

[1]Faculty of Geography, Yunnan Normal University, Kunming, China, [2]Geographic Information System Technology Engineering Research Centre for West-China Resources and Environment of Educational Ministry, Yunnan Normal University, Kunming, China, [3]State Key Laboratory of Estuarine and Coastal Research, East China Normal University, Shanghai, China, [4]Department of Geography, University College Cork, Cork, Ireland, [5]School of Big Data and Information Industry, Chongqing City Management College, Chongqing, China

Exposure to infected animals and their contaminated environments may be the primary cause of human infection with the H7N9 avian influenza virus. However, the transmission characteristics and specific role of various influencing factors in the spread of the epidemic are not clearly understood. Therefore, it is of great significance for scientific research and practical application to explore the influencing factors related to the epidemic. Based on the data of relevant influencing factors and case sample points, this study used the MaxEnt model to test the correlation between human infection with H7N9 avian influenza and influencing factors in China from 2013 to 2017, and scientifically simulated and evaluated the potential risk areas of human infection with H7N9 avian influenza in China. The simulation results show that the epidemic risk is increasing year by year, and the eastern and southeastern coasts have always been high-risk areas. After verification, the model simulation results are generally consistent with the actual outbreak of the epidemic. Population density was the main influencing factor of the epidemic, and the secondary influencing factors included vegetation coverage, precipitation, altitude, poultry slaughter, production value, and temperature. The study revealed the spatial distribution and diffusion rules of the H7N9 epidemic and clarified the key influencing factors. In the future, more variables need to be included to improve the model and provide more accurate support for prevention and control strategies.

KEYWORDS

H7N9, Maxent model, Influencing factors, risk simulation, China

1 Introduction

The first human case of avian influenza (H7N9) was detected in China in early 2013, followed by identifying the virus in local live poultry markets. At the beginning of the epidemic, the H7N9 avian influenza virus exhibited low pathogenic in poultry. However, the fatality rate of human infection with H7N9 avian influenza virus was significantly higher compared to that of seasonal influenza infection (Zhang et al., 2015). In early 2017, researchers found that a mutant strain was highly pathogenic to poultry and caused multiple outbreaks (Wu et al., 2021; Benmarhnia, 2020; Yu et al., 2014). Studies indicate that live poultry markets may contribute significantly to the transmission of H7N9 avian influenza to humans. This could be attributed to the ideal H7N9 avian influenza virus environment created by the traditional poultry breeding system with a semi-mixed breeding mode (Dong et al., 2015). Meanwhile, poultry farming systems are widespread in the southern coastal areas, recognized as high-risk areas for the spread of avian influenza viruses (Dong et al., 2017; Li et al., 2019; Shan et al., 2019). The outbreak of the H7N9 avian influenza among humans has posed a major threat to both the poultry industry and public health in China. As a result, several cities in southeastern China, including Shanghai, have taken steps to control the outbreak by gradually shutting down all local live poultry markets since April 4, 2013. Although previous studies have investigated the epidemiological features of human H7N9 avian influenza outbreaks and the general risk of disease outbreaks (Chong et al., 2016; Liu and Fang, 2015; Zhuang et al., 2013), no evidence of human-to-human transmission has been found (Bi et al., 2016; Zhou et al., 2018). Studies have found that the outbreak and transmission of H7N9 avian influenza to humans is likely related to poultry trade, vegetation cover, population density, and other factors (Shi et al., 2013; Wu et al., 2015; Zhou et al., 2020). Furthermore, other studies have shown that transmission of human infection with H7N9 avian influenza may be related to climate factors such as temperature, rainfall, and humidity (Fuller et al., 2014; Gao et al., 2020; Hu et al., 2015). In summary, human exposure to infected animals and their contaminated environment may be the primary cause of human infection with the H7N9 avian influenza virus. However, the transmission characteristics of human infection with the H7N9 avian influenza virus and the possible roles of various influencing factors in the transmission process are still unclear (Fang et al., 2013; Kim and Pak, 2019). Therefore, exploring the influencing factors that may be related to the epidemic is an important public health issue to be solved in recent years, which has good scientific research significance and practical application value.

The MaxEnt model is commonly used in biogeography, conservation biology, and ecology. It is used to identify environmental conditions that are related to the occurrence of a particular species and to estimate and predict the distribution of species in a specific region or under particular environmental conditions (Golding and Purse, 2016). Although few studies have utilized the MaxEnt model to assess potential risk areas and related influencing factors of human infection with H7N9 avian influenza, the MaxEnt model has been widely employed in public health research in recent years (Escobar and Craft, 2016; Wardrop et al., 2014). In particular, more and more attention has been paid to infectious diseases related to vector species, such as mosquito-borne diseases and tick-borne diseases (Bui et al., 2017; Liu et al., 2019; Wang et al., 2023), which are to some extent affected by climatic conditions that determine the distribution of vectors (Bui et al., 2017). Based on the MaxEnt model, this study tested the correlation between human infection with H7N9 avian influenza and its influencing factors in China from 2013 to 2017 and conducted scientific simulation and assessment of the potential risk areas for human infection with H7N9 avian influenza in China. The results of the study will help the government and relevant public health departments to formulate targeted epidemic prevention and surveillance strategies.

2 Materials and methods

2.1 Case data

The data on human infection with H7N9 avian influenza in China were from the Beijing Center for Disease Control and Prevention. From 2013 to 2017, a total of 1,474 people were infected with the H7N9 avian influenza virus in the country, including 155 in 2013, 333 in 2014, 196 in 2015, 265 in 2016, and 591 in 2017.

2.2 Poultry breeding data

Poultry breeding data for this study were obtained from the National Bureau of Statistics of China (https://www.stats.gov.cn/), and the poultry slaughter data and Poultry output data for different provinces in the 2013-2017 China Rural Statistical Yearbook were downloaded. In this study, the output value and vector data of poultry in related areas were converted into raster data by ArcGIS.

2.3 Meteorological data

The meteorological data in this paper are sourced from the Institute of Tibetan Plateau Research, Chinese Academy of Sciences. The spatial resolution of the data is 0.0083333° (about 1km). This dataset is generated from the global 0.5° meteorological dataset released by CRU and the global high-resolution climate dataset released by WorldClim and downscaled in China using the Delta spatial downscaling scheme. This study is based on the data sets of monthly precipitation, minimum temperature, and maximum temperature during 2013-2017.

2.4 Population data

China's population distribution is uneven, among which the population density in the southeast is relatively high, and the population density in the northwest is relatively low. In the process of population spatial data processing in China, this study first calculates the population distribution weight of land use type, nightlight data, and

settlement density, and then calculates the total weight of each county administrative unit based on the standardized treatment of the influence weights of the above three aspects. Then, based on the grid space calculation, the population quantity on the unit weight is combined with the total weight distribution map. Thus, population data can be spatialized. In this study, the population spatial distribution data of the 1 km grid was finally obtained using the method described above, which better reflects the spatial distribution of the population in China (Figure 1 Spatial distribution of population). The spatial distribution data of the population obtained in this study are grid data, each grid represents the number of population within the grid range (1 square kilometer), in the unit of person/square kilometer. The data format is gird (http://www.resdc.cn) (Xu, 2017).

2.5 Elevation data and vegetation index data

This research USES the elevation data (DEM) comes from us space shuttle endeavor radar topography SRTM (Shuttle Radar Topography Mission) data sets. The data set is a 500m precision data set generated by resampling the latest SRTMV4.1 data (http://www.resdc.cn). In addition, the China Vegetation Index (NDVI) spatial distribution data set used in this paper is SPOT/VEGETATIONNDVI satellite remote sensing data based on continuous time series. This dataset is the annual vegetation index dataset since 1998 generated by the maximum synthesis method (http://www.resdc.cn) (Xu, 2018).

2.6 Modeling methods

MaxEnt (version 3.4.1) used in this study is open-source software and can be used for scientific research free of charge (https://biodiversityinformatics.amnh.org/open_source/maxent/). The MaxEnt model can be used to predict the potential geographical distribution of species, and it has been proven to be effective in assessing the potential distribution of ecological or environmental-related diseases (Liu et al., 2018; Artun, 2019; Ma et al., 2019).

Based on relevant influencing factors and case sample points, this study used the MaxEnt model to simulate the potential risk areas of human infection with H7N9 avian influenza in China and assessed the risk probability of epidemic occurrence in relevant areas (Figure 2 Technical route). In the process of modeling, the maximum entropy principle and jackknife method were used to

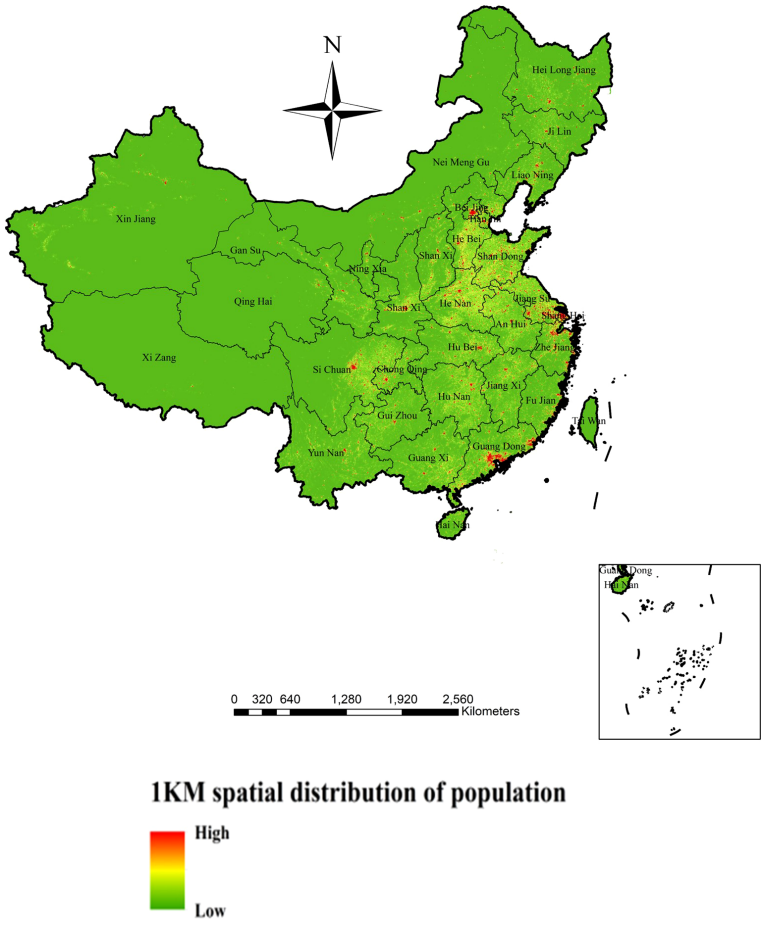

FIGURE 1
Spatial distribution data of population on a 1km grid.

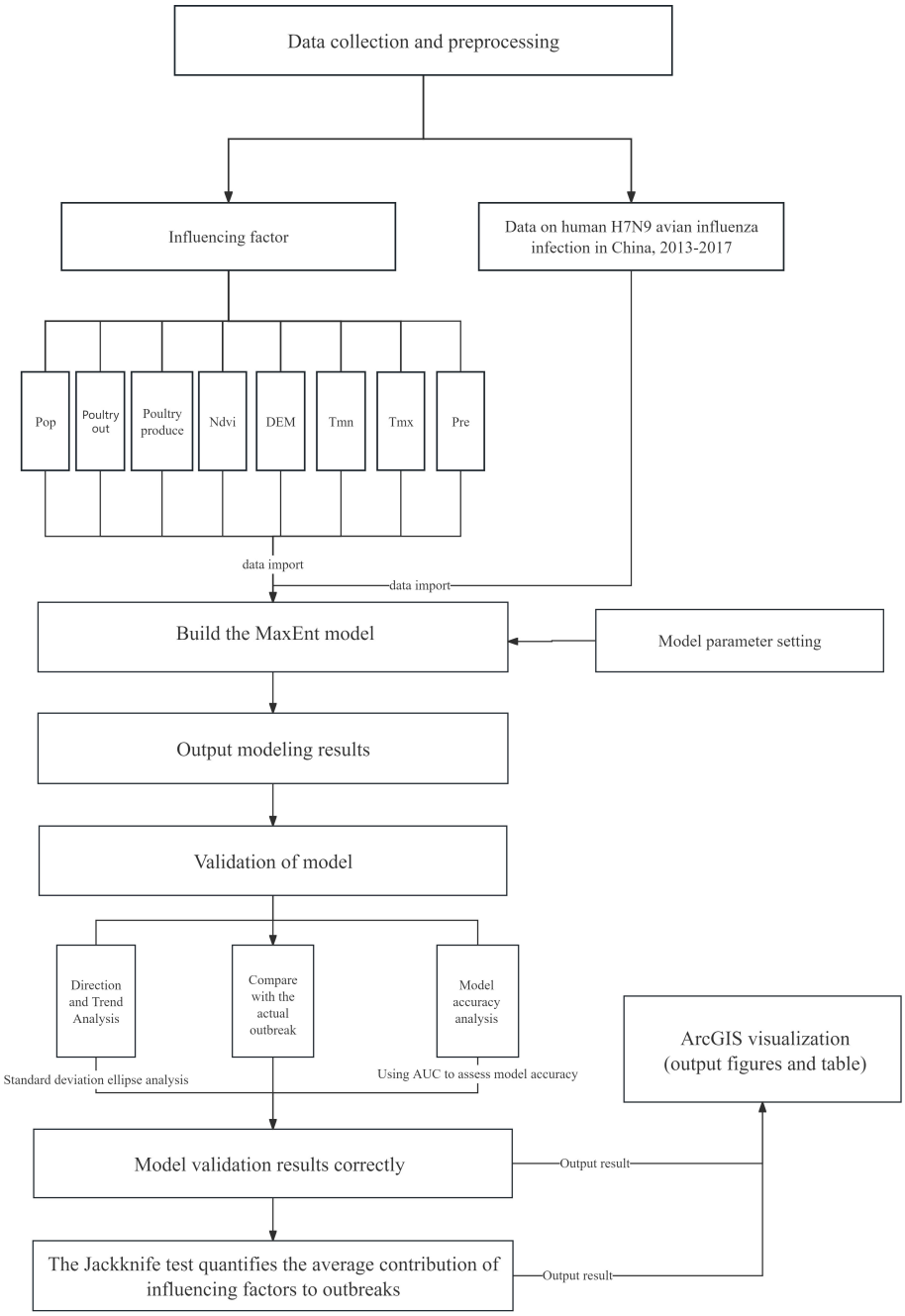

FIGURE 2
Technical route. In this study, we simulated the potential risk of an outbreak by building a MaxEnt model based on the outbreak data of human infection with the H7N9 avian influenza virus in China from 2013 to 2017 and environmental variables that may be related to the outbreak, including: Pre (average monthly precipitation), Tmx (average monthly maximum temperature), Tmn (average minimum temperature), DEM (altitude), Ndvi (vegetation coverage), Poultry produce (annual poultry).The MaxEnt model was used to simulate the potential risk areas of the outbreak, explore the influencing factors related to the outbreak and assess the risk probability of the outbreak in each area.

calculate the influence of each influencing factor to evaluate the impact of different influencing factors on the risk of human infection with H7N9 avian influenza. The data sample points used in this study were the location data of disease points from 2013 to 2017. To reduce the error, 75% of the epidemic data were selected for model training and 25% for model verification (Yuan et al., 2015). To clearly visualize the risk of human infection with H7N9 avian influenza in different regions of China, this study used four levels (Non-risk, low risk, medium risk, high risk) to represent varying degrees of risk. In this paper, the ROC characteristic curve was used to verify the model, and the ROC curve standard was defined as follows: The simulation result of AUC [0.5, 0.6] was "failure"; The simulation results of AUC [0.6, 0.7] were "poor". The simulation result of AUC [0.7, 0.8] is "average", the simulation result of AUC [0.8, 0.9] is "good", and the simulation result of AUC [0.9, 1.0] is "very good" (Ren et al., 2020).

3 Results

3.1 Simulation results of potential risk areas based on MaxEnt modeling

The simulation results of potential risk areas for human infection with H7N9 avian influenza in China based on the MaxEnt model show (Figure 3 Simulation results of potential risk areas). In 2013, the potential risk areas for human infection with H7N9 avian influenza were mainly distributed in Beijing, Hebei, Shandong, Shanxi, Henan, Jiangsu, Shanghai, Anhui, Hunan, Hubei, Zhejiang, Jiangxi, Sichuan, Fujian and other places; In 2014, the potential risk areas for human infection with H7N9 avian influenza were newly added in Xinjiang and some parts of Taiwan, and the risk of epidemic in Shandong, Guangxi and Hunan increased. In 2015, the potential risk areas for human infection with H7N9 avian influenza were mainly Guangdong, Shanghai, Heilongjiang, Xinjiang, Liaoning, Jilin, Sichuan, and other places; The potential risk areas for human infection with H7N9 avian influenza in 2016 indicate that the risk of epidemic in Xinjiang has weakened, while the risk of epidemic in Sichuan, Shandong, Henan, Jiangxi, Hunan and other places has increased. By 2017, the risk of epidemic occurrence was increasing in Guangxi, Guizhou, Sichuan, Heilongjiang, Jilin, Liaoning, Yunnan, Tibet, Qinghai, Gansu, Shaanxi and Inner Mongolia. In general, the risk of human infection with H7N9 avian influenza in China from 2013 to 2017 showed an increasing trend year by year, among which the eastern and southeastern coastal areas of China have always been high-risk areas of the epidemic, and the epidemic risk showed a clear trend of spreading from the eastern and southeastern coastal areas of China to the inland and western regions.

3.2 Verification and analysis of model simulation results

3.2.1 Direction and trend analysis

As can be seen in Figure 4 (Standard deviational ellipses analysis) during the period 2013-2016, in 2013, the mean center of the ellipse was located in Huangshan City, Anhui Province, and the ellipse was focused in the eastern region of China, mainly including Nanjing, Wuxi, and Suzhou in Jiangsu Province, as well as Chuzhou City, Anhui Province, Huzhou City, Zhejiang Province, and Shanghai City; In 2014, the mean center of the ellipse was focused in Shangrao City, Jiangxi Province, and the ellipse was confined to the eastern and partially central regions of China, mainly including Jiangsu Province, Anhui Province, Zhejiang Province (Hangzhou, Ningbo, and Shaoxing), Guangzhou, Shenzhen City in Guangdong Province, and Shanghai; In 2015, the average center of the ellipse was located in Quzhou City, Fujian Province, and the ellipse was confined to the eastern part of China, mainly including Jiangsu, Anhui, and Zhejiang Provinces (Wenzhou, Jiaxing, Huzhou, Quzhou, and Taizhou), Fujian Province (Fuzhou, Xiamen, Quanzhou, and Zhangzhou), as well as Guangdong Province (Shenzhen, Jiangmen, Meizhou, Shanwei and Dongguan) and Shanghai; In 2016, the mean center of the ellipse was located in Huangshan City, Anhui Province, and the ellipse was concentrated in the eastern part of China, which mainly included Jiangsu Province (Wuxi, Changzhou, and Suzhou),

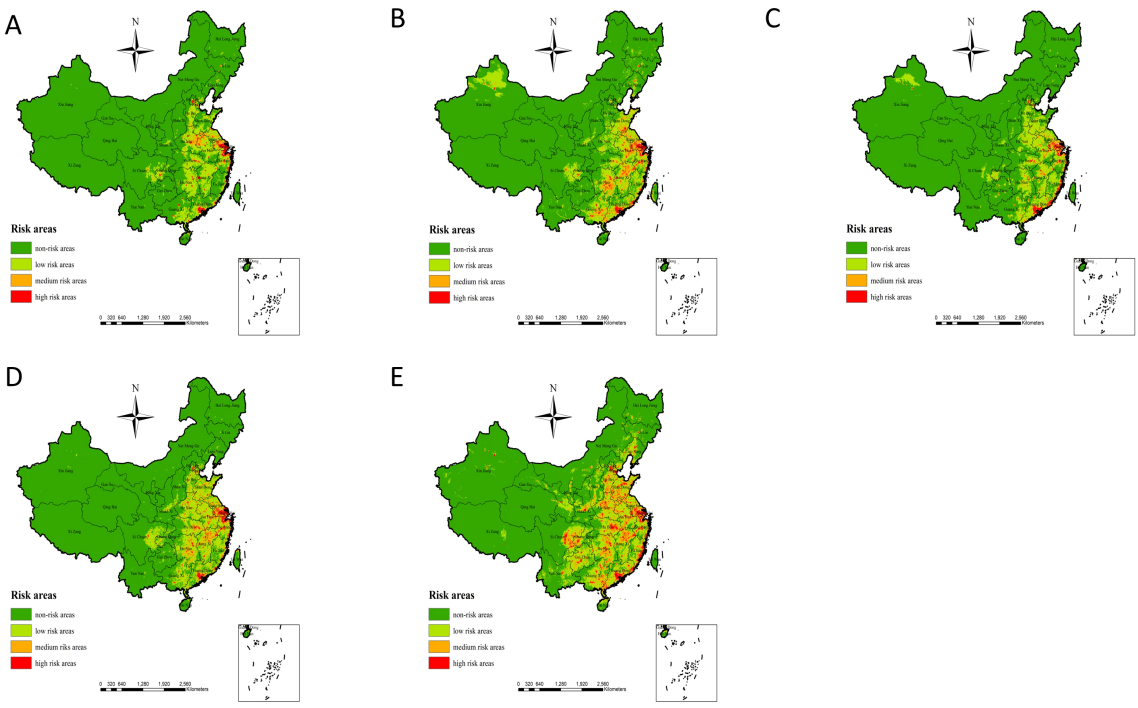

FIGURE 3
(A–E) represent the simulation results of potential risk areas for human infection with H7N9 in 2013, 2014, 2015, 2016 and 2017, respectively avian influenza in China.

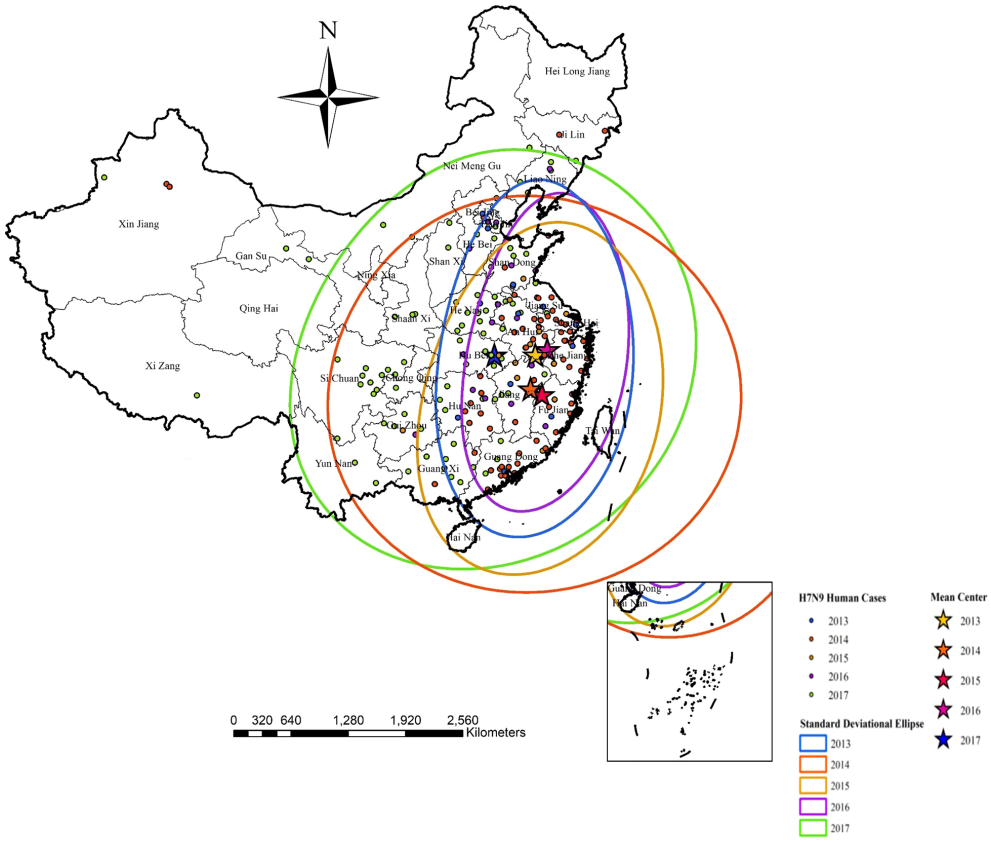

FIGURE 4
Illustrates clearly the mean centers and the directional trends of influenza A(H7N9) human cases from 2013 to 2017 by standard deviational ellipses.

Hefei City, Anhui Province, Zhejiang Province (Hangzhou and Wenzhou), and Shanghai; In 2017, the average center of the ellipse was located in Huangshi City, Hubei Province, and the ellipse was confined to eastern and most of central China, including Jiangsu Province (Suzhou City and Taizhou City), Anhui Province, Zhejiang Province (Ningbo City), Beijing City, Chengde City in Hebei Province, Chengdu City in Sichuan Province and Shanghai City.

3.2.2 Actual outbreaks in 2013-2017

The actual outbreaks of human H7N9 avian influenza outbreaks from 2013 to 2017 (Figure 5 Actual outbreak situation) demonstrated that, in 2013, Shanghai, Jiangsu, and Zhejiang were hardest hit by the H7N9 avian influenza outbreak with a high number of cases. In 2014, an outbreak of human H7N9 avian influenza occurred in the Xinjiang region, while the Zhejiang and Guangdong regions experienced an increase in cases. In 2015, the human infection with H7N9 avian influenza epidemic in the country exhibited a certain degree of a weakening trend, although the Guangdong region continued to experience the most severe outbreak, and the Zhejiang region also reported an increase in new cases. In 2016, the Jiangsu, Shanghai, and Zhejiang outbreaks were again serious, while the Guangdong region exhibited a certain degree of weakening. In 2017, the Guangxi, Guizhou, Hunan, Jiangxi, Guangdong, Beijing, and Hebei cases increased significantly, while outbreaks also occurred in Yunnan, Sichuan, Shaanxi, Shanxi, Gansu, and Guizhou (Figure 5 Actual outbreak situation). As can be seen from the results of the modeled risk assessment and the actual outbreaks of human H7N9 avian influenza outbreak risk (Figure 3 Simulation results of potential risk areas; Figure 5 Actual outbreak situation), the results of the model assessment and the actual incidence of this study are generally consistent with each other.

3.2.3 Accuracy analysis of epidemic risk model simulation

To further verify the risk simulation effect of the model, this study used AUC (area under the ROC curve) to evaluate the model accuracy, where the larger the value of AUC, the higher the accuracy of the model prediction. From Figure 6 (Analysis of model simulation accuracy), it can be seen that the AUC values of the model training set from 2013 to 2017 are 0.994, 0.989, 0.993, 0.985, and 0.977, respectively, and that of the model test set is 0.976, 0.991, 0.993, 0.992, and 0.954, respectively. It can be seen that the model constructed in this study has relatively good accuracy.

3.2.4 Average contribution of each influencing factor to the outbreak

The contribution rate of each influencing factor to the prediction model of human infection with H7N9 avian influenza is shown in Table 1. The results of this study showed that

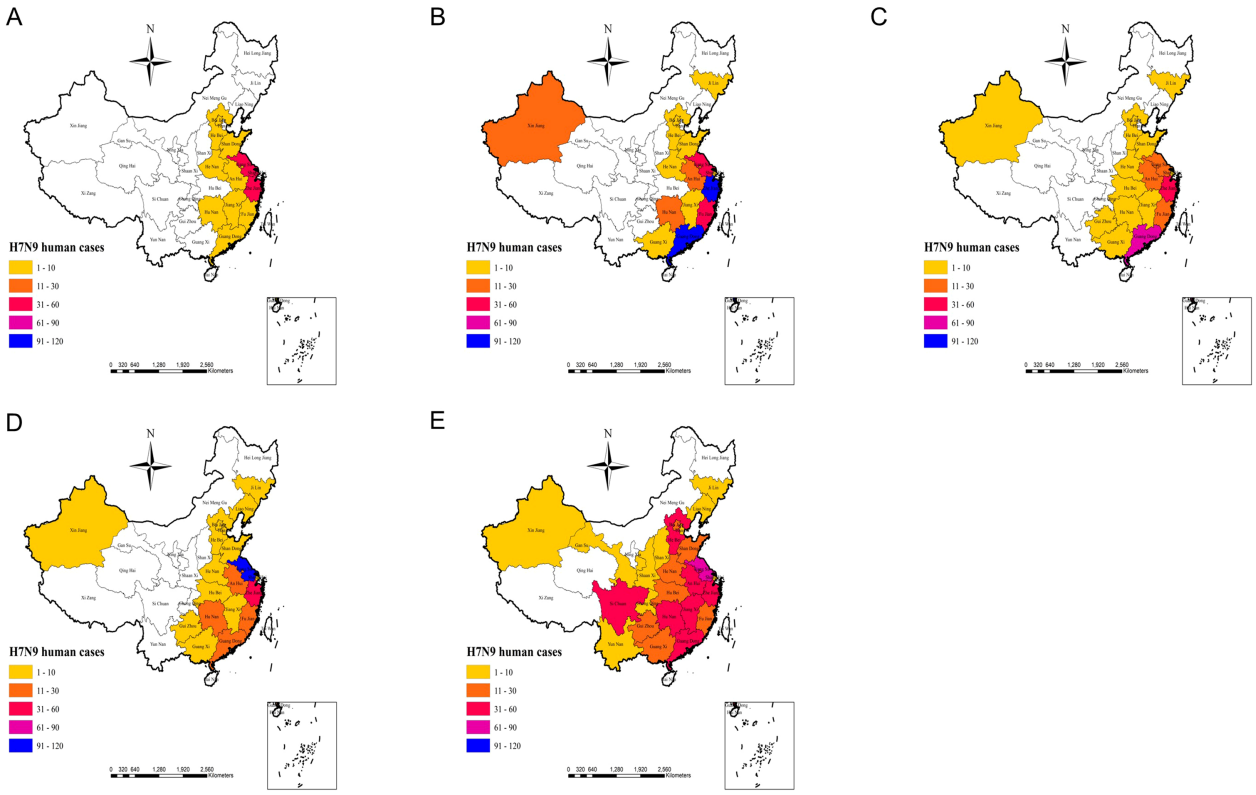

FIGURE 5
(A–E) represents the actual human H7N9 avian influenza outbreaks in China in 2013, 2014, 2015, 2016, and 2017 respectively.

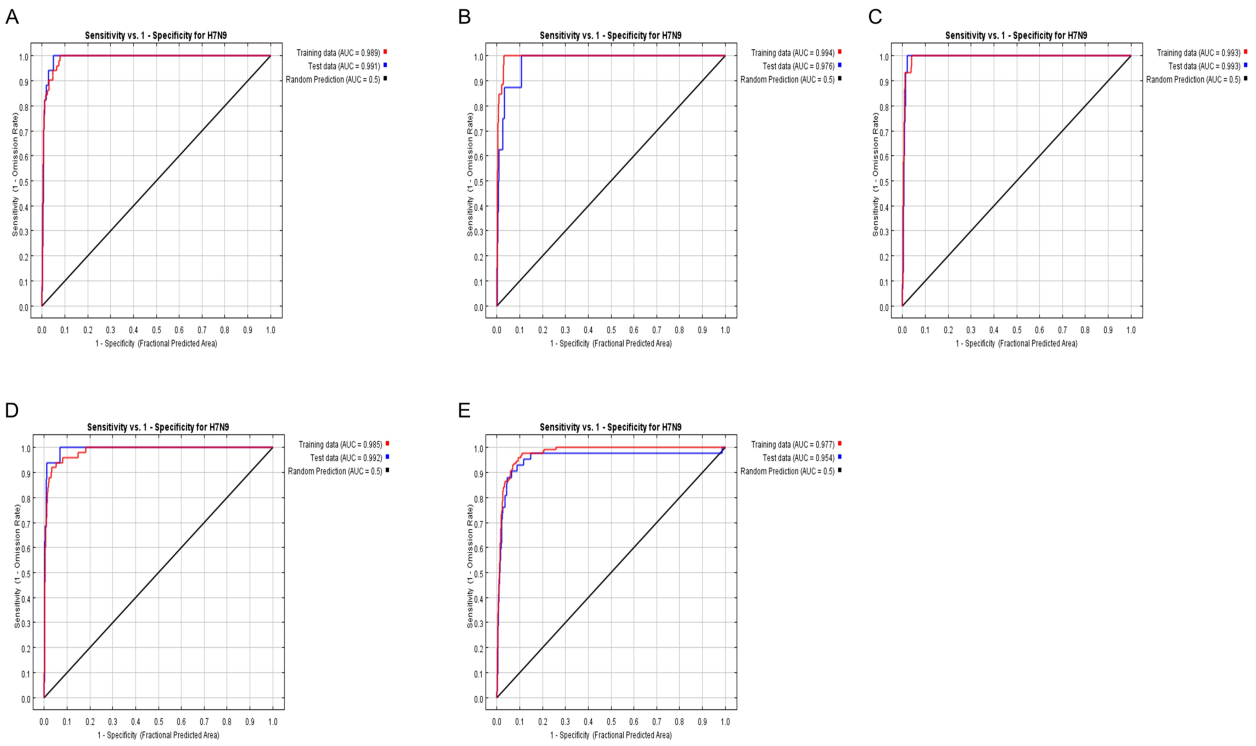

FIGURE 6
(A–E) representing 2013, 2014, 2015, 2016, 2017, the ROC curve and AUC values.

TABLE 1 Average contribution rate of each factor to H7N9 avian influenza epidemic from 2013 to 2017.

Variable	Percent contribution (%)	Permutation importance
Tmn	0.13	0.08
Pre	0.91	0.92
Tmx	0.36	1.39
Dem	0.64	18.88
Pop	72.96	34.2
Poultry produce	0.42	0.84
Ndvi	8.82	14.9
Poultry out	0.5	0.76

population density was the main influencing factor for the occurrence of H7N9 avian influenza in humans from 2013 to 2017 (72.96% Percent contribution and 34.2 Permutation importance). It was followed by vegetation cover index (8.82% Percent contribution and 14.9 Permutation importance), precipitation(0.91% Percent contribution and 0.92 Permutation importance), altitude (0.64% Percent contribution and 18.88 Permutation importance), poultry slaughter (0.5% Percent contribution and 0.76 Permutation importance) poultry production value (0.42% Percent contribution and 0.84 Permutation importance) and monthly average maximum temperature (0.36% Percent contribution and 1.39 Permutation importance) also had moderate effects on human H7N9 infection in avian influenza. Monthly average minimum temperature (0.13% Percent contribution and 0.08 Permutation importance) had no significant effect on human infection with H7N9 avian influenza (Table 1).

4 Discussion

We used MaxEnt to predict the potential distribution of human H7N9 avian influenza outbreaks in China because the MaxEnt model showed accurate predictive power in data-only simulations and evaluations. Its predictive power is superior to some classical modeling methods, such as random forest and logistic regression models, which generally show accurate predictive power in the simulation and evaluation of only data (Jia and Joyner, 2015). However, it turns out that MaxEnt's prediction is more accurate when the sample size is smaller, which is more appropriate for human H7N9 bird flu outbreak data (Shcheglovitova and Anderson, 2013; Bean et al., 2012; Wisz et al., 2008). Of course, no model is perfect, and it has its limitations. In order to ensure the accuracy of prediction results as much as possible during the calculation of MaxEnt model, a large number of external parameters need to be input, which leads to large workload in the early stage of data processing and complicated data calculation process. In addition, the accuracy of the model is highly dependent on the quality and integrity of the input data, and insufficient or biased data may lead to inaccurate prediction results (Aloufi, 2024).

Through the standard deviation ellipse analysis, the human infection with H7N9 avian influenza in China showed obvious characteristics of temporal and spatial clustering, and the distribution of cases in some natural years also showed a certain trend of diffusion direction and statistically significant spatio-temporal clustering. The epidemic had the characteristics of overall spread but local clustering. In the analysis, we integrated variables such as temperature, rainfall, altitude, population density, NDVI, annual poultry production, and poultry slaughter to simulate the regional risk distribution of human infection with H7N9 avian influenza in China based on the MaxEnt model.

The model showed that population density was the main influencing factor for human infection with H7N9 avian influenza from 2013 to 2017, followed by vegetation cover index, precipitation, altitude, poultry slaughter, poultry production value, and temperature. The more densely populated areas, the greater the risk of human infection with H7N9 bird flu outbreaks. This result indicates that these areas may be contaminated with the H7N9 avian influenza virus, and cases of H7N9 avian influenza virus infection in humans will likely occur. This may be due to the high mobility of densely populated areas, so people infected with H7N9 avian influenza epidemic. Vegetation coverage also has a greater impact on human infection with H7N9 avian influenza, which may be because areas with high vegetation coverage provide a favorable ecological environment for birds to inhabit, attracting a large number of birds to stay in the area. When the climate conditions in the area are conducive to the survival and reproduction of the H7N9 avian influenza virus, these areas with high vegetation coverage become dangerous sources of infection, thus increasing the probability of outbreaks. Precipitation and monthly maximum average temperature also had some effects on human infection with H7N9 avian influenza, but the monthly minimum temperature had little effect on human infection with H7N9 avian influenza. This may be due to the sensitivity of the H7N9 virus to climate, and the virus can survive for a longer time in a suitable environment.

According to our risk model, starting from Shanghai, high-risk areas for human transmission of H7N9 avian influenza were identified in the southeastern coastal areas and extended to the southwest. Shanghai and much of Guangdong have always been high-risk areas. Shanghai was the site of the first human outbreak of H7N9 avian influenza and still reflects a high risk (Xv et al., 2015). The reason for the outbreak of human H7N9 avian influenza in the eastern coastal areas may be that the local average temperature is very close to the temperature that is most suitable for the survival of avian influenza virus (H7N9); In addition, there are many live poultry processing factories and live poultry farms in these areas, and the traditional live poultry breeding system uses semi-mixed breeding methods, and poultry is the traditional carrier of H7N9 avian influenza virus, creating an ideal environment for the

transmission of H7N9 avian influenza virus, which also increases the risk of local residents coming into contact with poultry infected by H7N9 avian influenza virus. Inland, human H7N9 bird flu outbreak risk models show high risk in areas around the Yangtze River Delta, including its major tributaries such as Dongting Lake. These are migratory bird habitats and areas known to be at high risk for human transmission of H7N9 avian influenza (Bui et al., 2017; Liu et al., 2019; Wang et al., 2023). The eastern provinces (including Anhui, Jiangxi, Henan, Shandong, and Hubei) also contain some high-risk areas, but as can be seen from Figures 1–6, there are relatively few high-risk areas in these provinces. In these provinces, the driest months have very little rainfall, which may also increase the potential for the flu virus to spread from poultry to humans. This reminds us that in the dry season, we should strengthen the prevention of human infection with H7N9 avian influenza, and reduce the risk of poultry transmission of H7N9 avian influenza virus to humans. Vegetation coverage also has an impact on human infection with H7N9 avian influenza, which may be because the higher the vegetation coverage, the more suitable for wild birds to survive, which also provides a good way for the transmission of human infection with H7N9 avian influenza.

In our study, we also found that most high-risk areas from 2013 to 2016 were mainly concentrated in coastal areas such as Shanghai, Guangdong, Zhejiang, and Jiangsu. As of 2017, the epidemic has clearly spread from the eastern coastal areas to the western inland areas, and the outbreak has spread most seriously in 2017. It is worth noting that in 2017, the affected areas began to spread inland from the coastal areas. From 2013 to 2017, the central point of human infection with H7N9 avian influenza was mainly concentrated in Anhui, Fujian, Zhejiang, Jiangxi, and Hubei regions, and showed a trend of continuous westward spread in the eastern coastal areas. This shows that some southeastern coastal provinces and some central provinces have always been high-risk areas for human infection with H7N9 avian influenza, and gradually extending inland. Given this, epidemic prevention departments in these provinces should strengthen epidemic prevention measures to prevent the spread of the epidemic to the inland.

5 Conclusion

Based on the MaxEnt model, this study analyzed the spatial potential distribution of human infection with H7N9 avian influenza from 2013 to 2017 and the law of epidemic spread, and explored various influencing factors related to epidemic occurrence. Our research results can provide some auxiliary decision support for prevention work. Although the MaxEnt model provides some useful insights for the study of avian influenza virus, because the transmission of human H7N9 avian influenza virus is a rather complex process, we still need to incorporate more influencing factors into our model and expand the sample size in future work to improve the prediction accuracy and wide applicability of the model.

Data availability statement

The original contributions presented in the study are included in the article/supplementary material. Further inquiries can be directed to the corresponding authors.

Ethics statement

The study only used the data of human H7N9 infections in China to conduct spatial analysis and study the influencing factors of the epidemic. The studies were conducted in accordance with the local legislation and institutional requirements. The participants provided their written informed consent to participate in this study. Written informed consent was obtained from the individual(s) for the publication of any potentially identifiable images or data included in this article.

Author contributions

ZY: Formal analysis, Methodology, Software, Writing – original draft, Writing – review & editing. JW: Writing – review & editing, Conceptualization, Investigation, Validation. WD: Writing – review & editing, Funding acquisition, Project administration, Resources, Supervision. ZR: Investigation, Validation, Writing – review & editing, Data curation, Formal analysis, Methodology, Software.

Funding

The author(s) declare financial support was received for the research, authorship, and/or publication of this article. This research was supported by the National Natural Science Foundation of China (Grant Nos. 42161071, 41661087, 42161065, 41461038).This work was supported by the project funding of the “Support Program of Xingdian Talents”.

Conflict of interest

The authors declare that the research was conducted in the absence of any commercial or financial relationships that could be construed as a potential conflict of interest.

Publisher’s note

References

Aloufi, A. S. (2024). MaxEnt modeling of Klebsiella pneumoniae: predicting future distribution and evaluating the risk for public health. *Geomatics Natural Hazards Risk.* 15, 1. doi: 10.1080/19475705.2024.2417688

Artun, O. (2019). Ecological niche modeling for the prediction of cutaneous leishmaniasis epidemiology in current and projected future in Adana, Turkey. *J. vector borne diseases.* 56, 127–133. doi: 10.4103/0972-9062.263726

Bean, W. T., Stafford, R., and Brashares, J. S. (2012). The effects of small sample size and sample bias on threshold selection and accuracy assessment of species distribution models. *Ecography.* 35, 250–258. doi: 10.1111/j.1600-0587.2011.06545.x

Benmarhnia, T. (2020).). Linkages between air pollution and the health burden from COVID-19: methodological challenges and opportunities. *Am. J. Epidemiol.* 189, kwaa148. doi: 10.1093/aje/kwaa148

Bi, Y. H., Liu, J. Y., Xiong, H. F., Zhang, Y., Liu, D., Liu, Y. X., et al. (2016). A new reassortment of influenza A (H7N9) virus causing human infection in Beijin. *Sci. Rep.* 6, 26624. doi: 10.1038/srep26624

Bui, C. M., Gardner, L., Maclntyre, C. R., and Sarkar, S. (2017). Influenza A H5N1 and H7N9 in China: A spatial risk analysis. *PloS One* 12, 4. doi: 10.1371/journal.pone.0176903

Chong, K., Wang, X., Liu, S., Cai, J., Su, X., Zee, B. C., et al. (2016). Interpreting the transmissibility of the avian influenza A (H7N9) infection from 2013 to 2015 in Zhejiang Province,China. *Epidemiol. Infection.* 144, 8. doi: 10.1017/S0950268815002812

Dong, W., Yang, K., Xu, Q.-L., Liu, L., and Chen, J. (2017). Spatio-temporal pattern analysis for evaluation of the spread of human infections with avian influenza A(H7N9) virus in Chin-2014. *BMC Infect. Diseases.* 17, 704. doi: 10.1186/s12879-017-2781-2

Dong, W., Yang, K., Xu, Q.-L., and Yang, Y.-L. (2015). A predictive risk model for A (H7N9) human infections based on spatial-temporal autocorrelation and risk factors: Chin-2014. *Int. J. Environ. Res. Public Health* 12, 12. doi: 10.3390/ijerph121214981

Escobar, L. E., and Craft, M. E. (2016). Advances and limitations of disease biogeography using ecological niche modeling. *Front. Microbiol.* 7. doi: 10.3389/fmicb.2016.01174

Fang, L. Q., Li, X. L., Liu, K., Li, Y. J., Yao, H. W., Liang, S., et al. (2013). Mapping spread and risk of avian influenza A (H7N9) in China. *Environ. Res.* 3, 2722. doi: 10.1038/srep02722

Fuller, T., Havers, F., Xu, C. L., Fang, L. Q., Cao, W. C., Shu, Y. L., et al. (2014). Identifying areas with a high risk of human infection with the avian influenza A (H7N9) virus in East Asia. *J. Infection.* 69, 174–181. doi: 10.1016/j.jinf.2014.03.006

Gao, X., Huang, Y. R., Zheng, J. H., Xiao, J. H., and Wang, H. B. (2020). Impact of meteorological and geographical factors on the distribution of leishmaniasis's vector in mainland China. *Pest Manage. Science.* 76, 961–966. doi: 10.1002/ps.5604

Golding, N., and Purse, B. V. (2016). Fast and flexible Bayesian species distribution modelling using Gaussian processes. *Methods Ecol. Evolution.* 7, 598–608. doi: 10.1111/2041-210X.12523

Hu, W., Zhang, W., Huang, X., Clements, A., Mengersen, K., and Tong, S. L. (2015). Weather variability and influenza A (H7N9) transmission in Shanghai, China: A Bayesian spatial analysis. *Environ. Res.* 136, 405–412. doi: 10.1016/j.envres.2014.07.033

Jia, P., and Joyner, A. (2015). Human brucellosis occurrences in inner Mongolia, China: a spatio-temporal distribution and ecological niche modeling approach. *BMC Infect. diseases.* 15, 36. doi: 10.1109/ACCESS.2020.3037912

Kim, E., and Pak, S.-I. (2019). Application of species distribution model for predicting areas at risk of highly pathogenic avian influenza in the Republic of Korea. *J. Veterinary Clinics.* 36, 23–29. doi: 10.17555/jvc.2019.02.36.1.23

Li, Z., Fu, J. Y., Lin, G., and Jiang, D. (2019). Spatiotemporal variation and hotspot detection of the avian influenza A(H7N9) virus in Chin-2017. *Int. J. Of Enviormental Res. And Public Health* 16, 4. doi: 10.3390/ijerph16040648

Liu, B. Y., Jiao, Z. H., Ma, J., Gao, X., Xiao, J. H., Hayat, M. A., et al. (2019). Modelling the potential distribution of arbovirus vector Aedes aEgypti under current and future climate scenarios in Taiwan, China. *Pest Manage. Science.* 75, 11. doi: 10.1002/ps.5424

Liu, K. K., Sun, J. M., Liu, X. B., Li, R. Y., Wang, Y. G., Lu, L., et al. (2018). Spatiotemporal patterns and determinants of dengue at county level in China from 2005–2017. *Int. J. Infect. Diseases.* 77, 96–104. doi: 10.1016/j.ijid.2018.09.003

Liu, Z., and Fang, C.-T. (2015). A modeling study of human infections with avian influenza A H7N9 virus in mainland China. *Int. J. Infect. Diseases.* 41, 73–78. doi: 10.1016/j.ijid.2015.11.003

Ma, J., Gao, X., Liu, B. Y., Chen, H., Xiao, J. H., and Wang, H. B. (2019). Epidemiology and spatial distribution of bluetongue virus in Xinjiang, China. *PeerJ.* 7, e6514. doi: 10.7717/peerj.6514

Ren, Z. D., Yang, K., and Dong, W. (2020). Spatial analysis and risk assessment model research of arthritis based on risk factors: China 2013 and 2015. *IEEE Access.* 8, 206406–206417. doi: 10.1109/ACCESS.2020.3037912

Shan, X. Z., Lai, S. J., Liao, H. X., Li, Z. J., Lan, Y. J., Yang, W. Z., et al. (2019). The epidemic potential of avian influenza A (H7N9) virus in humans in mainland China: A two-stage risk analysis. *PloS One* 14, 4. doi: 10.1371/journal.pone.0215857

Shcheglovitova, M., and Anderson, R. P. (2013). Estimating optimal complexity for ecological niche models: A jackknife approach for species with small sample sizes. *Ecologigal Modelling.* 269, 9–17. doi: 10.1016/j.ecolmodel.2013.08.011

Shi, B. Y., Xia, S., Yang, G. J., Zhou, X. N., and Liu, J. M. (2013). Inferring the potential risks of H7N9 infection by spatiotemporally characterizing bird migration and poultry distribution in eastern China. *Infect. Dis. poverty.* 2, 8. doi: 10.1186/2049-9957-2-8

Wang, S. S., Liu, J. Y., Wang, B. Y., Wang, W. J., Cui, X. M., Jiang, J. F., et al. (2023). Geographical distribution of Ixodes persulcatus and associated pathogens: Analysis of integrated data from a China field survey and global published data. *One Health* 16, 10058. doi: 10.1016/j.onehlt.2023.100508

Wardrop, N. A., Geary, M., Osborne, P. E., and Atkinson, P. M. (2014). Interpreting predictive maps of disease: highlighting the pitfalls of distribution models in epidemiology. *Geospatial Health* 9, 237–246. doi: 10.4081/gh.2014.397

Wisz, M. S., Hijmans, R. J., Li, J., Peterson, A. T., Graham, C. H., and Guisan, A. (2008). Effects of sample size on the performance of species distribution models. *Diversity And Distributions.* 14, 763–773. doi: 10.1111/j.1472-4642.2008.00482.x

Wu, X. B., Lai, C. Q., and Ge, Z. Z. (2021). Spatio-temporal clustering, evolution, and autocorrelation effects of COVID-19 outbreaks in prefecture-level cities in China during the period of strict government control. *Gen. Geo_information Science.* 23, 246–258. doi: 10.12082/dqxxkx.2021.200362

Wu, J., Lau, E. H., Xing, Q. B., Zou, L. R., Zhang, H. B., Yen, H. L., et al. (2015). Seasonality of avian influenza A (H7N9) activity and risk of human A (H7N9) infections from live poultry markets. *J. Infection.* 71, 690–693. doi: 10.1016/j.jinf.2015.08.007

Xu, X. (2017). "Data from:Data registration and publishing system of Resource and Environmental Science Data Center of the Chinese Academy of Sciences," in *China population spatial distribution kilometer grid dataset*. (Beijing, China: Institute of Geographic Sciences and Natural Resources Research, Chinese Academy of Sciences). Available at: https://www.resdc.cn/ (accessed December 15, 2017).

Xu, X. (2018). "Data from:Data Registration and Publishing System of the Resource and Environmental Data Center of the Chinese Academy of Sciences," in *Spatial distribution dataset of annual vegetation index (NDVI) in China*. (Beijing, China: Institute of Geographic Sciences and Natural Resources Research, Chinese Academy of Sciences). Available at: https://www.resdc.cn/ (accessed October 8, 2018).

Xv, M., Cao, C. X., Li, Q., Jia, P., and Zhao, J. (2015). Ecological niche modeling of risk factors for H7N9 human infection in China. *Int. J. Environ. Res. Public Health* 13, 6. doi: 10.3390/ijerph13060600

Yu, H. J., Wu, J. T., Cowling, B. J., Liao, Q., Fang, V. J., Zhou, S., et al. (2014). Effect of closure of live poultry markets on poultry-to-person transmission of avian influenza A H7N9 virus: an ecological study. *Lancet* 383, 541–548. doi: 10.1016/S0140-6736(13)61904-2

Yuan, H. S., Wei, Y. L., and Wang, X. G. (2015). Maxent modeling for predicting the potential distribution of Sanghuang, an important group of medicinal fungi in China. *Fungal Ecology.* 17, 140–145. doi: 10.1016/j.funeco.2015.06.001

Zhang, Y., Feng, C., Ma, C., Yang, P., Tang, S., Lau, A., et al. (2015). The impact of temperature andhumidity measures on influenza A (H7N9) outbreaks-evidence from China. *Int. J. Infect. Dis.* 30, 122–124. doi: 10.1016/j.ijid.2014.11.010

Zhou, L., Chen, E. F., Bao, C. J., Xiang, N. J., Wu, J. B., Wu, S. G., et al. (2018). Clusters of human infection and human-to-human transmission of avian influenza A (H7N9) virus-2017. *Emerging Infect. Diseases.* 24, 2. doi: 10.3201/eid2402.171565

Zhou, X. Y., Gao, L., Wang, Y. M., Li, Y., Zhang, Y., Shen, C. J., et al. (2020). Geographical variation in the risk of H7N9 human infections in China: implications for risk-based surveillance. *Sci. Rep.* 10, 1. doi: 10.1038/s41598-020-66359-1

Zhuang, Q. Y., Wang, S. C., Wu, M. L., Liu, S., Jiang, W., Hou, G. Y., et al. (2013). Epidemiological and risk analysis of the H7N9 subtype influenza outbreak in China at its early stage. *Chin. Sci. Bulletin.* 58, 3183–3187. doi: 10.1007/s11434-013-5880-5

frontiers | Frontiers in Cellular and Infection Microbiology

TYPE Original Research
PUBLISHED 20 February 2025
DOI 10.3389/fcimb.2025.1498651

OPEN ACCESS

EDITED BY
Christy Rosaline Sundarraj,
National Institute of Research in Tuberculosis (ICMR), India

REVIEWED BY
Sam Ebenezer,
Sathyabama Institute of Science and Technology, India
Vignesh Sounderrajan,
Madurai Kamaraj University, India

*CORRESPONDENCE
Hongzhi Li
15517104660@163.com

RECEIVED 19 September 2024
ACCEPTED 27 January 2025
PUBLISHED 20 February 2025

CITATION
Li H, Gao X, Liu D, Li Z and Li J (2025) A new strategy improving TB diagnosis: stratified urine LAM test based on lymphocyte counts. *Front. Cell. Infect. Microbiol.* 15:1498651. doi: 10.3389/fcimb.2025.1498651

A new strategy improving TB diagnosis: stratified urine LAM test based on lymphocyte counts

Hongzhi Li[1,2,3]*, Xian Gao[1,2,3], Dandan Liu[1,2,3], Zhe Li[1,2,3] and Jing Li[1,2,3]

[1]Department of TB Diseases, Affiliated Infectious Diseases Hospital of Zhengzhou University, Zhengzhou, China, [2]Department of TB Diseases, Henan Infectious Diseases Hospital, Zhengzhou, China, [3]Department of TB Diseases, The Sixth People's Hospital of Zhengzhou, Zhengzhou, China

Background: Traditional lipoarabinomannan tests have limited sensitivity in HIV-negative individuals. Our aims were to compare chemiluminescence-based LAM (AIMLAM) and other diagnostic modalities in HIV-negative patients and to explore whether lymphocyte counts impact the sensitivity and costs of AIMLAM.

Methods: This is a prospective, cross-sectional, diagnostic accuracy study. Participants underwent testing with sputum acid-fast bacilli, sputum culture, GeneXpert, and AIMLAM. Their diagnostic efficiency and cost-effectiveness alone or under different lymphocyte count categories was evaluated.

Results: Using MRS as a reference, the sensitivities of different diagnostic methods were as follows: sputum smear 27.43%, sputum culture 45.13%, GeneXpert 74.34%, and AIMLAM 71.68%. Patients with lymphocyte counts <0.8 × 10^9/L were significantly more likely to have a positive AIMLAM result (OR = 9.431, 95% CI: 2.659–33.447, P = 0.001). The sensitivity of AIMLAM in patients with lymphocyte counts <0.8 × 10^9/L reached 93.02%. The overall cost of AIMLAM to detect a positive TB case was $129.82, lower than sputum culture ($136.10) and GeneXpert ($180.27). For patients with lymphocyte counts <0.8 × 10^9/L, the cost of AIMLAM was further reduced to $67.84 (a 47.74% decrease), which was lower than GeneXpert ($111.65) and sputum culture ($94.28).

Conclusion: AIMLAM showed promising diagnostic performance in HIV-negative patients. Stratifying patients using lymphocyte cell counting lifted the sensitivity and lowered the cost of LAM, offering a novel diagnostic strategy for tuberculosis in resource-limited settings.

KEYWORDS

tuberculosis, lipoarabinomannan, lymphocyte, diagnosis, biomarker

1 Introduction

Tuberculosis (TB) is an infectious disease caused by *Mycobacterium tuberculosis* (Mtb). It is ranked the second most deadly infectious disease after COVID-19. There were a total of 10.6 million cases of LTBI and 1.6 million deaths due to TB worldwide (World Health Organization, 2023). Among LTBI, 5%–10% would progress to active tuberculosis (ATB) (Ding et al., 2022).

For decades, sputum-based tests have remained the primary methods for diagnosis. However, only 75% of symptomatic patients and 10% of asymptomatic patients are able to produce sputum by themselves (Lissouba et al., 2021). Therefore, the WHO called for new non-sputum tests such as the urine test. The urine lipoarabinomannan (LAM) test is the most popular non-sputum test for TB diagnosis. LAM is a component of the cell envelope of Mtb (De et al., 2024), mediating host immune responses (Fukuda et al., 2013). After being released into the blood by Mtb, LAM reaches the kidneys and subsequently filters through the glomerular basement membrane into the urine (Bulterys et al., 2019). This lays the theoretical foundation for the detection of LAM in urine. The LAM test is promising for tuberculosis diagnosis, especially in people with HIV and in disseminated tuberculosis patients (Gupta-Wright et al., 2016).

Currently, the only commercially available LAM test kit is Alere's Determine TB LAM (AlereLAM), based on colloidal gold, with a limit of detection (LOD) of 500 pg/mL (García et al., 2019). The sensitivity of AlereLAM is 10.8%–18% in the HIV-negative population (Minion et al., 2011; Broger et al., 2020a) and 40% in people with HIV (Huerga et al., 2023). While another product Fujifilm SILVAMP TB LAM (FujiLAM) has been extensively researched, its variability between different lot numbers has hindered its application (Huerga et al., 2023). The sensitivity of FujiLAM in people with HIV has reached 70.7% (Broger et al., 2020a) and has been reported at 53% in the HIV-negative population (Broger et al., 2020a), thanks to the lowered LOD (30 pg/mL) (Broger et al., 2019). Reducing the LOD may be the main approach to improving sensitivity while ensuring stability and specificity. The new LAM test, based on chemiluminescence and urine concentration (AIMLAM), significantly improves the sensitivity of the LAM test. Studies have shown a sensitivity of 55% in HIV-negative populations. This will greatly enhance the diagnosis of TB in the general population.

In addition to lowering LOD to enhance sensitivity, employing immune status stratification strategies can also improve sensitivity. Mtb can replicate extensively within the body without sufficient immune capacity (Chandra et al., 2022), leading to an increased circulation of LAM. Immune suppression also reduces the formation of antigen–antibody complexes, resulting in more free LAM present in the circulation (Lawn, 2012). Therefore, in patients with immune deficiency and suppressed immunity, the concentration of LAM in the urine is much higher (Paris et al., 2017). The WHO recommends AlereLAM only to be used in people with HIV with $CD4^+$ T cells less than 200/mm^3. This stratification strategy based on $CD4^+$ T cells is based on immunity's critical role in the mechanism of LAM's emission to urine. However, in the general HIV-negative population, routine $CD4^+$ T-cell testing is not performed and there is a lack of immune stratification markers to fully assess the sensitivity and specificity of the LAM test.

In contrast, a complete blood count (CBC) is routinely performed, is cost-effective, and can provide an initial assessment of a patient's immune function (Gulati et al., 2022). $CD4^+$ T cells account for 23.78%–51.07% of lymphocytes (Silva et al., 2001). Studies have shown that both $CD4^+$ T-cell and $CD8^+$ T-cell lymphocytes are involved in the immune response against tuberculosis (Silva et al., 2001), and previous research has reported lower lymphocytes in TB patients (Luo et al., 2021). Lymphocyte counts may have similar effects to $CD4^+$ T-cell counts.

This study aims to explore whether lymphocyte counts can be used for immune stratification of HIV-negative TB patients. Additionally, the study will analyze the sensitivity and specificity of AIMLAM in tuberculosis patients with different immune stratifications and compare it with other methods.

2 Methods

2.1 Study design and participants

In this prospective, cross-sectional, double-blind diagnostic accuracy study, presumed tuberculosis patients from the Affiliated Infectious Diseases Hospital of Zhengzhou University from November 2023 to February 2024 were included. Collection of samples and diagnosis were performed before treatment. The sample size was calculated using PASS 21.0 based on the sensitivity and specificity of the AIMLAM test. According to our previous research, the prevalence of microbiological reference standard (MRS) TB in presumed TB patients was approximately 40%, the lowest acceptable sensitivity was 50%, and the expected sensitivity was 70%. Both acceptable and expected sensitivity were 95% and α was 0.05. Power ($1 - \beta$) was set at 0.9, and the dropout rate was 10% (Gao et al., 2024; Huang et al., 2023). Results showed that we needed to include 180 presumed cases of TB.

This study followed the Standards for Reporting of Diagnostic Accuracy (STARD) guideline. The study adhered to the Helsinki Declaration and was approved by the Medical Ethics Committee of the Sixth People's Hospital of Zhengzhou. The ethics number is IEC-KY-2023-48.

2.2 Participants

We included presumptive TB patients meeting the following criteria: 1) aged ≥18, men and women; 2) with symptoms of TB (cough of at least 2 weeks, unexplained fever, weight loss, night sweats); and 3) able to produce sputum and collected urine. Patients were excluded if they 1) had HIV and 2) were receiving tuberculosis treatment.

2.3 Definition

The definition of definite TB and possible TB was based on the "Diagnosis for pulmonary tuberculosis (WS 288-2017)"

(Commission, 2018) and the WHO tuberculosis guideline (World Health Organization, 2022). Definite TB was defined as Active tuberculosis (ATB), through TB culture or acid fast bacillusor or GeneXpert. Possible TB was defined as patients not meeting the criteria of definite TB but had X-ray positive, and they 1) had symptoms and signs or 2) were TST or IGRA or TB antibody positive. Non-TB was defined as patients not eligible for definite or possible TB.

Microbiological reference standard (MRS) is a benchmark diagnostic criterion based on direct microbiological evidence of infection. In tuberculosis diagnostics, MRS typically includes methods such as sputum smear microscopy, culture, and nucleic acid amplification tests (e.g., GeneXpert), which detect the presence of *Mycobacterium tuberculosis* directly (Shreffler and Huecker, 2020).

Composite reference standard (CRS) involves a composite of clinical assessments, including patient history, physical examinations, radiological findings, and sometimes histopathological evidence, to diagnose an infection (Shreffler and Huecker, 2020).

2.4 Sample collection

Sputum, urine, and blood were collected before any treatment was involved. Sterile, dry containers were used to collect three samples of sputum, including those obtained immediately, at night, and in the early morning. These were combined into one specimen, dissolved thoroughly in 5 mL of saline solution, and stored at 4°C for examination. Approximately 5 mL of midstream urine from the patient was collected in the morning and stored at 4°C for examination. Approximately 5 mL of fasting venous blood was collected and stored at room temperature.

2.5 Testing procedures

Urinary LAM detection was conducted using AIMLAM kits (Leide Biosciences Co., Ltd, Guangzhou, China) according to the user's manual (Zhang et al., 2023; Gao et al., 2024; Huang et al., 2023). The performers were blinded to the clinical information of the participants. This kit utilizes a chemiluminescent immunoassay to detect LAM in urine. LAM-specific antibodies immobilized on magnetic beads capture LAM, forming a complex of magnetic bead–antibody–antigen. Subsequently, the complex binds to a luminescent label, resulting in the formation of a magnetic bead–antibody–antigen–aminoluciferin label complex. Following separation and washing, a pre-triggering solution and a triggering solution were introduced to the reaction mixture, with the level of LAM in the test sample being directly proportional to the relative light unit value obtained.

The acid-fast stain (AFB) and microscopy were performed on sputum based on the Ziehl-Neelsen stain (van Deun et al., 2008). Sputum culture was performed according to protocols (Hanna et al., 1999) previously established based on the BACTEC™ MGIT™ 960 TB system (BD Diagnostic Systems, Sparks, MD, USA). GeneXpert was performed on 1.0 mL of sputum sample according to the user's instruction (Cepheid, Inc., Sunnyvale, CA, USA) (Giang Do et al., 2015). The performers of the above tests were masked to the AIMLAM results and clinical information of the participants.

2.6 Assessment of blood parameters

White blood cell count (WBC), granulocyte count, lymphocyte count, erythrocyte sedimentation rate (ESR), procalcitonin (PCT), and C-reactive protein (CRP) were determined using a fully automated hematology analyzer (Mindray BC-5180 CRP).

2.7 Statistics

All statistical analyses were conducted using SPSS 26.0. The diagnostic accuracy of AIMLAM compared with MRS and CRS was calculated. Continuous data were transformed into categorical data according to the following methods. Age was categorized using two cutoff values: 30 and 60 years. Blood cell count, ESR, PCT, and CRP were categorized based on commonly used clinical reference standards, as follows: WBC, 4–10 × 10^9/L; lymphocytes, 0.8–4 × 10^9/L; neutrophils, 1.8–6.3 × 10^9/L; monocytes, 0.1–0.6 × 10^9/L; ESR, 0–10 mm/h for men and 0–20 mm/h for women; CRP, 0–10 mg/L; and PCT, 0.5 ng/L. Because there were only three cases (1.21%) and one case (0.88%) in the high lymphocyte count group with LAM positive (LAM+) or LAM negative (LAM−), we grouped patients with normal and high lymphocyte counts into the ≥0.8 × 10^9/L category. Categorical data were expressed as frequencies and percentages.

2.8 Calculating sensitivity and specificity

Chi-square tests or Fisher's exact probability method was used for analysis. The sensitivity and specificity of each detection method were calculated based on MRS and CRS (Shreffler and Huecker, 2020; Kraef et al., 2022; Broger et al., 2020b).

Sensitivity = true positive cases/(true positive cases + false negative cases) × 100%.

Specificity = true negative cases/(true negative cases + false positive cases) × 100%.

2.9 Logistic regression analysis

MRS-positive patients were divided into two groups: LAM+ and LAM−. General data and blood indicators of the two groups were analyzed for differences. Logistic regression was employed to examine the association between lymphocyte count and AIMLAM. Model 1 included only lymphocyte count as the independent variable. Model 2 was adjusted for gender and age. Model 3 was further adjusted for factors in model 2 as well as diabetes and autoimmune diseases. Model 4 was additionally

adjusted for variables in model 3 and blood indicators showing statistically significant differences between LAM− and LAM+ individuals. Fagan nomography was used to demonstrate the clinical utility of AIMLAM in diagnosing TB patients from presumed TB patients.

2.10 Calculation of average cost per detected TB patient

The cost per detected TB patient was calculated as the total testing cost divided by the number of true positive cases. For all presumed TB patients, the average cost per person was determined using the formula (Aliyu et al., 2014; Gao et al., 2024):

(1) Average cost for all presumed TB patients:

Average cost = (total number of individuals × unit price)/ number of true positive cases

For patients with low lymphocyte counts, the average cost per person was also calculated.

The prices of all test reagents in this article are only applicable to the time of testing in this study. Currently, there is no confirmed price for AIMLAM. All costs were calculated based on the average exchange rate for the year 2023 (1 USD = 7.075 CNY), with the exchange rate sourced from the IRS website (https://www.irs.gov/individuals/international-taxpayers/yearly-average-currency-exchange-rates). A significance level of P <0.05 was considered statistically significant.

3 Results

3.1 Demographic characteristics

Initially, 335 patients were enrolled. Thirty-three people with HIV were excluded, 15 were excluded for not providing consent or withdrawing consent, 23 were excluded for extrapulmonary disease, 3 were excluded for receiving TB treatment, and 13 were excluded for lost follow-up. Finally, a total of 248 patients were included in the analysis. Among them, 113 were definite TB cases, 53 were possible TB cases, and 135 were non-TB (Figure 1). There were 131 men and 117 women. Fifty-three were less than 30 years old, 118 were 30–60 years old, and 77 were older than 60 years. Fifty-three cases (21.47%) had diabetes mellitus (DM), and 24 cases (9.68) had a history of TB. Sixty-one cases (24.6%), 184 cases (74.19%), and 3 cases (1.21%) had low, normal, and high lymphocyte counts, respectively. The distribution of sex, DM, monocytes, lymphocytes, ESR, PCT, and CRP was significantly different between groups (Supplementary Table 1).

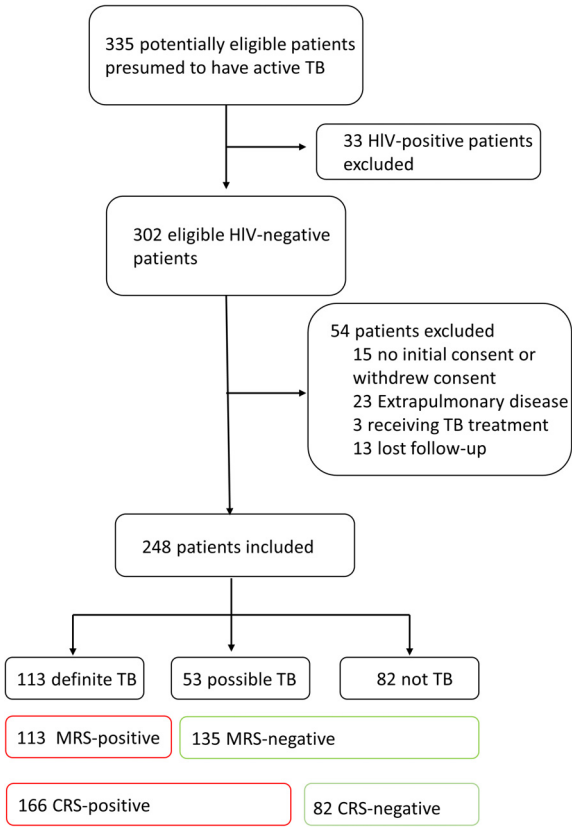

FIGURE 1
Flow diagram of patient selection.

3.2 Diagnostic performance of LAM

Using MRS, the sensitivity rates of AFB, culture, GeneXpert, and AIMLAM were 27.43%, 45.13%, 74.34%, and 71.68%, respectively. The sensitivity of AIMLAM was significantly higher than that of the AFB smear and culture but showed no significant difference compared to GeneXpert. The specificity of AFB, culture, and GeneXpert was 100%, as they compromised the MRS (Figure 2B). The specificity of AIMLAM was 95.56% (Figure 2A). Using CRS, the sensitivity rates of the AFB smear, culture, GeneXpert, and AIMLAM were 18.67%, 30.72%, 50.60%, and 51.20%, respectively. The specificity of the AFB smear, culture, and GeneXpert was 100%. The specificity of AIMLAM was 97.56% (Supplementary Figure 1).

3.3 Analysis of the risk factors of AIMLAM

Among the 113 definite TB patients, 81 were LAM-positive. Age, sex, comorbidity, and other serum variables were not statistically different between LAM+ patients and LAM− patients. The proportion of low neutrophils, low lymphocytes, high ESR, high PCT, and high CRP in the LAM+ TB group was significantly higher than that in the LAM− TB group. (Supplementary Table 2). In the unadjusted model (model 1), patients with low lymphocytes were more likely to have positive LAM results (OR = 9.431, 95% CI: 2.659–33.447, $P = 0.001$). When adjusted for sex and age (model 2), the OR was 9.562 (95% CI: 2.476–36.928, $P = 0.001$). When adjusted for factors in model 2 plus DM and TB history (model 3), the OR was 10.021 (95% CI: 2.555–39.297, $P = 0.001$). When adjusted for factors in model 3 plus neutrophils, ESR, and CRP (model 4), the OR was 5.992 (95% CI = 1.421–25.262, $P = 0.015$). Among the 135 MRS− cases, 6 were LAM positive. None of the factors listed were significantly different between LAM+ and LAM− patients (Table 1).

3.4 Comparison of the diagnostic performance of AIMLAM between different lymphocyte count categories

All presumed TB patients were grouped into $<0.8 \times 10^9$/L (64 out of 248) and $\geq 0.8 \times 10^9$/L (184 out of 248) according to their lymphocyte counts. In the $<0.8 \times 10^9$/L group, the sensitivity rates were 32.56%, 44.19%, 81.40%, and 93.02% for AFB, culture, GeneXpert, and AIMLAM, respectively. In the $\geq 0.8 \times 10^9$/L group, the sensitivity rates were 24.29%, 45.71%, 70.00%, and 58.57%, respectively. The sensitivity of AIMLAM in low lymphocyte patients was much higher than that in high lymphocyte patients ($P < 0.001$) (Table 2).

The Fagan nomogram was employed to evaluate the clinical value of AIMLAM in diagnosing TB. The Fagan nomogram showed posttest positive and negative probabilities of 93% and 20%, respectively, under a pretest probability set at 46% (Supplementary Figure 2).

A

Methods	Results	MRS		Sensitivity	Specificity	PPV	NPV	Kappa
		positive	negative					
AFB smear	positive	31	0	27.43%	100.00%	100.00%	62.21%	0.292
	negative	82	135					
Culture	positive	51	0	45.13%	100.00%	100.00%	68.53%	0.472
	negative	62	135					
GeneXpert	positive	84	0	74.34%	100.00%	100.00%	82.32%	0.759
	negative	29	135					
AIMLAM	positive	81	6	71.68%	95.56%	93.10%	80.12%	0.685
	negative	32	129					

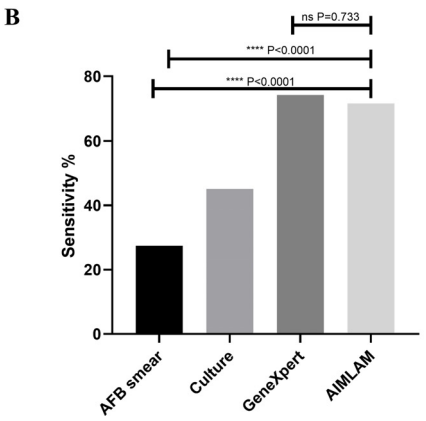

FIGURE 2
(A) Diagnostic performance of the four methods compared to MRS. **(B)** Sensitivity difference analysis of the four methods based on MRS. AFB, acid-fast bacillus; LAM, lipoarabinomannan; MRS, microbiological reference standard; PPV, positive predictive value; NPV, negative predictive value. ****, $P < 0.0001$; ns, $P > 0.05$. Sensitivity = true positive cases/(true positive cases + false negative cases) × 100%; Specificity, true negative cases/(true negative cases +false positive cases) × 100%; PPV, true positive cases/(true positive cases + false positive cases) × 100%; NPV, true negative cases/(true negative cases + false negative cases) × 100%.

10.3389/fcimb.2025.1498651

TABLE 1 Results of logistics regression.

Variables	MRS+				MRS−			
	β	OR	95% CI	*P*	β	OR	95% CI	*P*
Model 1								
Lymphocytes (low)	2.244	9.431	2.659–33.447	0.001	0.276	1.318	0.145–11.973	0.806
Model 2								
Lymphocytes (low)	2.258	9.562	2.476–36.928	0.001				
Sex (male)	0.023	1.023	0.409–2.559	0.961				
Age (30–60 years)	Ref	Ref	Ref	Ref	Ref	Ref	Ref	Ref
Age (<30 years)	−0.373	0.688	0.245–1.933	0.478				
Age (>60 years)	−0.269	0.764	0.234–2.492	0.655				
Model 3								
Lymphocytes (low)	2.305	10.021	2.555–39.297	0.001				
Age (30–60 years)	Ref	Ref	Ref	Ref	Ref	Ref	Ref	Ref
Age (<30 years)	−0.272	0.762	0.257–2.261	0.624				
Age (>60 years)	−0.179	0.836	0.252–2.778	0.770				
Sex (male)	0.025	1.025	0.4–2.626	0.959				
DM (yes)	−0.212	0.809	0.248–2.644	0.726				
TB history (yes)	−0.891	0.410	0.099–1.703	0.220				
Model 4								
Lymphocytes (low)	1.790	5.992	1.421–25.262	0.015				
Age (30–60 years)	Ref	Ref	Ref	Ref	Ref	Ref	Ref	Ref
Age (<30 years)	−0.318	0.727	0.224–2.363	0.596				
Age (>60 years)	−0.275	0.759	0.206–2.793	0.679				
Sex (male)	0.040	1.040	0.383–2.827	0.938				
DM (yes)	−0.145	0.865	0.25–2.999	0.819				
TB history (yes)	−1.045	0.352	0.079–1.574	0.172				
Neutrophils (low)	1.167	3.213	0.623–16.577	0.163				
ESR (high)	−0.001	0.999	0.23–4.336	0.999				
PCT (high)	0.439	1.551	0.375–6.412	0.545				
CRP (high)	0.678	1.971	0.459–8.456	0.361				

MRS, microbiological reference standard; ESR, erythrocyte sedimentation rate; PCT, procalcitonin; CRP, C-reactive protein.

3.5 Evaluating the cost-effectiveness of TB diagnosis across different lymphocyte levels (<0.8 × 10^9/L and ≥0.8 × 10^9/L)

For the cost-effectiveness analysis, without considering lymphocyte counts, the cost to detect a positive TB case was $48.40, $136.10, $180.27, and $129.82 for the AFB smear, culture, GeneXpert, and AIMLAM, respectively. After stratifying by lymphocyte counts, for patients with lymphocyte counts <0.8 × 10^9/L, AIMLAM testing emerged as the most cost-effective option (excluding the AFB smear), achieving a sensitivity of 93% and a specificity of 95%. In this group, the cost of AIMLAM to detect a positive TB case decreased to $67.84 (a 47.74% reduction), which was lower than GeneXpert ($111.65, a 38.06% reduction) and culture ($94.28, a 30.73% reduction). Conversely, for patients with lymphocyte counts ≥0.8 × 10^9/L, the difficulty of achieving a positive detection increased, and the most cost-effective diagnostic method was the AFB smear, followed by culture, AIMLAM, and finally GeneXpert (Table 3).

This stratification by lymphocyte counts highlights the optimal sequence of diagnostic methods for minimizing costs while maintaining diagnostic accuracy, offering valuable guidance for clinical decision-making. Since CBC testing is routinely performed in clinical practice, it does not contribute additional costs, further enhancing the practical utility of this approach.

TABLE 2 Diagnostic performance in different lymphocyte groups.

Methods	Results	<0.8 × 10^9/L			≥0.8 × 10^9/L			*P*
		MRS		Sensitivity	MRS		Sensitivity	
		Positive	Negative		Positive	Negative		
AFB smear	Positive	14	0	32.56%	17	0	24.29%	0.339
	Negative	29	21		53	114		
Culture	Positive	19	0	44.19%	32	0	45.71%	0.874
	Negative	24	21		38	114		
GeneXpert	Positive	35	0	81.40%	49	0	70.00%	0.178
	Negative	8	21		21	114		
AIMLAM	Positive	40	1	93.02%	41	5	58.57%	<0.001
	Negative	3	20		29	109		

Sensitivity = true positive cases/(true positive cases + false negative cases) × 100%.
AFB, acid-fast bacillus; LAM, lipoarabinomannan; MRS, microbiological reference standard; PPV, positive predictive value; NPV, negative predictive value.

4 Discussion

The main finding of this study was that the sensitivity of the LAM test in the HIV-negative population was 71.68% (MRS), which is comparable to GeneXpert and higher than AFB and culture. It is also higher than that reported in previous studies, mainly due to the reference standard used in these studies which was CRS (Gao et al., 2024; Zhang et al., 2023; Huang et al., 2023). The sensitivity of LAM was 51.2% when compared to the CRS, consistent with previous reports (Gao et al., 2024; Zhang et al., 2023; Huang et al., 2023). LAM is a tuberculosis pathogenetic test, and the accuracy of AIMLAM in diagnosing ATB is more accurately reflected by using MRS as a reference standard. Lowering the LOD can help improve detection rates (Huerga et al., 2023; Kraef et al., 2022; Broger et al., 2020b). This study also demonstrated that when the LAM detection limit was lowered to 1 pg/mL (Gao et al., 2024), the sensitivity increased from the original 10.8% (Huerga et al., 2023; Broger et al., 2020a) to 51.2% (reference CRS).

It has been extensively shown that urinary LAM concentration is influenced by immune function and immunosuppression, with bacterial proliferation and a subsequent increase in urinary LAM concentrations (Gupta-Wright et al., 2016). This suggests that, in addition to lowering the LOD to improve sensitivity, researchers can also increase LAM sensitivity by identifying and targeting immunosuppressed patients. The WHO recommends immunostratifying patients by $CD4^+$ T-cell count to analyze the diagnostic efficacy of LAM. The general sensitivity of AlereLAM was 9%–27% (Peter et al., 2016; Nakiyingi et al., 2014), and it increased dramatically in patients with $CD4^+$ T cells less than 200/mm^3 and 100/mm^3 (Peter et al., 2016), which means that lower immunity leads to higher sensitivity.

The lymphocyte count encompasses $CD4^+$ T cells, $CD8^+$ T cells, and B lymphocytes, all of which play critical roles in the immune response against TB infection (An et al., 2022). For HIV-negative patients, $CD4^+$ T-cell counts are not routinely measured, and lymphocyte count, as part of CBC, serves as the most convenient

TABLE 3 Price of detecting a TB case (US $).

Methods	Unit price ($)	True positive (*N*)	Total (*N*)	Overall ($)	Lymphocytes ($)					
					<0.8 × 10^9/L (change)			≥0.8 × 10^9/L (change)		
					True positive (*N*)	Total (*N*)	Overall ($)	True positive (*N*)	Total (*N*)	Overall ($)
AFB smear	6.05	31	248	48.40	14	64	27.66 (−42.85%)	17	184	65.48 (35.29%)
Culture	27.99	51	248	136.10	19	64	94.28 (−30.73%)	32	184	103.44 (24.00%)
GeneXpert	61.06	84	248	180.27	35	64	111.65 (−38.06%)	49	184	229.29 (27.20%)
AIMLAM	42.40	81	248	129.82	40	64	67.84 (−47.74%)	41	184	190.28 (46.57%)

Average cost = (total number of individuals × unit price)/number of true positive cases.
Change rate = (Overall (post-lymphocyte stratification) – Overall (pre-lymphocyte stratification))/Overall (pre-lymphocyte stratification) * 100%.
AFB, acid-fast bacillus; LAM, lipoarabinomannan.

method to assess the immune status of patients. Studies have indicated a decline in lymphocyte count among TB patients in the HIV-negative population (Li et al., 2023; Wang et al., 2015). In this study, we discovered that populations with a low lymphocyte count are more likely to be tested positive in the MRS+ population than those with normal and high lymphocyte counts (OR = 9.431, 95% CI: 2.659–33.447), consistent with previous reports (Li et al., 2023). It is suggested that lymphocyte count might serve as a viable surrogate marker for $CD4^+$ T cells specifically in HIV-negative individuals. In this study, the sensitivity of conventional TB diagnostic tests such as AFB smear, culture, and GeneXpert was notably higher in individuals with low lymphocyte counts compared to those with high lymphocyte counts. Remarkably, the sensitivity of the AIMLAM test was particularly noteworthy at 93.02%, surpassing that of other traditional tests. This heightened sensitivity associated with the LAM test in individuals with low lymphocyte counts is of paramount clinical significance. It implies that incorporating LAM testing into routine diagnostic protocols can substantially enhance the detection rate of TB patients with low lymphocyte counts, thereby mitigating missed diagnoses and treatment delays, ultimately improving clinical outcomes.

Moreover, the use of CBC, which includes lymphocyte counting, for immunostratification in TB diagnosis offers significant potential for cost reduction. Our study demonstrated that in patients with low lymphocyte counts ($<0.8 \times 10^9$/L), the cost of detecting one TB case decreased by 30.73% to 47.74% across various diagnostic modalities. Specifically, the cost for AIMLAM testing was reduced to $67.84, making it the second most cost-effective option after smear and significantly more economical than culture and GeneXpert. This dual benefit highlights the practical value of lymphocyte count-based immunostratification as a cost-effective diagnostic tool, particularly in resource-limited settings where the majority of TB cases occur (Organization, 2023). Importantly, CBC is a routine test with minimal additional cost, making it a practical option for widespread implementation.

In contrast, CD4 T-cell testing, while offering more specific immunological stratification, is rarely performed in HIV-negative populations due to its high cost (approximately $40 per test) and lack of routine applicability in this demographic. These factors limit its feasibility as a large-scale screening tool in non-HIV TB diagnosis. For patients with low lymphocyte counts identified via CBC, AIMLAM testing should be prioritized as a supplementary method alongside gold-standard diagnostics such as smear and culture, offering an optimal balance of cost-effectiveness and diagnostic accuracy.

For patients with lymphocyte counts $\geq 0.8 \times 10^9$/L, AIMLAM continues to demonstrate higher sensitivity compared to smear and culture, maintaining its diagnostic value. Although its cost-effectiveness is reduced in this group, it remains a valuable diagnostic modality with potential for broader applicability. Notably, if the cost of LAM testing were to decrease to $30 in the future, the cost of detecting a positive TB case in patients with low lymphocyte counts could be reduced further to $48. This would make AIMLAM not only the most cost-effective option but also more economical than the AFB smear, solidifying its role as a preferred diagnostic method in resource-limited settings.

Our study has limitations. On the one hand, the sample size for patients with low lymphocyte counts was relatively small. Larger sample sizes and multicenter trials are needed to validate the conclusion of high sensitivity in this subgroup. On the other hand, we did not compare the specific LAM test used in our study with the one recommended by the WHO. This limitation is partially due to the fact that Alere's marketing strategy does not include China, making it impossible to access their tests. Furthermore, our study focused solely on the HIV-negative population and did not conduct lymphocyte-based stratification in HIV-positive patients. Future studies are warranted to evaluate lymphocyte stratification in HIV-positive populations to ensure broader applicability and validate the potential of this approach across diverse patient groups.

The strengths of our study are as follows: the study was conducted in China which is among the high-burden countries. Therefore, the results of this study are eligible to be referenced in similar settings. Our study studied the impact of lymphocytes on both diagnostic efficiency and cost-effectiveness. High performance and low price might push the change of algorithm of TB diagnosis. Our study validates the efficacy of the new AIMLAM kit for the diagnosis of tuberculosis in an HIV-negative population.

5 Conclusion

New chemiluminescence-based LAM tests have the potential to diagnose all people with presumptive TB irrespective of HIV condition. After stratifying patients using lymphocyte cell counting, the sensitivity of AIMLAM significantly increased among patients with low lymphocyte counts, and the cost of detecting individual TB cases decreased significantly. Thanks to the accessibility of CBC and the high sensitivity of LAM testing, this provides a new strategy for the diagnosis of ATB, especially in resource-limited areas.

Data availability statement

The raw data supporting the conclusions of this article will be made available by the authors, without undue reservation.

Ethics statement

The studies involving humans were approved by the Medical Ethics Committee of the Sixth People's Hospital of Zhengzhou. The studies were conducted in accordance with the local legislation and institutional requirements. The participants provided their written informed consent to participate in this study.

Author contributions

HL: Conceptualization, Funding acquisition, Supervision, Writing – original draft. XG: Data curation, Formal Analysis, Writing – review & editing. DL: Data curation, Writing – review & editing. ZL: Formal Analysis, Writing – review & editing. JL: Formal Analysis, Writing – review & editing.

Funding

The author(s) declare that financial support was received for the research, authorship, and/or publication of this article. This work was supported by the Open Project of Clinical Medical Research Center of Infectious Diseases in Henan Province of 2024 (KFKT202408), Zhengzhou Science and Technology Benefit People Plan Project of 2023 (KJHM0018), and Henan Province Medical Science and Technology Research Plan Joint Construction Project: Analysis of Risk Factors and Construction of Risk Prediction Model for Drug-Resistant Tuberculosis in Henan Province (LHGJ20210691).

Acknowledgments

We are extremely grateful to all the participants and the performers of the tests. We also appreciate the assistance provided by Mr. Xiaotan Wang, Ms. Hongxia Wei, and Ms. Juanjuan Peng.

Conflict of interest

The authors declare that the research was conducted in the absence of any commercial or financial relationships that could be construed as a potential conflict of interest.

Publisher's note

Supplementary material

The Supplementary Material for this article can be found online at: https://www.frontiersin.org/articles/10.3389/fcimb.2025.1498651/full#supplementary-material

References

Aliyu, G., El-Kamary, S. S., Abimiku, A. L., Hungerford, L., Obasanya, J., and Blattner, W. (2014). Cost-effectiveness of point-of-care digital chest-x-ray in HIV patients with pulmonary mycobacterial infections in Nigeria. *BMC Infect. Dis.* 14, 1–8. doi: 10.1186/s12879-014-0675-0

An, H. R., Bai, X. J., Liang, J. Q., Wang, T., Wang, Z. Y., Xue, Y., et al. (2022). The relationship between absolute counts of lymphocyte subsets and clinical features in patients with pulmonary tuberculosis. *Clin. Respir. J.* 16, 369–379. doi: 10.1111/crj.13490

Broger, T., Nicol, M. P., Sigal, G. B., Gotuzzo, E., Zimmer, A. J., Surtie, S., et al. (2020a). Diagnostic accuracy of 3 urine lipoarabinomannan tuberculosis assays in HIV-negative outpatients. *J. Clin. Invest.* 130, 5756–5764. doi: 10.1172/JCI140461

Broger, T., Nicol, M. P., Székely, R., Bjerrum, S., Sossen, B., Schutz, C., et al. (2020b). Diagnostic accuracy of a novel tuberculosis point-of-care urine lipoarabinomannan assay for people living with HIV: a meta-analysis of individual in-and outpatient data. *PLoS Med.* 17, e1003113. doi: 10.1371/journal.pmed.1003113

Broger, T., Sossen, B., Du Toit, E., Kerkhoff, A. D., Schutz, C., Ivanova Reipold, E., et al. (2019). Novel lipoarabinomannan point-of-care tuberculosis test for people with HIV: a diagnostic accuracy study. *Lancet Infect. Dis.* 19, 852–861. doi: 10.1016/S1473-3099(19)30001-5

Bulterys, M. A., Wagner, B., Redard-Jacot, M., Suresh, A., Pollock, N. R., Moreau, E., et al. (2019). Point-of-care urine LAM tests for tuberculosis diagnosis: A status update. *J. Clin. Med.* 9(1):111. doi: 10.3390/jcm9010111

Chandra, P., Grigsby, S. J., and Philips, J. A. (2022). Immune evasion and provocation by Mycobacterium tuberculosis. *Nat. Rev. Microbiol.* 20, 750–766. doi: 10.1038/s41579-022-00763-4

Commission (2018). Tuberculosis classification (WS196—2017). *Electronic J. Emerging Infect. Dis.* 3, 2. doi: 10.19983/j.issn.2096-8493.2024055

De, K., Belardinelli, J. M., Pandurangan, A. P., Ehianeta, T., Lian, E., Palčeková, Z., et al. (2024). Lipoarabinomannan modification as a source of phenotypic heterogeneity in host-adapted Mycobacterium abscessus isolates. *Proc. Natl. Acad. Sci. U.S.A.* 121, e2403206121. doi: 10.1073/pnas.2403206121

Ding, C., Hu, M., Guo, W., Hu, W., Li, X., Wang, S., et al. (2022). Prevalence trends of latent tuberculosis infection at the global, regional, and country levels from 1990-2019. *Int. J. Infect. Dis.* 122, 46–62. doi: 10.1016/j.ijid.2022.05.029

Fukuda, T., Matsumura, T., Ato, M., Hamasaki, M., Nishiuchi, Y., Murakami, Y., et al. (2013). Critical roles for lipomannan and lipoarabinomannan in cell wall integrity of mycobacteria and pathogenesis of tuberculosis. *mBio* 4, e00472–e00412. doi: 10.1128/mBio.00472-12

Gao, M., Wu, Q., Wang, X., Sun, X., Li, M., and Bai, G. (2024). Advancements in LAM-based diagnostic kit for tuberculosis detection: enhancing TB diagnosis in HIV-negative individuals. *Front. Microbiol.* 15, 1367092. doi: 10.3389/fmicb.2024.1367092

García, J. I., Kelley, H. V., Meléndez, J., de León, R. A. A., Castillo, A., Sidiki, S., et al. (2019). Improved alere determine lipoarabinomannan antigen detection test for the diagnosis of human and bovine tuberculosis by manipulating urine and milk. *Sci. Rep.* 9, 18012. doi: 10.1038/s41598-019-54537-9

Giang Do, C., Duong, T. N., Ha, D. T., Nhan, H. T., Wolbers, M., Nhu, N. T., et al. (2015). Prospective evaluation of GeneXpert for the diagnosis of HIV- negative pediatric TB cases. *BMC Infect. Dis.* 15, 70. doi: 10.1186/s12879-015-0814-2

Gulati, G., Uppal, G., and Gong, J. (2022). Unreliable automated complete blood count results: causes, recognition, and resolution. *Ann. Lab. Med.* 42, 515–530. doi: 10.3343/alm.2022.42.5.515

Gupta-Wright, A., Peters, J. A., Flach, C., and Lawn, S. D. (2016). Detection of lipoarabinomannan (LAM) in urine is an independent predictor of mortality risk in patients receiving treatment for HIV-associated tuberculosis in sub-Saharan Africa: a systematic review and meta-analysis. *BMC Med.* 14, 53. doi: 10.1186/s12916-016-0603-9

Hanna, B. A., Ebrahimzadeh, A., Elliott, L. B., Morgan, M. A., Novak, S. M., Rusch-Gerdes, S., et al. (1999). Multicenter evaluation of the BACTEC MGIT 960 system for recovery of mycobacteria. *J. Clin. Microbiol.* 37, 748–752. doi: 10.1128/JCM.37.3.748-752.1999

Huang, L., Niu, Y., Zhang, L., Yang, R., and Wu, M. (2023). Diagnostic value of chemiluminescence for urinary lipoarabinomannan antigen assay in active tuberculosis: insights from a retrospective study. *Front. Cell. Infection Microbiol.* 13, 1291974. doi: 10.3389/fcimb.2023.1291974

Huerga, H., Bastard, M., Lubega, A. V., Akinyi, M., Antabak, N. T., Ohler, L., et al. (2023). Novel FujiLAM assay to detect tuberculosis in HIV-positive ambulatory patients in four African countries: a diagnostic accuracy study. *Lancet Glob Health* 11, e126–e135. doi: 10.1016/S2214-109X(22)00463-6

Kraef, C., Lindquist, E., Svensson, E., and Cambau, E. (2022). Diagnostic toolkit for tuberculosis: should we include urine lipoarabinomannan (LAM) detection in the WHO European Region? *Clin. Microbiol. Infection* 28, 1406–1408. doi: 10.1016/j.cmi.2022.06.022

Lawn, S. D. (2012). Point-of-care detection of lipoarabinomannan (LAM) in urine for diagnosis of HIV-associated tuberculosis: a state of the art review. *BMC Infect. Dis.* 12, 103. doi: 10.1186/1471-2334-12-103

Li, F., Chen, D., Zeng, Q., and Du, Y. (2023). Possible mechanisms of lymphopenia in severe tuberculosis. *Microorganisms* 11(11):2640. doi: 10.3390/microorganisms11112640

Lissouba, P., Akatukwasa, C., and Atieno, L. (2021). Perspectives and perceptions of urine sampling and urine-based TB testing among patients in Kenya and Uganda. *World Conference on Lung Health*. EP-27-366.

Luo, Y., Xue, Y., Tang, G., Cai, Y., Yuan, X., Lin, Q., et al. (2021). Lymphocyte-related immunological indicators for stratifying mycobacterium tuberculosis infection. *Front. Immunol.* 12, 658843. doi: 10.3389/fimmu.2021.658843

Minion, J., Leung, E., Talbot, E., Dheda, K., Pai, M., and Menzies, D. (2011). Diagnosing tuberculosis with urine lipoarabinomannan: systematic review and meta-analysis. *Eur. Respir. J.* 38, 1398–1405. doi: 10.1183/09031936.00025711

Nakiyingi, L., Moodley, V. M., Manabe, Y. C., Nicol, M. P., Holshouser, M., Armstrong, D. T., et al. (2014). Diagnostic accuracy of a rapid urine lipoarabinomannan test for tuberculosis in HIV-infected adults. *J. Acquir. Immune Defic. Syndr.* 66, 270–279. doi: 10.1097/QAI.0000000000000151

Organization, W. H (2022). *WHO consolidated guidelines on tuberculosis. Module 3: diagnosis. Tests for TB infection*. World Health Organization.

Organization, W. H (2023). *Global tuberculosis report 2023*. World Health Organization.

Paris, L., Magni, R., Zaidi, F., Araujo, R., Saini, N., Harpole, M., et al. (2017). Urine lipoarabinomannan glycan in HIV-negative patients with pulmonary tuberculosis correlates with disease severity. *Sci. Transl. Med.* 9(420):eaal2807. doi: 10.1126/scitranslmed.aal2807

Peter, J. G., Zijenah, L. S., Chanda, D., Clowes, P., Lesosky, M., Gina, P., et al. (2016). Effect on mortality of point-of-care, urine-based lipoarabinomannan testing to guide tuberculosis treatment initiation in HIV-positive hospital inpatients: a pragmatic, parallel-group, multicountry, open-label, randomised controlled trial. *Lancet* 387, 1187–1197. doi: 10.1016/S0140-6736(15)01092-2

Shreffler, J., and Huecker, M. R. (2020). Diagnostic testing accuracy: Sensitivity, specificity, predictive values and likelihood ratios. In: *StatPearls [Internet]*. Treasure Island (FL): StatPearls Publishing.

Silva, C. L., Bonato, V. L. D., Lima, K. M., Coelho-Castelo, A. A. M., Faccioli, L. H., Sartori, A., et al. (2001). Cytotoxic T cells and mycobacteria. *FEMS Microbiol. Lett.* 197, 11–18. doi: 10.1111/j.1574-6968.2001.tb10575.x

van Deun, A., Hossain, M. A., Gumusboga, M., and Rieder, H. L. (2008). Ziehl-Neelsen staining: theory and practice. *Int. J. Tuberc Lung Dis.* 12, 108–110.

Wang, J., Yin, Y., Wang, X., Pei, H., Kuai, S., Gu, L., et al. (2015). Ratio of monocytes to lymphocytes in peripheral blood in patients diagnosed with active tuberculosis. *Braz. J. Infect. Dis.* 19, 125–131. doi: 10.1016/j.bjid.2014.10.008

Zhang, Y., Chen, S., Wei, H., Zhong, Q., Yuan, Y., Wang, Y., et al. (2023). Breakthrough of chemiluminescence-based LAM urine test beyond HIV-positive individuals: Clinical diagnostic value of pulmonary tuberculosis in the general population. *Med. (Baltimore)* 102, e36371. doi: 10.1097/MD.0000000000036371

frontiers | Frontiers in Cellular and Infection Microbiology

TYPE Original Research
PUBLISHED 18 March 2025
DOI 10.3389/fcimb.2025.1531732

OPEN ACCESS

EDITED BY
Sam Ebenezer,
Sathyabama Institute of Science and Technology, India

REVIEWED BY
Saranya Somusundaram,
Dr. N.G.P. Arts and Science College, India
Tamilmaran Nagarajan,
Saveetha University, India

*CORRESPONDENCE
Xizhou Guan
gxz301@126.com

RECEIVED 20 November 2024
ACCEPTED 03 March 2025
PUBLISHED 18 March 2025

CITATION
Zhou Z, Liu S, Qu F, Wei Y, Song M and Guan X (2025) Development and validation of a clinical prediction model for pneumonia - associated bloodstream infections.
Front. Cell. Infect. Microbiol. 15:1531732.
doi: 10.3389/fcimb.2025.1531732

Development and validation of a clinical prediction model for pneumonia - associated bloodstream infections

Zhitong Zhou[1], Shangshu Liu[1], Fangzhou Qu[2], Yuanhui Wei[3], Manya Song[4] and Xizhou Guan[5]*

[1]The Graduate School, Liberation Army Medical College, Beijing, China, [2]Department of Cardiology, Shaanxi Provincial People's Hospital, Xian, Shanxi, China, [3]School of Medicine, Nankai University, Tianjin, China, [4]Department of Pulmonary and Critical Care Medicine, Liaocheng People's Hospital, Liaocheng, Shandong, China, [5]Department of Pulmonary and Critical Care Medicine, The Eighth Medical Centre, Chinese People's Liberation Army (PLA) General Hospital, Beijing, China

Purpose: The aim of this study was to develop a valuable clinical prediction model for pneumonia-associated bloodstream infections (PABSIs).

Patients and methods: The study retrospectively collected clinical data of pneumonia patients at the First Medical Centre of the Chinese People's Liberation Army General Hospital from 2019 to 2024. Patients who met the definition of pneumonia-associated bloodstream infections (PABSIs) were selected as the main research subjects. A prediction model for the probability of bloodstream infections (BSIs) in pneumonia patients was constructed using a combination of LASSO regression and logistic regression. The performance of the model was verified using several indicators, including receiver operating characteristic (ROC) curve, calibration curve, decision curve analysis (DCA) and cross validation.

Results: A total of 423 patients with confirmed pneumonia were included in the study, in accordance with the Inclusion Criteria and Exclusion Criteria. Of the patients included in the study, 73 developed a related bloodstream infection (BSI). A prediction model was constructed based on six predictors: long-term antibiotic use, invasive mechanical ventilation, glucocorticoids, urinary catheterization, vasoactive drugs, and central venous catheter placement. The areas under the curve (AUC) of the training set and validation set were 0.83 and 0.80, respectively, and the calibration curve demonstrated satisfactory agreement between the two.

Conclusion: This study has successfully constructed a prediction model for bloodstream infections associated with pneumonia cases, which has good stability and predictability and can help guide clinical work.

KEYWORDS

pneumonia, bloodstream infections, bacteremia, risk factor, early diagnosis, prediction model

1 Introduction

Pneumonia is a prevalent acute respiratory infection that primarily affects the alveoli and distal bronchial tree. Pneumonia is classified according to the source of infection, with the distinction between community-acquired pneumonia (CAP) and hospital-acquired pneumonia (HAP). The latter category includes ventilator-associated pneumonia (VAP) (Torres et al., 2021). The most prevalent clinical manifestations of the disease include cough, dyspnea, chest pain, sputum production, and fatigue (Metlay et al., 1997; Lamping et al., 2002). Pneumonia represents a significant public health concern, with high morbidity rates observed across all age groups and a strong association with both short- and long-term mortality. The 2019 Global Burden of Disease (GBD) study revealed that approximately 489 million individuals worldwide had been affected by lower respiratory tract infections (LRTIs), encompassing conditions such as pneumonia and bronchiolitis. The demographic groups most affected by these infections were children below five years of age and adults above 70 years of age (Abbafati et al., 2020). Bloodstream infections (BSIs) are serious systemic infections that can readily lead to sepsis and multiple organ dysfunction syndrome (MODS), and have a high mortality rate. Consequently, bloodstream infections have become a significant challenge to public health globally (Kern and Rieg, 2020). Pneumonia represents the most common cause of BSIs, accounting for approximately half of all cases (Angus and van der Poll, 2013). In the event that patients diagnosed with pneumonia fail to receive timely or appropriate treatment, they may develop bloodstream infections or even sepsis as their condition progresses. The incidence of bloodstream infections in modern respiratory wards has been increasing year on year, and this may be related to a number of factors, including an ageing population, increased use of immunosuppressants and rising antibiotic resistance. Severe complications of pneumonia, such as bacteremia and sepsis, represent a significant threat to patient survival.

The progressive advancement of data measurement technology and analytical methods is facilitating a gradual transition in the field of medicine from the era of evidence-based medicine to the era of precision medicine. As a consequence of this transition, the role of clinical prediction models is becoming increasingly significant within the field of healthcare, thereby facilitating the development of more sophisticated and tailored healthcare services. Logistic regression, a widely employed statistical technique, plays a pivotal role in the development of clinical prediction models. However, due to the relatively small sample sizes of some studies, problems such as overfitting are common in model construction, which limits the generalizability and practical application performance of the model. To address this challenge, LASSO regression (Least Absolute Shrinkage and Selection Operator) is an effective strategy that introduces a penalty term to reduce the number of variables in the model, thereby enhancing the stability, interpretability and predictive performance of the model. Consequently, an increasing number of researchers are employing LASSO in conjunction with logistic regression to develop more precise and dependable clinical prediction models.

Currently, there is a dearth of clinical research on bloodstream infections in patients with pneumonia, and there is no consensus on the definition of pneumonia-associated bloodstream infections. In light of these considerations, this study has been designed with the objective of addressing this clinical challenge with a view to preventing pneumonia patients from developing bloodstream infections, thereby avoiding the deterioration of their condition to sepsis. The ultimate objective is a reduction in mortality. The objective of this study is to facilitate an early diagnosis and timely treatment of pneumonia-associated bloodstream infections, with the aim of improving outcomes.

2 Patients and methods

2.1 Study subjects

This study employed a retrospective research design to collate data on inpatients diagnosed with pneumonia at the PLA General Hospital's First Medical Centre between May 2019 and May 2024.

The diagnostic criteria for pneumonia-associated bloodstream infections were as follows: (1) the patient presented with pneumonia as the initial symptom and a definitive diagnosis was reached; (2) the results of sputum and blood cultures were consistent with the same pathogen; and (3) all other potential sources of infection were excluded.

2.2 Inclusion criteria

The following inclusion criteria were employed:

1. Age > 18 years;
2. Pneumonia-associated clinical manifestations (any one of the following four manifestations is sufficient): (1) A recent cough with sputum or worsening of pre-existing respiratory symptoms, with or without purulent sputum, chest pain, dyspnea, and hemoptysis; (2) Fever; (3) Evidence of lung consolidation (voice raised, percussion dull) and/or wet rales; (4) Peripheral blood leukocyte count $>10\times10^9$/L or $<4\times10^9$/L, with or without nuclear shift to the left;
3. Chest imaging demonstrates the presence of new patchy infiltrates, lobular or segmental consolidation, ground-glass opacities, or interstitial changes, with or without pleural effusion;
4. Sputum and blood samples are obtained for culture.

2.3 Exclusion criteria

The exclusion criteria were as follows:

1. The patient was below the age of 18 years;
2. The diagnosis of pulmonary infection was uncertain;
3. Sputum and blood culture specimens were not obtained.

2.4 Study variables

The study collected patients' personal information and clinical data by searching the hospital's electronic medical record system. All baseline characteristics were recorded within a 24-hour period.

Data were collected from each patient for statistical analysis, including:(1) Demographic characteristics: sex, age, body mass index (BMI), date and time of admission; (2) Vital signs: body temperature, heart rate, respiratory rate, blood pressure (systolic and diastolic), and mean arterial pressure (MAP); (3) Personal lifestyle history: smoking and alcohol consumption; (4) History of chronic disease: Hypertension, Diabetes, coronary heart disease (CAD), Congestive Heart Failure, Atrial Fibrillation (AF), Arrhythmia, Hyperlipidemia, Cerebral Infarction, Chronic Respiratory Disease, Alzheimer's Disease, Parkinson's Disease, Thyroid Dysfunction, Renal Insufficiency, Benign Prostatic Hyperplasia (BPH), Gastrointestinal Bleeding, Chronic Gastritis, Reflux Esophagitis, Fatty Liver, Cirrhosis, Malignant Tumors, Hematologic Diseases, Lymphoma, Rheumatic Diseases of Immune System; (5) Surgical and treatment history: major surgery(Refers to surgery involving major organs or systems that carries a higher risk, longer recovery time, and may have a significant impact on the patient's quality of life. This includes, but is not limited to: heart surgery, brain surgery, organ removal, etc.), recent surgery(Refers to surgery that the patient has had within the last 2 weeks), long-term antibiotic treatment(Refers to the use of antibiotics for ≥2 weeks and ≥1 type), radiotherapy, chemotherapy, hemodialysis and organ transplant history; (6) Use of medical devices: nasogastric tube, urinary catheter, central venous catheter placement and drainage tube; (7) Implementation of nutritional support and therapeutic measures: Total parenteral nutrition, invasive mechanical ventilation, sedatives, anticoagulants, vasopressors and glucocorticoids; steroids; (8) Laboratory Indicators: Sputum and blood microbial culture, pH, PaO2, PaCO2, oxygenation index, bicarbonate, lactate, white blood cell count, neutrophil percentage, lymphocyte percentage, hemoglobin, platelet count, C-reactive protein (CRP), interleukin-6 (IL-6), procalcitonin (PCT), serum albumin, total serum albumin, alanine aminotransferase (ALT), aspartate aminotransferase (AST), total bilirubin, direct bilirubin, urea, serum creatinine, serum potassium concentration, serum sodium ion concentration, serum chloride ion concentration, prothrombin time (PT), activated partial thromboplastin time (APTT), prothrombin time activity (PTA), fibrinogen, D-dimer.

2.5 Missing data handling

To address the issue of missing data during the data processing stage, the following measures were implemented. In cases where more than 50% of the data was missing, the decision was taken to delete the entire data set. Secondly, if the proportion of missing values for a specific variable exceeded 21%, the variable was excluded from the analysis. In cases where missing values were present for variables within the remaining case data, multiple imputation techniques were employed to ensure the integrity and accuracy of the data analysis.

2.6 Sample size estimation

This study is a single-center, retrospective cohort design aimed at developing a multifactorial regression model to predict pneumonia-associated bloodstream infections (PABSI). The study population was selected based on the criterion of concordance between sputum and blood culture results. Given the limitations of clinical resources, sample size estimation was conducted with practical feasibility in mind, ensuring that the statistical requirements were met.

2.6.1 Requirements for multifactor regression analysis (Peduzzi guidelines)

A maximum of six outcome-related predictor variables were intended to be included in the model to balance explanatory power and predictive accuracy, while maintaining simplicity. According to the Peduzzi guideline, each predictor variable should correspond to at least 10 outcome events (EPV ≥ 10) to prevent overfitting and ensure the stability and accuracy of model estimates. Therefore, with six predictor variables, a minimum of 60 outcome events ($6 \times 10 = 60$) is required.

2.6.2 Calculation formula and process

To ensure adequate statistical power, sample size calculations were conducted as follows: assuming the incidence of bloodstream infection (BSI) in the exposed group (p_1) is 20% and in the unexposed group (p_2) is 5%, with a Type I error rate (α) set at 0.05 and a power (1 - β) of 80%. The sample size was calculated using the formula (Figure 1):

where $Z_{\alpha/2}$ is the critical value for the standard normal distribution (1.96 for $\alpha = 0.05$), and Z_β is the critical value for statistical power (0.84 for 80% power). The sample size was calculated as n = 84 to ensure the study would meet the statistical requirements.

Based on the above calculations, the minimum sample size required for this study was 146 cases, with 73 cases in each of the exposed and unexposed groups, to achieve 80% power.

2.7 Statistical processing

The statistical analysis was conducted using SPSS 26.0 and R 4.4.1. Quantitative data are expressed as mean ± standard deviation, and for non-normally distributed data, the median and interquartile range are employed. Categorical data are displayed as frequencies or percentages. In order to conduct a comparative analysis of continuous variables, the t-test or Mann-Whitney U test was employed. Similarly, the chi-square test or Fisher's exact test was

$$n = \frac{(p1 - p2)^2 (Z_{\alpha/2} + Z_\beta)^2 \cdot [p1(1 - p1) + p2(1 - p2)]}{(\text{standard deviation})^2}$$

FIGURE 1
Sample size calculation formula.

used for the comparison of categorical variables. The data was randomly divided into a training set and a validation set in a 1:1 ratio.

In the feature selection phase, a combination of LASSO regression and logistic regression was employed. Initially, all data were subjected to univariate logistic regression analysis to identify potentially pertinent variables with a P-value less than 0.05. Subsequently, LASSO regression was performed, and the 1 standard error (1se) rule was employed to ascertain the optimal penalty coefficient and exclude non-representative variables. Subsequently, a further multivariate logistic regression analysis was conducted to evaluate the independent effects of these variables on the outcome, with the corresponding odds ratios (OR) and 95% confidence intervals (CI) subsequently calculated.

Once the regression equation had been established, a line chart was employed to represent the prediction model. An ROC curve was constructed for the purpose of evaluating the model's performance, and the AUC value was calculated for the purpose of evaluating its diagnostic ability. The Hosmer-Lemeshow test was employed to evaluate the model's goodness of fit, while a calibration curve was plotted to assess the calibration effect of the model. Moreover, decision curve analysis (DCA) was employed to determine the clinical utility of the model. In this study, a statistically significant level was set at $P < 0.05$.

3 Results

3.1 Patient demographics

A total of 423 patients were enrolled in this study, including 211 patients in the training group and 212 patients in the test group. This sample size significantly exceeded the calculated minimum requirement, thereby ensuring the statistical validity of the study. All patient data were complete and suitable for analysis.

A comparison of the baseline data from the two cohorts revealed significant differences between the two groups with respect to partial pressure of arterial carbon dioxide ($Paco_2$; P = 0.036), lymphocyte percentage (P = 0.040), history of diabetes (P = 0.008), and use of drainage tubes (P = 0.025). No significant differences were identified for the remaining indicators (all p-values were greater than 0.05). For further details, please refer to Table 1.

3.2 Factor screening

In this study, a univariate logistic regression analysis was initially performed on all included variables, which encompassed demographic characteristics, vital signs, personal history of lifestyle habits, history of chronic diseases, history of surgery and treatment, use of medical equipment, nutrition and supportive care, use of drugs, and laboratory test indicators.

The results of the univariate logistic regression analysis demonstrated that the following variables were significantly associated with pneumonia-associated bloodstream infections (PABSIs) (P < 0.05): coronary heart disease, long-term use of antibiotics, nasogastric tube use, urinary catheter use, and central venous catheter, invasive mechanical ventilation, and sedative drug use, use of vasoactive drugs, use of glucocorticoids, body temperature, heart rate, diastolic blood pressure, and mean arterial pressure (MAP), oxygenation index, urea. For further details, please refer to Table 2.

The use of LASSO regression analysis identified six possible predictors that were found to be significantly associated with pneumonia-associated bloodstream infections (PABSIs) when the λ value was set to 1 standard error (1-se). The identified predictors were long-term antibiotic use, urinary catheter use, central venous catheterization, invasive mechanical ventilation, vasodilator use and glucocorticoid use. For further details, please refer to Figure 2.

Further multivariate logistic regression analysis was used to verify the six potential predictors selected by LASSO regression. The results of the analysis showed that the following factors were significantly associated with the risk of pneumonia-associated bloodstream infections (PABSIs): invasive mechanical ventilation, glucocorticoid use, use of long-term antibiotics, use of vasoactive drugs, urinary catheter use, and central venous catheter use. See Table 3 for details.

3.3 Construction of a prediction model

Based on the results of the multifactor logistic regression analysis, a prediction model was constructed to predict the risk of pneumonia-associated bloodstream infections. The model is presented visually in a line graph for ease of clinical application and interpretation. For further details, please refer to Figure 3.

3.4 Model evaluation

To comprehensively evaluate the performance of the nomogram we constructed, we used a number of statistical validation methods. These included receiver operating characteristic (ROC) curve analysis, area under the curve (AUC) calculation, calibration curve analysis and decision curve analysis (DCA). Together, these methods provide insight into the predictive accuracy of the nomogram, its calibration and its use in clinical decision making.

3.4.1 ROC curve and AUC analysis

In order to evaluate the discriminatory power of the nomogram that we had constructed, we initially employed a receiver operating characteristic (ROC) curve analysis. The area under the curve (AUC) values of the nomogram in the training and validation sets reached 0.83 and 0.80 (see Figure 4), respectively. These results demonstrate that the model exhibits excellent discriminative power on both the training and validation sets. The high AUC values also indicate that the model has high accuracy in identifying pneumonia-associated bloodstream infections (PABSIs).

10.3389/fcimb.2025.1531732

TABLE 1 Clinical characteristics and demographic of two groups.

Variables	Total (n = 423)	test (n = 212)	train (n = 211)	*P*
Age/year	79.00 (67.00, 87.00)	78.00 (64.75, 87.00)	80.00 (69.00, 87.00)	0.214
BMI	22.90 (20.85, 24.80)	23.19 (21.08, 25.00)	22.60 (20.35, 24.55)	0.101
Temperature/°C	36.60 (36.40, 36.80)	36.50 (36.40, 36.80)	36.60 (36.40, 36.80)	0.299
Heartbeat/BPM	82.00 (76.00, 93.00)	83.00 (77.75, 93.25)	82.00 (75.00, 90.50)	0.116
Respiratory rate/BPM	20.00 (19.00, 20.00)	20.00 (19.00, 20.00)	20.00 (19.00, 20.00)	0.957
Systolic pressure/mmHg,	128.00 (120.00, 139.00)	128.00 (119.75, 140.00)	128.00 (120.00, 139.00)	0.942
Diastolic pressure/mmHg	73.00 (65.00, 81.00)	73.00 (65.00, 81.00)	73.00 (66.00, 81.00)	0.473
MAP	91.67 (84.67, 99.83)	92.00 (84.00, 99.42)	91.33 (85.33, 100.67)	0.669
PH	7.43 (7.39, 7.47)	7.43 (7.39, 7.47)	7.43 (7.40, 7.47)	0.804
PaO_2/mmHg,	85.58 (73.90, 94.36)	85.75 (76.62, 95.55)	85.20 (71.00, 93.50)	0.196
$PaCo_2$/mmHg	37.28 (33.05, 40.16)	37.05 (32.93, 39.32)	37.79 (33.95, 40.80)	0.036
Oxygenation index	264.00 (227.00, 297.00)	264.86 (233.00, 297.50)	263.00 (221.00, 290.50)	0.217
HCO^{3-}/(mmol/L)	24.60 (23.20, 26.39)	24.50 (23.20, 26.05)	24.70 (23.18, 26.70)	0.414
Lac/(mmol/L)	1.56 (1.10, 2.08)	1.64 (1.10, 2.07)	1.42 (1.00, 2.09)	0.253
WBC/(10^9/L)	7.47 (5.55, 10.49)	7.42 (5.55, 10.52)	7.54 (5.56, 10.41)	0.993
N/%	0.76 (0.63, 0.85)	0.75 (0.62, 0.84)	0.77 (0.66, 0.86)	0.123
L/%	0.14 (0.08, 0.24)	0.15 (0.09, 0.26)	0.12 (0.07, 0.22)	0.040
Hb/(g/L)	120.00 (106.00, 134.50)	121.00 (107.00, 136.00)	119.00 (104.00, 132.50)	0.245
PLT/(10^9/L)	202.00 (153.50, 267.00)	204.00 (153.25, 259.00)	200.00 (154.00, 268.50)	0.928
CRP/(mg/dl)	2.31 (0.51, 6.70)	2.33 (0.49, 6.08)	2.25 (0.57, 6.77)	0.770
IL-6/(pg/ml)	27.17 (6.29, 90.51)	30.38 (6.19, 92.52)	24.42 (6.64, 89.66)	0.674
PCT	0.18 (0.07, 1.45)	0.18 (0.08, 1.44)	0.19 (0.07, 1.45)	0.821
Albumin/(g/L)	36.40 (33.10, 39.50)	36.50 (33.30, 39.90)	36.20 (33.00, 39.25)	0.231
Total albumin/(g/L)	67.10 (62.30, 72.40)	67.75 (63.40, 72.50)	66.30 (61.50, 71.90)	0.257
ALT/(U/L)	16.60 (11.20, 26.95)	17.40 (11.70, 27.95)	16.10 (10.55, 25.95)	0.186
AST/(U/L)	20.80 (16.00, 29.15)	20.60 (16.50, 29.07)	21.00 (15.50, 29.15)	0.482
Total bilirubin/(umol/L)	8.50 (5.70, 12.20)	8.40 (5.70, 12.12)	8.60 (5.80, 12.30)	0.573
Direct bilirubin/(umol/L)	3.30 (2.20, 5.20)	3.20 (2.20, 5.00)	3.30 (2.30, 5.40)	0.478
Urea/(mmol/L)	5.65 (4.27, 7.97)	5.42 (4.24, 7.50)	5.87 (4.29, 8.38)	0.326
Creatinine/(umol/L)	74.20 (59.80, 91.20)	75.05 (61.25, 91.32)	73.00 (58.95, 89.60)	0.451
K/(mmol/L)	3.78 (3.49, 4.20)	3.78 (3.48, 4.17)	3.79 (3.49, 4.22)	0.556
Na/(mmol/L)	136.80 (132.95, 140.00)	136.60 (133.20, 139.72)	136.90 (132.85, 140.30)	0.510
Cl/(mmol/L)	100.70 (96.90, 104.25)	100.60 (96.55, 103.62)	101.10 (97.05, 104.85)	0.306
PT/s	13.70 (12.90, 14.70)	13.60 (12.80, 14.62)	13.70 (13.00, 14.75)	0.233
APTT/s	36.40 (32.20, 40.70)	36.30 (32.00, 41.23)	36.40 (32.55, 40.00)	0.825
PTA	88.00 (78.00, 98.00)	89.00 (79.07, 99.00)	86.10 (76.00, 97.00)	0.161
Fib	4.52 (3.60, 5.64)	4.55 (3.71, 5.65)	4.49 (3.52, 5.63)	0.674
D-D/(ug/ml)	1.10 (0.52, 2.26)	1.05 (0.50, 2.08)	1.16 (0.55, 2.42)	0.336

(Continued)

10.3389/fcimb.2025.1531732

TABLE 1 Continued

Variables	Total (n = 423)	test (n = 212)	train (n = 211)	*P*
Outcome, n (%)				0.151
0	350 (82.74)	181 (85.38)	169 (80.09)	
1	73 (17.26)	31 (14.62)	42 (19.91)	
Sex, n (%)				0.793
1	262 (61.94)	130 (61.32)	132 (62.56)	
2	161 (38.06)	82 (38.68)	79 (37.44)	
Cigarette, n (%)				0.197
0	324 (76.60)	168 (79.25)	156 (73.93)	
1	99 (23.40)	44 (20.75)	55 (26.07)	
Alcohol, n (%)				0.600
0	345 (81.56)	175 (82.55)	170 (80.57)	
1	78 (18.44)	37 (17.45)	41 (19.43)	
Hypertension, n (%)				0.187
0	198 (46.81)	106 (50.00)	92 (43.60)	
1	225 (53.19)	106 (50.00)	119 (56.40)	
Diabetes, n (%)				0.008
0	300 (70.92)	138 (65.09)	162 (76.78)	
1	123 (29.08)	74 (34.91)	49 (23.22)	
Coronary Artery Disease, n (%)				0.718
0	312 (73.76)	158 (74.53)	154 (72.99)	
1	111 (26.24)	54 (25.47)	57 (27.01)	
Heart Failure, n (%)				0.371
0	418 (98.82)	208 (98.11)	210 (99.53)	
1	5 (1.18)	4 (1.89)	1 (0.47)	
Atrial Fibrillation, n (%)				0.235
0	395 (93.38)	201 (94.81)	194 (91.94)	
1	28 (6.62)	11 (5.19)	17 (8.06)	
Arrhythmia, n (%)				0.450
0	416 (98.35)	207 (97.64)	209 (99.05)	
1	7 (1.65)	5 (2.36)	2 (0.95)	
Hyperlipidemia, n (%)				0.092
0	376 (88.89)	183 (86.32)	193 (91.47)	
1	47 (11.11)	29 (13.68)	18 (8.53)	
Cerebral infarction, n (%)				0.683
0	350 (82.74)	177 (83.49)	173 (81.99)	
1	73 (17.26)	35 (16.51)	38 (18.01)	
Chronic respiratory disease, n (%)				0.146
0	367 (86.76)	189 (89.15)	178 (84.36)	

(Continued)

10.3389/fcimb.2025.1531732

TABLE 1 Continued

Variables	Total (n = 423)	test (n = 212)	train (n = 211)	*P*
1	56 (13.24)	23 (10.85)	33 (15.64)	
Alzheimer's disease, n (%)				0.357
0	390 (92.20)	198 (93.40)	192 (91.00)	
1	33 (7.80)	14 (6.60)	19 (9.00)	
Parkinsonism, n (%)				0.425
0	408 (96.45)	206 (97.17)	202 (95.73)	
1	15 (3.55)	6 (2.83)	9 (4.27)	
Gastrointestinal hemorrhage, n (%)				1.000
0	420 (99.29)	210 (99.06)	210 (99.53)	
1	3 (0.71)	2 (0.94)	1 (0.47)	
Chronic gastritis, n (%)				0.812
0	406 (95.98)	203 (95.75)	203 (96.21)	
1	17 (4.02)	9 (4.25)	8 (3.79)	
Gastroesophageal Reflux Disease, n (%)				0.496
0	414 (97.87)	209 (98.58)	205 (97.16)	
1	9 (2.13)	3 (1.42)	6 (2.84)	
Fatty liver, n (%)				1.000
0	421 (99.53)	211 (99.53)	210 (99.53)	
1	2 (0.47)	1 (0.47)	1 (0.47)	
Liver cirrhosis, n (%)				0.997
0	420 (99.29)	211 (99.53)	209 (99.05)	
1	3 (0.71)	1 (0.47)	2 (0.95)	
Malignant tumor, n (%)				0.179
0	355 (83.92)	183 (86.32)	172 (81.52)	
1	68 (16.08)	29 (13.68)	39 (18.48)	
Hematological Diseases, n (%)				0.593
0	409 (96.69)	204 (96.23)	205 (97.16)	
1	14 (3.31)	8 (3.77)	6 (2.84)	
Lymphoma, n (%)				0.994
0	414 (97.87)	208 (98.11)	206 (97.63)	
1	9 (2.13)	4 (1.89)	5 (2.37)	
Rheumatic immune system disease, n (%)				0.552
0	411 (97.16)	207 (97.64)	204 (96.68)	
1	12 (2.84)	5 (2.36)	7 (3.32)	
History of major surgery, n (%)				0.785
0	369 (87.23)	184 (86.79)	185 (87.68)	
1	54 (12.77)	28 (13.21)	26 (12.32)	
Hypothyroidism, n (%)				0.450

(Continued)

10.3389/fcimb.2025.1531732

TABLE 1 Continued

Variables	Total (n = 423)	test (n = 212)	train (n = 211)	*P*
0	416 (98.35)	207 (97.64)	209 (99.05)	
1	7 (1.65)	5 (2.36)	2 (0.95)	
Renal insufficiency, n (%)				0.199
0	390 (92.20)	199 (93.87)	191 (90.52)	
1	33 (7.80)	13 (6.13)	20 (9.48)	
Benign Prostatic Hyperplasia, n (%)				0.882
0	382 (90.31)	191 (90.09)	191 (90.52)	
1	41 (9.69)	21 (9.91)	20 (9.48)	
Peripheral Vascular Disease, n (%)				0.436
0	408 (96.45)	203 (95.75)	205 (97.16)	
1	15 (3.55)	9 (4.25)	6 (2.84)	
Long-term antibiotic use, n (%)				0.387
0	401 (94.80)	199 (93.87)	202 (95.73)	
1	22 (5.20)	13 (6.13)	9 (4.27)	
Radiotherapy or chemotherapy, n (%)				0.566
0	392 (92.67)	198 (93.40)	194 (91.94)	
1	31 (7.33)	14 (6.60)	17 (8.06)	
Dialysis, n (%)				0.996
0	418 (98.82)	210 (99.06)	208 (98.58)	
1	5 (1.18)	2 (0.94)	3 (1.42)	
Organ transplant, n (%)				1.000
0	420 (99.29)	210 (99.06)	210 (99.53)	
1	3 (0.71)	2 (0.94)	1 (0.47)	
Recent surgery, n (%)				0.499
0	421 (99.53)	210 (99.06)	211 (100.00)	
1	2 (0.47)	2 (0.94)	0 (0.00)	
Gastric tube, n (%)				0.975
0	299 (70.69)	150 (70.75)	149 (70.62)	
1	124 (29.31)	62 (29.25)	62 (29.38)	
Urinary tube, n (%)				0.709
0	326 (77.07)	165 (77.83)	161 (76.30)	
1	97 (22.93)	47 (22.17)	50 (23.70)	
Central venous catheter, n (%)				0.130
0	332 (78.49)	160 (75.47)	172 (81.52)	
1	91 (21.51)	52 (24.53)	39 (18.48)	
Drainage tube, n (%)				0.025
0	406 (95.98)	208 (98.11)	198 (93.84)	
1	17 (4.02)	4 (1.89)	13 (6.16)	

(Continued)

10.3389/fcimb.2025.1531732

TABLE 1 Continued

Variables	Total (n = 423)	test (n = 212)	train (n = 211)	*P*
Total Parenteral Nutrition, n (%)				1.000
0	418 (98.82)	209 (98.58)	209 (99.05)	
1	5 (1.18)	3 (1.42)	2 (0.95)	
Invasive mechanical ventilation, n (%)				0.846
0	398 (94.09)	199 (93.87)	199 (94.31)	
1	25 (5.91)	13 (6.13)	12 (5.69)	
Sedation, n (%)				0.637
0	405 (95.74)	202 (95.28)	203 (96.21)	
1	18 (4.26)	10 (4.72)	8 (3.79)	
Anticoagulant, n (%)				0.329
0	271 (64.07)	131 (61.79)	140 (66.35)	
1	152 (35.93)	81 (38.21)	71 (33.65)	
Vasoactive Drugs, n (%)				0.516
0	383 (90.54)	190 (89.62)	193 (91.47)	
1	40 (9.46)	22 (10.38)	18 (8.53)	
Glucocorticoid, n (%)				0.789
0	270 (63.83)	134 (63.21)	136 (64.45)	
1	153 (36.17)	78 (36.79)	75 (35.55)	

3.4.2 Calibration curve

In order to ascertain the predictive accuracy of the nomogram, a calibration curve analysis was conducted. The results are presented in Figure 5, which demonstrate that the nomogram exhibits robust predictive performance on both the training and validation sets. The calibration curve is in close proximity to the diagonal, indicating that the probability predicted by the model is highly consistent with the actual observed probability of event occurrence. These findings provide further confirmation of the model's predictive accuracy.

3.4.3 Decision curve analysis

Decision curve analysis (DCA) further verified the value of the nomogram in clinical applications, as shown in Figure 6. The results of the DCA showed that the model could achieve above average net benefits regardless of the threshold probability setting, indicating that the nomogram has significant advantages in clinical decision making.

3.4.4 Cross validation

To further validate the model, 5-fold cross-validation was performed. The AUC scores for each fold were as follows: 0.84, 0.77, 0.71, 0.87, and 0.82, with an average AUC of 0.80 ± 0.05. These results indicate that the model showed stable performance across different subsets of the data, with good generalizability. The cross-validation results further support the robustness and reliability of the predictive model.

4 Discussion

This study employed a combination of logistic regression and LASSO regression to develop a clinical prediction model for pneumonia-associated bloodstream infections (PABSIs) with notable success. The model employs clinical laboratory indicators and is trained and evaluated using medical record data. The model is capable of accurately predicting the risk of pneumonia patients developing bloodstream infections. The model demonstrated excellent performance on the training and validation sets, with AUC values of 0.83 and 0.80, respectively, confirming its excellent discrimination and prediction capabilities. Furthermore, the calibration curve and decision curve analysis demonstrate that the model exhibits high accuracy in actual prediction and clinical application, providing a robust foundation for clinical decision-making.

To ensure the adequacy of the sample size, this study performed sample size estimation based on the Peduzzi criteria, ensuring sufficient statistical power for the research. In the total sample, the number of outcome events per predictor variable was 12.17 (73 ÷ 6), which is significantly higher than the recommended minimum of 10 events per variable by the Peduzzi criterion, thereby ensuring the robustness and reliability of the model.

For variable selection, this study employed LASSO regression. By introducing a penalty term, LASSO regression effectively selects and shrinks variables, reducing the risk of over-parameterization and mitigating the overfitting problems commonly encountered

10.3389/fcimb.2025.1531732

TABLE 2 Univariate logistic regression.

Variables	β	S. E	Z	*P*	OR (95%CI)
Sex					
1					1.00 (Reference)
2	-0.64	0.38	-1.67	0.096	0.53 (0.25 ~ 1.12)
Cigarette					
0					1.00 (Reference)
1	0.30	0.38	0.80	0.421	1.36 (0.65 ~ 2.85)
Alcohol					
0					1.00 (Reference)
1	0.33	0.41	0.80	0.424	1.39 (0.62 ~ 3.13)
Hypertension					
0					1.00 (Reference)
1	0.16	0.35	0.46	0.648	1.17 (0.59 ~ 2.33)
Diabetes					
0					1.00 (Reference)
1	-0.13	0.42	-0.31	0.758	0.88 (0.39 ~ 1.99)
Coronary Artery Disease					
0					1.00 (Reference)
1	0.79	0.36	2.16	0.030	2.19 (1.08 ~ 4.46)
Heart Failure					
0					1.00 (Reference)
1	-13.18	882.74	-0.01	0.988	0.00 (0.00 ~ Inf)
Atrial Fibrillation					
0					1.00 (Reference)
1	-0.16	0.66	-0.24	0.808	0.85 (0.23 ~ 3.11)
Arrhythmia					
0					1.00 (Reference)
1	17.01	1029.12	0.02	0.987	24326759.34 (0.00 ~ Inf)
Hyperlipemia					
0					1.00 (Reference)
1	0.48	0.56	0.87	0.386	1.62 (0.54 ~ 4.83)
Cerebral infarction					
0					1.00 (Reference)
1	0.45	0.42	1.09	0.277	1.57 (0.69 ~ 3.56)
Chronic respiratory disease					
0					1.00 (Reference)
1	0.50	0.44	1.15	0.252	1.65 (0.70 ~ 3.87)

(Continued)

TABLE 2 Continued

Variables	β	S. E	Z	*P*	OR (95%CI)
Alzheimer's disease					
0					1.00 (Reference)
1	-0.31	0.65	-0.47	0.639	0.74 (0.20 ~ 2.65)
Parkinsonism					
0					1.00 (Reference)
1	-0.71	1.07	-0.66	0.508	0.49 (0.06 ~ 4.04)
Gastrointestinal hemorrhage					
0					1.00 (Reference)
1	-13.18	882.74	-0.01	0.988	0.00 (0.00 ~ Inf)
Chronic gastritis					
0					1.00 (Reference)
1	-15.22	848.37	-0.02	0.986	0.00 (0.00 ~ Inf)
Gastroesophageal Reflux Disease					
0					1.00 (Reference)
1	1.45	0.84	1.73	0.083	4.26 (0.83 ~ 21.90)
Fatty liver					
0					1.00 (Reference)
1	15.98	882.74	0.02	0.986	8731034.54 (0.00 ~ Inf)
Liver cirrhosis					
0					1.00 (Reference)
1	17.01	1029.12	0.02	0.987	24326759.33 (0.00 ~ Inf)
Malignant tumor					
0					1.00 (Reference)
1	-0.16	0.46	-0.34	0.735	0.86 (0.35 ~ 2.10)
Hematological Diseases					
0					1.00 (Reference)
1	0.72	0.88	0.82	0.413	2.06 (0.36 ~ 11.66)
Lymphoma					
0					1.00 (Reference)
1	0.01	1.13	0.01	0.996	1.01 (0.11 ~ 9.24)
Rheumatic immune system disease					
0					1.00 (Reference)
1	1.15	0.78	1.47	0.141	3.17 (0.68 ~ 14.76)
History of major surgery					
0					1.00 (Reference)
1	0.68	0.47	1.46	0.144	1.97 (0.79 ~ 4.91)

(Continued)

10.3389/fcimb.2025.1531732

TABLE 2 Continued

Variables	β	S. E	Z	*P*	OR (95%CI)
Hypothyroidism					
0					1.00 (Reference)
1	-14.19	1029.12	-0.01	0.989	0.00 (0.00 ~ Inf)
Renal insufficiency					
0					1.00 (Reference)
1	0.61	0.52	1.17	0.240	1.85 (0.66 ~ 5.13)
Benign Prostatic Hyperplasia					
0					1.00 (Reference)
1	-1.65	1.04	-1.58	0.114	0.19 (0.03 ~ 1.48)
Peripheral Vascular Disease					
0					1.00 (Reference)
1	0.72	0.88	0.82	0.413	2.06 (0.36 ~ 11.66)
Long-term antibiotic use					
0					1.00 (Reference)
1	2.82	0.82	3.42	<.001	16.70 (3.33 ~ 83.81)
Radiotherapy or chemotherapy					
0					1.00 (Reference)
1	0.57	0.56	1.01	0.311	1.77 (0.59 ~ 5.33)
Dialysis					
0					1.00 (Reference)
1	0.71	1.24	0.57	0.565	2.04 (0.18 ~ 23.01)
Organ transplant					
0					1.00 (Reference)
1	15.98	882.74	0.02	0.986	8731034.54 (0.00 ~ Inf)
Gastric tube					
0					1.00 (Reference)
1	1.14	0.36	3.19	0.001	3.12 (1.55 ~ 6.28)
Urinary tube					
0					1.00 (Reference)
1	1.85	0.37	4.94	<.001	6.37 (3.06 ~ 13.26)
Central venous catheter					
0					1.00 (Reference)
1	2.13	0.40	5.36	<.001	8.39 (3.85 ~ 18.26)
Drainage tube					
0					1.00 (Reference)
1	0.63	0.63	1.00	0.318	1.87 (0.55 ~ 6.40)

(Continued)

TABLE 2 Continued

Variables	β	S. E	Z	*P*	OR (95%CI)
Total Parenteral Nutrition					
0					1.00 (Reference)
1	17.01	1029.12	0.02	0.987	24326759.33 (0.00 ~ Inf)
Invasive mechanical ventilation					
0					1.00 (Reference)
1	4.09	1.06	3.85	<.001	59.61 (7.43 ~ 478.04)
Sedation					
0					1.00 (Reference)
1	3.51	1.09	3.24	0.001	33.60 (4.01 ~ 281.81)
Anticoagulant					
0					1.00 (Reference)
1	0.50	0.35	1.40	0.160	1.64 (0.82 ~ 3.28)
Vasoactive drug					
0					1.00 (Reference)
1	3.03	0.60	5.02	<.001	20.62 (6.33 ~ 67.20)
Glucocorticoid					
0					1.00 (Reference)
1	1.38	0.36	3.84	<.001	3.98 (1.96 ~ 8.06)
Age	0.01	0.01	0.43	0.664	1.01 (0.98 ~ 1.03)
BMI	0.06	0.04	1.41	0.158	1.06 (0.98 ~ 1.15)
Temperature	0.88	0.25	3.45	<.001	2.40 (1.46 ~ 3.95)
Heartbeat	0.05	0.01	3.62	<.001	1.05 (1.02 ~ 1.07)
Respiratory rate	0.08	0.10	0.85	0.396	1.09 (0.90 ~ 1.31)
Systolic pressure	0.01	0.01	1.30	0.193	1.01 (0.99 ~ 1.03)
Diastolic pressure	0.04	0.01	3.06	0.002	1.04 (1.02 ~ 1.07)
MAP	0.04	0.01	2.62	0.009	1.04 (1.01 ~ 1.06)
PH	-3.52	2.55	-1.38	0.168	0.03 (0.00 ~ 4.39)
PaO_2	0.01	0.01	1.76	0.079	1.01 (1.00 ~ 1.02)
$PaCo_2$	0.01	0.02	0.41	0.683	1.01 (0.96 ~ 1.06)
Oxygenation index	0.01	0.00	2.40	0.016	1.01 (1.01 ~ 1.01)
HCO^{3-}	-0.03	0.05	-0.54	0.586	0.97 (0.88 ~ 1.07)
Lac	0.16	0.11	1.42	0.156	1.17 (0.94 ~ 1.47)
WBC	-0.01	0.04	-0.22	0.827	0.99 (0.92 ~ 1.07)
N	1.06	1.23	0.86	0.390	2.88 (0.26 ~ 31.93)
L	-3.46	1.90	-1.83	0.068	0.03 (0.00 ~ 1.29)
Hb	-0.01	0.01	-0.76	0.450	0.99 (0.98 ~ 1.01)

(Continued)

10.3389/fcimb.2025.1531732

TABLE 2 Continued

Variables	β	S. E	Z	*P*	OR (95%CI)
Glucocorticoid					
PLT	-0.00	0.00	-1.62	0.105	1.00 (0.99 ~ 1.00)
CRP	0.03	0.03	1.03	0.305	1.03 (0.98 ~ 1.08)
IL-6	0.00	0.00	0.49	0.621	1.00 (1.00 ~ 1.00)
PCT	0.03	0.04	0.76	0.445	1.03 (0.95 ~ 1.11)
Album	-0.04	0.03	-1.28	0.201	0.96 (0.89 ~ 1.02)
Total albumin	-0.03	0.02	-1.38	0.167	0.97 (0.93 ~ 1.01)
ALT	0.00	0.00	1.49	0.137	1.00 (1.00 ~ 1.01)
AST	0.00	0.00	0.75	0.456	1.00 (1.00 ~ 1.01)
Total bilirubin	0.03	0.02	1.70	0.090	1.03 (1.00 ~ 1.07)
Direct bilirubin	0.06	0.03	1.77	0.076	1.06 (0.99 ~ 1.12)
Urea	0.10	0.03	2.99	0.003	1.10 (1.03 ~ 1.18)
Creatinine	0.00	0.00	1.54	0.124	1.00 (1.00 ~ 1.01)
K^+	0.26	0.32	0.80	0.423	1.30 (0.69 ~ 2.45)
Na^+	0.03	0.03	0.97	0.331	1.03 (0.97 ~ 1.08)
Cl^+	-0.00	0.03	-0.01	0.988	1.00 (0.95 ~ 1.05)
PT	0.03	0.05	0.60	0.548	1.03 (0.93 ~ 1.14)
APTT	0.02	0.01	1.44	0.151	1.02 (0.99 ~ 1.05)
PTA	-0.01	0.01	-0.58	0.559	0.99 (0.98 ~ 1.01)
Fib	-0.01	0.11	-0.12	0.903	0.99 (0.79 ~ 1.23)
D-D	0.07	0.06	1.07	0.286	1.07 (0.95 ~ 1.20)

with small sample sizes, thereby enhancing the model's predictive capability.

To further assess the robustness and accuracy of the model, the study used the Hosmer-Lemeshow test and calibration curves. The results indicated that the model exhibited good fit and strong predictive ability in both the training and validation sets. The validation set included 31 patients who developed pneumonia-associated bloodstream infections (PABSI), with an event-to-variable ratio of 5.17:1, which meets the basic requirements for regression analysis. The results from the validation set further reinforced the reliability and stability of the model.

In summary, this study ensured the robustness of the model through LASSO regression, Hosmer-Lemeshow test, and calibration curves, thus effectively assessing the risk of pneumonia-associated bloodstream infections.

The results of the study analysis identified several significant predictors associated with pneumonia-associated bloodstream infections (PABSIs), including long-term antibiotic use, use of urinary and central venous catheters, use of invasive mechanical ventilation, use of vasopressors, use of glucocorticoids, and use of urinary catheters.

In recent years, public health authorities and scientific societies around the world have articulated profound concern regarding the escalating issue of antimicrobial resistance (AMR). Antimicrobial resistance (AMR) has been widely acknowledged as a significant global health challenge of the 21st century (Tabah et al., 2023). In clinical practice, the misuse of antibiotics has been the subject of considerable attention, and their overuse has been identified as a significant contributing factor to the development of drug resistance (Read and Woods, 2014). The long-term use of antibiotics can result in selective changes to the structure of the human microbiota, whereby susceptible strains are suppressed or eliminated, while resistant strains survive and proliferate. This increase in selective pressure has resulted in an increase in the frequency of multidrug-resistant strains (Meng et al., 2021). These resistant strains demonstrate reduced susceptibility to the majority of antimicrobial drugs. As drug resistance increases, the treatment of lung infections becomes more challenging, leading to an increase in the prevalence of pneumonia-associated bloodstream infections. The results of the present study demonstrate a robust correlation

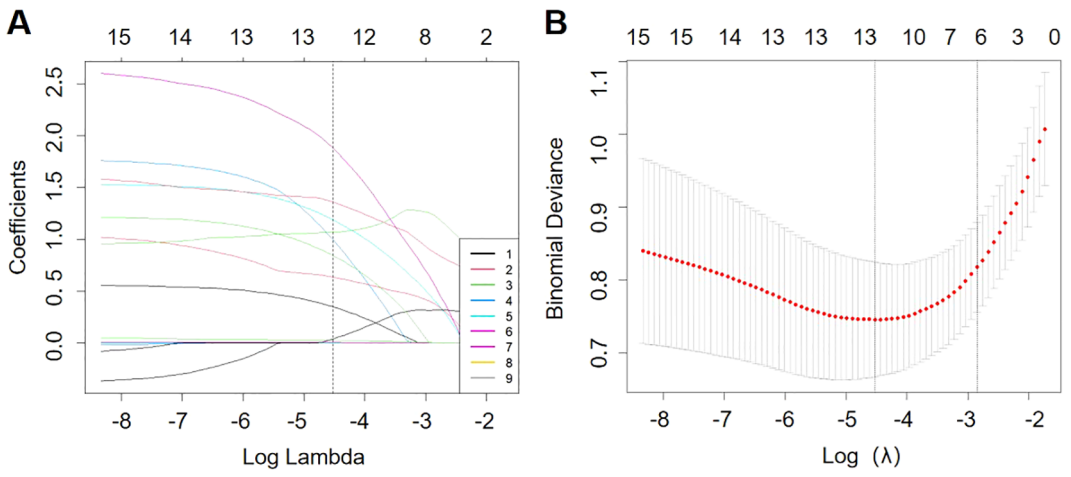

FIGURE 2
Overview of LASSO coefficients for 15 risk factors **(A)**. Six risk factors were selected using LASSO regression analysis **(B)**.

10.3389/fcimb.2025.1531732

TABLE 3 Multivariate logistic regression.

Variables	β	S. E	Z	*P*	OR (95%CI)
Intercept	-2.76	0.36	-7.67	<.001	0.06 (0.03 ~ 0.13)
Urinary tube					
0					1.00 (Reference)
1	0.88	0.54	1.62	0.106	2.40 (0.83 ~ 6.96)
Invasive mechanical ventilation					
0					1.00 (Reference)
1	2.54	1.17	2.18	0.030	12.71 (1.29 ~ 125.54)
Glucocorticoid					
0					1.00 (Reference)
1	1.28	0.43	2.96	0.003	3.61 (1.54 ~ 8.43)
Long-term antibiotic use					
0					1.00 (Reference)
1	1.89	1.05	1.79	0.073	6.62 (0.84 ~ 52.12)
Vasoactive drug					
0					1.00 (Reference)
1	1.53	0.92	1.66	0.096	4.61 (0.76 ~ 27.93)
Central venous catheter					
0					1.00 (Reference)
1	0.21	0.73	0.29	0.775	1.23 (0.30 ~ 5.13)

between long-term antibiotic utilization and pneumonia-associated bloodstream infections, which is consistent with the findings of prior studies in this area. Such an association may be attributed to a dysbiosis, or disruption, of the patient's endogenous flora, thereby elevating the risk of bloodstream infections among patients diagnosed with pneumonia. These findings have significant clinical implications, emphasizing the necessity for more precise and efficacious prevention and treatment strategies. The introduction of a defined daily dose (DDD) for each individual patient represents a crucial step in the effective management of those with pneumonia.

Device-associated infections have been shown to remain a significant challenge in clinical practice, primarily due to their high prevalence and potential for mortality (Blot et al., 2005; Li, 2015). In particular, urinary and central venous catheters provide a pathway for bacteria to enter the bloodstream, serving as a common conduit for hospital-acquired infections. In this study, we focused on the cohort of patients with pneumonia and found a notable association between urinary and central venous catheters and pneumonia-associated bloodstream infections after excluding other potential sources of bloodstream infections. This association may be due to the fact that patients with these catheters tend to have poorer overall health, higher disease severity and poorer prognosis. In addition, these patients often require prolonged periods of bed rest, which can affect their hemodynamic status.

Invasive mechanical ventilation is a fundamental aspect of respiratory and critical care medicine. It allows patients with respiratory distress to maintain adequate oxygenation and carbon dioxide elimination, thereby improving oxygenation and reducing the incidence of hypoxemia. In patients with fatigued or weak respiratory muscles, invasive mechanical ventilation can reduce the burden on the respiratory muscles and provide the necessary respiratory support for other treatments. However, the establishment of an artificial airway also deprives the patient of the airway's natural defense mechanisms, such as the ability to heat, humidify, and clear the inspired air. This increases the risk of airborne pathogens entering the patient's airways and lungs. In addition, prolonged use may result in tracheal damage (Eggimann and Pittet, 2001). Current research suggests that the presence of an endotracheal tube is the most significant risk factor for the development of ventilator-associated pneumonia (VAP) (Walaszek et al., 2016). The present study also identified invasive mechanical ventilation as a risk factor for the progression of pneumonia patients to pneumonia-associated bloodstream infections. Because the establishment of an artificial airway creates a direct pathway between the lungs and the outside world, increasing the possibility of invasion by pathogenic microorganisms from the outside world, it may further exacerbate pneumonia and thus increase the risk of bloodstream infections.

Vasopressors are of great importance in critical care medicine, particularly in the context of resuscitation and treatment of shock. These drugs can significantly improve the patient's hemodynamics, control blood pressure, and optimize blood flow to vital organs (Annane et al., 2018). In patients with pneumonia, pathogens of pulmonary infection, including bacteria, viruses or fungi, can enter the bloodstream through various mechanisms and cause bloodstream infections. During infection, pathogens such as viruses or bacteria can directly infect epithelial cells, causing cell death (Kenney et al., 2017). Tissue damage and inflammatory responses can lead to disruption of the alveolar-capillary barrier, allowing pathogens to cross the damaged lung tissue and enter the bloodstream (Long et al., 2022). In addition, the inflammatory response in the infected area may lead to local vasodilation and increased vascular permeability, facilitating pathogen invasion. Once the pathogen enters the blood stream, it can cause a systemic infection, which is a bloodstream infection. Studies have shown that the use of vasoactive drugs is significantly associated with the incidence of pneumonia-associated bloodstream infections. This may facilitate the occurrence of bloodstream infections by affecting the vasodilator and permeability properties of blood vessels due to damage to the alveolar-capillary barrier.

The pro-inflammatory mediator storm that critically ill patients with pulmonary infections may experience represents a complex pathological process in which an imbalance between pro- and anti-inflammatory mediators can lead to a variety of adverse effects (Li et al., 2020). Glucocorticoids help to attenuate the inflammatory response in critically ill patients by inhibiting the release of pro-inflammatory mediators, thereby regulating excessive immune responses and improving clinical symptoms (Patel et al., 2020). However, this treatment strategy may also suppress the patient's

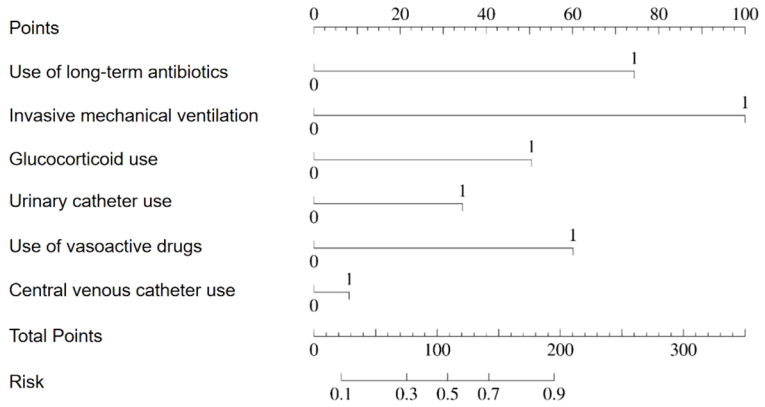

FIGURE 3
Nomogram for predicting the risk probability of pneumonia-associated bloodstream infections.

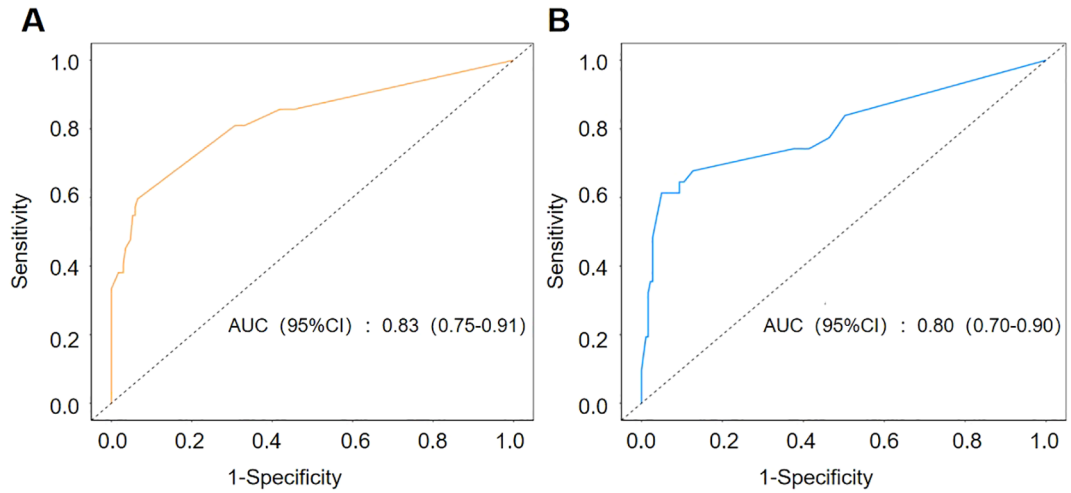

FIGURE 4
ROC curve of nomogram division with binomial verification of the training group **(A)** and test group **(B)**. The AUC of the training group and the test group was 0.83 and 0.80, respectively.

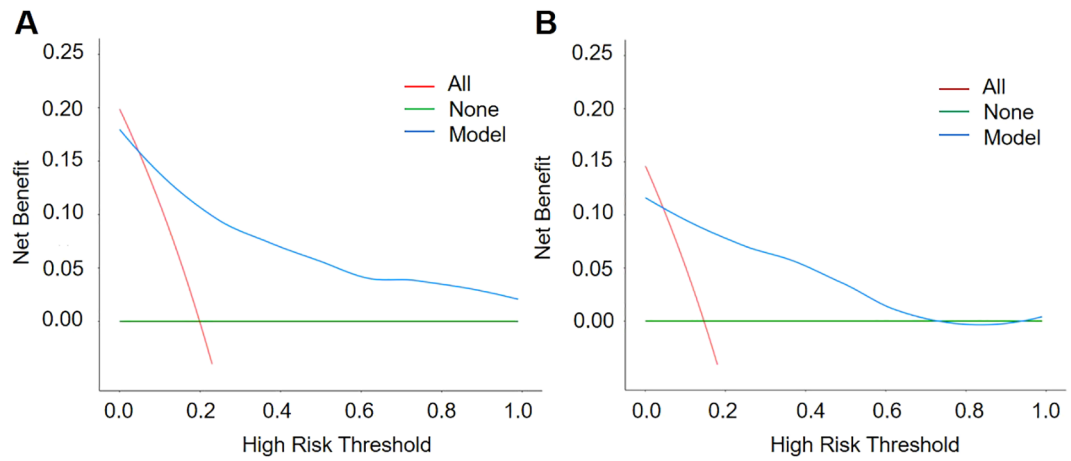

FIGURE 5
Calibration curve verifies the calibration of nomogram.

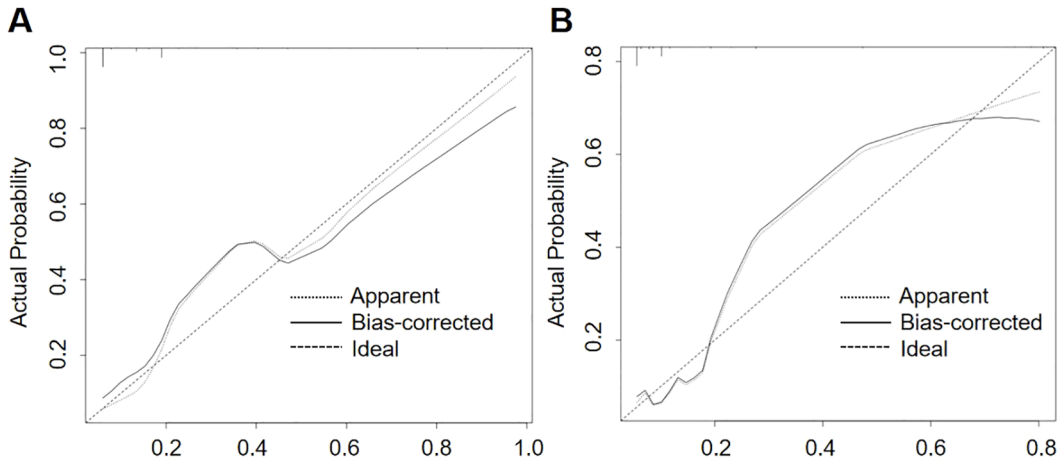

FIGURE 6
Decision Curve Analysis (DCA) curves of the training group **(A)** and the test group **(B)**. The net benefit of the nomogram was verified by the DCA curves of the two cohorts.

immune function, thereby reducing their ability to resist new infections. This may provide opportunities for invasion and spread of pathogenic microorganisms, and may even lead to immunosuppression and uncontrolled inflammatory responses. The results of this study demonstrate an increased likelihood of pneumonia-associated bloodstream infections in patients treated with glucocorticoids. This may be due to the immunosuppressive effects of glucocorticoids, which may increase the likelihood of such infections.

The particular advantage of this model over existing studies is that it combines the advantages of LASSO regression in feature selection with the strengths of logistic regression in predictive ability, thereby enhancing the stability and predictive accuracy of the model. This is evidenced by the high AUC and exemplary calibration curve performance of this model. In addition, this study focuses on the risk of pneumonia patients developing bloodstream infections, which is a critical aspect of pneumonia patient management. Given the current lack of research on individuals with pneumonia-associated bloodstream infections, this study seeks to assess the risk of such infections by developing a predictive model to facilitate the identification of early-stage pneumonia patients who may subsequently develop bloodstream infections. This will facilitate the implementation of prompt treatment measures and contribute to a reduction in mortality rates.

Although this model has demonstrated considerable efficacy in predicting pneumonia-associated bloodstream infections, it is important to acknowledge the limitations inherent in its evaluation. First, because this study used a retrospective cohort study design, there is a possibility of selection and information bias. Second, the study sample was derived from a single center, which may limit the generalizability of the model. Therefore, it is recommended that future studies use a multicenter prospective study design to further validate and optimize this model. Furthermore, future studies could explore the potential of combining this model with other biomarkers or imaging features to improve the accuracy of prediction and the value of clinical application. At the same time, external validation of the model and its applicability in different populations are important directions for future research.

5 Conclusion

In conclusion, the clinical prediction model for pneumonia-related bloodstream infections developed in this study, based on LASSO regression and logistic regression, provides clinicians with a precise risk assessment tool specifically for the management of pneumonia patients. The model not only has high predictive accuracy, but also has good calibration performance, which allows clinicians to identify high-risk patient groups early. The implementation of timely and effective preventive and treatment measures based on this tool is expected to significantly improve the clinical prognosis of patients.

Data availability statement

Ethical approval has been signed, and the data from this research project will be kept only by the researcher, will not be uploaded to public databases, and will not be shared with other researchers. Requests to access the datasets should be directed to ZZ, purple_zzt@163.com.

Ethics statement

The studies involving humans were approved by Ethics Committee of the First Medical Center of the PLA General Hospital (Approval No. S-603-01). The studies were conducted in accordance with the local legislation and institutional requirements. Written

informed consent for participation was not required from the participants or the participants' legal guardians/next of kin in accordance with the national legislation and institutional requirements.

Author contributions

ZZ: Data curation, Investigation, Methodology, Software, Validation, Writing – original draft, Formal analysis, Visualization. SL: Investigation, Methodology, Validation, Writing – review & editing, Formal Analysis. FQ: Formal analysis, Methodology, Validation, Writing – review & editing. YW: Investigation, Visualization, Writing – review & editing. MS: Methodology, Validation, Writing – review & editing. XG: Conceptualization, Project administration, Supervision, Writing – review & editing.

Funding

The author(s) declare that no financial support was received for the research and/or publication of this article.

Acknowledgments

The authors would like to express their gratitude to Dr. Changxin Liu for his assistance with the details of data collection. They would also like to acknowledge the valuable suggestions provided by Dr. Junyu Ding and Dr. Huijun Zhao regarding data analysis. Thanks to the Generative Artificial Intelligence Tool (Chat GPT) for assistance in embellishing the English expression. The tool uses GPT-4o sourced from OpenAI. All content edited through this tool has been checked for accuracy and plagiarism to ensure research rigor. Detailed records cannot be provided as the specific prompts for each interaction with GPT-4o were not recorded, but all content using the generated AI strictly followed academic norms, and the prompts were mainly related to text optimization, grammar checking, and language fluency enhancement to ensure compliance with academic standards.

Conflict of interest

The authors declare that the research was conducted in the absence of any commercial or financial relationships that could be construed as a potential conflict of interest.

Generative AI statement

The author(s) declare that Generative AI was used in the creation of this manuscript. Thank you for your review and attention to my submission. During the preparation of this manuscript, I utilized the generative AI tool (GPT-4o) to refine and optimize the English expression. It is important to note that I did not rely on this tool for content creation or to generate original ideas. All research data, analysis results, and discussions were independently conducted by me, and I have strictly adhered to academic standards.

Publisher's note

References

Abbafati, C., Abbas, K. M., Abbasi, M., Abbasifard, M., Abbasi-Kangevari, M., Abbastabar, H., et al. (2020). Global burden of 369 diseases and injuries in 204 countries and territories 1990-2019: a systematic analysis for the Global Burden of Disease Study 2019. *Lancet* 396, 1204–1222.

Angus, D. C., and van der Poll, T. (2013). Severe sepsis and septic shock. *New Engl. J. Med.* 369, 840–851. doi: 10.1056/NEJMra1208623

Annane, D., Ouanes-Besbes, L., de Backer, D., Du, B., Gordon, A. C., Hernández, G., et al. (2018). A global perspective on vasoactive agents in shock. *Intensive Care Med.* 44, 833–846. doi: 10.1007/s00134-018-5242-5

Blot, S. I., Depuydt, P., Annemans, L., Benoit, D., Hoste, E., de Waele, J. J., et al. (2005). Clinical and economic outcomes in critically ill patients with nosocomial catheter-related bloodstream infections. *Clin. Infect. Dis.* 41, 1591–1598. doi: 10.1086/497833

Eggimann, P., and Pittet, D. (2001). Infection control in the ICU. *Chest* 120, 2059–2093. doi: 10.1378/chest.120.6.2059

Kenney, A. D., Dowdle, J. A., Bozzacco, L., McMichael, T. M., St Gelais, C., Panfil, A. R., et al. (2017). Human genetic determinants of viral diseases. *Ann. Rev. Genet.* 51, 241–263. doi: 10.1146/annurev-genet-120116-023425

Kern, W. V., and Rieg, S. (2020). Burden of bacterial bloodstream infection-a brief update on epidemiology and significance of multidrug-resistant pathogens. *Clin. Microbiol. Infection* 26, 151–157. doi: 10.1016/j.cmi.2019.10.031

Lamping, D. L., Schroter, S., Marquis, P., Marrel, A., Duprat-Lomon, I., and Sagnier, P. P. (2002). The community-acquired pneumonia symptom questionnaire - A new, patient-based outcome measure to evaluate symptoms in patients with community-acquired pneumonia. *Chest* 122, 920–929. doi: 10.1378/chest.122.3.920

Li, H. M. (2015). Distribution and clinical characteristics of pathogenic bacteria causing catheter-related bloodstream infections. *Pakistan J. Pharm. Sci.* 28, 1163–1166.

Li, X., Chen, Z., Ji, N., and Zhang, M. (2020). Recent research progress of acute respiratory distress syndrome in COVID-19 patients. *Int. Respir. J.* 40, 1690–1696. doi: 10.3760/cma.j.cn131368-20200320-00195

Long, M. E., Mallampalli, R. K., and Horowitz, J. C. (2022). Pathogenesis of pneumonia and acute lung injury. *Clin. Sci.* 136, 747–769. doi: 10.1042/cs20210879

Meng, X., Fu, J., Zheng, Y., Qin, W., Yang, H., Cao, D., et al. (2021). Ten-year changes in bloodstream infection with acinetobacter baumannii complex in intensive care units in eastern China: A retrospective cohort study. *Front. Med. (Lausanne)* 8. doi: 10.3389/fmed.2021.715213

Metlay, J. P., Fine, M. J., Schulz, R., Marrie, T. J., Coley, C. M., Kapoor, W. N., et al. (1997). Measuring symptomatic and functional recovery in patients with community-acquired pneumonia. *J. Gen. Internal Med.* 12, 423–430. doi: 10.1046/j.1525-1497.1997.00074.x

Patel, S. K., Saikumar, G., Rana, J., Dhama, J., Yatoo, M. I., Tiwari, R., et al. (2020). Dexamethasone: A boon for critically ill COVID-19 patients? *Travel Med. Infect. Dis.* 37. doi: 10.1016/j.tmaid.2020.101844

Read, A. F., and Woods, R. J. (2014). Antibiotic resistance management. *Evol. Med. Public Health* 2014, 147. doi: 10.1093/emph/eou024

Tabah, A., Buetti, N., Staiquly, Q., Ruckly, S., Akova, M., Aslan, A. T., et al. (2023). Epidemiology and outcomes of hospital-acquired bloodstream infections in intensive care unit patients: the EUROBACT-2 international cohort study. *Intensive Care Med.* 49, 178–190. doi: 10.1007/s00134-022-06944-2

Torres, A., Cilloniz, C., Niederman, M. S., Menéndez, R., Chalmers, J. D., Wunderink, R. G., et al. (2021). Pneumonia. *Nat. Rev. Dis. Primers* 7. doi: 10.1038/s41572-021-00259-0

Walaszek, M., Kosiarska, A., Gniadek, A., Kolpa, M., Wolak, Z., Dobros, W., et al. (2016). The risk factors for hospital-acquired pneumonia in the Intensive Care Unit. *Przeglad epidemiologiczny* 70, 107–110.

frontiers | Frontiers in Cellular and Infection Microbiology

TYPE Mini Review
PUBLISHED 26 March 2025
DOI 10.3389/fcimb.2025.1554090

OPEN ACCESS

EDITED BY
Sam Ebenezer,
Institute of Science and Technology, India

REVIEWED BY
A Alwin Prem Anand,
University of Tübingen, Germany

*CORRESPONDENCE
Ana Margarida Vigário
anavig@staff.uma.pt

†These authors have contributed equally to this work

RECEIVED 08 January 2025
ACCEPTED 21 February 2025
PUBLISHED 26 March 2025

CITATION
Henriques P, Rosa A, Caldeira-Araújo H and Vigário AM (2025) Mouse models as a tool to study asymptomatic DENV infections. *Front. Cell. Infect. Microbiol.* 15:1554090. doi: 10.3389/fcimb.2025.1554090

Mouse models as a tool to study asymptomatic DENV infections

Paulo Henriques[1†], Alexandra Rosa[1†], Helena Caldeira-Araújo[1,2†] and Ana Margarida Vigário[1,3*†]

[1]Projecto Medicina, Faculdade de Ciências da Vida, Universidade da Madeira, Funchal, Portugal, [2]Centro de Química da Madeira (CQM), Universidade da Madeira, Funchal, Portugal, [3]Gulbenkian Institute for Molecular Medicine, Lisbon, Portugal

Asymptomatic outcome accounts for most dengue virus infections and is likely to play an important role in maintaining virus circulation, contributing to its dissemination and shortening inter-epidemic periods. While dengue immunopathogenesis, investigation of potential therapeutics, and vaccine efficacy have been widely studied, only recently have inapparent infections begun to be comprehensively addressed as an integral and important part of the puzzle that is dengue infection. Animal models are one of the tools utilized to study dengue and, among these, mouse models have played an important role in understanding both dengue pathogenesis and the hosts' initial immune response. However, these models have mostly focused on untangling the drivers of disease severity ignoring asymptomatic dengue virus infections. In this mini-review, the authors propose to provide a concise overview of the current state-of-the-art of existing mouse models with potential use for studying asymptomatic dengue virus infections, elaborating on the pros and cons of the several models. Variations in experimental conditions, such as altering the viral load of the inoculum or employing different virus entry routes, especially in mice with partial or transient blockade of the type I interferon response, might be sufficient to obtain both symptomatic and asymptomatic viremic mice. This would enable the study of factors involved in asymptomatic dengue virus infections.

KEYWORDS

dengue, mouse models, asymptomatic infections, inapparent infections, dengue virus, dengue fever, immune response

Introduction

Dengue virus (DENV) is a mosquito-borne flavivirus responsible for dengue, an emerging infectious disease that has become a major health concern in tropical and subtropical regions (reviewed in Halstead (2007); Guzman et al. (2010). Caused by any of its four circulating serotypes (DENV1 to DENV4), dengue usually manifests as either an undifferentiated febrile episode or classical Dengue Fever (DF) that can progress to more severe and potentially lethal Dengue Hemorrhagic Fever or Shock-Syndrome. Several signs and symptoms such as fever, headache, nausea, vomiting, myalgia, arthralgia, rash, and

leukopenia characterize DF, whilst, in the more severe cases, hemorrhage, plasma leakage, breathing difficulty, and organ dysfunction also occur. While much attention has been focused on symptomatic infections, most DENV infections are asymptomatic (Balmaseda et al., 2010; Johansson et al., 2014), as with many other flaviviruses. Asymptomatic DENV infections refer to infections with detectable viremia, but without any of the clinical symptoms described above, that are usually associated with DF. These may also include infections with very mild or non-specific symptoms that cannot be clearly attributed to DENV infection, sometimes globally referred to as inapparent dengue infections.

Understanding DENV infection and its outcomes remains challenging due to the complex nature of the virus, its intricate interactions with the host immune system (reviewed in (Guzman et al., 2010; Henriques et al., 2023), and the limitations of many of the existing mouse models.

DF is primarily associated with humans, where DENV is thought to evade the immune response by targeting key components of the type I Interferon (IFN) response. For instance, several DENV non-structural proteins have been described to disrupt type I IFN signaling in humans by degrading STAT2 (Jones et al., 2005; Mazzon et al., 2009; Ashour et al., 2010), inhibiting STAT1 phosphorylation (Muñoz-Jordán et al., 2003, 2005) or cleaving STING (Aguirre et al., 2012). Type I IFN signaling is critical for controlling viral replication during the early stages of infection, and its inhibition allows efficient viral replication in human cells. In contrast, DENV seems unable to evade the rodent immune response through the inhibition of type I IFN signaling (Yauch and Shresta, 2008), leading to their inherent resistance to DENV infection. As a result, dengue research has been hindered by the difficulty of establishing mouse models that reproducibly allow DENV infection and competently mimic the disease as it manifests in humans. Nevertheless, several immunocompetent, immunocompromised, and even humanized mouse models have been employed using different strategies and experimental designs to characterize specific features of DF pathogenesis, as well as, evaluate potential therapeutics and vaccine candidates, with varying degrees of success (reviewed in Chen and Diamond (2020) and Coronel-Ruiz et al. (2020)). Yet, asymptomatic DENV infections are the most common outcome in humans and are likely central to understanding the host factors influencing the clinical outcome. However, to our knowledge, asymptomatic DENV infections have been seldomly comprehensively addressed using mouse models, likely due to their limitations in achieving DENV infection and effective viremia without disease signs or animal mortality.

The authors hereby propose to briefly revisit the existing mouse models for studying DF pathogenesis, and to further objectively discuss the feasibility of using these models to study asymptomatic DENV infections.

Key assumptions and challenges in studying asymptomatic DENV infection using mouse models

Animal models rarely fully replicate the primary manifestations observed in human clinical infections. Nevertheless, in our understanding, if certain key assumptions can be met, we may be able to use mouse models to successfully investigate viral and host factors contributing to an asymptomatic outcome of DENV infection. Firstly, the appropriate mouse models must allow DENV infection to occur, ideally in all inoculated animals, with the least possible manipulation of their immune system. Secondly, the infection should be self-resolved within a few days without any manifestations/signs in its course. These models should then be compared with models in which, under similar experimental conditions, all animals develop viremia and DF signs. Alternatively, models could be set up where all the animals develop viremia, but only a proportion exhibit DF-associated signs. This would allow for comparative studies between animals with and without disease signs within the same model and experimental settings.

These theoretical assumptions lead us, however, to two important challenges to overcome. On the one hand, mouse models where all inoculated animals become infected need to be established while, at the same time, criteria and protocols must be defined to accurately confirm the establishment of infection. For instance, in some studies, animals did not have detectable infectious particles in their serum, as assessed by either RT-PCR or plaque assays, probably because the levels were below the test sensitivity, but viral RNA or infectious particles were present in various tissues (Shresta et al., 2004; Paes et al., 2005; Sridharan et al., 2013; Wilken et al., 2023) and/or seroconversion was identified (Shresta et al., 2004; Tan et al., 2010). On the other hand, it is crucial to define which behavioral signs and laboratory findings should be considered as indicative of DF, and which may be associated with asymptomatic infection. Mice with DF have hematological and biochemical alterations, such as leukopenia with lymphopenia, thrombocytopenia, and elevated aminotransferases and gamma-glutamyl transpeptidase. Asymptomatic or inapparent DENV infections are also expected to induce, at a certain extent, changes in at least some of these parameters, because of the immune response to the virus, and in some cases mild unspecific illness manifestations. In addition, the development and validation of a tool that allows the assessment of observable parameters would help to define the physiological state of the mice. For instance, the adaptation of SHIRPA test (**S**mithKline Beecham, **H**arwell, **I**mperial College, **R**oyal London Hospital, **p**henotype **a**ssessment), a battery of standardized tests used for qualitative behavioral and functional assessment in mouse studies to determine phenotypes based on scores, may be a useful tool to assess symptomatic DF in mice, and to a lesser extent, asymptomatic infections. Among the parameters to evaluate DF, we can suggest exploratory behavior (motor performance), muscular tone (limb strength), reflexes and self-preservation (touch escape and aggression), hygiene-related behavior (grooming) (Carroll et al., 2010) all as indicators of animal's general health and well-being, as they may relate to myalgia, arthralgia, headache, extreme fatigue, and/or malaise known to occur in human symptomatic infections. In addition, loss of weight may relate to loss of appetite, and/or gastrointestinal signs such as nausea, vomiting or diarrhea (Wilken et al., 2023). Some of these signs may be expected to change slightly in asymptomatic infections. Given the inter-individual variability observed in all animal models, adopting a scoring system based on the sum of major/minor criteria could be a reliable approach for both

behavioral signs and laboratory findings, that might include a cut-off score for asymptomatic infections.

Lessons from existing models for studying asymptomatic DENV infections

Immunocompetent mice

As mentioned above, immunocompetent mice such as A/J, C57BL/6 and BALB/c tend to be naturally resistant to DENV. However, their infection can be successfully achieved by manipulating experimental conditions, highly reliant on the used DENV strain (including mouse-adapted and non-mouse-adapted strains), the route of inoculation, and/or the size of the inoculum (Huang et al., 2000; Shresta et al., 2004; Paes et al., 2005; Chen et al., 2007; Gonçalves et al., 2012).

Although A/J mice seem to be more susceptible to DENV infection than other models (Huang et al., 2000), they may not be helpful for studying asymptomatic infections. Following DENV-2 intravenous inoculation, most animals develop paralysis, with detectable infectious particles in the central nervous system, increased hematocrit, leukopenia (Shresta et al., 2004), and transient thrombocytopenia (Huang et al., 2000), usually leading to death, even in the absence of signs. Neurological manifestations are uncommon in humans, and much less likely is that apparently asymptomatic infections could lead to death. Moreover, Shresta et al. (2004) reported that nearly half of A/J mice lacked disease signs, but these cannot be assumed to represent true asymptomatic as viremia was not tested in these animals.

In our opinion, the findings in C57BL/6 and BALB/c mice make them the more promising immunocompetent mice for establishing asymptomatic DENV infections. Intraperitoneal inoculation of a mouse-adapted DENV-1 caused viremia and detectable viral particles in the brain, kidney, and liver of C57BL/6 mice, along with thrombocytopenia, spleen hemorrhage, and liver damage, but no evident clinical signs (Gonçalves et al., 2012). Paes et al. (2005) reported that BALB/c mice, infected intraperitoneally with a non-mouse-adapted DENV-2 strain, developed liver pathology, as indicated by elevated ALT/AST levels and hepatic lesions, despite low viremia and the absence of other clinical symptoms.

Immunocompetent mice benefit from an intact immune system, and despite their limitations, we believe that an optimized combination of experimental conditions - such as the choice of DENV strain, inoculum size, and inoculation route - could aid in developing models to investigate certain mechanisms of asymptomatic DENV infections, as complementary evidence to findings in other models.

Mice with deficiencies in innate immune response

To overcome the inherent resistance of immunocompetent mice and to study different aspects of the DENV infection, animals with deficiencies in innate host defense responses have been used. AG129 mice, which lack receptors for both IFN type I (IFN-α/β) and type II (IFN-γ) on a 129/Sv or 129/SvEv background, have shown to be more susceptible to DENV infection than wildtype (WT) mice, presenting vascular leakage, changes in blood cell counts (platelets, lymphocytes, and erythrocytes), and rapidly developing severe disseminated disease or progressing to death (Johnson and Roehrig, 1999; Milligan et al., 2017; Sarathy et al., 2018; Chen and Diamond, 2020). Consequently, these models are likely to have limited use in the study of asymptomatic DENV infections. Nevertheless, they demonstrated that inoculation route, dose and viral strain influence the severity and type of clinical signs, with DENV-1 (Baldon et al., 2022) or low-passage DENV3 isolate reported as non-lethal in AG129 mice (Sarathy et al., 2018). However, it remains unclear whether lowering the inoculum dosage and/or using those isolates could produce asymptomatic infections in these animals. Conversely, *Ifnar*$^{-/-}$ (A129) mice typically exhibit greater resistance to DENV than AG129 and result in lower mortality (Shresta et al., 2004; Prestwood et al., 2012). Given their ability to support DENV infection while retaining IFN-γ signaling, *Ifnar*$^{-/-}$ mice have been useful in probing mechanisms of DENV pathogenesis in a less immunocompromised model (Shresta et al., 2004; Chen and Diamond, 2020). Notwithstanding, DENV could be detected in peripheral organs, including the liver and spleen, as well as in blood (Tan et al., 2010; Sarathy et al., 2015). Early DENV viral load seems to be limited by both IFN-α/β and IFN-γ receptors pathways (Shresta et al., 2004), while IFN-γ receptor also plays a critical role in late central nervous system infection clearance (Prestwood et al., 2012). Indeed, A129 mice had lower viral RNA in spinal cords and brains than AG129 mice confirming that IFN signaling has a role in protecting the central nervous system from DENV infection (Prestwood et al., 2012). Considering that A129 mice did not present clinical symptoms when infected with DENV-2, even though infectious particles were found in multiple tissues, this may be an interesting model to complement the study of asymptomatic DENV infection.

Likewise, *STAT1* and *STAT2*-deficient mice have also contributed to unraveling the initial IFN-mediated response to DENV infection. Shresta et al. (2005) observed that the initial viral clearance is STAT1-pathway-dependent, while later viral clearance and protection against DF is partially due to a STAT1-independent IFN response, where STAT2 seems to be involved (Perry et al., 2011) and to promote NK and B cells activation and MHC class I upregulation on macrophage and dendritic cells' surface. Also, inhibition of IFN-α and IFN-β production seems to be incomplete in these models, since detectable levels have been observed within a few hours post-infection (Perry et al., 2011).

In these models with an initial blockade of the type I IFN response, DENV inoculation resulted in detectable viremia, and allowed both symptomatic and asymptomatic outcomes in *Stat1*$^{-/-}$ mice (Shresta et al., 2005), while *Stat2*$^{-/-}$ mice were all asymptomatic (Perry et al., 2011). However, since most studies focus on specific disease phenotypes, such as death by paralysis, not all clinical signs representative of the full spectrum of the disease were screened for, and thus some may have been present but were not detected in *Stat2*$^{-/-}$ mice (Shresta et al., 2005; Perry et al., 2011). In the light of

these results, these models are also likely suitable for the study of asymptomatic DENV infections, targeted to immune responses that might be hampered in other models that completely inhibit the initial IFN response.

Perry et al. (2009) found that both *Cardif*$^{-/-}$ and WT C57BL/6 mice were susceptible to infection when intravenously injected with different inoculum doses of DENV-2 serotype, with no apparent signs of disease or mortality, while *Ifnar*$^{-/-}$ mice showed 100% mortality at the higher inoculum. However, *Cardif*$^{-/-}$ displayed 10-fold higher levels of DENV RNA in serum, bone marrow, and lymphoid tissues within the first 18 hours of infection, when compared to WT mice, supporting the essential role of Cardif in triggering IFN response, and the observed delay in IFN production in its absence. As far as we known, the *Cardif*$^{-/-}$model was not further explored in the context of dengue, likely because it did not display apparent disease signs, and most studies focus on pathogenesis of symptomatic dengue and vaccination strategies. However, this model fulfills the main assumptions we consider necessary for studying asymptomatic DENV infection, allowing a complementary approach, with immune response blockade at Cardif level. Possible improvements could be achieved by changing the serotype/strain, route, or dose of the inoculum, to verify the feasibility that a proportion of animals develop dengue signs.

Mice with transient suppression or conditional deletion of type I signaling

A transient suppression of the IFN-I signaling using MAR1-5A3, an anti-IFNAR1 monoclonal antibody, was shown to render WT mice more permissive to flavivirus replication and dissemination (Pinto et al., 2011; Lazear et al., 2016; Wilken et al., 2023), with limited influence on their adaptative immune response (Sheehan et al., 2006). Using this approach, Chuong et al. (2020) showed that C57BL/6J mice, pretreated with MAR1-5A3, and inoculated via a combined intradermal/subcutaneous route on the following day with low-passage isolates of DENV-1 or DENV-2, generated viremia and mild hematological changes, depending on the isolate, with no evident clinical signs being reported. Wilken et al. (2023) also demonstrated that C57BL/6J mice with MAR1-5A3 treatment prior to inoculation with a non-mouse-adapted DENV-2 strain exhibited no disease signs over 15 days, as measured by scores of weight loss, appearance, activity, and gastrointestinal symptoms. Animals sacrificed on day 5 showed splenomegaly, but no other gross pathological changes, and had detectable viral RNA in sera and visceral organs. In contrast, *Ifnar*$^{-/-}$ mice in this same study developed clinical signs of disease, such as rapid weight loss, and showed 1000-fold higher viral levels than WT MAR1-5A3-treated mice, 2-3 days post-infection (Wilken et al., 2023).

The strategy used in the above-mentioned studies seems to be a good basis for studying inapparent DENV infections, without genetic manipulation of the animals. An increasing dose of MAR1-5A3 or viral inoculum could potentially promote symptomatic infections in C57BL/6J mice, allowing the comparison of different study groups within the same model. Also, it would be interesting to compare with *Ifnar*$^{-/-}$ mice, under the same experimental conditions except for MAR1-5A3-treatment, since this immunocompromised model has a complete and permanent blockage at the same level of type I IFN signaling and could allow an insight over the entire spectrum of the infection, from asymptomatic to severe dengue.

Another possible approach is the conditional knockout of *Ifnar* in specific subsets of immune cells. This would render animals more permissive to infection but, at the same time, allowing type I IFN response in other cells to help in the resolution of the infection. Züst et al. (2014) showed that CD11c-Cre *Ifna*$^{rfl/fl}$ mice, which lack IFNAR expression primarily in dendritic cells, develop viremia with a slight loss of weight, but most mice recover completely when infected intraperitoneally with a non-mouse-adapted virus DENV-2. Although other signs of disease, such as hematological changes, were not assessed in this study, these could be suitable for studying asymptomatic infections.

Humanized mouse models

Humanized mouse models have also significantly advanced our understanding about diverse aspects of dengue infection (reviewed in Yuya et al. (2024)). Importantly, they have been shown to sustain DENV infection, with detectable viraemia and clinical signs such as erythema, thrombocytopenia and fever (reviewed in Yuya et al. (2024)). Once again, these findings vary according to the infecting genotype (Mota and Rico-Hesse, 2009; Frias-Staheli et al., 2014) and route of infection: subcutaneous inoculation leads to higher infection rate and prolonged viremia compared to intraperitoneal inoculation (Jaiswal et al., 2009), while mosquito-bite inoculation results in higher and sustained viremia, and more severe disease (Cox et al., 2012). Additionally, most studies showed that viremia in humanized mice is achieved with lower-dose DENV inoculum than in other models. Given their engraftment with human immune cells, humanized mouse models are among the closest resembling human DENV infection. By combining a low viral load with an inoculation route resulting in reduced viremia and clinical signs, they may offer valuable insights into asymptomatic DENV infection. Moreover, they may be used to infer differences in susceptibility to infection and immune response, due to intrinsic characteristics of different human engraftment donors. However, these models are not without limitations and pose several challenges that need to be overcome, including significant variability in engraftment success, which can hinder the replication of results, as well as their higher cost, time and labor, compared to other models.

Concluding remarks

Currently, no mouse model fully recapitulates the clinical spectra of human DENV infection. This is particularly relevant for the asymptomatic outcome, as studies have mainly focused on the most severe consequences and the protection associated with vaccines. For this reason, and since mice are inherently more resistant to infection by these viruses than humans, research has relied heavily on immunodeficient mice, which most often develop severe symptoms and/or die. However, immunocompetent mice

TABLE 1 Sumary of the most relevant models to study dengue and advantages and limitations of their use to study asymptomatic DENV infection.

	Mouse model	Background	DENV serotype	Inoculum	Entry route	Viremia (% mice)	Signs	References	Advantages and limitations of the potential use as asymptomatic model	
									Advantages	Limitations
Wild – type	A/J	A/J	DENV2	10^8 PFU	IV	+ / ns	transient thrombocymiddleenia; paralysis	Huang et al., 2000	immunocompetent mice; different inoculum dosage, DENV serotype and entry route may allow asymptomatic infections	neurological commitment is not a common manifestation in human infections
			DENV2	10^8 PFU	IV	0%	increased hematocrit; leukopenia; paralysis; death	Shresta et al., 2004		
	BALB/c	BALB/c	DENV2	10^4 $TCID_{50}$/ 0.2 ml	IP	75%	liver damage	Paes et al., 2005		
	C57BL/6	C57BL/6	DENV1	7.2×10^7 PFU	IP	100%	liver damage; thrombocymiddleenia; spleen hemorrhage	Gonçalves et al., 2012		
	MAR1-5A3	C57BL/6	DENV1	*ns*	ID/SC	100%	mild hematological changes; no signs of disease	Chuong et al., 2020	immunocompetent mice; transient blockade of type 1 IFN response; may allow asymptomatic infections	
		C57BL/6	DENV2	*ns*	ID/SC	100%	mild hematological changes; no signs of disease			
		C57BL/6	DENV2	10^6 PFU	SC	0%	no signs of disease; splenomegaly	Wilken et al., 2023		
Immunocompromised	AG129	129/SvEv	DENV2	10^6 PFU	IP	+ / ns	paralysis; blindness; death	Johnson and Roehrig, 1999		no asymptomatic infections are observed; paralysis and/or death are not common manifestations in human infections
		129/Sv	DENV2	10^7 - 10^2 PFU	IP	+ / ns	ruffled fur; lethargy; diarrhoea-lyke symptoms; death	Tan et al., 2010		
		129/Sv	DENV4	10^7 PFU	IP	100%	weight loss; limited motility; hunched posture; death	Sarathy et al., 2015		
		ns	DENV1	*ns*	IP	≥50%	vascular leakage; thrombocymiddleenia; leukopenia; increased hematocrit; death	Milligan et al., 2017		
		ns	DENV3	$10^{7.5}$ FFU	IP	+ / ns	weight loss; leukopenia; thrombocymiddleenia	Sarathy et al., 2018		
		ns	DENV1	10^6 PFU	IP	+ / ns	*ns*	Baldon et al., 2022		

(Continued)

10.3389/fcimb.2025.1554090

TABLE 1 Continued

	Mouse model	Background	DENV serotype	Inoculum	Entry route	Viremia (% mice)	Signs	References	Advantages and limitations of the potential use as asymptomatic model	
									Advantages	Limitations
	STAT1$^{-/-}$	129/SvEv	DENV2	10^8 PFU	IV	+ / ns	paralysis	Shresta et al., 2005	incomplete blockade of type 1 IFN response; allows asymptomatic infection	neurological commitment is not a common manifestation in human infections
			DENV1	4.4×10^4 PFU		*nd*	paralysis			
	Cardif $^{-/-}$	C57BL/6	DENV2	3×10^6 PFU	IV	+ / ns	no signs of disease	Perry et al., 2009		
	STAT2$^{-/-}$	129/SvEv	DENV2	2×10^5 PFU	IV	+ / ns	no signs of disease	Perry et al., 2011		
	A129	129/Sv	DENV2	3×10^6 PFU	IV	+ / ns	no signs of disease	Prestwood et al., 2012		
Humanized	RAG2$^{-/-}\gamma_c^{-/-}$	BALB/c	DENV2	10^6 PFU	IP/SC	≥50%	fever	Kuruvilla et al., 2007	allows the study of human cells' response to DENV; may allow asymptomatic infection	low replicability due to grafting variability; high cost
	NOD-*scid* *IL2rγ*^{null}(NSG)	NOD	DENV2	10^6 PFU	IP/SC	0 - 100%	weight loss; ruffled fur; hunched back posture; rash	Jaiswal et al., 2009		
		NOD	DENV2	10^6 PFU	SC	+ / ns	erythema; fever; thrombocymiddleenia	Mota and Rico-Hesse, 2009		
	NSG-BLT HLA-A2	NOD	DENV2	10^6 PFU	SC	100%	weight loss; ruffled fur; hunched back posture	Jaiswal et al., 2012		
	NSG-BLT	NOD	DENV2	1×10^6 $TCID_{50}$	IV	20 - 40%	weight loss; ruffler fur; hunching; thrombocymiddleenia	Frias-Staheli et al., 2014		

ns, not specified; nd, not determined; IV, intravenous; ID, intradermal; IP, intraperitoneal; SC, subcutaneous; PFU, plaque forming unit; FFU, focus forming unit.

10.3389/fcimb.2025.1554090

together with transiently immunocompromised mice on type I IFN signaling, have the potential to become good models for studying asymptomatic infections, as long as inoculation routes, virus strains, and doses are adapted (Table 1). Indeed, some authors have already highlighted the potential of some of these models (Baldon et al., 2022; Wilken et al., 2023). As of this point, the main obstacle to establishing a universal model to study asymptomatic infections appears to be the greatly variable results, which mainly depend on the strain used and/or the number of *in vitro* passages. In addition, in order to be able to study asymptomatic infections using mouse models, establishing precise and standardized methods to detect infection and protocols to assess the signs of disease/infection that accurately distinguish dengue fever from asymptomatic infection in mice are also important challenges to overcome.

Author contributions

PH: Writing – original draft, Writing – review & editing. AR: Writing – original draft, Writing – review & editing. HC: Writing – original draft, Writing – review & editing. AV: Conceptualization, Writing – original draft, Writing – review & editing.

Funding

The author(s) declare that no financial support was received for the research and/or publication of this article.

Acknowledgments

We thank Catarina Luis for participating in a discussion concerning Cardif$^{-/-}$ mouse models. We apologize to all authors whose work was not cited due to constraints on the number of references.

Conflict of interest

The authors declare that the research was conducted in the absence of any commercial or financial relationships that could be construed as a potential conflict of interest.

Generative AI statement

The author(s) declare that no Generative AI was used in the creation of this manuscript.

Publisher's note

References

Aguirre, S., Maestre, A. M., Pagni, S., Patel, J. R., Savage, T., Gutman, D., et al. (2012). DENV inhibits type I IFN production in infected cells by cleaving human STING. *PLoS Pathog.* 8, e1002934. doi: 10.1371/journal.ppat.1002934

Ashour, J., Morrison, J., Laurent-Rolle, M., Belicha-Villanueva, A., Plumlee, C. R., Bernal-Rubio, D., et al. (2010). Mouse STAT2 restricts early dengue virus replication. *Cell Host Microbe* 8, 410–421. doi: 10.1016/j.chom.2010.10.007

Baldon, L. V. R., Mendonça, S. F. D., Ferreira, F. V., Rezende, F. O., Amadou, S. C. G., Leite, T. H. J. F., et al. (2022). AG129 mice as a comprehensive model for the experimental assessment of mosquito vector competence for arboviruses. *Pathogens* 11, 879. doi: 10.3390/pathogens11080879

Balmaseda, A., Standish, K., Mercado, J. C., Matute, J. C., Tellez, Y., Saborío, S., et al. (2010). Trends in patterns of dengue transmission over 4 years in a pediatric cohort study in Nicaragua. *J. Infect. Dis.* 201, 5–14. doi: 10.1086/648592

Carroll, R. W., Wainwright, M. S., Kim, K.-Y., Kidambi, T., Gómez, N. D., Taylor, T., et al. (2010). A rapid murine coma and behavior scale for quantitative assessment of murine cerebral malaria. *PLoS One* 5, e13124. doi: 10.1371/journal.pone.0013124

Chen, H.-C., Hofman, F. M., Kung, J. T., Lin, Y.-D., and Wu-Hsieh, B. A. (2007). Both virus and tumor necrosis factor alpha are critical for endothelium damage in a mouse model of dengue virus-induced hemorrhage. *J. Virol.* 81, 5518. doi: 10.1128/JVI.02575-06

Chen, R. E., and Diamond, M. S. (2020). Dengue mouse models for evaluating pathogenesis and countermeasures. *Curr. Opin. Virol.* 43, 50–58. doi: 10.1016/j.coviro.2020.09.001

Chuong, C., Bates, T. A., Akter, S., Werre, S. R., LeRoith, T., and Weger-Lucarelli, J. (2020). Nutritional status impacts dengue virus infection in mice. *BMC Biol.* 18, 106. doi: 10.1186/s12915-020-00828-x

Coronel-Ruiz, C., Gutiérrez-Barbosa, H., Medina-Moreno, S., Velandia-Romero, M. L., Chua, J. V., Castellanos, J. E., et al. (2020). Humanized mice in dengue research: A comparison with other mouse models. *Vaccines (Basel)* 8, 39. doi: 10.3390/vaccines8010039

Cox, J., Mota, J., Sukupolvi-Petty, S., Diamond, M. S., and Rico-Hesse, R. (2012). Mosquito bite delivery of dengue virus enhances immunogenicity and pathogenesis in humanized mice. *J. Virol.* 86, 7637–7649. doi: 10.1128/JVI.00534-12

Frias-Staheli, N., Dorner, M., Marukian, S., Billerbeck, E., Labitt, R. N., Rice, C. M., et al. (2014). Utility of humanized BLT mice for analysis of dengue virus infection and antiviral drug testing. *J. Virol.* 88, 2205–2218. doi: 10.1128/JVI.03085-13

Gonçalves, D., de Queiroz Prado, R., Almeida Xavier, E., Cristina de Oliveira, N., da Matta Guedes, P. M., da Silva, J. S., et al. (2012). Imunocompetent mice model for dengue virus infection. *Sci. World J.* 2012, 525947. doi: 10.1100/2012/525947

Guzman, M. G., Halstead, S. B., Artsob, H., Buchy, P., Farrar, J., Gubler, D. J., et al. (2010). Dengue: a continuing global threat. *Nat. Rev. Microbiol.* 8, S7–16. doi: 10.1038/nrmicro2460

Halstead, S. B. (2007). Dengue. *Lancet* 370, 1644–1652. doi: 10.1016/S0140-6736(07)61687-0

Henriques, P., Rosa, A., Caldeira-Araújo, H., Soares, P., and Vigário, A. M. (2023). Flying under the radar – impact and factors influencing asymptomatic DENV infections. *Front. Cell. Infect. Microbiol.* 13. doi: 10.3389/fcimb.2023.1284651

Huang, K.-J., Li, S.-Y. J., Chen, S.-C., Liu, H.-S., Lin, Y.-S., Yeh, T.-M., et al. (2000). Manifestation of thrombocytopenia in dengue-2-virus-infected mice. *J. Gen. Virol.* 81, 2177–2182. doi: 10.1099/0022-1317-81-9-2177

Jaiswal, S., Pazoles, P., Woda, M., Shultz, L. D., Greiner, D. L., Brehm, M. A., et al. (2012). Enhanced humoral and HLA-A2-restricted dengue virus-specific T-cell responses in humanized BLT NSG mice. *Immunology* 136, 334–343. doi: 10.1111/j.1365-2567.2012.03585.x

Jaiswal, S., Pearson, T., Friberg, H., Shultz, L. D., Greiner, D. L., Rothman, A. L., et al. (2009). Dengue virus infection and virus-specific HLA-A2 restricted immune responses in humanized NOD-scid IL2rgammanull mice. *PLoS One* 4, e7251. doi: 10.1371/journal.pone.0007251

Johansson, M. A., Vasconcelos, P. F. C., and Staples, J. E. (2014). The whole iceberg: estimating the incidence of yellow fever virus infection from the number of severe cases. *Trans. R. Soc Trop. Med. Hyg.* 108, 482–487. doi: 10.1093/trstmh/tru092

Johnson, A. J., and Roehrig, J. T. (1999). New mouse model for dengue virus vaccine testing. *J. Virol.* 73, 783–786. doi: 10.1128/JVI.73.1.783-786.1999

Jones, M., Davidson, A., Hibbert, L., Gruenwald, P., Schlaak, J., Ball, S., et al. (2005). Dengue virus inhibits alpha interferon signaling by reducing STAT2 expression. *J. Virol.* 79, 5414–5420. doi: 10.1128/JVI.79.9.5414-5420.2005

Kuruvilla, J. G., Troyer, R. M., Devi, S., and Akkina, R. (2007). Dengue virus infection and immune response in humanized RAG2$^{-/-}\gamma c^{-/-}$ (RAG-hu) mice. *Virology* 369, 143–152. doi: 10.1016/j.virol.2007.06.005

Lazear, H. M., Govero, J., Smith, A. M., Platt, D. J., Fernandez, E., Miner, J. J., et al. (2016). A mouse model of Zika virus pathogenesis. *Cell Host Microbe* 19, 720–730. doi: 10.1016/j.chom.2016.03.010

Mazzon, M., Jones, M., Davidson, A., Chain, B., and Jacobs, M. (2009). Dengue virus NS5 inhibits interferon-alpha signaling by blocking signal transducer and activator of transcription 2 phosphorylation. *J. Infect. Dis.* 200, 1261–1270. doi: 10.1086/605847

Milligan, G. N., Sarathy, V. V., White, M. M., Greenberg, M. B., Campbell, G. A., Pyles, R. B., et al. (2017). A lethal model of disseminated dengue virus type 1 infection in AG129 mice. *J. Gen. Virol.* 98, 2507–2519. doi: 10.1099/jgv.0.000923

Mota, J., and Rico-Hesse, R. (2009). Humanized mice show clinical signs of dengue fever according to infecting virus genotype. *J. Virol.* 83, 8638–8645. doi: 10.1128/jvi.00581-09

Muñoz-Jordán, J. L., Laurent-Rolle, M., Ashour, J., Martínez-Sobrido, L., Ashok, M., Lipkin, W. I., et al. (2005). Inhibition of alpha/beta interferon signaling by the NS4B protein of flaviviruses. *J. Virol.* 79, 8004–8013. doi: 10.1128/JVI.79.13.8004-8013.2005

Muñoz-Jordán, J. L., Sánchez-Burgos, G. G., Laurent-Rolle, M., and García-Sastre, A. (2003). Inhibition of interferon signaling by dengue virus. *Proc. Natl. Acad. Sci. U. S. A.* 100, 14333–14338. doi: 10.1073/pnas.2335168100

Paes, M. V., Pinhão, A. T., Barreto, D. F., Costa, S. M., Oliveira, M. P., Nogueira, A. C., et al. (2005). Liver injury and viremia in mice infected with dengue-2 virus. *Virology* 338, 236–246. doi: 10.1016/j.virol.2005.04.042

Perry, S. T., Buck, M. D., Lada, S. M., Schindler, C., and Shresta, S. (2011). STAT2 mediates innate immunity to dengue virus in the absence of STAT1 via the type I interferon receptor. *PLoS Pathog.* 7, e1001297. doi: 10.1371/journal.ppat.1001297

Perry, S. T., Prestwood, T. R., Lada, S. M., Benedict, C. A., and Shresta, S. (2009). Cardif-mediated signaling controls the initial innate response to dengue virus in *vivo*. *J. Virol.* 83, 8276–8281. doi: 10.1128/JVI.00365-09

Pinto, A. K., Daffis, S., Brien, J. D., Gainey, M. D., Yokoyama, W. M., Sheehan, K. C. F., et al. (2011). A temporal role of type I interferon signaling in CD8+ T cell maturation during acute west Nile virus infection. *PLoS Pathog.* 7, e1002407. doi: 10.1371/journal.ppat.1002407

Prestwood, T. R., May, M. M., Plummer, E. M., Morar, M. M., Yauch, L. E., and Shresta, S. (2012). Trafficking and replication patterns reveal splenic macrophages as major targets of dengue virus in mice. *J. Virol.* 86, 12138–12147. doi: 10.1128/JVI.00375-12

Sarathy, V. V., Infante, E., Li, L., Campbell, G. A., Wang, T., Paessler, S., et al. (2015). Characterization of lethal dengue virus type 4 (DENV-4) TVP-376 infection in mice lacking both IFN-α/β and IFN-γ receptors (AG129) and comparison with the DENV-2 AG129 mouse model. *J. Gen. Virol.* 96, 3035–3048. doi: 10.1099/jgv.0.000246

Sarathy, V. V., White, M., Li, L., Kaiser, J. A., Campbell, G. A., Milligan, G. N., et al. (2018). Characterization of a murine model of non-lethal, symptomatic dengue virus infection. *Sci. Rep.* 8, 4900. doi: 10.1038/s41598-018-22618-w

Sheehan, K. C. F., Lai, K. S., Dunn, G. P., Bruce, A. T., Diamond, M. S., Heutel, J. D., et al. (2006). Blocking monoclonal antibodies specific for mouse IFN-alpha/beta receptor subunit 1 (IFNAR-1) from mice immunized by *in vivo* hydrodynamic transfection. *J. Interferon Cytokine Res.* 26, 804–819. doi: 10.1089/jir.2006.26.804

Shresta, S., Kyle, J. L., Robert Beatty, P., and Harris, E. (2004). Early activation of natural killer and B cells in response to primary dengue virus infection in A/J mice. *Virology* 319, 262–273. doi: 10.1016/j.virol.2003.09.048

Shresta, S., Sharar, K. L., Prigozhin, D. M., Snider, H. M., Beatty, P. R., and Harris, E. (2005). Critical roles for both STAT1-dependent and STAT1-independent pathways in the control of primary dengue virus infection in mice1. *J. Immunol.* 175, 3946–3954. doi: 10.4049/jimmunol.175.6.3946

Sridharan, A., Chen, Q., Tang, K. F., Ooi, E. E., Hibberd, M. L., and Chen, J. (2013). Inhibition of megakaryocyte development in the bone marrow underlies dengue virus-induced thrombocytopenia in humanized mice. *J. Virol.* 87, 11648–11658. doi: 10.1128/JVI.01156-13

Tan, G. K., Ng, J. K. W., Trasti, S. L., Schul, W., Yip, G., and Alonso, S. (2010). A non mouse-adapted dengue virus strain as a new model of severe dengue infection in AG129 mice. *PLoS Negl. Trop. Dis.* 4, e672. doi: 10.1371/journal.pntd.0000672

Wilken, L., Stelz, S., Prajeeth, C. K., and Rimmelzwaan, G. F. (2023). Transient blockade of type I interferon signalling promotes replication of dengue virus strain D2Y98P in adult wild-type mice. *Viruses* 15, 814. doi: 10.3390/v15040814

Yauch, L. E., and Shresta, S. (2008). Mouse models of dengue virus infection and disease. *Antiviral Res.* 80, 87–93. doi: 10.1016/j.antiviral.2008.06.010

Yuya, W., Yuansong, Y., Susu, L., Chen, L., Yong, W., Yining, W., et al. (2024). Progress and challenges in development of animal models for dengue virus infection. *Emerg. Microbes Infect.* 13, 2404159. doi: 10.1080/22221751.2024.2404159

Züst, R., Toh, Y.-X., Valdés, I., Cerny, D., Heinrich, J., Hermida, L., et al. (2014). Type I interferon signals in macrophages and dendritic cells control dengue virus infection: implications for a new mouse model to test dengue vaccines. *J. Virol.* 88, 7276–7285. doi: 10.1128/JVI.03827-13

frontiers | Frontiers in Cellular and Infection Microbiology

TYPE Original Research
PUBLISHED 03 April 2025
DOI 10.3389/fcimb.2025.1499154

OPEN ACCESS

EDITED BY
Krupakar Parthasarathy,
Sathyabama Institute of Science and Technology, India

REVIEWED BY
Pei Lu,
University of Texas Southwestern Medical Center, United States
Swayam Prakash,
University of California, Irvine, United States

*CORRESPONDENCE
Ya Fu
hzxfy@fjmu.edu.cn
Liang Wang
52069878@qq.com
Jialin Song
jialinson@fjmu.edu.cn

†These authors have contributed equally to this work

RECEIVED 20 September 2024
ACCEPTED 03 March 2025
PUBLISHED 03 April 2025

CITATION
Xu Y, Tang M, Guo Z, Lin Y, Guo H, Fang F, Lin L, Shi Y, Lai L, Pan Y, Tang X, You W, Li Z, Song J, Wang L, Cai W and Fu Y (2025) A model based on PT-INR and age serves as a promising predictor for evaluating mortality risk in patients with SARS-CoV-2 infection. *Front. Cell. Infect. Microbiol.* 15:1499154. doi: 10.3389/fcimb.2025.1499154

A model based on PT-INR and age serves as a promising predictor for evaluating mortality risk in patients with SARS-CoV-2 infection

Yongjie Xu[1,2,3,4,5,6†], Minjie Tang[1,2,3,4,5,6], Zhaopei Guo[1,2,3,4,5†], Yanping Lin[7†], Hongyan Guo[1,2,3,4,5], Fengling Fang[1,2,3,4,5], Lin Lin[1,2,3,4,5], Yue Shi[1,2,3,4,5], Lu Lai[1,2,3,4,5], Yan Pan[1,2,3,4,5], Xiangjun Tang[1,2,3,4,5], Weiquan You[1,2,3,4,5†], Zishun Li[7], Jialin Song[8*], Liang Wang[9*], Weidong Cai[1,2,3,4,5,6] and Ya Fu[1,2,3,4,5*]

[1]Department of Laboratory Medicine, The First Affiliated Hospital, Fujian Medical University, Fuzhou, China, [2]Department of Laboratory Medicine, National Regional Medical Center, Binhai Campus of the First Affiliated Hospital, Fujian Medical University, Fuzhou, China, [3]Fujian Key Laboratory of Laboratory Medicine, The First Affiliated Hospital, Fujian Medical University, Fuzhou, China, [4]Gene Diagnosis Research Center, The First Affiliated Hospital, Fujian Medical University, Fuzhou, China, [5]Department of Laboratory Medicine, National Reginal Medical Center, Binhai Campus of the First Affiliated Hospital, Fujian Medical University, Fuzhou, China, [6]Department of Blood Transfusion, The First Affiliated Hospital, Fujian Medical University, Fuzhou, China, [7]Department of Laboratory Medicine, The Third Hospital of Xiamen, Xiamen, China, [8]Medical Research Center, Fujian Maternity and Child Health Hospital, Fuzhou, Fujian, China, [9]Department of Hepatopancreatobiliary Surgery, The First Affiliated Hospital, Fujian Medical University, Fuzhou, China, [10]Department of Laboratory Medicine, the Affiliated Hospital of Putian University, Putian University, Putian, China

COVID-19 caused by the coronavirus SARS-CoV-2 has resulted in a global pandemic. Considering some patients with COVID-19 rapidly develop respiratory distress and hypoxemia, early assessment of the prognosis for COVID-19 patients is important, yet there is currently a lack of research on a comprehensive multi-marker approach for disease prognosis assessment. Here, we utilized a large sample of hospitalized individuals with COVID-19 to systematically compare the clinical characteristics at admission and developed a nomogram model that was used to predict prognosis. In all cases, those with pneumonia, older age, and higher PT-INR had a poor prognosis. Besides, pneumonia patients with older age and higher PT-INR also had a poor prognosis. A nomogram model incorporating presence of pneumonia, age and PT-INR could evaluate the prognosis in all patients with SARS-CoV-2 infections well, while a nomogram model incorporating age and PT-INR could evaluate the prognosis in those with pneumonia well. Together, our study establishes a prognostic prediction model that aids in the timely identification of patients with poor prognosis and helps facilitate the improvement of treatment strategies in clinical practice in the future.

KEYWORDS

PT-INR, age, predictor, mortality, SARS-CoV-2

Introduction

COVID-19, short for a novel coronavirus disease, is a severe acute respiratory syndrome caused by the coronavirus SARS-CoV-2, resulting in a global pandemic defined by the Director-General of the World Health Organization (WHO) on March 11, 2020 (Rothan and Byrareddy, 2020; Rubin et al., 2020). The pathogen of this disease belongs to the beta genus of coronaviruses and is mainly transmitted through respiratory droplets and close contact, and the general population is susceptible to it (Wang et al., 2020).

Although most patients have a good prognosis, some patients rapidly develop respiratory distress and hypoxemia after the onset of the disease, leading to the development of acute respiratory distress syndrome (ARDS), and even multiple organ failure, of which the mortality rate is relatively high (Gilbert et al., 2020). Based on the severity of the condition, COVID-19 can be classified into four categories: mild, moderate, severe, and critical. Early identification of potential severe cases, preventing the progression from mild or moderate to severe or critical, as well as assessing the prognosis and predicting the outcome of COVID-19, pose significant challenges in clinical practice.

Several indicators have been reported to be associated with the prognosis of COVID-19. Throughout the course of infection, the persistently low count of eosinophils could have fatal consequences (Chen et al., 2020; Zhao et al., 2021). Significantly elevated levels of IL-6 were associated with adverse clinical outcomes (Coomes and Haghbayan, 2020). Additionally, age, gender, and hypertension were also associated with the severity of the disease (Shi et al., 2020). Nevertheless, there is currently a lack of research on a comprehensive multi-marker approach for disease prognosis assessment. Although there are already various early warning scoring systems that can comprehensively assess the severity of patients' conditions and predict clinical outcomes, such as the National Early Warning Score version 2 (NEWS2) and the Acute Physiology and Chronic Health Evaluation II (APACHE II) scoring systems, prognostic prediction models based on specific clinical indicators are equally important and effective. These models can serve as supplements to early warning scoring systems, thereby enhancing the accuracy of predictions.

Therefore, this study aims to utilize data from a large cohort of hospitalized COVID-19 patients to systematically compare the clinical characteristics of different prognostic groups at the time of admission. Our objective is to develop a standardized prognostic prediction model that incorporates patients' age and PT-INR data upon admission, in order to provide accurate predictive capabilities for different prognostic groups. Through this research, we hope to establish an effective prognostic prediction tool that will assist clinicians in timely identifying patients with poor prognoses, ultimately improving treatment strategies in the future.

Methods

Study design and population

The study population included hospitalized patients diagnosed with COVID-19 at our hospital. The training cohort consisted of patients who were discharged or deceased between December 1, 2022, and January 31, 2023, while the validation cohort included patients who were discharged or deceased between April 1, 2023, and April 30, 2023. Data collection was conducted through the hospital's electronic medical record system, and the relevant data were compiled into spreadsheets and reviewed by senior physicians. The collected information included the patients' age, gender, diagnosis at the time of admission, presence of pneumonia, laboratory test results, and prognosis. For the sample size calculation, we set the significance level at 0.05, the statistical power at 0.80, the expected effect size at 0.8, and the loss percentage at 20%, resulting in a final sample size of 554 participants. According to the guidelines and standards set by the World Health Organization (WHO) regarding COVID-19 (O. World Health, 2021), the diagnostic criteria for confirmed cases include the presence of one of the following microbiological evidence based on suspected cases: 1) The patient exhibits acute respiratory infection symptoms, such as fever, cough, fatigue, shortness of breath, sore throat, muscle or joint pain, headache, and loss of smell or taste; 2) Positive results for the novel coronavirus nucleic acid via real-time fluorescent RT-PCR testing; 3) Viral gene sequencing showing high homology with known novel coronaviruses; 4) A history of contact with confirmed COVID-19 cases within the past 14 days, or travel or residence in areas experiencing severe outbreaks; 5) Chest X-ray or CT scans revealing pneumonia or other lung lesions associated with COVID-19. The criteria for excluding COVID-19 typically include the following aspects: 1) Clinical Symptoms: Patients who do not exhibit COVID-19-related symptoms (such as fever, cough, shortness of breath, fatigue, muscle or joint pain, sore throat, headache, loss of taste or smell, etc.) usually do not meet the criteria for a COVID-19 diagnosis. 2) Test Results: If PCR or rapid antigen test results are negative, and the patient's symptoms or clinical history do not align with COVID-19, then a COVID-19 diagnosis should also be excluded. 3) Other Causes: If the patient's symptoms can be explained by other known causes (such as influenza, other respiratory viral infections, or bacterial pneumonia), and relevant tests confirm this, then a diagnosis of COVID-19 can be ruled out. 4) Epidemiological Background: An absence of epidemiological risk factors for COVID-19 (such as no contact with confirmed cases or recent travel to areas with high incidence of the disease) can also serve as a basis for exclusion from the diagnosis. 5) Imaging Studies: If X-ray or CT imaging does not show typical lesions associated with COVID-19, the patient may also be considered for exclusion from a COVID-19 diagnosis. Based on the clinical treatment outcomes, we categorized the patients into four groups: Cured Group: Patients who had a complete resolution of their condition after clinical treatment. Improved Group: Patients who showed significant improvement in their symptoms following treatment. Unimproved Group: This group includes a portion of patients whose condition did not improve and actually worsened after treatment. In these cases, family members chose to discontinue treatment, leading to the patient's discharge against medical advice. Deceased Group: Patients who passed away during the course of clinical treatment. In our study, patients were categorized into two groups based on their clinical outcomes following treatment: "Effective Treatment" and "Ineffective Treatment." Patients classified as having received "Effective Treatment" were those who demonstrated

significant improvement in symptoms and met the discharge criteria during our observation/data collection period (this includes patients from both the "Cured" and "Improved" groups). In contrast, "Ineffective Treatment" refers to patients who did not meet these criteria within the specified observation period (this includes patients from both the "Unimproved" and "Deceased" groups). The written consent was obtained from each patient and the study was approved by the Ethics Committee of the First Affiliated Hospital of Fujian Medical University. Ethics Committee Approval Number: MTCA, ECFAH of FMU〔2015〕No. 084-2.

Nomogram model construction and prognosis evaluation

In the training cohort, the one-way analysis of variance (ANOVA) was used to compare the differences in various clinical indicators among the cured, improved, unimproved, and dead groups. Indicators with significantly statistical differences were further filtered by lasso regression and logistic regression analysis. We further simplified the complex logistic regression model into a visualized nomogram by using the rms package of R. Subsequently, the efficiency of the visualized nomogram was evaluated by calibration curve and receiver operating characteristic (ROC) curve. The calibration curve was used to compare the association between actual outcomes and predicted probabilities. The ROC curve was used to assess the discriminative ability of the nomogram and then the area under the curve (AUC). Nomogram scores are utilized to predict the patient's 30-day clinical outcomes during hospitalization. Cumulative events of effective treatment within 30 days of hospitalization based on cox regression analysis were visualized by using the survminer and ggplot2 packages of R.

Statistical analysis

Statistical differences were evaluated by one-way analysis of variance (ANOVA), chi-squared test (Fisher's exact test was used when needed), lasso regression, logist regression, and cox regression with IBM SPSS Statistics software (Version 22.0.0; IBM, Armonk, New York, USA) and R (version 4.1.0 http://www.r-project.org). All P values were two-tailed. $P < 0.05$ was considered to be statistically significant.

Results

Clinical characteristics of COVID-19 patients

The study enrolled a total of 1134 hospitalized patients who were infected with COVID-19, including 823 cases in the training set and 311 cases in the validation set (Figure 1). Among these 823 patients in the training set, 89 succumbed to the disease, 293 successfully recovered, while the remaining 441 individuals were still undergoing treatment at the time of their enrollment in the study. The clinical data of patients with different prognoses at admission in the training set are shown in Table 1. By anlysing the differences in the clinical characteristics among the cured, improved, unimproved and dead groups, significant differences in 38 indexes by ANOVA

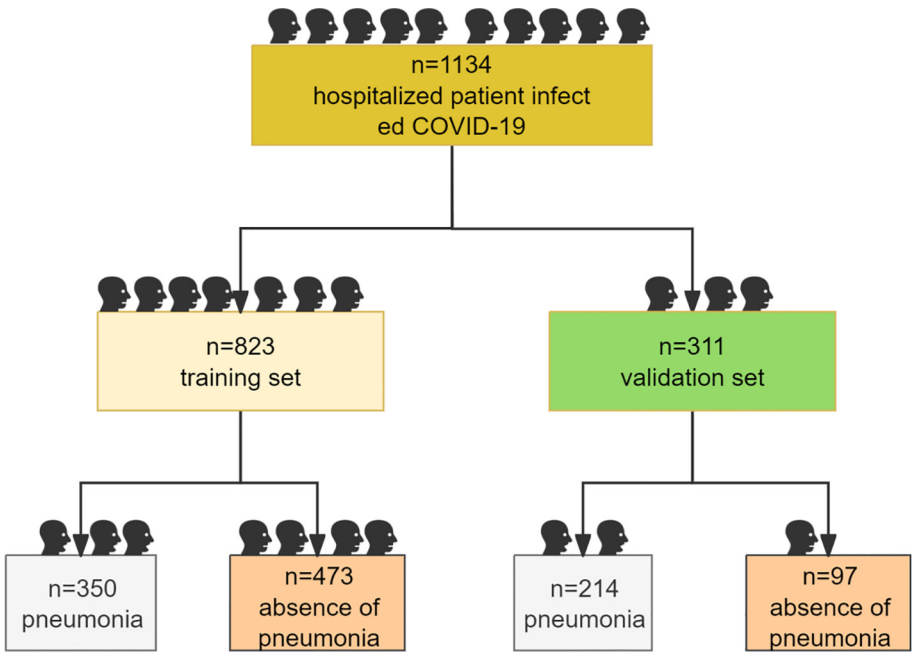

FIGURE 1
Study flow diagram.

10.3389/fcimb.2025.1499154

TABLE 1 Clinical characteristics of patients infected with COVID-19.

Hospital discharge status	Cured (n = 293)	Improved (n = 424)	Unimproved (n = 17)	Dead (n = 89)	χ^2/ F/U	P
Gender					8.97	0.0297
male	167 (57.00%)	272 (65.15%)	12 (70.59%)	65 (73.03%)		
female	126 (43.00%)	152 (34.85%)	5 (29.41%)	24 (26.97%)		
Presence/Absence of pneumonia					140.62	<0.0001
yes	64 (21.84%)	199 (46.93%)	6 (35.29%)	81 (91.01%)		
no	229 (78.16%)	225 (53.07%)	11 (64.71%)	8 (8.99%)		
Age (year)	56.59 ± 17.68	62.97 ± 16.55	63.06 ± 16.28	73.42 ± 11.89	25.10	<0.0001
PT (s)	13.09 ± 5.98	13.18 ± 2.00	13.50 ± 2.70	15.04 ± 4.36	5.61	0.0008
PT-INR	1.09 ± 0.18	1.14 ± 0.20	1.17 ± 0.28	1.34 ± 0.48	25.52	<0.0001
APTT (s)	33.52 ± 7.86	34.87 ± 10.44	36.64 ± 12.25	41.47 ± 16.95	13.11	<0.0001
Fg (g/L)	3.64 ± 1.43	4.01 ± 1.55	3.65 ± 1.09	4.51 ± 2.14	7.75	<0.0001
TT(s)	17.90 ± 4.79	17.95 ± 2.86	19.25 ± 3.56	19.39 ± 9.69	2.81	0.0387
WBC (10^9/L)	7.96 ± 5.30	7.50 ± 3.69	10.03 ± 12.44	8.96 ± 4.45	3.66	0.0122
%NEUT (%)	69.62 ± 14.65	69.07 ± 14.01	59.80 ± 16.02	79.07 ± 12.32	15.89	<0.0001
#NEUT (10^9/L)	5.67 ± 3.73	5.45 ± 3.58	6.20 ± 7.60	7.38 ± 4.40	6.31	0.0003
%LYMPH (%)	19.78 ± 12.36	20.14 ± 11.14	27.49 ± 14.09	13.03 ± 9.86	12.52	<0.0001
#LYMPH (10^9/L)	1.51 ± 3.70	1.33 ± 0.77	2.05 ± 1.73	0.94 ± 0.64	1.92	0.1255
%MONO (%)	5.85 ± 2.46	5.81 ± 2.42	6.30 ± 2.20	4.84 ± 1.83	4.88	0.0023
#MONO (10^9/L)	0.43 ± 0.24	0.40 ± 0.20	0.55 ± 0.56	0.42 ± 0.24	2.72	0.0433
%EOS (%)	1.20 (0.00-20.70)	1.35 (0.00-19.40)	1.70 (0.00-5.00)	0.30 (0.00-4.90)	20.84	<0.001
#EOS (10^9/L)	0.08 (0.00-2.89)	0.09 (0.00-1.46)	0.12 (0.01-0.33)	0.02 (0.00-0.28)	20.35	<0.001
%BASO (%)	0.57 ± 0.64	0.58 ± 0.62	0.81 ± 0.89	0.45 ± 0.73	1.89	0.1303
#BASO (10^9/L)	0.05 ± 0.14	0.04 ± 0.04	0.17 ± 0.53	0.04 ± 0.05	7.10	0.0001
%LUC (%)	2.47 ± 1.92	2.55 ± 2.20	3.94 ± 6.53	1.93 ± 1.64	4.42	0.0043
#LUC (10^9/L)	0.19 ± 0.33	0.16 ± 0.10	1.07 ± 3.81	0.14 ± 0.09	13.84	<0.0001
RBC (10^{12}/L)	4.01 ± 0.91	3.95 ± 0.86	4.05 ± 0.90	3.74 ± 0.89	2.13	0.0946
HGB (g/l)	120.19 ± 26.21	118.02 ± 25.37	122.24 ± 27.93	111.74 ± 24.44	2.62	0.0496
HCT	0.36 ± 0.08	0.36 ± 0.07	0.38 ± 0.08	0.34 ± 0.07	3.12	0.0255
MCV (fL)	91.70 ± 8.05	91.71 ± 7.57	93.09 ± 7.04	91.31 ± 8.41	0.26	0.8580
MCH (Pg)	30.23 ± 3.06	30.05 ± 2.97	30.05 ± 2.95	30.14 ± 2.91	0.24	0.8695
MCHC (g/l)	329.42 ± 15.17	327.25 ± 14.91	325.24 ± 9.60	330.19 ± 16.22	1.92	0.1244
RDW (%)	14.59 ± 2.34	14.77 ± 2.30	14.35 ± 1.95	14.43 ± 1.81	0.85	0.4679
PLT (10^9/L)	226.21 ± 114.64	241.15 ± 121.44	228.47 ± 83.27	201.46 ± 92.75	3.20	0.0229
MPV (fL)	9.01 ± 1.34	9.00 ± 1.29	9.38 ± 1.34	9.42 ± 1.37	3.01	0.0294
PDW (fL)	52.34 ± 9.45	51.77 ± 9.42	54.46 ± 8.13	53.63 ± 9.86	1.31	0.2698
PCT	0.20 ± 0.09	0.21 ± 0.10	0.21 ± 0.08	0.18 ± 0.08	2.49	0.0589
MPC (g/l)	255.29 ± 20.30	254.58 ± 19.69	251.53 ± 17.20	249.28 ± 20.23	2.25	0.0810

(Continued)

10.3389/fcimb.2025.1499154

TABLE 1 Continued

Hospital discharge status	Cured (n = 293)	Improved (n = 424)	Unimproved (n = 17)	Dead (n = 89)	χ^2/ F/U	P
TBIL (μmol/L)	11.76 ± 17.99	12.92 ± 28.02	9.41 ± 5.99	10.17 ± 12.28	0.48	0.6960
DBIL (μmol/L)	6.33 ± 16.11	8.00 ± 25.17	4.69 ± 4.22	5.59 ± 10.41	0.63	0.5965
IBIL (μmol/L)	5.70 ± 5.67	4.93 ± 4.91	4.72 ± 3.38	4.58 ± 4.10	1.81	0.1445
TP (g/L)	64.71 ± 8.83	63.35 ± 8.92	62.45 ± 6.47	59.59 ± 8.53	7.79	<0.0001
ALB (g/L)	38.56 ± 6.58	37.59 ± 6.90	37.43 ± 6.27	34.03 ± 5.93	10.48	<0.0001
GLO (g/L)	26.09 ± 7.02	25.76 ± 4.99	25.02 ± 3.80	25.56 ± 5.26	0.39	0.7631
A/G	1.62 ± 1.21	1.51 ± 0.36	1.54 ± 0.40	1.38 ± 0.35	2.51	0.0575
ALT (U/L)	17.00 (1.00-227.00)	18.00 (1.00-1210.00)	16.00 (5.00-56.00)	19.00 (1.00-999.00)	2.21	0.137
AST (U/L)	21.00 (1.00-235.00)	21.00 (6.00-773.00)	19.00 (12.00-58.00)	26.00 (8.00-1714.00)	6.92	0.009
ALT/AST	1.05 ± 2.74	0.88 ± 0.47	0.80 ± 0.40	0.86 ± 0.59	0.66	0.5764
GGT (U/L)	54.62 ± 91.10	65.35 ± 121.95	26.82 ± 17.43	47.28 ± 54.88	1.60	0.1891
LDH (U/L)	194.00 (97.00-757.00)	193.50 (87.00-5425.00)	186.00 (126.00-1131.00)	243.00 (123.00-2246.00)	19.92	<0.001
ALP (U/L)	96.99 ± 103.30	104.74 ± 121.36	83.00 ± 62.73	80.51 ± 33.96	1.43	0.2315
CK (U/L)	71.00 (5.00-6830.00)	72.50 (6.00-13938.00)	76.00 (30.00-453.00)	139.00 (11.00-14514.00)	6.73	0.009
CKMB (U/L)	14.00 (3.00-94.00)	14.00 (4.00-442.00)	13.00 (8.00-27.00)	16.00 (5.00-369.00)	12.85	<0.001
UREA (mmol/L)	6.73 ± 7.01	7.04 ± 6.20	6.54 ± 3.34	10.44 ± 9.51	7.11	0.0001
CREA (μmol/L)	70.00 (0.06-1477.00)	72.00 (27.00-1613.00)	85.00 (48.00-157.00)	70.00 (14.00-1273.00)	0.03	0.858
UREA/CREA	0.82 ± 12.66	0.08 ± 0.03	0.07 ± 0.03	0.09 ± 0.04	0.60	0.6158
UA (μmol/L)	305.75 ± 120.19	310.25 ± 129.92	329.54 ± 121.34	313.11 ± 149.77	0.25	0.8627
GLU (mmol/L)	6.45 ± 3.03	6.77 ± 3.55	6.38 ± 3.05	8.54 ± 4.49	8.43	<0.0001
TC (mmol/L)	4.11 ± 1.23	4.12 ± 1.24	3.91 ± 1.29	3.67 ± 1.22	3.49	0.0153
TG (mmol/L)	1.32 ± 0.80	1.40 ± 0.78	1.20 ± 0.39	1.46 ± 1.63	0.84	0.4727
HDL-C (mmol/L)	1.12 ± 0.39	1.07 ± 0.39	1.09 ± 0.45	1.03 ± 0.39	1.70	0.1661
HDL-C/TC	0.29 ± 0.21	0.27 ± 0.09	0.28 ± 0.09	0.29 ± 0.10	1.96	0.1186
LDL-C (mmol/L)	2.56 ± 1.02	2.56 ± 1.06	2.48 ± 1.08	2.18 ± 1.09	3.56	0.0141
VLDL-C (mmol/L)	0.60 ± 0.37	0.63 ± 0.35	0.54 ± 0.18	0.66 ± 0.74	0.77	0.5113
APOA1 (g/L)	1.14 ± 0.36	1.11 ± 0.36	1.12 ± 0.37	0.98 ± 0.36	4.08	0.0069
APOB (g/L)	0.91 ± 0.30	0.93 ± 0.29	0.86 ± 0.30	0.86 ± 0.33	1.89	0.1306
APOA1/APOB	1.36 ± 0.56	1.29 ± 0.56	1.40 ± 0.56	1.26 ± 0.65	1.35	0.2559
CA (mmol/L)	2.19 ± 0.19	2.17 ± 0.20	2.18 ± 0.15	2.07 ± 0.16	9.65	<0.0001
P (mmol/L)	1.15 ± 0.31	1.11 ± 0.33	1.09 ± 0.27	1.15 ± 0.50	0.83	0.4778
MG (mmol/L)	1.01 ± 1.73	0.91 ± 0.11	0.95 ± 0.08	0.92 ± 0.15	0.56	0.6437
CO2CP (mmol/L)	24.81 ± 3.57	24.65 ± 4.25	24.84 ± 3.24	22.64 ± 4.40	7.17	<0.0001
K (mmol/L)	6.02 ± 9.35	5.60 ± 4.96	6.73 ± 6.44	5.14 ± 3.53	0.58	0.6283

(Continued)

TABLE 1 Continued

Hospital discharge status	Cured (n = 293)	Improved (n = 424)	Unimproved (n = 17)	Dead (n = 89)	χ^2/ F/U	P
NA (mmol/L)	130.96 ± 33.76	131.51 ± 33.53	124.25 ± 45.13	132.51 ± 28.71	0.31	0.8206
CL (mmol/L)	103.93 ± 11.48	104.90 ± 11.12	108.56 ± 13.61	103.80 ± 11.55	1.26	0.2856
AG (mmol/L)	19.24 ± 23.07	18.92 ± 22.66	22.82 ± 32.74	18.11 ± 19.46	0.22	0.8836
GFR (ml/min/1.73m^2)	86.62 ± 30.01	78.97 ± 31.93	68.59 ± 34.24	73.84 ± 36.85	2.57	0.0529

numerical variables are represented using the mean ± standard deviation.PT, prothrombin time; PT-INR, prothrombin time-international normalized ratio; APTT, activated partial thromboplastin time; Fg, fibrinogen; TT, prothrombin time; WBC, white blood cell; %NEUT, percentage of neutrophils; #NEUT, neutrophil count; %LYMPH, percentage of lymphocytes; #LYMPH, lymphocyte count; %MONO, percentage of mononuclear cells; #MONO, monocyte count.; %EO, eosinophil percentage; #EO, eosinophil count; %BASO, basophil percentage; #BASO, basophil count; %LUC, percentage of unstained macrophages; #LUC, unstained macrophage count; RBC, red blood cell; HGB, hemoglobin; HCT, hematocrit; MCV, mean erythrocyte volume; MCH, mean erythrocyte hemoglobin volume; MCHC, mean erythrocyte hemoglobin concentration; RDW, erythrocyte distribution width; PLT, platelet; MPV, mean platelet volume; PDW, platelet distribution width; PCT, platelet specific volume; MPC, mean platelet component concentration; TBIL, total bilirubin; DBIL, direct bilirubin; IBIL, indirect bilirubin; TP, total protein; ALB, albumin; GLO, globulin; A/G, albumin-to-globulin ratio; ALT, alanine aminotransferase; AST, aspartate aminotransferase; ALT/AST, alanine aminotransferase to aspartate aminotransferase ratio; GGT, gamma-glutaminyl transferase; LDH, lactate dehydrogenase; ALP, alkaline phosphatase; CK, creatine kinase; CKMB, creatine kinase isoenzyme; UREA, urea; CREA, creatinine; UREA/CREA, urea to creatinine ratio; UA, uric acid; GLU, glucose; TC, total cholesterol; TG, triglyceride; HDL-C, high-density lipoprotein cholesterol; HDL-C/TC, ratio of high-density lipoprotein cholesterol to total cholesterol; LDL-C, low-density lipoprotein cholesterol; VLDL-C, very low-density lipoprotein cholesterol; APOA1, apolipoprotein A1; APOB, apolipoprotein B; APOA1/APOB, apolipoprotein A1 to apolipoprotein B ratio; CA, calcium; P, phosphorus; MG, magnesium; CO2CP, carbon dioxide binding capacity; K, potassium; NA, sodium; CL, chloride; AG, anion gap; GFR. Glomerular filtration rate.

were observed across above 4 groups. The results shown that gender was associated with prognosis ($P = 0.0297$), and male patients have a poorer prognosis compared with female ones (Dead: male vs female, 73.03% vs 26.97%. Unimproved: male vs female, 70.59% vs 29.41%). Moreover, patients with pneumonia in this study also had the poorer prognosis compared with those without pneumonia ($P < 0.0001$. Dead: pneumonia vs non-pneumonia, 91.01% vs 8.99%). In addition, the elevated levels of 18 factors were found correlated to the poorer prognosis, while the declining levels of the other 18 factors were correlated to the poorer prognosis, In addition, the elevated levels of 18 biochemical and clinical factors were found to be correlated to the poorer prognosis as detailed in table.

Presence/Absence of pneumonia, age and PT-INR at admission are potential predictors for prognosis post COVID-19 infection

To evaluate factors associated with prognosis post COVID-19 infection, patients in this study were classified into effective-treatment group versus ineffective-treatment group. The effective group included cured and improved patients, while the ineffective group included unimproved and dead patients. One case was excluded from the analysis due to missing the data about duration of hospitalization. The lasso regression was used to initially screen the prognosis-related factors from above 38 indexes with significant difference among the cured, improved, unimproved and dead patients (Table 1, Figures 2A, B). Consequently, 19 of 38 indexes were selected for the subsequent analysis, including gender, presence/absence of pneumonia, age, PT-INR, APTT, Fg, #NEUT, %MONO, %EOS, #LUC, PLT, ALB, AST, LDH, CK, GLU, TCHO, CA, CO_2CP. The logist regression was employed to analyze the probability of using these 19 indexes for predicting the prognosis. It was shown that except #LUC, 18 of 19 indexed were all significantly different between effective-treatment and ineffective-treatment groups by univariate analysis of cox regression, while only 3 indexes —— presence/absence of pneumonia(mean OR = 3.783, $P < 0.001$), age (mean OR = 1.029, $P = 0.001$) and PT-INR (mean OR = 3.286, $P = 0.007$) —— were significantly different between effective-treatment and ineffective-treatment groups by multivariate analysis of cox regression (Figure 2C). Further, these aforementioned 3 predictors were integrated to develop a nomogram model that could be used to evaluate the prognosis (Figure 2D). The observed and predicted values of this model exhibited a high level of agreement, indicating a reliable performance of the model (Figure 2E). Using the scores marked by the nomogram model, the receiver operating characteristic (ROC) curves were generated between the effective-treatment and ineffective-treatment groups (Figure 2F). The areas under the curve (AUC) of model scores, presence/absence of pneumonia, age and PT-INR were respectively 0.802, 0.727, 0.697 and 0.710, suggesting that the model could effectively predict the prognosis post COVID-19 infection. The cox regression analysis was employed to further enhance the reliability of the model in predicting patient prognosis by evaluating the cumulative events of treatment effectiveness within 30 days of hospitalization (Figures 2G-J). The findings indicated that younger age (low vs high, mean HR = 0.70, $P < 0.001$), lower PT-INR levels (low vs high, mean HR = 0.64, $P < 0.001$), and the absence of pneumonia (pneumonia vs absence of pneumonia, mean HR = 2.13 or absence of pneumonia vs pneumonia, mean HR = 1/2.13 = 0.47, $P < 0.001$) were correlated with a more favorable prognosis within 30 days of hospitalization. Furthermore, patients with lower model scores also exhibited improved outcomes within 30 days of hospitalization (low vs high, mean HR = 0.45, $P < 0.001$).

Age and PT-INR at admission are potential predictors for prognosis in patients with pneumonia post COVID-19 infection

To further obtain factors associated with recovery post COVID-19 infection in 350 patients with pneumonia, the differences in the clinical characteristics were analyzed among the cured, improved, unimproved

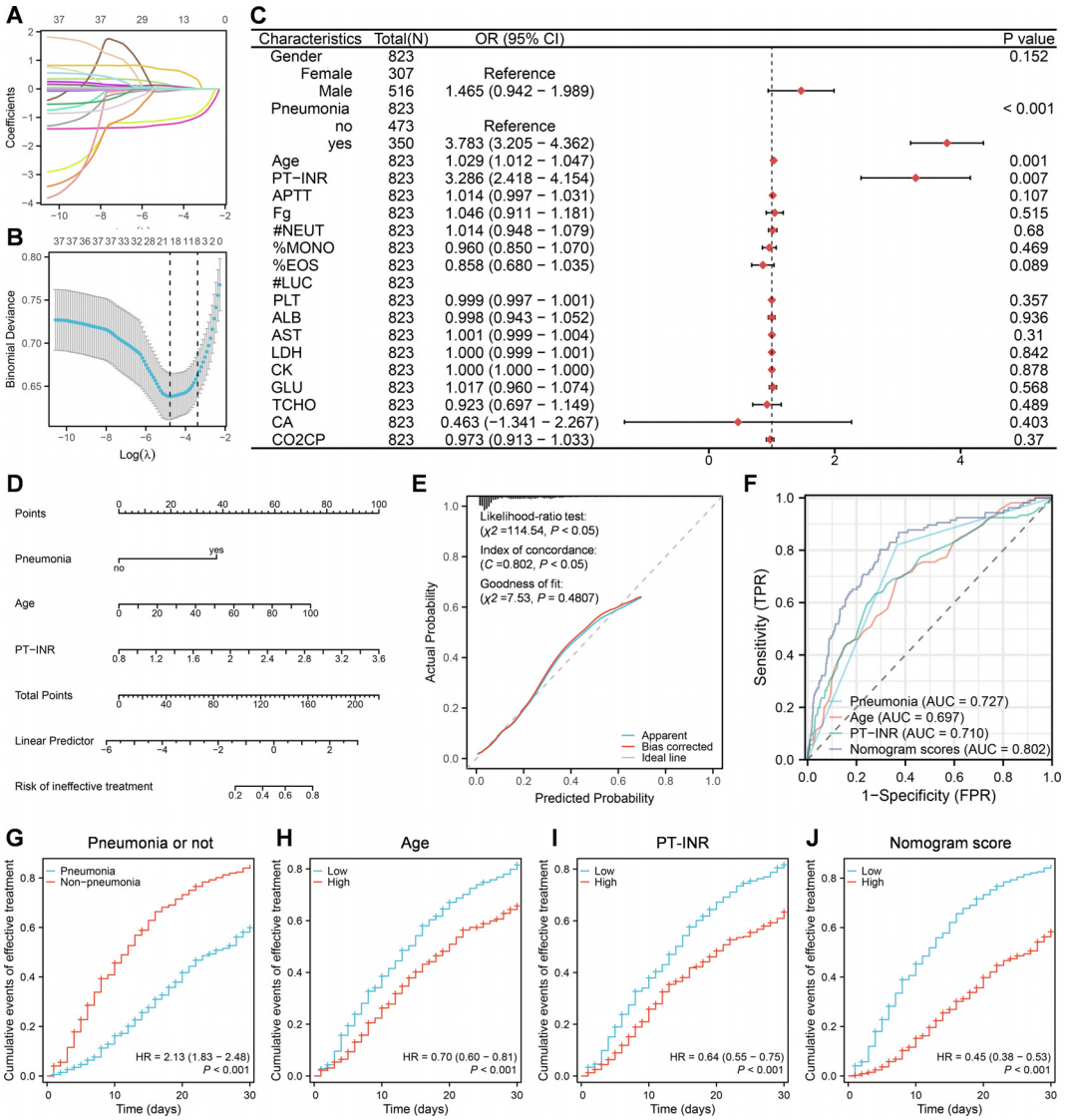

FIGURE 2
A nomogram model built based on pneumonia, age and PT-INR at admission for predicting prognosis post COVID-19 infection. **(A, B)** Lasso regression analysis. **(C)** Multivariate logistic regression analysis. **(D)** Construction of nomogram model based on multivariate logistic regression analysis. **(E)** Construction of calibration curves for the nomogram model. **(F)** Construction of ROC curves for nomogram scores, presence/absence of pneumonia, age, and PT-INR, respectively. **(G-J)** Cumulative events of effective treatment within 30 days of hospitalization based on cox regression analysis.

and dead groups, and a total of 23 indicators were found to have statistically significant differences (Table 2). The lasso regression was also used to screen the recovery-related factors from aforementioned 23 indexes with significant difference by ANOVA among the cured group, uncured group and dead group (Figures 3A, B). 11 of 23 indexes were selected for the subsequent analysis, including age, PT-INR, APTT, WBC, %MONO, %EOS, %LUC, LDH, UREA/CREA, CA and CO_2CP (Figure 3C). The logistic regression was used to analyze the feasibility of using these 11 indexes for assessing the probability of recovery post COVID-19 infection, and the results demonstrated that except #LUC, 10 of 11 indexed were all significantly different between effective-treatment and ineffective-treatment groups by univariate analysis of cox regression, while only 2 indexes; age (mean OR = 1.042, $P < 0.001$) and PT-INR (mean OR = 2.742, $P = 0.04$); were significantly different between effective-treatment and ineffective-treatment groups by multivariate analysis of cox regression (Figure 3C). Subsequently, a nomogram model incorporating age and PT-INR was constructed to assess the prognosis (Figure 3D). The calibration curve showed that the observed and predicted values of this model exhibited a high level of agreement, indicating a reliable performance of the model (Figure 3E). Using the scores marked by the nomogram model, ROC curves were generated between the effective-treatment and ineffective-treatment groups (Figure 3F). The areas under the curve (AUC) of model scores, age and PT-INR were respectively 0.701, 0.639 and 0.665. The cox regression analysis was also employed to evaluate the cumulative events of treatment effectiveness within 30 days of hospitalization in patients with pneumonia (Figures 3G-I). The findings indicated that younger age (low vs high, mean HR = 0.73,

10.3389/fcimb.2025.1499154

TABLE 2 Clinical characteristics of pneumonia patients infected with COVID-19.

Hospital discharge status	Cured (n = 64)	Improved (n = 199)	Unimproved (n = 6)	Dead (n = 81)	χ^2/F	*P*
Gender					0.74	0.8640
male	43	139	5	57		
female	21	60	1	24		
Age (year)	62.31 ± 13.64	68.37 ± 15.05	75.33 ± 10.56	73.91 ± 11.40	8.71	<0.0001
PT (s)	13.42 ± 2.88	13.55 ± 2.30	16.03 ± 3.08	14.94 ± 4.52	5.46	0.0011
PT-INR	1.17 ± 0.31	1.18 ± 0.23	1.44 ± 0.33	1.33 ± 0.45	6.03	0.0005
APTT (s)	34.02 ± 8.30	36.08 ± 9.49	46.85 ± 15.88	40.39 ± 16.90	5.59	0.0009
Fg (g/L)	4.18 ± 1.76	4.33 ± 1.67	3.75 ± 1.16	4.67 ± 2.12	1.28	0.2813
TT(s)	18.90 ± 9.51	18.07 ± 2.81	21.70 ± 5.13	19.33 ± 10.14	1.19	0.3126
WBC (10^9/L)	7.72 ± 3.68	7.86 ± 3.63	15.71 ± 19.31	9.00 ± 4.63	7.01	0.0001
%NEUT (%)	74.54 ± 12.59	72.50 ± 12.59	54.63 ± 15.30	78.91 ± 12.55	9.77	<0.0001
#NEUT (10^9/L)	6.02 ± 3.64	5.93 ± 3.48	8.57 ± 10.38	7.41 ± 4.57	3.45	0.0168
%LYMPH (%)	15.94 ± 10.27	17.41 ± 9.73	29.73 ± 15.36	13.12 ± 10.12	7.13	0.0001
#LYMPH (10^9/L)	1.02 ± 0.59	1.22 ± 0.70	3.32 ± 2.40	0.94 ± 0.66	21.11	<0.0001
%MONO (%)	5.49 ± 1.91	5.70 ± 2.66	6.83 ± 2.73	4.88 ± 1.85	3.00	0.0307
#MONO (10^9/L)	0.41 ± 0.21	0.41 ± 0.22	0.86 ± 0.85	0.42 ± 0.25	6.76	0.0002
%EO (%)	1.39 ± 1.61	1.69 ± 2.19	1.42 ± 1.22	0.77 ± 1.04	4.70	0.0031
#EO (10^9/L)	0.08 ± 0.09	0.12 ± 0.17	0.14 ± 0.11	0.05 ± 0.06	4.21	0.0061
%BASO (%)	0.39 ± 0.26	0.50 ± 0.36	1.23 ± 1.43	0.46 ± 0.75	5.47	0.0011
#BASO (10^9/L)	0.03 ± 0.02	0.04 ± 0.04	0.41 ± 0.88	0.04 ± 0.05	21.68	<0.0001
%LUC (%)	2.24 ± 1.19	2.22 ± 1.17	6.80 ± 10.90	1.95 ± 1.72	12.76	<0.0001
#LUC (10^9/L)	0.15 ± 0.07	0.15 ± 0.08	2.79 ± 6.40	0.14 ± 0.09	22.85	<0.0001
RBC (10^{12}/L)	3.69 ± 1.00	3.90 ± 0.90	4.04 ± 1.06	3.77 ± 0.87	1.07	0.3616
HGB (g/l)	111.69 ± 28.52	116.70 ± 26.41	122.83 ± 39.21	112.90 ± 23.92	0.95	0.4155
HCT	0.34 ± 0.08	0.36 ± 0.08	0.38 ± 0.11	0.34 ± 0.07	1.47	0.2228
MCV (fL)	92.49 ± 8.01	91.78 ± 7.54	93.93 ± 10.12	91.36 ± 8.17	0.40	0.7560
MCH (Pg)	30.56 ± 3.06	30.13 ± 2.95	30.15 ± 3.52	30.19 ± 2.76	0.36	0.7806
MCHC (g/l)	330.20 ± 15.55	327.81 ± 15.53	320.83 ± 8.42	330.64 ± 16.05	1.34	0.2614
RDW (%)	14.60 ± 2.38	14.70 ± 2.16	15.25 ± 2.93	14.35 ± 1.71	0.69	0.5562
PLT (10^9/L)	203.83 ± 90.68	228.82 ± 111.09	262.00 ± 84.23	205.73 ± 95.19	1.83	0.1406
MPV (fL)	8.95 ± 1.15	9.24 ± 1.41	10.32 ± 1.64	9.37 ± 1.35	2.47	0.0621
PDW (fL)	51.67 ± 10.81	53.00 ± 9.41	56.72 ± 8.38	53.74 ± 9.14	0.87	0.4596
PCT	0.18 ± 0.07	0.20 ± 0.09	0.27 ± 0.09	0.19 ± 0.08	3.24	0.0222
MPC (g/l)	254.45 ± 20.41	251.60 ± 19.42	244.67 ± 20.37	248.10 ± 20.00	1.49	0.2168
TBIL (μmol/L)	14.77 ± 22.92	11.12 ± 18.62	13.33 ± 7.34	9.59 ± 11.81	1.05	0.3714
DBIL (μmol/L)	9.04 ± 20.66	6.14 ± 14.94	7.63 ± 6.19	5.18 ± 10.08	0.85	0.4660
IBIL (μmol/L)	5.74 ± 4.01	4.98 ± 5.62	5.70 ± 3.85	4.42 ± 4.10	0.86	0.4599
TP (g/L)	63.10 ± 11.05	62.08 ± 8.88	62.92 ± 4.58	59.43 ± 8.07	2.33	0.0739
ALB (g/L)	36.75 ± 6.60	36.24 ± 6.90	37.88 ± 4.78	33.90 ± 5.75	3.19	0.0238
GLO (g/L)	26.35 ± 9.53	25.84 ± 4.77	25.03 ± 3.06	25.53 ± 5.22	0.26	0.8514

(Continued)

10.3389/fcimb.2025.1499154

TABLE 2 Continued

Hospital discharge status	Cured (n = 64)	Improved (n = 199)	Unimproved (n = 6)	Dead (n = 81)	χ^2/F	*P*
A/G	1.50 ± 0.40	1.44 ± 0.35	1.54 ± 0.30	1.38 ± 0.36	1.38	0.2485
ALT (U/L)	22.36 ± 18.13	30.69 ± 53.94	20.00 ± 18.80	49.78 ± 132.65	1.84	0.1390
AST (U/L)	27.84 ± 21.25	36.22 ± 45.90	26.50 ± 17.26	74.86 ± 250.85	2.27	0.0807
ALT/AST	0.86 ± 0.43	0.88 ± 0.50	0.83 ± 0.62	0.87 ± 0.60	0.05	0.9866
GGT (U/L)	57.20 ± 98.70	62.82 ± 112.37	38.33 ± 24.87	49.94 ± 56.75	0.42	0.7409
LDH (U/L)	232.67 ± 120.10	257.91 ± 159.38	335.17 ± 390.73	345.56 ± 342.67	4.28	0.0055
ALP (U/L)	93.53 ± 79.07	98.88 ± 95.72	114.17 ± 101.34	81.38 ± 35.13	0.98	0.4012
CK (U/L)	182.16 ± 405.56	357.27 ± 1227.93	130.83 ± 160.69	538.94 ± 1762.04	1.02	0.3838
CKMB (U/L)	18.67 ± 13.41	22.82 ± 39.19	15.50 ± 6.06	29.38 ± 51.20	1.05	0.3719
UREA (mmol/L)	7.86 ± 9.67	8.01 ± 7.15	6.10 ± 3.00	10.48 ± 9.24	2.14	0.0946
CREA (μmol/L)	105.97 ± 164.58	109.06 ± 123.96	98.00 ± 28.12	149.73 ± 213.14	1.50	0.2142
UREA/CREA	0.08 ± 0.04	0.08 ± 0.03	0.07 ± 0.03	0.09 ± 0.04	3.46	0.0166
UA (μmol/L)	309.25 ± 125.89	318.34 ± 143.07	345.07 ± 118.17	311.92 ± 150.50	0.17	0.9148
GLU (mmol/L)	7.03 ± 2.75	7.64 ± 4.49	6.12 ± 2.18	8.62 ± 4.58	2.11	0.0986
TC (mmol/L)	3.89 ± 1.30	4.04 ± 1.30	3.45 ± 1.18	3.71 ± 1.14	1.69	0.1690
TG (mmol/L)	1.24 ± 0.75	1.39 ± 0.69	1.22 ± 0.53	1.51 ± 1.69	0.85	0.4664
HDL-C (mmol/L)	1.00 ± 0.34	1.02 ± 0.39	0.91 ± 0.30	1.04 ± 0.38	0.29	0.8353
HDL-C/TC	0.27 ± 0.09	0.26 ± 0.09	0.27 ± 0.07	0.29 ± 0.10	1.51	0.2113
LDL-C (mmol/L)	2.49 ± 1.11	2.52 ± 1.10	2.18 ± 0.95	2.19 ± 1.04	1.95	0.1219
VLDL-C (mmol/L)	0.56 ± 0.34	0.63 ± 0.31	0.55 ± 0.24	0.68 ± 0.77	0.85	0.4680
APOA1 (g/L)	1.01 ± 0.35	1.05 ± 0.35	1.04 ± 0.31	0.99 ± 0.36	0.64	0.5931
APOB (g/L)	0.89 ± 0.32	0.93 ± 0.29	0.80 ± 0.29	0.87 ± 0.32	1.32	0.2687
APOA1/APOB	0.51 ± 0.06	0.52 ± 0.04	0.41 ± 0.17	0.65 ± 0.07	0.28	0.8372
CA (mmol/L)	2.13 ± 0.18	2.15 ± 0.22	2.20 ± 0.13	2.07 ± 0.15	3.39	0.0183
P (mmol/L)	1.12 ± 0.34	1.09 ± 0.36	1.10 ± 0.25	1.14 ± 0.48	0.37	0.7739
MG (mmol/L)	0.90 ± 0.13	0.92 ± 0.12	0.91 ± 0.04	0.92 ± 0.15	0.46	0.7095
CO2CP (mmol/L)	24.73 ± 3.60	24.14 ± 4.13	24.08 ± 3.66	22.62 ± 4.23	3.81	0.0105
K (mmol/L)	5.82 ± 5.53	5.60 ± 4.80	4.63 ± 0.64	5.23 ± 3.69	0.28	0.8398
NA (mmol/L)	129.46 ± 37.06	131.48 ± 33.99	139.22 ± 2.57	131.84 ± 29.99	0.19	0.9061
CL (mmol/L)	104.97 ± 10.94	105.33 ± 11.70	103.23 ± 3.93	103.89 ± 12.05	0.34	0.7959
AG (mmol/L)	19.97 ± 24.16	19.64 ± 23.67	11.90 ± 3.42	18.56 ± 20.27	0.27	0.8459
GFR (ml/min/1.73m^2)	77.16 ± 32.59	75.00 ± 32.61	67.45 ± 17.94	73.03 ± 37.13	0.28	0.8403

numerical variables are represented using the mean ± standard deviation. PT, prothrombin time; PT-INR, prothrombin time-international normalized ratio; APTT, activated partial thromboplastin time; Fg, fibrinogen; TT, prothrombin time; WBC, white blood cell; %NEUT, percentage of neutrophils; #NEUT, neutrophil count; %LYMPH, percentage of lymphocytes; #LYMPH, lymphocyte count; %MONO, percentage of mononuclear cells; #MONO, monocyte count.; %EO, eosinophil percentage; #EO, eosinophil count; %BASO, basophil percentage; #BASO, basophil count; %LUC, percentage of unstained macrophages; #LUC, unstained macrophage count; RBC, red blood cell; HGB, hemoglobin; HCT, hematocrit; MCV, mean erythrocyte volume; MCH, mean erythrocyte hemoglobin volume; MCHC, mean erythrocyte hemoglobin concentration; RDW, erythrocyte distribution width; PLT, platelet; MPV, mean platelet volume; PDW, platelet distribution width; PCT, platelet specific volume; MPC, mean platelet component concentration; TBIL, total bilirubin; DBIL, direct bilirubin; IBIL, indirect bilirubin; TP, total protein; ALB, albumin; GLO, globulin; A/G, albumin-to-globulin ratio; ALT, alanine aminotransferase; AST, aspartate aminotransferase; ALT/AST, alanine aminotransferase to aspartate aminotransferase ratio; GGT, gamma-glutaminyl transferase; LDH, lactate dehydrogenase; ALP, alkaline phosphatase; CK, creatine kinase; CKMB, creatine kinase isoenzyme; UREA, urea; CREA, creatinine; UREA/CREA, urea to creatinine ratio; UA, uric acid; GLU, glucose; TC, total cholesterol; TG, triglyceride; HDL-C, high-density lipoprotein cholesterol; HDL-C/TC, ratio of high-density lipoprotein cholesterol to total cholesterol; LDL-C, low-density lipoprotein cholesterol; VLDL-C, very low-density lipoprotein cholesterol; APOA1, apolipoprotein A1; APOB, apolipoprotein B; APOA1/APOB, apolipoprotein A1 to apolipoprotein B ratio; CA, calcium; P, phosphorus; MG, magnesium; CO2CP, carbon dioxide binding capacity; K, potassium; NA, sodium; CL, chloride; AG, anion gap; GFR. Glomerular filtration rate.

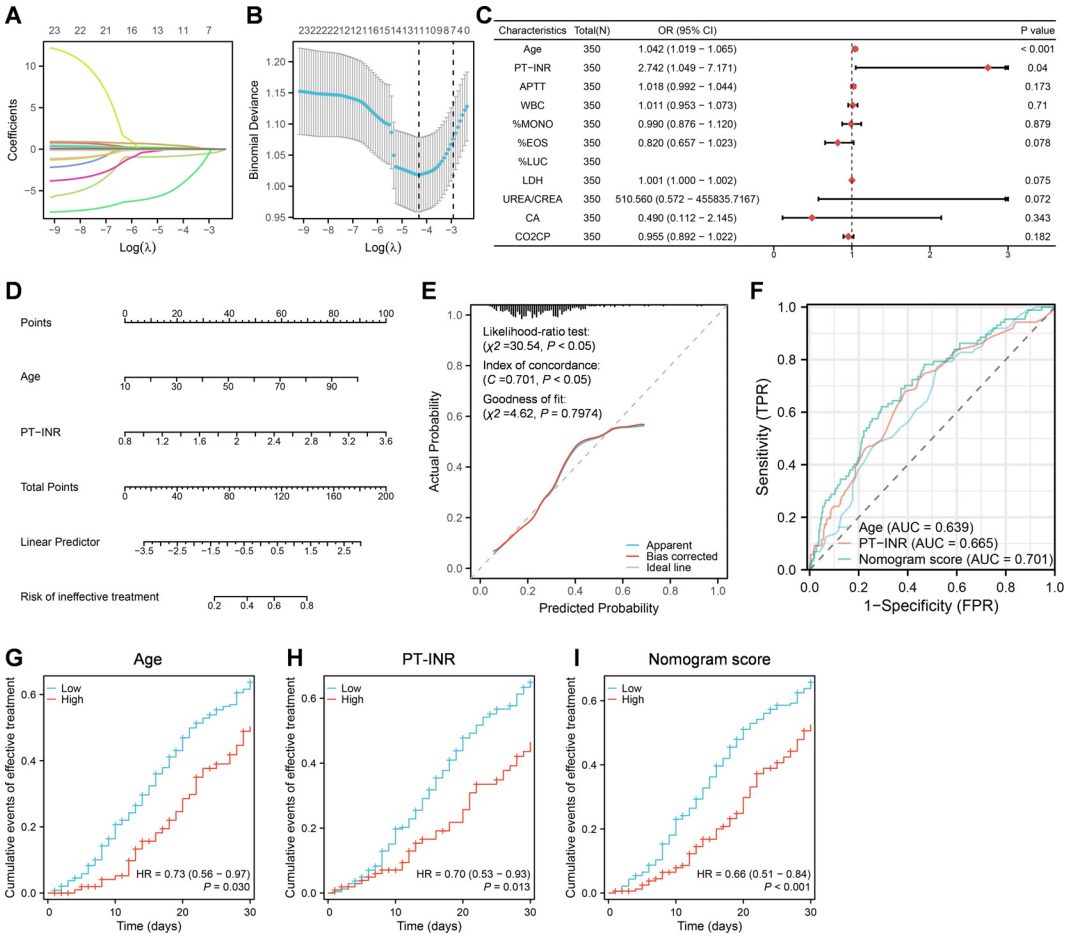

FIGURE 3
A nomogram model built based on age and PT-INR at admission for predicting prognosis post COVID-19 infection in patients with pneumonia. **(A, B)** Lasso regression analysis. **(C)** Multivariate logistic regression analysis. **(D)** Construction of nomogram model based on multivariate logistic regression analysis. **(E)** Construction of calibration curves for the nomogram model. **(F)** Construction of ROC curves for nomogram scores, age, and PT-INR, respectively. **(G-I)** Cumulative events of effective treatment within 30 days of hospitalization based on cox regression analysis.

P = 0.030) and lower PT-INR levels (low vs high, mean HR = 0.70, P = 0.013) were correlated with a more favorable prognosis within 30 days of hospitalization in patients with pneumonia. Furthermore, pneumonia patients with lower model scores also exhibited improved outcomes within 30 days of hospitalization (low vs high, mean HR = 0.66, $P < 0.001$).

30 The constructed nomogram model is validated for evaluating prognosis within 30 days of hospitalization in 311 patients post COVID-19 infection

Furthermore, we utilized the constructed nomogram models to evaluate the prognosis of 311 patients in the validation set within 30 days of hospitalization. The cox regression analysis was employed to analyze prognosis by evaluating the cumulative events of treatment effectiveness within 30 days of hospitalization (Figure 4). The findings indicated that in all 311 patients, younger age (low vs high, mean HR = 0.57, $P < 0.001$), lower PT-INR levels (low vs high, mean HR = 0.69, P = 0.003), and the absence of pneumonia (pneumonia vs absence of pneumonia, mean HR = 1.74 or absence of pneumonia vs pneumonia, mean HR = 1/1.74 = 0.57, $P < 0.001$) were correlated with a more favorable prognosis within 30 days of hospitalization (Figure 4A). Furthermore, patients with lower model scores exhibited improved outcomes within 30 days of hospitalization (low vs high, mean HR = 0.54, $P < 0.001$) (Figure 4A). Moreover, in patients with pneumonia, except PT-INR, the younger age (low vs high, mean HR = 0.59, $P < 0.001$) and lower model scores (low vs high, mean HR = 0.55, $P < 0.001$) were also correlated with a more favorable prognosis within 30 days of hospitalization (Figure 4B).

Discussion

The outbreak of coronavirus disease 2019 (COVID-19) caused by severe acute respiratory syndrome coronavirus 2 (SARS-CoV-2) has resulted in high morbidity and mortality rates worldwide. As of December 19, 2021, COVID-19 has impacted 273 million people and resulted in over 5.3 million deaths (Zhang et al., 2022). SARS-

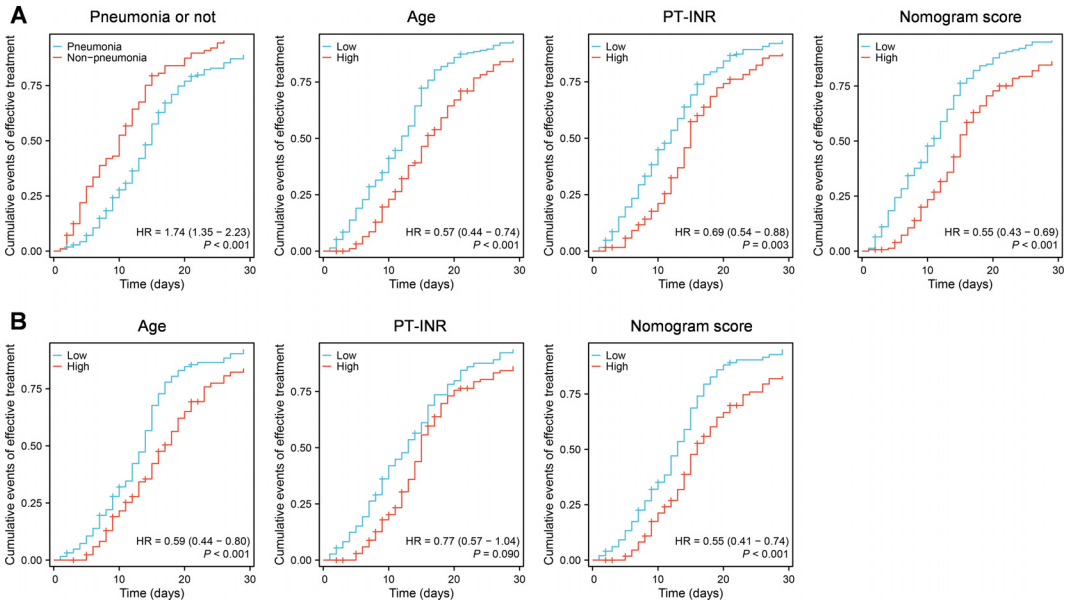

FIGURE 4
The validation of the constructed nomogram models for evaluating prognosis. **(A)** The validation of the constructed nomogram model incorporating the presence of presence/absence of pneumonia, age and PT-INR. **(B)** The validation of the constructed nomogram model incorporating age and PT-INR.

CoV-2 infection may initially be asymptomatic, until severe pneumonia, respiratory distress, organ dysfunction, and even death occur (Li et al., 2020), raising questions regarding the risks and protective factors of COVID-19. In this study, we utilized large-scale clinical data to compare the differences in clinical characteristics among different prognostic groups at admission and attempted to develop a model for predicting patient outcomes.

This study compared the clinical characteristics of different prognostic groups at admission and found a correlation between the presence of presence/absence of pneumonia, gender, age, and 35 laboratory biomarkers with clinical outcomes (Table 1). In addition, to further explore death - related factors, we divided the subjects in Tables 1 and 2 into a death group and a non-death group (including the cured, improved, and unimproved groups), and created Tables 3 and 4 as Supplementary Materials. Our current study demonstrated that older age, male gender, and the presence of pneumonia were closely associated with poor prognosis, consistent with previous research findings (Fauci et al., 2020). COVID-19 has been reported to cause coagulation dysfunction, characterized by significant elevation of D-dimer and fibrinogen, mild thrombocytopenia, and mild prolongation of PT/APTT (Lim and McRae, 2021). In this study, we found elevation of fibrinogen and PT-INR, reduction of PLT, and prolongation of PT, APTT and TT in patients with a poor prognosis. Some researchers have reported that COVID-19 could also cause alterations in hemogram of patients (Wang et al., 2020; Zhao et al., 2021). The current study displayed that significant reduction of %EOS, #EOS, %LYMPH, and %MONO but significant elevation of % NEUT and #NEUT at admission in dead cases. Besides, we also identified several biochemical indicators at admission, including TP, ALB, ALT, AST, LDH, CK, CKMB, UREA, CREA, GLU, TC, LDL-C, APOA1, CA, and CO_2CP, that exhibited significant alterations in patients with adverse prognosis, particularly in fatal cases. These biochemical changes suggested that multi-organ involvement might be a major contributing factor to poor prognosis in patients. Together, these observations provide a detailed analysis of the clinical characteristic differences at admission among different prognostic groups, offering a data-driven support for clinicians in assessing the severity of patients' conditions.

Based on the analysis of variance, lasso regression, and logistic regression, we found that the presence of pneumonia, older age, and higher PT-INR at admission were the most important prognostic indicators for COVID-19 patients. Moreover, older age and higher PT-INR were also important prognostic indicators for COVID-19 patients with pneumonia. Although the prognostic indicators for patients with COVID-19 and pneumonia show limited predictive capability, with individual AUC values for age and PT-INR falling below 0.7, our study demonstrates that by constructing a multivariable model that incorporates both age and PT-INR, the overall predictive ability of the model exceeds 0.7. This indicates that while the predictive power of certain individual factors may be limited, their combination in a multivariable model can significantly enhance predictive performance. This underscores the importance of utilizing multivariable models in clinical predictions. Clearly, existing studies have shown that the presence of pneumonia is one of the main causes of mortality in COVID-19 patients (Wiersinga et al., 2020; Zhang et al., 2022). The findings of O'Driscoll et al. demonstrated that in the population studied, the fatality rate of SARS-CoV-2 infection increased with age, beginning as early as 5 years old (O'Driscoll et al., 2021), which highlighted the significant influence of age on the prognosis of SARS-CoV-2 infection and was consistent with the experimental outcomes in our study. Similar to our findings, several studies reported a

significant increase in PT-INR in COVID-19 patients with poor prognosis (Aminasnafi et al., 2022; Ceci et al., 2023; Wu et al., 2023), suggesting that liver involvement might be a major factor contributing to COVID-19 mortality. Collectively, these findings highlight the close relationship between age, PT-INR, and poor prognosis in COVID-19 patients, and it is the first to establish a predictive model based on age and PT-INR. Several studies (Martin-Rodriguez et al., 2022; Wibisono et al., 2022) have demonstrated that the National Early Warning Score version 2 (NEWS2) can effectively predict clinical deterioration and hospitalization outcomes in COVID-19 patients, particularly in emergency and inpatient settings. Its simplicity and ease of use make it an ideal tool for initial screening in clinical practice. However, based on the analyses presented in Supplementary Figures S1 and S2, we found that the ROC score of the NEWS2 assessment from our observed case records was lower than that of our model, indicating that our study's model has relatively good predictive performance. Our study has several limitations. It is currently a single-center retrospective study, and further validation of our model's efficacy will require a multicenter approach. Additionally, due to incomplete data collection, we were unable to conduct a correlation analysis between the symptoms of COVID-19 patients and the severity of their condition.

In conclusion, this study emphasizes the strong correlation between age, PT-INR at hospital admission, and patient prognosis. The prognostic model developed based on age and PT-INR can effectively identify patients at higher risk of poor outcomes. Our findings enhance the understanding of COVID-19 disease characteristics and provide valuable guidance for clinical management and treatment.

Data availability statement

The raw data supporting the conclusions of this article will be made available by the authors, without undue reservation.

Ethics statement

The studies involving humans were approved by the Ethics Committee of the First Affiliated Hospital of Fujian Medical University. The studies were conducted in accordance with the local legislation and institutional requirements. Written informed consent for participation was not required from the participants or the participants' legal guardians/next of kin in accordance with the national legislation and institutional requirements.

Author contributions

YX: Formal Analysis, Investigation, Writing – original draft. MT: Data curation, Validation, Resources, Writing – review & editing. ZG: Formal Analysis, Writing – original draft. YL: Funding acquisition, Investigation, Writing – original draft. HG: Writing – review & editing. FF: Writing – review & editing. LLi: Data curation, Writing – review & editing. YS: Data curation, Writing – review & editing. LLa: Software, Writing – review & editing. YP: Validation, Writing – review & editing. XT: Validation, Writing – review & editing. WY: Software, Writing – review & editing. ZL: Visualization, Writing – review & editing. JS: Writing – review & editing. LW: Writing – review & editing. WC: Data curation, Validation, Resources, Writing – review & editing. YF: Funding acquisition, Methodology, Writing – review & editing.

Funding

The author(s) declare that financial support was received for the research and/or publication of this article. This work was supported by grants from the National Natural Science Foundation (82202596), Joint Funds for the Innovation of Science and Technology, Fujian Province (2023Y9022), and Fujian Provincial Natural Science Foundation of China (2020J05281, 2022D009).

Acknowledgments

We thank all the participants who agreed to take part in this study.

Conflict of interest

The authors declare that the research was conducted in the absence of any commercial or financial relationships that could be construed as a potential conflict of interest.

Publisher's note

Supplementary material

The Supplementary Material for this article can be found online at: https://www.frontiersin.org/articles/10.3389/fcimb.2025.1499154/full#supplementary-material

References

Aminasnafi, A., Heidari, S., Alisamir, M., Mirkarimi, M., Namehgoshayfard, N., and Pezeshki, S. M. S. (2022). Hematologic evaluation of children with COVID-19 infection: mortality biomarkers. *Clin. Lab.* 68 (4). doi: 10.7754/Clin.Lab.2021.210746

Ceci, F. M., Ferraguti, G., Lucarelli, M., Angeloni, A., Bonci, E., Petrella, C., et al. (2023). Investigating biomarkers for COVID-19 morbidity and mortality. *Curr. topics medicinal Chem.* 23, 1196–1210. doi: 10.2174/1568026623666230222094517

Chen, R., Sang, L., Jiang, M., Yang, Z., Jia, N., Fu, W., et al. (2020). Longitudinal hematologic and immunologic variations associated with the progression of COVID-19 patients in China. *J. Allergy Clin. Immunol.* 146, 89–100. doi: 10.1016/j.jaci.2020.05.003

Coomes, E. A., and Haghbayan, H. (2020). Interleukin-6 in Covid-19: A systematic review and meta-analysis. *Rev. Med. Virol.* 30, 1–9. doi: 10.1002/rmv.v30.6

Fauci, A. S., Lane, H. C., and Redfield, R. R. (2020). Covid-19 — Navigating the uncharted. *New Engl. J. Med.* 382, 1268–1269. doi: 10.1056/NEJMe2002387

Gilbert, M., Pullano, G., Pinotti, F., Valdano, E., Poletto, C., Boelle, P. Y., et al. (2020). Preparedness and vulnerability of African countries against importations of COVID-19: a modelling study. *Lancet (London England)* 395, 871–877. doi: 10.1016/S0140-6736(20)30411-6

Li, G., Fan, Y., Lai, Y., Han, T., Li, Z., Zhou, P., et al. (2020). Coronavirus infections and immune responses. *J. Med. Virol.* 92, 424–432. doi: 10.1002/jmv.25685

Lim, M. S., and McRae, S. (2021). COVID-19 and immunothrombosis: Pathophysiology and therapeutic implications. *Crit. Rev. Oncology/Hematol.* 168, 103529. doi: 10.1016/j.critrevonc.2021.103529

Martin-Rodriguez, F., Sanz-Garcia, A., Ortega, G. J., Delgado-Benito, J. F., Garcia Villena, E., Mazas-Perez-Oleaga, C., et al. (2022). One-on-one comparison between qCSI and NEWS scores for mortality risk assessment in patients with COVID-19. *Ann. Med.* 54, 646–654. doi: 10.1080/07853890.2022.2042590

O'Driscoll, M., Ribeiro Dos Santos, G., Wang, L., Cummings, D. A. T., Azman, A. S., Paireau, J., et al. (2021). Age-specific mortality and immunity patterns of SARS-CoV-2. *Nature* 590, 140–145. doi: 10.1038/s41586-020-2918-0

O. World Health (2021). *COVID-19 clinical management: living guidance, 25 January 2021* (Geneva: World Health Organization).

Rothan, H. A., and Byrareddy, S. N. (2020). The epidemiology and pathogenesis of coronavirus disease (COVID-19) outbreak. *J. Autoimmun.* 109, 102433. doi: 10.1016/j.jaut.2020.102433

Rubin, E. J., Baden, L. R., and Morrissey, S. (2020). Audio interview: A look at covid-19 prevention and care in 2020. *New Engl. J. Med.* 383, e147. doi: 10.1056/NEJMe2036225

Shi, Y., Yu, X., Zhao, H., Wang, H., Zhao, R., and Sheng, J. (2020). Host susceptibility to severe COVID-19 and establishment of a host risk score: findings of 487 cases outside Wuhan. *Crit. Care* 24, 108. doi: 10.1186/s13054-020-2833-7

Wang, D., Hu, B., Hu, C., Zhu, F., Liu, X., Zhang, J., et al. (2020). Clinical characteristics of 138 hospitalized patients with 2019 novel coronavirus-infected pneumonia in Wuhan, China. *JAMA* 323, 1061–1069. doi: 10.1001/jama.2020.1585

Wibisono, E., Hadi, U., Bramantono,, Arfijanto, M. V., Rusli, M., Rahman, B. E., et al. (2022). National early warning score (NEWS) 2 predicts hospital mortality from COVID-19 patients. *Ann. Med. Surg. (Lond)* 76, 103462. doi: 10.1016/j.amsu.2022.103462

Wiersinga, W. J., Rhodes, A., Cheng, A. C., Peacock, S. J., and Prescott, H. C. (2020). Pathophysiology, transmission, diagnosis, and treatment of coronavirus disease 2019 (COVID-19). *Jama* 324, 782. doi: 10.1001/jama.2020.12839

Wu, P. J., Feng, I. C., Lai, C. C., Ho, C. H., Kan, W. C., Sheu, M. J., et al. (2023). The mortality of hospitalized patients with COVID-19 and non-cirrhotic chronic liver disease: a retrospective multi-center study. *PeerJ* 11, e16582. doi: 10.7717/peerj.16582

Zhang, J.-j., Dong, X., Liu, G.-h., and Gao, Y.-d. (2022). Risk and protective factors for COVID-19 morbidity, severity, and mortality. *Clin. Rev. Allergy Immunol.* 64, 90–107. doi: 10.1007/s12016-022-08921-5

Zhao, L., Zhang, Y. P., Yang, X., and Liu, X. (2021). Eosinopenia is associated with greater severity in patients with coronavirus disease 2019. *Allergy* 76, 562–564. doi: 10.1111/all.14455

frontiers | Frontiers in Cellular and Infection Microbiology

TYPE Review
PUBLISHED 08 May 2025
DOI 10.3389/fcimb.2025.1572547

OPEN ACCESS

EDITED BY
Shakila Harshavardhan,
Madurai Kamaraj University, India

REVIEWED BY
Ana Margarida Vigário,
Universidade da Madeira, Portugal
Shainaba A Saadhali,
National Institute of Research in Tuberculosis (ICMR), India

*CORRESPONDENCE
Garima Khare
garimakhare@south.du.ac.in

†These authors have contributed equally to this work

RECEIVED 07 February 2025
ACCEPTED 04 April 2025
PUBLISHED 08 May 2025

CITATION
Nangpal P, Nagpal NL, Angrish N and Khare G (2025) Model systems to study *Mycobacterium tuberculosis* infections: an overview of scientific potential and impediments.
Front. Cell. Infect. Microbiol. 15:1572547.
doi: 10.3389/fcimb.2025.1572547

Model systems to study *Mycobacterium tuberculosis* infections: an overview of scientific potential and impediments

Prachi Nangpal, Neha Lalwani Nagpal†, Nupur Angrish† and Garima Khare*

Department of Biochemistry, University of Delhi, New Delhi, India

Despite years of global efforts to combat tuberculosis (TB), *Mycobacterium tuberculosis* (*Mtb*), the causative agent of this disease, continues to haunt the humankind making TB elimination a distant task. To comprehend the pathogenic nuances of this organism, various *in vitro, ex vivo* and *in vivo* experimental models have been employed by researchers. This review focuses on the salient features as well as pros and cons of various model systems employed for TB research. *In vitro* and *ex vivo* macrophage infection models have been extensively used for studying *Mtb* physiology. Animal models have provided us with great wealth of information and have immensely contributed to the understanding of TB pathogenesis and host responses during infection. Additionally, they have been used for evaluation of anti-mycobacterial drug therapy as well as for determining the efficacy of potential vaccine candidates. Advancements in various 'omics' based approaches have enhanced our understanding about the host-pathogen interface. Although animal models have been the cornerstone to TB research, none of them is ideal that gives us a complete picture of human infection, disease and progression. Further, the review also discusses about the newer systems including three dimensional (3D)-tissue models, lung-on-chip infection model, *in vitro* TB granuloma model and their limitations for studying TB. Thus, converging information gained from various *in vitro* and *ex vivo* models in tandem with *in vivo* experiments will ultimately bridge the gap that exists in understanding human TB.

KEYWORDS

tuberculosis, animal models, omics-based approaches, host-pathogen interactions, cellular models

1 Introduction

Tuberculosis (TB) remains a leading cause of death by a single infectious agent, claiming an estimated 1.09 million deaths among HIV-negative people and an estimated 161,000 deaths among HIV-positive people in the year 2023 (WHO Global TB report, 2024). A total of 1.25 million deaths in 2023 was observed, which was lower than the number of deaths observed in the year 2019. However, this reduction in total number of TB deaths was calculated to be 23% between 2015 and 2023, which is far from the desired milestone of the WHO End TB Strategy (a 75% reduction between 2015 and 2025) (WHO End Strategy). Unawareness among the common people is one of the main causes for non-compliance and non-adherence observed to the TB treatment, which often leads to emergence of multidrug and extensively drug-resistant strains. In 2023, 400,000 individuals developed MDR/RR-TB worldwide, with 150,000 deaths due to multidrug-resistant TB. Thus, elimination of TB is an urgent matter and requires global efforts to attain the targets of 90% reduction in TB incidence, with fewer than 100 cases per million people by 2035, as per the WHO End TB Strategy (WHO End Strategy). Achieving these targets demand the requirement of developing novel and effective TB vaccines, improved diagnostic measures and better therapeutics.

Mycobacterium tuberculosis (*Mtb*) is an extremely successful pathogen that has daunted the mankind since ages. The wide clinical outcomes that are experienced on *Mtb* infection complicate our understanding on the host-pathogen interface as well as the immune responses required to eliminate the pathogen. Few individuals do not get infected at all despite being exposed to *Mtb* reflecting the importance of strong innate immune defenses (Figure 1) (Stead et al., 1990; van Crevel et al., 2002; Simmons et al., 2018; Kroon et al., 2020; Boom et al., 2021; Aiello et al., 2023). However, most of the individuals who get infected with *Mtb*, enter into latency (LTBI) and control the infection in a few intact granulomas. These individuals are tuberculin skin test (TST) positive and about 5-10% of these individuals are at risk of developing active TB during their lifetime (van Crevel et al., 2002; Bucsan et al., 2019). Besides, certain other underlying health conditions including diabetes, HIV infection or immunotherapies pose a significant risk of reactivation TB in LTBI individuals (Miller and Ernst, 2009; Kwan and Ernst, 2011; Ai et al., 2016; Bucsan et al., 2019; Tezera et al., 2020a; Salindri et al., 2021). 5-10% of the

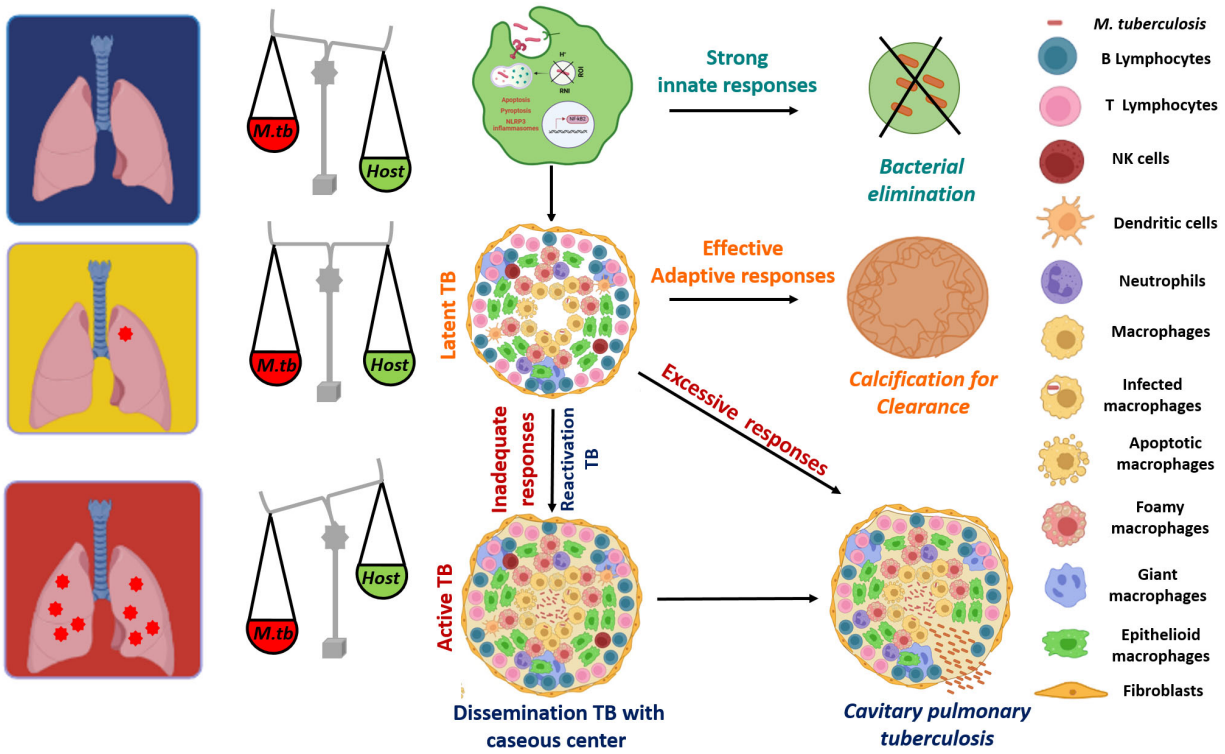

FIGURE 1
A wide spectrum of clinical fates of *Mtb* infection: Alveolar macrophages are the first cells to get exposed to *Mtb* and hence are the most important line of defense that decides the fate of the infection. Many individuals do not get infected with *Mtb*, due to the robust innate immunity that leads to an efficient activation of macrophages, resulting in a stronger anti-mycobacterial response and elimination of the pathogen. However, most of the individuals who get infected with *Mtb* enter into latency (Latent TB) and an effective adaptive response is able to control the infection in a few intact granulomas consisting of various immune cells that act as safeguards to contain the infection. With a successful adaptive response, some latent individuals also sterilize the infection via calcification. Some 5-10% of infected individuals develop active TB with cavitary pulmonary tuberculosis becoming a potential source of transmitting the pathogen to other uninfected individuals. In addition, ~ 90% of the active TB cases are results of reactivation of latent infections, due to the immune comprised status (HIV infection, anti-TNF-α therapies) of these individuals and thus, with inadequate immune responses, granulomas become necrotic with a caseous center (soft, cheese-like appearance), which results in dissemination of the infection to other parts of the host system. The figure is prepared by using BioRender.com.

individuals who get infected with *Mtb* develop the active full-borne disease and are potential sources of transmitting the pathogen to the uninfected individual (Acharya et al., 2020).

Mtb is transmitted to the uninfected host via the aerosols propelled by the patient's cough. The bacilli reaches the alveoli where it infects the alveolar macrophages, the first cells to get exposed to the pathogen. Recognition of *Mtb* by various PRRs (pattern recognition receptors) leads to phagocytosis of pathogen and induction of a plethora of innate responses (Liu et al., 2017; Chai et al., 2020; Boom et al., 2021; Chandra et al., 2022). Subsequently, macrophage activation stimulates the anti-mycobacterial defenses including acidification of the infected phagosomes, ROI and RNI stress, apoptosis and production of proinflammatory cytokines (Liu et al., 2017; Boom et al., 2021). However, being a smart pathogen, *Mtb* has premeditated its machinery to evade the host antibacterial artillery and finally persist inside macrophages as an intracellular pathogen. Various *Mtb* proteins are known to inhibit the assembly as well as the acquisition of the NADPH oxidase on the infected phagosomes, thereby reducing the generation of reactive oxygen species (Sun et al., 2013; Köster et al., 2017; Srivastava et al., 2019). It has also devised its own detoxification system based on *katG* to quench the oxidative radicals (Ng et al., 2004). In addition, *Mtb* expresses proteins that prevent the fusion of phagosomes to lysosomes, thus, stalling the delivery of the bacteria to the lysosomes (Puri et al., 2013; Pradhan et al., 2018). *Mtb* also encodes proteins that help the pathogen survive the acidic conditions faced inside the phagosomes (Vandal et al., 2009; Singh et al., 2019). Besides, virulent *Mtb* induces necrosis of infected macrophages in order to enhance its spread to other macrophages to ultimately increase bacterial replication (Divangahi et al., 2013). The pathogen induced dysregulation of the antibacterial responses mark the rapid division of *Mtb* until the adaptive immune responses come into the picture.

Following the macrophage infection, other innate cells such as neutrophils, dendritic cells and natural killer cells also traffic to the site of infection in an attempt to effectively control the pathogen (Ravesloot-Chávez et al., 2021; Sankar and Mishra, 2023). Dendritic cells are key players in disseminating the bacteria to the draining lymph node where they present *Mtb* antigens to prime the T cells (Marino et al., 2004). Following priming, an adaptive immune response is mounted, which includes the involvement of various immune cells like CD4+, CD8+ T and B-cells. Moreover, CD4+ T cell responses play a major role in anti-TB immunity, as depletion of these cells such as in the case of HIV infection, renders an individual more susceptible to tuberculosis. These CD4+ T cells differentiate further leading to the generation of effector and memory T cells. Trafficking of these effector T cells and other immune cells to the lungs initiate the cell-mediated responses that ultimately lead to granuloma formation (Chandra et al., 2022). Granulomas are pivotal to TB immunity, which are well-organized and structured complex, comprising of collection of various immune cells such as macrophages, neutrophils and lymphocytes surrounded by fibrinogen and collagen (Chai et al., 2020). As the infection progresses, macrophages within the granulomas mature to differentiate into various phenotypes including differentiated or epithelioid macrophages, foamy macrophages, and multinucleated (or Langhans) giant cells (MNGCs) (Ndlovu and Marakalala, 2016; Chai et al., 2020). A successful adaptive response will either control the infection within these stable granulomas (latent TB) or sometimes even sterilize the infection leading to sclerotic and calcified granulomas (Chandra et al., 2022). In latent infections, granulomas halt the bacterial replication and spread, however, are unable to eliminate the pathogen (Luies and Du Preez, 2020; Alsayed and Gunosewoyo, 2023). Thus, *Mtb* can survive in this conducive niche in a non-replicating state for decades (Luies and Du Preez, 2020; Alsayed and Gunosewoyo, 2023). These individuals are at a lifetime risk of reactivation, which is estimated to be around 5-10%, with most of the reactivation TB cases observed to be within the first five years of initial infection (WHO; Martin et al., 2021). Infact, ~90% of the active TB cases are due to reactivation of latent infections (Jilani et al., 2020; Martin et al., 2021). In individuals with inadequate adaptive response in case of HIV infections, newborns or people undertaking anti-TNF-α therapies, granulomas become necrotic with a caseous center (soft, cheese-like appearance), which results in dissemination of the infection to other parts of the host (Solovic et al., 2010; Tornheim and Dooley, 2017; Chandra et al., 2022). Moreover, an excessive immune response can be detrimental rather than beneficial for the host, leading to worsened pathology, which is associated with cavitary pulmonary disease (Figure 1) (Comstock et al., 1974; Kaufmann, 2003; Tezera et al., 2020b). Infact, it is observed that as granuloma matures, *Mtb* influences the differentiation of the macrophages to foamy phenotype characterized by the accumulation of lipid bodies (Singh et al., 2012; Agarwal et al., 2021). These lipid bodies, which are induced by the pathogen by modulating lipolysis of the neutral lipids serve as both a nutrient source and a privileged niche for its replication (Singh et al., 2012). Thus, these foamy macrophages contribute to both bacterial sustenance and tissue pathology, which ultimately leads to cavitation. Thus, an inadequate immune response or an excessive host response leads to different forms of active TB (Tezera et al., 2020b). Due to such wide variety of clinical presentations that can be experienced upon *Mtb* infections, we currently lack knowledge about the immunological determinants that can distinguish between protection and pathology (Figure 1). The lack of information on the protective responses that can lead to containment or elimination of the pathogen along with those that can be detrimental to the host is a significant roadblock to the development of novel preventive vaccines against TB.

Animal models have been instrumental in providing a platform to increase our repertoire of knowledge on immune mechanisms and pathology driving factors. Much of our learning about the bacterial as well as host traits involved in TB infection and progression have come from the experiments conducted in various animal models. Although several animal models for TB exist including mouse, guinea pigs, non-human primates (NHPs) and rabbits etc., unfortunately, none of them recapitulates the complete picture of the pathological features of human TB disease. In this review, an attempt has been made to describe the pros and cons of various animal models along with a comparison of

the respective pathological features they demonstrate and their usage for various aspects of TB research. Further, advancements made in the "omics-based approaches" have also been extremely beneficial in giving us insights into various host-pathogen interactions that are useful in developing host-directed therapies, are also discussed in the review.

2 *In vivo* models for TB research

Human samples from various healthy individuals and TB patients (active, latent, household contacts) are definitely the preferred choice for gaining real insights into various stages of *Mtb* infection. However, the limitations associated with human samples are the availability issues, the invasive procedures required to obtain the biopsies and ethical regulations that confine their usage (Soldevilla et al., 2022). Experimental animal models have been paramount in TB research and have provided valuable information about the pathogenesis as well as TB immunity. Apart from advancing knowledge on basic sciences, they have also been extensively employed as powerful research tools for translational research, including vaccine and drug testing. For instance, mouse model of experimental TB has been employed for rapid screening of compounds for their anti-TB activity due to the ease of delivering drugs orally. Moreover, guinea pigs are considered suitable for vaccine testing because of the immunological similarities they share with human disease. Infact, NHPs display clinical symptoms as well as granuloma structures similar to a human TB patient, making them a pragmatic and rational choice for studying immunological parameters and mechanisms (Zhan et al., 2017).

2.1 Mouse

Till date, the mouse (*Mus musculus*) model has been the most extensively employed animal system, not only for TB research but also for studying many other communicable and non-communicable diseases, due to the huge practical and cost-effective advantage it brings along. Additionally, the major reasons for its broad usage are: (i) the huge genomic similarity it shares with human genome, (ii) tools for genetic manipulation and (iii) the availability of several genetic knockout mouse strains. These knockout strains have provided us useful information on identification of various genetic factors associated with TB susceptibility, various innate and adaptive immune mechanisms and host-pathogen interactions.

Cost definitely plays an important role in the wide utility of mice for conducting various kinds of research, especially in context to TB, where requirement of BSL3 facility adds additional expense. Besides, the ease of handling and genetically manipulating these animals have provided further advantage in recognizing the importance of host responses, particularly T cell immunity required for protection against TB infection. For instance, mice deficient in CD4+ T cells have impaired ability to control *Mtb* and succumb to the disease much faster than the wild type mice (Caruso et al., 1999). Additionally, mice that are unable to produce T-bet (T-box transcription factor essential to Th1-cell generation), which is associated with reduced production of IFN-γ and increased production of IL-10 and accumulation of multinucleated cells in the lungs, are susceptible to virulent *Mtb* infection (Sullivan et al., 2005). In addition, many other immune cells contributing towards host response to *Mtb* infection have been identified in the mouse model, including γδTCR T cells, NK cells and iNKT cells (Orme and Ordway, 2016).

Toll like receptors (TLRs) are family of pattern recognition receptors (PRRs) that are involved in the recognition of various pattern associated molecular patterns (PAMPs) on the invading pathogen and mounting the downstream inflammatory response. TLRs are very well studied in mice to understand their function in TB resistance. For example, TLR4-/- deficient C3H/HeJ mice showed higher bacterial burden, reduced macrophage recruitment, higher IL-10 levels and higher neutrophil counts, leading to excessive lung inflammation and reduced survival (Abel et al., 2002; Park et al., 2020). It was also demonstrated that TLR2 and TLR9 work in cooperation to provide protection against TB. A TLR2/9 double knockout mice showed increased susceptibility to *Mtb* infection, which was related to defective proinflammatory cytokine production and impaired IFN-γ recall responses, along with altered lung pathology (Bafica et al., 2005). These results from various mice studies have been extended in humans, as polymorphisms in these TLR genes result in enhanced susceptibility to TB in various populations (Ogus et al., 2004; Zaki et al., 2012; Torres-García et al., 2013; Jafari et al., 2016). Several other PRRs, including C-type lectin receptors and NOD like receptors have also been shown to be important for innate immunity, by using murine models (Divangahi et al., 2008; Wilson et al., 2015).

Other genetically modified mice have also been used to study various components of signaling cascades involved in host responses to TB. Most of the TLRs work via stimulation of the MyD88 downstream protein that leads to NFκB activation, resulting in production of proinflammatory cytokines. Thus, MyD88-/- deficient mice displayed markedly increased bacterial burden, exacerbated pulmonary inflammation and necrosis (Scanga et al., 2004). These mice also showed a reduced survival time of 42 days post *Mtb* challenge, in comparison to wild type infected mice, that showed a survival time of >180 days (Scanga et al., 2004). Much of our knowledge about various other immune components such as cytokines like IFN-γ, TNF-α, IL-12 etc., has been determined in mice, in part due to the availability of large number of immunological reagents and antibodies, standardized assays and use of flow cytometry technique. Low-dose *Mtb* infection of IFN-γ-/- deficient mice, either via aerosols or intravenously resulted in an increased number of acid fast bacilli along with heightened pathological damage and succumbed to disease faster (Cooper et al., 1993; Flynn et al., 1993). In yet another study, the use of murine model established the essentiality of TNF-α and its receptor in TB immunity (Flynn et al., 1995). Murine models have been used to establish the role of many other cytokines of innate and adaptive

immunity, including IL-12, IL-17 and IL-23 (Cooper et al., 2002; Méndez-Samperio, 2010; Okamoto et al., 2010; Torrado and Cooper, 2010; Khader et al., 2011). Infact, it was observed that children with genetic defects in IL-12/23–IFN-γ axis showed Mendelian susceptibility to mycobacterial and other infectious diseases (Filipe-Santos et al., 2006). Further, the discovery of inhalation chambers marked a new era of TB research and enabled us to study *Mtb* infection cycle through its natural route of aerosol infection.

Mice strains used for laboratory purposes for studying various infectious diseases are inbred population, which results in less heterogeneity and are generally genetically homogenous (Soldevilla et al., 2022). Several inbred strains of mice exhibit genetic variations that influence the outcome of the infection. The most commonly used mice strains are BALB/c, C57BL/6, C3HeB/FeJ, DBA/2 and 129/Sv. In general, mice are tolerant hosts and depending on which lineage is employed for the study, one can determine the degree of resistance to *Mtb* infections based on parameters like bacterial load, pathological damage and survival time (Mitsos et al., 2000; Eruslanov et al., 2005; Yan et al., 2006; Yang et al., 2021). BALB/c and C57BL/6 mice are more resistant to *Mtb* infection and demonstrate a mean survival time (MST) of more than 300 days to intravenous or aerosol *Mtb* infection (Medina and North, 1998; Beamer and Turner, 2005). On the other hand, C3HeB/FeJ, DBA/2 and 129/Sv mice are more susceptible to TB, displaying an MST of 150 days or less (Medina and North, 1998; Beamer and Turner, 2005). The differences in the susceptibility towards *Mtb* infection have been attributed to several genomic loci. Initial studies identified *Bcg (Ity, Lsh)* locus on mouse chromosome 1 to be involved in controlling the replication of antigenically unrelated intracellular pathogens in macrophages (Vidal et al., 1993; Malo et al., 1994). *NRAMP* (Natural resistance associated macrophage protein-1) was identified as one of the candidate genes belonging to the *BCG* locus. This gene encodes for a macrophage-specific transport protein, and a single mutation of glycine to aspartic acid at position 105 was observed to be associated with the susceptibility phenotype (Bcg^s) in various inbred mouse strains (Vidal et al., 1993; Malo et al., 1994). Two distinct phenotypes exist: BCG^s (susceptible) and BCG^r (resistant) to infection with various pathogens including *Salmonella typhimurium*, *mycobacterial* species and *Leishmania donovani* (Plant and Glynn, 1976; Bradley, 1977; Gros et al., 1981; Goto et al., 1989). Later it was shown that NRAMP-1 does not play a role in protection against virulent *Mtb* challenge in various mice (Medina and North, 1996; Medina and North, 1998; North et al., 1999). Although the mutation in *NRAMP-1* does not influence *Mtb* infection, it has been shown that polymorphism in the human ortholog of *NRAMP-1* play a role in human TB susceptibility in certain populations (Bellamy et al., 1998; Cervino et al., 2000; Gao et al., 2000; Ryu et al., 2000).

By crossing the inbred strains and generating the F1 and F2 hybrids, many other genetic loci were mapped. Kramnik et al. identified a new locus, *sst1* (*super susceptibility to tuberculosis-1*), by analyzing the F2 hybrids (highly susceptible C3HeB/FeJ X C57BL/6 resistant mice), which mapped on chromosome 1 (Kramnik et al., 2000). This locus was found to be distinct from that of *Nramp1*. The *sst1* locus functions to control granuloma formation and necrosis in the lungs, reducing the pulmonary damage (Kramnik et al., 2000). Subsequent studies found *ipr1* gene to be present in *sst1* locus responsible for the resistance to *Mtb* infection (Pan et al., 2005). Moreover, Yan et al. demonstrated that *sst1* locus was associated with mechanisms that were independent of inducible NO synthase in innate immunity, rather than activation and migration of Th1 cells to the lungs (Yan et al., 2007). To extend the study in humans, polymorphisms in *SP110* (the human homolog of *lpr1* gene) were correlated with susceptibility to TB disease in various West African populations (Tosh et al., 2006; Chang et al., 2018). In another study, DBA/2 mouse strain, which is highly susceptible to *Mtb* infection, exhibits progressive bacterial replication, neutrophil-dependent pulmonary damage, extensive necrosis and finally early death. The susceptibility loci were identified to chromosome 1 (designated as Tuberculosis resistance locus (*Trl-1*), 3 (*Trl-2*) and 7 (*Trl-3*) by quantitative trait loci (QTL) mapping, that results in reduced MST on intravenous challenge (Mitsos et al., 2000). Subsequently, respiratory infection of F2 hybrids (DBA/2 x C57Bl/6) with *Mtb* H37Rv revealed a major locus on chromosome 19 (*Trl-4*) to be involved in bacterial replication in the lungs (Mitsos et al., 2003). These variations at the genetic level also lead to differences in pulmonary lesions and TB-associated pathologies among these various inbred mouse strains.

BALB/c and C57BL/6 (B6) mice have been infected through the natural route of infection i.e. via aerosols, by using inhalation chambers. High-dose of aerosol infection, usually implanting more than 5000 bacterial CFU per lung, causes death in these resistant mice within 3-4 weeks of *Mtb* challenge (Rhoades et al., 1997; Hunter et al., 2023). However, moderate or low-dose of aerosol infection i.e. implanting 500-1000 CFU or 50-100 CFU per lung, allows *Mtb* to replicate exponentially for the first 2-4 weeks post-infection. During this period, infection enters into the long chronic phase with controlled replication and limited pathological damage (Rhoades et al., 1997; Turner et al., 2001; Hunter et al., 2023). This phase usually lasts for around 6 months, after which mice eventually start to succumb to TB disease (Rhoades et al., 1997; Turner et al., 2001; Hunter et al., 2023).

One of the drawbacks of these two murine models is that they fail to develop necrotic and hypoxic granulomas like in human disease. Rhoades et al. demonstrated that B6 mice infected with *Mtb*, regardless of the dose of the inoculum showed similar pathological profile in the lungs (Rhoades et al., 1997). During the course of disease progression, the granulomatous response in all the mice, irrespective of the dose of infection, falls into five categories as described by Rhoades et al., with predominantly fused and foamy macrophages surrounded by loose aggregates of lymphocytes. As the infection progresses into the chronic phase, these loosely bound lymphocytes dissipate and spread across the entire lung section. The non-necrotizing small foci formed are characterized by interstitial fibrosis rich granulomas and thickened alveolar septae. Infact, even with high dose of infection,

central necrosis was not observed, unlike in the case of granulomas observed in human patients with active TB (Rhoades et al., 1997).

Although BALB/c and B6 mice strains have been extensively employed for therapeutic testing of various anti-TB drugs and regimens, there are varying differences in the pathological responses, which do not coincide with the pulmonary lesions observed in human patient. This discrepancy leads to distinct effects of the various anti-TB drugs tested in these animal models. Microenvironments inside human granulomas, which are highly necrotic and hypoxic, influence the bacterial physiology and metabolism that can make the pathogen drug tolerant thereby impacting efficacy of the treatment (Driver et al., 2012; Irwin et al., 2016). Moreover, *Mtb* largely remains intracellular in mice granulomas in contrast to what is observed in human TB granulomas, where they are largely extracellular (Eum et al., 2010; Hoff et al., 2011). Thus, the efficacy of the drugs in terms of their ability to penetrate the fibrotic and necrotic centers, to work under hypoxic conditions and to show inhibitory effects on extracellular bacteria (which are metabolically distinct than intracellular bacteria) cannot be evaluated in these resistant models (Irwin et al., 2014).

Thus, the failure to develop necrotic and hypoxic granulomas has encouraged the use of other animal models for drug testing. The use of C3HeB/FeJ mouse model that was discovered by Igor Kramnik's group is being encouraged for drug testing (Kramnik et al., 2000). These mice have genetic mutation in the interferon-inducible 75 (*ifi75*) gene, which is an isoform of *ipr1*, making them highly susceptible to *Mtb* infection (Pan et al., 2005). C3HeB/FeJ mice develop large, caseating granulomas in the lungs, which are hypoxic following low dose aerosol infection with *Mtb* (Kramnik et al., 2000; Harper et al., 2012). Moreover, these lesions contain abundant extracellular bacilli and are enclosed by foamy macrophages containing intracellular bacilli (Driver et al., 2012; Harper et al., 2012). Infact, as the disease progresses, these lesions also show fibrosis (Harper et al., 2012). Thus, all these pathological features resemble human pulmonary lesions and represent conditions that prevail in human TB. Moreover, efficacy of various clinical anti-TB drugs were compared in both BALB/c and Kramnik mice infected with *Mtb* (Driver et al., 2012). It was observed that Kramnik mice exhibited less efficacy to monotherapy with drugs such as isoniazid (INH), rifampicin (RIF), linezolid (LZD), or pyrazinamide (PZA) than BALB/c mice. More than 99% bacteria were eliminated from BALB/c mice following PZA treatment, while no reduction in bacilli number was observed in C3He/FeJ mice (Driver et al., 2012). Further, *Mtb* infection of NOS2-/- deficient mice that are incapable of producing nitric oxide (NO) in immune cells also developed necrotic and hypoxic granulomas (Gengenbacher et al., 2017). While INH treatment of these infected mice induced drug-tolerant population with the start of the necrotic lesions, other drugs, such as pretomanid, delamanid and BTZ043 showed bactericidal activity independent of pulmonary pathology (Gengenbacher et al., 2017). Thus, these susceptible models represent a realistic tool for assessing various anti-TB drugs due to their ability to represent TB lesions pathologically similar to humans.

2.2 Guinea pigs

Guinea pigs (*Cavea porcellus*) represent one of the closest models to humans to study TB related pathology. During the 19th century, these small animals were employed to study TB and diphtheria (Padilla-Carlin et al., 2008). Infact, the famous Koch postulates were developed by using guinea pig model and are now considered essential prerequisites for identification of the causative agent of any infectious disease (Padilla-Carlin et al., 2008). Apart from using guinea pigs as model for TB, they have been widely used to study other infectious diseases such as sexually transmitted diseases, infections related to *Staphylococcus aureus* and *Legionnaires* disease (Padilla-Carlin et al., 2008). Moreover, the causative agents of both TB and diphtheria were identified by using guinea pigs, efforts of which led to Noble Prizes (Koch, 1882; Behring, 1890).

Guinea pigs share a number of immunological and hormonal features with humans, including pulmonary structure and physiology, response to corticosteroids, requirement for an exogenous supply of vitamin C and delayed-type hypersensitivity (DTH) reaction after getting exposed to any infection (Gell and Benacerraf, 1961; Claman, 1972; Ganguly et al., 1976; McMurray, 1994; Meurs et al., 2006; Padilla-Carlin et al., 2008). While gene technology advancements can produce gene knockout or knock-in lines easily in murine model, such protocols are not available for guinea pigs. Besides, the myriad of immunological reagents that are readily available for mice are unavailable for guinea pigs. Nevertheless, other methodologies including various bioassays, antibody blocking and molecular techniques to study relative gene expression are being developed to learn about various components of immune response (Kawahara et al., 2002; Yamamoto et al., 2002; Jeevan et al., 2003; Yamada et al., 2005; Banasik et al., 2019). Infact, the importance of CD1-restricted T cells in *Mtb* infections were identified in guinea pigs (Hiromatsu et al., 2002). Jain and Dey et al. developed an oligonucleotide microarray in guinea pigs to study the global transcription profile to identify disease specific signatures for pulmonary TB (Jain et al., 2012). Ordway and the group used quantitative polymerase chain reaction (qPCR) along with flow cytometry to monitor changes in lymphocyte populations in guinea pigs (Ordway et al., 2007). The group also showed that clinical strains of *Mtb* elicit different kind of immune responses, especially the induction of regulatory T cells by highly virulent strains in comparison to laboratory strains (Shang et al., 2011). Despite these tools, the immunological reagents required to monitor immune responses to vaccine candidates in guinea pigs are limited, confining their use towards protection studies (Clark et al., 2015). Nevertheless, guinea pigs remain a popular model for studying TB primarily because they are highly susceptible to TB and can get infected with aerosols at very low dose (10-30 bacilli), mimicking the human situation. During the first 3-4 weeks of infection, *Mtb* progressively grows in guinea pig lungs (active phase) before the onset of adaptive immunity and subsequent containment of the bacterial replication (Smith et al., 1970; Turner et al., 2003). Granulomas are a trademark of TB disease that defines the outcome of the infection. Early during the

infection, guinea pigs show small lesions in their lungs, often situated near the airways that consist of mainly macrophages, neutrophils and few lymphocytes (Hunter et al., 2023). At this stage, typically two weeks post-infection, lymphangitis is also observed in infected guinea pigs (Basaraba et al., 2006). By 15-20 days of infection, a typical granuloma in guinea pigs is developed consisting of epithelioid and foamy macrophages (Turner et al., 2003). This is further encapsulated by layers of lymphocytes mainly CD4+ and CD8+ T cells and subsequently calcification takes place to contain the infection and prevent bacterial spread (Turner et al., 2003). Unlike the mouse model, where the distribution of CD4+ and CD8+ T cells is discrete, these T cells are situated at the periphery in guinea pig granulomas. Finally, by 4 weeks of post-challenge, central necrosis is evident with many extracellular bacteria (Ordway et al., 2007; Hunter et al., 2023) As the disease progresses with time, infiltration of various inflammatory cells in the granulomas lead to replacement of normal lung parenchyma disrupting the local blood supply and compression of adjacent blood vessels, which lead to tissue hypoxia (Via et al., 2008; Orme and Basaraba, 2014). With time, the central necrotic core begins to show signs of wound repair, including fibrosis and dystrophic calcification (Orme and Basaraba, 2014). These remarkably similar pathological features shared with human TB disease, make guinea pigs one of the most suitable models for drug testing and vaccine efficacy assessment.

Guinea pigs are considered the gold standard for TB vaccine evaluation and serve as an initial guide. Infact, almost every vaccine candidate has been tested for its protective efficacy in this animal model before entering any clinical set up. The efficacy of various vaccine candidates and regimens can be easily assessed in guinea pigs by monitoring the reduction in the bacterial counts in the lung and spleen as well as changes in pathological damage (Williams et al., 2009). Moreover, weight loss is an indicator of the disease progression and survival time is one of the most significant parameter for vaccine efficacy (Williams et al., 2009). According to the EU cluster of TB vaccine evaluation forum, three doses of aerosol challenge are employed for vaccine efficacy testing (Williams et al., 2005). Under low dose aerosol challenge i.e., 5-10 bacilli per lung, the MST of guinea pigs infected with virulent *Mtb* is around 20 weeks (Reddy et al., 2012; Khare et al., 2013), whereas medium dose of infection i.e., ~20-50 bacilli per lung leads to rapid progression of the disease and animals succumb to TB by 30 weeks (Brandt et al., 2004; Williams et al., 2009). While high dose challenge of ~ 500-1000 bacilli, animals die within 8 to 20 weeks (Williams et al., 2005; Clark et al., 2015). Although high dose is not clinically relevant, there are few vaccines, which have been tested at this dose (Jain et al., 2008).

The main focus of evaluating the protective efficacy is to show that the new vaccine candidate imparts better protection than BCG control in guinea pigs. Many different kinds of vaccines are developed based on various approaches, such as recombinant BCG, live attenuated vaccines, DNA vaccines, subunit vaccines and atypical mycobacterial strains. Several of these vaccine candidates, which are being assessed in various stages of clinical development were initially tested for their protective efficacy in guinea pigs (Brandt et al., 2004; Martin et al., 2006). In general, BCG is employed as positive control in every efficacy experiment, which reduces the bacterial counts significantly by 1.5 to 2.0 $\log_{10}$ and effectively prolongs the survival time in comparison to unvaccinated control under low-dose challenge (Grover et al., 2009; Nangpal et al., 2017). Thus, any new vaccine candidate that shows better efficacy in comparison to BCG vaccination stands a chance to go further for downstream development.

In addition, various *Mtb* knockout strains are employed for infection of guinea pigs, not only to study their role in virulence and survival of the pathogen, but also to validate these virulence factors as important drug targets. Many *Mtb* genes involved in cell wall biosynthesis, DNA related processes, acidic resistance genes, energy metabolism, evasion of host immunity and iron uptake systems etc., have been validated *in vivo* in guinea pigs as crucial drug targets (Singh et al., 2003; Reddy et al., 2013; Chai et al., 2020). Guinea pigs also played an important role in identifying several auxotrophic *Mtb* mutants that were shown to be attenuated in these animals, as potential vaccine candidates. For instance, *bioA* mutant of *Mtb*, administered either via aerosols or intradermally, shows severe attenuation in guinea pigs (Kar et al., 2017). Immunization of guinea pigs with *Mtb*ΔbioA induced significant protection against an *Mtb* challenge, when compared with the unvaccinated animals (Kar et al., 2017). Likewise, *Mtb*ΔleuDΔpanCD auxotrophic strain, carrying two independent deletions in the essential *leuD* (Rv2987c) and *panCD* (Rv3602c and Rv3601c) loci, was shown to be immunogenic and protected guinea pigs against aerosol challenge of *Mtb* (Sampson et al., 2004).

Thus, to summarize, guinea pigs have provided us with valuable information about the pathogenesis of *Mtb* as well as virulence determinants of the pathogen. They have served as an initial platform for evaluation the efficacy of many new vaccines candidates and development of new immunological reagents and tools will help in increasing the usage of guinea pigs in future research.

2.3 Non-human primates

Non-Human Primates (NHPs) hold an evolutionary significance and share similar characteristics of TB disease to those observed in humans, making them the most reliable choice to evaluate TB vaccines. However, most of the new vaccines that are tested in NHP model are initially screened in guinea pigs and mouse for preliminary evaluation to eliminate the non-promising candidates that do not show their worth in small animals. Very few laboratories worldwide employ NHP model for conducting TB-related studies, primarily because of the high maintenance costs, handling issues, ethical limitations and the mandatory need for biocontainment facility. Different NHP species exist that are employed for studying various aspects of TB research. The clinical spectrum of TB infections in humans is vast and can be observed in NHP model as different animals show varied outcomes, including latent infection, dissemination and pneumonia (Laddy et al., 2018). Infact, the granulomas observed in NHPs also become

caseous with further liquefaction and subsequent cavitation (Laddy et al., 2018). Rhesus macaques (*Macaca mulatta*, RM) and Cynomolgus macaques (*Macaca fascicularis*, CM) are the two most commonly used NHP species for TB research. Most of the initial TB studies in the Golden Age in 1970s, were conducted in Indian RMs, which were focused on understanding the efficacy and immunogenicity of BCG vaccine (Barclay et al., 1970; Baram et al., 1971). Infact, there was one study which showed the use of ethambutol and isoniazid as TB drugs in RMs (Schmidt, 1966). After two decades of dedicated research on RMs, the use of CM was identified for TB-related studies, and since then, extensive research has been conducted on these two species to assess efficacy of novel TB vaccines, determine the therapeutic efficacy of new anti-TB drugs and understand TB pathogenesis in great detail.

These old-world monkeys (RM and CM) have been known to get infected with *Mtb* and develop human-like disease, however, the new world monkeys (*Callithrix jacchus*, the common marmoset) are also now employed for studying TB pathology (Via et al., 2013). These monkey strains vary in their susceptibility to *Mtb* infections and clinical outcomes. RM are more susceptible to *Mtb* infections than CM, which develop both active as well as latent tuberculosis (Maiello et al., 2018). Moreover, ultra-low-dose aerosol *Mtb* challenge along with stereological techniques to determine bacterial burden also demonstrated that RMs are more susceptible than CMs (Sharpe et al., 2016). The very first report of using CM was published by Walsh et al. in 1996, which showed that high dose of intratracheal *Mtb* challenge led to progressive fatal infection in Philippine cynomolgus monkey (Walsh et al., 1996). On the other hand, low-dose of challenge developed a chronic, slowly progressive, localized form of pulmonary TB with significant number of CMs able to contain the infection (Walsh et al., 1996). Later, low-dose challenge (10-25 CFU of *Mtb* Erdman) administered intrabronchially resulted in active disease in ~50% of CM animals, while remaining half of the animals showed no evidence of disease for 15-20 months of the study and remained clinically latent (Capuano et al., 2003; Lin et al., 2009). Infact, the same group, in their subsequent studies demonstrated that LTBI monkeys could reactivate on treatment with anti-tumor necrosis factor (anti-TNF) or depletion of CD4+ T cell or simian immunodeficiency virus (SIV) coinfection (Diedrich et al., 2010; Lin et al., 2010; Lin et al., 2012b).

Although RMs are highly susceptible to *Mtb* infections, one of the reports show evidence of latent infection in these species (Gormus et al., 2004). It was observed that RMs infected either via the aerosols or through intrabronchial instillation show similar clinical outcomes in terms of disease burden, however, exhibit variations in the pathology (Sibley et al., 2016). Both RM and CM have been employed for TB vaccine studies. It was shown that BCG vaccination of CM provided better protection to animals against *Mtb* infection in comparison to BCG immunized RM (Langermans et al., 2001). Infact, the worth of MVA85A vaccine as a booster vaccine and SO2 vaccine strain (live attenuated, phoP deficient *Mtb* mutant strain) was observed in RMs. The study showed that both the regimens involving either the SO2 strain or BCG-primed RMs boosted with MVA85A showed significant protection with reduced pathological damage and chest X-ray scores against *Mtb* Erdman challenge (Verreck et al., 2009). Moreover, the most advanced TB vaccine *MTB*VAC, which is also live attenuated *Mtb* based vaccine, was tested in RMs. A single intradermal administration of *MTB*VAC resulted in protection of these animals against aerosol challenge of *Mtb* as observed by significantly reduced pathological damage as shown by *in vivo* medical imaging, gross pathology lesion counts and pathology scores (White et al., 2021). Moreover, the immune parameters measured matched the profile that were determined in humans vaccinated with *MTB*VAC (White et al., 2021).

CMs have also been employed for TB vaccine studies especially in context to reactivation TB. For instance, multistage vaccine H56, is a subunit-based vaccine comprising of Ag85B and ESAT-6 (acute phase secretory *Mtb* proteins) fused with Rv2660c (the nutrient stress-induced antigen), given along with adjuvant IC31, was able to boost the protection of BCG-primed CMs by significantly reducing the clinical disease progression against *Mtb* challenge in CM. It was also observed that reactivation of latent infection was prevented in these vaccinated CM (Lin et al., 2012a). Another subunit vaccine M72f, formulated with AS02A adjuvant was evaluated in CMs (Reed et al., 2009). Animals immunized in BCG priming and boosting with M72f/AS02A vaccine regimen imparted better protection in comparison to BCG alone vaccination against *Mtb* challenge as measured by pathological assessment and survival time (Reed et al., 2009).

Apart from being employed for TB vaccine efficacy and immunogenicity studies, macaques are also being used for studying various aspects of TB pathogenesis, including factors that contribute to reactivation TB and various important host-pathogen interactions. For instance, transcriptomics of TB granulomatous lesions of RM with active TB was performed and it was found that early stages of infection are characterized by high levels of immune pathways related to proinflammatory cytokines, which are indeed required to contain immunopathological damage. However, during the late stages, lesions showed reduced inflammatory responses (Mehra et al., 2010). Such host profiles can be helpful in identifying markers of latency and reactivation (Mehra et al., 2010). Moreover, macaques have been successfully employed to identify important genes of *Mtb* that play crucial role in the virulence of the pathogen. *Mtb* SigH is a stress-induced transcriptional factor that is important for the pathogens survival under various *in vitro* conditions including heat, oxidative-stress, envelope damage and hypoxia. *Mtb*ΔSigH mutant strain was found to generate stronger innate responses in bone marrow derived macrophages (BMDMs) isolated from RMs in comparison to wild type *Mtb* (Dutta et al., 2012). In their subsequent study, NHPs were challenged with *Mtb* or *Mtb*ΔSigH mutant and the disease progression was monitored in both groups by using clinical, pathological, microbiological, and immunological parameters (Mehra et al., 2012). It was observed that NHPs infected with *Mtb* alone exhibited higher bacillary load along with granulomatous immunopathological damage. Moreover, all the animals rapidly succumbed to TB disease. On the contrary, NHPs exposed to the *Mtb*ΔSigH mutant did not exhibit acute tuberculosis and survived

the entire duration of the study (Mehra et al., 2012), thus, validating the importance of SigH in providing survival advantage to pathogen *in vivo*, making it a potential drug target.

Macaques are also an excellent model to study TB/SIV (simian immunodeficiency virus) coinfection, especially in context to understanding reactivation TB, since people with HIV and latent TB have higher risk of developing TB in comparison to HIV-negative latently infected individuals (Mukadi et al., 1993; Post et al., 1995). SIV infection serves as a counterpart to HIV in NHPs and have been used in number of studies employing both RM and CM. For example, SIV infection of all latently infected CM induced reactivation TB, with a variable time to reactivation (up to 11 months post-SIV), which was correlated to depletion of peripheral T cells during acute SIV infection rather than viral load (Diedrich et al., 2010). Similarly, *Mtb* infection of RM (~500 CFU *Mtb* CDC1551 via a head-only aerosol method) induced latent aymptomatic infections in these NHPs. Coinfection of the latently infected RMs with SIV significantly induced reactivation TB and showed significantly higher body temperature, CRP levels and body weight loss than the *Mtb* monoinfected group (Mehra et al., 2011). In another study published by Mattila et al., the group investigated multifunctional T cell profile and granuloma T cell responses in reactivated TB in CM model of HIV–*Mtb* coinfection (Mattila et al., 2011). They found differences in the multifunctional T cell responses in animals showing reactivation <17 weeks than in animals that reactivated >26 weeks (Mattila et al., 2011).

Thus, to recapitulate, macaques offer several advantages for being the closest to humans anatomically and physiologically. Besides, the remarkable similarities they share with human TB, representing the wide spectrum of clinical manifestations, makes these animals the most suitable for conducting TB vaccine efficacy as well as TB drug screening studies. HIV/TB coinfection is also a major health concern, and while small animals can be infected with *Mtb*, they are not the hosts for HIV infections and hence, NHPs represent an excellent model for studying TB and AIDS coinfections.

2.4 Rabbits

Rabbits (*Oryctolagus cuniculus*) have been used historically for studying various human diseases, including syphilis, TB, HIV-AIDS and acute hepatic failure etc. In 1920, Lurie and his team worked extensively on these animals to study the immunopathogenesis of TB by inbreeding various susceptible and resistant strains of rabbit and defined various pathological features, which were human like from formation of granulomas to caseous necrosis and cavitation (Lurie, 1928; Dannenberg, 2001; Dannenberg, 2009). However, these lines of rabbits no longer exist and have become extinct. The most common rabbit breed available now is the New Zealand White (NZW) rabbits, which have also been employed as models to study various aspects of TB pathology, latent tuberculosis, spinal TB and TB meningitis (Flynn et al., 2008; Manabe et al., 2008; Kaplan and Tsenova, 2010; Yue et al., 2022; Esteves et al., 2018). In general, the outbred strains of rabbits are more resistant to *Mtb* and recover within 4 to 6 months of infection (Heppleston, 1949; Lurie et al., 1952). Infact, rabbits are more resistant to *Mtb* infection in comparison to guinea pigs and mice (Gupta and Katoch, 2005). While these outbred New Zealand white rabbits are naturally resistant to *Mtb* infections, *M. bovis* infection leads to cavitary disease, which is fatal (Converse et al., 1996). The response of NZW rabbits to infection varies with *Mtb* strains being used (Manabe et al., 2003). One of the studies compared the three different strains of *Mtb*: Erdman, H37Rv, and CDC1551 for their ability to cause disease in rabbits (Manabe et al., 2003). It was observed that *Mtb* Erdman was the most virulent strain, which required the least number of bacteria to form a visible tubercle at 5 weeks post-infection in comparison to H37Rv. While most of the rabbits infected with *Mtb* H37Rv recovered within 4 to 6 months, several Erdman infected rabbits showed caseous tubercles with two of the rabbits having cavitary lesions (Manabe et al., 2003). Rabbits infected with HN878, a hyper-virulent *Mtb* strain, show heterogeneous lesions within the same animals as observed in humans (Flynn et al., 2008; Subbian et al., 2011b). CDC1551, a clinical isolate of *Mtb*, causes latent infections in rabbits, although these animals did not show any evidence of spontaneous reactivation unless immunosuppressants like corticosteroids were administered (Subbian et al., 2012). In addition, inbred strains of NZW rabbits are more susceptible to infections in comparison to outbred rabbits, giving an opportunity to understand the mechanisms underlying resistance to TB (Dorman et al., 2004). Unlike the murine model, necrotic granulomas observed in rabbit lungs also show evidence of hypoxic microenvironment (Via et al., 2008). Thus, rabbits represent a suitable model for TB related studies as it can mimic various prominent pathological features of human TB.

Rabbits infected with HN878 strain leads to TB disease with similar pathological characteristics as humans and thus, are used for studying kinetics, penetration and distribution of standard anti-TB drugs (Kjellsson et al., 2012; Via et al., 2012; Rifat et al., 2018). In one of the studies, by using onlinear mixed-effects pharmacokinetic modeling approach, it was found that INH, RIF and PYZ were much less concentrated in lesions than in plasma, while moxifloxacin was able to very well partition into lung and granulomas (Kjellsson et al., 2012). A study published by Rifat et al. measured the tissue drug distribution and penetration ability of two rifamycin antibiotics (rifampin and rifapentine) by using pharmacokinetic-pharmacodynamic (PK/PD) modeling (Rifat et al., 2018). They used rabbit model of experimental TB to show that both drugs were able to penetrate different lung lesions as well as the fibrotic wall of cavitary lesions and exhibited a penetration coefficient of ≥1 when compared to plasma (Rifat et al., 2018). However, rifampin was able to penetrate the necrotic core i.e., caseum much efficiently than rifapentine (Rifat et al., 2018). These studies also correlated well with clinical data wherein patients with cavitary lung lesions were not benefitted from rifapentine treatment (Rifat et al., 2018). Rabbits have also been employed to study the effect of immune modulation on treatment outcomes (Subbian et al., 2011a; Datta et al., 2015).

While rabbits are a model systems for studying pulmonary TB, they are also explored to understand pathogenesis of

extrapulmonary TB, including spinal TB and TB meningitis (Tsenova et al., 1998; Jia et al., 2024). Although the rabbit model is considered suitable for conducting TB research, the limited availability of validated immune reagents and the requirement of larger biocontainment facility restricts its use. Table 1 summarizes the features of various animal model systems employed for TB research, highlighting their advantages, disadvantages and their applications.

3 Omics-based approaches to understand pathogenesis via animal models

Omics-based technologies are approaches, which aim to measure and evaluate an ensemble of biomolecules together in order to understand the contribution of each molecule under investigation. They offer the advantage of being unsupervised, making them a less biased methodology that can reveal new insights into the query being addressed. Genomics, transcriptomics, proteomics, metabolomics and lipidomics are some of the commonly employed techniques which allow researchers to delve into the fundamentals of infection biology and pathogenesis (Figure 2). Besides, these techniques can be used to explore molecular mechanisms underlying a disease, understand the basis of drug resistance and also host response to an infection (Khan et al., 2019).

In addition, omics-based technology provides avenues for identifying biomarkers with therapeutic or diagnostic potentials, for rational drug designing and for developing novel vaccines (Ahamad et al., 2022; Guha et al., 2024). In particular, discovery of host signatures by comparing diseased versus uninfected groups has helped to identify diagnostic biomarkers (Burel et al., 2019). Such study designs have provided opportunities to explore host genes, proteins, metabolites or pathways that get altered upon infection, thereby gaining mechanistic understanding of the disease and providing a platform for designing host-directed therapeutics. Besides, these approaches have also been employed to elucidate global alterations that take place in the host post-treatment with a drug, giving a holistic view with regard to the

TABLE 1 Animal models employed for TB research: *pros and cons*.

Animal Model	Strains available	Advantages	Disadvantages	Applications	References
Mouse (Mus musculus)	Resistant strains: • BALB/C • C57BL/6 Susceptible strains: • C3HeB/FeJ, • DBA/2 • 129/Sv	• Cost effective • Ease of handling • Availability of knock out mice strains • Availability of immunonological reagents • Limited capacity required for housing	• Differences in the TB associated pathological features such as granuloma structure which is different in mouse as compared to human. • Do not form necrotic cores in TB lesions unlike human TB granulomas except in C3HeB/FeJ model	• TB immune response studies • Drug efficacy studies • PK-PD studies • Vaccine efficacy and immunogenicity studies • Vaccine safety studies	(Rhoades et al., 1997; Medina and North, 1998; Kramnik et al., 2000; Beamer and Turner, 2005; Pan et al., 2005; Eum et al., 2010; Hoff et al., 2011; Driver et al., 2012; Harper et al., 2012)
Guinea Pigs (Cavea porcellus)	• Dunkin Hartley	• Cost effective • Highly susceptible to tuberculosis infection • Form necrotic cores in granulomas similar to that in humans	• Non availability of immunological reagents thus, are not extensively used for studying immune parameters • Does not develop latency	• Vaccine efficacy studies • Studies related to identification of *Mtb* virulence determinants	(Turner et al., 2003; Via et al., 2008; Orme and Basaraba, 2014; Hunter et al., 2023)
Non-Human Primates	• Rhesus macaques (Macaca mulatta) • Cynomolgus macaques (Macaca fascicularis) • Callithrix jacchus, the common marmoset	• Shows similar clinical outcomes to TB infections as humans • Share similar immune response and pathological features like that observed in human TB • Can develop LTBI on *Mtb* infections	• High maintenance costs • Handling issues • Ethical limitations • Requirement of large housing capacity	• Evaluation of efficacy of novel TB vaccines • Evaluation of therapeutic efficacy of new anti-TB drugs • Studies related to TB pathogenesis • TB-HIV co-infection studies	(Barclay et al., 1970; Baram et al., 1971; Gormus et al., 2004; Diedrich et al., 2010; Mattila et al., 2011; Mehra et al., 2011; Via et al., 2013; Sibley et al., 2016; Laddy et al., 2018; Bucsan et al., 2019)
Rabbits (Oryctolagus cuniculus)	• New Zealand White (NZW)	• TB granulomas form necrotic cores and are hypoxic • Evidence of liquefaction and cavitation as observed in human TB	• High maintenance costs • Resistant to laboratory strains like H37Rv and Erdman • Requirement of large housing and bio-containment facility	• Drug and vaccine efficacy studies • Studies related to TB pathology and latent tuberculosis, • Model to study spinal TB and TB meningitis	(Tsenova et al., 1998; Manabe et al., 2003; Via et al., 2008; Subbian et al., 2011b; Jia et al., 2024)

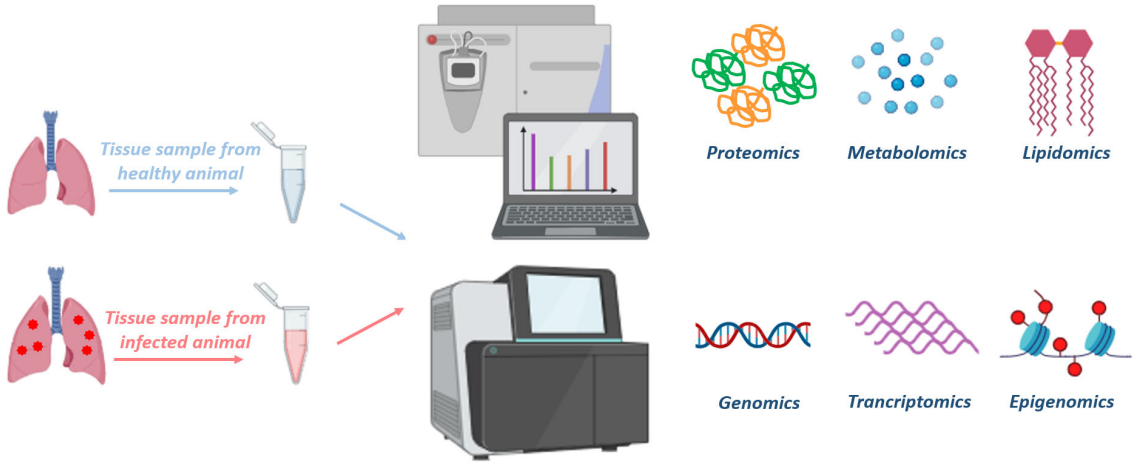

FIGURE 2
Multiple omics-based approaches to understand disease biology: Various tissue samples can be collected to isolate different biological molecules (DNA, RNA, metabolites, proteins and lipids) from animals. These tissue samples can be processed and subjected to mass spectrometry or NGS platforms to perform various omics-based approaches, such as proteomics, metabolomics, lipidomics, genomics, transcriptomics, epigenomics, respectively. Analysis of the omics data allow us to compare the differences between the disease progression and characteristics of healthy vs diseased or treated vs untreated tissue samples. Moreover, integration of multi-omics data would help us in understanding the complete spectrum of the disease, allowing the discovery of therapeutic targets and disease-biomarkers. The figure is prepared by using BioRender.com.

mechanism of action of the molecule and revealing new insights into drug activity.

Mtb infections are complex, with the host undergoing various changes at genomic, transcriptomic, and proteomic levels during the course of the disease. Additionally, the host deploys various metabolic strategies to limit the supply of nutrients to the pathogen and, in turn, limit bacterial growth. Although, to understand TB pathogenesis, *in vitro* models have been developed to represent various features of the *in vivo* conditions, such as low oxygen levels (Rustad et al., 2008), low nutrients (Betts et al., 2002) and the addition of exogenous stresses (Stewart et al., 2002; Deb et al., 2009). However, they cannot fully mimic the microenvironment that *Mtb* faces inside host cells. While macrophages have been employed for several *ex-vivo Mtb* infection experiments, the absence of interacting immune cells (eg. T cells, natural killer cells, dendritic cells) as well as the lack of the ability to form a granulomatous structure are major shortcomings of using this cell culture system (Schnappinger et al., 2003; Cappelli et al., 2006; Rachman et al., 2006a; Fontán et al., 2008; Tailleux et al., 2008; Ward et al., 2010). It is convincing to believe that *in vivo* models can closely mimic the multifarious milieu as seen in human lungs. Thus, conducting large-scale expression profiling experiments using animal models is a rational approach to identify genes required for pathogen clearance.

Transcriptomics allows quantifying the abundance and differential expression of various transcripts of an organism exposed to different conditions. Understanding the transcriptome is the key for connecting information attained from genomics to protein target expression (Talaat et al., 2004; Rachman et al., 2006b; Talaat et al., 2007). This can be applied for the identification of responses to infection or to drug exposure, and further, characterize potentially druggable pathways. Additionally, RNA profiling of both the pathogen and the host lays the basis for understanding interactions at the host-pathogen interface (Westermann et al., 2017). Host transcriptomics is one of the leading approaches to discover immune signatures between uninfected and infected host samples, which can pave the way for identification of novel biomarkers. In addition, transcriptomics also allows detection of infection-associated antigens, such as circulating and secreted host RNA (miRNA, lncRNA), blood cell-produced RNA or bacterial secreted RNA (van den Esker and Koets, 2019). Transcriptome analysis of blood samples isolated from C3HeB/FeJ mice infected with HN878 strain of *Mtb* revealed a signature that was associated with high type I interferons, activation and recruitment of neutrophils and a reduction in B lymphocyte, NK cells and T-cell effector responses, all of which leads to TB in humans (Moreira-Teixeira et al., 2020).

In another study, RNA sequencing was employed to determine the changes that occur in the host transcriptome upon *Mtb* infection. The authors had demonstrated that *Mtb* strain lacking the MenT3 and MenT4 toxins (*MtbΔment3Δment4)*, displayed severe attenuation in BALB/c mice as well as in guinea pigs (Gosain et al., 2024). Detailed host RNA-seq analysis of lung tissues, revealed increased transcripts levels of proteins that were associated with calcium signaling, apoptotic pathway and autophagy in mice infected with the mutant strain, as compared to wild type infected mice. Moreover, inflammatory responses were much reduced in animals infected with the *MtbΔment3Δment4* mutant (Gosain et al., 2024). Thus, *in vivo* RNA sequencing identified differentially expressed genes upon infection with *Mtb* and help in elucidation of the possible mechanisms behind the attenuation of the mutant strain inside the host (Gosain et al., 2024).

Since *Mtb* infection leads to alterations in the host metabolome, characterization of such changes is important as it may result in identification of host-protective pathways and thus, aid in the

development of host-directed therapies (Vrieling et al., 2020). Metabolomics offers advantages for the identification of low molecular weight metabolites (catabolites as well as anabolites) that are altered in response to various pathophysiological events in both *in vitro* and *in vivo* animal models, as well as in human patients (Frediani et al., 2014; Lau et al., 2015; Borah et al., 2021). The identified metabolites can be employed as biomarkers for diagnosis or trustworthy markers that can distinguish between unhealthy or healthly status, and for the evaluation of potential therapeutics.

In another study, TB granulomatous lung tissues were employed to evaluate the metabolic status with respect to host response in guinea pigs infected with low-dose *Mtb* H37Rv infection. Metabolite profiling performed by using 1H HRMAS (high resolution magic angle spinning) NMR spectroscopy led to the unambiguous identification of 20 distinct host metabolites involved in various cellular pathways, such as anaerobic glycolysis and TCA cycle as the infection progressed (Somashekar et al., 2011). Lactate is produced by anerobic glycolysis and its levels were found to increase from 15 days onwards (Somashekar et al., 2011). Accumulation of lactate can be considered as an index of hypoxia developed inside the granulomatous tissue as well as host tissue necrosis (Via et al., 2008; Kraut and Madias, 2014). Similarly, the increasing levels of reduced glutathione (GSH) were also observed which is considered as a measure of oxidative stress as the disease progresses. Moreover, the GSH redox system is one of the most important antioxidant defense systems for maintaining redox homeostasis in lung cells (Venketaraman et al., 2005). This study also suggested that *Mtb* utilizes host lipids for *in vivo* growth as evident from the increased levels of phosphocholine (PC), glycerophosphocholine (GPC) and a concomitant depletion of phosphatidylcholine (PtC) observed with the disease progression, indicating that free fatty acids so produced could act as carbon and energy source for intracellular *Mtb* metabolism (Somashekar et al., 2011).

Further, global metabolic changes were studied in *Mtb* H37Rv infected C57BL/6 mice by extracting metabolites from the infected lungs at 4 weeks and 8 weeks post-infection (Fernández-García et al., 2020). This untargeted MS-based lung metabolomic study revealed that high levels of trimethylamine-N-oxide (TMAO) may be undesirable for the host and may probably impact *Mtb* growth positively. Similarly, increased levels of kynurenine was also observed, which is a tryptophan degradation metabolite involved in immunomodulation. This may again exert deleterious effects on the host immune system, as it is known that inhibiting the activity of indoleamine 2,3-dioxygenase (IDO) promotes TB infection control (Routy et al., 2016; Gautam et al., 2018). A shift in metabolism towards fatty acid oxidation was observed, as evident from the depleting carbohydrates at 4-week time point as well as increasing carnitines at 9-week time point. This shift describes the ability of *Mtb* to modify host macrophages from an inflammatory phenotype to an anti-inflammatory one (Huang et al., 2015; Gaber et al., 2017). Apart from these, metabolites pertaining to amino acids, polyamines and oxido-reductive stress were also found to be modulated upon *Mtb* infection in the host (Fernández-García et al., 2020).

In another study, 1H NMR-based metabolomics was employed to conduct global profiling to characterize the responses induced in C57BL/6 mice upon virulent *Mtb* infection (Shin et al., 2011). Various metabolites associated with amino acid and nucleotide metabolism, membrane phospholipids, glycolysis and the antioxidative stress elements were found to be altered in the host upon infection. Glycogen and glucose levels were observed to be decreased, while lactate levels were elevated in the infected mice. *Mtb* can survive in a low glucose environment because it can interplay the carbon source between the β-oxidation of lipids and the glyoxylate pathway to replenish the TCA cycle intermediates (Sharma et al., 2000; Lorenz and Fink, 2001; Serafini et al., 2019). Indeed, succinate was found to be increased significantly in the organs of *Mtb* infected mice when compared to the naïve mice. Intermediates of pyrimidine and purine metabolism were found to be increased in infected mice, suggesting that active cell division takes place in *Mtb* infected organs, especially in the lungs (Reyes et al., 1982; Simmonds et al., 1997; Berg et al., 2002; Chaudhary et al., 2004; Daniel et al., 2007; Hyde, 2007; Weljie et al., 2007). Further, this was the first report to demonstrate that itaconate was increased in the lungs infected with *Mtb*. Though the reason remains unclear, it was suggested by the authors that it can inhibit isocitrate lyase, which acts as a main enzyme in the glyoxylate pathway of *Mtb* (Hillier and Charnetzky, 1981; Berg et al., 2002; Daniel et al., 2007; Shin et al., 2011).

A NMR-based metabolite profiling of lung tissues of guinea pigs infected with *Mtb* W-Beijing strains led to the identification of 16 metabolites involved in carbohydrate, membrane lipids and amino acid metabolisms that were altered (Somashekar et al., 2012). For instance, levels of lactate, choline compounds, nicotinamide, and glutamate were significantly reduced, while formate and acetate were shown to be high in the infected serum samples (Somashekar et al., 2012). The observed signatures were attributed to hypoxic TB lesions, the Warburg effect or the production of free radicals in response to infection (Venketaraman et al., 2005; Lenaerts et al., 2007; Dakubo and Dakubo, 2010; Somashekar et al., 2012; Qualls and Murray, 2016).

It has been reported that treatment with methionine sulfoximine (MSO), an irreversible inhibitor of glutamine synthetase enzymes, leads to a reduction in the bacterial load in the *Mtb* infected guinea pigs (Harth and Horwitz, 2003; Tullius et al., 2003; Harth et al., 2005). Evidences of JHU083, a glutamine (Gln) metabolism antagonist drug, has been shown to reprogramme the host immune-metabolic signatures as well as improve effector T-cell responses in various murine tumor models (Rais et al., 2016; Leone et al., 2019; Oh et al., 2020). These observations, led to the hypothesis that JHU083, apart from directly possessing antibacterial activity, may also serve as a host-directed therapy against TB by reprogramming Gln metabolism. Further, it was shown that administration of JHU083 reduced the lung bacillary load by 1.9 $\log_{10}$ CFU at 5-weeks post-treatment compared to untreated mice, and consequently prolonged the survival of

animals significantly. Moreover, LC/MS-based metabolomics of total lung tissues from untreated, JHU083-treated and RIF-treated animals led to the identification of 144 metabolites, with the most notable changes in the arginine metabolism, with a 1.4-fold increase in citrulline levels in JHU083 treated mice (Parveen et al., 2023).

A multi-tissue metabolite profiling study was conducted by using gas chromatography and mass spectrometry (GCMS) in female C57BL/6 mice (2 and 5 months old) infected with low-dose aerosol infection of *Mtb* H37Rv. It was demonstrated that distinct tissue metabolomic profiles existed between the mice of different age groups after infection, despite the lung bacillary load being similar till 6-weeks post-challenge in both the groups. In particular, a deregulated tissue-specific amino acid metabolism signature was observed in mice of different age groups, with the signature being more pronounced in the 5-months old mice. Additionally, it was proposed that the older age group mice could more efficiently control the infection due to reduced levels of mannose detected in their lungs, which is one of the sugars that is required for *Mtb* growth. The authors also suggested that targeting amino acid metabolic pathways could be helpful in developing adjunctive therapies (Pahwa et al., 2024). Considering the above-mentioned studies, it seems that metabolomics could be a potentially valuable tool in enhancing our understanding of TB disease by determining unique metabolic signatures that arise in specific conditions and also aid in the development of adjunctive host therapies against TB.

Since its inception, proteomics has gained considerable attention as it provides detailed insights into cellular processes, which cannot be apprehended by genomics or transcriptomics (Southan, 2004; Gengenbacher et al., 2014; Bisht et al., 2019). Proteomic profiling allows identification of proteins, which get altered upon specific conditions such as, after infection or upon treatment, thereby, aiding in identification of biomarkers for diagnosis, treatment or prevention of a disease (Kanabalan et al., 2021). However, due to the complexity of analyses and its sensitivity, the application of proteomics has yet to reach a translational stage for *in vivo* investigations pertaining to TB. Despite, these limitations, the variations observed between mRNA abundance (transcriptomics) and the corresponding protein levels indicate that proteomics provides a distinct and more correlated analysis that explains physiological responses to *Mtb* infection in true terms (Vogel and Marcotte, 2012; Bespyatykh et al., 2017).

A proteomics study conducted to define detailed molecular maps of human granulomas using LC-MS-MS led to the identification of ~3000 proteins and some lipids in the lungs of human TB subjects and *Mtb* infected NZW rabbits (Marakalala et al., 2016). The results suggested that different compartments within granulomas exhibit unique molecular signatures. It was observed that the center of granulomas has a proinflammatory milieu with the abundance of LTA4H and TNF-α, ROS mediators alongside antimicrobial effectors like cathelicidin along with proinflammatory eicosanoids. In contrast, the caseous center displayed an anti-inflammatory environment. Importantly, the data obtained was consistent across human and rabbit tissue samples. It was thus, proposed that balance between anti-inflammatory and proinflammatory mediators determines the outcome of infection (Marakalala et al., 2016).

Moreover, a mouse model has also been applied for validation of proteomics data generated from human samples. A study conducted using free-solution isoelectric focusing combined with high resolution LTQ Orbitrap Velos mass spectrometry to identify *Mtb* specific antigens from TB infected human lung tissues resulted in the identification of six *Mtb*-associated peptides. Out of these, a 34 amino acid peptide, PKAp (serine/threonine–protein kinase), was found to elicit *Mtb*-specific cellular responses with enhanced proliferation of CD8+ T-cell along with a strong cytotoxic lymphocyte (CTL) response. C57BL/6 female mice were immunized with PKAp peptide to validate the above results and it was observed that cellular levels of IFN-γ were increased in both the lungs and spleen without resulting in any immunopathogenesis. The results indicated that PKAp could be considered as a novel antigen, which can be used for development of vaccines (Yu et al., 2015).

To recapitulate, we believe that multi-omics can be employed to project a comprehensive landscape of a disease including differentiating between active and latent TB infections, predicting the risk of disease progression, or detecting markers that may be specifically associated with drug resistant TB infections. Hence, a system biology approach integrating global genomic, transcriptional, proteomic, and metabolomic profiles would provide a complete view of the disease and give in-depth information about the host-pathogen interactions. This would ultimately allow for more efficient diagnosis, enable the identification of novel anti-TB therapeutics, and pave the way for the development of personalized treatment options as well as host-directed therapies (Hasin et al., 2017; Goff et al., 2020; Guha et al., 2024).

4 Cellular models for studying tuberculosis

For many years, various animal models have been employed for studying complexities of TB infection, including granuloma formulation, host-pathogen interactions and latency. However, none of these models recapitulates the disease's heterogeneity as it manifests in human. There has always been purpose-oriented use of *in vivo* models aimed at addressing specific scientific questions. While these models remain imperative for advancing our understanding of TB, it is important to consider the ethical issues related with the use of animals and to follow the principle of 3R (replace, reduce and refine) when conducting animal experiments (Franco and Rezzani, 2024).

In the recent years, *in vitro* models have emerged as powerful tools to investigate the interactions between the host and *Mtb*. These models often provide valuable insights that are challenging to achieve with animal models, further strengthening our research efforts in this critical area.

4.1 Cell lines and two-dimensional *in vitro* models

Given the crucial role of macrophages during *Mtb* infection, numerous studies have focused on *in vitro* models of infection to understand the pathogen's behavior within the host. These include primary macrophages, immortalized cell lines and induced pluripotent stem cells (Keiser and Purdy, 2017). These models have been instrumental in studying the various strategies adapted by *Mtb* to survive within the host, such as phagosome maturation arrest, modulation of host cell death pathways, resistance to anti-mycobacterial compounds, alterations in the host signaling pathways and granuloma formation (Jordao et al., 2008; Keiser and Purdy, 2017).

Immortalized murine macrophage cell lines, such as RAW264.7 and J774 as well as primary cells like BMDMs, are predominant choice for *Mtb* infection studies. Both RAW264.7 and J774 are adherent macrophage cells derived from BALB/c mice, which can produce various TB associated cytokines, including TNF-α, IL-6 and IFN-β as well as release nitric oxide (NO) in response to bacterial infection and various other stimuli (Raschke et al., 1978; Stuehr and Marletta, 1987; Adams et al., 1993; Perez et al., 2000; Indrigo et al., 2003; Rao et al., 2005; Rao et al., 2006). It is well-established that NO produced by nitric oxide synthase 2 (NOS2), is critical host defense mechanism in controlling TB infection (Gross et al., 2014).

Primary macrophages derived from C57BL/6 mice and various knockout mice strains have been useful for studying the role of specific proteins and pathways involved in innate immunity. For example, primary cells isolated from mice deficient in NADPH oxidase and NOS2 were useful for studying the role of various detoxifying systems in mycobacteria (Bogdan, 2015). *Mtb* encodes several detoxifying genes, such as *sodA*, *katG*, NADH-dependent peroxidase, *aphC*, *aphD*, *dlaT* and *lpd* and mutations in these genes were shown to severely impair bacterial growth (Dussurget et al., 2001; Edwards et al., 2001; Ng et al., 2004; Shi and Ehrt, 2006). Additionally, several studies in macrophages have elucidated the role of *Mtb* cell wall lipids and components of ESX-1 secretion system in phagosome maturation arrest (Vergne et al., 2004; Pethe et al., 2004; MacGurn and Cox, 2007).

In addition to murine models, human monocytic cell lines, such as U937 and THP-1 are widely used for studying *Mtb* biology *in vitro*. Amongst these, human monocytic leukemia cell line, THP-1 is most extensively studied due to its ease of culturing, yielding unlimited number of cells for conducting different experiments. Differentiation of THP-1 cells into macrophages can be stimulated via phorbol 12-myristate 13-acetate (PMA), after which they become adherent, exhibit lysozyme activity, express macrophage-specific surface markers and increase their phagocytosis ability (Tsuchiya et al., 1982; Schwende et al., 1996; Daigneault et al., 2010). It is well-documented that *Mtb* induces the differentiation of macrophages to foamy macrophages *in vivo*. Thus, *in vitro* differentiation of THP-1 into foamy macrophages would serve as an excellent tool to investigate host-pathogen interactions and *Mtb* pathogenesis (Peyron et al., 2008). Several protocols are available for converting THP-1 cells into foamy macrophages by incubating them under hypoxic conditions or exposing the cell culture to fatty acids, lipoproteins or surfactant lipids (Deng et al., 2023). In addition, dormancy has also been studied in lipid loaded THP-1-derived macrophages by incubating cells under hypoxic conditions. It was observed that within these macrophages, bacteria lose their acid-fastness and become phenotypically resistant to anti-TB drugs, features that are considered indicative of a dormant state of the pathogen (Daniel et al., 2011).

Alternatively, macrophages can be extracted from healthy human donors as peripheral blood monocyte cells (PBMCs), which can be differentiated into macrophages by using granulocyte-macrophage colony-stimulating factor (GM-CSF) or macrophage colony-stimulating factor (M-CSF) or human serum (Portevin et al., 2011; Vogt and Nathan, 2011). Although, the properties of these differentiated cells are different from tissue resident cells, their use is cost-effective due to the ease of access to PBMCs. These macrophages respond to *Mtb* infection by releasing immune mediators such as TNF, IL-6 and IL-10 (Wang et al., 2010). While most studies of macrophage-pathogen interactions are focused at single cell level, these intracellular assays do not fully represent the heterogeneous microenvironment of granuloma formation (Yuan and Sampson, 2018). As such, several researchers have utilized PBMCs to develop *in vitro* 2D model to study human mycobacterial granulomas.

One such model, developed in study by Puissegur et al. demonstrated the formation of *in vitro* granulomas with morphological features and differentiation pattern similar to those of natural granulomas. They observed progressive macrophage recruitment around mycobacterial antigen- coated artificial beads or live bacteria, which further differentiated into multinucleated giant cells and epithelioid macrophages fused with surrounding macrophages and lymphocytes. This model enhanced our understanding of cell differentiation and cellular recruitment, and it could serve as a foundation for evaluating the granuloma-inducing ability of newer vaccine candidates compared to BCG (Puissegur et al., 2004).

To further understand the potential mechanisms of early granuloma formation and establishment, Guirado et al. developed an *in vitro* granuloma model from PBMCs and autologous serum. Their work showed that granuloma formation in patients with latent TB infection (LTBI) differed from those in naive individuals, with significant alterations in bacterial growth, cytokine production and lipid body accumulation. Additionally, the study highlighted unique bacterial transcriptional signatures in LTBI individuals, wherein *Mtb* exhibited a metabolic shift towards increased expression of genes involved in TCA cycle, fatty acid degradation, glyoxylate shunt and gluconeogenesis. This model greatly enhanced our fundamentals about the pathophysiology of human TB granulomas, facilitating the identification of new potential biomarkers (Guirado et al., 2015). However, this model fails to address the factors that influence the kinetics and stability of granuloma, such as the absence of fibroblasts and extracellular matrix (ECM) components. In addition, *in vitro* granuloma models have been utilized for evaluating the activity of anti-tubercular compounds in high-content screening set ups. The study showed significant differences in the minimum inhibitory

concentration (MIC) of compounds against the extracellular bacteria versus bacteria within granulomas (Silva-Miranda et al., 2015).

Despite their extensive use in screening potential anti-mycobacterial molecules and investigating *Mtb* infection dynamics and immune responses, most of these *in vitro* studies rely on monolayers of cell cultured on flat surfaces. Thus, these models lack physiological microenvironment and fail to mimic the tissue architecture, receptor topography and gradients of oxygen, nutrients, and metabolites as well as the three-dimensional (3D) interactions between different cell types found *in vivo*. Furthermore, these models exhibit altered morphology, gene expression and have limited ability to replicate the complex immune responses such as interactions between macrophages, dendritic cells and T cells that occur *in vivo* (Franco and Rezzani, 2024). Consequently, the recent years have witnessed a significant focus on the development of 3D *in vitro* models that can better replicate the *in vivo* tissue microenvironment. These models offer the opportunity to study complex cellular interactions and provides a more physiologically relevant tissue microenvironment for studying immune responses and cell behavior under various stress conditions.

4.2 3D *in vitro* granuloma models

Several studies have explained 3D *in vitro* model of *Mtb* granulomas, in which infected primary human cells were co-cultured with various matrices (Bhavanam et al., 2016). Seitzer and Gerdes reported the first 3D granuloma model by infecting PBMCs seeded in agarose-coated well with *Mtb* H37Rv or *M. bovis* at different multiplicities of infection (MOIs). They observed the formation of cell aggregates at MOI of only 1:50 (bacteria/cells) after 4 days of incubation, while higher MOI resulted in small aggregates with higher number of dead cells. Their model displayed many phenotypic features representative of granulomas, such as aggregation of primary monocytes, B-cells, T-cells, presence of macrophages, multinucleated giant cells and necrotic areas (Seitzer and Gerdes, 2003).

To study this process further, Birkness et al. combined blood lymphocytes, autologous macrophages and *Mtb* in ultra-low attachment tissue culture plates, resulting in the formation of small, round aggregates. To mimic the natural infection process, they added non-adherent PBMCs on day 2 and day 5 post-infection and observed small aggregates of CD68+ epithelioid macrophages and CD3+ lymphocytes, similar to what is observed in clinical specimens (Birkness et al., 2007). Immunological analysis of the supernatant from these infected cells revealed the presence of several cytokines involved in human granuloma formation, including IL-6, IL-8, IFN-γ and TNFα. Additionally, they found that the addition of these cytokines significantly enhance the formation of aggregates. These studies provide valuable tools for studying immunological changes during bacterial infection and granuloma formation. However, these models did not provide insight into the establishment of dormancy inside granulomas and reactivation of disease (Birkness et al., 2007).

Further, Kapoor et al. employed a different approach to develop an *in vitro* model of TB granuloma by culturing human PBMCs in a collagen matrix with a low-dose of *Mtb* to study dormancy and resuscitation upon immune suppression. This model demonstrated several features similar to *in vivo* human TB granulomas, such as formation of multinucleated giant cells, reduction in CD4+ T-cell counts and secretion of various cytokines and chemokines. *Mtb* within these granulomas displayed several characteristics of dormancy, including, loss of acid-fastness, lipid bodies accumulation, tolerance to rifampicin and changes in the gene expression profile. Notably, they observed reactivation of dormant *Mtb* upon immune suppression by using anti-TNFα monoclonal antibodies (Kapoor et al., 2013). Despite its strength in studying latency, this model is relatively low throughput and faces limitation in studying dynamics over time due to technical challenges. Additionally, the requirement for collagenase for removal of the cells from the ECM for downstream processing also restricts its utility (Elkington et al., 2019). Recently, a study by Berry et al. introduced a novel microscale *in vitro* granuloma platform to study the signaling of soluble factors between granuloma and its surrounding microenvironment following infection. Using an open microfluidic stacks platform, they cultured *M. bovis* BCG infected monocyte-derived macrophages that could be integrated with different microenvironment cues through spatial and temporal stacking. This system resulted in generation of 3D cell aggregates encapsulating *Mtb* that secreted increased levels of proinflammatory cytokines, such as IL-6, VEGF and TNFα. They further extended their study by co-culturing human vascular endothelial cells with *Mtb*-infected macrophages to understand the role of granuloma associated angiogenesis (Berry et al., 2020). Additionally, several other studies have employed 3D *in vitro* granuloma model to study other mycobacterial diseases caused by other *M. leprae, M. bovis* and *M. avium subsp. paratuberculosis* (Puissegur et al., 2004; Birkness et al., 2007; Kapoor et al., 2013; Wang et al., 2013).

4.3 Multicellular lung tissue model

The studies described above do not fully account for the diverse cell types that are present in a *Mtb* infected lung tissue. To address this gap, researchers have developed *in vitro* human lung tissue models to study early granuloma formation (BéruBé et al., 2011; Hoang et al., 2012; Parasa et al., 2014; Braian et al., 2015; Parasa et al., 2017). The development of first human lung tissue model to study granuloma formation was reported by Parasa et al., who introduced *Mtb*-infected macrophages into an established *in vitro* lung tissue model. They observed the clustering of macrophages at the site of infection, suggesting the formation of early TB granuloma. This study also demonstrated that ESAT-6, component of ESX-1 secretion system, is required for early granuloma formation as *Mtb* mutant strain lacking RD1 region or ESAT-6 was unable to induce clustering of macrophages (Parasa et al., 2014). This finding is consistent with previous *in vivo* studies providing a unique platform to study host-pathogen interactions for the development of new therapeutic strategies (Davis and Ramakrishnan, 2009; Parasa et al., 2014).

In addition to this, researchers have investigated the role of host matrix metalloproteases (MMPs) in the formation of granuloma and bacterial growth within *Mtb* infected tissue. Human lung-derived cells and primary human monocyte-derived macrophages were utilized to model tissue lung model, which showed upregulation of several MMPs, including MMP-1, MMP-3, MMP-9 and MMP-12. Further, the use of marimastat, a global MMP inhibitor, in *Mtb*-infected lung tissue model resulted in reduction of mycobacterial growth and granuloma formation. A drawback to this study, however, is the use of global MMP inhibitor, which does not provide information into the specific role of individual MMPs in granuloma formation. Similar results regarding the involvement of MMPs at the site of necrosis and tissue damage have been observed in several animal models and in human lung tissue biopsies from patients with TB (Parasa et al., 2017).

Another notable study by Braian et al. showed the development of 3D lung model consisting of human lung-specific epithelial cells, *Mtb*-infected primary macrophages or monocytes seeded onto a matrix of collagen embedded fibroblasts prepared on a transwell filter. Exposure of the culture to air resulted in the stratification of epithelial cells and secretion of mucus at the apical surface. This model was particularly useful for 3D visualization of the entire lung tissue and for studying the migration of immune cells in the tissue during granuloma formation.

However, these studies have some limitations that include their inability to translate into high throughput platforms and the absence of other immune cells such as neutrophils and lymphocytes, which are typically present in a granuloma structures. Addressing these limitations could further strengthen the use of these models in understanding intricacies of disease.

4.4 Bioelectrospray 3D model

Workman et al. employed the bioelectrospray method to produce customizable microspheres containing extracellular matrix (ECM) components and THP-1 cells. Cell encapsulation within microsphere was achieved using a biocompatible cross-linking polymer, alginate, in a calcium chloride gelling bath. This system offers the advantage of easy downstream analysis as cells can be quickly released from the spheres using EDTA or sodium citrate. The researchers investigated the effect of various parameters such as voltage, flow rate and nozzle size on the size and stability of the microspheres. They compared the size of spheres generated with or without collagen addition to alginate, highlighting the role of ECM in host-pathogen interaction (Workman et al., 2014).

Subsequently, in another study it was demonstrated that *Mtb* has lower proliferation rate in collagen-containing microspheres (Tezera et al., 2017). The group also observed increased apoptosis, altered energy balance and secretion of various proinflammatory cytokines (IL-1β, TNF-α, IFN-γ, IL-6, IL-8 and MCP-1) in the presence of collagen, all of which favors host ability to control infection. The study further investigated several emerging therapeutic interventions, including the effects of cytokine supplementation on microspheres, host-directed therapy through PGE2 augmentation and immunoaugmentation with ESAT-6 and CFP-10 specific T cell lines. These findings align with several *in vivo* studies, positioning this system to serve as powerful tool for discerning the protective and pathological immune responses (Tezera et al., 2017). Additionally, bioelectrospray 3D model of TB granuloma formation has been used to investigate the mechanisms of immunopathology in TB, by specifically examining the role of MMP inhibitor in matrix degradation (Walker et al., 2017).

Apart from this, bioengineering approach have been employed to compare the sensitivity of *Mtb* to PZA in standard culture conditions versus within the 3D microspheres. Notably, the researchers observed upregulation of multiple stress-related mycobacterial genes at day 14 as well as rapid killing of bacteria by PZA inside these microspheres (Bielecka et al., 2017). This system is highly versatile, wherein cell numbers can be modulated along with changes in the composition of ECM, size of sphere, challenge dose and the surrounding media, making it a promising tool for addressing various human infections. One of the major advantages of this microsphere system is its integration potential with microfluidic platform, enabling the study of antibiotic response modulation over time to replicate the drug pharmacokinetics observed in patients during treatment. In their preliminary screening, they developed a microfluidic system with two inlets and one exit channel, facilitating smooth flow of medium through wells containing encapsulated microspheres. They demonstrated dose-dependent killing of *Mtb* with a stepwise increase in rifampicin concentration, which was consistent with clinical findings in patients (Barrila et al., 2010; Pasipanodya et al., 2013; Bielecka et al., 2017).

Like other models, this system also has some limitations, especially, the lack of vasculature, and incorporation of other immune cells once cells are embedded within the microspheres. Furthermore, the anatomical constraints that occur during infection are lost due to absence of spatial organisation seen in the lung, which makes it difficult to fully replicate complexity of granuloma. Hence, to better mimic these features, modifications such as dual encapsulation system are needed to replicate multiple microenvironments such as the caseous central core and hypoxic conditions, in order to more effectively study TB immunopathogenesis (Elkington et al., 2019; Franco and Rezzani, 2024).

4.5 Organoids

Advances in the stem cell biology have created an exciting opportunity to grow human tissues in dishes that closely resemble organs *in vitro*. Organoids are self-organizing, multicellular 3D aggregates that mimic structure, function, cellular heterogeneity and behavior of human tissues *in vitro* (Iakobachvili and Peters, 2017). These organoids can be derived from either adult stem cells (ASCs), embryonic stem cells, induced pluripotent stem cells (iPSCs) or tissue biopsies. Stem cells have the capacity for self-renewal and the source of these stem cells have profound impact on

the types of cells present in the resulting organoids. For instance, organoids derived from ASCs are generally polarized, cystic structures consisting mostly of epithelial cells, whereas organoids derived from iPSCs tend to be more complex, containing both epithelial and non-epithelial cell types (Dichtl et al., 2024; Franco and Rezzani, 2024). Additionally, lung organoids derived from adult tissue biopsies or bronchoalveolar lavage fluid include a wide range of cells such as basal, club, goblet and ciliated cells. Organoid technology has proven useful in studying in infectious diseases, enabling researchers to better understand the host responses, pathogen survival and cell tropism (Mills and Estes, 2016; Heo et al., 2018; Hui et al., 2018; Sachs et al., 2019; Bagayoko et al., 2021).

Human airway organoids (AOs) have been used to investigate the very early steps of mycobacterial infection, particularly those caused by *Mtb* and *M. abscessus* (Mabs). Researchers have observed differences in the replication potential, cytokines secretion profile and antimicrobial peptides between these pathogens inside AOs. While the growth of *Mtb* was controlled, Mabs readily replicated more freely inside the lumen of AOs, highlighting the hospitable environment of the airways for non-tuberculous mycobacteria (NTM). Further, they attempted to co-culture human monocyte-derived macrophages with *M. bovis* BCG infected organoids and observed the movement of macrophages within the matrix towards the bacteria-containing organoids. However, this model does not fully mimic the *in vivo* environment, as macrophages were not able to traverse the basal side of hAOs to reach lumen for clearing the bacteria (Iakobachvili et al., 2022).

Recently, a group had developed a 3D human lung organoids (hLOs) model derived from human pluripotent stem cells (hPSCs). These organoids exhibited a hollow lumen structure similar to that of alveolar sacs. The model was used to study *Mtb* infection in lung epithelial cells and human macrophages by microinjecting fluorescently labelled bacteria and macrophages into the lumen of hLOs. A key advantage of this model is its ability to maintain the 3D structure and sustain the bacterial populations even after multiple passages. In addition, they have evaluated the inhibitory effects of known anti-TB drugs, rifampicin and bedaquiline, and observed a reduction in *Mtb* H37Rv growth in hLOs at each passage. This model has been utilized to explore host-directed therapies by knocking down the host genes (such as MFN2 and HERPUD1), which resulted in a significant reduction in inflammatory cytokines and intracellular *Mtb* growth, consistent with pervious findings (Lee et al., 2019; Son et al., 2023; Kim et al., 2024).

Despite the promising potential of lung organoids in TB research, there are some challenges that need to be addressed before they can be used more systematically. For example, to study host-pathogen interactions more efficiently in a lung-like environment, it is essential to incorporate macrophages and other cell types that can replicate granuloma formation. Furthermore, introduction of vasculature is necessary to create more dynamic microenvironment, allowing for better control of experimental conditions. Currently, lung organoids lack an air-liquid-mucosa interface due to their closed, cystic structure. This limitation can be overcome by using alternative microfluidic cell culture platform, such as the Lung- on-a-chip technology (Nadkarni et al., 2016; Fonseca et al., 2017).

4.6 Lung-on-chip

The integration of microfluidic and micro-fabricated biosystems with innovations in biological approaches has led to the development of organ-on-chip (OoC) platforms. These systems are engineered to replicate complex physiological processes of human organs that allow more accurate and ethical alternatives to animal models. Various OoC devices have been developed to model human tissues, such as the lung, intestine, heart, kidney, liver, blood vessels and blood-brain barrier (Low et al., 2021; Bhatia and Ingber, 2014). In general, each OoC platform has some defining features, including 3D microarchitecture, the integration of multiple cell types and the incorporation of relevant biomechanical forces that mimic the specific tissue environment (Shrestha et al., 2020).

One of the earliest and most notable OoC is the "Lung-on-chip" model, developed by Huh and colleagues. This model is designed to mimic the 3D structure, microenvironment and physiological processes of human lungs, including breathing movements. The system is constructed using a soft lithography-based micro-fabrication technology to create 3D micro-channel in which human alveolar epithelial cells and pulmonary micro-vascular endothelial cells were are seeded on the opposite side of culture chambers. These cells are separated by micro-porous elastomeric membrane, which mimics the alveolar-capillary interface. Subsequently, vacuum suction was applied to induce mechanical stretching of the adherent cell layers, simulating the physiological breathing motions. This proof-of-concept biomimetic system has been instrumental for conducting nano-toxicology studies and modelling complex human disease processes (Huh et al., 2010; Huh et al., 2012; Huh, 2015).

In addition to this, a human lung "small airway-on-a-chip" model has been developed by Benam et al., to study respiratory disorders, such as asthma and chronic obstructive pulmonary disease (COPD). This system includes a differentiated, mucociliary bronchial epithelium in the upper layer and an underlying micro-vascular endothelium. Fluid flow is applied to the endothelial layer, mimicking blood circulation. This model offers a powerful tool for studying both human pathophysiology and evaluating the efficacy of drugs, that can complement the preclinical research in animal models (Benam et al., 2016; Bielecka and Elkington, 2018).

Recent advancements in the field include a "Lung-on-chip" model of *Mtb* infection developed by Thacker et al. This model utilizes time-lapse microscopy to study dynamics of *Mtb* infection in alveolar epithelial cells and macrophages at an air-liquid interface, allowing for high-resolution spatiotemporal analysis. The study also examined the role of pulmonary surfactants, molecules produced by lungs to normal functioning and to respond to TB infection. The researchers found that *Mtb* grew slowly in the lung and immune cells in the presence of surfactant, indicating the protective role of surfactants in TB. This may be due

to role of surfactants in pulling out proteins and fats from the surface of *Mtb*, hindering the bacteria's ability to infect host cells. The study further indicated that pulmonary surfactant replacement formulations may serve as host-directed therapies to enhance the immune responses against TB (Thacker et al., 2020).

These advancements in lung-on-chip technology offer significant potential for TB research, particularly in the development of novel therapeutic approaches. However, further exploration is needed to address the technical hurdles and complexities associated with the disease. Refinements in these models would not only improve our understanding of respiratory diseases but also lay the groundwork for more effective drug discovery and personalized therapeutics in the future.

5 Concluding remarks

The capacity of an individual to clear TB infection involves a well-coordinated innate and adaptive immune response systems and thus, it is important to understand the immune response and heterogeneity associated with the disease. This review describes various *in vitro* and *in vivo* model systems to provide a comprehensive overview of the different aspects of TB research including drug discovery, vaccine development and host-pathogen interactions. Animal models remain at forefront in providing a wealth of information about host genes associated with susceptibility to TB, the immunopathogenesis of *Mtb* infection, various immune cells and responses and identification of crucial bacterial virulence determinants.

The murine model has played a significant role in TB research in identification of various important susceptibility loci to TB infections. Infact, the advent of genetic engineering and molecular techniques has allowed investigators to develop knockout and transgenic mice, leading to the identification of key immune components required for TB immunity. Moreover, most of the new TB drugs are evaluated for their therapeutic efficacy in mouse model of tuberculosis. Guinea pigs have underpinned the TB vaccine development program, providing the initial platform to identify potential vaccine candidates. Many different kinds of vaccine regimens based on recombinant BCG vaccine, auxotrophic mutants, subunit vaccines, DNA and viral vectored vaccines have been evaluated in guinea pig model of tuberculosis to establish the preliminary proof of their efficacy. NHP model of tuberculosis is an expensive system but is the closest representative to human TB. Thus, most of the promising vaccines are evaluated for their protective efficacy and immunogenicity in this model before the vaccine candidate is allowed to progress to clinical trials.

The use of animal systems have been extended to the recent omics-based technologies. With the advancements in next-generation sequencing techniques and mass spectrometry, various biomarkers and host gene signatures that differentiate between different clinical forms of TB or predict the prognosis of the disease and the treatment outcome can now be identified. Further, the review also describes the *in vitro* 2D and 3D models that have been employed to understand granuloma formation, cell surface expression of markers and the secretion of various cytokines and chemokines associated with TB. Thus, the conjugation of advanced cellular models with other "omics" approaches and *in vivo* models will offer new insights into the host-pathogen interactions, establishing a strong foundation for the development of novel therapeutic and vaccination strategies.

Author contributions

PN: Conceptualization, Writing – original draft, Writing – review & editing. NN: Writing – original draft. NA: Writing – original draft. GK: Conceptualization, Funding acquisition, Writing – review & editing.

Funding

The author(s) declare that no financial support was received for the research and/or publication of this article.

Acknowledgments

PN is grateful to ICMR-Department of Health and Research for the fellowship. NN and NA are thankful to University Grant Commission (UGC) and Council of Scientific and Industrial Research (CSIR) for the fellowships. GK and PN acknowledge the financial assistance received from the Department of Biotechnology, Govt. of India, New Delhi (BT/PR32697/MED/29/1471/2019), Institution of Eminence, University of Delhi (IoE-DU/MRP/2022/056) and ICMR-DHR (R.12013/13/2023-HR) for the work contributed and elaborated in this review.

Conflict of interest

The authors declare that the research was conducted in the absence of any commercial or financial relationships that could be construed as a potential conflict of interest.

Generative AI statement

The author(s) declare that no Generative AI was used in the creation of this manuscript.

Publisher's note

References

Abel, B., Thieblemont, N., Quesniaux, V. J., Brown, N., Mpagi, J., Miyake, K., et al. (2002). Toll-like receptor 4 expression is required to control chronic Mycobacterium tuberculosis infection in mice. *J. Immunol.* 169, 3155–3162. doi: 10.4049/jimmunol.169.6.3155

Acharya, B., Acharya, A., Gautam, S., Ghimire, S. P., Mishra, G., Parajuli, N., et al. (2020). Advances in diagnosis of Tuberculosis: an update into molecular diagnosis of Mycobacterium tuberculosis. *Mol. Biol. Rep.* 47, 4065–4075. doi: 10.1007/s11033-020-05413-7

Adams, L. B., Fukutomi, Y., and Krahenbuhl, J. L. (1993). Regulation of murine macrophage effector functions by lipoarabinomannan from mycobacterial strains with different degrees of virulence. *Infect. Immun.* 61, 4173–4181. doi: 10.1128/iai.61.10.4173-4181.1993

Agarwal, P., Gordon, S., and Martinez, F. O. (2021). Foam cell macrophages in tuberculosis. *Front. Immunol.* 12, 775326. doi: 10.3389/fimmu.2021.775326

Ahamad, N., Gupta, S., and Parashar, D. (2022). Using omics to study leprosy, tuberculosis, and other mycobacterial diseases. *Front. Cell. Infect. Microbiol.* 12, 792617. doi: 10.3389/fcimb.2022.792617

Ai, J. W., Ruan, Q. L., Liu, Q. H., and Zhang, W. H. (2016). Updates on the risk factors for latent tuberculosis reactivation and their managements. *Emerg. microb. infect.* 5, 1–8. doi: 10.1038/emi.2016.10

Aiello, A., Najafi-Fard, S., and Goletti, D. (2023). Initial immune response after exposure to Mycobacterium tuberculosis or to SARS-COV-2: similarities and differences. *Front. Immunol.* 14, 1244556. doi: 10.3389/fimmu.2023.1244556

Alsayed, S. S., and Gunosewoyo, H. (2023). Tuberculosis: pathogenesis, current treatment regimens and new drug targets. *Int. J. Mol. Sci.* 24, 5202. doi: 10.3390/ijms24065202

(2024). *WHO Global TB report*. Available online at: https://www.who.int/teams/global-tuberculosis-programme/tb-reports/global-tuberculosis-report-2024 (Accessed February 5, 2025).

Bafica, A., Scanga, C. A., Feng, C. G., Leifer, C., Cheever, A., and Sher, A. (2005). TLR9 regulates Th1 responses and cooperates with TLR2 in mediating optimal resistance to Mycobacterium tuberculosis. *J. Exp. Med.* 202, 1715–1724. doi: 10.1084/jem.20051782

Bagayoko, S., Leon-Icaza, S. A., Pinilla, M., Hessel, A., Santoni, K., Péricat, D., et al. (2021). Host phospholipid peroxidation fuels ExoU-dependent cell necrosis and supports Pseudomonas aeruginosa-driven pathology. *PloS Pathog.* 17, e1009927. doi: 10.1371/journal.ppat.1009927

Banasik, B. N., Perry, C. L., Keith, C. A., Bourne, N., Schäfer, H., and Milligan, G. N. (2019). Development of an anti-Guinea pig CD4 monoclonal antibody for depletion of CD4+ T cells *in vivo*. *J. immunol. Methods* 474, 112654. doi: 10.1016/j.jim.2019.112654

Baram, P., Soltysik, L., and Condoulis, W. (1971). The *in vitro* assay of tuberculin hypersensitivity in Macaca mulatta sensitized with Bacille Calmette Guerin cell wall vaccine and/or infected with virulent Mycobacterium tuberculosis. *Lab. Anim. Sci.* 21 (5), 727–733. doi: 10.1159/000460011

Barclay, W. R., Anacker, R. L., Brehmer, W., Leif, W., and Ribi, E. (1970). Aerosol-induced tuberculosis in subhuman primates and the course of the disease after intravenous BCG vaccination. *Infect. Immun.* 2, 574–582. doi: 10.1128/iai.2.5.574-582.1970

Barrila, J., Radtke, A. L., Crabbé, A., Sarker, S. F., Herbst-Kralovetz, M. M., Ott, C. M., et al. (2010). Organotypic 3D cell culture models: using the rotating wall vessel to study host–pathogen interactions. *Nat. Rev. Microbiol.* 8, 791–801. doi: 10.1038/nrmicro2423

Basaraba, R. J., Dailey, D. D., McFarland, C. T., Shanley, C. A., Smith, E. E., McMurray, D. N., et al. (2006). Lymphadenitis as a major element of disease in the Guinea pig model of tuberculosis. *Tuberculosis* 86, 386–394. doi: 10.1016/j.tube.2005.11.003

Beamer, G. L., and Turner, J. (2005). Murine models of susceptibility to tuberculosis. *Archivum Immunol. Et Therapiae Experimentalis-English Edit.* 53, 469.

Behring, E. V. (1890). Ueber das Zustandekommen der Diphtherie-Immunität und der Tetanus-Immunität bei Thieren. *Dtsch. Med. Wschr.* 16, 1145–1147. doi: 10.1055/s-0029-1207609

Bellamy, R., Ruwende, C., Corrah, T., McAdam, K. P., Whittle, H. C., and Hill, A. V. (1998). Variations in the NRAMP1 gene and susceptibility to tuberculosis in West Africans. *New Engl. J. Med.* 338, 640–644. doi: 10.1056/NEJM199803053381002

Benam, K. H., Villenave, R., Lucchesi, C., Varone, A., Hubeau, C., Lee, H. H., et al. (2016). Small airway-on-a-chip enables analysis of human lung inflammation and drug responses *in vitro*. *Nat. Methods* 13, 151–157. doi: 10.1038/nmeth.3697

Berg, I. A., Filatova, L. V., and Ivanovsky, R. N. (2002). Inhibition of acetate and propionate assimilation by itaconate via propionyl-CoA carboxylase in isocitrate lyase-negative purple bacterium Rhodospirillum rubrum. *FEMS Microbiol. Lett.* 216, 49–54. doi: 10.1111/j.1574-6968.2002.tb11413.x

Berry, S. B., Gower, M. S., Su, X., Seshadri, C., and Theberge, A. B. (2020). A modular microscale granuloma model for immune-microenvironment signaling studies *in vitro*. *Front. bioeng. Biotechnol.* 8, 931. doi: 10.3389/fbioe.2020.00931

BéruBé, K., Gibson, C., Job, C., and Prytherch, Z. (2011). Human lung tissue engineering: a critical tool for safer medicines. *Cell Tissue bank.* 12, 11–13. doi: 10.1007/s10561-010-9204-6

Bespyatykh, J. A., Shitikov, E. A., and Ilina, E. N. (2017). Proteomics for the investigation of mycobacteria. *Acta Naturae (англоязычная версия)* 9, 15–25. doi: 10.32607/20758251-2017-9-1-15-25

Betts, J. C., Lukey, P. T., Robb, L. C., McAdam, R. A., and Duncan, K. (2002). Evaluation of a nutrient starvation model of Mycobacterium tuberculosis persistence by gene and protein expression profiling. *Mol. Microbiol.* 43 (3), 717–731. doi: 10.1046/j.1365-2958.2002.02779.x

Bhatia, S. N., and Ingber, D. E. (2014). Microfluidic organs-on-chips. *Nat. Biotechnol.* 32, 760–772. doi: 10.1038/nbt.2989

Bhavanam, S., Rayat, G. R., Keelan, M., Kunimoto, D., and Drews, S. J. (2016). Understanding the pathophysiology of the human TB lung granuloma using *in vitro* granuloma models. *Future Microbiol.* 11, 1073–1089. doi: 10.2217/fmb-2016-0005

Bielecka, M. K., and Elkington, P. (2018). Advanced cellular systems to study tuberculosis treatment. *Curr. Opin. Pharmacol.* 42, 16–21. doi: 10.1016/j.coph.2018.06.005

Bielecka, M. K., Tezera, L. B., Zmijan, R., Drobniewski, F., Zhang, X., Jayasinghe, S., et al. (2017). A bioengineered three-dimensional cell culture platform integrated with microfluidics to address antimicrobial resistance in tuberculosis. *MBio* 8, 10–1128. doi: 10.1128/mbio.02073-16

Birkness, K. A., Guarner, J., Sable, S. B., Tripp, R. A., Kellar, K. L., Bartlett, J., et al. (2007). An *in vitro* model of the leukocyte interactions associated with granuloma formation in Mycobacterium tuberculosis infection. *Immunol. Cell Biol.* 85, 160–168. doi: 10.1038/sj.icb.7100019

Bisht, D., Sharma, D., Sharma, D., Singh, R., and Gupta, V. K. (2019). Recent insights into Mycobacterium tuberculosis through proteomics and implications for the clinic. *Expert Rev. Proteomics* 16, 443–456. doi: 10.1080/14789450.2019.1608185

Bogdan, C. (2015). Nitric oxide synthase in innate and adaptive immunity: an update. *Trends Immunol.* 36, 161–178. doi: 10.1016/j.it.2015.01.003

Boom, W. H., Schaible, U. E., and Achkar, J. M. (2021). The knowns and unknowns of latent Mycobacterium tuberculosis infection. *J. Clin. Invest.* 131 (3), e136222. doi: 10.1172/JCI136222

Borah, K., Xu, Y., and McFadden, J. (2021). Dissecting host-pathogen interactions in TB using systems-based omic approaches. *Front. Immunol.* 12, 762315. doi: 10.3389/fimmu.2021.762315

Bradley, D. J. (1977). Regulation of Leishmania populations within the host. II. genetic control of acute susceptibility of mice to Leishmania donovani infection. *Clin. Exp. Immunol.* 30, 130.

Braian, C., Svensson, M., Brighenti, S., Lerm, M., and Parasa, V. R. (2015). A 3D human lung tissue model for functional studies on Mycobacterium tuberculosis infection. *J. Visual. Exper.: JoVE* 104), 53084. doi: 10.3791/53084

Brandt, L., Skeiky, Y. A., Alderson, M. R., Lobet, Y., Dalemans, W., Turner, O. C., et al. (2004). The protective effect of the Mycobacterium bovis BCG vaccine is increased by coadministration with the Mycobacterium tuberculosis 72-kilodalton fusion polyprotein Mtb72F in M. tuberculosis-infected Guinea pigs. *Infect. Immun.* 72, 6622–6632. doi: 10.1128/IAI.72.11.6622-6632.2004

Bucsan, A. N., Mehra, S., Khader, S. A., and Kaushal, D. (2019). The current state of animal models and genomic approaches towards identifying and validating molecular determinants of Mycobacterium tuberculosis infection and tuberculosis disease. *Pathog. Dis.* 77, ftz037. doi: 10.1093/femspd/ftz037

Burel, J. G., Babor, M., Pomaznoy, M., Lindestam Arlehamn, C. S., Khan, N., Sette, A., et al. (2019). Host transcriptomics as a tool to identify diagnostic and mechanistic immune signatures of tuberculosis. *Front. Immunol.* 10, 221. doi: 10.3389/fimmu.2019.00221

Cappelli, G., Volpe, E., Grassi, M., Liseo, B., Colizzi, V., and Mariani, F. (2006). Profiling of Mycobacterium tuberculosis gene expression during human macrophage infection: upregulation of the alternative sigma factor G, a group of transcriptional regulators, and proteins with unknown function. *Res. Microbiol.* 157, 445–455. doi: 10.1016/j.resmic.2005.10.007

Capuano, S. V. III, Croix, D. A., Pawar, S., Zinovik, A., Myers, A., Lin, P. L., et al. (2003). Experimental Mycobacterium tuberculosis infection of cynomolgus macaques closely resembles the various manifestations of human M. tuberculosis infection. *Infect. Immun.* 71, 5831–5844. doi: 10.1128/IAI.71.10.5831-5844.2003

Caruso, A. M., Serbina, N., Klein, E., Triebold, K., Bloom, B. R., and Flynn, J. L. (1999). Mice deficient in CD4 T cells have only transiently diminished levels of IFN-γ, yet succumb to tuberculosis. *J. Immunol.* 162, 5407–5416. doi: 10.4049/jimmunol.162.9.5407

Cervino, A. C. L., Lakiss, S., Sow, O., and Hill, A. V. S. (2000). Allelic association between the NRAMP1 gene and susceptibility to tuberculosis in Guinea–Conakry. *Ann. Hum. Genet.* 64, 507–512. doi: 10.1046/j.1469-1809.2000.6460507.x

Chai, Q., Wang, L., Liu, C. H., and Ge, B. (2020). New insights into the evasion of host innate immunity by Mycobacterium tuberculosis. *Cell. Mol. Immunol.* 17, 901–913. doi: 10.1038/s41423-020-0502-z

Chandra, P., Grigsby, S. J., and Philips, J. A. (2022). Immune evasion and provocation by Mycobacterium tuberculosis. *Nat. Rev. Microbiol.* 20, 750–766. doi: 10.1038/s41579-022-00763-4

Chang, S. Y., Chen, M. L., Lee, M. R., Liang, Y. C., Lu, T. P., Wang, J. Y., et al. (2018). SP110 polymorphisms are genetic markers for vulnerability to latent and active tuberculosis infection in Taiwan. *Dis. Markers* 2018 (1), 4687380. doi: 10.1155/2018/4687380

Chaudhary, K., Darling, J. A., Fohl, L. M., Sullivan, W. J., Donald, R. G., Pfefferkorn, E. R., et al. (2004). Purine salvage pathways in the apicomplexan parasite Toxoplasma gondii. *J. Biol. Chem.* 279, 31221–31227. doi: 10.1074/jbc.M404232200

Claman, H. N. (1972). Corticosteroids and lymphoid cells. *New Engl. J. Med.* 287, 388–397. doi: 10.1056/NEJM197208242870806

Clark, S., Hall, Y., and Williams, A. (2015). Animal models of tuberculosis: Guinea pigs. *Cold Spring Harbor Perspect. Med.* 5, a018572. doi: 10.1101/cshperspect.a018572

Comstock, G. W., Livesay, V. T., and Woolpert, S. F. (1974). The prognosis of a positive tuberculin reaction in childhood and adolescence. *Am. J. Epidemiol.* 99, 131–138. doi: 10.1093/oxfordjournals.aje.a121593

Converse, P. J., Dannenberg, A. M., Estep, J. E., Sugisaki, K., Abe, Y., Schofield, B. H., et al. (1996). Cavitary tuberculosis produced in rabbits by aerosolized virulent tubercle bacilli. *Infect. Immun.* 64, 4776–4787. doi: 10.1128/iai.64.11.4776-4787.1996

Cooper, A. M., Dalton, D. K., Stewart, T. A., Griffin, J. P., Russell, D. G., and Orme, I. M. (1993). Disseminated tuberculosis in interferon gamma gene-disrupted mice. *J. Exp. Med.* 178, 2243–2247. doi: 10.1084/jem.178.6.2243

Cooper, A. M., Kipnis, A., Turner, J., Magram, J., Ferrante, J., and Orme, I. M. (2002). Mice lacking bioactive IL-12 can generate protective, antigen-specific cellular responses to mycobacterial infection only if the IL-12 p40 subunit is present. *J Immunol.* 168 (3), 1322–1327. doi: 10.4049/jimmunol.168.3.1322

Daigneault, M., Preston, J. A., Marriott, H. M., Whyte, M. K., and Dockrell, D. H. (2010). The identification of markers of macrophage differentiation in PMA-stimulated THP-1 cells and monocyte-derived macrophages. *PloS One* 5, e8668. doi: 10.1371/journal.pone.0008668

Dakubo, G. D., and Dakubo, G. D. (2010). The Warburg phenomenon and other metabolic alterations of cancer cells. *Mitochondr. Genet. Cancer* 1, 39–66. doi: 10.1007/978-3-642-11416-8

Daniel, J., Maamar, H., Deb, C., Sirakova, T. D., and Kolattukudy, P. E. (2011). Mycobacterium tuberculosis uses host triacylglycerol to accumulate lipid droplets and acquires a dormancy-like phenotype in lipid-loaded macrophages. *PloS Pathog.* 7, e1002093. doi: 10.1371/journal.ppat.1002093

Daniel, J., Oh, T. J., Lee, C. M., and Kolattukudy, P. E. (2007). AccD6, a member of the Fas II locus, is a functional carboxyltransferase subunit of the acyl-coenzyme A carboxylase in Mycobacterium tuberculosis. *J. bacteriol.* 189, 911–917. doi: 10.1128/JB.01019-06

Dannenberg, A. M. Jr. (2001). Pathogenesis of pulmonary Mycobacterium bovis infection: basic principles established by the rabbit model. *Tuberculosis* 81, 87–96. doi: 10.1054/tube.2000.0260

Dannenberg, A. M. Jr. (2009). Liquefaction and cavity formation in pulmonary TB: a simple method in rabbit skin to test inhibitors. *Tuberculosis* 89, 243–247. doi: 10.1016/j.tube.2009.05.006

Datta, M., Via, L. E., Kamoun, W. S., Liu, C., Chen, W., Seano, G., et al. (2015). Anti-vascular endothelial growth factor treatment normalizes tuberculosis granuloma vasculature and improves small molecule delivery. *Proc. Natl. Acad. Sci.* 112, 1827–1832. doi: 10.1073/pnas.1424563112

Davis, J. M., and Ramakrishnan, L. (2009). The role of the granuloma in expansion and dissemination of early tuberculous infection. *Cell* 136, 37–49. doi: 10.1016/j.cell.2008.11.014

Deb, C., Lee, C. M., Dubey, V. S., Daniel, J., Abomoelak, B., Sirakova, T. D., et al. (2009). A novel *in vitro* multiple-stress dormancy model for Mycobacterium tuberculosis generates a lipid-loaded, drug-tolerant, dormant pathogen. *PloS One* 4, e6077. doi: 10.1371/journal.pone.0006077

Deng, L., Kersten, S., and Stienstra, R. (2023). Triacylglycerol uptake and handling by macrophages: From fatty acids to lipoproteins. *Prog. Lipid Res.* 92, 101250. doi: 10.1016/j.plipres.2023.101250

Dichtl, S., Posch, W., Wilflingseder, D., et al (2024). The breathtaking world of human respiratory *in vitro* models: Investigating lung diseases and infections in 3D models, organoids, and lung-on-chip. *Eur. J. Immunol.* 54, 2250356. doi: 10.1002/eji.202250356

Diedrich, C. R., Mattila, J. T., Klein, E., Janssen, C., Phuah, J., Sturgeon, T. J., et al. (2010). Reactivation of latent tuberculosis in cynomolgus macaques infected with SIV is associated with early peripheral T cell depletion and not virus load. *PloS One* 5, e9611. doi: 10.1371/journal.pone.0009611

Divangahi, M., Behar, S. M., and Remold, H. (2013). Dying to live: how the death modality of the infected macrophage affects immunity to tuberculosis. *Adv Exp Med Biol.* 783, 103–120. doi: 10.1007/978-1-4614-6111-1

Divangahi, M., Mostowy, S., Coulombe, F., Kozak, R., Guillot, L., Veyrier, F., et al. (2008). NOD2-deficient mice have impaired resistance to Mycobacterium tuberculosis infection through defective innate and adaptive immunity. *J. Immunol.* 181, 7157–7165. doi: 10.4049/jimmunol.181.10.7157

Dorman, S. E., Hatem, C. L., Tyagi, S., Aird, K., Lopez-Molina, J., Pitt, M. L. M., et al. (2004). Susceptibility to tuberculosis: clues from studies with inbred and outbred New Zealand White rabbits. *Infect. Immun.* 72, 1700–1705. doi: 10.1128/IAI.72.3.1700-1705.2004

Driver, E. R., Ryan, G. J., Hoff, D. R., Irwin, S. M., Basaraba, R. J., Kramnik, I., et al. (2012). Evaluation of a mouse model of necrotic granuloma formation using C3HeB/FeJ mice for testing of drugs against Mycobacterium tuberculosis. *Antimicrob. Agents chemother.* 56, 3181–3195. doi: 10.1128/AAC.00217-12

Dussurget, O., Stewart, G., Neyrolles, O., Pescher, P., Young, D., and Marchal, G. (2001). Role of Mycobacterium tuberculosis copper-zinc superoxide dismutase. *Infect. Immun.* 69, 529–533. doi: 10.1128/IAI.69.1.529-533.2001

Dutta, N. K., Mehra, S., Martinez, A. N., Alvarez, X., Renner, N. A., Morici, L. A., et al. (2012). The stress-response factor SigH modulates the interaction between Mycobacterium tuberculosis and host phagocytes. *PloS One* 7, e28958. doi: 10.1371/journal.pone.0028958

Edwards, K. M., Cynamon, M. H., Voladri, R. K., Hager, C. C., DeStefano, M. S., Tham, K. T., et al. (2001). Iron-cofactored superoxide dismutase inhibits host responses to Mycobacterium tuberculosis. *Am. J. respiratory Crit. Care Med.* 164, 2213–2219. doi: 10.1164/ajrccm.164.12.2106093

Elkington, P., Lerm, M., Kapoor, N., Mahon, R., Pienaar, E., Huh, D., et al. (2019). *In vitro* granuloma models of tuberculosis: potential and challenges. *J. Infect. Dis.* 219, 1858–1866. doi: 10.1093/infdis/jiz020

Eruslanov, E. B., Lyadova, I. V., Kondratieva, T. K., Majorov, K. B., Scheglov, I. V., Orlova, M. O., et al. (2005). Neutrophil responses to Mycobacterium tuberculosis infection in genetically susceptible and resistant mice. *Infect. Immun.* 73, 1744–1753. doi: 10.1128/IAI.73.3.1744-1753.2005

Esteves, P. J., Abrantes, J., Baldauf, H. M., BenMohamed, L., Chen, Y., Christensen, N., et al. (2018). The wide utility of rabbits as models of human diseases. *Exp. Mol. Med.* 50, 1–10. doi: 10.1038/s12276-018-0094-1

Eum, S. Y., Kong, J. H., Hong, M. S., Lee, Y. J., Kim, J. H., Hwang, S. H., et al. (2010). Neutrophils are the predominant infected phagocytic cells in the airways of patients with active pulmonary TB. *Chest* 137, 122–128. doi: 10.1378/chest.09-0903

Fernández-García, M., Rey-Stolle, F., Boccard, J., Reddy, V. P., García, A., Cumming, B. M., et al. (2020). Comprehensive examination of the mouse lung metabolome following Mycobacterium tuberculosis infection using a multiplatform mass spectrometry approach. *J. Proteome Res.* 19, 2053–2070. doi: 10.1021/acs.jproteome.9b00868

Filipe-Santos, O., Bustamante, J., Chapgier, A., Vogt, G., de Beaucoudrey, L., Feinberg, J., et al. (2006). Inborn errors of IL-12/23-and IFN-γ-mediated immunity: molecular, cellular, and clinical features. *Semin. Immunol.* 18, 347–361. doi: 10.1016/j.smim.2006.07.010

Flynn, J. L., Chan, J., Triebold, K. J., Dalton, D. K., Stewart, T. A., and Bloom, B. R. (1993). An essential role for interferon gamma in resistance to Mycobacterium tuberculosis infection. *J. Exp. Med.* 178, 2249–2254. doi: 10.1084/jem.178.6.2249

Flynn, J. L., Goldstein, M. M., Chan, J., Triebold, K. J., Pfeffer, K., Lowenstein, C. J., et al. (1995). Tumor necrosis factor-α is required in the protective immune response against Mycobacterium tuberculosis in mice. *Immunity* 2, 561–572. doi: 10.1016/1074-7613(95)90001-2

Flynn, J. L., Tsenova, L., Izzo, A., and Kaplan, G. (2008). "Experimental animal models of tuberculosis," in S. H.E. Kaufmann, P. van Helden, E. Rubin and W. J. Britton. *Handbook of tuberculosis* (Hoboken, NJ: Wiley-Blackwell) 2, 389–426.

Fonseca, K. L., Rodrigues, P. N., Olsson, I. A. S., and Saraiva, M. (2017). Experimental study of tuberculosis: From animal models to complex cell systems and organoids. *PloS Pathog.* 13, e1006421. doi: 10.1371/journal.ppat.1006421

Fontán, P., Aris, V., Ghanny, S., Soteropoulos, P., and Smith, I. (2008). Global transcriptional profile of Mycobacterium tuberculosis during THP-1 human macrophage infection. *Infect. Immun.* 76 (2), 717–725. doi: 10.1128/IAI.00974-07

Franco, C., and Rezzani, R. (2024). Methods and models for studying mycobacterium tuberculosis in respiratory infections. *Int. J. Mol. Sci.* 26, 18. doi: 10.3390/ijms26010018

Frediani, J. K., Jones, D. P., Tukvadze, N., Uppal, K., Sanikidze, E., Kipiani, M., et al. (2014). Plasma metabolomics in human pulmonary tuberculosis disease: a pilot study. *PloS One* 9, e108854. doi: 10.1371/journal.pone.0108854

Gaber, T., Strehl, C., and Buttgereit, F. (2017). Metabolic regulation of inflammation. *Nat. Rev. Rheumatol.* 13, 267–279. doi: 10.1038/nrrheum.2017.37

Ganguly, R., Durieux, M. F., and Waldman, R. H. (1976). Macrophage function in vitamin C-deficient Guinea pigs. *Am. J. Clin. Nutr.* 29, 762–765. doi: 10.1093/ajcn/29.7.762

Gao, P. S., Fujishima, S., Mao, X. Q., Remus, N., Kanda, M., Enomoto, T., et al. (2000). Genetic variants of NRAMP1 and active tuberculosis in Japanese populations. *Clin. Genet.* 58 (1), 74–6. doi: 10.1034/j.1399-0004.2000.580113.x

Gautam, U. S., Foreman, T. W., Bucsan, A. N., Veatch, A. V., Alvarez, X., Adekambi, T., et al. (2018). *In vivo* inhibition of tryptophan catabolism reorganizes the tuberculoma and augments immune-mediated control of Mycobacterium tuberculosis. *Proc. Natl. Acad. Sci.* 115, E62–E71. doi: 10.1073/pnas.1711373114

Gell, P. G. H., and Benacerraf, B. (1961). Studies on hypersensitivity: IV. The relationship between contact and delayed sensitivity: A study on the specificity of cellular immune reactions. *J. Exp. Med.* 113, 571–585. doi: 10.1084/jem.113.3.571

Gengenbacher, M., Duque-Correa, M. A., Kaiser, P., Schuerer, S., Lazar, D., Zedler, U., et al. (2017). NOS2-deficient mice with hypoxic necrotizing lung lesions predict outcomes of tuberculosis chemotherapy in humans. *Sci. Rep.* 7, 8853. doi: 10.1038/s41598-017-09177-2

Gengenbacher, M., Mouritsen, J., Schubert, O. T., Aebersold, R., and Kaufmann, S. H. (2014). Mycobacterium tuberculosis in the proteomics era. *Mol. Genet. Mycobacteria* 2, 239–260. doi: 10.1128/microbiolspec.MGM2-0020-2013

Goff, A., Cantillon, D., Muraro Wildner, L., and Waddell, S. J. (2020). Multi-omics technologies applied to tuberculosis drug discovery. *Appl. Sci.* 10, 4629. doi: 10.3390/app10134629

Gormus, B. J., Blanchard, J. L., Alvarez, X. H., and Didier, P. J. (2004). Evidence for a rhesus monkey model of asymptomatic tuberculosis. *J. Med. primatol.* 33, 134–145. doi: 10.1111/j.1600-0684.2004.00062.x

Gosain, T. P., Chugh, S., Rizvi, Z. A., Chauhan, N. K., Kidwai, S., Thakur, K. G., et al. (2024). Mycobacterium tuberculosis strain with deletions in menT3 and menT4 is attenuated and confers protection in mice and Guinea pigs. *Nat. Commun.* 15, 5467. doi: 10.1038/s41467-024-49246-5

Goto, Y., Buschman, E., and Skamene, E. (1989). Regulation of host resistance to Mycobacterium intracellulare *in vivo* and *in vitro* by the Bcg gene. *Immunogenetics*. 30 (3), 218–221. doi: 10.1007/BF02421210

Gros, P., Skamene, E., and Forget, A. (1981). Genetic control of natural resistance to Mycobacterium bovis (BCG) in mice. *J. Immunol. (Baltimore Md.: 1950)* 127, 2417–2421. doi: 10.4049/jimmunol.127.6.2417

Gross, T. J., Kremens, K., Powers, L. S., Brink, B., Knutson, T., Domann, F. E., et al. (2014). Epigenetic silencing of the human NOS2 gene: rethinking the role of nitric oxide in human macrophage inflammatory responses. *J. Immunol.* 192, 2326–2338. doi: 10.4049/jimmunol.1301758

Grover, A., Taylor, J., Troudt, J., Keyser, A., Arnett, K., Izzo, L., et al. (2009). Kinetics of the immune response profile in Guinea pigs after vaccination with Mycobacterium bovis BCG and infection with Mycobacterium tuberculosis. *Infect. Immun.* 77, 4837–4846. doi: 10.1128/IAI.00704-09

Guha, P., Dutta, S., Murti, K., Charan, J. K., Pandey, K., Ravichandiran, V., et al. (2024). The integration of omics: A promising approach to personalized tuberculosis treatment. *Med. Omics* 12, 100033. doi: 10.1016/j.meomic.2024.100033

Guirado, E., Mbawuike, U., Keiser, T. L., Arcos, J., Azad, A. K., Wang, S. H., et al. (2015). Characterization of host and microbial determinants in individuals with latent tuberculosis infection using a human granuloma model. *MBio* 6, 10–1128. doi: 10.1128/mBio.02537-14

Gupta, U. D., and Katoch, V. M. (2005). Animal models of tuberculosis. *Tuberculosis* 85, 277–293. doi: 10.1016/j.tube.2005.08.008

Harper, J., Skerry, C., Davis, S. L., Tasneen, R., Weir, M., Kramnik, I., et al. (2012). Mouse model of necrotic tuberculosis granulomas develops hypoxic lesions. *J. Infect. Dis.* 205, 595–602. doi: 10.1093/infdis/jir786

Harth, G., and Horwitz, M. A. (2003). Inhibition of Mycobacterium tuberculosis glutamine synthetase as a novel antibiotic strategy against tuberculosis: demonstration of efficacy in *vivo*. *Infect. Immun.* 71, 456–464. doi: 10.1128/IAI.71.1.456-464.2003

Harth, G., Masleša-Galić, S., Tullius, M. V., and Horwitz, M. A. (2005). All four Mycobacterium tuberculosis glnA genes encode glutamine synthetase activities but only GlnA1 is abundantly expressed and essential for bacterial homeostasis. *Mol. Microbiol.* 58, 1157–1172. doi: 10.1111/j.1365-2958.2005.04899.x

Hasin, Y., Seldin, M., and Lusis, A. (2017). Multi-omics approaches to disease. *Genome Biol.* 18, 1–15. doi: 10.1186/s13059-017-1215-1

Heo, I., Dutta, D., Schaefer, D. A., Iakobachvili, N., Artegiani, B., Sachs, N., et al. (2018). Modelling Cryptosporidium infection in human small intestinal and lung organoids. *Nat. Microbiol.* 3, 814–823. doi: 10.1038/s41564-018-0177-8

Heppleston, A. G. (1949). Quantitative air-borne tuberculosis in the rabbit: The course of human type infection. *J. Exp. Med.* 89, 597. doi: 10.1084/jem.89.6.597

Hillier, S., and Charnetzky, W. (1981). Glyoxylate bypass enzymes in Yersinia species and multiple forms of isocitrate lyase in Yersinia pestis. *J. bacteriol.* 145, 452–458. doi: 10.1128/jb.145.1.452-458.1981

Hiromatsu, K., Dascher, C. C., LeClair, K. P., Sugita, M., Furlong, S. T., Brenner, M. B., et al. (2002). Induction of CD1-restricted immune responses in Guinea pigs by immunization with mycobacterial lipid antigens. *J. Immunol.* 169, 330–339. doi: 10.4049/jimmunol.169.1.330

Hoang, A. T. N., Chen, P., Juarez, J., Sachamitr, P., Billing, B., Bosnjak, L., et al. (2012). Dendritic cell functional properties in a three-dimensional tissue model of human lung mucosa. *Am. J. Physiology-Lung Cell. Mol. Physiol.* 302, L226–L237. doi: 10.1152/ajplung.00059.2011

Hoff, D. R., Ryan, G. J., Driver, E. R., Ssemakulu, C. C., De Groote, M. A., Basaraba, R. J., et al. (2011). Location of intra-and extracellular M. tuberculosis populations in lungs of mice and Guinea pigs during disease progression and after drug treatment. *PloS One* 6, e17550. doi: 10.1371/journal.pone.0017550

Huang, Z., Luo, Q., Guo, Y., Chen, J., Xiong, G., Peng, Y., et al. (2015). Mycobacterium tuberculosis-induced polarization of human macrophage orchestrates the formation and development of tuberculous granulomas in *vitro*. *PloS One* 10, e0129744. doi: 10.1371/journal.pone.0129744

Huh, D. (2015). A human breathing lung-on-a-chip. *Ann. Am. Thoracic Soc.* 12, S42–S44. doi: 10.1513/AnnalsATS.201410-442MG

Huh, D., Leslie, D. C., Matthews, B. D., Fraser, J. P., Jurek, S., Hamilton, G. A., et al. (2012). A human disease model of drug toxicity–induced pulmonary edema in a lung-on-a-chip microdevice. *Sci. Trans. Med.* 4, 159ra147. doi: 10.1126/scitranslmed.3004249

Huh, D., Matthews, B. D., Mammoto, A., Montoya-Zavala, M., Hsin, H. Y., and Ingber, D. E. (2010). Reconstituting organ-level lung functions on a chip. *Science* 328, 1662–1668. doi: 10.1126/science.1188302

Hui, K. P., Ching, R. H., Chan, S. K., Nicholls, J. M., Sachs, N., Clevers, H., et al. (2018). Tropism, replication competence, and innate immune responses of influenza virus: an analysis of human airway organoids and ex-vivo bronchus cultures. *Lancet Respiratory Med.* 6, 846–854. doi: 10.1016/S2213-2600(18)30236-4

Hunter, L., Ruedas-Torres, I., Agulló-Ros, I., Rayner, E., and Salguero, F. J. (2023). Comparative pathology of experimental pulmonary tuberculosis in animal models. *Front. Vet. Sci.* 10, 1264833. doi: 10.3389/fvets.2023.1264833

Hyde, J. E. (2007). Targeting purine and pyrimidine metabolism in human apicomplexan parasites. *Curr. Drug Targets* 8, 31–47. doi: 10.2174/138945007779315524

Iakobachvili, N., Leon-Icaza, S. A., Knoops, K., Sachs, N., Mazères, S., Simeone, R., et al. (2022). Mycobacteria–host interactions in human bronchiolar airway organoids. *Mol. Microbiol.* 117, 682–692. doi: 10.1111/mmi.v117.3

Iakobachvili, N., and Peters, P. J. (2017). Humans in a dish: the potential of organoids in modeling immunity and infectious diseases. *Front. Microbiol.* 8, 2402. doi: 10.3389/fmicb.2017.02402

Indrigo, J., Hunter, R. L. Jr., and Actor, J. K. (2003). Cord factor trehalose 6, 6′-dimycolate (TDM) mediates trafficking events during mycobacterial infection of murine macrophages. *Microbiology* 149, 2049–2059. doi: 10.1099/mic.0.26226-0

Irwin, S. M., Gruppo, V., Brooks, E., Gilliland, J., Scherman, M., Reichlen, M. J., et al. (2014). Limited activity of clofazimine as a single drug in a mouse model of tuberculosis exhibiting caseous necrotic granulomas. *Antimicrob. Agents chemother.* 58, 4026–4034. doi: 10.1128/AAC.02565-14

Irwin, S. M., Prideaux, B., Lyon, E. R., Zimmerman, M. D., Brooks, E. J., Schrupp, C. A., et al. (2016). Bedaquiline and pyrazinamide treatment responses are affected by pulmonary lesion heterogeneity in Mycobacterium tuberculosis infected C3HeB/FeJ mice. *ACS Infect. Dis.* 2, 251–267. doi: 10.1021/acsinfecdis.5b00127

Jafari, M., Nasiri, M. R., Sanaei, R., Anoosheh, S., Farnia, P., Sepanjnia, A., et al. (2016). The NRAMP1, VDR, TNF-α, ICAM1, TLR2 and TLR4 gene polymorphisms in Iranian patients with pulmonary tuberculosis: A case–control study. *Infect. Genet. Evol.* 39, 92–98. doi: 10.1016/j.meegid.2016.01.013

Jain, R., Dey, B., Dhar, N., Rao, V., Singh, R., Gupta, U. D., et al. (2008). Enhanced and enduring protection against tuberculosis by recombinant BCG-Ag85C and its association with modulation of cytokine profile in lung. *PloS One* 3, e3869. doi: 10.1371/journal.pone.0003869

Jain, R., Dey, B., and Tyagi, A. K. (2012). Development of the first oligonucleotide microarray for global gene expression profiling in Guinea pigs: defining the transcription signature of infectious diseases. *BMC Genomics* 13, 1–11. doi: 10.1186/1471-2164-13-520

Jeevan, A., Yoshimura, T., Lee, K. E., and McMurray, D. N. (2003). Differential expression of gamma interferon mRNA induced by attenuated and virulent Mycobacterium tuberculosis in Guinea pig cells after Mycobacterium bovis BCG vaccination. *Infect. Immun.* 71, 354–364. doi: 10.1128/IAI.71.1.354-364.2003

Jia, J., Zhang, M., Cao, Z., Hu, X., Lei, S., Zhang, Y., et al. (2024). The rabbit model for spinal tuberculosis: An overview. *J. Orthop. Surg.* 32, 10225536241266703. doi: 10.1177/10225536241266703

Jilani, T. N., Avula, A., Zafar Gondal, A., and Siddiqui, A. H. (2020). "Active Tuberculosis," in *StatPearls* (StatPearls Publishing, Treasure Island, FL, USA).

Jordao, L., Bleck, C. K., Mayorga, L., Griffiths, G., and Anes, E. (2008). On the killing of mycobacteria by macrophages. *Cell. Microbiol.* 10, 529–548. doi: 10.1111/j.1462-5822.2007.01067.x

Kanabalan, R. D., Lee, L. J., Lee, T. Y., Chong, P. P., Hassan, L., Ismail, R., et al. (2021). Human tuberculosis and Mycobacterium tuberculosis complex: A review on genetic diversity, pathogenesis and omics approaches in host biomarkers discovery. *Microbiol. Res.* 246, 126674. doi: 10.1016/j.micres.2020.126674

Kaplan, G., and Tsenova, L. (2010). "Pulmonary tuberculosis in the rabbit," in *A color atlas of comparative pathology of pulmonary tuberculosis* (Boca Raton, FL), vol. 107, 130.

Kapoor, N., Pawar, S., Sirakova, T. D., Deb, C., Warren, W. L., and Kolattukudy, P. E. (2013). Human granuloma *in vitro* model, for TB dormancy and resuscitation. *PloS One* 8, e53657. doi: 10.1371/journal.pone.0053657

Kar, R., Nangpal, P., Mathur, S., Singh, S., and Tyagi, A. K. (2017). bioA mutant of Mycobacterium tuberculosis shows severe growth defect and imparts protection against tuberculosis in Guinea pigs. *PloS One* 12, e0179513. doi: 10.1371/journal.pone.0179513

Kaufmann, S. H. (2003). A short history of Robert pp.Koch's fight against tuberculosis: those who do not remember the past are condemned to repeat it. *Tuberculosis (Edinb)*. 83, 86–90. doi: 10.1016/s1472-9792(02)00064-1

Kawahara, M., Nakasone, T., and Honda, M. (2002). Dynamics of gamma interferon, interleukin-12 (IL-12), IL-10, and transforming growth factor β mRNA expression in primary Mycobacterium bovis BCG infection in Guinea pigs measured by a real-time fluorogenic reverse transcription-PCR assay. *Infect. Immun.* 70, 6614–6620. doi: 10.1128/IAI.70.12.6614-6620.2002

Keiser, T. L., and Purdy, G. E. (2017). Killing Mycobacterium tuberculosis *in vitro*: what model systems can teach us. *Microbiol. Spectr.* 5, 10–1128. doi: 10.1128/microbiolspec.TBTB2-0028-2016

Khader, S. A., Guglani, L., Rangel-Moreno, J., Gopal, R., Fallert Junecko, B. A., Fountain, J. J., et al. (2011). IL-23 is required for long-term control of Mycobacterium tuberculosis and B cell follicle formation in the infected lung. *J. Immunol.* 187, 5402–5407. doi: 10.4049/jimmunol.1101377

Khan, M. M., Ernst, O., Manes, N. P., Oyler, B. L., Fraser, I. D., Goodlett, D. R., et al. (2019). Multi-omics strategies uncover host–pathogen interactions. *ACS Infect. Dis.* 5, 493–505. doi: 10.1021/acsinfecdis.9b00080

Khare, G., Reddy, P. V., Sidhwani, P., and Tyagi, A. K. (2013). KefB inhibits phagosomal acidification but its role is unrelated to M. tuberculosis survival in host. *Sci. Rep.* 3, 3527. doi: 10.1038/srep03527

Kim, S. Y., Choi, J. A., Choi, S., Kim, K. K., Song, C. H., and Kim, E. M. (2024). Advances in an *in vitro* tuberculosis infection model using human lung organoids for host-directed therapies. *PloS Pathog.* 20, e1012295. doi: 10.1371/journal.ppat.1012295

Kjellsson, M. C., Via, L. E., Goh, A., Weiner, D., Low, K. M., Kern, S., et al. (2012). Pharmacokinetic evaluation of the penetration of antituberculosis agents in rabbit pulmonary lesions. *Antimicrob. Agents chemother.* 56, 446–457. doi: 10.1128/AAC.05208-11

Koch, R. (1882). Aetiologie der tuberculose. *Berlin Klin Wochenschr* 19, 221–230.

Köster, S., Upadhyay, S., Chandra, P., Papavinasasundaram, K., Yang, G., Hassan, A., et al. (2017). Mycobacterium tuberculosis is protected from NADPH oxidase and LC3-associated phagocytosis by the LCP protein CpsA. *Proc. Natl. Acad. Sci.* 114, E8711–E8720. doi: 10.1073/pnas.1707792114

Kramnik, I., Dietrich, W. F., Demant, P., and Bloom, B. R. (2000). Genetic control of resistance to experimental infection with virulent Mycobacterium tuberculosis. *Proc. Natl. Acad. Sci.* 97, 8560–8565. doi: 10.1073/pnas.150227197

Kraut, J. A., and Madias, N. E. (2014). Lactic acidosis. *New Engl. J. Med.* 371, 2309–2319. doi: 10.1056/NEJMra1309483

Kroon, E. E., Kinnear, C. J., Orlova, M., Fischinger, S., Shin, S., Boolay, S., et al. (2020). An observational study identifying highly tuberculosis-exposed, HIV-1-positive but persistently TB, tuberculin and IGRA negative persons with M. tuberculosis specific antibodies in Cape Town, South Africa. *EBioMedicine* 61, 103053. doi: 10.1016/j.ebiom.2020.103053

Kwan, C. K., and Ernst, J. D. (2011). HIV and tuberculosis: a deadly human syndemic. *Clin. Microbiol. Rev.* 24, 351–376. doi: 10.1128/CMR.00042-10

Laddy, D. J., Bonavia, A., Hanekom, W. A., Kaushal, D., Williams, A., Roederer, M., et al. (2018). Toward tuberculosis vaccine development: recommendations for nonhuman primate study design. *Infect. Immun.* 86, 10–1128. doi: 10.1128/IAI.00776-17

Langermans, J. A., Andersen, P., van Soolingen, D., Vervenne, R. A., Frost, P. A., van der Laan, T., et al. (2001). Divergent effect of bacillus Calmette–Guerin (BCG) vaccination on Mycobacterium tuberculosis infection in highly related macaque species: Implications for primate models in tuberculosis vaccine research. *Proc. Natl. Acad. Sci.* 98, 11497–11502. doi: 10.1073/pnas.201404898

Lau, S. K., Lam, C. W., Curreem, S. O., Lee, K. C., Lau, C. C., Chow, W. N., et al. (2015). Identification of specific metabolites in culture supernatant of Mycobacterium tuberculosis using metabolomics: exploration of potential biomarkers. *Emerg. microb. infect.* 4, 1–10. doi: 10.1038/emi.2015.6

Lee, J., Choi, J. A., Cho, S. N., Son, S. H., and Song, C. H. (2019). Mitofusin 2-deficiency suppresses Mycobacterium tuberculosis survival in macrophages. *Cells* 8, 1355. doi: 10.3390/cells8111355

Lenaerts, A. J., Hoff, D., Aly, S., Ehlers, S., Andries, K., Cantarero, L., et al. (2007). Location of persisting mycobacteria in a Guinea pig model of tuberculosis revealed by r207910. *Antimicrob. Agents chemother.* 51, 3338–3345. doi: 10.1128/AAC.00276-07

Leone, R. D., Zhao, L., Englert, J. M., Sun, I. M., Oh, M. H., Sun, I. H., et al. (2019). Glutamine blockade induces divergent metabolic programs to overcome tumor immune evasion. *Science* 366, 1013–1021. doi: 10.1126/science.aav2588

Lin, P. L., Dietrich, J., Tan, E., Abalos, R. M., Burgos, J., Bigbee, C., et al. (2012a). The multistage vaccine H56 boosts the effects of BCG to protect cynomolgus macaques against active tuberculosis and reactivation of latent Mycobacterium tuberculosis infection. *J. Clin. Invest.* 122, 303–314. doi: 10.1172/JCI46252

Lin, P. L., Myers, A., Smith, L. K., Bigbee, C., Bigbee, M., Fuhrman, C., et al. (2010). Tumor necrosis factor neutralization results in disseminated disease in acute and latent Mycobacterium tuberculosis infection with normal granuloma structure in a cynomolgus macaque model. *Arthritis Rheuma.* 62, 340–350. doi: 10.1002/art.27271

Lin, P. L., Rodgers, M., Smith, L. K., Bigbee, M., Myers, A., Bigbee, C., et al. (2009). Quantitative comparison of active and latent tuberculosis in the cynomolgus macaque model. *Infect. Immun.* 77, 4631–4642. doi: 10.1128/IAI.00592-09

Lin, P. L., Rutledge, T., Green, A. M., Bigbee, M., Fuhrman, C., Klein, E., et al. (2012b). CD4 T cell depletion exacerbates acute Mycobacterium tuberculosis while reactivation of latent infection is dependent on severity of tissue depletion in cynomolgus macaques. *AIDS Res. Hum. retroviruses* 28, 1693–1702. doi: 10.1089/aid.2012.0028

Liu, C. H., Liu, H., and Ge, B. (2017). Innate immunity in tuberculosis: host defense vs pathogen evasion. *Cell. Mol. Immunol.* 14, 963–975. doi: 10.1038/cmi.2017.88

Lorenz, M. C., and Fink, G. R. (2001). The glyoxylate cycle is required for fungal virulence. *Nature* 412, 83–86. doi: 10.1038/35083594

Low, L. A., Mummery, C., Berridge, B. R., Austin, C. P., and Tagle, D. A. (2021). Organs-on-chips: into the next decade. *Nat. Rev. Drug Discov.* 20, 345–361. doi: 10.1038/s41573-020-0079-3

Luies, L., and Du Preez, I. (2020). The echo of pulmonary tuberculosis: mechanisms of clinical symptoms and other disease-induced systemic complications. *Clin. Microbiol. Rev.* 33, 10–1128. doi: 10.1128/CMR.00036-20

Lurie, M. B. (1928). The fate of human and bovine tubercle bacilli in various organs of the rabbit. *J. Exp. Med.* 48, 155–182. doi: 10.1084/jem.48.2.155

Lurie, M. B., Abramson, S., and Heppleston, A. G. (1952). On the response of genetically resistant and susceptible rabbits to the quantitative inhalation of human type tubercle bacilli and the nature of resistance to tuberculosis. *J. Exp. Med.* 95, 119. doi: 10.1084/jem.95.2.119

MacGurn, J. A., and Cox, J. S. (2007). A genetic screen for Mycobacterium tuberculosis mutants defective for phagosome maturation arrest identifies components of the ESX-1 secretion system. *Infect. Immun.* 75, 2668–2678. doi: 10.1128/IAI.01872-06

Maiello, P., DiFazio, R. M., Cadena, A. M., Rodgers, M. A., Lin, P. L., Scanga, C. A., et al. (2018). Rhesus macaques are more susceptible to progressive tuberculosis than cynomolgus macaques: a quantitative comparison. *Infect. Immun.* 86, 10–1128. doi: 10.1128/IAI.00505-17

Malo, D., Vogan, K., Vidal, S., Hu, J., Cellier, M., Schurr, E., et al. (1994). Haplotype mapping and sequence analysis of the mouse Nramp gene predict susceptibility to infection with intracellular parasites. *Genomics* 23, 51–61. doi: 10.1006/geno.1994.1458

Manabe, Y. C., Dannenberg, A. M. Jr., Tyagi, S. K., Hatem, C. L., Yoder, M., Woolwine, S. C., et al. (2003). Different strains of Mycobacterium tuberculosis cause various spectrums of disease in the rabbit model of tuberculosis. *Infect. Immun.* 71, 6004–6011. doi: 10.1128/IAI.71.10.6004-6011.2003

Manabe, Y. C., Kesavan, A. K., Lopez-Molina, J., Hatem, C. L., Brooks, M., Fujiwara, R., et al. (2008). The aerosol rabbit model of TB latency, reactivation and immune reconstitution inflammatory syndrome. *Tuberculosis* 88, 187–196. doi: 10.1016/j.tube.2007.10.006

Marakalala, M. J., Raju, R. M., Sharma, K., Zhang, Y. J., Eugenin, E. A., Prideaux, B., et al. (2016). Inflammatory signaling in human tuberculosis granulomas is spatially organized. *Nat. Med.* 22, 531–538. doi: 10.1038/nm.4073

Marino, S., Pawar, S., Fuller, C. L., Reinhart, T. A., Flynn, J. L., and Kirschner, D. E. (2004). Dendritic cell trafficking and antigen presentation in the human immune response to Mycobacterium tuberculosis. *J. Immunol.* 173, 494–506. doi: 10.4049/jimmunol.173.1.494

Martin, D. R., Sibuyi, N. R., Dube, P., Fadaka, A. O., Cloete, R., Onani, M., et al. (2021). Aptamer-based diagnostic systems for the rapid screening of TB at the point-of-care. *Diagnostics* 11, 1352. doi: 10.3390/diagnostics11081352

Martin, C., Williams, A., Hernandez-Pando, R., Cardona, P. J., Gormley, E., Bordat, Y., et al. (2006). The live Mycobacterium tuberculosis phoP mutant strain is more attenuated than BCG and confers protective immunity against tuberculosis in mice and Guinea pigs. *Vaccine* 24, 3408–3419. doi: 10.1016/j.vaccine.2006.03.017

Mattila, J. T., Diedrich, C. R., Lin, P. L., Phuah, J., and Flynn, J. L. (2011). Simian immunodeficiency virus-induced changes in T cell cytokine responses in cynomolgus macaques with latent Mycobacterium tuberculosis infection are associated with timing of reactivation. *J. Immunol.* 186, 3527–3537. doi: 10.4049/jimmunol.1003773

McMurray, D. N. (1994). Guinea pig model of tuberculosis. *Tubercul.: pathogen. protect. control*, 135–147. doi: 10.1128/9781555818357

Medina, E., and North, R. J. (1996). Evidence inconsistent with a role for the Bcg gene (Nramp1) in resistance of mice to infection with virulent Mycobacterium tuberculosis. *J. Exp. Med.* 183, 1045–1051. doi: 10.1084/jem.183.3.1045

Medina, E., and North, R. J. (1998). Resistance ranking of some common inbred mouse strains to Mycobacterium tuberculosis and relationship to major histocompatibility complex haplotype and Nramp1 genotype. *Immunology* 93, 270–274. doi: 10.1046/j.1365-2567.1998.00419.x

Mehra, S., Golden, N. A., Dutta, N. K., Midkiff, C. C., Alvarez, X., Doyle, L. A., et al. (2011). Reactivation of latent tuberculosis in rhesus macaques by coinfection with simian immunodeficiency virus. *J. Med. primatol.* 40, 233–243. doi: 10.1111/j.1600-0684.2011.00485.x

Mehra, S., Golden, N. A., Stuckey, K., Didier, P. J., Doyle, L. A., Russell-Lodrigue, K. E., et al. (2012). The Mycobacterium tuberculosis stress response factor SigH is required for bacterial burden as well as immunopathology in primate lungs. *J. Infect. Dis.* 205, 1203–1213. doi: 10.1093/infdis/jis102

Mehra, S., Pahar, B., Dutta, N. K., Conerly, C. N., Philippi-Falkenstein, K., Alvarez, X., et al. (2010). Transcriptional reprogramming in nonhuman primate (rhesus macaque) tuberculosis granulomas. *PloS One* 5, e12266. doi: 10.1371/journal.pone.0012266

Méndez-Samperio, P. (2010). Role of interleukin-12 family cytokines in the cellular response to mycobacterial disease. *Int. J. Infect. Dis.* 14, e366–e371. doi: 10.1016/j.ijid.2009.06.022

Meurs, H., Santing, R. E., Remie, R., van der Mark, T. W., Westerhof, F. J., Zuidhof, A. B., et al. (2006). A Guinea pig model of acute and chronic asthma using permanently instrumented and unrestrained animals. *Nat. Protoc.* 1, 840–847. doi: 10.1038/nprot.2006.144

Miller, E. A., and Ernst, J. D. (2009). Anti-TNF immunotherapy and tuberculosis reactivation: another mechanism revealed. *J. Clin. Invest.* 119, 1079–1082. doi: 10.1172/JCI39143

Mills, M., and Estes, M. K. (2016). Physiologically relevant human tissue models for infectious diseases. *Drug Discov. Today* 21, 1540–1552. doi: 10.1016/j.drudis.2016.06.020

Mitsos, L. M., Cardon, L. R., Fortin, A., Ryan, L., LaCourse, R., North, R. J., et al. (2000). Genetic control of susceptibility to infection with Mycobacterium tuberculosis in mice. *Genes Immun.* 1, 467–477. doi: 10.1038/sj.gene.6363712

Mitsos, L. M., Cardon, L. R., Ryan, L., LaCourse, R., North, R. J., and Gros, P. (2003). Susceptibility to tuberculosis: a locus on mouse chromosome 19 (Trl-4) regulates Mycobacterium tuberculosis replication in the lungs. *Proc. Natl. Acad. Sci.* 100, 6610–6615. doi: 10.1073/pnas.1031727100

Moreira-Teixeira, L., Tabone, O., Graham, C. M., Singhania, A., Stavropoulos, E., Redford, P. S., et al. (2020). Mouse transcriptome reveals potential signatures of protection and pathogenesis in human tuberculosis. *Nat. Immunol.* 21, 464–476. doi: 10.1038/s41590-020-0610-z

Mukadi, Y., Perriëns, J. H., St Louis, M. E., Brown, C., Ryder, R. W., Portaels, F., et al. (1993). Spectrum of immunodeficiency in HIV-1-infected patients with pulmonary tuberculosis in Zaire. *Lancet* 342, 143–146. doi: 10.1016/0140-6736(93)91346-N

Nadkarni, R. R., Abed, S., and Draper, J. S. (2016). Organoids as a model system for studying human lung development and disease. *Biochem. Biophys. Res. Commun.* 473, 675–682. doi: 10.1016/j.bbrc.2015.12.091

Nangpal, P., Bahal, R. K., and Tyagi, A. K. (2017). Boosting with recombinant MVA expressing M. tuberculosis α-crystallin antigen augments the protection imparted by BCG against tuberculosis in Guinea pigs. *Sci. Rep.* 7, 17286. doi: 10.1038/s41598-017-17587-5

Ndlovu, H., and Marakalala, M. J. (2016). Granulomas and inflammation: host-directed therapies for tuberculosis. *Front. Immunol.* 7, 434. doi: 10.3389/fimmu.2016.00434

Ng, V. H., Cox, J. S., Sousa, A. O., MacMicking, J. D., and McKinney, J. D. (2004). Role of KatG catalase-peroxidase in mycobacterial pathogenesis: countering the phagocyte oxidative burst. *Mol. Microbiol.* 52, 1291–1302. doi: 10.1111/j.1365-2958.2004.04078.x

North, R. J., LaCourse, R., Ryan, L., and Gros, P. (1999). Consequence of Nramp1 deletion to Mycobacterium tuberculosis infection in mice. *Infect. Immun.* 67, 5811–5814. doi: 10.1128/IAI.67.11.5811-5814.1999

Ogus, A. C., Yoldas, B., Ozdemir, T., Uguz, A., Olcen, S., Keser, I., et al. (2004). The Arg753GLn polymorphism of the human toll-like receptor 2 gene in tuberculosis disease. *Eur. Respiratory J.* 23, 219–223. doi: 10.1183/09031936.03.00061703

Oh, M. H., Sun, I. H., Zhao, L., Leone, R. D., Sun, I. M., Xu, W., et al. (2020). Targeting glutamine metabolism enhances tumor-specific immunity by modulating suppressive myeloid cells. *J. Clin. Invest.* 130, 3865–3884. doi: 10.1172/JCI131859

Okamoto, Y., Umemura, M., Yahagi, A., O'Brien, R. L., Ikuta, K., Kishihara, K., et al. (2010). Essential role of IL-17A in the formation of a mycobacterial infection-induced granuloma in the lung. *J. Immunol.* 184, 4414–4422. doi: 10.4049/jimmunol.0903332

Ordway, D., Palanisamy, G., Henao-Tamayo, M., Smith, E. E., Shanley, C., Orme, I. M., et al. (2007). The cellular immune response to Mycobacterium tuberculosis infection in the Guinea pig. *J. Immunol.* 179, 2532–2541. doi: 10.4049/jimmunol.179.4.2532

Orme, I. M., and Basaraba, R. J. (2014). The formation of the granuloma in tuberculosis infection. *Semin. Immunol.* 26, 601–609. doi: 10.1016/j.smim.2014.09.009

Orme, I. M., and Ordway, D. J. (2016). Mouse and Guinea pig models of tuberculosis. *Microbiol. Spectr.* 4, 10–1128. doi: 10.1128/microbiolspec.TBTB2-0002-2015

Padilla-Carlin, D. J., McMurray, D. N., and Hickey, A. J. (2008). The Guinea pig as a model of infectious diseases. *Comp. Med.* 58, 324–340.

Pahwa, F., Chaudhary, S., Dayal, A., and Nanda, R. K. (2024). Lung Mycobacterium tuberculosis infection perturbs metabolic pathways in non-pulmonary tissues. *bioRxiv*, 2024–2002. doi: 10.1101/2024.02.09.579656

Pan, H., Yan, B. S., Rojas, M., Shebzukhov, Y. V., Zhou, H., Kobzik, L., et al. (2005). Ipr1 gene mediates innate immunity to tuberculosis. *Nature* 434, 767–772. doi: 10.1038/nature03419

Parasa, V. R., Muvva, J. R., Rose, J. F., Braian, C., Brighenti, S., and Lerm, M. (2017). Inhibition of tissue matrix metalloproteinases interferes with Mycobacterium tuberculosis-induced granuloma formation and reduces bacterial load in a human lung tissue model. *Front. Microbiol.* 8, 2370. doi: 10.3389/fmicb.2017.02370

Parasa, V. R., Rahman, M. J., Ngyuen Hoang, A. T., Svensson, M., Brighenti, S., and Lerm, M. (2014). Modeling Mycobacterium tuberculosis early granuloma formation in experimental human lung tissue. *Dis. Models Mech.* 7, 281–288. doi: 10.1242/dmm.013854

Park, J., Kim, H., Kwon, K. W., Choi, H. H., Kang, S. M., Hong, J. J., et al. (2020). Toll-like receptor 4 signaling-mediated responses are critically engaged in optimal host protection against highly virulent Mycobacterium tuberculosis K infection. *Virulence* 11, 430–445. doi: 10.1080/21505594.2020.1766401

Parveen, S., Shen, J., Lun, S., Zhao, L., Alt, J., Koleske, B., et al. (2023). Glutamine metabolism inhibition has dual immunomodulatory and antibacterial activities against Mycobacterium tuberculosis. *Nat. Commun.* 14, 7427. doi: 10.1038/s41467-023-43304-0

Pasipanodya, J. G., McIlleron, H., Burger, A., Wash, P. A., Smith, P., and Gumbo, T. (2013). Serum drug concentrations predictive of pulmonary tuberculosis outcomes. *J. Infect. Dis.* 208, 1464–1473. doi: 10.1093/infdis/jit352

Perez, R. L., Roman, J., Roser, S., Little, C., Olsen, M., Indrigo, J., et al. (2000). Cytokine message and protein expression during lung granuloma formation and resolution induced by the mycobacterial cord factor trehalose-6, 6′-dimycolate. *J. Interfer. Cytok. Res.* 20, 795–804. doi: 10.1089/10799900050151067

Pethe, K., Swenson, D. L., Alonso, S., Anderson, J., Wang, C., and Russell, D. G. (2004). Isolation of Mycobacterium tuberculosis mutants defective in the arrest of phagosome maturation. *Proc. Natl. Acad. Sci.* 101, 13642–13647. doi: 10.1073/pnas.0401657101

Peyron, P., Vaubourgeix, J., Poquet, Y., Levillain, F., Botanch, C., Bardou, F., et al. (2008). Foamy macrophages from tuberculous patients' granulomas constitute a nutrient-rich reservoir for M. *tubercul. persist. PloS Pathog.* 4, e1000204. doi: 10.1371/journal.ppat.1000204

Plant, J., and Glynn, A. A. (1976). Genetics of resistance to infection with Salmonella typhimurium in mice. *J. Infect. Dis.* 133, 72–78. doi: 10.1093/infdis/133.1.72

Portevin, D., Gagneux, S., Comas, I., and Young, D. (2011). Human macrophage responses to clinical isolates from the Mycobacterium tuberculosis complex discriminate between ancient and modern lineages. *PloS Pathog.* 7, e1001307. doi: 10.1371/journal.ppat.1001307

Post, F. A., Wood, R., and Pillay, G. P. (1995). Pulmonary tuberculosis in HIV infection: radiographic appearance is related to CD4+ T-lymphocyte count. *Tubercle Lung Dis.* 76, 518–521. doi: 10.1016/0962-8479(95)90527-8

Pradhan, G., Shrivastva, R., and Mukhopadhyay, S. (2018). Mycobacterial PknG targets the Rab7l1 signaling pathway to inhibit phagosome–lysosome fusion. *J. Immunol.* 201, 1421–1433. doi: 10.4049/jimmunol.1800530

Puissegur, M. P., Botanch, C., Duteyrat, J. L., Delsol, G., Caratero, C., and Altare, F. (2004). An *in vitro* dual model of mycobacterial granulomas to investigate the molecular interactions between mycobacteria and human host cells. *Cell. Microbiol.* 6, 423–433. doi: 10.1111/j.1462-5822.2004.00371.x

Puri, R. V., Reddy, P. V., and Tyagi, A. K. (2013). Secreted acid phosphatase (SapM) of Mycobacterium tuberculosis is indispensable for arresting phagosomal maturation and growth of the pathogen in Guinea pig tissues. *PloS One* 8, e70514. doi: 10.1371/journal.pone.0070514

Qualls, J. E., and Murray, P. J. (2016). Immunometabolism within the tuberculosis granuloma: amino acids, hypoxia, and cellular respiration. *Semin. immunopathol.* 38, 139–152. doi: 10.1007/s00281-015-0534-0

Rachman, H., Strong, M., Schaible, U., Schuchhardt, J., Hagens, K., Mollenkopf, H., et al. (2006a). Mycobacterium tuberculosis gene expression profiling within the context of protein networks. *Microb. infect.* 8, 747–757. doi: 10.1016/j.micinf.2005.09.011

Rachman, H., Strong, M., Ulrichs, T., Grode, L., Schuchhardt, J., Mollenkopf, H., et al. (2006b). Unique transcriptome signature of Mycobacterium tuberculosis in pulmonary tuberculosis. *Infect. Immun.* 74, 1233–1242. doi: 10.1128/IAI.74.2.1233-1242.2006

Rais, R., Jancarik, A., Tenora, L., Nedelcovych, M., Alt, J., Englert, J., et al. (2016). Discovery of 6-diazo-5-oxo-l-norleucine (DON) prodrugs with enhanced CSF delivery in monkeys: a potential treatment for glioblastoma. *J. med. Chem.* 59, 8621–8633. doi: 10.1021/acs.jmedchem.6b01069

Rao, V., Fujiwara, N., Porcelli, S. A., and Glickman, M. S. (2005). Mycobacterium tuberculosis controls host innate immune activation through cyclopropane modification of a glycolipid effector molecule. *J. Exp. Med.* 201, 535–543. doi: 10.1084/jem.20041668

Rao, V., Gao, F., Chen, B., Jacobs, W. R., and Glickman, M. S. (2006). Trans-cyclopropanation of mycolic acids on trehalose dimycolate suppresses Mycobacterium tuberculosis–induced inflammation and virulence. *J. Clin. Invest.* 116, 1660–1667. doi: 10.1172/JCI27335

Raschke, W. C., Baird, S., Ralph, P., and Nakoinz, I. (1978). Functional macrophage cell lines transformed by Abelson leukemia virus. *Cell* 15, 261–267. doi: 10.1016/0092-8674(78)90101-0

Ravesloot-Chávez, M. M., Van Dis, E., and Stanley, S. A. (2021). The innate immune response to Mycobacterium tuberculosis infection. *Annu. Rev. Immunol.* 39, 611–637. doi: 10.1146/annurev-immunol-093019-010426

Reddy, P. V., Puri, R. V., Chauhan, P., Kar, R., Rohilla, A., Khera, A., et al. (2013). Disruption of mycobactin biosynthesis leads to attenuation of Mycobacterium tuberculosis for growth and virulence. *J. Infect. Dis.* 208, 1255–1265. doi: 10.1093/infdis/jit250

Reddy, P. V., Puri, R. V., Khera, A., and Tyagi, A. K. (2012). Iron storage proteins are essential for the survival and pathogenesis of Mycobacterium tuberculosis in THP-1 macrophages and the Guinea pig model of infection. *J. bacteriol.* 194, 567–575. doi: 10.1128/JB.05553-11

Reed, S. G., Coler, R. N., Dalemans, W., Tan, E. V., DeLa Cruz, E. C., Basaraba, R. J., et al. (2009). Defined tuberculosis vaccine, Mtb72F/AS02A, evidence of protection in

cynomolgus monkeys. *Proc. Natl. Acad. Sci.* 106, 2301–2306. doi: 10.1073/pnas.0712077106

Reyes, P., Rathod, P. K., Sanchez, D. J., Mrema, J. E., Rieckmann, K. H., and Heidrich, H. G. (1982). Enzymes of purine and pyrimidine metabolism from the human malaria parasite, Plasmodium falciparum. *Mol. Biochem. parasitol.* 5, 275–290. doi: 10.1016/0166-6851(82)90035-4

Rhoades, E. R., Frank, A. A., and Orme, I. M. (1997). Progression of chronic pulmonary tuberculosis in mice aerogenically infected with virulent Mycobacterium tuberculosis. *Tubercle Lung Dis.* 78, 57–66. doi: 10.1016/S0962-8479(97)90016-2

Rifat, D., Prideaux, B., Savic, R. M., Urbanowski, M. E., Parsons, T. L., Luna, B., et al. (2018). Pharmacokinetics of rifapentine and rifampin in a rabbit model of tuberculosis and correlation with clinical trial data. *Sci. Trans. Med.* 10, eaai7786. doi: 10.1126/scitranslmed.aai7786

Routy, J. P., Routy, B., Graziani, G. M., and Mehraj, V. (2016). The kynurenine pathway is a double-edged sword in immune-privileged sites and in cancer: implications for immunotherapy. *Int. J. Tryptop. Res.* 9, IJTR–S38355. doi: 10.4137/IJTR.S38355

Rustad, T. R., Harrell, M. I., Liao, R., and Sherman, D. R. (2008). The enduring hypoxic response of Mycobacterium tuberculosis. *PloS One* 3, e1502. doi: 10.1371/journal.pone.0001502

Ryu, S., Park, Y. K., Bai, G. H., Kim, S. J., Park, S. N., and Kang, S. (2000). 3′ UTR polymorphisms in the NRAMP1 gene are associated with susceptibility to tuberculosis in Koreans. *Int. J. Tubercul. Lung Dis.* 4, 577–580.

Sachs, N., Papaspyropoulos, A., Zomer-van-Ommen, D. D., Heo, I., Böttinger, L., Klay, D., et al. (2019). Long-term expanding human airway organoids for disease modeling. *EMBO J.* 38, e100300. doi: 10.15252/embj.2018100300

Salindri, A. D., Haw, J. S., Amere, G. A., Alese, J. T., Umpierrez, G. E., and Magee, M. J. (2021). Latent tuberculosis infection among patients with and without type-2 diabetes mellitus: results from a hospital case-control study in Atlanta. *BMC Res. Notes* 14, 252. doi: 10.1186/s13104-021-05662-0

Sampson, S. L., Dascher, C. C., Sambandamurthy, V. K., Russell, R. G., Jacobs, W. R. Jr., Bloom, B. R., et al. (2004). Protection elicited by a double leucine and pantothenate auxotroph of Mycobacterium tuberculosis in Guinea pigs. *Infect. Immun.* 72, 3031–3037. doi: 10.1128/IAI.72.5.3031-3037.2004

Sankar, P., and Mishra, B. B. (2023). Early innate cell interactions with Mycobacterium tuberculosis in protection and pathology of tuberculosis. *Front. Immunol.* 14, 1260859. doi: 10.3389/fimmu.2023.1260859

Scanga, C. A., Bafica, A., Feng, C. G., Cheever, A. W., Hieny, S., and Sher, A. (2004). MyD88-deficient mice display a profound loss in resistance to Mycobacterium tuberculosis associated with partially impaired Th1 cytokine and nitric oxide synthase 2 expression. *Infect. Immun.* 72, 2400–2404. doi: 10.1128/IAI.72.4.2400-2404.2004

Schmidt, L. H. (1966). Studies on the antituberculous activity of ethambutol in monkeys. *Ann. New York Acad. Sci.* 135, 747–758. doi: 10.1111/j.1749-6632.1966.tb45520.x

Schnappinger, D., Ehrt, S., Voskuil, M. I., Liu, Y., Mangan, J. A., Monahan, I. M., et al. (2003). Transcriptional adaptation of Mycobacterium tuberculosis within macrophages: insights into the phagosomal environment. *J. Exp. Med.* 198, 693–704. doi: 10.1084/jem.20030846

Schwende, H., Fitzke, E., Ambs, P., and Dieter, P. (1996). Differences in the state of differentiation of THP-1 cells induced by phorbol ester and 1, 25-dihydroxyvitamin D3. *J. Leuco. Biol.* 59, 555–561. doi: 10.1002/jlb.59.4.555

Seitzer, U., and Gerdes, J. (2003). Generation and characterization of multicellular heterospheroids formed by human peripheral blood mononuclear cells. *Cells Tissues Organs* 174, 110–116. doi: 10.1159/000071151

Serafini, A., Tan, L., Horswell, S., Howell, S., Greenwood, D. J., Hunt, D. M., et al. (2019). Mycobacterium tuberculosis requires glyoxylate shunt and reverse methylcitrate cycle for lactate and pyruvate metabolism. *Mol. Microbiol.* 112, 1284–1307. doi: 10.1111/mmi.v112.4

Shang, S., Harton, M., Tamayo, M. H., Shanley, C., Palanisamy, G. S., Caraway, M., et al. (2011). Increased Foxp3 expression in Guinea pigs infected with W-Beijing strains of M. tuberculosis. *Tuberculosis* 91, 378–385. doi: 10.1016/j.tube.2011.06.001

Sharma, V., Sharma, S., Zu Bentrup, K. H., McKinney, J. D., Russell, D. G., Jacobs, W. R., et al. (2000). Structure of isocitrate lyase, a persistence factor of Mycobacterium tuberculosis. *Nat. Struct. Biol.* 7, 663–668. doi: 10.1038/77964

Sharpe, S., White, A., Gleeson, F., McIntyre, A., Smyth, D., Clark, S., et al. (2016). Ultra low dose aerosol challenge with Mycobacterium tuberculosis leads to divergent outcomes in rhesus and cynomolgus macaques. *Tuberculosis* 96, 1–12. doi: 10.1016/j.tube.2015.10.004

Shi, S., and Ehrt, S. (2006). Dihydrolipoamide acyltransferase is critical for Mycobacterium tuberculosis pathogenesis. *Infect. Immun.* 74, 56–63. doi: 10.1128/IAI.74.1.56-63.2006

Shin, J. H., Yang, J. Y., Jeon, B. Y., Yoon, Y. J., Cho, S. N., Kang, Y. H., et al. (2011). 1H NMR-based metabolomic profiling in mice infected with Mycobacterium tuberculosis. *J. Proteome Res.* 10, 2238–2247. doi: 10.1021/pr101054m

Shrestha, J., Razavi Bazaz, S., Aboulkheyr Es, H., Yaghobian Azari, D., Thierry, B., Ebrahimi Warkiani, M., et al. (2020). Lung-on-a-chip: the future of respiratory disease models and pharmacological studies. *Crit. Rev. Biotechnol.* 40, 213–230. doi: 10.1080/07388551.2019.1710458

Sibley, L., Dennis, M., Sarfas, C., White, A., Clark, S., Gleeson, F., et al. (2016). Route of delivery to the airway influences the distribution of pulmonary disease but not the outcome of Mycobacterium tuberculosis infection in rhesus macaques. *Tuberculosis* 96, 141–149. doi: 10.1016/j.tube.2015.11.004

Silva-Miranda, M., Ekaza, E., Breiman, A., Asehnoune, K., Barros-Aguirre, D., Pethe, K., et al. (2015). High-content screening technology combined with a human granuloma model as a new approach to evaluate the activities of drugs against Mycobacterium tuberculosis. *Antimicrob. Agents chemother.* 59, 693–697. doi: 10.1128/AAC.03705-14

Simmonds, H. A., Duley, J. A., Fairbanks, L. D., and McBride, M. B. (1997). When to investigate for purine and pyrimidine disorders. Introduction and review of clinical and laboratory indications. *J. inherit. Metab. Dis.* 20, 214–226. doi: 10.1023/A:1005308923168

Simmons, J. D., Stein, C. M., Seshadri, C., Campo, M., Alter, G., Fortune, S., et al. (2018). Immunological mechanisms of human resistance to persistent Mycobacterium tuberculosis infection. *Nat. Rev. Immunol.* 18, 575–589. doi: 10.1038/s41577-018-0025-3

Singh, S., Goswami, N., Tyagi, A. K., and Khare, G. (2019). Unraveling the role of the transcriptional regulator VirS in low pH–induced responses of Mycobacterium tuberculosis and identification of VirS inhibitors. *J. Biol. Chem.* 294, 10055–10075. doi: 10.1074/jbc.RA118.005312

Singh, V., Jamwal, S., Jain, R., Verma, P., Gokhale, R., and Rao, K. V. (2012). Mycobacterium tuberculosis-driven targeted recalibration of macrophage lipid homeostasis promotes the foamy phenotype. *Cell host Microbe* 12, 669–681. doi: 10.1016/j.chom.2012.09.012

Singh, R., Rao, V., Shakila, H., Gupta, R., Khera, A., Dhar, N., et al. (2003). Disruption of mptpB impairs the ability of Mycobacterium tuberculosis to survive in Guinea pigs. *Mol. Microbiol.* 50, 751–762. doi: 10.1046/j.1365-2958.2003.03712.x

Smith, D. W., McMurray, D. N., Wiegeshaus, E. H., Grover, A. A., and Harding, G. E. (1970). Host-parasite relationships in experimental airborne tuberculosis: IV. Early events in the course of infection in vaccinated and nonvaccinated Guinea pigs. *Am. Rev. Respiratory Dis.* 102, 937–949. doi: 10.1164/arrd.1970.102.6.937

Soldevilla, P., Vilaplana, C., and Cardona, P. J. (2022). Mouse models for Mycobacterium tuberculosis pathogenesis: show and do not tell. *Pathogens* 12, 49. doi: 10.3390/pathogens12010049

Solovic, I., Sester, M., Gomez-Reino, J. J., Rieder, H. L., Ehlers, S., Milburn, H. J., et al. (2010). The risk of tuberculosis related to tumour necrosis factor antagonist therapies: a TBNET consensus statement. *Eur. Respir. J.* (2011) 36, 1185–1206. doi: 10.1183/09031936.00028510

Somashekar, B. S., Amin, A. G., Rithner, C. D., Troudt, J., Basaraba, R., Izzo, A., et al. (2011). Metabolic profiling of lung granuloma in Mycobacterium tuberculosis infected Guinea pigs: ex vivo 1H magic angle spinning NMR studies. *J. Proteome Res.* 10, 4186–4195. doi: 10.1021/pr2003352

Somashekar, B. S., Amin, A. G., Tripathi, P., MacKinnon, N., Rithner, C. D., Shanley, C. A., et al. (2012). Metabolomic signatures in Guinea pigs infected with epidemic-associated W-Beijing strains of Mycobacterium tuberculosis. *J. Proteome Res.* 11, 4873–4884. doi: 10.1021/pr300345x

Son, S. H., Lee, J., Cho, S. N., Choi, J. A., Kim, J., Nguyen, T. D., et al. (2023). Herp regulates intracellular survival of Mycobacterium tuberculosis H37Ra in macrophages by regulating reactive oxygen species-mediated autophagy. *Mbio* 14, e01535–e01523. doi: 10.1128/mbio.01535-23

Southan, C. (2004). Has the yo-yo stopped? An assessment of human protein-coding gene number. *Proteomics* 4, 1712–1726. doi: 10.1002/pmic.200300700

Srivastava, S., Battu, M. B., Khan, M. Z., Nandicoori, V. K., and Mukhopadhyay, S. (2019). Mycobacterium tuberculosis PPE2 protein interacts with p67phox and inhibits reactive oxygen species production. *J. Immunol.* 203, 1218–1229. doi: 10.4049/jimmunol.1801143

Stead, W. W., Senner, J. W., Reddick, W. T., and Lofgren, J. P. (1990). Racial differences in susceptibility to infection by Mycobacterium tuberculosis. *N. Engl. J. Med.* 322, 422–427. doi: 10.1056/NEJM199002153220702

Stewart, G. R., Wernisch, L., Stabler, R., Mangan, J. A., Hinds, J., Laing, K. G., et al. (2002). Dissection of the heat-shock response in Mycobacterium tuberculosis using mutants and microarrays. *Microbiology* 148, 3129–3138. doi: 10.1099/00221287-148-10-3129

Stuehr, D. J., and Marletta, M. A. (1987). Synthesis of nitrite and nitrate in murine macrophage cell lines. *Cancer Res.* 47, 5590–5594.

Subbian, S., Tsenova, L., O'Brien, P., Yang, G., Koo, M. S., Peixoto, B., et al. (2011a). Phosphodiesterase-4 inhibition combined with isoniazid treatment of rabbits with pulmonary tuberculosis reduces macrophage activation and lung pathology. *Am. J. Pathol.* 179, 289–301. doi: 10.1016/j.ajpath.2011.03.039

Subbian, S., Tsenova, L., O'Brien, P., Yang, G., Kushner, N. L., Parsons, S., et al. (2012). Spontaneous latency in a rabbit model of pulmonary tuberculosis. *Am. J. Pathol.* 181, pp.1711–1724. doi: 10.1016/j.ajpath.2012.07.019

Subbian, S., Tsenova, L., Yang, G., O'Brien, P., Parsons, S., Peixoto, B., et al. (2011b). Chronic pulmonary cavitary tuberculosis in rabbits: a failed host immune response. *Open Biol.* 1, 110016. doi: 10.1098/rsob.110016

Sullivan, B. M., Jobe, O., Lazarevic, V., Vasquez, K., Bronson, R., Glimcher, L. H., et al. (2005). Increased susceptibility of mice lacking T-bet to infection with

Mycobacterium tuberculosis correlates with increased IL-10 and decreased IFN-γ production. *J. Immunol.* 175, 4593–4602. doi: 10.4049/jimmunol.175.7.4593

Sun, J., Singh, V., Lau, A., Stokes, R. W., Obregón-Henao, A., Orme, I. M., et al. (2013). Mycobacterium tuberculosis nucleoside diphosphate kinase inactivates small GTPases leading to evasion of innate immunity. *PloS Pathog.* 9, e1003499. doi: 10.1371/journal.ppat.1003499

Tailleux, L., Waddell, S. J., Pelizzola, M., Mortellaro, A., Withers, M., Tanne, A., et al. (2008). Probing host pathogen cross-talk by transcriptional profiling of both Mycobacterium tuberculosis and infected human dendritic cells and macrophages. *PloS One* 3, e1403. doi: 10.1371/journal.pone.0001403

Talaat, A. M., Ward, S. K., Wu, C. W., Rondon, E., Tavano, C., Bannantine, J. P., et al. (2007). Mycobacterial bacilli are metabolically active during chronic tuberculosis in murine lungs: insights from genome-wide transcriptional profiling. *J. bacteriol.* 189 (11), 4265–4274. doi: 10.1128/JB.00011-07

Talaat, A. M., Lyons, R., Howard, S. T., and Johnston, S. A. (2004). The temporal expression profile of Mycobacterium tuberculosis infection in mice. *Proc. Natl. Acad. Sci.* 101, 4602–4607. doi: 10.1073/pnas.0306023101

Tezera, L. B., Bielecka, M. K., Chancellor, A., Reichmann, M. T., Shammari, B. A., Brace, P., et al. (2017). Dissection of the host-pathogen interaction in human tuberculosis using a bioengineered 3-dimensional model. *Elife* 6, e21283. doi: 10.7554/eLife.21283

Tezera, L. B., Bielecka, M. K., Ogongo, P., Walker, N. F., Ellis, M., Garay-Baquero, D. J., et al. (2020a). Anti-PD-1 immunotherapy leads to tuberculosis reactivation via dysregulation of TNF-α. *Elife* 9, e52668. doi: 10.7554/eLife.52668

Tezera, L. B., Mansour, S., and Elkington, P. (2020b). Reconsidering the optimal immune response to Mycobacterium tuberculosis. *Am. J. respiratory Crit. Care Med.* 201, 407–413. doi: 10.1164/rccm.201908-1506PP

Thacker, V. V., Dhar, N., Sharma, K., Barrile, R., Karalis, K., and McKinney, J. D. (2020). A lung-on-chip model of early Mycobacterium tuberculosis infection reveals an essential role for alveolar epithelial cells in controlling bacterial growth. *Elife* 9, e59961. doi: 10.7554/eLife.59961.sa2

Tornheim, J. A., and Dooley, K. E. (2017). Tuberculosis associated with HIV infection. *Microbiol. Spectr.* 5, 10–1128. doi: 10.1128/microbiolspec.TNMI7-0028-2016

Torrado, E., and Cooper, A. M. (2010). IL-17 and Th17 cells in tuberculosis. *Cytok. Growth factor Rev.* 21, 455–462. doi: 10.1016/j.cytogfr.2010.10.004

Torres-García, D., Cruz-Lagunas, A., García-Sancho-Figueroa, M. C., Fernández-Plata, R., Baez-Saldaña, R., Mendoza-Milla, C., et al. (2013). Variants in toll-like receptor 9 gene influence susceptibility to tuberculosis in a Mexican population. *J. Trans. Med.* 11, 1–8. doi: 10.1186/1479-5876-11-220

Tosh, K., Campbell, S. J., Fielding, K., Sillah, J., Bah, B., Gustafson, P., et al. (2006). Variants in the SP110 gene are associated with genetic susceptibility to tuberculosis in West Africa. *Proc. Natl. Acad. Sci.* 103, 10364–10368. doi: 10.1073/pnas.0603340103

Tsenova, L., Sokol, K., Victoria, H. F., and Kaplan, G. (1998). A combination of thalidomide plus antibiotics protects rabbits from mycobacterial meningitis-associated death. *J. Infect. Dis.* 177, 1563–1572. doi: 10.1086/jid.1998.177.issue-6

Tsuchiya, S., Kobayashi, Y., Goto, Y., Okumura, H., Nakae, S., Konno, T., et al. (1982). Induction of maturation in cultured human monocytic leukemia cells by a phorbol diester. *Cancer Res.* 42, 1530–1536.

Tullius, M. V., Harth, G., and Horwitz, M. A. (2003). Glutamine synthetase GlnA1 is essential for growth of Mycobacterium tuberculosis in human THP-1 macrophages and Guinea pigs. *Infect. Immun.* 71, 3927–3936. doi: 10.1128/IAI.71.7.3927-3936.2003

Turner, O. C., Basaraba, R. J., and Orme, I. M. (2003). Immunopathogenesis of pulmonary granulomas in the Guinea pig after infection with Mycobacterium tuberculosis. *Infect. Immun.* 71, 864–871. doi: 10.1128/IAI.71.2.864-871.2003

Turner, J., Gonzalez-Juarrero, M., Saunders, B. M., Brooks, J. V., Marietta, P., Ellis, D. L., et al. (2001). Immunological basis for reactivation of tuberculosis in mice. *Infect. Immun.* 69, 3264–3270. doi: 10.1128/IAI.69.5.3264-3270.2001

van Crevel, R., Ottenhoff, T. H., and van der Meer, J. W. (2002). Innate immunity to Mycobacterium tuberculosis. *Clin. Microbiol. Rev.* 15, 294–309. doi: 10.1128/CMR.15.2.294-309.2002

Vandal, O. H., Roberts, J. A., Odaira, T., Schnappinger, D., Nathan, C. F., and Ehrt, S. (2009). Acid-susceptible mutants of Mycobacterium tuberculosis share hypersusceptibility to cell wall and oxidative stress and to the host environment. *J. bacteriol.* 191, 625–631. doi: 10.1128/JB.00932-08

van den Esker, M. H., and Koets, A. P. (2019). Application of transcriptomics to enhance early diagnostics of mycobacterial infections, with an emphasis on Mycobacterium avium ssp. paratuberculosis. *Vet. Sci.* 6, 59. doi: 10.3390/vetsci6030059

Venketaraman, V., Dayaram, Y. K., Talaue, M. T., and Connell, N. D. (2005). Glutathione and nitrosoglutathione in macrophage defense against Mycobacterium tuberculosis. *Infect. Immun.* 73, 1886–1889. doi: 10.1128/IAI.73.3.1886-1889.2005

Vergne, I., Fratti, R. A., Hill, P. J., Chua, J., Belisle, J., and Deretic, V. (2004). Mycobacterium tuberculosis phagosome maturation arrest: mycobacterial phosphatidylinositol analog phosphatidylinositol mannoside stimulates early endosomal fusion. *Mol. Biol. Cell* 15(2), 751–760. doi: 10.1091/mbc.E03-05-0307

Verreck, F. A., Vervenne, R. A., Kondova, I., van Kralingen, K. W., Remarque, E. J., Braskamp, G., et al. (2009). MVA. 85A boosting of BCG and an attenuated, phoP deficient M. tuberculosis vaccine both show protective efficacy against tuberculosis in rhesus macaques. *PloS One* 4, e5264. doi: 10.1371/journal.pone.0005264

Via, L. E., Lin, P. L., Ray, S. M., Carrillo, J., Allen, S. S., Eum, S. Y., et al. (2008). Tuberculous granulomas are hypoxic in Guinea pigs, rabbits, and nonhuman primates. *Infect. Immun.* 76, 2333–2340. doi: 10.1128/IAI.01515-07

Via, L. E., Schimel, D., Weiner, D. M., Dartois, V., Dayao, E., Cai, Y., et al. (2012). Infection dynamics and response to chemotherapy in a rabbit model of tuberculosis using [18F] 2-fluoro-deoxy-D-glucose positron emission tomography and computed tomography. *Antimicrob. Agents chemother.* 56, 4391–4402. doi: 10.1128/AAC.00531-12

Via, L. E., Weiner, D. M., Schimel, D., Lin, P. L., Dayao, E., Tankersley, S. L., et al. (2013). Differential virulence and disease progression following Mycobacterium tuberculosis complex infection of the common marmoset (Callithrix jacchus). *Infect. Immun.* 81, 2909–2919. doi: 10.1128/IAI.00632-13

Vidal, S. M., Malo, D., Vogan, K., Skamene, E., and Gros, P. (1993). Natural resistance to infection with intracellular parasites: isolation of a candidate for Bcg. *Cell* 73, 469–485. doi: 10.1016/0092-8674(93)90135-D

Vogel, C., and Marcotte, E. M. (2012). Insights into the regulation of protein abundance from proteomic and transcriptomic analyses. *Nat. Rev. Genet.* 13, 227–232. doi: 10.1038/nrg3185

Vogt, G., and Nathan, C. (2011). *In vitro* differentiation of human macrophages with enhanced antimycobacterial activity. *J. Clin. Invest.* 121, 3889–3901. doi: 10.1172/JCI57235

Vrieling, F., Kostidis, S., Spaink, H. P., Haks, M. C., Mayboroda, O. A., Ottenhoff, T. H., et al. (2020). Analyzing the impact of Mycobacterium tuberculosis infection on primary human macrophages by combined exploratory and targeted metabolomics. *Sci. Rep.* 10, 7085. doi: 10.1038/s41598-020-62911-1

Walker, N. F., Wilkinson, K. A., Meintjes, G., Tezera, L. B., Goliath, R., Peyper, J. M., et al. (2017). Matrix degradation in human immunodeficiency virus type 1–Associated tuberculosis and tuberculosis immune reconstitution inflammatory syndrome: a prospective observational study. *Clin. Infect. Dis.* 65, 121–132. doi: 10.1093/cid/cix231

Walsh, G. P., Tan, E. V., Dela Cruz, E. C., Abalos, R. M., Villahermosa, L. G., Young, L. J., et al. (1996). The Philippine cynomolgus monkey (Macaca fasicularis) provides a new nonhuman primate model of tuberculosis that resembles human disease. *Nat. Med.* 2, 430–436. doi: 10.1038/nm0496-430

Wang, H., Maeda, Y., Fukutomi, Y., and Makino, M. (2013). An *in vitro* model of Mycobacterium leprae induced granuloma formation. *BMC Infect. Dis.* 13, 1–10. doi: 10.1186/1471-2334-13-279

Wang, C., Peyron, P., Mestre, O., Kaplan, G., van Soolingen, D., Gao, Q., et al. (2010). Innate immune response to Mycobacterium tuberculosis Beijing and other genotypes. *PloS One* 5, e13594. doi: 10.1371/journal.pone.0013594

Ward, S. K., Abomoelak, B., Marcus, S. A., and Talaat, A. M. (2010). Transcriptional profiling of Mycobacterium tuberculosis during infection: lessons learned. *Front. Microbiol.* 1, 121. doi: 10.3389/fmicb.2010.00121

Weljie, A. M., Dowlatabadi, R., Miller, B. J., Vogel, H. J., and Jirik, F. R. (2007). An inflammatory arthritis-associated metabolite biomarker pattern revealed by 1H NMR spectroscopy. *J. Proteome Res.* 6, 3456–3464. doi: 10.1021/pr070123j

Westermann, A. J., Barquist, L., and Vogel, J. (2017). Resolving host–pathogen interactions by dual RNA-seq. *PloS Pathog.* 13, e1006033. doi: 10.1371/journal.ppat.1006033

White, A. D., Sibley, L., Sarfas, C., Morrison, A., Gullick, J., Clark, S., et al. (2021). MTBVAC vaccination protects rhesus macaques against aerosol challenge with M. tuberculosis and induces immune signatures analogous to those observed in clinical studies. *NPJ Vacc.* 6, 4. doi: 10.1038/s41541-020-00262-8

WHO *Tuberculosis (TB): Latent Tuberculosis Infection (LTBI)—FAQs*. Available online at: https://www.who.int/tb/areas-of-work/preventive-care/ltbi/faqs/en/ (Accessed May 26 2021).

WHO End Strategy. Available online at: https://www.who.int/teams/global-tuberculosis-programme/the-end-tb-strategy.

Williams, A., Hall, Y., and Orme, I. M. (2009). Evaluation of new vaccines for tuberculosis in the Guinea pig model. *Tuberculosis* 89, 389–397. doi: 10.1016/j.tube.2009.08.004

Williams, A., Hatch, G. J., Clark, S. O., Gooch, K. E., Hatch, K. A., Hall, G. A., et al. (2005). Evaluation of vaccines in the EU TB Vaccine Cluster using a Guinea pig aerosol infection model of tuberculosis. *Tuberculosis* 85, 29–38. doi: 10.1016/j.tube.2004.09.009

Wilson, G. J., Marakalala, M. J., Hoving, J. C., Van Laarhoven, A., Drummond, R. A., Kerscher, B., et al. (2015). The C-type lectin receptor CLECSF8/CLEC4D is a key component of anti-mycobacterial immunity. *Cell host Microbe* 17, 252–259. doi: 10.1016/j.chom.2015.01.004

Workman, V. L., Tezera, L. B., Elkington, P. T., and Jayasinghe, S. N. (2014). Controlled generation of microspheres incorporating extracellular matrix fibrils for three-dimensional cell culture. *Adv. Funct. mater.* 24, 2648–2657. doi: 10.1002/adfm.201303891

Yamada, H., Udagawa, T., Mizuno, S., Hiramatsu, K., and Sugawara, I. (2005). Newly designed primer sets available for evaluating various cytokines and iNOS mRNA

expression in Guinea pig lung tissues by RT-PCR. *Exp. Anim.* 54, 163–172. doi: 10.1538/expanim.54.163

Yamamoto, T., Jeevan, A., Ohishi, K., Nojima, Y., Umemori, K., Yamamoto, S., et al. (2002). A new assay system for Guinea pig interferon biological activity. *J. interfer. cytok. Res.* 22, 793–797. doi: 10.1089/107999002320271387

Yan, B. S., Kirby, A., Shebzukhov, Y. V., Daly, M. J., and Kramnik, I. (2006). Genetic architecture of tuberculosis resistance in a mouse model of infection. *Genes Immun.* 7, 201–210. doi: 10.1038/sj.gene.6364288

Yan, B. S., Pichugin, A. V., Jobe, O., Helming, L., Eruslanov, E. B., Gutiérrez-Pabello, J. A., et al. (2007). Progression of pulmonary tuberculosis and efficiency of bacillus Calmette-Guerin vaccination are genetically controlled via a common sst1-mediated mechanism of innate immunity. *J. Immunol.* 179, 6919–6932. doi: 10.4049/jimmunol.179.10.6919

Yang, H. J., Wang, D., Wen, X., Weiner, D. M., and Via, L. E. (2021). One size fits all? Not in *in vivo* modeling of tuberculosis chemotherapeutics. *Front. Cell. Infect. Microbiol.* 11, 613149. doi: 10.3389/fcimb.2021.613149

Yu, Y., Jin, D., Hu, S., Zhang, Y., Zheng, X., Zheng, J., et al. (2015). A novel tuberculosis antigen identified from human tuberculosis granulomas*. *Mol. Cell. Proteomics* 14, 1093–1103. doi: 10.1074/mcp.M114.045237

Yue, X., Zhu, X., Wu, L., and Shi, J. (2022). A comparative study of a rabbit spinal tuberculosis model constructed by local direct infection via the posterior lateral approach. *Sci Rep.* 12 (1), 12853. doi: 10.1038/s41598-022-16624-2

Yuan, T., and Sampson, N. S. (2018). Hit generation in TB drug discovery: from genome to granuloma. *Chem. Rev.* 118, 1887–1916. doi: 10.1021/acs.chemrev.7b00602

Zaki, H. Y., Leung, K. H., Yiu, W. C., Gasmelseed, N., Elwali, N. E. M., and Yip, S. P. (2012). Common polymorphisms in TLR4 gene associated with susceptibility to pulmonary tuberculosis in the Sudanese. *Int. J. tubercul. Lung Dis.* 16, 934–940. doi: 10.5588/ijtld.11.0517

Zhan, L., Tang, J., Sun, M., and Qin, C. (2017). Animal models for tuberculosis in translational and precision medicine. *Front. Microbiol.* 8, 717. doi: 10.3389/fmicb.2017.00717

frontiers | Frontiers in Cellular and Infection Microbiology

TYPE Review
PUBLISHED 30 May 2025
DOI 10.3389/fcimb.2025.1588446

OPEN ACCESS

EDITED BY
Sam Ebenezer,
Sathyabama Institute of Science and Technology, India

REVIEWED BY
Konda Mani Saravanan,
Bharath Institute of Higher Education and Research, India
Deepu Pandita,
Government Department of School Education, India

*CORRESPONDENCE
Farah Al-Marzooq
f.almarzooq@uaeu.ac.ae
Mushtak T. S. Al-Ouqaili
ph.dr.mushtak_72@uoanbar.edu.iq

†These authors have contributed equally to this work

RECEIVED 05 March 2025
ACCEPTED 28 April 2025
PUBLISHED 30 May 2025

CITATION
Al-Ouqaili MTS, Ahmad A, Jwair NA and Al-Marzooq F (2025) Harnessing bacterial immunity: CRISPR-Cas system as a versatile tool in combating pathogens and revolutionizing medicine.
Front. Cell. Infect. Microbiol. 15:1588446.
doi: 10.3389/fcimb.2025.1588446

Harnessing bacterial immunity: CRISPR-Cas system as a versatile tool in combating pathogens and revolutionizing medicine

Mushtak T. S. Al-Ouqaili [1*†], Amna Ahmad [2†], Noor A. Jwair [3] and Farah Al-Marzooq [2*]

[1]Department of Microbiology, College of Medicine, University of Anbar, Ramadi, Anbar Governorate, Iraq, [2]Department of Microbiology and Immunology, College of Medicine and Health Sciences, United Arab Emirates University, Al-Ain, United Arab Emirates, [3]Anbar Health Directorate, Department of Public Health, Anbar Governorate, Ramadi, Iraq

Clustered Regularly Interspaced Short Palindromic Repeats (CRISPR) technology has emerged as an adaptable instrument for several uses. The CRISPR–Cas system employs Cas proteins and programmable RNA molecules to guide the recognition and cleavage of specific DNA regions, permitting accurate genome editing. It is derived from the bacterial immune system and allows for accurate and efficient modification of DNA sequences. This technique provides unparalleled gene editing, control, and precise alteration opportunities. This review aims to offer a comprehensive update of the core concepts of the CRISPR–Cas system and recent progress, while also providing an overview of the significant applications in diverse fields such as microbiology and medicine. The CRISPR–Cas9 gene editing technique has facilitated substantial advancements in comprehending gene function, simulating diseases, and creating innovative therapeutics. CRISPR-based therapeutics present a hopeful prospect for addressing intricate ailments, including genetic disorders, malignancies, and infectious diseases, as they serve as viable substitutes for conventional pharmaceuticals. In microbiology, this method serves as a diagnostic and therapeutic tool that proves highly efficient in eliminating bacteria that have developed resistance to various antibiotics. Despite its significant potential, CRISPR encounters ethical, safety, and regulatory obstacles that necessitate meticulous deliberation. Concerns regarding off-target effects, poor delivery to target tissues, and unwanted side effects emphasize the necessity to thoroughly examine the technology. It is necessary to balance the advantages and difficulties CRISPR presents. Consequently, more rigorous preclinical and clinical experiments are essential before using it in humans.

KEYWORDS

gene editing, CRISPR-Cas, Cas9, innovative therapeutics, infections

1 Introduction to CRISPR–Cas systems

In 1987, Yoshizumi Ishino and his team from Osaka University in Japan were the first to identify CRISPR in *E. coli*, announcing the existence of CRISPR in bacteria. Subsequently, Francisco Mojica, a Spanish scientist, together with his colleagues, characterized the CRISPR sequence and introduced the term "clustered regularly interspaced short palindromic repeats" (CRISPR) to refer to it as a bacterial immune system (Jacinto et al., 2020). However, the functionality and importance of CRISPR in prokaryotes were realized later in the mid-2000s, leading to the development of a revolutionary genetic engineering tool. Emmanuelle Charpentier and Jennifer Doudna discovered CRISPR–Cas by chance while studying how bacteria defend against viruses. This tool, often described as a pair of genetic scissors, allows for the precise editing of genes. The inventors realized that this natural process could be harnessed to cut out faulty genes and replace them with healthy genes, paving the way for the future of medicine (Strzyz, 2020). The inventors documented the existence of a second short RNA, known as the trans activator CRISPR RNA (tracrRNA), which plays a vital role in the CRISPR–Cas system. They effectively reconstructed all the essential CRISPR–Cas chemicals for precise cutting of the target and suggested merging CRISPR RNA (crRNA) and tracrRNA into a single guide RNA (sgRNA). This was the first suggestion that these tools could be used for RNA-programmable genome editing through RNA-guided DNA cutter cleavage systems (Kim and Kim, 2014). Doudna also contributed to understanding protein structures involved in the DNase activity and RNA processing of the CRISPR–Cas system. In recognition of their ground-breaking work, the 2020 Nobel Prize in Chemistry was awarded to them (Uyhazi and Bennett, 2021). Together, they became the first women to share a Nobel Prize for their work in discovering and transforming CRISPR into a gene-editing technology (Ledford and Callaway, 2020). Since the discovery of this system, vast advances in technology have enabled its application in various fields of biotechnology and medicine, including microbiology. Therefore, this review aims to provide a snapshot of the recent advances of this innovative tool and its various applications.

2 Overview of CRISPR–Cas system and its components

CRISPR–Cas system enables accurate and targeted modification of genes, granting unparalleled authority in changing genetic information (Adli, 2018). CRISPR is an abbreviation for "Clustered Regularly Interspaced Short Palindromic Repeats," which refers to a specific sequence of DNA in prokaryotes, found in 88% of archaea and 39% of bacteria, in both Gram-positive and Gram-negative bacteria (Barrangou, 2015). These sequences demonstrate palindromic repeats, meaning they read the same from 5' to 3' on one DNA strand and from 3' to 5' on the complementary strand (Tsui and Li, 2015). Bacteria employ a defense mechanism using CRISPR to recognize foreign DNA elements, which are similar to adaptive immunity in humans. The unique sequences between the palindromic repeats, called spacers, which are fragments taken from foreign DNA and stored in the CRISPR system. These spacers are derived from mobile genetic elements (MGEs), such as bacteriophages, transposons, or plasmids, that have previously infected bacteria (Hille and Charpentier, 2016). The identification of the spacers in the CRISPR system by sequencing provided evidence supporting the concept that bacteria may use this mechanism as a defense to detect foreign DNA fragments (Bikard and Barrangou, 2017).

Cas, an abbreviation for "CRISPR-associated protein," is an enzyme that uses CRISPR sequences to recognize and impair particular DNA strands that are complementary to the ones present in the CRISPR spacer sequences (as shown in Figure 1) (Zhang et al., 2014). The complex formed by the Cas protein and CRISPR sequences is known as CRISPR–Cas, which can be used to defend against foreign genomes. The CRISPR–Cas adaptive immune system is used naturally by bacteria to protect themselves from foreign DNA originating from bacteriophage invasion, conjugation, or transformation (Azangou-Khyavy et al., 2020). Thus, these sequences play a significant role as weapons in fighting against foreign genes to support adaptive bacterial immunity (Barrangou et al., 2007).

The CRISPR–Cas system components are shown in Figure 1.

As shown in Figure 1, the CRISPR locus (28–37 bp) contains repeats of palindromic DNA, with a leader rich in AT (Hille and Charpentier, 2016). The spacer (32–38 bp) is located between DNA repeats and contains a piece of foreign genome (e.g., viral genome) that previously invaded the bacteria (Barrangou and Marraffini, 2014). Cas genes are located near the CRISPR locus, giving Cas enzymes their position. There are fewer than 50 units of CRISPR arrays and spacers in bacteria (Tyson and Banfield, 2008). Apart from CRISPR arrays, Cas genes have short sequences. There are ninety-three Cas genes in all, grouped into thirty-five families based on how similar the enzymes they encode are to one another. Eleven of the 35 families are part of the Cas core, which is made up of the enzymes Cas1 through Cas9 (Koonin and Makarova, 2019). CRISPR–Cas systems are divided into two categories. Class 1 systems use a combination of numerous Cas proteins to destroy the invading genome, whereas class 2 systems use a single large Cas protein for this purpose. Types II, V, and VI are further categorized into class 2, while types I, III, and IV are categorized into class 1 (Wright et al., 2016). The six groups are further divided into 19 subtypes (Westra et al., 2016). The CRISPR–Cas systems are comprised of three unique types, namely types I, II, and III. The classification is determined by the unique genes that each type

Abbreviations: CRISPR, Clustered Regularly Interspaced Short Palindromic Repeats; Cas, CRISPR-associated protein; MGEs, mobile genetic elements; crRNA, CRISPR RNA; tracrRNA, trans-activator CRISPR RNA; sgRNA, single guide RNA; PAM, protospacer adjacent motifs; ZFNs, Zinc finger nucleases; TALENs, Transcriptional activator-like effector nucleases; TKIs, Tyrosine kinase inhibitors; IC50, half-maximal inhibitory concentration; KO, knockout; SHERLOCK, Specific High-sensitivity Enzymatic Reporter unlocking; AMR, antimicrobial resistance; MRSA, methicillin-resistant *Staphylococcus aureus*.

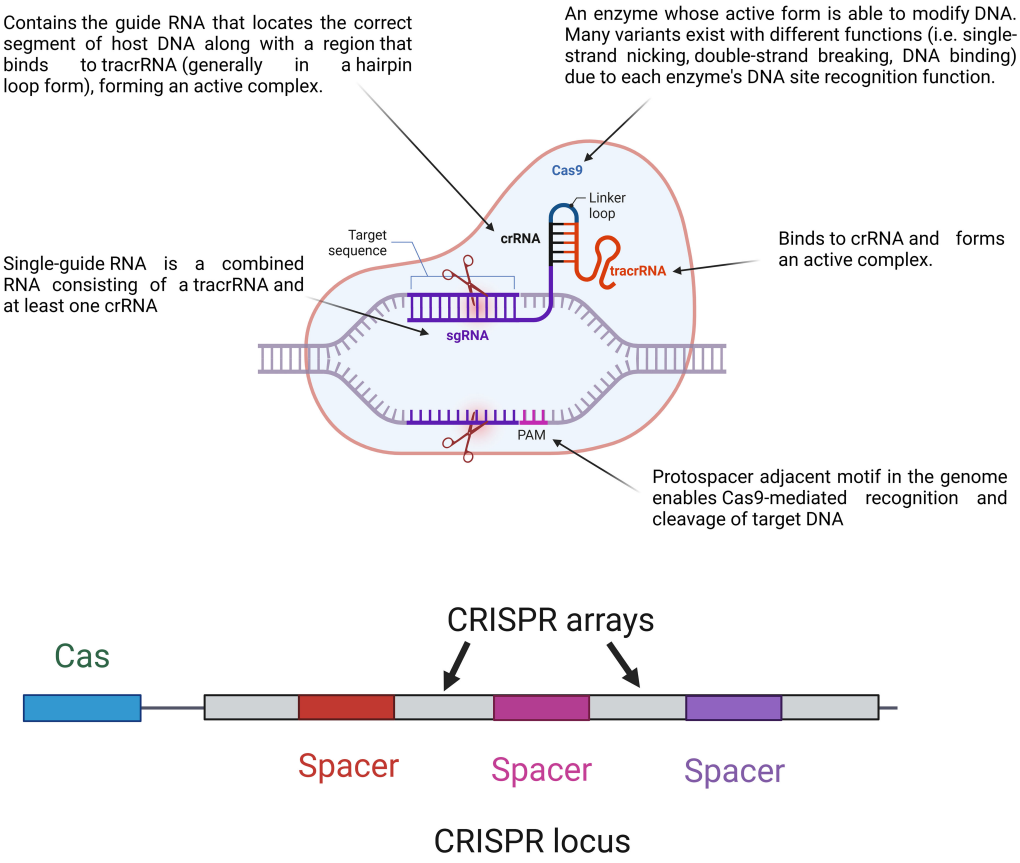

FIGURE 1
Major components of the CRISPR–Cas system and their loci. The CRISPR locus contains *cas* genes and CRISPR arrays made up of repeat and spacer sequences. During immunity, a single guided RNA (sgRNA), which combines a crRNA and tracrRNA, guides the Cas9 protein to the target DNA sequences. Cas9 forms an active complex with the sgRNA and recognizes the protospacer adjacent motif (PAM) on the target DNA, enabling precise DNA cleavage. This mechanism allows for targeted genome editing by directing Cas9 to specific DNA sites for modification.

possesses. Cas3, Cas9, and Cas10 are correspondingly present in types I, II, and III. Recognizing that all types and subtypes of CRISPR systems consistently contain the proteins Cas1 and Cas2 is crucial. These two proteins are essential for preserving the function of spacers (Shabbir et al., 2016). The most important types of CRISPR systems are listed in Table 1.

3 Mechanisms and functional diversity of CRISPR–Cas system

3.1 Core components and functional motifs

Genetic analysis of foreign nucleic acid regions, specifically protospacers, has revealed that their elimination is not random. Usually, it is located near protospacer adjacent motifs (PAMs), which are brief DNA sequences (usually 2–6 base pairs in length) positioned one nucleotide downstream of the complementary region of the guide RNA (Mojica et al., 2009). The CRISPR system, namely CRISPR–Cas9, cleaves foreign DNA sections that are situated downstream of the PAM sequence (Vorontsova et al., 2015). Research has demonstrated that PAMs are essential for the acquisition of spacers in type I and type II CRISPR–Cas systems, but they are not required in type III systems (Sonmez, 2021). A mechanism in the CRISPR system regulates the size of the spacer when protospacers are cut near a PAM sequence (Shah et al., 2013). The PAM sequence is present in the foreign nucleic acid of viruses and plasmids, but it is lacking from the bacterial CRISPR locus since it is not a part of bacterial DNA. If the PAM sequence comes before Cas9, it cannot attach to or break the target genome. Consequently, the PAM region is required to prevent Cas enzymes from damaging the CRISPR locus (Swarts et al., 2012). Guide RNA (gRNA), a small RNA sequence not translated into protein, is required for this process. gRNA binds to a complementary foreign DNA sequence. The gRNA is composed of CRISPR RNA (crRNA) and trans-activating CRISPR RNA (tracrRNA) (Kouranova et al., 2016). Its length ranges from 17 to 24 nucleotides, and it has a GC percentage of 40-80%. Increasing this percentage strengthens the binding between the RNA and the foreign DNA (Konstantakos et al., 2022). The mechanism becomes less selective, and the RNA binds to multiple regions in the genome when the length decreases to less than 17 nucleotides (Konstantakos et al., 2022). The gRNA forms a complex with the Cas9 protein and guides it to cleave a specific

10.3389/fcimb.2025.1588446

TABLE 1 Major and minor CRISPR–Cas variants (types and subtypes), their presumed roles, and signature genes. Known functions are listed for each type and subtype, while some are not well defined (ND).

Class	Cas type	Cas subtype	Signature protein (s)	Function
1	I	–	Cas3	The HD domain of single-stranded DNA nuclease and ATP-dependent helicase
		I-A	Cas8a, Cas5	Cas8, PAM recognition and targeting foreign DNA Cas5 crRNA processing/maintenance
		I-B	Cas8b	PAM recognition/targeting
		I-C	Cas8c	
		I-D	Cas10d	Contains region similar to palm domain of nucleic acid polymerases/nucleotide cyclases
		I-E	Cse1, Cse2	PAM recognition/targeting via Cse1
		I-F	Csy1, Csy2, Csy3	PAM recognition/targeting via Csy1
		I-G	GSU0054	PAM recognition/targeting
	III	–	Cas10	Cas10d/Cse1 homolog; stabilizes interference complex by binding target RNA
		III-A	Csm2	ND
		III-B	Cmr5	
		III-C	Cas10 or Csx11	
		III-D	Csx10	
		III-E	–	
		III-F		
	IV	–	Csf1	
		IV-A	–	
		IV-B		
		IV-C		
2	II	–	Cas9	HNH & RuvC nucleases for DSBs/SSBs; facilitates spacer acquisition during adaptation
		II-A	Csn2	Ring-form DNA binding protein; involved in primed adaptation
		II-B	Cas4	Endonuclease working with Cas1/Cas2 to create spacer sequences
		II-C	–	Distinguished by the lack of Csn2 or Cas4
	V	–	Cas12	RuvC nuclease activity, lacks HNH domain
		V-A	Cas12a (Cpf1)	
		V-B	Cas12b (C2c1)	
		V-C	Cas12c (C2c3)	
		V-D	Cas12d (CasY)	
		V-E	Cas12e (CasX)	
		V-F	Cas12f (Cas14, C2c10)	
		V-G	Cas12g	
		V-H	Cas12h	
		V-I	Cas12i	

(Continued)

TABLE 1 Continued

Class	Cas type	Cas subtype	Signature protein (s)	Function
		V-K	Cas12k (C2c5)	
		V-U	C2c4, C2c8, C2c9	
	VI	–	Cas13	RNA-guided RNase
		VI-A	Cas13a (C2c2)	
		VI-B	Cas13b	
		VI-C	Cas13c	
		VI-D	Cas13d	

location in foreign DNA using complementary base pairing between the RNA and foreign DNA (Jiang and Doudna, 2017).

The novel spacers are inserted in a specific direction in a CRISPR array (Pourcel et al., 2005), ideally situated close to the sequence of the leader. The new spacer obtained after infection is inserted between the first and second repeats of the CRISPR array in the *E. coli* type I-E system, and the first repeat next to the leader sequence is duplicated (Yosef et al., 2012).

According to Charpentier and Doudna's 2012 study, the CRISPR gene-editing mechanism consists of a guide molecule that functions as a GPS and locates and binds to a particular gene location on a virus's DNA. Furthermore, the DNA is cut by the CRISPR-associated protein (Cas), which functions as a molecular scissor (Westermann et al., 2021). Selective targeting of a specific DNA sequence is the first step in genome editing. Cas9 and guide RNA work together to form a complex that can recognize target sequences. Recent research has shown that Cas9 can prevent viruses from altering host DNA. Without guide RNA, Cas9 is inactive (Jinek et al., 2014). A single strand that forms a T shape with one tetraloop and two or three stem-loops makes up the guide RNA in CRISPR systems. The guide RNA's 5' end is made to match the target DNA sequence. Cas9 works a conformational shift that turns it from inactive to active when the guide RNA attaches to it. While the exact reason for this conformational shift is unknown, steric interactions or weakened bonds between RNA bases and protein side chains may be responsible for it (Jinek et al., 2014). Once activated, Cas9 searches for target DNA by attaching to regions that match its PAM sequence (Sternberg et al., 2014). Cas9 unwound the bases just upstream of the PAM and couples them with the correct region on the guide RNA. If the complementary region and target area precisely match, the RuvC and HNH nuclease domains of Cas9 will cut the target DNA after the third nucleotide base upstream of the PAM (Anders et al., 2014).

3.2 Stages of CRISPR–Cas activity

There are three steps for CRISPR–Cas activity against foreign DNA, which are shown in Figure 2.

Step 1 (spacer acquisition): This step happens when a bacteriophage inserts nucleic acid, the initial stage involves separating a portion of the phage genome and inserting it into a CRISPR array in a spacer position between repeated palindromic sequences (sandwiched form) (Pawluk et al., 2018). This step is the same for all three types (I, II, III) when nucleic acid is first inserted by a bacteriophage into a bacterial cell. In the initial stage of the immune response, the phage genome is broken down, a small piece is removed (usually from the area near the PAM region), and this piece is inserted into a DNA spacer near the CRISPR locus. Cas genes have a role in the CRISPR process. Cas1 and Cas2 are ubiquitous in all CRISPR–Cas systems, suggesting their importance in spacer acquisition. These genes' mutations support the theory by demonstrating that any deletion of Cas1 or Cas2 hinders the acquisition of spacers without impacting the CRISPR system (Dugar et al., 2013).

Step 2 (crRNA processing or biogenesis): In this step, CRISPR RNA (crRNA) is produced by the transcription of one strand of DNA that is complementary to the coding strand. Complementary sequences from both viral genome sequences and CRISPR repeats compose crRNAs (Marraffini and Sontheimer, 2010). The three distinct CRISPR system types each contain one of three forms of crRNA:

Type I: CRISPR repeats form loops, and the mRNA is cleaved by the Cas6e and Cas6f enzymes to produce small RNA fragments. Each fragment is composed of a CRISPR sequence as a loop and viral genome sequence, and these two fragments are referred to as crRNAs (Gesner et al., 2011).

Type II: In this type, there is another player called tracrRNA (shown in Figure 3), which is composed of multiple RNA segments bound to CRISPR repeats. The mRNA is cleaved by Cas9 and RNAseIII enzymes to produce multiple segments of CRISPR repeats and viral genome sequences along with crRNA. This complex is called tracrRNA.

Type III: In this type, Cas6 directly cleaves mRNA, resulting in crRNAs containing CRISPR repeats and viral genome sequences (Sashital et al., 2011).

Step 3 (interference): This step occurs due to the complex formation between crRNA and Cas proteins. This complex can recognize the PAM sequence in the bacteriophage genome. The presence of a PAM increases specificity because not only does the spacer recognize the PAM region, but the Cas proteins also recognize the PAM sequence (Gleditzsch et al., 2019). There is a slight difference in this step among the different types of CRISPR systems:

10.3389/fcimb.2025.1588446

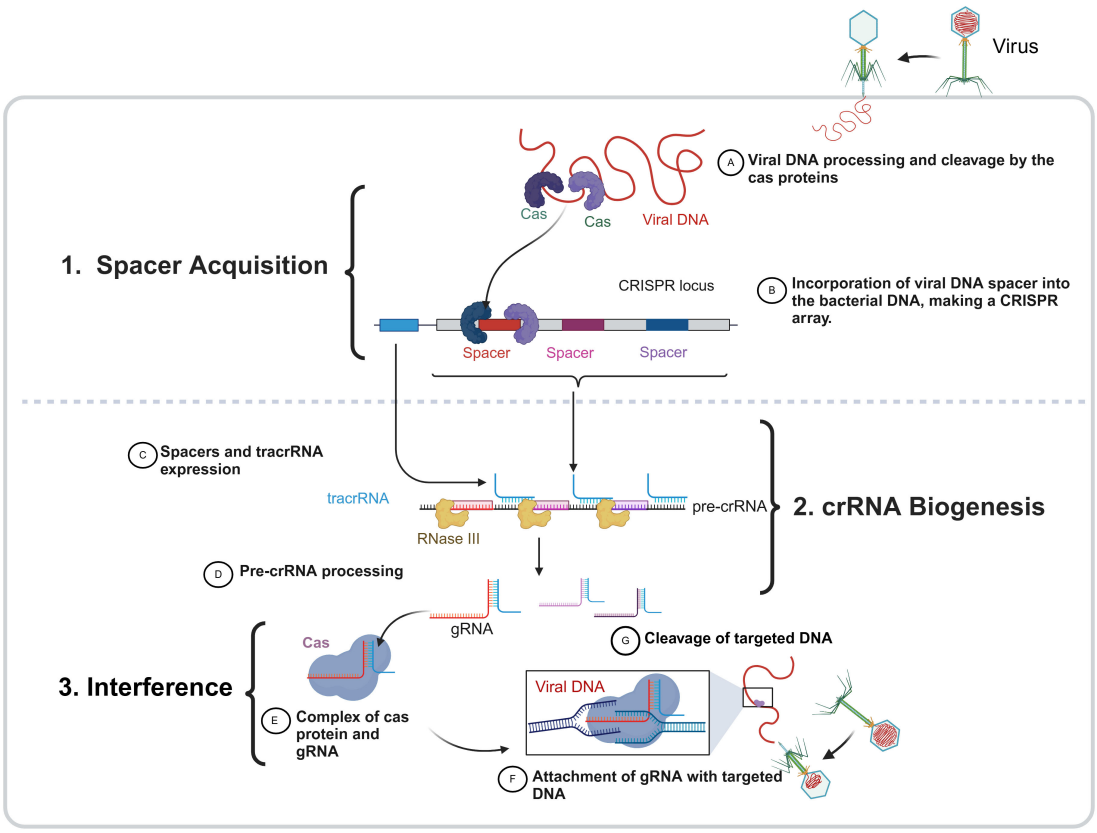

FIGURE 2
The three phases of the bacterial CRISPR–Cas function. The CRISPR-Cas immune system in bacteria operates through three main stages: (1) spacer acquisition, (2) crRNA biogenesis, (3) interference. During spacer acquisition, foreign DNA (viral DNA as an example) is recognized and cleaved by Cas proteins, and the resulting fragments are integrated into the bacterial genome at the CRISPR locus as a new spacer, forming a CRISPR array that serves as a genetic memory of past infections. In the crRNA biogenesis phase, the CRISPR array is transcribed into a precursor CRISPR RNA (pre-crRNA), which is processed by RNaseIII in the presence of a trans-activating crRNA (tracrRNA), producing mature guide RNAs (gRNAs) that carry spacer sequences. In the final interference stage, these gRNAs associate with Cas proteins to form an active surveillance complex that scans for complementary sequences in invading DNA. Upon target recognition, the Cas-gRNA complex binds to the complementary foreign DNA, leading to its cleavage and degradation.

Type I: When the virus infects the bacteria for the second time, a segment of the lower strand adjacent to the PAM becomes complementary to the RNA in the CRISPR complex. This activates a cascade of Cas enzymes (Figure 3), which is a complex and not yet fully understood process. Ultimately, this cascade recruits Cas3 to cleave the viral genome into smaller fragments, preventing further invasion of the bacteria by the virus (Brouns et al., 2008).

Type II: The main player in this type is the Cas9 complex, which contains crRNA that recognizes the PAM sequence of the viral genome. Cas9 itself undergoes a double-strand break at the same site (Jinek et al., 2012).

Type III: This type is relatively simple, as no PAM exists. The viral genome binds to complementary RNA, and the Cas cascade degrades the viral DNA (Hale et al., 2009), as described in Figure 3.

When a bacteriophage (a virus that infects bacteria) attaches itself to the bacterial surface, it injects its own genome into the bacterial cell. This viral genome forces the cell to produce viral proteins and enzymes, altering the entire cell machinery. However, the CRISPR system prevents this from occurring again. Therefore, this form of memory in the CRISPR system helps avoid the same bacteriophage from invading the cell again. As such, CRISPR acts naturally as an adaptive immune system. Humans and animals have developed intricate immune systems to combat viral infections, but single-cell bacteria utilize CRISPR to identify and eliminate viral genetic material, preventing its replication (Rentmeister, 2015). The functions of CRISPR–Cas components based on their classes and types are illustrated in Figure 3.

4 CRISPR–Cas system advantages over older gene editing tools

Programmable nucleases such as zinc finger nucleases (ZFNs) and transcriptional activator-like effector nucleases (TALENs) were used for genome editing before the CRISPR–Cas9 system's launch. They also act as molecular scissors, which can cut DNA at the desired location within the genome, leading to targeted DNA double-strand breaks (DSBs), causing genomic modifications (Rahman et al., 2011; Bhardwaj and Nain, 2021). Figure 4 shows the key features differentiating these three technologies. Compared with other gene

10.3389/fcimb.2025.1588446

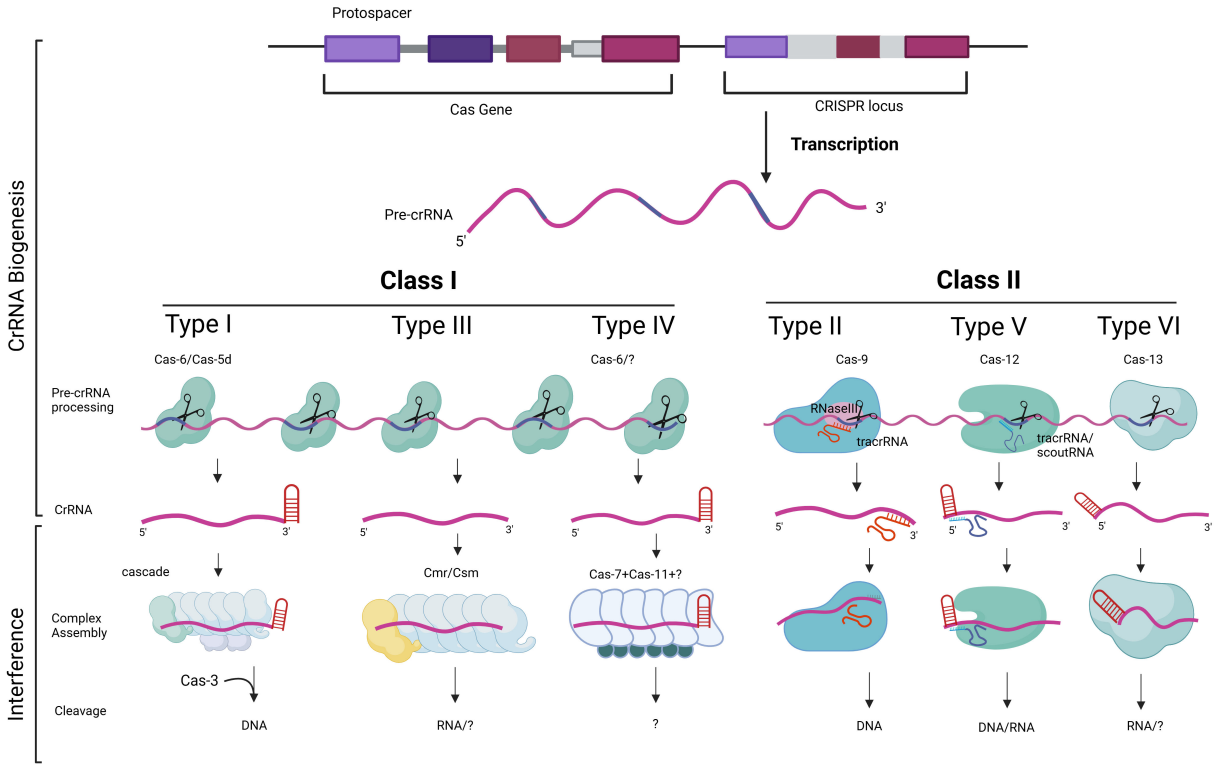

FIGURE 3
The diversity in the function of CRISPR–Cas components. The biogenesis and processing of CRISPR RNA (crRNA) and tracrRNA in CRISPR–Cas immunity are illustrated. The CRISPR-Cas system is primarily classified into Class I and Class II, based on their structural and mechanistic components. The CRISPR locus consists of repeating sequences interspaced with spacer sequences. Transcription produces a pre-crRNA which is processed by different Cas proteins depending on the CRISPR–Cas type. Class I systems (types I, III and IV) uses multi-protein complexes, such as Cas6 or Cas5d, for crRNA maturation and target recognition. Class II systems (types II, V and VI) uses a single Cas9 protein binds tracrRNA and pre-crRNA, facilitating cleavage by RNase III, resulting in mature crRNAs that guide Cas9 for targeted DNA cleavage. Types V and VI, associated with Cas12 and Cas13, respectively, use different accessory RNAs, such as tracrRNA or scoutRNA, for crRNA maturation, enabling the targeting and cleavage of DNA or RNA. This mechanistic diversity highlights the adaptability and specialization of CRISPR-Cas systems in prokaryotic immune defense.

editing tools, CRISPR has demonstrated superior efficiency, ease of design, cost-effectiveness, and time efficiency (Zhu, 2022).

Compared to ZFNs and TALENs, the CRISPR–Cas system has the benefit of using only single-stranded RNA (sgRNA) for editing, while other systems use proteins to identify specific genomic regions. CRISPR–Cas system stands out due to its cost-effectiveness, with potential for multiplexing. As a single Cas9 enzyme can be guided by multiple different sgRNAs supplied concurrently, researchers can target several genes or genomic sites within the same cell or organism with relative ease. This capability is extremely valuable for studying complex genetic interactions, dissecting biological pathways, engineering complex traits, or developing multi-targeted therapeutic strategies. Multiplexing with ZFNs or TALENs, requiring multiple unique protein pairs, is far more cumbersome, expensive, and less scalable (Aljabali et al., 2024). Another important feature is versatility, as the core CRISPR-Cas system is remarkably adaptable, since some Cas types, such as Cas9 protein can be modified to create variants with altered functions, leading to wider application (Villiger et al., 2024). Further, it exhibits high, robust efficiency in mediating DSBs and subsequent gene editing across a wide range of cell types and organisms. While ZFNs and TALENs can also be efficient, CRISPR often achieves high rates of modification with less optimization. Crucially, the simple and easy design, synthesis and use of sgRNA has led to the widespread acceptance of genome editing and enabled researchers to perform a wide range of genome alterations, including changing genes in living cells and species (Van Kampen and Van Rooij, 2019). These advantages lead to shortened experimental timelines from target selection to functional validation compared to the protein-based tools.

These advantages make it a powerful tool for gene editing across various fields, despite some challenges that ongoing advancements can overcome. One of these challenges is low specificity in some cases due to the short target recognition sequences as compared to the other gene editing tools, which have better specificity owing to their longer DNA recognition sites, especially for TALENs (Bhardwaj and Nain, 2021).

5 Applications of the CRISPR–Cas system

CRISPR–Cas systems are available in various forms and have been discovered, developed, and used to modify genes. In 2012,

10.3389/fcimb.2025.1588446

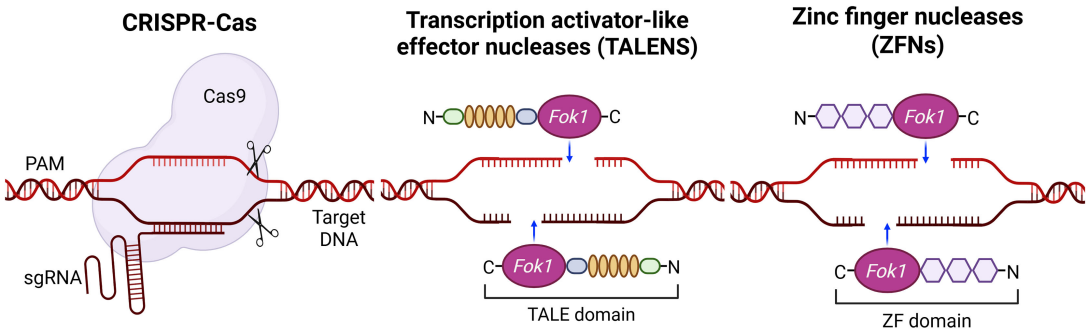

First Discovered	2012	2010	1996
Origin	Bacterial adaptive immune system	Plant pathogen proteins	Zinc finger DNA-binding domains
Guide mechanism	RNA-guided (sgRNA)	Protein-guided (TALE proteins)	Protein-guided (zinc finger proteins)
Cleavage Component	Cas9 Nuclease (HNH & RuvC domains)	FokI Nuclease Dimer	FokI Nuclease Dimer
Target recognition	20+ bp RNA-DNA complementarity + PAM	30-40 bp protein-DNA recognition	18-36 bp protein-DNA recognition
Component size	Small (~4.2 kb for Cas9)	Large (~3 kb per TALEN)	Medium (~1 kb per ZFN)
Design complexity	Low (simple sgRNA design)	Medium (modular assembly required)	High (complex protein engineering)
Assembly time	1-2 days (fast)	5-7 days (moderate)	Weeks to months (slow)
Multiplexing capability	High (multiple targets simultaneously)	Limited	Limited
Efficiency	High to Very High	High	Moderate to High (Variable)
Cost	Low	Medium	High
Specificity	Moderate to High (Improving)	High	Moderate
Off-target risk	Moderate to high	Low to moderate	Low to moderate
Approved Therapies	Emerging	Limited	Limited
Applications	Dominant in research, expanding in therapeutics	Precision editing, certain therapeutic applications	Few gene therapy applications

FIGURE 4
Comparison of CRISPR–Cas with other genome editing tools, including Zinc finger nucleases (ZFNs) and transcriptional activator-like effector nucleases (TALENs). CRISPR–Cas is an RNA-guided system that uses a single guide RNA to direct the Cas9 nucleases to specific DNA sequences through RNA-DNA complementarity and protospacer adjacent motif (PAM). It is characterized by a small component size, low design complexity, fast assembly time, high multiplexing capability, and high efficacy, with low cost and improved specificity. TALENs rely on protein-guided DNA recognition via TALE proteins and require the assembly of large constructs. Although TALENs offer high specificity and efficiency, they are limited in multiplexing and involve moderate design complexity and assembly time. ZFNs function through protein-DNA recognition using zinc finger domains and FokI nucleases dimers. This system demands complex protein engineering, has slower assembly, and limited flexibility. While all three systems exhibit varying degrees of off-target risk and therapeutic use, CRISPR-Cas currently dominates research and is rapidly expanding in clinical applications. In contrast, TALENs and ZFNs are primarily applied in precision editing with limited therapeutic adoption.

Jennifer Doudna and Emmanuelle Charpentier launched innovative studies by suggesting that the bacterial CRISPR–Cas9 system could serve as a customizable tool for modifying the genetic makeup of humans and other animal species. They exploited the inherent biological capacity of microorganisms and employed it in manipulating bacteria's genetic makeup through genetic engineering (Uyhazi and Bennett, 2021). This powerful molecular scalpel allows scientists to target any desired piece of DNA and conduct genome editing. Almost any scientist can use this technology to quickly and easily alter DNA in any way they desire. Another advantage is the rapid delivery of results (Zhao et al., 2016). CRISPR's simplicity is its distinctive beauty. It may be readily tailored to specifically target any desired gene, whether it is present in plants, animals, microorganisms, or humans.

This approach is highly significant in the fields of biotechnology and medicine due to its ability to enable accurate, cost-effective, and uncomplicated editing of genomes, both in laboratory settings and within living organisms. CRISPR has a wide range of applications, including facilitating the study of biology, aiding in diagnostics, and assisting in developing new treatments. It is also used to improve crop yields, produce biofuels, and create organs that can be transplanted (Koonin, 2018). It can be used to develop new pharmaceuticals, food products, and genetically modified organisms and to manage infections. CRISPR/Cas is also being explored for gene therapy, particularly in treating genetic diseases and cancer.

Scientists have successfully employed CRISPR technology in the laboratory to precisely alter the genes of various creatures, including fruit flies, fish, mice, plants, and even human cells (Crudele and Chamberlain, 2018). These modifications have extended beyond applications related to bacterial immune responses (Crudele and Chamberlain, 2018). Below is an up-to-date summary of various medical applications of this technology, which are also summarized in Figure 5.

Table 2 provides a comprehensive overview of the most significant CRISPR-based therapies in clinical development. It summarizes the clinical trials on CRISPR-based therapies, their current stages of clinical development, and potential applications against various diseases. Since 2017, CRISPR-based therapies have achieved significant clinical milestones, highlighted by the US Food and Drug Administration (FDA) approval of the first CRISPR treatment (CASGEVY™) for sickle cell disease and β-thalassemia in 2023 (Adashi et al., 2024). *In vivo* preclinical studies have also shown potential; for instance, various CRISPR-edited CAR-T cell therapies have demonstrated promising safety and anti-tumor effects (Lei et al., 2024), with CB-010 achieving a complete response rate of 100% in early B-cell malignancy trials (Tao et al., 2024). The pipeline is steadily growing, featuring early advancements in tailored therapies such as diabetes treatments via insulin production from gene-edited islet cells (Bevacqua et al., 2024). Further preclinical developments address other conditions like Duchenne muscular dystrophy and cystic fibrosis, all focusing on somatic (non-heritable) applications rather than germline editing (Polcz and Lewis, 2016).

5.1 CRISPR gene editing and the future of medicines

CRISPR technology is being applied across various medical domains, including the treatment of hereditary diseases, cancer, and infectious diseases. It enables personalized medicine by allowing for precise gene editing and the development of targeted therapies. Gene silencing and editing using CRISPR involves using a guide RNA that matches the DNA area of interest to lead the molecular machinery to cleave both strands of the targeted DNA. Gene silencing occurs when the cell tries to fix damaged DNA but frequently introduces mistakes that interfere with the functioning of the gene, resulting in its silence. During gene editing, a repair template that includes a precise sequence alteration is injected into the cell and incorporated into the DNA as part of the repair process. As a result, the specific DNA undergoes modifications that result in the acquisition of this new sequence (Zhang et al., 2021b).

Numerous researchers are intrigued by the prospect of employing CRISPR technology due to its encouraging preliminary results in the laboratory. There are many examples of the successful use of this approach in managing diseases, such as hereditary disorders. Several years ago, the first evidence demonstrating that CRISPR could be used to repair a faulty gene and reverse the symptoms of a disease in a living animal was published (Kannan and Ventura, 2015). For liver disease, various gene therapy approaches with specific gene targets have emerged as appealing treatment options for monogenic disorders or multifactorial disorders (Cozmescu et al., 2021). In the case of maladaptive protein expression, gene function can be disabled using the CRISPR–Cas system. For instance, blocking transthyretin can be used as a therapy for amyloidosis. Additionally, gene defects can be corrected by restoring the normal functions of liver enzymes such as fumarylacetoacetate hydrolase or alpha-1 antitrypsin (Adlat et al., 2023). Researchers have shown that a patient with a rare liver condition (Crigler–Najjar syndrome) could be cured with a single gene therapy in trials conducted on human patients (D'antiga et al., 2023). Crigler-Najjar syndrome is an inherited disorder caused by a lack of the gene UGT1A1 (as shown in Figure 5A). This leads to a deficiency or absence of the enzyme UDP-glucuronosyltransferase, which is necessary for the liver to convert unconjugated bilirubin into a form that can be eliminated from the body. In the subsequent study, individuals diagnosed with Crigler–Najjar syndrome successfully restored the expression of the liver enzyme UGT1A1 with the application of gene therapy.

A liver-targeting CRISPR–Cas9 delivery nanosystem was developed in a newly published study to delete the proprotein convertase subtilisin/kexin type 9 (Pcsk9) gene, which is linked to the pathophysiology of dyslipidemia. When this technique was applied in a mouse model, atherosclerosis was prevented, and cholesterol was significantly reduced (Xu et al., 2024a).

However, in the treatment of Sickle Cell disorder (SCD), CRISPR technology has emerged as a transformative tool for gene editing by reactivating fetal hemoglobin (HbF) through targeted disruption of repressor binding sites. Frati, Giacomo et al. findings

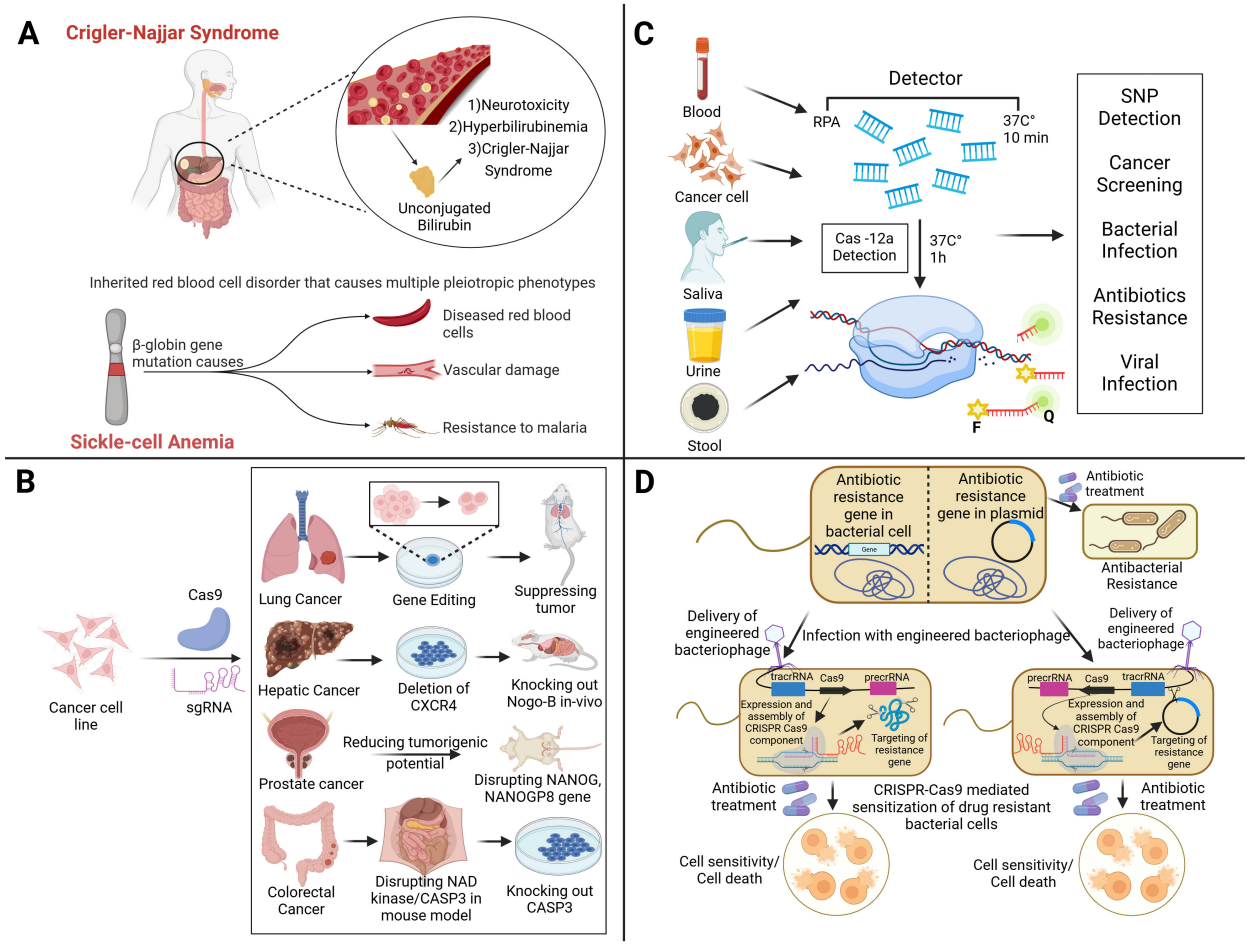

FIGURE 5
The diverse applications of CRISPR-based technologies in genetic disorders, diagnostics, cancer therapy, and antimicrobial resistance, which highlight its impact on precision medicine and infectious disease control. **(A)** CRISPR holds therapeutic potential for Crigler-Najjar Syndrome and sickle-cell anemia by targeting disease-causing mutations, such as those in β-globin gene, responsible for abnormal red blood cells and associated complications. In cancer therapy **(B)**, CRISPR-Cas9 facilitates targeted gene editing to suppress tumors by modifying oncogenic pathways, for example, by deleting CXCR4 in lung cancer, disrupting NANOG in prostate cancer, and knocking out CASP3 in colorectal cancer therapy, reducing tumorigenic potential across multiple cancer types. For diagnostics **(C)**, CRISPR-Cas12a enables rapid and sensitive detection of single-nucleotide polymorphisms (SNPs), cancer biomarkers, bacterial and viral pathogens, and antibiotic resistance markers using bodily fluids like blood, saliva, urine, and stool. In addressing antibiotic resistance **(D)**, engineered bacteriophages carrying CRISPR-Cas systems can be used to specifically target and cleave resistance genes within bacterial chromosomes or plasmids, restoring bacterial susceptibility to antibiotics and leading to cell death.

showed that SCD hematopoietic stem and progenitor cells (HSPCs) exhibit higher gene editing efficiency than healthy donor cells, potentially due to differences in DNA repair mechanisms or chromatin accessibility influenced by chronic inflammation. Despite this advantage, SCD HPSCs show reduced engraftment and heightened sensitivity to cellular stress induced by the CRISPR–Cas9 procedure, underscoring the need for optimized protocols and comprehensive safety assessments. Off-targets, large deletions, and chromosomal rearrangements present challenges, highlighting the importance of high-fidelity Cas-9 variants and DSB free technologies such as base and prime editing to minimize unintended mutations. While DSB-free approaches show precision in reducing genomic stability, their efficiency in SCD cells remains limited. Moving forward, the integration of novel delivery methods, single-cell analyses, and improved editing strategies will enhance the safety and efficacy of CRISPR therapies, accelerating their transition into clinical practice to provide durable and personalized treatment for patients with SCD and other genetic disorders (Frati et al., 2024).

5.2 CRISPR in oncology and resistance to anti-cancer drugs

CRISPR–Cas9 has been applied experimentally to edit genomes to explore tumor occurrence, development, and metastasis, and to repair mutations or knock out specific genes involved in cancer. It has shown promise in enhancing the efficacy of cancer immunotherapy. Moreover, the application of the CRISPR–Cas9 system enables the deletion of functional domains within drug resistance genes, offering a strategy to combat anti-cancer drug resistance (Figure 5B). Several scientists have developed

TABLE 2 Clinical trials on CRISPR-based therapies, target and mechanisms of each therapy, current stages of clinical development, and potential applications against various diseases.

Disease/ Condition	Therapy Name/ Identifier	Target/ Mechanism	Year Started	Phase	Key Results/Status	Clinical trials	References
Sickle Cell Disease & β-thalassemia	CRISPR–Cas9-edited CD34+ cells (CTX001/ exa-cel/CASGEVY)	BCL11A gene to increase fetal hemoglobin (HbF)	2018	Approved	FDA approval (Dec 2023); patients who are transfusion-independent with sustained HbF levels	NCT03745287; NCT03655678	(Frangoul et al., 2021)
Cancer (Multiple Myeloma, Solid Tumors)	CRISPR-edited T cells (CTX110, CTX120, CTX130)	Allogeneic CAR-T targeting CD19, BCMA, CD70	2019	Phase 1/2	Encouraging safety profile and anti-tumor activity	NCT04035434; NCT04244656	(Stadtmauer et al., 2020)
Cancer (Advanced Solid Tumors)	CRISPR-edited T cells	PD-1 knockout in autologous TILs	2019	Phase 1	Demonstrated feasibility and safety; modest clinical responses	NCT02793856; NCT03399448	(Stadtmauer et al., 2020)
HIV	CCR5 gene-edited CD34+ cells	CCR5 gene knockout to prevent HIV infection	2017	Phase 1/2	Demonstrated safety; limited efficacy	NCT03164135	(Xu et al., 2019)
Leber Congenital Amaurosis 10 (LCA10)	EDIT-101 (AGN-151587)	CEP290 gene correction via subretinal injection	2019	Phase 1/2	Evidence of editing, vision improvements in some patients	NCT03872479	(Maeder et al., 2019)
Transthyretin Amyloidosis	NTLA-2001	*In vivo* CRISPR to reduce TTR protein production	2020	Phase 1	Sustained reduction in serum TTR levels (>80%) after single dose	NCT04601051	(Gillmore et al., 2021)
Hereditary Angioedema	NTLA-2002	Kallikrein (KLKB1) gene knockout	2022	Phase 1/2	>90% reduction in attack rate; sustained effect	NCT05120830	(Longhurst et al., 2024)
Mucopolysaccharidosis Type I (MPS I)	SB-318	Zinc finger nuclease targeting albumin locus for IDS enzyme expression	2017	Phase 1/2	Evidence of *in vivo* genome editing; modest increases in enzyme levels	NCT02702115	(Harmatz et al., 2022; Nan et al., 2020)
Acute Myeloid Leukemia	FT819	CRISPR-engineered iPSC-derived CAR-T cells targeting CD19	2022	Phase 1	First iPSC-derived CAR-T cell therapy	NCT04629729	(Park et al., 2020)
Metastatic Gastrointestinal Cancers	Neoantigen-targeted T cells (NeoTCR-P1)	CRISPR-engineered TCR T cells targeting personalized neoantigens	2021	Phase 1	First personalized engineered TCR-T cells; demonstrated T cell persistence	NCT03970382	(Borgers et al., 2025)
Relapsed/Refractory B-cell Malignancies	CB-010	Allogeneic anti-CD19 CAR-T with additional edits for enhanced persistence	2021	Phase 1	100% CR rate in initial cohort	NCT04637763	(Nastoupil et al., 2022)
Type 1 Diabetes	VCTX210/ VX-880	Gene-edited pancreatic islet cells in device	2022	Phase 1/2	Ongoing; early evidence of insulin production	NCT04786262	(Vertex, 2024)
Duchenne Muscular Dystrophy	IM-267 (formerly CRISPR-SKIP)	Exon skipping strategy targeting dystrophin	2024	Preclinical	Moving toward clinical trials	NCT not yet assigned	(Min et al., 2019)
Cystic Fibrosis	CTX003	Correction of CFTR mutations	2023	Preclinical	Moving toward clinical trials	NCT not yet assigned	(Hodges and Conlon, 2019)
Advanced Mycosis Fungoides and Sézary Syndrome	Allogeneic CD70-CAR-T cells	CRISPR-engineered CAR-T targeting CD70	2022	Phase 1	Early-stage trial	NCT04502446	(Aftimos et al., 2017)

instruments that can successfully eliminate genes connected to resistance to drugs in cancer. Tyrosine kinase inhibitors (TKIs) block several targets and signaling pathways to prevent the growth and metastasis of tumors. While TKIs can be used as a treatment strategy for patients, long-term usage of them may cause resistance (Metibemu et al., 2019). Drug responsiveness may be enhanced by targeting genes linked to TKI resistance. Imatinib is one specific TKI that kills cells in conditions like gastrointestinal stromal tumors (GISTs) and chronic myeloid leukemia (CML). However, imatinib-treated cancer cells may become resistant to the medication, preventing it from killing the cells. Utilizing CRISPR gene editing technology to prevent the emergence of imatinib resistance has been covered in several studies. To increase the susceptibility of resistant cell lines linked to chronic myeloid leukemia (K562 and KCL22) to imatinib, CRISPR was utilized to repress genes including hTERT, miR-21, miRNA182, bcr-abl, and KDM6 (Zhang et al., 2021a; Shirani-Bidabadi et al., 2023). The half-maximal inhibitory concentration (IC50) of imatinib was considerably lower in K562/G01 cells when the expression of miR-21 decreased than in wild-type (WT) cells (Zhang et al., 2020). In another study, removing KDM6A increased the drug's cellular sensitivity and reduced imatinib's IC50 (from 1.15 to 0.24 μM) (Zhang et al., 2021a). Three K562 cell lines with decreased hTERT had GI50s (50% of maximal inhibition of cell growth) compared to the control, reducing imatinib's efficacy (Grandjenette et al., 2020). CRISPR gene editing techniques can be used to combat resistance to additional TKI medications, including erlotinib, sorafenib, and ibritumomab. A concrete example of this can be observed in the capacity to modify the resistance to erlotinib in the non-small cell lung cancer (NSCLC) HCC827 cell line through the decrease of miR-214 expression and its subsequent target LHX6. The sensitivity to erlotinib was higher in miR-214 knockout cells (1.22 μM erlotinib IC50) and miR-214/LHX6 knockout cells (2.25 μM erlotinib) as compared to control cells (3.38 μM erlotinib IC50) (Liao et al., 2017). Several cancer types have documented resistance to antimitotic drugs such as vinca alkaloids or taxanes (Shirani-Bidabadi et al., 2023). Drug resistance has been associated with human epididymis protein-4 (HE4/WFDC2), a small secretory protein that is increased in ovarian cancer. When paclitaxel was administered to ovarian cancer cells with HE4 deletion, the survival rate of the KO cells decreased significantly; it reduced from 73.9% in normal cells to 65.9% in CRISPR-knockout cells (Ribeiro et al., 2016). Elevated Aurora-B expression in non-small cell lung cancer has been linked to cisplatin and paclitaxel resistance. To investigate this possibility, CRISPR was used to remove Aurora-B from the A549 paclitaxel-resistant (A549/PTX) cell line. Upon exposure to different doses of paclitaxel, A549/PTX WT cells exhibited increased resistance and proliferation. However, the proliferation and resistance of prA549/PTX mutant cells substantially decreased at high doses of paclitaxel. There has been talk of deleting Rsf-1, an overexpressed histone-binding protein linked to several cancers, including lung cancer, as a potential tactic to combat paclitaxel resistance. The loss of RSF1 reduced the mobility and propagation of H460 and H1299 cells and enhanced cell mortality, making them more susceptible to paclitaxel. The tumor volume was lower in the H460 cell xenograft mice treated with paclitaxel (13.0 ± 9.2 mm3) compared to the H460 cell xenograft mice treated with paclitaxel (49.4 ± 14.5 mm3). The creation of xenograft animal models employing H460 Rsf-1 KO cells served as an example of this. Atypical chemokine receptor 3 (ACKR3), a member of the G protein-coupled receptor (GPCR) superfamily, is widely expressed in a wide range of cancers, particularly in methotrexate-resistant prostate cancer tissue. The application of CRISPR-mediated ACKR3 deletion reduced the viability of DU145R and PC3R cells to around 60% and 70%, respectively, of the control when the cells were exposed to docetaxel. Doxorubicin is an anthracycline that has shown promise in treating many cancers, including breast cancer. Nevertheless, taking it could cause tumors to proliferate and treatment resistance to develop (Shirani-Bidabadi et al., 2023).

Another study introduces a novel methodology that can identify genes involved in multidrug resistance and CRISPR–Cas9 resistant cancer cell lines, and reveals critical gene networks through differential gene expression analysis. Gene regulatory network (GRN) construction using FSSEM highlights key genes like UHMK1, MGST3, and USP9X, directly linked to drug resistance, while non-coding RNAs like ESRG and LINC00664 exhibit regulatory roles in lung cancer resistance. Though none of the genes directly associated with CRISPR–Cas9 resistance were identified. However, the pathways involved in transcription and proliferation regulation show potential influences on CRISPR efficiency. The tissue-specific nature of resistance, demonstrated by the distinct GRNs for lung and intestinal cancer, underscores the importance of tailoring future research to specific cancer types. Expanding datasets and exploring non-coding gene functions will enhance understanding of resistance mechanisms, ultimately improving CRISPR-based therapies and advancing personalized cancer treatment.

5.3 Sharpening the edge in infectious disease diagnosis and treatment

CRISPR technology has emerged as a transformative tool in infectious disease detection and treatment. By leveraging the gene-editing capabilities of CRISPR–Cas systems, researchers are developing innovative diagnostic and therapeutic approaches that promise to enhance the management of infectious diseases (Figures 5C, D).

5.3.1 CRISPR-based diagnostics for infections

CRISPR-Cas systems have been utilized to create rapid, accurate, and portable diagnostic tools that can detect infectious agents directly from clinical samples. Scientists have discovered that Cas13, a close relative of Cas9, can also be used to detect diseases. Cas13 searches for viral RNA using an RNA guide in its natural environment. Once its viral target is identified, Cas13 becomes activated (Kellner et al., 2019). In certain situations, it cuts any RNA it encounters, a process known as collateral cleavage. Researchers at the McGovern Institute, Broad Institute, and Harvard University have harnessed this mechanism to create specific high-sensitivity

enzymatic reporter unlocking (SHERLOCK), an exceptionally sensitive tool for detecting human infectious diseases (as described in Figure 6C). Currently, SHERLOCK can be adapted to detect any genetic signature, including those associated with cancer, in virtually any location. Cas9, Cas13, and Cas12 are just a few examples of natural biological systems (shown in Figure 6) that scientists have modified to combat genetic and infectious diseases (Mustafa and Makhawi, 2021).

CRISPR–Cas12 system has been used to detect SARS-CoV-2, which caused the famous COVID-19 global pandemic. Scientists have developed an assay called SARS-CoV-2 DNA Endonuclease-Targeted CRISPR Trans Reporter (DETECTR). Initially, viral genomic material extracted from nasopharyngeal or oropharyngeal swabs undergoes a series of reverse transcription (as in Figure 6A) and isothermal amplification using loop-mediated amplification. Finally, Cas12 detects coronavirus sequences with the aid of a FAM-biotin reporter molecule, which is visualized by lateral flow strips designed to capture labeled nucleic acids (Broughton et al., 2020).

Interestingly, Cas12a-based sensing technology was also used to detect mutations in SARS-CoV-2, which represent challenges in the virus detection. Cas12a-based RT-PCR combined with a CRISPR on-site rapid detection system (RT-CORDS) platform was utilized to detect the key mutations in SARS-CoV-2 variants, such as 69/70 deletion, N501Y, and D614G. This novel assay designed type-specific crRNAs to identify wild-type (crRNA-W) and mutant (crRNA-M) virus sequences. Indeed, CRISPR tools can be helpful in the epidemiological monitoring of the spread of novel escape viral variants, besides their valuable role in clinical diagnostics (Marqués et al., 2021; He et al., 2022).

Other novel assays, such as all-in-one dual CRISPR-Cas12a (AIOD-CRISPR), were designed for ultrasensitive and visual detection of SARS-CoV-2. In the latter assay, two CRISPR RNAs

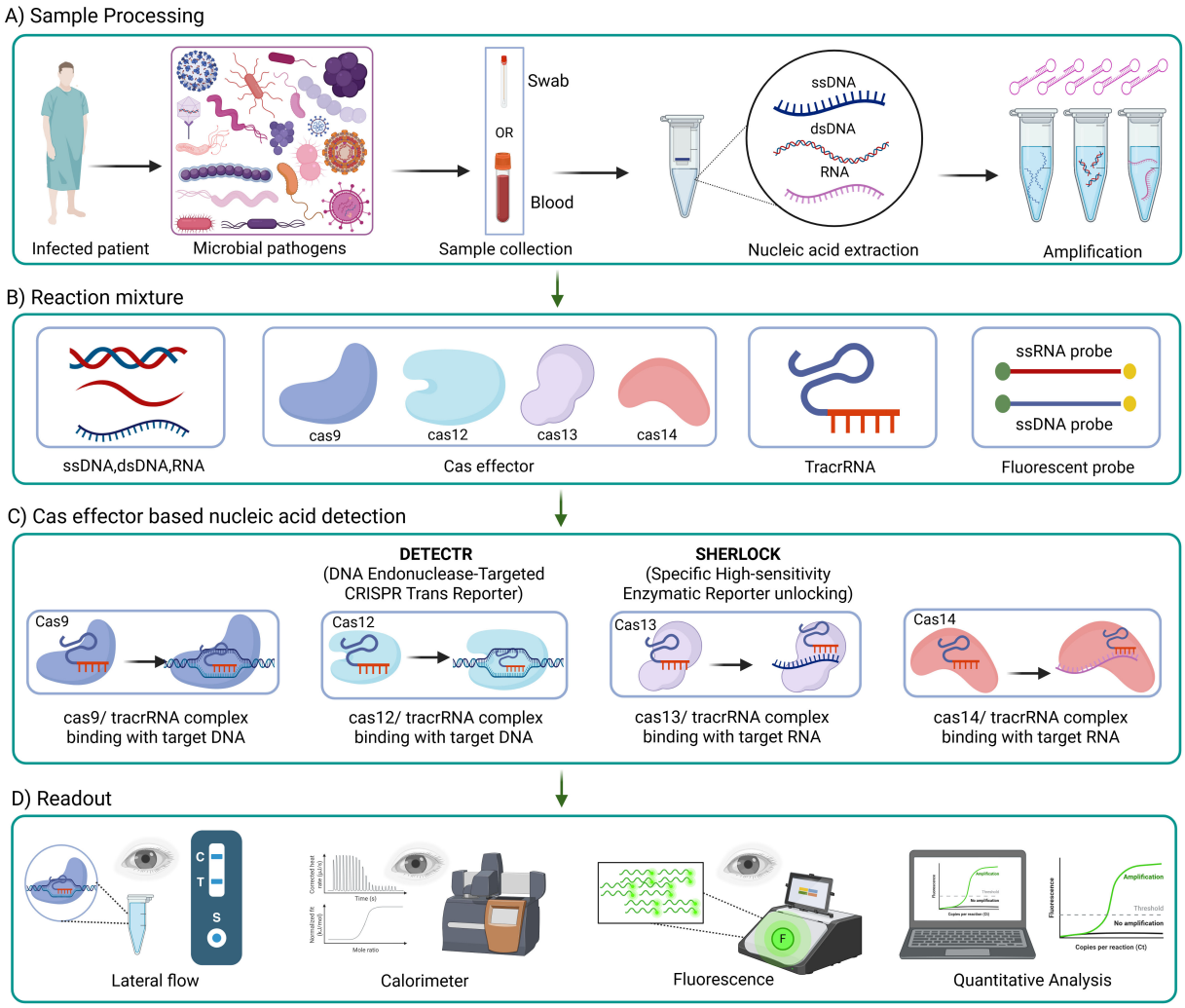

FIGURE 6
Workflow of CRISPR-based diagnostics for infections. CRISPR-based tools detects infections through four main steps; **(A)** a sample (like a swab or blood) is collected from an infected patient, and DNA or RNA is extracted and amplifies; **(B)** the reaction mixture includes Cas protein (like Cas9, Cas12, Cas13 and Cas14), guide RNAs and a reaction detector (example, fluorescent probes); **(C)** Cas proteins, paired with guide RNAs, recognize specific genetic targets, DNA or RNA, and trigger a signal using systems like DETECTR or SHERLOCK; **(D)** the results is then read using methods such as lateral flow strips, fluorescence, color changes, or computer based quantitative analysis.

without a PAM site were developed to achieve highly sensitive, specific, and robust detection of viral nucleic acids in clinical samples (Ding et al., 2020).

Technologies such as SHERLOCK and DETECTR allow ultrasensitive detection of pathogens. These innovative CRISPR-based diagnostic tests are promising as they present the potential for future development of point-of-care diagnostics, offering an alternative to conventional PCR methods. This can help rapidly identify infectious diseases without requiring extensive laboratory infrastructure (as shown in Figure 6). Future CRISPR-based diagnostics can be designed to be inexpensive, user-friendly, and capable of providing results quickly. The ability to perform these tests on multiple specimen types further enhances their utility in diverse clinical settings, including resource-limited areas whereby traditional diagnostics are impractical due to their need for sophisticated equipment and trained personnel.

5.3.2 CRISPR-based therapeutics for infections: recent developments in CRISPR-Cas-based antimicrobials

CRISPR technology is being explored for its potential to target and cleave pathogenic DNA or RNA sequences, offering a novel approach to treating infectious diseases. Antimicrobial agents, whether synthetic or natural, are crucial substances that can effectively eliminate or hinder the growth of infectious microbes. The discovery of antibiotics has saved millions of lives; however, the increase in antibiotic resistance is causing further infectious diseases to become incurable. Antimicrobial resistance (AMR), as defined by the World Health Organization (WHO), is a worldwide problem resulting from various contributing causes, including insufficient hygiene, ineffective management, and overuse of antibiotics. This problem leads to an increase in rates of illness and mortality, an increase in expenses, and a prolongation of infectious disease durations. Conventional antimicrobial medications have become ineffective due to AMR. Producing these traditional antibiotics requires significant time and a substantial financial investment. Research on next-generation alternatives, specifically CRISPR–Cas9, has been driven by the challenges presented by existing antibacterial drugs (Getahun et al., 2022).

Shortly after the discovery of CRISPR–Cas, scientists recognized the potential of CRISPR as an antibiotic, which has recently garnered increasing attention (Aqeel and Raza, 2017; Owaid and Al-Ouqaili, 2025). The application of genome editing to the treatment of infectious diseases has the potential to revolutionize medicine. Because the essential step needed to target and cut different DNA sequences is the selective deletion of the plasmid encoding the targeted gene, CRISPR–Cas technology is especially attractive (Zhou et al., 2019). CRISPR can serve as an antibacterial agent by using either a pathogen-centric method or a gene-centric technique as described in Figure 6D, contingent upon the specific gene's position. A pathogen-focused technique involves the precise targeting of specific regions on the bacterial chromosome. This method selectively eradicates the specific harmful strain and induces the demise of bacterial cells, while preserving the survival of other beneficial bacteria (Pursey et al., 2018). On the other hand, the gene-focused strategy focuses on a plasmid that contains AMR genes. This method results in plasmid removal and bacterial antibiotic re-sensitization (Tagliaferri et al., 2020). Given that AMR genes frequently migrate and have the potential to move across various bacterial species, eliminating AMR genes regardless of the host's genetic makeup may be a successful therapy (Bhattacharyya and Mukherjee, 2020).

Since the CRISPR–Cas system is widely found in bacteria and archaea, efforts are being made to separate, enhance, and create delivery systems for this system. Researchers aim to develop RNA-guided nucleases that can efficiently target a wider variety of bacterial strains, including infections that are resistant to several drugs. Targeting particular DNA regions associated with antibiotic resistance genes and bacterial pathogens, the Cas9 nuclease is injected into microbial populations by a variety of mechanisms, such as bacteriophages, conjugative plasmid-carrying bacteria, and polymer-derivatized CRISPR nano-complexes (Gholizadeh et al., 2020).

For AMR, CRISPR–Cas can be utilized using three overarching methodologies: (i) It can target and cut genes that are particular to certain species to treat sudden illnesses. This involves using the desired bacteria while keeping the host's microbiome unchanged (Gomaa et al., 2014; Owaid and Al-Ouqaili, 2024); (ii) The process can be targeted to cleave genes that cause medication resistance, thereby killing bacteria that carry these genes while keeping the viable wild-type susceptible clones intact, thus removing the pathogens from patients (Bikard et al., 2014); or (iii it can be employed to suppress or alter resistance genes by inducing changes that render the resistance genes non-functional while keeping the bacteria alive. This process is referred to as re-sensitization (Wang et al., 2018).

Scientists have attempted the exploitation of CRISPR–Cas system to neutralize AMR genes. This system, an effective bacterial defense mechanism, may be customized to precisely identify and cleave DNA sequences, providing a promising approach to address antibiotic resistance as described in Figure 6D. This approach makes use of repeat-enclosed RNA-based spacers to guide Cas proteins to DNA at particular locations, enabling the development of an adaptable tool that can target a variety of genes. Recent studies have shown that it can be lethal to intentionally or unintentionally target specific bacterial genome sequences with the CRISPR–Cas system, causing irreversible chromosomal damage and ultimately cell death (Jwair et al., 2023).

Researchers used the type I-E CRISPR–Cas system of *E. coli* in a study to specifically target crucial sites in the genomes of various strains. The findings demonstrated that it was possible to effectively eradicate bacterial strains by focusing on various sites within the genome, including individual genes. A different strategy was to remove methicillin-resistant *Staphylococcus aureus* (MRSA) strains from a mixed bacterial community by enclosing the plasmid in phage capsids, or a Cas9 phagemid. The Cas9 phagemid demonstrated efficacy in specifically targeting tetracycline-resistant plasmids and effectively decreasing the proportion of MRSA strains within the population (Brouns et al., 2008).

In another investigation, scientists introduced the Cas9 nuclease into bacteria to target specific antibiotic resistance genes using conjugative plasmids and M13-based phagemids. This technique demonstrated how the CRISPR–Cas system can distinguish

between susceptible and resistant strains by significantly reducing the number of viable cells in the resistant strains. The findings highlight the potential of CRISPR-based technologies to target and eliminate antibiotic-resistant bacteria, offering a promising prospect in the ongoing fight against infections caused by bacteria (Rasheed et al., 2000, 2013).

In a study by Kang et al., 2017, a non-viral delivery method for the CRISPR–Cas system was introduced (Kang et al., 2017). The scientists employed a cationic polymer called branched polyethyleneimine (bPEI), sgRNA that targets *mecA*, and a Cas9 nano-complex. Improved Cas9 translocation into MRSA strains is demonstrated by this method. When compared to native Cas9 combined with bPEI and native Cas9 mixed with lipofectamine, a carrier that is widely used for gene delivery in mammalian cells, the Cas9-bPEI complex showed more bacterial uptake. The MRSA strains that were treated exhibited reduced growth on oxacillin-containing agar media, indicating that this technique can inhibit the development and survival of bacteria. Using Cas9 phagemids, which are plasmids made to be enclosed in phage capsids, was another important tactic. Researchers have created a CRISPR–Cas9 phagemid to target particular ARGs in MRSA strains (Bikard et al., 2014; Kang et al., 2017). Tetracycline-resistant plasmids in MRSA were effectively eradicated by the phagemid, which resulted in a marked reduction in bacterial proliferation. Similar to this, Citorik et al. (2014) used phagemids to target crucial genes in strains of bacteria resistant to antibiotics, which significantly decreased the number of viable cells (Citorik et al., 2014). These studies highlight the potential of phagemids as effective tools in CRISPR-based antimicrobial strategies. Phagemids have disadvantages despite their benefits, which include decreased plasmid content and targeted death. One disadvantage is that, once infected, phagemids do not multiply to generate other phages. Hence, a higher dosage is needed for treatment. Furthermore, their vast population and restricted host range might prevent them from being widely used. On the other hand, the use of a single nuclease with several guide RNAs to target distinct plasmids or chromosomal sequences is made possible by programmed Cas9-mediated death. This strategy demonstrates its adaptability in altering bacterial populations by potentially reducing resistant clones and minimizing the transmission of antibiotic-resistance or virulence plasmids. Moreover, the ability of the CRISPR–Cas system to modulate complex bacterial communities has been explored. Studies have demonstrated its effectiveness in selectively removing bacteria with specific genomes, reducing the prevalence of unwanted genes such as virulence loci or antibiotic resistance genes. The efficiency of Cas9 phagemids was also tested in an *in vivo* mouse model, where topical treatment significantly reduced the proportion of infected cells (Gholizadeh et al., 2020).

There have been many successful attempts to use CRISPR–Cas in managing AMR bacteria. Recent studies have reported effective eradication of AMR bacteria by specifically targeting efflux pumps (Chikkareddy, 2024). Nine specific sgRNAs were designed to target the components of the AcrAB-TolC efflux pump in *Escherichia coli* in a recent study, which showed increased susceptibility to multiple drugs, such as rifampicin, erythromycin and tetracycline, in bacterial cells with repressed efflux pump genes (Wan et al., 2022).

Moreover, several resistance genes, such as those for ciprofloxacin (*grlA, grlB*), gentamicin (*aacA*), and methicillin (*mecA*), were knocked out in MRSA using CRISPR–Cas9 technology. This study showed a noteworthy shift in the direction of antibiotic susceptibility. Another work demonstrated that pathogenic *Escherichia coli* may successfully cure *IncF* plasmids using the CRISPR–Cas9 technology. Since *IncF* plasmids contain a variety of AMR determinants, removing them from bacteria aids in the restoration of their antibiotic-susceptible status (Chen et al., 2024).

A recent study by Wang et al. introduced an innovative strategy termed as ATTACK (AssociaTes TA and CRISPR-Cas to kill) for combating multi-drug resistant (MDR) bacterial pathogens. This approach protects the CreTA module, a CRISPR regulated toxin-antitoxin (TA) system that naturally safeguards CRISPR-Cas components within the host. The underlying mechanisms are based on programmed cell death upon CRISPR-Cas inactivation. The researchers demonstrated two key mechanisms: first, the CreT component specifically targets multiple small RNAs essential for the initiation of protein synthesis; second, the CreA molecule acts as a guide RNA, directing the CRISPR-Cas complex to target CreT. The ATTACK system utilizes these elements such that, in the event of CRISPR-Cas system inactivation within MDR pathogens, CreTA is activated to induce bacterial cell death (Wang et al., 2023). Chen et al. developed an optimized CRISPR interference (CRISPRi) system based on the type I-F subtype, referred to as CSYi, for gene silencing applications in clinical isolates of *Pseudomonas Aeruginosa*. This system enabled functional characterization of resistance determinants, and notably, the researcher identified the regulatory role of CzcR in controlling efflux pump gene expression, which plays a critical role in the multi-drug resistance phenotype of *P. aeruginosa* (Chen et al., 2023). Additionally, Sheng et al. uncovered a novel resistance mechanism whereby insertion sequences (ISs) integrate into Cas genes, resulting in the inactivation of CRISPR-Cas systems. This insertional mutagenesis effectively transforms a bacterial defense mechanism, impairing its function. Their findings underscore the role of OS elements in disrupting CRISPR-Cas integrity, as demonstrated in *E. coli* isolates (Sen and Mukhopadhyay, 2024). Furthermore, Locus Biosciences (Morrisville, NC, USA) carried out the first clinical trial employing a CRISPR-Cas3 system delivered via phage to target *E. coli* causing urinary tract infections, yielding favorable safety and tolerability results (Kim et al., 2024).

Finally, it is important to consider the advantages of CRISPR-Cas-based antimicrobials over traditional antibiotics, as depicted in Figure 7. The development of CRISPR-Cas systems as versatile antimicrobials holds significant promise, allowing for the targeted attack of pathogens, even those resistant to conventional antibiotics. These intelligent tools can be tailored to disrupt essential bacterial genes, virulence factors, or specific antibiotic resistance genes, potentially reestablishing antibiotic efficacy or directly eradicating harmful bacteria while safeguarding beneficial microbiota (Uddin et al., 2021). Scientists have recently harnessed these powerful biological tools that hold enormous potential to treat infectious

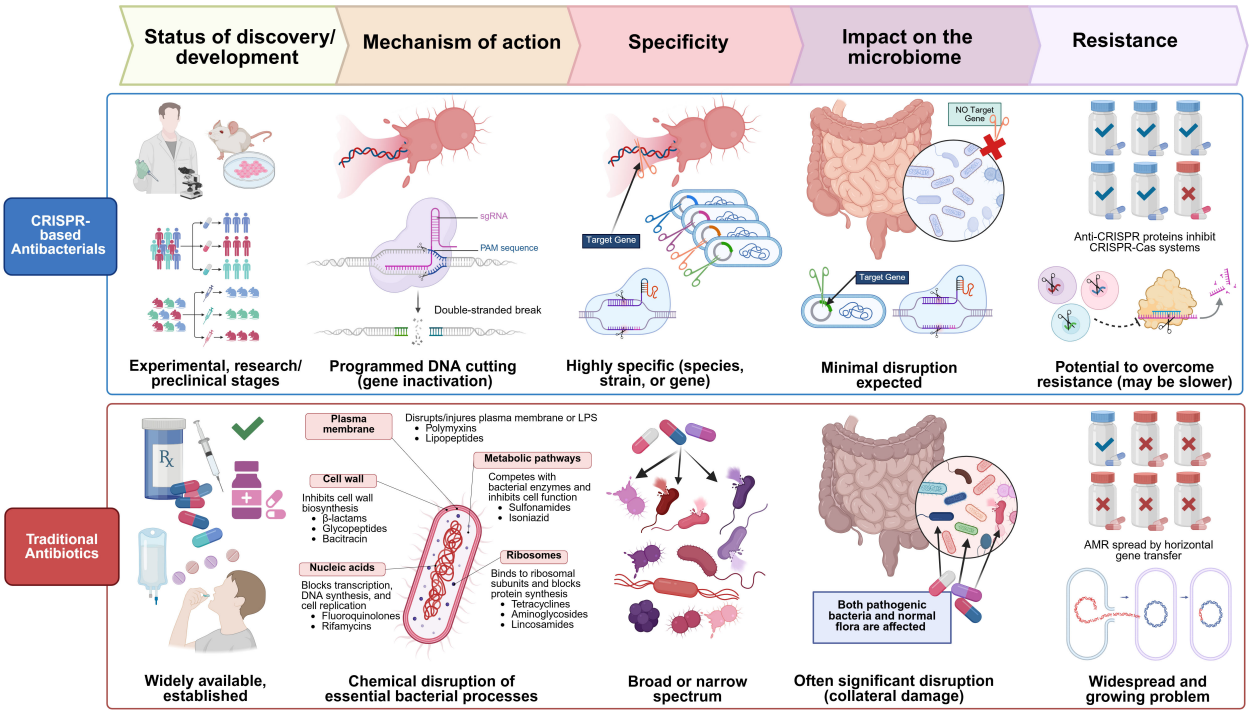

FIGURE 7
Comparative overview of CRISPR-based antibacterials and traditional antibiotics across five key aspects: development stage, mechanism of action, specificity, microbiome impact, and resistance. Traditional antibiotics, widely available and clinically established, exert their antibacterial effect through chemical disruption of essential bacterial processes, including inhibition of cell wall synthesis, protein translation, and DNA replication. These drugs display either broad or narrow-spectrum activity but often lead to significant collateral damage to the host microbiota. Furthermore, the widespread emergence of antimicrobial resistance (AMR), frequently driven by horizontal gene transfer, poses a major clinical challenge. In contrast, CRISPR-based antibacterials are in early research and preclinical stages. They function via sequence-specific, RNA-guided DNA cleavage, enabling precise gene inactivation. Their high specificity allows targeting of particular bacterial species or even strains, minimizing off-target effects and preserving the host microbiome. Although anti-CRISPR proteins may confer resistance, the potential to overcome such resistance exists, limiting resistance to CRISPR-based antibacterials.

diseases, potentially enabling the development of more targeted antibiotics that solely attack disease-causing bacterial strains. This is linked to the unique mechanism of action and selectivity of these gene editing tools over broad-spectrum antibiotics, which can damage a wide range of bacteria, including the beneficial microbiota (Mayorga-Ramos et al., 2023).

5.4 Precision editing by next-generation CRISPR tools: base editors and prime editors

CRISPR-Cas systems can be adapted for a wide range of applications, including base editing and prime editing.

Base editing is evolving as a precise alternative to traditional CRISPR-Cas9. It signifies a groundbreaking breakthrough in genome editing technology, enabling accurate nucleotide substitutions. They comprise a nuclease-deficient Cas9 (usually nCas9 or dCas9) linked to a DNA deaminase enzyme. The Cas component directs the editor to the target location through an sgRNA, while the deaminase chemically alters a specific base within a small editing window close to the target site. This allows the deaminase to introduce specific point mutations into DNA without creating double-strand breaks (DSBs) or relying on donor DNA templates and repair efficiency (Wang et al., 2022). Early clinical translation efforts are focusing on diseases where precise edits of specific mutations are needed. Key therapeutic uses include rectifying harmful point mutations in genetic disorders, as shown in clinical trials for hypercholesterolemia by targeting PCSK 9 (Hoekstra and Van Eck, 2024), and HbF gene in sickle cell disease (Zeballos and Gaj, 2021). Recent advancements showcase dual-function editors capable of implementing specific combinations of nucleotide alterations simultaneously, along with engineered variants that exhibit markedly reduced off-target activity (Liang et al., 2022). These features establish base editing as a revolutionary technique in both research and therapeutic genomic medicine.

Prime editors signify a notable advancement in precision genome editing technology, which is more versatile than base editors. This technique allows for improved flexibility by integrating new genetic sequences into the genome with accuracy (Zeballos and Gaj, 2021). This search-and-replace system can execute all possible base-to-base conversions, small insertions, and precise deletions with fewer off-target effects compared to traditional CRISPR methods (Anzalone et al., 2019). It is capable of addressing multiple mutations without requiring donor

templates and without generating direct DSBs. Prime editors comprise a Cas9 nickase attached to a reverse transcriptase (RT) enzyme. Guided by a specialized prime editing guide RNA (pegRNA), this system not only identifies the target site but also includes an RT template sequence that encodes the desired modification. The process starts with the nCas9 making a cut in one DNA strand at the target location, followed by pegRNA binding to the nicked strand. The RT then utilizes the pegRNA template to synthesize a new DNA strand incorporating the edit. Ultimately, cellular mechanisms resolve the intermediate structure to integrate the change into both DNA strands (Xu et al., 2024b).

Noteworthy therapeutic applications include rectifying pathogenic mutations in multiple diseases, such as cystic fibrosis (Bulcaen et al., 2024), Duchenne muscular dystrophy (Happi Mbakam et al., 2022), and metabolic disorders like phenylketonuria (Brooks et al., 2023). Recently, the FDA approved the use of prime editing in a phase 1/2 clinical trial for pediatric and adult patients with chronic granulomatosis disease, a rare immunodeficiency resulting from mutations in genes that impact phagocyte function (Biotechnology, 2024).

6 Hurdles in using CRISPR–Cas technology for therapeutic purposes

CRISPR has been recognized as a versatile and adaptable tool for molecular and clinical research and gene therapy approaches (Saber et al., 2020). It has been used in drug resistance research applications, such as gene function screening, resistant model creation, and molecular mechanism exploration (Yang et al., 2021). However, scientific, economic, and regulatory challenges face new genomic technologies, including CRISPR technology (Pacia et al., 2024). Several concerns confront this groundbreaking tool for genome editing:

6.1 Safety concerns

The main downside of CRISPR is its off-target cleavage of DNA sequences (Balon et al., 2022), which can decrease the efficiency of gene editing (Yang et al., 2021). The off-target effect occurs when Cas acts on untargeted genomic loci, leading to random cleavage at undesired sites, which can cause several adverse outcomes. These sites are often gRNA-dependent, since Cas9 can tolerate up to 3 mismatches between gRNA and genomic DNA (Guo et al., 2023). Modifying Cas9 and optimizing the gRNA can help mitigate off-target effects (Balon et al., 2022). Indeed, designing specific gRNAs for CRISPR-Cas systems can be performed with the aid of artificial intelligence (AI) models, which can increase the precision, specificity, and efficiency by predicting off-target scores (Dixit et al., 2023; Dai et al., 2024). Engineering Cas9 proteins can help to improve their specificity in binding to gRNA-matched genomic regions, ensuring perfect guide-target complementarity. Furthermore, these engineered variants of Cas9 have fewer mutagenic and immunogenic adverse effects (Kovalev et al., 2024). Another limitation of the CRISPR technique is the requirement for a PAM near the DNA target site. Efforts have been made to develop engineered nucleases that require less or no PAM. Recent research has shown that PAM-relaxed variants of Cas9 are improved by increased specificity and activity (Kovalev et al., 2024).

Gene therapy has the potential to cause immunotoxicity. The bacterial origin of the CRISPR system can trigger immunogenicity as it can be recognized as foreign by the human immune system (Ewaisha and Anderson, 2023). Selection of non-cross-reactive CRISPR types from non-ubiquitous organisms can be considered to overcome the effect of pre-existing immunity. The immune system may also react to the Cas9 protein, leading to the elimination of genetically modified cells. Further work is necessary to develop a remedy, such as using a recombinant Cas9 protein that blocks T-cell activation as described in Figure 8.

Viral vectors used for delivery can induce an adverse immune response, which poses a significant challenge. For example, adenoviruses, widely used viral vectors for the delivery of gene therapy (Wold and Toth, 2013), can induce cross-reactive adaptive immune responses with different serotypes of the same virus (Kovalev et al., 2024). Viral vector tissue tropism can be used for targeting desired disease sites, lowering the risk of systemic immune responses. *In silico* prediction of the immunogenicity of CRISPR therapeutics can be helpful in light of the advances in various tools that can leverage AI for efficient design with fewer adverse reactions. Enabling the effective and secure transportation of the CRISPR–Cas9 system into targeted cells presents a significant challenge (Balon et al., 2022).

One additional challenge that this innovative technology faces is the lack of secure and effective distribution channels; thus, safe delivery methods are required. CRISPR delivery employs three main categories of carriers: physical transfer, viral vectors, and non-viral vectors (shown in Figure 8). Microinjection and electroporation are well-established techniques used for the physical delivery of drugs, and ongoing scientific research is focused on hydrodynamic delivery systems (Zhang et al., 2021c). Adeno-associated viruses (AAVs), full-sized adenoviruses, and lentiviruses are commonly used as viral vectors to transport genetic material. Viruses serve as the primary vehicle for delivering CRISPR–Cas9 into living organisms. Non-viral vectors do not receive the same level of awareness as viral vectors, but they provide unique advantages that have attracted scientific research (Shirani-Bidabadi et al., 2023). Scientists are creating nano-carriers that specifically transport CRISPR–Cas9 to cancerous tumors. Self-assembled nanoparticles are chosen for their ability to pack and protect efficiently. Nano-carriers possess the ability to contain reactive molecules, hence enhancing the processes of circulation, absorption, and targeting. Additionally, they can exhibit delivery patterns that are sensitive to stimuli, so allowing gene editing. Nanotechnology has improved the effectiveness of cancer therapy and minimized the unwanted consequences of CRISPR–Cas9 treatment (Shirani-Bidabadi et al., 2023).

6.2 Ethical concerns

There are ethical concerns when implementing CRISPR–Cas technology in preclinical or clinical trials. The primary issue is

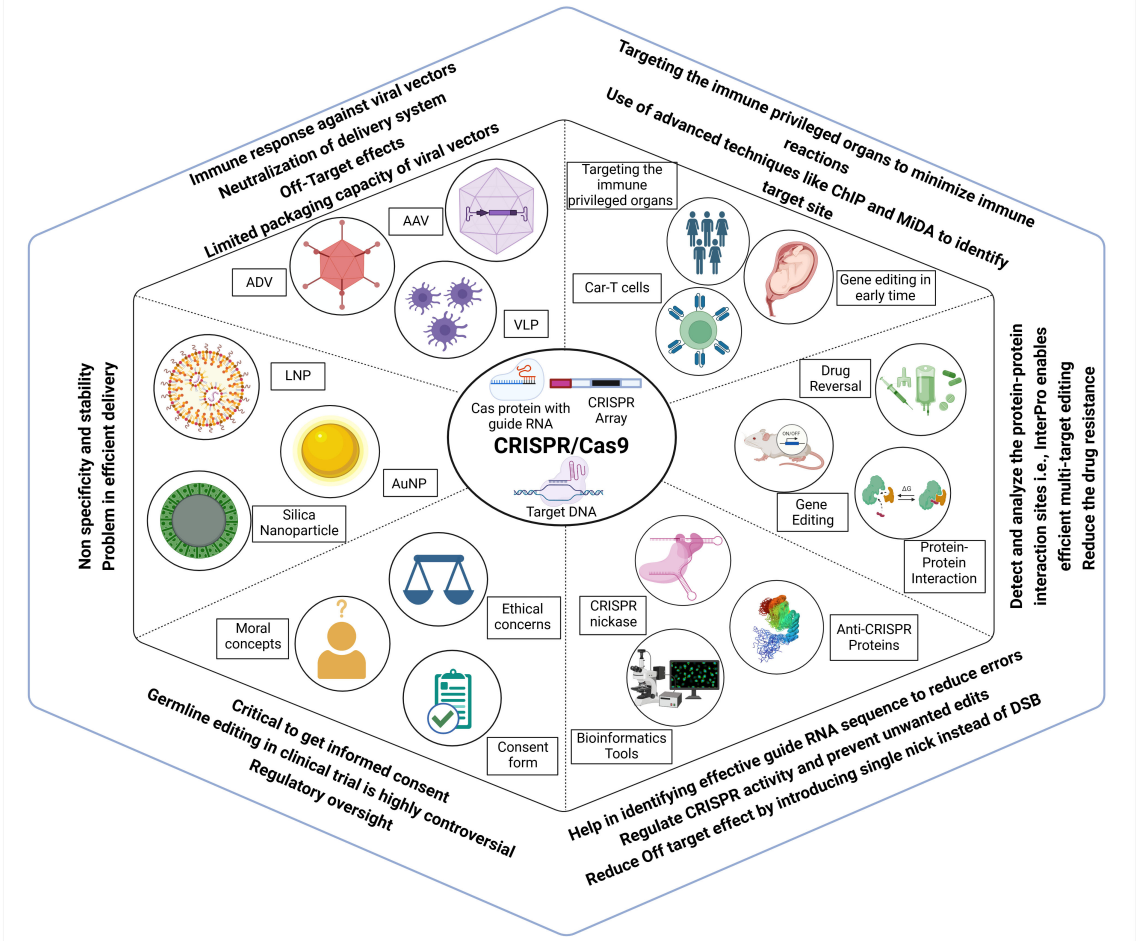

FIGURE 8
Challenges, ethical considerations and advancements associated with CRISPR Cas genome editing. Efficient delivery of CRISPR components remains a major hurdle, with vectors such as AAV, ADV, VLPs, and various nanoparticles limited by immune responses, off-target effects, and low stability. These issues can be mitigated by targeting immune-privileged organs, using early-stage gene editing, and applying advanced site identification tools. CRISPR application extends beyond gene correction to include drug resistance reversal, modulation of protein-protein interactions, and multi-target effects, and avoiding double-strand breaks. AI and bioinformatics tools assist in designing effective guide RNAs to enhance target specificity and minimize unwanted edits. However, germline editing remains highly controversial, requiring strict regulatory oversight, ethical reflection, comprehensive informed consent, and controlled clinical trials.

related to apprehensions over off-target effects, adverse consequences, inadequate editing, and lower efficacy of the treatment in comparison to conventional therapeutic drugs (Kotagama et al., 2019). Furthermore, one of the most contentious ethical issues is the potential for using CRISPR technology in human germline editing (shown in Figure 8), which entails making alterations to sperm, eggs, or embryos that can be inheritable. This situation raises concerns regarding unforeseen and undesirable consequences, as well as the moral implications associated with the modification of human genetics (Ben Ouagrham-Gormley and Fye-Marnien, 2019).

In 2017, Ma et al. reported the first therapeutic germline intervention, which involved creating modified zygotes by fertilizing healthy oocytes with sperm from a carrier of a mutation linked to hypertrophic cardiomyopathy. Utilizing CRISPR–Cas9, they corrected the genetic defect in these zygotes, resulting in mutation-free, viable embryos (Ma et al., 2017). This germline intervention was conducted for research purposes, demonstrating the feasibility of correcting gene mutations in viable human embryos through genome editing techniques, and also proved the efficiency, accuracy, and safety of this method (Rubeis and Steger, 2018). This method can also be used for other inheritable traits as a way to prevent diseases. As a potential life-saving treatment, it offers advantages that surpass its risks. So far, no clinical trials involving humans have taken place, and the embryos produced were solely for research, not for implantation in the womb. The ongoing debate centers on the moral implications of modifying genomic material in a way that these edits could be passed on to future generations (Brokowski, 2018).

Notably, a Chinese research team conducted an unauthorized trial involving germline editing using CRISPR-Cas9 to create embryos resistant to HIV from an infected father. In 2018, Dr. He Jiankui sought to alter both copies of the CCR5 gene, allegedly intending to render the future babies' white blood cells incapable of

contracting HIV. Consequently, two twin girls were born with genetically modified traits that grant them immunity to HIV. There are also concerns that modifications to the CCR5 gene may impact brain development and potentially enhance cognitive abilities (Raposo, 2019). This was not part of an approved clinical trial, resulting in severe backlash and his incarceration. In December 2019, the Chinese doctor was convicted of illegal medical practices and received a three-year prison sentence (Alonso and Savulescu, 2021).

Before starting any clinical trial focused on human germline editing, it is vital to gather extensive preclinical safety data, conduct ethical assessments, obtain regulatory approvals, and achieve wide societal consensus. Establishing global ethical standards and guidelines is imperative for managing CRISPR applications, particularly in the context of human germline editing. This requires working together with international organizations to maintain biosecurity and prevent misuse (Dieuliis and Giordano, 2018). Continuous research and open dialogue among scientists, ethicists, and policymakers are essential for addressing the ethical and safety challenges associated with CRISPR technology. This collaborative approach guarantees that the technology is utilized in a responsible and safe manner (Aljabali et al., 2024).

6.3 Resistance progression against CRISPR-Cas

CRISPR technology faces resistance challenges both in human applications and bacterial systems. The emergence of resistance poses a significant challenge to the effective application of CRISPR-Cas technologies. Bacteria use various mechanisms to defend against CRISPR, which play a key role in the continuous co-evolutionary battle between prokaryotes and their viral predators, impacting the advancement of CRISPR-based antimicrobials significantly (Uribe et al., 2021).

In the context of phage interactions, resistance can rapidly arise through the accumulation of point mutations within the target sequence of the CRISPR-Cas system (Tao et al., 2018). A similar phenomenon may occur when targeting antibiotic resistance genes, particularly under conditions of positive selection, such as the presence of antibiotics for which the resistance gene provides protection. Furthermore, resistance may develop through the disruption or deletion of essential Cas genes, impairing the ability of the system to cleave target DNA, or through the loss of targeting spacers critical for CRISPR functionality (Common et al., 2020). Apart from point mutation, resistance can also arise through the selection of anti-CRISPR genes (Kadkhoda et al., 2024). These genes encode small proteins capable of binding and inhibiting key components of the CRISPR-Cas immune machinery. Till now, more than 50 unique families of anti-CRISPR (*acr*) genes have been identified, targeting both type I and type II CRISPR-Cas system (Chaudhary et al., 2018).

Another cause of resistance against CRISPR-Cas system is the microbial ecosystems present in the environmental niches, as well as within human hosts (Watson et al., 2023). These microbial ecosystems are extraordinarily diverse and structurally intricate. These natural microbial communities form unique, distinct microbiomes, each comprising billions of bacterial cells representing thousands of species per gram of sample. Such diversity poses a considerable challenge when deploying CRISPR-Cas system for combating antimicrobial resistance. Although CRISPR-Cas technologies have shown significant promise in eradicating pathogenic bacteria or restoring antibiotic sensitivity in resistant strains, current research has primarily been confined to simplified, near-clonal bacterial populations. Only a limited number of *in vivo* investigations, mostly utilizing murine models, have attempted to target Gram-negative pathogens within the gastrointestinal tract to impede their colonization (Geinoro et al., 2024).

Moreover, anticipating the ecological consequences of CRISPR-Cas antimicrobial interventions within complex microbial communities remains a substantial hurdle. Targeted depletion of a specific strain may inadvertently disrupt microbial homeostasis (dysbiosis), creating ecological niches that can be exploited by opportunistic or harmful species. As a result, the broader implications of eliminating antimicrobial resistance within these multifaceted microbial ecosystems must be rigorously assessed prior to the clinical or environmental application of CRISPR-Cas based antimicrobials (Kadkhoda et al., 2024).

Similarly, human cells can show resistance to CRISPR, often noted as low editing efficiency that leads to unintended outcomes due to the poor interplay between the editing tool and the human cell. As a result, only a small fraction of the target cell population displays the desired genetic modification. This can be attributed to DNA repair pathway alterations, as cells can modify their DNA repair mechanisms in ways that reduce CRISPR editing efficiency (Liao et al., 2024). Additionally, the activation of p53-mediated responses may be another contributing factor. CRISPR-induced DNA double-strand breaks can activate p53, a tumor suppressor protein, leading to cell cycle arrest or apoptosis. This process effectively favors the survival of cells with impaired p53 pathways, enabling them to divide even in the presence of DNA damage (Conti and Di Micco, 2018). Pre-existing genetic variations also play a role, as the natural genetic polymorphisms in target sequences or PAM sites can prevent CRISPR recognition and cutting (Hirakawa et al., 2020). Editing may not take place in all cells within a population or even on all alleles in a single cell, resulting in a mosaic mixture of edited, partially edited, and unedited cells. This incomplete editing can compromise therapeutic efficacy, particularly if a high percentage of corrected cells is essential for phenotypic rescue (Hirakawa et al., 2020; Yang et al., 2021).

7 Strategies for overcoming the obstacles to enhance the delivery of CRISPR–Cas

Multiple challenges have emerged in implementing the CRISPR–Cas system in medical microbiology applications. Therefore, several methodologies have been examined and evaluated to tackle these issues.

An approach to enhance the delivery of CRISPR–Cas involves the use of conjugative plasmids, which can be further enhanced by screening for additional plasmids with a broader range of hosts. The researchers intentionally chose conjugative plasmids from the *Enterobacteriaceae* family to target pathogenic bacteria in the gut. The researchers discovered plasmids that exhibit improved DNA transfer efficiency within the gut microbiota. Consequently, scientists have developed a genetically engineered probiotic strain capable of utilizing exceptionally effective plasmids for transmitting the CRISPR–Cas system. This strain can eradicate chloramphenicol-resistant *E. coli* germs in mice (Neil et al., 2021). Conjugation is a less effective method of removing resistant species or those with specific genetic traits than phage delivery, nevertheless, it can still be more effective in some cases. This is because certain conjugative plasmids have the capacity for replication and a wide range of hosts. It is essential to design a delivery system that works with a broad variety of hosts, especially when applying the CRISPR–Cas system in complex microbial communities. Because the reaction of bacterial groups to this application is unknown, careful monitoring and analysis of the ecological consequences of the CRISPR–Cas system are essential. With the help of this study, researchers will be able to better comprehend how the removal of drug-resistance genes affects the frequency of other bacterial species in the community. Phage engineering shows promise as a strategy to overcome the constraints of current phages in delivering CRISPR–Cas antimicrobial agents. Scientists have integrated the CRISPR–Cas system into the genetic material of a phage, resulting in a modified bacteriophage. This system has two benefits: first, is the phage's specific affinity for the target initiates the demise of pathogenic cells by employing an abortive infection pathway during phage invasion. Secondly, the introduction of the CRISPR–Cas system into the specific pathogen results in the removal of the target gene and induces apoptosis in the harmful bacteria (Shukla et al., 2021). Researchers have used this technique to eradicate multidrug resistance genes from *K. pneumoniae* by modifying the *Klebsiella* virulent bacteriophage phiKpS2. However, administering the CRISPR–Cas system using phages does not precisely mimic phage therapy and has similar challenges. Furthermore, the application of a phage system that incorporates CRISPR–Cas to restore susceptibility in antibiotic-resistant bacteria by antibiotic therapy results in the eradication of antibiotic-resistant mutants that evade treatment. Yosef et al. have developed a method that uses temperate phages to deliver the CRISPR–Cas system into bacterial cells to address the challenges posed by antibiotic-resistant bacteria. The CRISPR spacers utilized in this method are precisely designed to selectively target genes that are associated with antibiotic resistance and lytic phages. When the CRISPR–Cas phage system is introduced into the samples, bacteria that are capable of integrating phage DNA into their own DNA restore their susceptibility to antibiotics. On the other hand, bacteria without this capability are susceptible to the damaging actions of lytic phages (Kundar and Gokarn, 2022). Integrating several phages to stop the creation of resistant mutants and improve the effectiveness of treatment approaches is feasible since pathogenic bacteria can evolve and become resistant to manufactured phages.

However, the anti-CRISPR activity of *acr* genes can be countered by some CRISPR–Cas systemic changes that can negate the effects of anti-CRISPR proteins. It is also feasible to produce CRISPR variants that are insensitive to Acr proteins to solve the problem of accessing Acr proteins. Similarly, several strategies can improve the toxicity and efficacy of Cas9 nucleases in various bacterial hosts, such as mixing alternative Cas proteins with Cas9.

Furthermore, a large repertoire of strategies has been developed to improve specificity (high-fidelity Cas, better gRNAs), favoring precise repair (base/prime editing), developing stealthier delivery systems, and managing host immune responses. Combating bacterial resistance, particularly for CRISPR antimicrobials, requires anticipating evolution through multiplex targeting, careful target selection, and robust delivery methods capable of overcoming bacterial defenses while addressing the threat of Acr proteins. Vigilance regarding off-target effects, immunogenicity, and the emergence of resistance remains paramount as these technologies move further into clinical settings. Utilizing current technological advancements could aid in overcoming challenges related to obtaining regulatory approval for the CRISPR–Cas system's implementation in the real world (Kundar and Gokarn, 2022).

8 Conclusions and future perspectives

Undoubtedly, CRISPR has become a valuable gene-editing tool offering unprecedented precision and versatility in manipulating genetic material, although there is still much to learn about it. CRISPR–Cas gene editing technology has a wide range of valuable applications, which could potentially replace conventional treatments and has the potential to advance next-generation diagnostic platforms. Its future perspectives are vast and promising, spanning various fields in medicine. There is enough interest in the field to support the establishment of several biotech start-ups aiming to treat human diseases with CRISPR-inspired technologies. The future use of CRISPR–Cas technologies offer significant potential for both medical applications and genome editing in the majority, if not all, species. As we progress from modifying the genomes of model organisms to humans, numerous ethical issues must be considered; thus, it is crucial to carefully consider both the benefits and challenges associated with this groundbreaking tool. We are only beginning to grasp how the CRISPR revolution will impact our future. The future development of this technology will allow for a more personalized approach to targeted treatment for various illnesses, but indeed, this needs more research. Therefore, conducting more thorough preclinical and clinical trials before implementing this technology in human treatments is essential.

Author contributions

MA-O: Conceptualization, Data curation, Formal analysis, Investigation, Methodology, Resources, Software, Supervision, Validation, Visualization, Writing – original draft, Writing –

review & editing. AA: Formal analysis, Investigation, Methodology, Resources, Software, Visualization, Writing – review & editing. NJ: Conceptualization, Data curation, Formal analysis, Investigation, Methodology, Resources, Writing – original draft. FA-M: Conceptualization, Data curation, Formal analysis, Funding acquisition, Investigation, Methodology, Project administration, Resources, Software, Supervision, Validation, Visualization, Writing – original draft, Writing – review & editing.

Funding

The author(s) declare that financial support was received for the research and/or publication of this article. This project is supported by a Strategic Research Program grant (G00004973) from UAE University (awarded to Farah Al-Marzooq).

Acknowledgments

Figures were prepared using Biorender (https://www.biorender.com/ (accessed on 25 April 2025).

Conflict of interest

The authors declare that the research was conducted in the absence of any commercial or financial relationships that could be construed as a potential conflict of interest.

Generative AI statement

The author(s) declare that no Generative AI was used in the creation of this manuscript.

Publisher's note

References

Adashi, E. Y., Gruppuso, P. A., and Cohen, I. G. (2024). CRISPR therapy of sickle cell disease: the dawning of the gene editing era. *Am. J. Med.* 137, 390–392. doi: 10.1016/j.amjmed.2023.12.018

Adlat, S., Vázquez Salgado, A. M., Lee, M., Yin, D., and Wangensteen, K. J. (2023). Emerging and potential use of CRISPR in human liver disease. *Hepatology*. doi: 10.1097/hep.0000000000000578

Adli, M. (2018). The CRISPR tool kit for genome editing and beyond. *Nat. Commun.* 9, 1911. doi: 10.1038/s41467-018-04252-2

Aftimos, P., Rolfo, C., Rottey, S., Offner, F., Bron, D., Maerevoet, M., et al. (2017). Phase I dose-escalation study of the anti-CD70 antibody ARGX-110 in advanced malignancies. *Clin. Cancer Res.* 23, 6411–6420.

Aljabali, A., El-Tanani, M., and Tambuwala, M. M. (2024). Principles of CRISPR-Cas9 technology: Advancements in genome editing and emerging trends in drug delivery. *J. Drug Deliv. Sci. Technol.* 92, 105338. doi: 10.1016/j.jddst.2024.105338

Alonso, M., and Savulescu, J. (2021). He Jiankui´s gene-editing experiment and the non-identity problem. *Bioethics* 35, 563–573. doi: 10.1111/bioe.12878

Anders, C., Niewoehner, O., Duerst, A., and Jinek, M. (2014). Structural basis of PAM-dependent target DNA recognition by the Cas9 endonuclease. *Nature* 513, 569–573. doi: 10.1038/nature13579

Anzalone, A. V., Randolph, P. B., Davis, J. R., Sousa, A. A., Koblan, L. W., Levy, J. M., et al. (2019). Search-and-replace genome editing without double-strand breaks or donor DNA. *Nature* 576, 149–157. doi: 10.1038/s41586-019-1711-4

Aqeel, M., and Raza, A. (2017). CRISPR/cas9: an emerging revolution in therapeutics. *Int. J. Appl. Biol. Forensics.* 1, 1–4.

Azangou-Khyavy, M., Ghasemi, M., Khanali, J., Boroomand-Saboor, M., Jamalkhah, M., Soleimani, M., et al. (2020). CRISPR/cas: from tumor gene editing to T cell-based immunotherapy of cancer. *Front. Immunol.* 11. doi: 10.3389/fimmu.2020.02062

Balon, K., Sheriff, A., Jacków, J., and Łaczmański, Ł. (2022). Targeting cancer with CRISPR/cas9-based therapy. *Int. J. Mol. Sci.* 23, 573. doi: 10.3390/ijms23010573

Barrangou, R. (2015). The roles of CRISPR-Cas systems in adaptive immunity and beyond. *Curr. Opin. Immunol.* 32, 36–41. doi: 10.1016/j.coi.2014.12.008

Barrangou, R., Fremaux, C., Deveau, H., Richards, M., Boyaval, P., Moineau, S., et al. (2007). CRISPR provides acquired resistance against viruses in prokaryotes. *Science* 315, 1709–1712. doi: 10.1126/science.1138140

Barrangou, R., and Marraffini, L. A. (2014). CRISPR-Cas systems: Prokaryotes upgrade to adaptive immunity. *Mol. Cell* 54, 234–244. doi: 10.1016/j.molcel.2014.03.011

Ben Ouagrham-Gormley, S., and Fye-Marnien, S. R. (2019). "Is CRISPR a security threat?," in *Defense Against Biological Attacks: Volume I*. Eds. S. K. Singh and J. H. Kuhn (Springer International Publishing, Cham), 233–251.

Bevacqua, R. J., Zhao, W., Merheb, E., Kim, S. H., Marson, A., Gloyn, A. L., et al. (2024). Multiplexed CRISPR gene editing in primary human islet cells with Cas9 ribonucleoprotein. *iScience*. 27 (1), 108693. doi: 10.1101/2023.09.16.558090

Bhardwaj, A., and Nain, V. (2021). TALENs-an indispensable tool in the era of CRISPR: a mini review. *J. Genet. Eng. Biotechnol.* 19, 125. doi: 10.1186/s43141-021-00225-z

Bhattacharyya, S., and Mukherjee, A. (2020). "CRISPR: the revolutionary gene editing tool with far-reaching applications," in *Biotechnology Business - Concept to Delivery*. Ed. A. Saxena (Springer International Publishing, Cham), 47–56.

Bikard, D., and Barrangou, R. (2017). Using CRISPR-Cas systems as antimicrobials. *Curr. Opin. Microbiol.* 37, 155–160. doi: 10.1016/j.mib.2017.08.005

Bikard, D., Euler, C. W., Jiang, W., Nussenzweig, P. M., Goldberg, G. W., Duportet, X., et al. (2014). Exploiting CRISPR-Cas nucleases to produce sequence-specific antimicrobials. *Nat. Biotechnol.* 32, 1146–1150. doi: 10.1038/nbt.3043

Biotechnology, N. (2024). FDA clears prime editors for testing in humans. *Nat. Biotechnol.* 42, 691–691. doi: 10.1038/s41587-024-02264-6

Borgers, J. S. W., Lenkala, D., Kohler, V., Jackson, E. K., Linssen, M. D., Hymson, S., et al. (2025). Personalized, autologous neoantigen-specific T cell therapy in metastatic melanoma: a phase 1 trial. *Nat. Med.*.

Brokowski, C. (2018). Do CRISPR germline ethics statements cut it? *Crispr. J.* 1, 115–125. doi: 10.1089/crispr.2017.0024

Brooks, D. L., Whittaker, M. N., Qu, P., Musunuru, K., Ahrens-Nicklas, R. C., and Wang, X. (2023). Efficient *in vivo* prime editing corrects the most frequent phenylketonuria variant, associated with high unmet medical need. *Am. J. Hum. Genet.* 110, 2003–2014. doi: 10.1016/j.ajhg.2023.10.005

Broughton, J. P., Deng, X., Yu, G., Fasching, C. L., Servellita, V., Singh, J., et al. (2020). CRISPR–cas12-based detection of SARS-coV-2. *Nat. Biotechnol.* 38, 870–874. doi: 10.1038/s41587-020-0513-4

Brouns, S. J., Jore, M. M., Lundgren, M., Westra, E. R., Slijkhuis, R. J., Snijders, A. P., et al. (2008). Small CRISPR RNAs guide antiviral defense in prokaryotes. *Science* 321, 960–964. doi: 10.1126/science.1159689

Bulcaen, M., Kortleven, P., Liu, R. B., Maule, G., Dreano, E., Kelly, M., et al. (2024). Prime editing functionally corrects cystic fibrosis-causing CFTR mutations in human organoids and airway epithelial cells. *Cell Rep. Med.* 5, 101544. doi: 10.1016/j.xcrm.2024.101544

Chaudhary, K., Chattopadhyay, A., and Pratap, D. (2018). Anti-CRISPR proteins: Counterattack of phages on bacterial defense (CRISPR/Cas) system. *J. Cell Physiol.* 233, 57–59. doi: 10.1002/jcp.25877

Chen, S., Cao, H., Xu, Z., Huang, J., Liu, Z., Li, T., et al. (2023). A type I-F CRISPRi system unveils the novel role of CzcR in modulating multidrug resistance of

Pseudomonas aeruginosa. *Microbiol. Spectr.* 11, e0112323. doi: 10.1128/spectrum.01123-23

Chen, L., Peirano, G., Yen, K., Wang, B., Terlecky, A., Devinney, R., et al. (2024). CRISPR-Cas9-mediated IncF plasmid curing in extraintestinal pathogenic Escherichia coli. *Microbiol. Spectr.* 12, e0369223. doi: 10.1128/spectrum.03692-23

Chikkareddy, A. (2024). *How can the CRISPR system be utilized as an innovative approach to combat antibiotic resistance by specifically targeting efflux pumps in bacteria*? doi: 10.58445/rars.867

Citorik, R. J., Mimee, M., and Lu, T. K. (2014). Sequence-specific antimicrobials using efficiently delivered RNA-guided nucleases. *Nat. Biotechnol.* 32, 1141–1145. doi: 10.1038/nbt.3011

Common, J., Sünderhauf, D., Van Houte, S., and Westra, E. R. (2020). Diversity in CRISPR-based immunity protects susceptible genotypes by restricting phage spread and evolution. *J. Evol. Biol.* 33, 1097–1108. doi: 10.1111/jeb.13638

Conti, A., and Di Micco, R. (2018). p53 activation: a checkpoint for precision genome editing? *Genome Med.* 10, 66. doi: 10.1186/s13073-018-0578-6

Cozmescu, A. C., Counsell, J., and Gissen, P. (2021). Gene therapies targeting the liver. *J. Hepatol.* 74, 235–236. doi: 10.1016/j.jhep.2020.08.003

Crudele, J. M., and Chamberlain, J. S. (2018). Cas9 immunity creates challenges for CRISPR gene editing therapies. *Nat. Commun.* 9, 3497. doi: 10.1038/s41467-018-05843-9

D'antiga, L., Beuers, U., Ronzitti, G., Brunetti-Pierri, N., Baumann, U., Giorgio, A. D., et al. (2023). Gene therapy in patients with the crigler–najjar syndrome. *New Engl. J. Med.* 389, 620–631. doi: 10.1056/NEJMoa2214084

Dai, M., Li, X., Zhang, Q., Liang, T., Huang, X., and Fu, Q. (2024). Health research in the era of artificial intelligence: Advances in gene-editing study. *Med. Plus.* 1, 100027. doi: 10.1016/j.medp.2024.100027

Dieuliis, D., and Giordano, J. (2018). Gene editing using CRISPR/Cas9: implications for dual-use and biosecurity. *Protein Cell* 9, 239–240. doi: 10.1007/s13238-017-0493-4

Ding, X., Yin, K., Li, Z., Lalla, R. V., Ballesteros, E., Sfeir, M. M., et al. (2020). Ultrasensitive and visual detection of SARS-CoV-2 using all-in-one dual CRISPR-Cas12a assay. *Nat. Commun.* 11, 4711. doi: 10.1038/s41467-020-18575-6

Dixit, S., Kumar, A., Srinivasan, K., Vincent, P., and Ramu Krishnan, N. (2023). Advancing genome editing with artificial intelligence: opportunities, challenges, and future directions. *Front. Bioeng. Biotechnol.* 11. doi: 10.3389/fbioe.2023.1335901

Dugar, G., Herbig, A., Förstner, K. U., Heidrich, N., Reinhardt, R., Nieselt, K., et al. (2013). High-resolution transcriptome maps reveal strain-specific regulatory features of multiple campylobacter jejuni isolates. *PloS Genet.* 9, e1003495. doi: 10.1371/journal.pgen.1003495

Ewaisha, R., and Anderson, K. S. (2023). Immunogenicity of CRISPR therapeutics-Critical considerations for clinical translation. *Front. Bioeng. Biotechnol.* 11. doi: 10.3389/fbioe.2023.1138596

Frangoul, H., Altshuler, D., Cappellini, M. D., Chen, Y. S., Domm, J., Eustace, B. K., et al. (2021). CRISPR-Cas9 gene editing for sickle cell disease and β-thalassemia. *N. Engl. J. Med.* 384, 252–260.

Frati, G., Brusson, M., Sartre, G., Mlayah, B., Felix, T., Chalumeau, A., et al. (2024). Safety and efficacy studies of CRISPR-Cas9 treatment of sickle cell disease highlights disease-specific responses. *Mol. Ther.* 32, 4337–4352. doi: 10.1016/j.ymthe.2024.07.015

Geinoro, T., Chala, G., and Mulugeta, W. (2024). Exploiting crispr-cas system to combat antibiotic resistance: A review. *Global Vet.* 26, 25–36. doi: 10.5829/idosi.gv.2024.25.3

Gesner, E. M., Schellenberg, M. J., Garside, E. L., George, M. M., and Macmillan, A. M. (2011). Recognition and maturation of effector RNAs in a CRISPR interference pathway. *Nat. Struct. Mol. Biol.* 18, 688–692. doi: 10.1038/nsmb.2042

Getahun, Y. A., Ali, D. A., Taye, B. W., and Alemayehu, Y. A. (2022). Multidrug-resistant microbial therapy using antimicrobial peptides and the CRISPR/cas9 system. *Vet. Med. (Auckl).* 13, 173–190. doi: 10.2147/vmrr.S366533

Gillmore, J. D., Gane, E., Taubel, J., Kao, J., Fontana, M., Maitland, M. L., et al. (2021). CRISPR-Cas9 in vivo gene editing for transthyretin amyloidosis. *N. Engl. J. Med.* 385, 493–502.

Gholizadeh, P., Köse, Ş., Dao, S., Ganbarov, K., Tanomand, A., Dal, T., et al. (2020). How CRISPR-cas system could be used to combat antimicrobial resistance. *Infect. Drug Resist.* 13, 1111–1121. doi: 10.2147/idr.S247271

Gleditzsch, D., Pausch, P., Müller-Esparza, H., Özcan, A., Guo, X., Bange, G., et al. (2019). PAM identification by CRISPR-Cas effector complexes: diversified mechanisms and structures. *RNA Biol.* 16, 504–517. doi: 10.1080/15476286.2018.1504546

Gomaa, A. A., Klumpe, H. E., Luo, M. L., Selle, K., Barrangou, R., and Beisel, C. L. (2014). Programmable removal of bacterial strains by use of genome-targeting CRISPR-Cas systems. *mBio* 5, e00928–e00913. doi: 10.1128/mBio.00928-13

Grandjenette, C., Schnekenburger, M., Gaigneaux, A., Gérard, D., Christov, C., Mazumder, A., et al. (2020). Human telomerase reverse transcriptase depletion potentiates the growth-inhibitory activity of imatinib in chronic myeloid leukemia stem cells. *Cancer Lett.* 469, 468–480. doi: 10.1016/j.canlet.2019.11.017

Guo, C., Ma, X., Gao, F., and Guo, Y. (2023). Off-target effects in CRISPR/Cas9 gene editing. *Front. Bioeng. Biotechnol.* 11. doi: 10.3389/fbioe.2023.1143157

Hale, C. R., Zhao, P., Olson, S., Duff, M. O., Graveley, B. R., Wells, L., et al. (2009). RNA-guided RNA cleavage by a CRISPR RNA-Cas protein complex. *Cell* 139, 945–956. doi: 10.1016/j.cell.2009.07.040

Happi Mbakam, C., Rousseau, J., Tremblay, G., Yameogo, P., and Tremblay, J. P. (2022). Prime editing permits the introduction of specific mutations in the gene responsible for duchenne muscular dystrophy. *Int. J. Mol. Sci.* 23, 6160. doi: 10.3390/ijms23116160

Harmatz, P., Prada, C. E., Burton, B. K., Lau, H., Kessler, C. M., Cao, L., et al. (2022). First-in-human in vivo genome editing via AAV–zinc-finger nucleases for mucopolysaccharidosis I/II and hemophilia B. *Mol. Ther.* 30, 3587–3600.

He, C., Lin, C., Mo, G., Xi, B., Li, A. A., Huang, D., et al. (2022). Rapid and accurate detection of SARS-CoV-2 mutations using a Cas12a-based sensing platform. *Biosensors. Bioelectron.* 198, 113857. doi: 10.1016/j.bios.2021.113857

Hille, F., and Charpentier, E. (2016). CRISPR-Cas: biology, mechanisms and relevance. *Philos. Trans. R. Soc. B.: Biol. Sci.* 371, 20150496. doi: 10.1098/rstb.2015.0496

Hirakawa, M. P., Krishnakumar, R., Timlin, J. A., Carney, J. P., and Butler, K. S. (2020). Gene editing and CRISPR in the clinic: current and future perspectives. *Biosci. Rep.* 40, BSR20200127. doi: 10.1042/bsr20200127

Hodges, C. A., and Conlon, R. A. (2019). Delivering on the promise of gene editing for cystic fibrosis. *Genes Dis.* 6, 97–108.

Hoekstra, M., and Van Eck, M. (2024). Gene editing for the treatment of hypercholesterolemia. *Curr. Atheroscl. Rep.* 26, 139–146. doi: 10.1007/s11883-024-01198-3

Jacinto, F. V., Link, W., and Ferreira, B. I. (2020). CRISPR/Cas9-mediated genome editing: From basic research to translational medicine. *J. Cell Mol. Med.* 24, 3766–3778. doi: 10.1111/jcmm.14916

Jiang, F., and Doudna, J. A. (2017). CRISPR-cas9 structures and mechanisms. *Annu. Rev. Biophys.* 46, 505–529. doi: 10.1146/annurev-biophys-062215-010822

Jinek, M., Chylinski, K., Fonfara, I., Hauer, M., Doudna, J. A., and Charpentier, E. (2012). A programmable dual-RNA-guided DNA endonuclease in adaptive bacterial immunity. *Science* 337, 816–821. doi: 10.1126/science.1225829

Jinek, M., Jiang, F., Taylor, D. W., Sternberg, S. H., Kaya, E., Ma, E., et al. (2014). Structures of Cas9 endonucleases reveal RNA-mediated conformational activation. *Science* 343, 1247997. doi: 10.1126/science.1247997

Jwair, N. A., Al-Ouqaili, M. T. S., and Al-Marzooq, F. (2023). Inverse association between the existence of CRISPR/cas systems with antibiotic resistance, extended spectrum β-lactamase and carbapenemase production in multidrug, extensive drug and pandrug-resistant klebsiella pneumoniae. *Antibiot. (Basel).* 12, 980. doi: 10.3390/antibiotics12060980

Kadkhoda, H., Gholizadeh, P., Samadi Kafil, H., Ghotaslou, R., Pirzadeh, T., Ahangarzadeh Rezaee, M., et al. (2024). Role of CRISPR-Cas systems and anti-CRISPR proteins in bacterial antibiotic resistance. *Heliyon* 10, e34692. doi: 10.1016/j.heliyon.2024.e34692

Kannan, R., and Ventura, A. (2015). The CRISPR revolution and its impact on cancer research. *Swiss Med. Wkly.* 145, w14230. doi: 10.4414/smw.2015.14230

Kang, Y. K., Kwon, K., Ryu, J. S., Lee, H. N., Park, C., and Chung, H. J. (2017). Nonviral genome editing based on a polymer-derivatized CRISPR nanocomplex for targeting bacterial pathogens and antibiotic resistance. *Bioconjug. Chem.* 28, 957–967. doi: 10.1021/acs.bioconjchem.6b00676

Kellner, M. J., Koob, J. G., Gootenberg, J. S., Abudayyeh, O. O., and Zhang, F. (2019). SHERLOCK: nucleic acid detection with CRISPR nucleases. *Nat. Protoc.* 14, 2986–3012. doi: 10.1038/s41596-019-0210-2

Kim, H., and Kim, J.-S. (2014). A guide to genome engineering with programmable nucleases. *Nat. Rev. Genet.* 15, 321–334. doi: 10.1038/nrg3686

Kim, P., Sanchez, A. M., Penke, T. J. R., Tuson, H. H., Kime, J. C., Mckee, R. W., et al. (2024). Safety, pharmacokinetics, and pharmacodynamics of LBP-EC01, a CRISPR-Cas3-enhanced bacteriophage cocktail, in uncomplicated urinary tract infections due to Escherichia coli (ELIMINATE): the randomised, open-label, first part of a two-part phase 2 trial. *Lancet Infect. Dis.* 24, 1319–1332. doi: 10.1016/s1473-3099(24)00424-9

Konstantakos, V., Nentidis, A., Krithara, A., and Paliouras, G. (2022). CRISPR-Cas9 gRNA efficiency prediction: an overview of predictive tools and the role of deep learning. *Nucleic Acids Res.* 50, 3616–3637. doi: 10.1093/nar/gkac192

Koonin, E. V. (2018). Open questions: CRISPR biology. *BMC Biol.* 16, 95. doi: 10.1186/s12915-018-0565-9

Koonin, E. V., and Makarova, K. S. (2019). Origins and evolution of CRISPR-Cas systems. *Philos. Trans. R. Soc. B.: Biol. Sci.* 374, 20180087. doi: 10.1098/rstb.2018.0087

Kotagama, O. W., Jayasinghe, C. D., and Abeysinghe, T. (2019). Era of genomic medicine: A narrative review on CRISPR technology as a potential therapeutic tool for human diseases. *BioMed. Res. Int.* 2019, 1369682. doi: 10.1155/2019/1369682

Kouranova, E., Forbes, K., Zhao, G., Warren, J., Bartels, A., Wu, Y., et al. (2016). CRISPRs for optimal targeting: delivery of CRISPR components as DNA, RNA, and protein into cultured cells and single-cell embryos. *Hum. Gene Ther.* 27, 464–475. doi: 10.1089/hum.2016.009

Kovalev, M. A., Davletshin, A. I., and Karpov, D. S. (2024). Engineering Cas9: next generation of genomic editors. *Appl. Microbiol. Biotechnol.* 108, 209. doi: 10.1007/s00253-024-13056-y

Kundar, R., and Gokarn, K. (2022). CRISPR-cas system: A tool to eliminate drug-resistant gram-negative bacteria. *Pharmaceuticals* 15, 1498. doi: 10.3390/ph15121498

Ledford, H., and Callaway, E. (2020). Pioneers of revolutionary CRISPR gene editing win chemistry Nobel. *Nature* 586, 346–347. doi: 10.1038/d41586-020-02765-9

Lei, T., Wang, Y., Zhang, Y., Yang, Y., Cao, J., Huang, J., et al. (2024). Leveraging CRISPR gene editing technology to optimize the efficacy, safety and accessibility of CAR T-cell therapy. *Leukemia* 38, 2517–2543. doi: 10.1038/s41375-024-02444-y

Liang, Y., Xie, J., Zhang, Q., Wang, X., Gou, S., Lin, L., et al. (2022). AGBE: a dual deaminase-mediated base editor by fusing CGBE with ABE for creating a saturated mutant population with multiple editing patterns. *Nucleic Acids Res.* 50, 5384–5399. doi: 10.1093/nar/gkac353

Liao, J., Lin, J., Lin, D., Zou, C., Kurata, J., Lin, R., et al. (2017). Down-regulation of miR-214 reverses erlotinib resistance in non-small-cell lung cancer through up-regulating LHX6 expression. *Sci. Rep.* 7, 781. doi: 10.1038/s41598-017-00901-6

Liao, H., Wu, J., Vandusen, N. J., Li, Y., and Zheng, Y. (2024). CRISPR-Cas9-mediated homology-directed repair for precise gene editing. *Mol. Ther. Nucleic Acids* 35, 102344. doi: 10.1016/j.omtn.2024.102344

Longhurst, H. J., Lindsay, K., Petersen, R. S., Fijen, L. M., Gurugama, P., Maag, D., et al. (2024). CRISPR-Cas9 in vivo gene editing of KLKB1 for hereditary angioedema. *N. Engl. J. Med.* 390, 432–441.

Ma, H., Marti-Gutierrez, N., Park, S.-W., Wu, J., Lee, Y., Suzuki, K., et al. (2017). Correction of a pathogenic gene mutation in human embryos. *Nature* 548, 413–419. doi: 10.1038/nature23305

Maeder, M. L., Stefanidakis, M., Wilson, C. J., Baral, R., Barrera, L. A., Bounoutas, G. S., et al. (2019). Development of a gene-editing approach to restore vision loss in Leber congenital amaurosis type 10. *Nat. Med.* 25, 229–233.

Marqués, M.-C., Ruiz, R., Montagud-Martínez, R., Márquez-Costa, R., Albert, S., Domingo-Calap, P., et al. (2021). CRISPR-cas12a-based detection of SARS-coV-2 harboring the E484K mutation. *ACS Synthetic. Biol.* 10, 3595–3599. doi: 10.1021/acssynbio.1c00323

Marraffini, L. A., and Sontheimer, E. J. (2010). CRISPR interference: RNA-directed adaptive immunity in bacteria and archaea. *Nat. Rev. Genet.* 11, 181–190. doi: 10.1038/nrg2749

Mayorga-Ramos, A., Zúñiga-Miranda, J., Carrera-Pacheco, S. E., Barba-Ostria, C., and Guamán, L. P. (2023). CRISPR-cas-based antimicrobials: design, challenges, and bacterial mechanisms of resistance. *ACS Infect. Dis.* 9, 1283–1302. doi: 10.1021/acsinfecdis.2c00649

Metibemu, D. S., Akinloye, O. A., Akamo, A. J., Ojo, D. A., Okeowo, O. T., and Omotuyi, I. O. (2019). Exploring receptor tyrosine kinases-inhibitors in Cancer treatments. *Egyptian. J. Med. Hum. Genet.* 20, 35. doi: 10.1186/s43042-019-0035-0

Min, Y. L., Bassel-Duby, R., and Olson, E. N. (2019). CRISPR correction of Duchenne muscular dystrophy. *Annu. Rev. Med.* 70, 239–255.

Mojica, F. J. M., Díez-Villaseñor, C., García-Martínez, J., and Almendros, C. (2009). Short motif sequences determine the targets of the prokaryotic CRISPR defence system. *Microbiol. (Reading).* 155, 733–740. doi: 10.1099/mic.0.023960-0

Mustafa, M. I., and Makhawi, A. M. (2021). SHERLOCK and DETECTR: CRISPR-cas systems as potential rapid diagnostic tools for emerging infectious diseases. *J. Clin. Microbiol.* 59, e00745-20. doi: 10.1128/jcm.00745-20

Nan, H., Park, C., and Maeng, S. (2020). Mucopolysaccharidoses I and II: Brief review of therapeutic options and supportive/palliative therapies. *Biomed Res. Int.* 2020, 2408402.

Nastoupil, L. J., O'Brien, S., Holmes, H. E., Dsouza, L., Hart, D., Matsuda, E., et al. (2022). P1455: First-in-human trial of CB-010, a CRISPR-edited allogeneic anti-CD19 CAR -T cell therapy with a PD-1 knock out, in patients with relapsed or refractory B cell non-Hodgkin lymphoma (ANTLER study). *Hemasphere* 6.

Neil, K., Allard, N., Roy, P., Grenier, F., Menendez, A., Burrus, V., et al. (2021). High-efficiency delivery of CRISPR-Cas9 by engineered probiotics enables precise microbiome editing. *Mol. Syst. Biol.* 17, e10335. doi: 10.15252/msb.202110335

Owaid, H. A., and Al-Ouqaili, M. T. S. (2024). Molecular and bacteriological investigations for the co-existence CRISPR/Cas system and β-lactamases of types extended-spectrum and carbapenemases in Multidrug, extensive drug and Pandrug-Resistant Klebsiella pneumoniae. *Saudi. J. Biol. Sci.* 31, 104022. doi: 10.1016/j.sjbs.2024.104022

Owaid, H. A., and Al-Ouqaili, M. T. S. (2025). Molecular characterization and genome sequencing of selected highly resistant clinical isolates of Pseudomonas aeruginosa and its association with the clustered regularly interspaced palindromic repeat/Cas system. *Heliyon* 11, e41670. doi: 10.1016/j.heliyon.2025.e41670

Pacia, D. M., Brown, B. L., Minssen, T., and Darrow, J. J. (2024). CRISPR-phage antibacterials to address the antibiotic resistance crisis: scientific, economic, and regulatory considerations. *J. Law Biosci.* 11, lsad030. doi: 10.1093/jlb/lsad030

Park, J. H., Jain, N., Chen, A., McGuirk, J. P., Diaz, M., Valamehr, B., et al. (2020). A phase I study of FT819, a first-of-kind, off-the-shelf, iPSC-derived TCR-less CD19 CAR T cell therapy for the treatment of relapsed/refractory B-cell malignancies. *Blood* 136, 15–16.

Pawluk, A., Davidson, A. R., and Maxwell, K. L. (2018). Anti-CRISPR: discovery, mechanism and function. *Nat. Rev. Microbiol.* 16, 12–17. doi: 10.1038/nrmicro.2017.120

Polcz, S., and Lewis, A. (2016). CRISPR-Cas9 and the non-germline non-controversy. *J. Law Biosci.* 3, 413–425. doi: 10.1093/jlb/lsw016

Pourcel, C., Salvignol, G., and Vergnaud, G. (2005). CRISPR elements in Yersinia pestis acquire new repeats by preferential uptake of bacteriophage DNA, and provide additional tools for evolutionary studies. *Microbiol. (Reading).* 151, 653–663. doi: 10.1099/mic.0.27437-0

Pursey, E., Sünderhauf, D., Gaze, W. H., Westra, E. R., and Van Houte, S. (2018). CRISPR-Cas antimicrobials: Challenges and future prospects. *PloS Pathog.* 14, e1006990. doi: 10.1371/journal.ppat.1006990

Rahman, S. H., Maeder, M. L., Joung, J. K., and Cathomen, T. (2011). Zinc-finger nucleases for somatic gene therapy: the next frontier. *Hum. Gene Ther.* 22, 925–933. doi: 10.1089/hum.2011.087

Raposo, V. L. (2019). The first chinese edited babies: A leap of faith in science. *JBRA. Assist. Reprod.* 23, 197–199. doi: 10.5935/1518-0557.20190042

Rasheed, J. K., Anderson, G. J., Yigit, H., Queenan, A. M., Doménech-Sánchez, A., Swenson, J. M., et al. (2000). Characterization of the extended-spectrum beta-lactamase reference strain, Klebsiella pneumoniae K6 (ATCC 700603), which produces the novel enzyme SHV-18. *Antimicrob. Agents Chemother.* 44, 2382–2388. doi: 10.1128/aac.44.9.2382-2388.2000

Rasheed, J. K., Kitchel, B., Zhu, W., Anderson, K. F., Clark, N. C., Ferraro, M. J., et al. (2013). New delhi metallo-β-lactamase-producing enterobacteriaceae, United States. *Emerg. Infect. Dis.* 19, 870–878. doi: 10.3201/eid1906.121515

Rentmeister, A. (2015). CRISPR craze conquers the RNA world: precise manipulation of DNA and RNA based on a bacterial defense system. *Angewandte. Chemie. Int. Edition.* 54, 4710–4712. doi: 10.1002/anie.201500563

Ribeiro, J. R., Schorl, C., Yano, N., Romano, N., Kim, K. K., Singh, R. K., et al. (2016). HE4 promotes collateral resistance to cisplatin and paclitaxel in ovarian cancer cells. *J. Ovarian Res.* 9, 28. doi: 10.1186/s13048-016-0240-0

Rubeis, G., and Steger, F. (2018). Risks and benefits of human germline genome editing: An ethical analysis. *Asian Bioeth. Rev.* 10, 133–141. doi: 10.1007/s41649-018-0056-x

Saber, A., Liu, B., Ebrahimi, P., and Haisma, H. J. (2020). CRISPR/Cas9 for overcoming drug resistance in solid tumors. *Daru* 28, 295–304. doi: 10.1007/s40199-019-00240-z

Sashital, D. G., Jinek, M., and Doudna, J. A. (2011). An RNA-induced conformational change required for CRISPR RNA cleavage by the endoribonuclease Cse3. *Nat. Struct. Mol. Biol.* 18, 680–687. doi: 10.1038/nsmb.2043

Sen, D., and Mukhopadhyay, P. (2024). Antimicrobial resistance (AMR) management using CRISPR-Cas based genome editing. *Gene Genome Editing.* 7, 100031. doi: 10.1016/j.ggedit.2024.100031

Shabbir, M., Hao, H., Shabbir, M. Z., Wu, Q., Sattar, A., and Yuan, Z. (2016). Bacteria vs. Bacteriophages: parallel evolution of immune arsenals. *Front. Microbiol.* 7. doi: 10.3389/fmicb.2016.01292

Shah, S. A., Erdmann, S., Mojica, F. J., and Garrett, R. A. (2013). Protospacer recognition motifs: mixed identities and functional diversity. *RNA Biol.* 10, 891–899. doi: 10.4161/rna.23764

Shirani-Bidabadi, S., Tabatabaee, A., Tavazohi, N., Hariri, A., Aref, A. R., Zarrabi, A., et al. (2023). CRISPR technology: A versatile tool to model, screen, and reverse drug resistance in cancer. *Eur. J. Cell Biol.* 102, 151299. doi: 10.1016/j.ejcb.2023.151299

Shukla, A., Jani, N., Polra, M., Kamath, A., and Patel, D. (2021). CRISPR: the multidrug resistance endgame? *Mol. Biotechnol.* 63, 676–685. doi: 10.1007/s12033-021-00340-9

Sonmez, Y. E. (2021). CRISPR-Cas: a brief overview. *Kidneys* 10, 2–3. doi: 10.22141/2307-1257.10.1.2021.227199

Stadtmauer, E. A., Fraietta, J. A., Davis, M. M., Cohen, A. D., Weber, K. L., Lancaster, E., et al. (2020). CRISPR-engineered T cells in patients with refractory cancer. *Science* 367.

Sternberg, S. H., Redding, S., Jinek, M., Greene, E. C., and Doudna, J. A. (2014). DNA interrogation by the CRISPR RNA-guided endonuclease Cas9. *Nature* 507, 62–67. doi: 10.1038/nature13011

Strzyz, P. (2020). CRISPR-cas9 wins nobel. *Nat. Rev. Mol. Cell Biol.* 21, 714. doi: 10.1038/s41580-020-00307-9

Swarts, D. C., Mosterd, C., Van Passel, M. W. J., and Brouns, S. J. J. (2012). CRISPR interference directs strand specific spacer acquisition. *PloS One* 7, e35888. doi: 10.1371/journal.pone.0035888

Tagliaferri, T. L., Guimarães, N. R., Pereira, M. D. P. M., Vilela, L. F. F., Horz, H.-P., Dos Santos, S. G., et al. (2020). Exploring the potential of CRISPR-cas9 under challenging conditions: facing high-copy plasmids and counteracting beta-lactam resistance in clinical strains of enterobacteriaceae. *Front. Microbiol.* 11. doi: 10.3389/fmicb.2020.00578

Tao, R., Han, X., Bai, X., Yu, J., Ma, Y., Chen, W., et al. (2024). Revolutionizing cancer treatment: enhancing CAR-T cell therapy with CRISPR/Cas9 gene editing technology. *Front. Immunol.* 15. doi: 10.3389/fimmu.2024.1354825

Tao, P., Wu, X., and Rao, V. (2018). Unexpected evolutionary benefit to phages imparted by bacterial CRISPR-Cas9. *Sci. Adv.* 4, eaar4134. doi: 10.1126/sciadv.aar4134

Tsui, T. K., and Li, H. (2015). Structure principles of CRISPR-cas surveillance and effector complexes. *Annu. Rev. Biophys.* 44, 229–255. doi: 10.1146/annurev-biophys-060414-033939

Tyson, G. W., and Banfield, J. F. (2008). Rapidly evolving CRISPRs implicated in acquired resistance of microorganisms to viruses. *Environ. Microbiol.* 10, 200–207. doi: 10.1111/j.1462-2920.2007.01444.x

Uddin, T. M., Chakraborty, A. J., Khusro, A., Zidan, B. R. M., Mitra, S., Emran, T. B., et al. (2021). Antibiotic resistance in microbes: History, mechanisms, therapeutic strategies and future prospects. *J. Infect. Public Health* 14, 1750–1766. doi: 10.1016/j.jiph.2021.10.020

Uribe, R. V., Rathmer, C., Jahn, L. J., Ellabaan, M. M. H., Li, S. S., and Sommer, M. O. A. (2021). Bacterial resistance to CRISPR-Cas antimicrobials. *Sci. Rep.* 11, 17267. doi: 10.1038/s41598-021-96735-4

Uyhazi, K. E., and Bennett, J. (2021). A CRISPR view of the 2020 nobel prize in chemistry. *J. Clin. Invest.* 131, e145214. doi: 10.1172/jci145214

Van Kampen, S. J., and Van Rooij, E. (2019). CRISPR craze to transform cardiac biology. *Trends Mol. Med.* 25, 791–802. doi: 10.1016/j.molmed.2019.06.008

Vertex. (2024). Vertex announces positive results from ongoing Phase 1/2 study of VX-880 for the treatment of type 1 diabetes presented at the American Diabetes Association 84th Scientific Sessions. *Vertex Pharmaceuticals*. Available online at: https://investors.vrtx.com/news-releases/news-release-details/vertex-announces-positive-results-ongoing-phase-12-study-vx-880.

Villiger, L., Joung, J., Koblan, L., Weissman, J., Abudayyeh, O. O., and Gootenberg, J. S. (2024). CRISPR technologies for genome, epigenome and transcriptome editing. *Nat. Rev. Mol. Cell Biol.* 25, 464–487. doi: 10.1038/s41580-023-00697-6

Vorontsova, D., Datsenko, K. A., Medvedeva, S., Bondy-Denomy, J., Savitskaya, E. E., Pougach, K., et al. (2015). Foreign DNA acquisition by the I-F CRISPR-Cas system requires all components of the interference machinery. *Nucleic Acids Res.* 43, 10848–10860. doi: 10.1093/nar/gkv1261

Wan, X., Li, Q., Olsen, R. H., Meng, H., Zhang, Z., Wang, J., et al. (2022). Engineering a CRISPR interference system targeting AcrAB-TolC efflux pump to prevent multidrug resistance development in Escherichia coli. *J. Antimicrob. Chemother.* 77, 2158–2166. doi: 10.1093/jac/dkac166

Wang, S.-W., Gao, C., Zheng, Y.-M., Yi, L., Lu, J.-C., Huang, X.-Y., et al. (2022). Current applications and future perspective of CRISPR/Cas9 gene editing in cancer. *Mol. Cancer* 21, 57. doi: 10.1186/s12943-022-01518-8

Wang, R., Shu, X., Zhao, H., Xue, Q., Liu, C., Wu, A., et al. (2023). Associate toxin-antitoxin with CRISPR-Cas to kill multidrug-resistant pathogens. *Nat. Commun.* 14, 2078. doi: 10.1038/s41467-023-37789-y

Wang, Y., Wang, S., Chen, W., Song, L., Zhang, Y., Shen, Z., et al. (2018). CRISPR-cas9 and CRISPR-assisted cytidine deaminase enable precise and efficient genome editing in klebsiella pneumoniae. *Appl. Environ. Microbiol.* 84, e01834–e01818. doi: 10.1128/AEM.01834-18

Watson, B. N. J., Pursey, E., Gandon, S., and Westra, E. R. (2023). Transient eco-evolutionary dynamics early in a phage epidemic have strong and lasting impact on the long-term evolution of bacterial defences. *PloS Biol.* 21, e3002122. doi: 10.1371/journal.pbio.3002122

Westermann, L., Neubauer, B., and Köttgen, M. (2021). Nobel Prize 2020 in Chemistry honors CRISPR: a tool for rewriting the code of life. *Pflügers. Archiv. - Eur. J. Physiol.* 473, 1–2. doi: 10.1007/s00424-020-02497-9

Westra, E. R., Dowling, A. J., Broniewski, J. M., and Van Houte, S. (2016). Evolution and ecology of CRISPR. *Annu. Rev. Ecol. Evol. Syst.* 47, 307–331. doi: 10.1146/annurev-ecolsys-121415-032428

Wold, W. S., and Toth, K. (2013). Adenovirus vectors for gene therapy, vaccination and cancer gene therapy. *Curr. Gene Ther.* 13, 421–433. doi: 10.2174/15665232136661311250950 46

Wright, A. V., Nuñez, J. K., and Doudna, J. A. (2016). Biology and applications of CRISPR systems: harnessing nature's toolbox for genome engineering. *Cell* 164, 29–44. doi: 10.1016/j.cell.2015.12.035

Xu, W., Zhang, S., Qin, H., and Yao, K. (2024b). From bench to bedside: cutting-edge applications of base editing and prime editing in precision medicine. *J. Trans. Med.* 22, 1133. doi: 10.1186/s12967-024-05957-3

Xu, C., Zhang, X., Yang, W., Gao, S., Zhao, N., Li, P., et al. (2024a). Effective prevention of atherosclerosis by non-viral delivery of CRISPR/Cas9. *Nano. Today* 54, 102097. doi: 10.1016/j.nantod.2023.102097

Xu, L., Wang, J., Liu, Y., Xie, L., Su, B., Mou, D., et al. (2019). CRISPR-edited stem cells in a patient with HIV and acute lymphocytic leukemia. *N. Engl. J. Med.* 381, 1240–1247.

Yang, Y., Xu, J., Ge, S., and Lai, L. (2021). CRISPR/cas: advances, limitations, and applications for precision cancer research. *Front. Med. (Lausanne)* 8. doi: 10.3389/fmed.2021.649896

Yosef, I., Goren, M. G., and Qimron, U. (2012). Proteins and DNA elements essential for the CRISPR adaptation process in Escherichia coli. *Nucleic Acids Res.* 40, 5569–5576. doi: 10.1093/nar/gks216

Zeballos, C. M., and Gaj, T. (2021). Next-generation CRISPR technologies and their applications in gene and cell therapy. *Trends Biotechnol.* 39, 692–705. doi: 10.1016/j.tibtech.2020.10.010

Zhang, L., Li, Y., Wang, Q., Chen, Z., Li, X., Wu, Z., et al. (2020). The PI3K subunits, P110α and P110β are potential targets for overcoming P-gp and BCRP-mediated MDR in cancer. *Mol. Cancer* 19, 10. doi: 10.1186/s12943-019-1112-1

Zhang, S., Shen, J., Li, D., and Cheng, Y. (2021c). Strategies in the delivery of Cas9 ribonucleoprotein for CRISPR/Cas9 genome editing. *Theranostics* 11, 614–648. doi: 10.7150/thno.47007

Zhang, C., Shen, L., Zhu, Y., Xu, R., Deng, Z., Liu, X., et al. (2021a). KDM6A promotes imatinib resistance through YY1-mediated transcriptional upregulation of TRKA independently of its demethylase activity in chronic myelogenous leukemia. *Theranostics* 11, 2691–2705. doi: 10.7150/thno.50571

Zhang, F., Wen, Y., and Guo, X. (2014). CRISPR/Cas9 for genome editing: progress, implications and challenges. *Hum. Mol. Genet.* 23, R40–R46. doi: 10.1093/hmg/ddu125

Zhang, R., Xu, W., Shao, S., and Wang, Q. (2021b). Gene silencing through CRISPR interference in bacteria: current advances and future prospects. *Front. Microbiol.* 12. doi: 10.3389/fmicb.2021.635227

Zhao, D., Yuan, S., Xiong, B., Sun, H., Ye, L., Li, J., et al. (2016). Development of a fast and easy method for Escherichia coli genome editing with CRISPR/Cas9. *Microbial. Cell Factories.* 15, 205. doi: 10.1186/s12934-016-0605-5

Zhou, Q., Zhan, H., Liao, X., Fang, L., Liu, Y., Xie, H., et al. (2019). A revolutionary tool: CRISPR technology plays an important role in construction of intelligentized gene circuits. *Cell Prolif.* 52, e12552. doi: 10.1111/cpr.12552

Zhu, Y. (2022). Advances in CRISPR/cas9. *BioMed. Res. Int.* 2022, 9978571. doi: 10.1155/2022/9978571

frontiers | Frontiers in Cellular and Infection Microbiology

TYPE Review
PUBLISHED 30 June 2025
DOI 10.3389/fcimb.2025.1595076

OPEN ACCESS

EDITED BY
Sam Ebenezer,
Sathyabama Institute of Science and Technology, India

REVIEWED BY
Vijay Srinivasan,
Texas A and M University, United States
Afsal Kolloli,
Rutgers University, United States

*CORRESPONDENCE
Damien Portevin
damien.portevin@swisstph.ch

RECEIVED 17 March 2025
ACCEPTED 04 June 2025
PUBLISHED 30 June 2025

CITATION
Schmidiger S and Portevin D (2025) Experimental dissection of tuberculosis protective immunity: a human perspective. *Front. Cell. Infect. Microbiol.* 15:1595076. doi: 10.3389/fcimb.2025.1595076

Experimental dissection of tuberculosis protective immunity: a human perspective

Sarah Schmidiger[1,2] and Damien Portevin[1,2]*

[1]Department of Medical Parasitology & Infection Biology, Swiss Tropical and Public Health Institute, Allschwil, Switzerland, [2]Faculty of Science, University of Basel, Basel, Switzerland

Mycobacterium tuberculosis (*Mtb*), the causative agent of tuberculosis (TB), has plagued humankind for millennia. Claiming 1.25 million lives in 2023, TB remains the worldwide leading cause of death from a single-infectious agent. Improved vaccines, diagnostics and treatment regimens for drug-susceptible and drug-resistant cases are paramount to attain the goals of the WHO's End TB Strategy. Our knowledge gap in protective immunity in TB impedes the development of such new vaccines and host-directed interventions. *Mtb* is a pathogen highly adapted to humans and primarily infects the lungs. Access to relevant specimens is invasive, preventing ample human TB studies, which therefore mostly rely on peripheral blood specimens and biopsies. Thus, there is a need for relevant surrogates. In recent years, *in vivo*, *in vitro*, and *in silico* systems have arisen to approach and model different aspects of TB pathogenesis. Moving away from cell-line infections and classical animal models, TB research has advanced to genetically diverse mice, 3D organoid cultures and computational modelling. We will review current TB models and discuss their applicability to decipher protective human immunity, understand disease progression, transmission, as well as evaluate vaccine candidates and unravel host-directed therapeutic approaches.

KEYWORDS

tuberculosis, immunology & infectious diseases, human, model, systems immunology

Introduction

Tuberculosis (TB) elimination remains an ambitious target. Despite extensive research, this ancient disease keeps claiming 143 lives every hour, making *Mycobacterium tuberculosis* (*Mtb*) the leading single-infectious killer (WHO, 2024). The WHO has outlined a strategy to end the global TB epidemic by 2035. This includes reducing mortality by 95% and incidence by 90% compared to 2015. To reach those goals, we urgently need new vaccines, improved drug regimens and innovative, host-directed interventions. Owing to ethical restrictions as well as limited access to *in situ* samples, human TB studies are scarce. Thus, there is a need for appropriate surrogates that allow us to decipher protective traits against this pathogen, which after millennia of co-evolution is highly adapted to humans. Intriguingly, while a substantial proportion of the human population is thought to be latently infected (estimates ranging between 25 and <10%

(Houben and Dodd, 2016; Schwalb et al., 2024)), only <5% of encounters with *Mtb* result in active TB disease (Behr et al., 2018). Progression to active disease is dependent on the strain, the age and the intensity of exposure (Sloot et al., 2014; De Jong et al., 2008). In contrast, most current infection systems fail to capture the 90-95% of protective outcomes. Hence, several susceptibility traits to TB, such as impaired T cell function or IL-12/IFN-γ and TNF-α signaling, have successfully been dissected by combining research in animals, humans and *in vitro* systems with epidemiological data (Scriba et al., 2017; Bustamante et al., 2014; Wallis, 2007). We have further come to realize that environmental factors (e.g. nutrition, economic status) may be as influential as genetic and immunological ones (Bhargava et al., 2023). Historically, studying resistance to disease over susceptibility has greatly contributed to improving public health by delivering the smallpox vaccine (developed after observing cowpox-exposed milkmaids resisted the disease) and CCR5-inhibitors for HIV treatment (after realizing that individuals carrying a CCR5 variant are HIV-resistant). A similar approach could be useful for TB too, for our understanding of TB protective traits is very limited. With ongoing efforts to recruit and characterize natural or vaccine-induced "resister" cohorts, research into TB resistance is gaining momentum. We here review recent *in vivo*, *in vitro* and *in silico* approaches that may capture and dissect protective traits in TB, which in turn could be leveraged for vaccine and host-directed therapy (HDT) drug design. Particularly, we emphasize the potential of human-based *in vitro* approaches, combined with advanced technologies and computational modeling, as promising tools to characterize protective immune mechanisms and to serve as clinical platforms for vaccine and drug development.

In vivo studies

In vivo studies in animals

The first experimental infections of guinea pigs with *Mtb* date back to 1882, when Robert Koch identified *Mtb* as the causative agent of TB. Since, animal models ranging from amoeba and zebra fish, over rodents to cattle and non-human primates have been invaluable to increase our understanding of TB pathogenesis. Animal models for TB have been extensively reviewed elsewhere (Ernst, 2012; Dube et al., 2020; Singh and Gupta, 2018; Williams and Orme, 2016; Bucsan et al., 2019) and more specifically in light of vaccine (Gong et al., 2020) and chemotherapy (Yang et al., 2021) development. Here, we will emphasize limitations and advantages of selected animal models to study protective immunity in human TB and discuss ongoing efforts in overcoming their caveats.

Mtb is one of several TB-causing pathogens, collectively known as the *Mycobacterium tuberculosis* complex (MTBC). The MTBC encompasses 10 lineages infecting humans, with lineages 1 to 4 accounting for 99% of TB cases, and nine animal infecting ones (Goig et al., 2025). Zoonotic TB can occur in humans, e.g. infection with the bovine pathogen *Mycobacterium bovis* following ingestions of unpasteurized milk (Olea-Popelka et al., 2017), which adds to the global TB burden in areas of human contact with live-stock. Rare instances of TB reactivation from latent *M. bovis* infection have been reported (Capoferri et al., 2024). While TB also exists in animals, MTBC strains that infect humans are highly restricted to their host and failed to induce lung lesions in cattle (Villarreal-Ramos et al., 2018). *Mtb* has plagued and coevolved with humans for thousands of years (Gagneux, 2012). In that regard, experiments conducted in animals, aiming to decipher TB in humans, can legitimately be criticized to "pervade the field" (Scriba et al., 2017). Due to the global spread of institutional facilities and availability of an arsenal of genetic and immunological tools, mice constitute the most commonly used model in TB *in vivo* studies (Figure 1). This is yet very concerning, as mice are no natural host for *Mtb* and are not naturally infected by any MTBC member. Nonetheless and as elegantly reviewed elsewhere (Ernst, 2012), animals can serve as surrogates of specific stages in the "immunological life cycle" of tuberculosis. Guinea pigs and mice model the delayed onset of adaptive immunity, rabbits capture necrosis and lung cavitation, NHPs and mice reproduce the impact of CD4 T cell defects or NHPs and cattle allow to study latency and reactivation. Mouse breeds used in TB research include susceptible (C3HeB/FeJ, DBA/2, 129/Sv) and resistant (BALB/c and C57BL/6) mice (Soldevilla et al., 2022). However, a common denominator across mouse models is that they cannot eliminate the infection and do not reflect the large majority (>95%) of human infection outcomes. Efforts to develop mouse models that may better reflect human TB pathogenesis are being pursued (Yang et al., 2021). In 2021, Kevin Urdahl's group reported an ultra-low dose (ULD) aerosol challenge model (Plumlee et al., 2021). Unlike other infection models, ULD-infected mice responded heterogeneously to infection and remarkably showed singular, organized granulomas. Furthermore, the authors were able to extract blood transcriptional signatures that correlated with disease severity in NHPs and predict TB risk in humans. Aside from optimized infection doses, advances are being made to account for genetic diversity. Collaborative cross (CC) or diversity outbred (DO) mice are deployed to address how the genetic background may influence immune responses and vaccine efficacy (Saul et al., 2019). The use of humanized mice, in which human immune cells are engrafted into immunodeficient mice, is also emerging and their applications recently reviewed (Mcdonald et al., 2024). Humanized mice have been utilized in TB research as promising tools in the assessment of drugs (Arrey et al., 2019), bacteriophage therapy (Yang et al., 2024), innovative vaccines strategies (Afkhami et al., 2023), and to dissect HIV-*Mtb* co-infection (Bohórquez et al., 2024; Calderon et al., 2013). Together, these advanced murine models hold promise in overcoming some of the caveats of standard mouse research for TB, e.g. more diverse infection outcomes, while still benefitting from genetic manipulation avenues. ULD, CC and DO mice may provide valuable data for vaccine development (Wang et al., 2024) and new insights into protective or detrimental immune traits. However, their use – together making up a mere 0.25% of publications - is still in its infancy (Figure 1).

Despite its importance for human interventions, the transmission feature of human TB disease is understudied (Behr

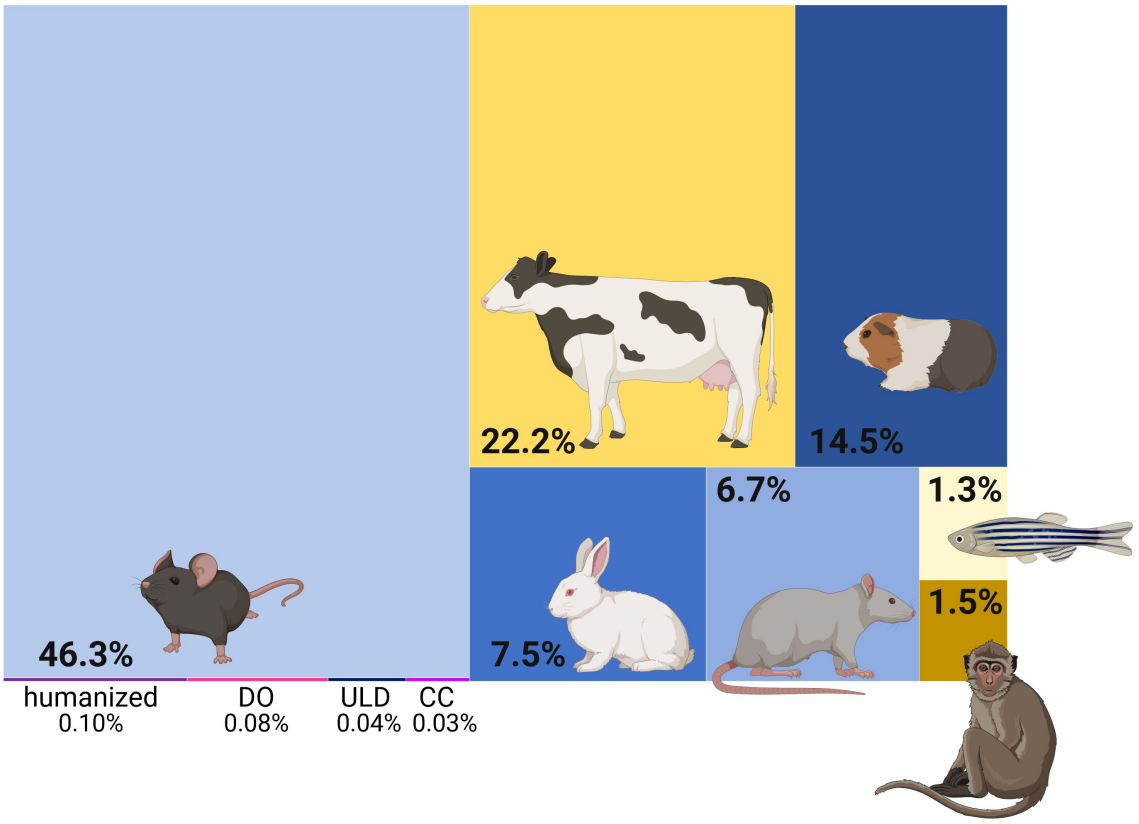

FIGURE 1
Tuberculosis *in vivo* studies in animals. Treemap representing the proportion of publications using the respective animal models. Yellow shades indicate challenge models of natural host-pathogen pairs. DO diversity outbred; ULD ultra-low dose; CC collaborative cross. Generated with biorender.com; Based on a PubMed search on 21.11.24 using the queries: "tuberculosis" AND ("mice" OR "mouse") | ("mice" OR "mouse") AND ("ULD" OR "ultra-low dose") | ("mice" OR "mouse") AND ("collaborative cross") | ("mice" OR "mouse") AND ("diversity outbred" OR "DO") | ("mice" OR "mouse") AND ("humanized mice") | "cattle" | ("guinea pigs" OR "guinea pig") | ("rabbits" OR "rabbit") | ("rats" OR "rat") | ("zebrafish" OR "zebra fish") | ("NHPs" OR "NHP" OR "non-human primate*" OR "nonhuman primate*").

et al., 2020). Nevertheless, guinea pigs are particularly susceptible to *Mtb* infection and like humans; they can transmit the disease via aerosols (Lurie, 1930). An intriguing study revealed that a glycolipid component of the *Mtb* cell wall (sulfolipid-1) is able to induce cough in guinea pigs (Ruhl et al., 2020). Rabbits constitute important models in TB research, which has been reviewed elsewhere (Bucsan et al., 2019). Noteworthy, the rabbit was the first animal model able to mimic HIV-immune reconstitution inflammatory syndrome (IRIS) using corticosteroids (Manabe et al., 2008). Besides, rabbit infection with *Mtb* notably allowed studying the dynamics of cavitary disease and found a significant degree of molecular and pathological correlates with humans (Kübler et al., 2015). Studies in zebra fish (infected with *M. marinum*) and cattle (infected with *M. bovis*) provide an interesting opportunity to study TB in the context of natural host-pathogen pairs; the former being much easier to use and the latter genetically closer to humans. Interestingly, the zebra fish model has provided mechanistic insights into human bone TB. In an elegant study ignited by a TB outbreak with atypical rates of disseminated and skeletal TB, Saelens et al. linked occurrence of bone TB to increased macrophage motility, dependent on the presence of *esxM* (Saelens et al., 2022). This gene is present in its full length in ancestral lineages, while modern lineages carry a truncated form. This discrepancy, in conjunction with host factors (Rachwal et al., 2024), supports the association of particular ancient lineages with extra-pulmonary TB (EPTB) (Click et al., 2012; Du et al., 2023). Models of natural host-pathogen pairs also allow assessing the conservation of protective or susceptibility traits across different species. This is particularly relevant as zoonotic TB associated to *M. bovis* infections can cause human deaths (Capoferri et al., 2024) and *M. marinum* can cause skin infections in humans (Gonçalves et al., 2022). Non-human primates (comprising cynomolgus monkeys, rhesus monkeys and marmosets (Yang et al., 2021)) display TB pathology and disease spectrum closely resembling those of humans (Scanga and Flynn, 2014), likely rendering them the most relevant model of human TB. Cynomolgus macaques (Capuano et al., 2003) are particularly suitable to study latent infection (O'Garra et al., 2013). However, financial, logistical and ethical concerns imped the wide adoption of these models. Nonetheless, NHPs have proven highly valuable in highlighting human-like heterogeneity of disease presentation across animals and across individual granulomas within a single animal (Lin et al., 2014). Recently, NHP studies yielded further insights into correlates of protection associated with the presence of

a NK cell subset in the lungs of latently infected macaques (Esaulova et al., 2021). Comparison of low and high-burden granulomas in cynomolgus macaques also suggested correlates of bacterial clearance associated to the accumulation of T_H17 and cytotoxic T cells (Gideon et al., 2022). Interestingly, a parallel study also identified cytotoxic signatures to be associated with protection (Winchell et al., 2023). Hansen et al. made a breakthrough by demonstrating unprecedented sterilizing immunity following vaccination with a cytomegalovirus-vectored TB vaccine (RhCMV/TB) (Hansen et al., 2018). Later, similar successes were achieved using an intra-venous (IV) BCG vaccination route (Darrah et al., 2020; Larson et al., 2023). IV BCG vaccination induced protective humoral responses (IgM titers, complement) and NK cell activation in a dose-dependent manner (Irvine et al., 2024). In a separate study, the recruitment and priming of alveolar macrophages and polyfunctional T cells characterized the lung response of protected animals (Peters et al., 2025). Another study demonstrated the necessity of CD4 T and innate CD8 lymphocytes, but not adaptive CD8 lymphocytes, for IV BCG-mediated protection (Simonson et al., 2025). Altogether, recent data collected through the IV BCG approach in NHPs suggest that a plethora of immune players is likely required to synergize for protection.

Overall, animal models have proven valuable to dissect different aspects of TB pathogenesis (Soldevilla et al., 2022). However, controversy remains in the extent of translatability of these findings across different models and, most importantly, to humans (Warren et al., 2015). One of few studies directly comparing immune responses to *in vivo Mtb* infection across DO mice, NHPs and humans found a great degree of overlap of genes differentially expressed during TB disease (Ahmed et al., 2020). Yet, animal models are raising controversial conclusions. For example, a study in mice found a therapeutic potential of MAIT T cells, where their expansion induced by an antigen increased bacterial control (Sakai et al., 2021a); however, in NHPs, the same treatment induced exhaustion of MAIT T cells (Sakai et al., 2021b). *In vitro* models (detailed in the sections below), have highlighted further similarities and discrepancies. Corroborating Ahmed et al., a recent preprint found human and murine alveolar macrophage responses to *Mtb* infection to be majorly conserved; however, they also identified several pathways (e.g. cholesterol, IFN genes) that differ between the two species (Dill-Mcfarland et al., 2025). Other studies have highlighted that rapamycin-induced autophagy restricts *Mtb* replication in murine (Gutierrez et al., 2004), while it would promote it in human macrophages (Andersson et al., 2016). This lack of total translatability is inevitable, given the inherent, irrevocable differences between animals and humans, and the respective TB pathogeneses. While advanced animal models retain relevance as *in vivo* surrogates and will remain an essential tool in pre-clinical safety assessment, scientific efforts are being made to focus translational TB research on human-based approaches. In that perspective, we will now review available approaches aiming at identifying protective traits in humans or human-based systems.

Human *in vivo* studies

Studying TB in humans is challenged by legitimate ethical considerations and the particularly invasive access to the primary infection sites (lung, lymph nodes, bones or brain), making diseased and non-diseased specimens globally scarce. Consequently, most *in situ* specimens are derived from biopsies or lung/lymph node resections that mostly reflect late stages of failed immune responses and do not allow studying the early onset of disease nor protective traits. Nonetheless, such specimens have provided valuable insights into the spatial organization (Marakalala et al., 2016) of late-stage human TB granulomas, as well as unexpected immunoregulatory features (McCaffrey et al., 2022).

To understand protective immunity, it appears paramount to study infection and ensuing pathogenesis from its earliest onset. Such investigations have become possible through controlled human infection model (CHIM) studies (Pollard et al., 2012) that have already yielded exciting results in vaccine efficacy and drug assessment for the Malaria field (Sauerwein et al., 2011). In TB, the first CHIM trial was conducted over a decade ago, first with intra-dermal (Minassian et al., 2012) and later aerosol-administration of a live-attenuated BCG vaccine strain (Satti et al., 2024). Currently, conditionally replicating *Mtb* strains are being explored as a BCG replacement (Wang et al., 2024; Balasingam et al., 2024). Specifically, a triple-kill-switch *Mtb* strain may present a safe and more physiological candidate for CHIM studies (Wang et al., 2025), holding promise to propel TB vaccine development. While mainly used to assess vaccine efficacy, insights into protective immunity are expected to arise from samples collected alongside CHIM studies. Similarly, a growing body of investigations benefit from existing vaccination cohorts to seek biomarkers of (i) correlates of protection, by identifying vaccine-induced markers that are respectively absent and present in individuals that later progressed or not to active disease; (ii) correlates of risk, with markers whose presence/absence are respectively associated with a low or a high risk of disease, reviewed in (Scriba et al., 2017; Walzl et al., 2011). Yet, vaccination cohorts do not allow identification of naturally occurring protective traits that do not necessarily overlap with vaccine-induced correlates of protection. In that context, the identification of "TB resisters" sparked new hope in the identification of protective traits in human TB. Resisters are defined as individuals repeatedly exposed to *Mtb* that do not harbor detectable immune-reactivity to mycobacterial antigens by TST and/or IGRA testing (Simmons et al., 2018). Study of resister phenotypes is hampered by limitations in the classification of resisters, linked to the lack of tools to assess and estimate the degree of exposure, which is under the influence of the index case's TB disease status, including bacillary load, cough and strain diversity affecting transmission rate (Simmons et al., 2018). Yet, TB resistance in the absence of adaptive immune memory supports an exceptional potency of innate myeloid responses, which have been shown to be epigenetically regulated in a cohort of health care workers (Zhang et al., 2021). Evidence from historical and contemporary studies suggest that the frequency of resisters is

below 10%, although high inter-study variability is observed (Simmons et al., 2018). Recent data suggest that this figure may be over-estimated due to IFN-γ independent and regulatory responses, such as those characterizing the T cell response of household contacts in Kampala (Sun et al., 2024). Further research is necessary to untangle the importance of the various mechanisms supporting natural resistance to *Mtb* infection; and potentially exploit them in host-directed therapeutic approaches. Such approaches may encompass training innate immune responses, and/or boosting IFN-γ-independent cellular mechanisms mediated by lipid-specific MAIT or γδ T cells at the instar of peptide-specific T cells measured in IGRAs. Furthermore, B cells and antibodies might play an additive role (Simmons et al., 2018). Investigation of these resister phenotypes constitutes exquisite translational research for which data from human-based *in vitro* systems may nicely complement animal challenge models. Specimens of resister cohorts may indeed be subjected to an arsenal of *in vitro* tools (described in the section below) to extract features and demonstrate mechanisms of TB resistance.

In summary, human *in vivo* studies encompassing vaccine and drug trials, resister cohorts and controlled human infections are generating a multitude of specimens that can now be used in human-based *in vitro* approaches to further dissect protective traits (Figure 2). This is of particular relevance, since human trials are lengthy and costly. It is thus paramount to make informed choices on bio-banking relevant specimens to pursue the most promising leads. We will now seek to outline the newest advances in that respect.

Human *ex vivo* and *in vitro* studies

This section highlights human-derived TB *in vitro* studies, summarized in Table 1. *In vitro* infections of macrophages to study TB date back to the 1940s (Lurie, 1942). Since then, technological advances surged from alveolar and foamy macrophages, over bilayer systems and 3D granuloma models all the way to lung tissues and stem cell-derived organoids, even extending to entire organs (Figure 2). *In vitro* approaches based on human specimens hold great promise to assess comorbidities and incorporate the complex dimension of human genetic diversity. Some are scalable and might find applications for drug screening.

Single-cell systems

Mtb can survive and thrive in the very cells deployed for its clearance. Consequently, macrophages have long been the center of attention in TB research. Numerous infection systems exist to study the host-pathogen interaction between *Mtb* and macrophage host cells.

Cell lines

The human monocytic leukemia THP-1 cell line can be differentiated into macrophages and has been widely used in immunological studies of monocyte and macrophage functions (Shah et al., 2022). THP-1s are easy to culture and economic to maintain. Assays are readily scalable and allow for large-scale drug screening on intracellular bacteria (Rankine-Wilson et al., 2022). Yet, THP-1s do not account for human genetic diversity and as a cancerous cell-line have limited physiological relevance.

Primary cells

Cellular TB immunology research is very often conducted on human macrophages derived from blood monocytes (MDM), whose polarization and ultimate phenotypes upon *Mtb* infection vary with specific culture conditions (Vogt and Nathan, 2011; Murray, 2017). *Mtb* infection of MDMs has elucidated distinct immune escape and protection mechanisms, such as inhibition of phagosome-lysosome fusion (Armstrong and Hart, 1971), phagosome escape (Van Der Wel et al., 2007) and autophagy (Gutierrez et al., 2004). However, since *Mtb* transmits via aerosols, the first cells to be infected *in vivo*, are alveolar macrophages (AMs), which have distinct characteristics and responses to *Mtb* infection than MDMs (Campo et al., 2024; Tomlinson et al., 2012; Papp et al., 2018). AMs can be isolated from bronchioalveolar lavage (BAL) specimens (Dodd et al., 2016); albeit, in limited numbers. Hence, differentiation of blood monocytes into alveolar-like macrophages facilitates ample study of human alveolar macrophage functions (Pahari et al., 2023, 2024). Another macrophage phenotype commonly observed in TB granulomas consists of foamy macrophages (FMs), which result through lipid droplets accumulation. FMs provide a niche for *Mtb* dormancy and persistence and can be differentiated from monocytes in response to mycolic acids (Peyron et al., 2008) or hypoxia (Daniel et al., 2011). Their study has provided insights into the interconnected macrophage and *Mtb* lipid metabolism associated with *Mtb* dormancy and TB reactivation (Daniel et al., 2011; Santucci et al., 2016).

Stem cells

The discovery of inducible-pluripotent stem cells (iPSC) continues to revolutionize medical research (Shi et al., 2017; Cerneckis et al., 2024). iPSCs are expandable, genetically editable and can be differentiated into most organ-specific cell types, all while retaining the genetic background of the original donor (Shi et al., 2017). Gutierrez' lab used CRISPR-Cas9 edited iPSC-derived macrophages to identify a role for *ATG14* (a gene involved in autophagy) as a regulator of phagosome-lysosome fusion (Aylan et al., 2023). This study demonstrates the utility of iPSCs to study *Mtb*-macrophage interaction at single-gene level, which was previously not possible in primary human cells. In combination with *Mtb* reporter strains (detailed below), iPSC-derived macrophages allow for high-throughput assessment of such host-pathogen interactions, as well as assessment of drug penetration, toxicity and efficiency. Furthermore, iPSC can be derived from patients, opening avenues for personalized medicine and cell therapy (Shi et al., 2017; Cerneckis et al., 2024). Finally, iPSC (and other stem cells) make the generation of (patient-specific) organoids possible. The implications of organoids in disease research are discussed below.

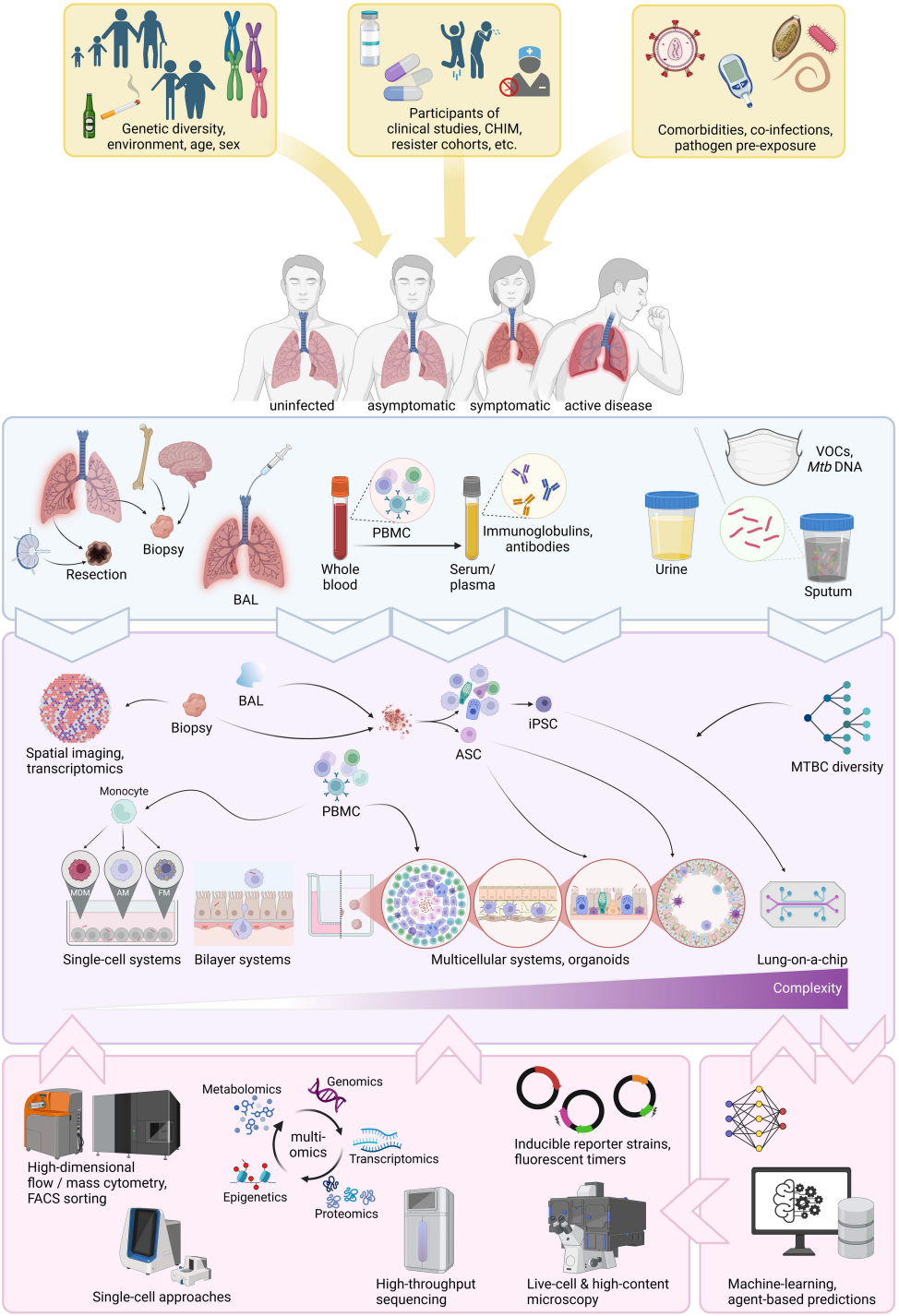

FIGURE 2
Overview of current human-based approaches to decipher protective immunity. Sources of human diversity, co-factors, co-morbidities, co-infections and disease spectrum (yellow boxes and arrows). Sources of human specimens (light blue box). Human specimens obtainable from those sources and *in vitro* approaches human specimens can be used for (purple box). Cutting-edge technologies and computational approaches that can be applied to *in vitro* systems (pink boxes). CHIM, controlled human infection model; BAL, broncho-alveolar lavage fluid; PBMC, peripheral blood mononuclear cell; VOCs, volatile organic compounds; ASC, adult stem cell; iPCS, inducible pluripotent stem cell; MDM, monocyte-derived macrophage; AM, alveolar macrophages; FM, foamy macrophage; FACS, fluorescence-activated cell sorting. Generated with biorender.com.

TABLE 1 Overview of human *in vitro* TB infection systems.

Model (ascending complexity)	Technical difficulty	Cell source	Can be donor-specific	Applications*	Reference(s)
THP-1	–	Cell line	NO	H-P interaction; drug-screening (HTS)	Shah et al., 2022
MDM	+	PBMC	YES	H-P interaction; drug-screening (HTS)	Vogt and Nathan, 2011
AM	++	PBMC	YES	H-P interaction; innate alveolar response	Pahari et al., 2024
FM	++	PBMC	YES	H-P interaction; *Mtb* persistence	Daniel et al., 2011; *reviewed by* Santucci et al., 2016
iPSC	++	PBMC, BAL	YES	H-P interaction; role of specific genes; drug-screening (HTS)	Aylan et al., 2023
Alveolar barrier	++	Cell line, PBMC	(YES)	Innate alveolar responses	Birkness et al., 1999; Bermudez et al., 2002
2D granuloma models	+	PBMC	YES	Innate and adaptive responses; drug-screening (HTS); HDT	Puissegur et al., 2004; Guirado et al., 2015
3D granuloma models	++(+)	PBMC	YES	Innate and adaptive responses; *Mtb* resuscitation; HDT	Kapoor et al., 2013; Tezera et al., 2017; Arbués et al., 2020b; *reviewed by* Elkington et al., 2019
Spheroid granulomas	+++	BAL, PBMC	YES	Innate and adaptive responses; HDT	Kotze et al., 2021
Miniaturized TB spheroids	+++	THP-1/PBMC, cell line fibroblasts	YES	Innate and adaptive responses; HDT	Mukundan et al., 2021a
ALI-PBEC	++++	Human lung tissue	YES	Innate alveolar responses; HDT	Barclay et al., 2023
Experimental human lung tissue	++++	Cell line fibroblasts, epithelial cells, PBMC	(YES)	Innate alveolar responses; HIV co-infection; drug-screening; HDT	Hoang et al., 2012 *model*; Parasa et al., 2014 *Mtb application*
Human bronchial airway organoid model	+++++	Human lung tissue (ASC)	YES	Innate alveolar responses, HDT	Iakobachvili et al., 2022
Human lung organoid	+++++	Human pluripotent stem cells (H9 cell line)	(YES)*	Innate alveolar responses; drug-screening; HDT	Kim et al., 2024
Lung-on-a-chip	★★★★★	Primary murine lung epithelial and endothelial cells, BM	(YES)*	Innate alveolar responses; drug-screening; HDT	Huh et al., 2010 *model*; Thacker et al., 2020 *Mtb application*

*can be combined with MTBC diversity.
ALI-PBEC, air-liquid interface model of human primary bronchial epithelial cells; ASC, adult stem cells; HTS, high-throughput screening; HDT, host-directed therapy; PBMC, peripheral blood mononuclear cells; H-P, host-pathogen. (YES) partially, because cell lines involved; (YES)* theoretically feasible but not yet done for *Mtb*.
Symbols represent technical difficulty from very easy (-) to highly demanding (+++++) and extraordinarily demanding (stars).

Dual-culture systems

Modeling the first cellular interaction with *Mtb* in the alveolar space seems of particular relevance to elucidate how an infection can be favored or cleared prior to the onset of an adaptive immune response. A system modelling the alveolar barrier was first developed in 1999 (Birkness et al., 1999). Human lung epithelial type II pneumocytes were cultured with endothelial cells in a two-chamber transwell system. The addition of macrophages allowed the characterization of multiple scenarios of *Mtb* translocation across the cellular bilayer (Bermudez et al., 2002). Interestingly, a similar model was transposed for *M. bovis* infections (Lee et al., 2020; Lee and Chambers, 2019). More advanced systems modeling the alveolar space are discussed in the 'complex models' section below. In addition, T cell/macrophage dual-culture systems were notably used to highlight the poor recognition of M2-like infected MDMs by *Mtb*-specific autologous T cells (Gail et al., 2023) or the antimicrobial activity of granulysin delivered upon degranulation of γδ T cell clones onto *Mtb*-infected macrophages (Stenger et al., 1998).

Multi-cellular systems

Primary cell profiling

Direct assessment of primary cells (mostly of blood origin) has been leveraged to improve TB diagnostics, assess the impact of co-morbidities and -infections (HIV and diabetes cohorts, helminth co-infections) or to identify immune correlates of protection in vaccine trials. These studies analyzed whole blood, peripheral blood

mononuclear cell (PBMC), as well as BAL specimens *in vitro* directly (e.g. by single-cell RNA sequencing) or following infection or stimulation with relevant antigens (Scriba et al., 2017; Walzl et al., 2011). In a pillar study using whole-blood transcriptome analysis, an interferon-driven neutrophil signature associated with active TB disease (Berry et al., 2010). Issued from relevant clinical cohorts, such samples provided valuable insights for disease prediction. However, the potential for mechanistic investigation remains limited, unless combined with *in vitro* models detailed below.

In vitro and *ex vivo* granulomas

Granulomas constitute the hallmark of human TB immune reactions. These aggregates of immune and non-immune cells form to physically contain *Mtb*, which may be cleared resulting in a fibrotic or calcified lesion. Otherwise, *Mtb* may persist in a non-replicating state or continue to replicate and eventually exploit the expansion of the granulomatous response to leak into the airways and spread (Ehlers and Schaible, 2012). As such, granulomas hold potential to be tuned towards protectiveness by host-directed interventions. The first granuloma-like structures were generated from PPD-coated beads (Puissegur et al., 2004). Since then, several granuloma models have been developed (Kapoor et al., 2013; Guirado et al., 2015; Tezera et al., 2017), and previously reviewed (Elkington et al., 2019). *In vitro* granuloma models have provided insights into the capacity of LTBI over healthy controls to better control *Mtb* growth (Guirado et al., 2015; Crouser et al., 2017), and to promote *Mtb* dormancy or resuscitation upon exposure to TNF-α antagonists (Kapoor et al., 2013; Arbués et al., 2020a; Tezera et al., 2020). 3D granuloma models restore antimicrobial susceptibility to pyrazinamide (Bielecka et al., 2017) and capture the variable impact of *Mtb* genetic diversity (Arbués et al., 2025). 3D models (Kapoor et al., 2013; Arbués et al., 2020b), unlike 2D ones (Guirado et al., 2015), generate a hypoxic environment that specifically induces *Mtb* to exhibit dormant-like features (Arbués et al., 2021). However, matrix and electrospray 3D technologies (Tezera et al., 2017) hamper the high-throughput-capacity of these models. In contrast, 2D granuloma models are easier to use, which makes them more suitable for drug screening-platforms.

Spheroid models

A spheroid model leveraged magnetic cell levitation to generated three-dimensional spheroid granulomas from primary human AMs infected with BCG as "innate" spheroids or with autologous T cells to generate "adaptive" spheroids (Kotze et al., 2021). Interestingly – and unlike the granuloma models described above – spheroids form even in absence of infection and the architecture is altered upon infection by containing an AM-rich core and a cuff of T cells. A miniaturized TB spheroid model allows formation of granuloma-like structures without addition of an extracellular matrix from both cell lines (THP-1, Jurkat) and primary cells (PBMCs) (Mukundan et al., 2021a, 2021). This model may include fibroblasts and was used to study disruption of granuloma formation following HIV co-infection.

Alveolar interface systems

Characterizing the alveolar microenvironment and the interaction of epithelial cells with *Mtb* and immune cells is crucial to decipher host-pathogen interactions at the onset of infection. An air-liquid interface model of human primary bronchial epithelial cells (ALI-PBEC) was used to compare the infection of epithelial cells across mycobacterial species (Barclay et al., 2023). These ALI-PBECs incorporate a mixture of PBEC cells from various donors to account for human diversity. Interestingly, this model demonstrated that alveolar cells' secretome attracts neutrophils, highlighting an immune regulatory function in response to infection. Besides, an experimental human lung tissue model of epithelial cells and fibroblasts that produces extra-cellular matrix (ECM) and secretes mucus, was used to study dendritic cell function and monocyte migration, revealing that granuloma formation was dependent on ESAT-6 secretion by mycobacteria (Parasa et al., 2014; Hoang et al., 2012).

Complex models: from organoids to organs-on-a-chip

While multicellular systems can account for genetic diversity and assess interactions between various immune cells, they do not apprehend the structural features of the lung (Kim et al., 2024). Organoids are functional 3D *in vitro* replicates of human organs that self-organize and self-renew (Clevers, 2016). They constitute very promising platforms that can bridge between animal models and human clinical trials (Thangam et al., 2024), thereby contributing to reducing animal use (3R) and research costs. They can be induced from embryonic/pluripotent (ESC), induced pluripotent (iPSC) or organ-specific adult stem cells (ASC) (Clevers, 2016). For lung organoids, one distinguishes alveolar, airway and whole-lung organoids. The application of these systems covers everything from basic research to regenerative medicine. Importantly, organoids can be generated from healthy and ill tissues to establish differential biomarker expression and further our understanding of disease pathophysiology and cure through drug screening. Regarding the latter, patient-specific ASC-derived organoids are of particular relevance to test personalized interventions. iPSC-derived organoids on the other hand, allow for genetic recombination of progenitor cells prior their differentiation and assessment of the functional contributions of the knock-in or knock-out out genes. In recent years, organoids have gained momentum as tools to model infectious diseases. For TB, a human bronchial airway organoid model was used to demonstrate the increased fitness of *M. abscessus* over *Mtb* to invade the airway microenvironment (Iakobachvili et al., 2022). Besides, human lung organoids (LOs) based on a human pluripotent stem cell line allowed the assessment of long-term replication of *Mtb* within THP-1 cells following LO micro-injection (up to 31 days) and were used to validate the potential of two promising HDT pathways in a knock-down approach (Kim et al., 2024). Albeit based on cell lines, this model holds great

potential to study protective responses by incorporating ASC/iPSC as well as autologous primary human macrophages and other immune cells of individuals suffering from or resisting TB.

The most advanced *in vitro* systems are organs-on-a-chip, which are microfluidic devices allowing renewal of "body" fluids that are being widely adopted in different fields of research to allow for mechanistic dissection of human diseases and drug treatment (Ingber, 2022). Lungs-on-a-chip can recapitulate the alveolar-capillary interface, with organ-level functions such as breathing-type movements and inflammatory responses to pathogens (Huh et al., 2010). Until a few years ago, organoids and lungs on-a-chip had not yet been used for TB research (Fonseca et al., 2017). Recently, using a murine-based lung-on-a-chip, Thacker et al. demonstrated the protective role of surfactant, an essential factor that cannot be knocked-out in *in vivo* systems, in the control of *Mtb* replication (Thacker et al., 2020). Their findings shed light on the increased TB susceptibility of elderly and smokers. In combination with a mouse *in vivo* model and agent-based modelling, they further enlightened dynamics of *Mtb* cording (Mishra et al., 2023). The translational potential of human-based lungs-on-a-chip to study human pathophysiology in TB is underlined by its recent development and use to demonstrate the implication of endothelial cells damage in the pathogenesis of coronavirus infection (Thacker et al., 2021).

Advanced experimental technologies

Several cutting-edge technologies are being progressively implemented into the various experimental systems to mechanistically dissect their outputs (Figure 2). Advances in single-cell RNA sequencing for TB research has been reviewed recently (Pan et al., 2023). Moreover, high-dimensional (spatial) mass cytometry and spectral flow-cytometry, as well as high-throughput and live-cell microscopy are being applied to the TB research field (Aylan et al., 2023; Silva-Miranda et al., 2015; McCaffrey et al., 2022; Ogongo et al., 2024). These tools are now commercialized as kits enabling standardized and reproducible read-outs for clinical studies and allowing data concatenation and comparison across sites (e.g. Standard Biotools' MDIPA, BD Rhapsody Targeted human immune gene panel). The body of cloud-based platforms offered by companies developing these kits is almost systematic while sequencing costs are dropping substantially, rendering these systems more accessible.

Computational tools to analyze high-dimensional data are also growing by the day. These tools are openly shared on web-based platforms (GitHub, Bioconductor, …) and generously maintained by their developers, encouraging a fruitful, collaborative environment, promoting advances in scientific research globally. Many come with step-wise guides or examples, making them easy to use, even for non-computational experts.

Remarkably, an array of reporter *Mtb* strains has been constructed and generously shared upon request to track bacteria while reporting on their viability or response to immunological stresses (Abramovitch, 2018; Aylan et al., 2023; Bryson et al., 2019; Sukumar et al., 2014). Fluorescent *Mtb* strains greatly facilitate microscopy-based high-throughput read-outs. Furthermore, barcoded *Mtb* strains were built to demonstrate that single bacteria lead to individual granulomas in NHPs (Martin et al., 2017; Bromley et al., 2024). Like knockout mutants, *Mtb* reporter strains provided substantial insights into the host-pathogen interaction occurring in their respective models, by delivering complex microbiological endpoints associated to immunological responses or environments.

In silico approaches

Beyond wet-lab systems, the computational field has delivered algorithms and deep-learning models that can be trained with experimental and clinical data to infer immune cell interaction and predict drug efficacy (Linderman and Kirschner, 2015). As such, computational models hold great potential to guide research and tailor funding towards the most promising leads (Linderman and Kirschner, 2015). A hybrid multi-scale model of granuloma formation (called *GranSim*) integrated experimental and computational modeling to study cytotoxic and regulatory signaling dynamics in granulomas (Warsinske et al., 2017), as well as to study granuloma-associated fibrosis, predicting a potential role for macrophage-to-myofibroblast transformation (Evans et al., 2021). A further development of this model, *HostSim*, integrates multiple physiological and time scales, tracking cellular, granuloma, organ and whole-host events (Joslyn et al., 2022). *HostSim* may provide valuable predictions of understudied lymph node granuloma dynamics (Krupinsky et al., 2025) and even allow conducting virtual clinical trials (Michael et al., 2024). *In silico* approaches seem especially promising when integrated with multi-omics read-outs of experimental models to reproduce an observed phenotype (Chen et al., 2023). In an elegant approach, an agent-based model fed with data from advanced *in vitro* systems was used to assess the immunological determinants enabling better control of *Mtb* growth by macrophages in a spheroid granuloma model (Kotze et al., 2021; Petrucciani et al., 2024).

Discussion

Further considerations and future perspectives

iPSC limitations

The opportunities awarded by the possible use of stem cells to study infectious diseases appear endless. Nevertheless, some limitations may likely arise, as iPSC-derived macrophage function was notably found to differ depending on culture conditions, which ultimately affected *Mtb* growth (Bussi et al., 2024). It is presumable that organoid functions will be affected similarly and preclude usage of unphysiological conditions to increase a translation potential of the generated data *in vivo*.

Strain variation

Likewise, and often overlooked, the selection of the infecting strain may be consequential. Clinical and epidemiological data indicate that the strain genetic background may influence the nature and extent of TB disease (Peters et al., 2020). *Mtb* global phylogenetic diversity contrasts the limited diversity of strains used in TB research, which is mostly conducted on a handful of laboratory-adapted *Mtb* strains (e.g. H37Ra, H37Rv, Erdman, CDC1551, HN878) (Gagneux and Small, 2007) or related species (e.g. *M. bovis* BCG, *M. smegmatis*, *M. marinum*, *M. avium*). While this enables comparison of findings across laboratories, *Mtb* strain variation has implications for the efficacy of TB vaccines, diagnostics and host-directed therapeutics (Tientcheu et al., 2017). Clinical *Mtb* strains can be routinely isolated and identified from sputum samples, as well as less invasive tongue swaps or mask samples that are being investigated to improve TB diagnosis (Nogueira et al., 2022). Ideally, this variable will be systematically included while advancing immunological studies into complex cellular systems, as previously appreciated within simpler experimental systems (Portevin et al., 2011; Reiling et al., 2013; Wang et al., 2010; Arbués et al., 2025; Hiza et al., 2024; Romagnoli et al., 2018).

Co-prevalent microorganisms

Gut microbiome dysbiosis as well as co-infections, such as helminths, are gaining recognition as potent influencers of immune responses to vaccination and *Mtb* infection (Cadmus et al., 2020; Eribo et al., 2020; Feng et al., 2025). Microbiome interactions may be particularly relevant in further understanding the contribution of innate-like lymphoid (ILC) and mucosa-associated invariant T cells – two cell types tightly linked to microbiota (Mori et al., 2021) –, to TB protective immunity. Therein, microbiota might constitute a point of manipulating mucosal responses towards protectiveness. An in-depth overview of the interactions between microbiomes and tuberculosis has been provided elsewhere (Mori et al., 2021; Namasivayam et al., 2018).

Epigenetics

Another emerging concept relates to epigenetic changes resulting from BCG vaccination and chronic infections (such as TB), which respectively increase non-specific protection through innate immune training (Ziogas et al., 2025) or promote post-TB morbidity and mortality (Abhimanyu et al., 2024; Bobak et al., 2022). Recent findings in guinea pigs and humans indicate that *Mtb* infection induces premature epigenetic aging, which could support post-

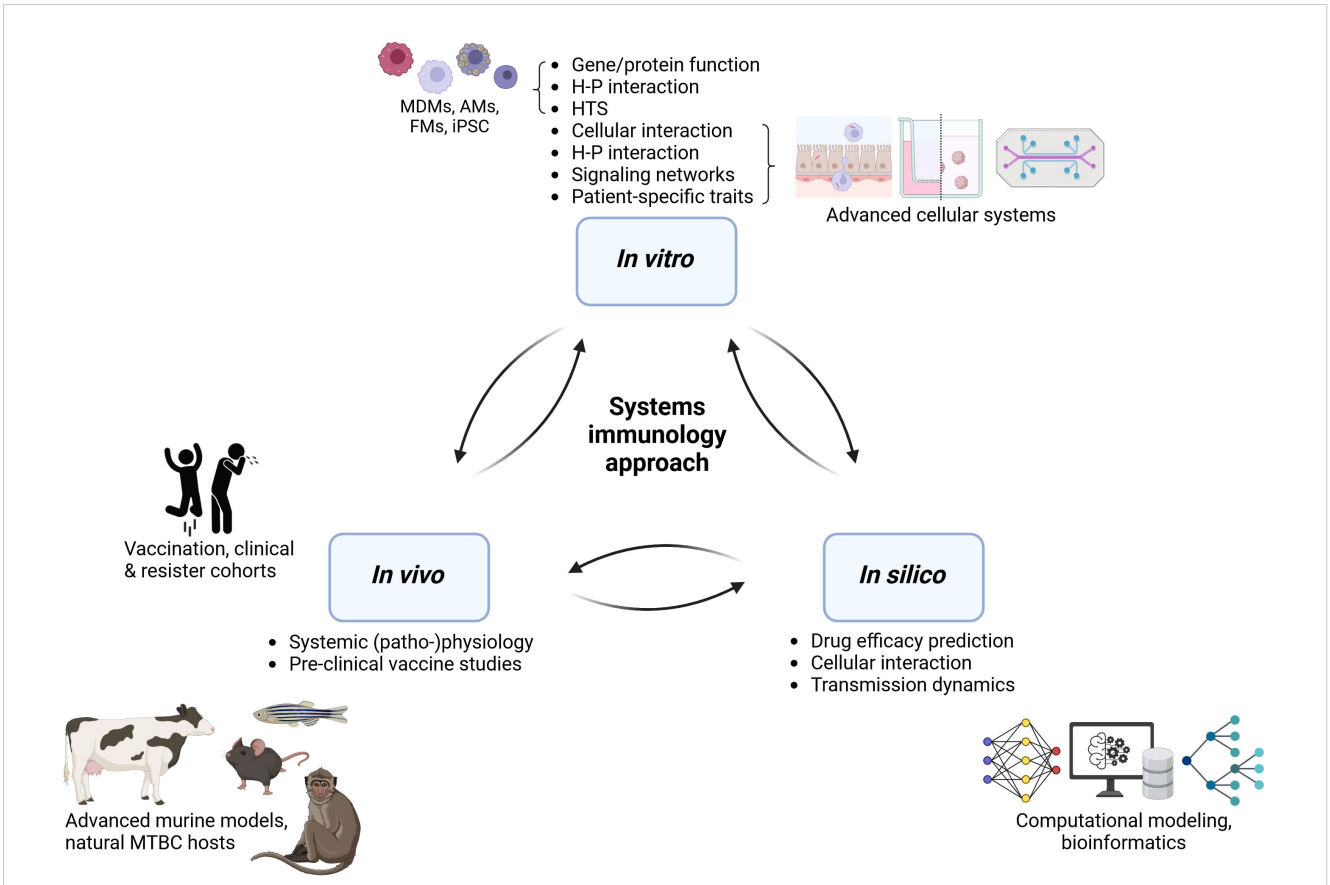

FIGURE 3
An integrative approach to decipher human protective immunity in TB. H-P, host-pathogen; HTS, high-throughput screening; MDMs, monocyte-derived macrophages; AM, alveolar macrophages; FM, foamy macrophages; iPSC, induced pluripotent stem cells; MTBC, *Mycobacterium tuberculosis complex*. Generated with biorender.com.

disease morbidity (Bobak et al., 2022). Metabolic responses, e.g. tricarboxylic acid (TCA) cycle (Abhimanyu et al., 2024), are crystallizing as important drivers of these epigenetic changes. Particularly in the elderly, epigenetic remodeling by host-directed immunomodulation constitutes a promising therapeutic approach (Romero-Rodríguez et al., 2025). Interestingly, epigenetic changes have been associated with resisters' monocytes in independent studies (Zhang et al., 2021; Seshadri et al., 2017). TB research should further investigate epigenetic changes occurring following *Mtb* infection, the effect of these changes on subsequent immune responses and their potential suitability for therapeutic intervention.

Concluding remarks

TB immunological research has to distinguish between protective immunity in terms of (i) natural protection against primary infection, (ii) vaccine-induced protection against infection or disease, (iii) natural or vaccine-induced protection against disease progression. How different samples and models may facilitate the identification of correlates of protection for vaccine development has been recently reviewed by Wang et al., 2024. Advanced *in vitro* approaches were not featured, and we aimed to cover this gap in the present review.

Individual models of TB immunology cannot capture all facets of human TB pathology. However, they allow us to perform mechanistic investigations of specific factors and to evaluate the impact of human diversity. An ultimate model would likely integrate multiple approaches, shining light on protective immune traits from all necessary angles (Figure 3). We posit that an iterative systems approach is necessary to dissect the many facets of human protective immunity in TB, where *in vitro*, *in vivo*, and *in silico* approaches are gradually being integrated. Collective efforts should extract the most of human *in vitro* studies by sharing and making use of clinical samples and combining the generated data with fast-growing computational modeling field in order to: (1) Extract protective traits from human-based *in vitro* systems, aided by computational modeling. (2) Perform mechanistic investigations in advanced multi-cellular organoid systems that may feed predictive *in silico* models to capture the spectrum of human outcomes in TB. (3) Translate and confirm findings *in vivo* in animal models prior scale-up for clinical safety and efficacy evaluation in human trials. Such an integrative, collaborative approach may pave the way for innovative interventions needed to reduce TB burden globally.

Author contributions

SS: Visualization, Writing – original draft, Conceptualization, Writing – review & editing. DP: Writing – review & editing, Conceptualization, Supervision, Funding acquisition.

Funding

The author(s) declare that financial support was received for the research and/or publication of this article. SS's PhD salary costs were supported by the Swiss National Science Foundation (Project numbers 197838 and 213514).

Acknowledgments

We would like to thank the members of our group for inspiring discussions and apologize to all scientists whose work we missed or could not include due to space limitations.

Conflict of interest

The authors declare that the research was conducted in the absence of any commercial or financial relationships that could be construed as a potential conflict of interest.

Generative AI statement

The author(s) declare that no Generative AI was used in the creation of this manuscript.

Publisher's note

References

Abhimanyu,, Longlax, S. C., Nishiguchi, T., Ladki, M., Sheikh, D., Martinez, A. L., et al. (2024). TCA metabolism regulates DNA hypermethylation in LPS and *Mycobacterium tuberculosis*-induced immune tolerance. *Proc. Natl. Acad. Sci. U.S.A.* 121, e2404841121. doi: 10.1073/pnas.2404841121

Abramovitch, R. B. (2018). *Mycobacterium tuberculosis* reporter strains as tools for drug discovery and development. *IUBMB Life* 70, 818–825. doi: 10.1002/iub.v70.9

Afkhami, S., D'agostino, M. R., Vaseghi-Shanjani, M., Lepard, M., Yang, J. X., Lai, R., et al. (2023). Intranasal multivalent adenoviral-vectored vaccine protects against replicating and dormant *M.tb* in conventional and humanized mice. *NPJ Vaccines* 8, 25. doi: 10.1038/s41541-023-00623-z

Ahmed, M., Thirunavukkarasu, S., Rosa, B. A., Thomas, K. A., Das, S., Rangel-Moreno, J., et al. (2020). Immune correlates of tuberculosis disease and risk translate across species. *Sci. Transl. Med.* 12. doi: 10.1126/scitranslmed.aay0233

Andersson, A.-M., Andersson, B., Lorell, C., Raffetseder, J., Larsson, M., and Blomgran, R. (2016). Autophagy induction targeting mTORC1 enhances *Mycobacterium tuberculosis* replication in HIV co-infected human macrophages. *Sci. Rep.* 6, 28171. doi: 10.1038/srep28171

Arbués, A., Brees, D., Chibout, S. D., Fox, T., Kammüller, M., and Portevin, D. (2020a). TNF-α antagonists differentially induce TGF-β1-dependent resuscitation of

dormant-like *Mycobacterium tuberculosis*. *PloS Pathog.* 16, e1008312. doi: 10.1371/journal.ppat.1008312

Arbués, A., Kammüller, M., and Portevin, D. (2020b). Generating Three-dimensional Human Granulomas *in vitro* to Study *Mycobacterium tuberculosis*-host Interaction. *Bio-protocol* 10, e3820. doi: 10.21769/BioProtoc.3820

Arbués, A., Schmidiger, S., Kammüller, M., and Portevin, D. (2021). Extracellular matrix-induced GM-CSF and hypoxia promote immune control of *mycobacterium tuberculosis* in human *in vitro* granulomas. *Front. Immunol.* 12, 727508. doi: 10.3389/fimmu.2021.727508

Arbués, A., Schmidiger, S., Reinhard, M., Borrell, S., Gagneux, S., and Portevin, D. (2025). Soluble immune mediators orchestrate protective *in vitro* granulomatous responses across *Mycobacterium tuberculosis* complex lineages. *eLife*. doi: 10.7554/eLife.99062.4.sa3

Armstrong, J. A., and Hart, P. D. (1971). Response of cultured macrophages to *Mycobacterium tuberculosis*, with observations on fusion of lysosomes with phagosomes. *J. Exp. Med.* 134, 713–740. doi: 10.1084/jem.134.3.713

Arrey, F., Löwe, D., Kuhlmann, S., Kaiser, P., Moura-Alves, P., Krishnamoorthy, G., et al. (2019). Humanized mouse model mimicking pathology of human tuberculosis for *in vivo* evaluation of drug regimens. *Front. Immunol.* 10, 89. doi: 10.3389/fimmu.2019.00089

Aylan, B., Bernard, E. M., Pellegrino, E., Botella, L., Fearns, A., Athanasiadi, N., et al. (2023). ATG7 and ATG14 restrict cytosolic and phagosomal *Mycobacterium tuberculosis* replication in human macrophages. *Nat. Microbiol.* 8, 803–818. doi: 10.1038/s41564-023-01335-9

Balasingam, S., Dheda, K., Fortune, S., Gordon, S. B., Hoft, D., Kublin, J. G., et al. (2024). Review of current tuberculosis human infection studies for use in accelerating tuberculosis vaccine development: A meeting report. *J. Infect. Dis.* 230, e457–e464. doi: 10.1093/infdis/jiae238

Barclay, A. M., Ninaber, D. K., Van Veen, S., Hiemstra, P. S., Ottenhoff, T. H. M., van der Does, A. M., et al. (2023). Airway epithelial cells mount an early response to mycobacterial infection. *Front. Cell Infect. Microbiol.* 13, 1253037. doi: 10.3389/fcimb.2023.1253037

Behr, M. A., Edelstein, P. H., and Ramakrishnan, L. (2018). Revisiting the timetable of tuberculosis. *Bmj* 362, k2738. doi: 10.1136/bmj.k2738

Behr, M. A., Edelstein, P. H., and Ramakrishnan, L. (2020). SLeuthing tuberculous cough. *Cell* 181, 230–232. doi: 10.1016/j.cell.2020.03.057

Bermudez, L. E., Sangari, F. J., Kolonoski, P., Petrofsky, M., and Goodman, J. (2002). The efficiency of the translocation of *Mycobacterium tuberculosis* across a bilayer of epithelial and endothelial cells as a model of the alveolar wall is a consequence of transport within mononuclear phagocytes and invasion of alveolar epithelial cells. *Infect. Immun.* 70, 140–146. doi: 10.1128/IAI.70.1.140-146.2002

Berry, M. P., Graham, C. M., Mcnab, F. W., Xu, Z., Bloch, S. A., Oni, T., et al. (2010). An interferon-inducible neutrophil-driven blood transcriptional signature in human tuberculosis. *Nature* 466, 973–977. doi: 10.1038/nature09247

Bhargava, A., Bhargava, M., Meher, A., Benedetti, A., Velayutham, B., Sai Teja, G., et al. (2023). Nutritional supplementation to prevent tuberculosis incidence in household contacts of patients with pulmonary tuberculosis in India (RATIONS): a field-based, open-label, cluster-randomised, controlled trial. *Lancet* 402, 627–640. doi: 10.1016/S0140-6736(23)01231-X

Bielecka, M. K., Tezera, L. B., Zmijan, R., Drobniewski, F., Zhang, X., Jayasinghe, S., et al. (2017). A bioengineered three-dimensional cell culture platform integrated with microfluidics to address antimicrobial resistance in tuberculosis. *mBio* 8. doi: 10.1128/mBio.02073-16

Birkness, K. A., Deslauriers, M., Bartlett, J. H., White, E. H., King, C. H., and Quinn, F. D. (1999). An *in vitro* tissue culture bilayer model to examine early events in *Mycobacterium tuberculosis* infection. *Infect. Immun.* 67, 653–658. doi: 10.1128/IAI.67.2.653-658.1999

Bobak, C. A., Abhimanyu,, Natarajan, H., Gandhi, T., Grimm, S. L., Nishiguchi, T., et al. (2022). Increased DNA methylation, cellular senescence and premature epigenetic aging in Guinea pigs and humans with tuberculosis. *Aging (Albany NY)* 14, 2174–2193. doi: 10.18632/aging.203936

Bohórquez, J. A., Adduri, S., Ansari, D., John, S., Florence, J., Adejare, O., et al. (2024). A novel humanized mouse model for HIV and tuberculosis co-infection studies. *Front. Immunol.* 15, 1395018. doi: 10.3389/fimmu.2024.1395018

Bromley, J. D., Ganchua, S. K. C., Nyquist, S. K., Maiello, P., Chao, M., Borish, H. J., et al. (2024). $CD4^+$ T cells re-wire granuloma cellularity and regulatory networks to promote immunomodulation following *Mtb* reinfection. *Immunity* 57, 2380–2398.e6. doi: 10.1016/j.immuni.2024.08.002

Bryson, B. D., Rosebrock, T. R., Tafesse, F. G., Itoh, C. Y., Nibasumba, A., Babunovic, G. H., et al. (2019). Heterogeneous GM-CSF signaling in macrophages is associated with control of *Mycobacterium tuberculosis*. *Nat. Commun.* 10, 2329. doi: 10.1038/s41467-019-10065-8

Bucsan, A. N., Mehra, S., Khader, S. A., and Kaushal, D. (2019). The current state of animal models and genomic approaches towards identifying and validating molecular determinants of *Mycobacterium tuberculosis* infection and tuberculosis disease. *Pathog. Dis.* 77. doi: 10.1093/femspd/ftz037

Bussi, C., Lai, R., Athanasiadi, N., and Gutierrez, M. G. (2024). Physiologic medium renders human iPSC-derived macrophages permissive for *M. tuberculosis* by rewiring organelle function and metabolism. *mBio* 15, e0035324. doi: 10.1128/mbio.00353-24

Bustamante, J., Boisson-Dupuis, S., Abel, L., and Casanova, J. L. (2014). Mendelian susceptibility to mycobacterial disease: genetic, immunological, and clinical features of inborn errors of IFN-γ immunity. *Semin. Immunol.* 26, 454–470. doi: 10.1016/j.smim.2014.09.008

Cadmus, S. I., Akinseye, V. O., Taiwo, B. O., Pinelli, E. O., Van Soolingen, D., and Rhodes, S. G. (2020). Interactions between helminths and tuberculosis infections: Implications for tuberculosis diagnosis and vaccination in Africa. *PloS Negl. Trop. Dis.* 14, e0008069. doi: 10.1371/journal.pntd.0008069

Calderon, V. E., Valbuena, G., Goez, Y., Judy, B. M., Huante, M. B., Sutjita, P., et al. (2013). A humanized mouse model of tuberculosis. *PloS One* 8, e63331. doi: 10.1371/journal.pone.0063331

Campo, M., Dill-Mcfarland, K. A., Peterson, G. J., Benson, B., Skerrett, S. J., and Hawn, T. R. (2024). Human alveolar and monocyte-derived human macrophage responses to *mycobacterium tuberculosis*. *J. Immunol.* 213, 161–169. doi: 10.4049/jimmunol.2300885

Capoferri, G., Ghielmetti, G., Glatz, B., Mutke, M. R., Tzankov, A., Stephan, R., et al. (2024). Disseminated, fatal reactivation of bovine tuberculosis in a patient treated with adalimumab: a case report and review of the literature. *Infection*. doi: 10.1007/s15010-024-02364-0

Capuano, S. V. 3rd, Croix, D. A., Pawar, S., Zinovik, A., Myers, A., Lin, P. L., et al. (2003). Experimental *Mycobacterium tuberculosis* infection of cynomolgus macaques closely resembles the various manifestations of human *M. tuberculosis* infection. *Infect. Immun.* 71, 5831–5844. doi: 10.1128/IAI.71.10.5831-5844.2003

Cerneckis, J., Cai, H., and Shi, Y. (2024). Induced pluripotent stem cells (iPSCs): molecular mechanisms of induction and applications. *Signal Transduction Targeted Ther.* 9, 112. doi: 10.1038/s41392-024-01809-0

Chen, C., Wang, J., Pan, D., Wang, X., Xu, Y., Yan, J., et al. (2023). Applications of multi-omics analysis in human diseases. *MedComm* 4, e315. doi: 10.1002/mco2.v4.4

Clevers, H. (2016). Modeling development and disease with organoids. *Cell* 165, 1586–1597. doi: 10.1016/j.cell.2016.05.082

Click, E. S., Moonan, P. K., Winston, C. A., Cowan, L. S., and Oeltmann, J. E. (2012). Relationship between *Mycobacterium tuberculosis* phylogenetic lineage and clinical site of tuberculosis. *Clin. Infect. Dis.* 54, 211–219. doi: 10.1093/cid/cir788

Crouser, E. D., White, P., Caceres, E. G., Julian, M. W., Papp, A. C., Locke, L. W., et al. (2017). A novel *in vitro* human granuloma model of sarcoidosis and latent tuberculosis infection. *Am. J. Respir. Cell Mol. Biol.* 57, 487–498. doi: 10.1165/rcmb.2016-0321OC

Daniel, J., Maamar, H., Deb, C., Sirakova, T. D., and Kolattukudy, P. E. (2011). *Mycobacterium tuberculosis* uses host triacylglycerol to accumulate lipid droplets and acquires a dormancy-like phenotype in lipid-loaded macrophages. *PloS Pathog.* 7, e1002093. doi: 10.1371/journal.ppat.1002093

Darrah, P. A., Zeppa, J. J., Maiello, P., Hackney, J. A., Wadsworth, M. H., Hughes, T. K., et al. (2020). Prevention of tuberculosis in macaques after intravenous BCG immunization. *Nature* 577, 95–102. doi: 10.1038/s41586-019-1817-8

De Jong, B. C., Hill, P. C., Aiken, A., Awine, T., Martin, A., Adetifa, I. M., et al. (2008). Progression to Active Tuberculosis, but Not Transmission, Varies by *Mycobacterium tuberculosis* Lineage in The Gambia. *J. Infect. Dis.* 198, 1037–1043. doi: 10.1086/591504

Dill-Mcfarland, K. A., Peterson, G., Lim, P. N., Skerrett, S., Hawn, T. R., Rothchild, A. C., et al. (2025). Shared and distinct responses of human and murine alveolar macrophages and monocyte-derived macrophages to *Mycobacterium tuberculosis*. *bioRxiv 2025.02.28.640814*. doi: 10.1101/2025.02.28.640814

Dodd, C. E., Pyle, C. J., Glowinski, R., Rajaram, M. V., and Schlesinger, L. S. (2016). CD36-mediated uptake of surfactant lipids by human macrophages promotes intracellular growth of *mycobacterium tuberculosis*. *J. Immunol.* 197, 4727–4735. doi: 10.4049/jimmunol.1600856

Du, D. H., Geskus, R. B., Zhao, Y., Codecasa, L. R., Cirillo, D. M., Van Crevel, R., et al. (2023). The effect of *M. tuberculosis* lineage on clinical phenotype. *PloS Glob Public Health* 3, e0001788. doi: 10.1371/journal.pgph.0001788

Dube, D., Sharma, R., Mody, N., Gupta, M., Agrawal, U., and Vyas, S. P. (2020). "Chapter 2 - Animal models of tuberculosis," in *Animal biotechnology*, *2nd ed*. Eds. A. S. Verma and A. Singh (Academic Press, Boston).

Ehlers, S., and Schaible, U. E. (2012). The granuloma in tuberculosis: dynamics of a host-pathogen collusion. *Front. Immunol.* 3, 411. doi: 10.3389/fimmu.2012.00411

Elkington, P., Lerm, M., Kapoor, N., Mahon, R., Pienaar, E., Huh, D., et al. (2019). *In vitro* granuloma models of tuberculosis: potential and challenges. *J. Infect. Dis.* 219, 1858–1866. doi: 10.1093/infdis/jiz020

Eribo, O. A., Du Plessis, N., Ozturk, M., Guler, R., Walzl, G., and Chegou, N. N. (2020). The gut microbiome in tuberculosis susceptibility and treatment response: guilty or not guilty? *Cell Mol. Life Sci.* 77, 1497–1509. doi: 10.1007/s00018-019-03370-4

Ernst, J. D. (2012). The immunological life cycle of tuberculosis. *Nat. Rev. Immunol.* 12, 581–591. doi: 10.1038/nri3259

Esaulova, E., Das, S., Singh, D. K., Choreño-Parra, J. A., Swain, A., Arthur, L., et al. (2021). The immune landscape in tuberculosis reveals populations linked to disease and latency. *Cell Host Microbe* 29, 165–178.e8. doi: 10.1016/j.chom.2020.11.013

Evans, S., Butler, J. R., Mattila, J. T., and Kirschner, D. E. (2021). Systems biology predicts that fibrosis in tuberculous granulomas may arise through macrophage-to-myofibroblast transformation. *PloS Comput. Biol.* 16, e1008520. doi: 10.1371/journal.pcbi.1008520

Feng, Y., De Jong, S. E., Oliveira, A. P. B. N., Samaha, H., Yang, F., Hu, M., et al. (2025). Antibiotic-induced gut microbiome perturbation alters the immune responses to the rabies vaccine. *Cell Host Microbe* 33, 705–718.e5. doi: 10.1016/j.chom.2025.03.015

Fonseca, K. L., Rodrigues, P. N. S., Olsson, I. A. S., and Saraiva, M. (2017). Experimental study of tuberculosis: From animal models to complex cell systems and organoids. *PloS Pathog.* 13, e1006421. doi: 10.1371/journal.ppat.1006421

Gagneux, S. (2012). Host-pathogen coevolution in human tuberculosis. *Philos. Trans. R Soc. Lond B Biol. Sci.* 367, 850–859. doi: 10.1098/rstb.2011.0316

Gagneux, S., and Small, P. M. (2007). Global phylogeography of *Mycobacterium tuberculosis* and implications for tuberculosis product development. *Lancet Infect. Dis.* 7, 328–337. doi: 10.1016/S1473-3099(07)70108-1

Gail, D. P., Suzart, V. G., Du, W., Kaur Sandhu, A., Jarvela, J., Nantongo, M., et al. (2023). *Mycobacterium tuberculosis* impairs human memory CD4+ T cell recognition of M2 but not M1-like macrophages. *iScience* 26, 107706. doi: 10.1016/j.isci.2023.107706

Gideon, H. P., Hughes, T. K., Tzouanas, C. N., Wadsworth, M. H. 2nd, Tu, A. A., Gierahn, T. M., et al. (2022). Multimodal profiling of lung granulomas in macaques reveals cellular correlates of tuberculosis control. *Immunity* 55, 827–846.e10. doi: 10.1016/j.immuni.2022.04.004

Goig, G. A., Windels, E. M., Loiseau, C., Stritt, C., Biru, L., Borrell, S., et al. (2025). Ecology, global diversity and evolutionary mechanisms in the *Mycobacterium tuberculosis* complex. *Nat. Rev. Microbiol.* doi: 10.1038/s41579-025-01159-w

Gonçalves, I. C., Furtado, I., Gonçalves, M. J., and Xará, S. (2022). *Mycobacterium marinum* cutaneous infection: A series of three cases and literature review. *Cureus* 14, e31787. doi: 10.7759/cureus.31787

Gong, W., Liang, Y., and Wu, X. (2020). Animal models of tuberculosis vaccine research: an important component in the fight against tuberculosis. *BioMed. Res. Int.* 2020, 4263079. doi: 10.1155/2020/4263079

Guirado, E., Mbawuike, U., Keiser, T. L., Arcos, J., Azad, A. K., Wang, S. H., et al. (2015). Characterization of host and microbial determinants in individuals with latent tuberculosis infection using a human granuloma model. *mBio* 6, e02537–e02514. doi: 10.1128/mBio.02537-14

Gutierrez, M. G., Master, S. S., Singh, S. B., Taylor, G. A., Colombo, M. I., and Deretic, V. (2004). Autophagy is a defense mechanism inhibiting BCG and *Mycobacterium tuberculosis* survival in infected macrophages. *Cell* 119, 753–766. doi: 10.1016/j.cell.2004.11.038

Hansen, S. G., Zak, D. E., Xu, G., Ford, J. C., Marshall, E. E., Malouli, D., et al. (2018). Prevention of tuberculosis in rhesus macaques by a cytomegalovirus-based vaccine. *Nat. Med.* 24, 130–143. doi: 10.1038/nm.4473

Hiza, H., Zwyer, M., Hella, J., Arbués, A., Sasamalo, M., Borrell, S., et al. (2024). Bacterial diversity dominates variable macrophage responses of tuberculosis patients in Tanzania. *Sci. Rep.* 14, 9287. doi: 10.1038/s41598-024-60001-0

Hoang, A. T. N., Chen, P., Juarez, J., Sachamitr, P., Billing, B., Bosnjak, L., et al. (2012). Dendritic cell functional properties in a three-dimensional tissue model of human lung mucosa. *Am. J. Physiology-Lung Cell. Mol. Physiol.* 302, L226–L237. doi: 10.1152/ajplung.00059.2011

Houben, R. M., and Dodd, P. J. (2016). The global burden of latent tuberculosis infection: A re-estimation using mathematical modelling. *PloS Med.* 13, e1002152. doi: 10.1371/journal.pmed.1002152

Huh, D., Matthews, B. D., Mammoto, A., Montoya-Zavala, M., Hsin, H. Y., and Ingber, D. E. (2010). Reconstituting organ-level lung functions on a chip. *Science* 328, 1662–1668. doi: 10.1126/science.1188302

Iakobachvili, N., Leon-Icaza, S. A., Knoops, K., Sachs, N., Mazères, S., Simeone, R., et al. (2022). Mycobacteria-host interactions in human bronchiolar airway organoids. *Mol. Microbiol.* 117, 682–692. doi: 10.1111/mmi.v117.3

Ingber, D. E. (2022). Human organs-on-chips for disease modelling, drug development and personalized medicine. *Nat. Rev. Genet.* 23, 467–491. doi: 10.1038/s41576-022-00466-9

Irvine, E. B., Darrah, P. A., Wang, S., Wang, C., Mcnamara, R. P., Roederer, M., et al. (2024). Humoral correlates of protection against *Mycobacterium tuberculosis* following intravenous BCG vaccination in rhesus macaques. *iScience* 27, 111128. doi: 10.1016/j.isci.2024.111128

Joslyn, L. R., Linderman, J. J., and Kirschner, D. E. (2022). A virtual host model of *Mycobacterium tuberculosis* infection identifies early immune events as predictive of infection outcomes. *J. Theor. Biol.* 539, 111042. doi: 10.1016/j.jtbi.2022.111042

Kapoor, N., Pawar, S., Sirakova, T. D., Deb, C., Warren, W. L., and Kolattukudy, P. E. (2013). Human granuloma *in vitro* model, for TB dormancy and resuscitation. *PloS One* 8, e53657. doi: 10.1371/journal.pone.0053657

Kim, S. Y., Choi, J. A., Choi, S., Kim, K. K., Song, C. H., and Kim, E. M. (2024). Advances in an *in vitro* tuberculosis infection model using human lung organoids for host-directed therapies. *PloS Pathog.* 20, e1012295. doi: 10.1371/journal.ppat.1012295

Kotze, L. A., Beltran, C. G. G., Lang, D., Loxton, A. G., Cooper, S., Meiring, M., et al. (2021). Establishment of a patient-derived, magnetic levitation-based, three-dimensional spheroid granuloma model for human tuberculosis. *mSphere* 6, e0055221. doi: 10.1128/mSphere.00552-21

Krupinsky, K. C., Michael, C. T., Nanda, P., Mattila, J. T., and Kirschner, D. (2025). Distinguishing multiple roles of T cell and macrophage involvement in determining lymph node fates during *Mycobacterium tuberculosis* infection. *PloS Comput. Biol.* 21, e1013033. doi: 10.1371/journal.pcbi.1013033

Kübler, A., Luna, B., Larsson, C., Ammerman, N. C., Andrade, B. B., Orandle, M., et al. (2015). *Mycobacterium tuberculosis* dysregulates MMP/TIMP balance to drive rapid cavitation and unrestrained bacterial proliferation. *J. Pathol.* 235, 431–444. doi: 10.1002/path.4432

Larson, E. C., Ellis-Connell, A. L., Rodgers, M. A., Gubernat, A. K., Gleim, J. L., Moriarty, R. V., et al. (2023). Intravenous Bacille Calmette-Guérin vaccination protects simian immunodeficiency virus-infected macaques from tuberculosis. *Nat. Microbiol.* 8, 2080–2092. doi: 10.1038/s41564-023-01503-x

Lee, D., and Chambers, M. (2019). A co-culture model of the bovine alveolus. *F1000Res* 8, 357. doi: 10.12688/f1000research

Lee, D. F., Stewart, G. R., and Chambers, M. A. (2020). Modelling early events in *Mycobacterium bovis* infection using a co-culture model of the bovine alveolus. *Sci. Rep.* 10, 18495. doi: 10.1038/s41598-020-75113-6

Lin, P. L., Ford, C. B., Coleman, M. T., Myers, A. J., Gawande, R., Ioerger, T., et al. (2014). Sterilization of granulomas is common in active and latent tuberculosis despite within-host variability in bacterial killing. *Nat. Med.* 20, 75–79. doi: 10.1038/nm.3412

Linderman, J. J., and Kirschner, D. E. (2015). *In silico* models of *M. tuberculosis* infection provide a route to new therapies. *Drug Discov. Today Dis. Models* 15, 37–41. doi: 10.1016/j.ddmod.2014.02.006

Lurie, M. B. (1930). Experimental epidemiology of tuberculosis: air-borne contagion of tuberculosis in an animal room. *J. Exp. Med.* 51, 743–751. doi: 10.1084/jem.51.5.743

Lurie, M. B. (1942). Studies on the mechanism of immunity in tuberculosis: the fate of tubercle bacilli ingested by mononuclear phagocytes derived from normal and immunized animals. *J. Exp. Med.* 75, 247–268. doi: 10.1084/jem.75.3.247

Manabe, Y. C., Kesavan, A. K., Lopez-Molina, J., Hatem, C. L., Brooks, M., Fujiwara, R., et al. (2008). The aerosol rabbit model of TB latency, reactivation and immune reconstitution inflammatory syndrome. *Tuberculosis (Edinb)* 88, 187–196. doi: 10.1016/j.tube.2007.10.006

Marakalala, M. J., Raju, R. M., Sharma, K., Zhang, Y. J., Eugenin, E. A., Prideaux, B., et al. (2016). Inflammatory signaling in human tuberculosis granulomas is spatially organized. *Nat. Med.* 22, 531–538. doi: 10.1038/nm.4073

Martin, C. J., Cadena, A. M., Leung, V. W., Lin, P. L., Maiello, P., Hicks, N., et al. (2017). Digitally barcoding *mycobacterium tuberculosis* reveals *in vivo* infection dynamics in the macaque model of tuberculosis. *mBio* 8. doi: 10.1128/mBio.00312-17

Mccaffrey, E. F., Donato, M., Keren, L., Chen, Z., Delmastro, A., Fitzpatrick, M. B., et al. (2022). The immunoregulatory landscape of human tuberculosis granulomas. *Nat. Immunol.* 23, 318–329. doi: 10.1038/s41590-021-01121-x

Mcdonald, K., Rodriguez, A., and Muthukrishnan, G. (2024). Humanized mouse models of bacterial infections. *Antibiotics (Basel)* 13. doi: 10.3390/antibiotics13070640

Michael, C. T., Almohri, S. A., Linderman, J. J., and Kirschner, D. E. (2024). A framework for multi-scale intervention modeling: virtual cohorts, virtual clinical trials, and model-to-model comparisons. *Front. Syst. Biology Volume* 3, 2023. doi: 10.3389/fsysb.2023.1283341

Minassian, A. M., Satti, I., Poulton, I. D., Meyer, J., Hill, A. V., and Mcshane, H. (2012). A human challenge model for *Mycobacterium tuberculosis* using *Mycobacterium bovis* bacille Calmette-Guerin. *J. Infect. Dis.* 205, 1035–1042. doi: 10.1093/infdis/jis012

Mishra, R., Hannebelle, M., Patil, V. P., Dubois, A., Garcia-Mouton, C., Kirsch, G. M., et al. (2023). Mechanopathology of biofilm-like *Mycobacterium tuberculosis* cords. *Cell* 186, 5135–5150.e28. doi: 10.1016/j.cell.2023.09.016

Mori, G., Morrison, M., and Blumenthal, A. (2021). Microbiome-immune interactions in tuberculosis. *PloS Pathog.* 17, e1009377. doi: 10.1371/journal.ppat.1009377

Mukundan, S., Bhatt, R., Lucas, J., Tereyek, M., Chang, T. L., Subbian, S., et al. (2021a). 3D host cell and pathogen-based bioassay development for testing anti-tuberculosis (TB) drug response and modeling immunodeficiency. *Biomol Concepts* 12, 117–128. doi: 10.1515/bmc-2021-0013

Mukundan, S., Singh, P., Shah, A., Kumar, R., O'neill, K. C., Carter, C. L., et al. (2021b). *In vitro* miniaturized tuberculosis spheroid model. *Biomedicines* 9. doi: 10.3390/biomedicines9091209

Murray, P. J. (2017). Macrophage polarization. *Annu. Rev. Physiol.* 79, 541–566. doi: 10.1146/annurev-physiol-022516-034339

Namasivayam, S., Sher, A., Glickman, M. S., and Wipperman, M. F. (2018). The microbiome and tuberculosis: early evidence for cross talk. *mBio* 9. doi: 10.1128/mBio.01420-18

Nogueira, B. M. F., Krishnan, S., Barreto-Duarte, B., Araújo-Pereira, M., Queiroz, A. T. L., Ellner, J. J., et al. (2022). Diagnostic biomarkers for active tuberculosis: progress and challenges. *EMBO Mol. Med.* 14, e14088. doi: 10.15252/emmm.202114088

O'garra, A., Redford, P. S., Mcnab, F. W., Bloom, C. I., Wilkinson, R. J., and Berry, M. P. (2013). The immune response in tuberculosis. *Annu. Rev. Immunol.* 31, 475–527. doi: 10.1146/annurev-immunol-032712-095939

Ogongo, P., Tran, A., Marzan, F., Gingrich, D., Krone, M., Aweeka, F., et al. (2024). High-parameter phenotypic characterization reveals a subset of human Th17 cells that preferentially produce IL-17 against *M. tuberculosis* antigen. *Front. Immunol.* 15, 1378040. doi: 10.3389/fimmu.2024.1378040

Olea-Popelka, F., Muwonge, A., Perera, A., Dean, A. S., Mumford, E., Erlacher-Vindel, E., et al. (2017). Zoonotic tuberculosis in human beings caused by *Mycobacterium bovis* - a call for action. *Lancet Infect. Dis.* 17, e21–e25. doi: 10.1016/S1473-3099(16)30139-6

Pahari, S., Arnett, E., Simper, J., Azad, A., Guerrero-Arguero, I., Ye, C., et al. (2023). A new tractable method for generating human alveolar macrophage-like cells *in vitro* to study lung inflammatory processes and diseases. *mBio* 14, e0083423. doi: 10.1128/mbio.00834-23

Pahari, S., Neehus, A.-L., Trapnell, B. C., Bustamante, J., Casanova, J.-L., and Schlesinger, L. S. (2024). Protocol to develop human alveolar macrophage-like cells from mononuclear cells or purified monocytes for use in respiratory biology research. *STAR Protoc.* 5, 103061. doi: 10.1016/j.xpro.2024.103061

Pan, J., Chang, Z., Zhang, X., Dong, Q., Zhao, H., Shi, J., et al. (2023). Research progress of single-cell sequencing in tuberculosis. *Front. Immunol.* 14, 1276194. doi: 10.3389/fimmu.2023.1276194

Papp, A. C., Azad, A. K., Pietrzak, M., Williams, A., Handelman, S. K., Igo, R. P. Jr., et al. (2018). AmpliSeq transcriptome analysis of human alveolar and monocyte-derived macrophages over time in response to *Mycobacterium tuberculosis* infection. *PloS One* 13, e0198221. doi: 10.1371/journal.pone.0198221

Parasa, V. R., Rahman, M. J., Ngyuen Hoang, A. T., Svensson, M., Brighenti, S., and Lerm, M. (2014). Modeling *Mycobacterium tuberculosis* early granuloma formation in experimental human lung tissue. *Dis. Model. Mech.* 7, 281–288. doi: 10.1242/dmm.013854

Peters, J. M., Irvine, E. B., Makatsa, M. S., Rosenberg, J. M., Wadsworth, M. H., Hughes, T. K., et al. (2025). High-dose intravenous BCG vaccination induces enhanced immune signaling in the airways. *Sci. Adv.* 11, eadq8229. doi: 10.1126/sciadv.adq8229

Peters, J. S., Ismail, N., Dippenaar, A., Ma, S., Sherman, D. R., Warren, R. M., et al. (2020). Genetic diversity in *mycobacterium tuberculosis* clinical isolates and resulting outcomes of tuberculosis infection and disease. *Annu. Rev. Genet.* 54, 511–537. doi: 10.1146/annurev-genet-022820-085940

Petrucciani, A., Hoerter, A., Kotze, L., Du Plessis, N., and Pienaar, E. (2024). *In silico* agent-based modeling approach to characterize multiple *in vitro* tuberculosis infection models. *PloS One* 19, e0299107. doi: 10.1371/journal.pone.0299107

Peyron, P., Vaubourgeix, J., Poquet, Y., Levillain, F., Botanch, C., Bardou, F., et al. (2008). Foamy macrophages from tuberculous patients' granulomas constitute a nutrient-rich reservoir for *M. tuberculosis* persistence. *PloS Pathog.* 4, e1000204. doi: 10.1371/journal.ppat.1000204

Plumlee, C. R., Duffy, F. J., Gern, B. H., Delahaye, J. L., Cohen, S. B., Stoltzfus, C. R., et al. (2021). Ultra-low dose aerosol infection of mice with *mycobacterium tuberculosis* more closely models human tuberculosis. *Cell Host Microbe* 29, 68–82.e5. doi: 10.1016/j.chom.2020.10.003

Pollard, A. J., Savulescu, J., Oxford, J., Hill, A. V., Levine, M. M., Lewis, D. J., et al. (2012). Human microbial challenge: the ultimate animal model. *Lancet Infect. Dis.* 12, 903–905. doi: 10.1016/S1473-3099(12)70292-X

Portevin, D., Gagneux, S., Comas, I., and Young, D. (2011). Human macrophage responses to clinical isolates from the *Mycobacterium tuberculosis* complex discriminate between ancient and modern lineages. *PloS Pathog.* 7, e1001307. doi: 10.1371/journal.ppat.1001307

Puissegur, M. P., Botanch, C., Duteyrat, J. L., Delsol, G., Caratero, C., and Altare, F. (2004). An *in vitro* dual model of mycobacterial granulomas to investigate the molecular interactions between mycobacteria and human host cells. *Cell Microbiol.* 6, 423–433. doi: 10.1111/j.1462-5822.2004.00371.x

Rachwal, N., Idris, R., Dreyer, V., Richter, E., Wichelhaus, T. A., Niemann, S., et al. (2024). Pathogen and host determinants of extrapulmonary tuberculosis among 1035 patients in Frankfurt am Main, Germany 2008-2023. *Clin. Microbiol. Infect.* doi: 10.1016/j.cmi.2024.11.009

Rankine-Wilson, L., Rens, C., Sahile, H. A., and Av-Gay, Y. (2022). *Mycobacterium tuberculosis* infection of THP-1 cells: A model for high content analysis of intracellular growth and drug susceptibility. *Methods Mol. Biol.* 2427, 73–82. doi: 10.1007/978-1-0716-1971-1_7

Reiling, N., Homolka, S., Walter, K., Brandenburg, J., Niwinski, L., Ernst, M., et al. (2013). Clade-specific virulence patterns of *Mycobacterium tuberculosis* complex strains in human primary macrophages and aerogenically infected mice. *mBio* 4. doi: 10.1128/mBio.00250-13

Romagnoli, A., Petruccioli, E., Palucci, I., Camassa, S., Carata, E., Petrone, L., et al. (2018). Clinical isolates of the modern *Mycobacterium tuberculosis* lineage 4 evade host defense in human macrophages through eluding IL-1beta-induced autophagy. *Cell Death Dis.* 9, 624. doi: 10.1038/s41419-018-0640-8

Romero-Rodríguez, D. P., Díaz-Alvarado, C. A., Rocha-González, H. I., and Juárez, E. (2025). Control of *Mycobacterium tuberculosis* infection in the elderly: Is there a role for epigenetic reprogramming reversal? *Biofactors* 51, e2151. doi: 10.1002/biof.v51.1

Ruhl, C. R., Pasko, B. L., Khan, H. S., Kindt, L. M., Stamm, C. E., Franco, L. H., et al. (2020). *Mycobacterium tuberculosis* sulfolipid-1 activates nociceptive neurons and induces cough. *Cell* 181, 293–305.e11. doi: 10.1016/j.cell.2020.02.026

Saelens, J. W., Sweeney, M. I., Viswanathan, G., Xet-Mull, A. M., Jurcic Smith, K. L., Sisk, D. M., et al. (2022). An ancestral mycobacterial effector promotes dissemination of infection. *Cell* 185, 4507–4525.e18. doi: 10.1016/j.cell.2022.10.019

Sakai, S., Kauffman, K. D., Oh, S., Nelson, C. E., Barry, C. E., and Barber, D. L. (2021a). MAIT cell-directed therapy of *Mycobacterium tuberculosis* infection. *Mucosal Immunol.* 14, 199–208. doi: 10.1038/s41385-020-0332-4

Sakai, S., Lora, N. E., Kauffman, K. D., Dorosky, D. E., Oh, S., Namasivayam, S., et al. (2021b). Functional inactivation of pulmonary MAIT cells following 5-OP-RU treatment of non-human primates. *Mucosal Immunol.* 14, 1055–1066. doi: 10.1038/s41385-021-00425-3

Santucci, P., Bouzid, F., Smichi, N., Poncin, I., Kremer, L., De Chastellier, C., et al. (2016). Experimental models of foamy macrophages and approaches for dissecting the mechanisms of lipid accumulation and consumption during dormancy and reactivation of tuberculosis. *Front. Cell Infect. Microbiol.* 6, 122. doi: 10.3389/fcimb.2016.00122

Satti, I., Marshall, J. L., Harris, S. A., Wittenberg, R., Tanner, R., Lopez Ramon, R., et al. (2024). Safety of a controlled human infection model of tuberculosis with aerosolised, live-attenuated *Mycobacterium bovis* BCG versus intradermal BCG in BCG-naive adults in the UK: a dose-escalation, randomised, controlled, phase 1 trial. *Lancet Infect. Dis.* 24, 909–921. doi: 10.1016/S1473-3099(24)00143-9

Sauerwein, R. W., Roestenberg, M., and Moorthy, V. S. (2011). Experimental human challenge infections can accelerate clinical malaria vaccine development. *Nat. Rev. Immunol.* 11, 57–64. doi: 10.1038/nri2902

Saul, M. C., Philip, V. M., Reinholdt, L. G., and Chesler, E. J. (2019). High-diversity mouse populations for complex traits. *Trends Genet.* 35, 501–514. doi: 10.1016/j.tig.2019.04.003

Scanga, C. A., and Flynn, J. L. (2014). Modeling tuberculosis in nonhuman primates. *Cold Spring Harb. Perspect. Med.* 4, a018564. doi: 10.1101/cshperspect.a018564

Schwalb, A., Dodd, P., Rickman, H. M., Ugarte-Gil, C., Horton, K. C., and Houben, R. M. G. J. (2024). Estimating the global burden of viable *mycobacterium tuberculosis* infection. *Lancet Preprint*. doi: 10.2139/ssrn.5017943

Scriba, T. J., Coussens, A. K., and Fletcher, H. A. (2017). Human immunology of tuberculosis. *Microbiol. Spectr.* 5. doi: 10.1128/microbiolspec.TBTB2-0016-2016

Seshadri, C., Sedaghat, N., Campo, M., Peterson, G., Wells, R. D., Olson, G. S., et al. (2017). Transcriptional networks are associated with resistance to *Mycobacterium tuberculosis* infection. *PloS One* 12, e0175844. doi: 10.1371/journal.pone.0175844

Shah, P. T., Tufail, M., Wu, C., and Xing, L. (2022). THP-1 cell line model for tuberculosis: A platform for *in vitro* macrophage manipulation. *Tuberculosis (Edinb)* 136, 102243. doi: 10.1016/j.tube.2022.102243

Shi, Y., Inoue, H., Wu, J. C., and Yamanaka, S. (2017). Induced pluripotent stem cell technology: a decade of progress. *Nat. Rev. Drug Discov.* 16, 115–130. doi: 10.1038/nrd.2016.245

Silva-Miranda, M., Ekaza, E., Breiman, A., Asehnoune, K., Barros-Aguirre, D., Pethe, K., et al. (2015). High-content screening technology combined with a human granuloma model as a new approach to evaluate the activities of drugs against *Mycobacterium tuberculosis*. *Antimicrob. Agents Chemother.* 59, 693–697. doi: 10.1128/AAC.03705-14

Simmons, J. D., Stein, C. M., Seshadri, C., Campo, M., Alter, G., Fortune, S., et al. (2018). Immunological mechanisms of human resistance to persistent *Mycobacterium tuberculosis* infection. *Nat. Rev. Immunol.* 18, 575–589. doi: 10.1038/s41577-018-0025-3

Simonson, A. W., Zeppa, J. J., Bucsan, A. N., Chao, M. C., Pokkali, S., Hopkins, F., et al. (2025). Intravenous BCG-mediated protection against tuberculosis requires CD4+ T cells and CD8α+ lymphocytes. *J. Exp. Med.* 222. doi: 10.1084/jem.20241571

Singh, A. K., and Gupta, U. D. (2018). Animal models of tuberculosis: Lesson learnt. *Indian J. Med. Res.* 147, 456–463. doi: 10.4103/ijmr.IJMR_554_18

Sloot, R., Schim van der Loeff, M. F., Kouw, P. M., and Borgdorff, M. W. (2014). Risk of tuberculosis after recent exposure. A 10-year follow-up study of contacts in Amsterdam. *Am. J. Respir. Crit. Care Med.* 190, 1044–1052. doi: 10.1164/rccm.201406-1159OC

Soldevilla, P., Vilaplana, C., and Cardona, P. J. (2022). Mouse models for *mycobacterium tuberculosis* pathogenesis: show and do not tell. *Pathogens* 12. doi: 10.3390/pathogens12010049

Stenger, S., Hanson, D. A., Teitelbaum, R., Dewan, P., Niazi, K. R., Froelich, C. J., et al. (1998). An antimicrobial activity of cytolytic T cells mediated by granulysin. *Science* 282, 121–125. doi: 10.1126/science.282.5386.121

Sukumar, N., Tan, S., Aldridge, B. B., and Russell, D. G. (2014). Exploitation of *Mycobacterium tuberculosis* reporter strains to probe the impact of vaccination at sites of infection. *PloS Pathog.* 10, e1004394. doi: 10.1371/journal.ppat.1004394

Sun, M., Phan, J. M., Kieswetter, N. S., Huang, H., Yu, K. K. Q., Smith, M. T., et al. (2024). Specific CD4+ T cell phenotypes associate with bacterial control in people who 'resist' infection with *Mycobacterium tuberculosis*. *Nat. Immunol.* 25, 1411–1421. doi: 10.1038/s41590-024-01897-8

Tezera, L. B., Bielecka, M. K., Chancellor, A., Reichmann, M. T., Shammari, B. A., Brace, P., et al. (2017). Dissection of the host-pathogen interaction in human tuberculosis using a bioengineered 3-dimensional model. *Elife* 6. doi: 10.7554/eLife.21283

Tezera, L. B., Bielecka, M. K., Ogongo, P., Walker, N. F., Ellis, M., Garay-Baquero, D. J., et al. (2020). Anti-PD-1 immunotherapy leads to tuberculosis reactivation via dysregulation of TNF-alpha. *Elife* 9. doi: 10.7554/eLife.52668.sa2

Thacker, V. V., Dhar, N., Sharma, K., Barrile, R., Karalis, K., and Mckinney, J. D. (2020). A lung-on-chip model of early *Mycobacterium tuberculosis* infection reveals an essential role for alveolar epithelial cells in controlling bacterial growth. *Elife* 9. doi: 10.7554/eLife.59961.sa2

Thacker, V. V., Sharma, K., Dhar, N., Mancini, G. F., Sordet-Dessimoz, J., and Mckinney, J. D. (2021). Rapid endotheliitis and vascular damage characterize SARS-CoV-2 infection in a human lung-on-chip model. *EMBO Rep.* 22, e52744. doi: 10.15252/embr.202152744

Thangam, T., Parthasarathy, K., Supraja, K., Haribalaji, V., Sounderrajan, V., Rao, S. S., et al. (2024). Lung organoids: systematic review of recent advancements and its future perspectives. *Tissue Eng. Regener. Med.* 21, 653–671. doi: 10.1007/s13770-024-00628-2

Tientcheu, L. D., Koch, A., Ndengane, M., Andoseh, G., Kampmann, B., and Wilkinson, R. J. (2017). Immunological consequences of strain variation within the *Mycobacterium tuberculosis* complex. *Eur. J. Immunol.* 47, 432–445. doi: 10.1002/eji.201646562

Tomlinson, G. S., Booth, H., Petit, S. J., Potton, E., Towers, G. J., Miller, R. F., et al. (2012). Adherent human alveolar macrophages exhibit a transient pro-inflammatory profile that confounds responses to innate immune stimulation. *PloS One* 7, e40348. doi: 10.1371/journal.pone.0040348

Van Der Wel, N., Hava, D., Houben, D., Fluitsma, D., Van Zon, M., Pierson, J., et al. (2007). *M. tuberculosis* and *M. leprae* translocate from the phagolysosome to the cytosol in myeloid cells. *Cell* 129, 1287–1298. doi: 10.1016/j.cell.2007.05.059

Villarreal-Ramos, B., Berg, S., Whelan, A., Holbert, S., Carreras, F., Salguero, F. J., et al. (2018). Experimental infection of cattle with *Mycobacterium tuberculosis* isolates shows the attenuation of the human tubercle bacillus for cattle. *Sci. Rep.* 8, 894. doi: 10.1038/s41598-017-18575-5

Vogt, G., and Nathan, C. (2011). *In vitro* differentiation of human macrophages with enhanced antimycobacterial activity. *J. Clin. Invest.* 121, 3889–3901. doi: 10.1172/JCI57235

Wallis, R. S. (2007). Reactivation of latent tuberculosis by TNF blockade: the role of interferon γ. *J. Invest. Dermatol. Symposium Proc.* 12, 16–21. doi: 10.1038/sj.jidsymp.5650031

Walzl, G., Ronacher, K., Hanekom, W., Scriba, T. J., and Zumla, A. (2011). Immunological biomarkers of tuberculosis. *Nat. Rev. Immunol.* 11, 343–354. doi: 10.1038/nri2960

Wang, J., Fan, X. Y., and Hu, Z. (2024). Immune correlates of protection as a game changer in tuberculosis vaccine development. *NPJ Vaccines* 9, 208. doi: 10.1038/s41541-024-01004-w

Wang, C., Peyron, P., Mestre, O., Kaplan, G., Van Soolingen, D., Gao, Q., et al. (2010). Innate immune response to *Mycobacterium tuberculosis* Beijing and other genotypes. *PloS One* 5, e13594. doi: 10.1371/journal.pone.0013594

Wang, X., Su, H., Wallach, J. B., Wagner, J. C., Braunecker, B. J., Gardner, M., et al. (2025). Engineered *Mycobacterium tuberculosis* triple-kill-switch strain provides controlled tuberculosis infection in animal models. *Nat. Microbiol.* 10, 482–494. doi: 10.1038/s41564-024-01913-5

Warren, H. S., Tompkins, R. G., Moldawer, L. L., Seok, J., Xu, W., Mindrinos, M. N., et al. (2015). Mice are not men. *Proc. Natl. Acad. Sci.* 112, E345–E345. doi: 10.1073/pnas.1414857111

Warsinske, H. C., Pienaar, E., Linderman, J. J., Mattila, J. T., and Kirschner, D. E. (2017). Deletion of TGF-β1 increases bacterial clearance by cytotoxic T cells in a tuberculosis granuloma model. *Front. Immunol.* 8, 1843. doi: 10.3389/fimmu.2017.01843

WHO (2024). Global tuberculosis report 2024. Geneva: World Health Organization; 2024. Licence: CC BY-NC-SA 3.0 IGO.

Williams, A., and Orme, I. M. (2016). Animal models of tuberculosis: an overview. *Microbiol. Spectr.* 4. doi: 10.1128/microbiolspec.tbtb2-0004-2015

Winchell, C. G., Nyquist, S. K., Chao, M. C., Maiello, P., Myers, A. J., Hopkins, F., et al. (2023). CD8+ lymphocytes are critical for early control of tuberculosis in macaques. *J. Exp. Med.* 220. doi: 10.1084/jem.20230707

Yang, F., Labani-Motlagh, A., Bohorquez, J. A., Moreira, J. D., Ansari, D., Patel, S., et al. (2024). Bacteriophage therapy for the treatment of *Mycobacterium tuberculosis* infections in humanized mice. *Commun. Biol.* 7, 294. doi: 10.1038/s42003-024-06006-x

Yang, H. J., Wang, D., Wen, X., Weiner, D. M., and Via, L. E. (2021). One size fits all? Not in *in vivo* modeling of tuberculosis chemotherapeutics. *Front. Cell Infect. Microbiol.* 11, 613149. doi: 10.3389/fcimb.2021.613149

Zhang, F., Yu, S., Chai, Q., Wang, J., Wu, T., Liu, R., et al. (2021). HDAC6 contributes to human resistance against *Mycobacterium tuberculosis* infection via mediating innate immune responses. *FASEB J.* 35, e22009. doi: 10.1096/fj.202100614R

Ziogas, A., Novakovic, B., Ventriglia, L., Galang, N., Tran, K. A., Li, W., et al. (2025). Long-term histone lactylation connects metabolic and epigenetic rewiring in innate immune memory. *Cell*. doi: 10.1016/j.cell.2025.03.048

frontiers | Frontiers in Cellular and Infection Microbiology

TYPE Original Research
PUBLISHED 10 July 2025
DOI 10.3389/fcimb.2025.1552556

OPEN ACCESS

EDITED BY
Sam Ebenezer,
Sathyabama Institute of Science and Technology, India

REVIEWED BY
Tamilmaran Nagarajan,
Saveetha University, India
Johnson Christdas,
American College, Madurai, India

*CORRESPONDENCE
Yu Hu
huyusdu@163.com

†These authors have contributed equally to this work

RECEIVED 28 December 2024
ACCEPTED 09 May 2025
PUBLISHED 10 July 2025

CITATION
Peng Z, Gao X, He M, Dong X, Wang D, Dai Z, Yu D, Sun H, Tian J and Hu Y (2025) Computed tomography-based radiomics prediction model for differentiating invasive pulmonary aspergillosis and *Pneumocystis jirovecii* pneumonia. *Front. Cell. Infect. Microbiol.* 15:1552556. doi: 10.3389/fcimb.2025.1552556

Computed tomography-based radiomics prediction model for differentiating invasive pulmonary aspergillosis and *Pneumocystis jirovecii* pneumonia

Zhiguo Peng[1†], Xingzhe Gao[2†], Miao He[3], Xinyue Dong[4], Dongdong Wang[5], Zhengjun Dai[6], Dexin Yu[5], Huaibin Sun[1], Jun Tian[1] and Yu Hu[7*]

[1]Department of Organ Transplantation, Qilu Hospital, Cheeloo College of Medicine, Shandong University, Jinan, China, [2]Department of Anesthesiology, Qilu Hospital (Qingdao), Cheeloo College of Medicine, Shandong University, Qingdao, China, [3]Department of Medical Oncology, Qilu Hospital (Qingdao), Cheeloo College of Medicine, Shandong University, Qingdao, China, [4]Department of Oncology, Qilu Hospital of Shandong University, Dezhou Hospital, Dezhou, China, [5]Department of Radiology, Qilu Hospital, Cheeloo College of Medicine, Shandong University, Jinan, China, [6]Scientific Research Department, Huiying Medical Technology Co., Ltd, Beijing, China, [7]Department of Oncology, Qilu Hospital, Cheeloo College of Medicine, Shandong University, Jinan, China

Background: *Pneumocystis jirovecii* and *Aspergillus fumigatus* are important pathogens that cause fungal pulmonary infections. Because the manifestations of *P. jirovecii* pneumonia (PJP) or invasive pulmonary aspergillosis (IPA) are difficult to differentiate on computed tomography (CT) images and the treatment of the two diseases is different, correct imaging for diagnosis is highly significant. The present study developed and validated the diagnostic performance of a CT-based radiomics prediction model for differentiating IPA from PJP.

Methods: In total, 97 patients, 51 with IPA and 46 with PJP, were included in this study. Each patient underwent a non-enhanced chest CT examination. All the patients were randomly divided into two cohorts, training and validation, at a ratio of 7:3 using random seeds automatically generated using the RadCloud platform. Image segmentation, feature extraction, and radiomic feature selection were performed on the RadCloud platform. The regions of interest (ROIs) were manually segmented, including the consolidation area with the surrounding ground-glass opacity (GGO) area and the consolidation area alone. Six supervised-learning classifiers were used to develop a CT-based radiomics prediction model, which was estimated using the receiver operating characteristic (ROC) curve, area under the curve (AUC), sensitivity, specificity, precision, and F1-score. The radiomics score was also calculated to compare the prediction performance.

Results: Classifiers trained with the consolidation area and surrounding GGO area as the ROI showed better prediction efficacy than classifiers trained using only the consolidation area as the ROI. The XGBoost model performed better

than the other classifiers and radiomics scores in the validation cohort, with an AUC of 0.808 (95% CI, 0.655–0.961).

Conclusions: This radiomics model can effectively assist in the differential diagnosis of PJP and IPA. The consolidation area with the surrounding GGO area was more suitable for ROI segmentation.

KEYWORDS

invasive pulmonary aspergillosis, *Pneumocystis jirovecii* pneumonia, discriminant model, radiomics, CT

Introduction

Invasive pulmonary aspergillosis (IPA) is among the most severe disorders and has the highest mortality rate among all types of pulmonary aspergillosis (Dai et al., 2013). IPA characteristically occurs in immunocompromised individuals, including those with long-term neutropenia, hematological malignancies, or solid organ or hematopoietic stem cell transplantation. IPA is difficult to diagnose and treat and can cause symptoms such as coughing, chest pain, hemoptysis, severe breathing difficulties, and even respiratory failure (Schweer et al., 2016).

Pneumocystis jirovecii is a specific fungal pathogen that can cause *P. jirovecii* pneumonia (PJP), a severe opportunistic pneumonia, in immunocompromised patients, including those with organ transplantation, cancer, and malignant hematological diseases (Avino et al., 2016). The typical symptoms of PJP include fever, cough, and hypoxemia, which can rapidly aggravate and lead to severe respiratory failure. Non-enhanced chest computed tomography (CT) is often used to diagnose patients with suspected PJP or IPA.

Typical CT manifestations of IPA include nodules, ground-glass opacities (GGOs), segmental consolidations, pleural effusions, or cavities (Kuhlman et al., 1988). Typical imaging findings of PJP include ground-glass density shadows in the lungs, which are diffusely distributed, scattered, or interlaced with the normal lung tissue. GGOs in the lungs can merge into nodular or massive consolidated opacities. However, the manifestations of PJP and IPA are non-specific and are sometimes difficult to differentiate clinically (Roux et al., 2014). Because the manifestations of PJP or IPA are difficult to differentiate on CT images, and the treatment of the two diseases is quite different, correct imaging for diagnosis may allow for early initiation of treatment before microbiological confirmation and significantly improve prognosis.

In cases where distinguishing between PJP and IP caused by *Aspergillus fumigatus* remains challenging based on galactomannan (GM) assay, β-D-glucan (BDG) testing, and macroscopic imaging findings, a nuanced diagnostic approach is warranted. Both GM antigen (specific to *Aspergillus*) and BDG (elevated in PJP and other fungal infections) exhibit overlapping limitations: BDG lacks species specificity, while GM sensitivity may decline in non-neutropenic hosts or with prophylactic antifungal use. Radiologically, atypical presentations, such as diffuse ground-glass opacities mimicking PJP in early IPA or focal consolidation overlapping with bacterial pneumonia, further obscure differentiation.

To resolve this diagnostic ambiguity, integrating host immune status with ancillary biomarkers is critical. For example, profound CD4 + lymphopenia (<200/μL) strongly favors PJP in patients with HIV, whereas prolonged neutropenia or hematopoietic stem cell transplantation heightens IPA probability. Molecular assays [e.g., *P. jirovecii* PCR on bronchoalveolar lavage fluid (BALF) or *Aspergillus*-specific PCR] enhance pathogen detection when conventional methods are inconclusive. Histopathological confirmation via biopsy, demonstrating *Pneumocystis* cysts (methenamine silver stain) or septate hyphae with acute-angle branching (Grocott's stain), remains the diagnostic gold standard but is often limited by procedural risks.

Ultimately, a tiered diagnostic algorithm combining risk stratification, serial biomarker monitoring, and advanced imaging techniques (e.g., dynamic contrast-enhanced CT for IPA) is essential to mitigate misdiagnosis and guide timely, species-directed therapy.

Radiomics is an emerging imaging technology designed to convert clinical digital images into high-dimensional, mineable data via high-throughput extraction of the quantitative features (Gillies et al., 2016). This technique has been applied to predict pathological classification and differential diagnosis or to assess gene expression, response to therapy, and disease prognosis (Limkin et al., 2017).

To the best of our knowledge, this study is the first to investigate the role of radiomics in improving early differential diagnosis between IPA and PJP. The purpose of our study was to investigate the feasibility of using a CT-based radiomics model to differentiate IPA from PJP.

Materials and methods

Patient population

Patient information and data from the Picture Archiving and Communication System (PACS) in Qilu Hospital of Shandong

University from September 2013 to May 2022 were collected. Patients with a positive metagenomic next-generation sequencing (mNGS) result obtained using BALF as the detection sample and a non-enhanced thorax CT scan were included. The inclusion criteria were as follows: (1) *P. jirovecii* or *Aspergillus* infection was confirmed using mNGS, and the corresponding treatment was effective; (2) Regular dosage of non-enhanced chest CT revealed that the lesions were mainly consolidations and GGOs. The exclusion criteria were as follows: (1) The imaging diagnosis and evaluation were consistent with the mNGS analysis reports; (2) Motion artifacts in CT images, poor image quality, and large differences in scanning conditions; (3) The pathogen was not confirmed due to ineffective treatment or clinical suspicion of a mixed infection; (4) Other pneumonia, illness, or unconfirmed pneumonia. Finally, 97 patients, including 46 in the PJP group and 51 in the IPA group, were included in this retrospective study. Prior information on sample size can be obtained from previous studies. A review analyzing the sample size of some studies using radiomics showed that in a total of 87 studies that were included in the final report, most had sample sizes above 50 patients, with a median cohort size of 101 (Dercle et al., 2022). Therefore, 97 patients were deemed adequate for this study. Data on their clinical characteristics, including sex and age at diagnosis, were also collected. According to a classic review, the ratio used in practice ranges from 60:40 to 90:10 (Shur et al., 2021). As in many other studies, a one-third proportion represents a trade-off between having sufficient data in the training set to ensure that the model has sufficient predictive power and a sufficiently large test dataset to ensure that the predicted performance estimate is accurate (Chen et al., 2022; Jiang et al., 2022; Zheng et al., 2022). All the patients were randomly divided into training and validation cohorts at a ratio of 7:3 using random seeds automatically generated by the RadCloud platform. No differences were observed between the training and validation sets.

This study was approved by the Medical Ethics Committee of Qilu Hospital of Shandong University (KYLL-202209-016).

Image acquisition

All thoracic CT images were obtained with a Siemens SOMATOM Definition AS 64-slice spiral CT, scanning from the thoracic inlet to the diaphragm, with the following parameter settings: tube voltage 120KV, tube current 250–400mA/s (automatic tube current modulation was used); 18–35cm field of view; 512×512 reconstruction matrix; 5mm slice thickness, 1.0s scanning time.

Image segmentation and feature extraction

A flowchart of patient recruitment and radiomics is shown in Figure 1. All CT images were saved in the Digital Imaging and Communications in Medicine (DICOM) format and were uploaded to the RadCloud (Version 7.2, Huiying Medical Technology Beijing Co., Ltd) (Yayuan et al., 2021) platform (https://mics.huiyihuiying.com/login?redirect=%2F, Huiying Medical Technology Co., Ltd). RadCloud's module is based on the pseudo-random number algorithm from the Python language's random library. By fixing the seed, it can ensure the division of the training and testing sets, thereby ensuring the reproducibility of experimental results. The random seed value used in this research was 803. It uses cloud computing, big data analysis, and machine learning algorithms to manage the DICOM imaging data on cloud platforms. We employed the RadCloud platform because the convenience of its remote operation. Many high-quality studies have been based on the RadCloud platform (Cangir et al., 2022; Wang et al., 2022; Zhao et al., 2022).

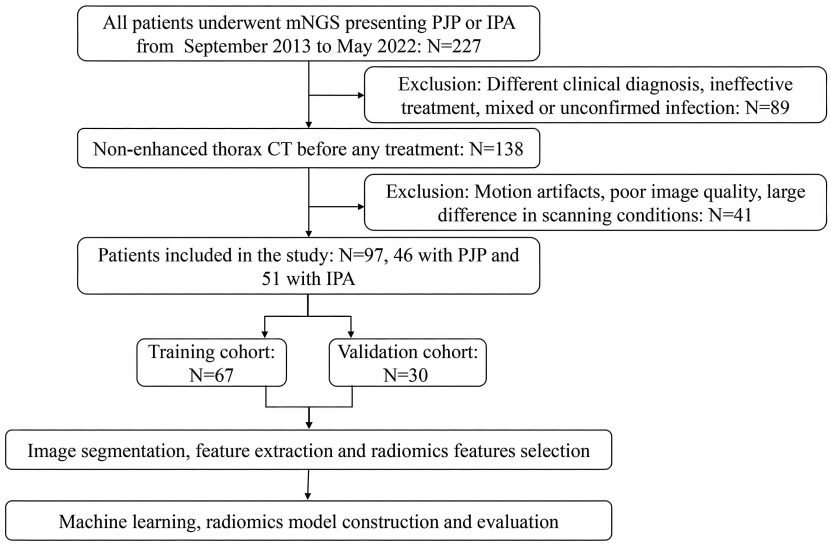

FIGURE 1
Flowchart of patient recruitment and radiomics model construction.

The regions of interest (ROIs) were manually marked by a radiologist with 5 years of experience and then re-examined by another radiologist with more than 10 years of experience. The radiologists were blinded to the patients' diagnoses. If there were any contradictions, the senior radiologists evaluated the ROI again to reach an agreement. To better separate the consolidation and surrounding GGO areas from normal lung tissues, we chose the lung window during ROI segmentation. One image that contained the most typical lesion area was selected for each patient and separated as the ROI. Two methods were used to mark the ROIs in each patient. The first method included only the consolidation area. Cavities were included, but the adjacent mediastinum, pleura, and pleural effusion were avoided in the ROIs. In the second method, the consolidation areas with surrounding GGO areas were included. The ROI delineation in the PJP and IPA CT images is presented in Figure 2. Finally, 97 ROIs were segmented from the 97 patients. After 3 months, 30 cases were randomly selected, and the two radiologists repeated the segmentation to evaluate the inter- and intra-examiner reliability. Radiomic features were automatically extracted by the platform.

Radiomic feature selection and radiomics model building

For each CT sequence in each image,1,409 radiomic features were extracted using the RadCloud platform. The obtained features were divided into three categories. First-order statistics consisted of 270 descriptors that quantitatively delineate the distribution of voxel intensities within the CT image through commonly used and basic metrics. The shape- and size-based features contained 14 three-dimensional features that reflected the shape and size of the region. Texture features that can quantify regional heterogeneity differences include 1125 textural features such as the grey-level run-length (GLRLM), grey-level co-occurrence (GLCM), grey-level size zone (GLSZM), neighboring gray-tone difference (NGTDM), and grey-level dependence matrices (GLDM).

The values of the radiomic features were normalized using the z-score method, and stable features with an ICC >0.75 were retained and normalized for subsequent analysis. Dimensionality reduction and the selection of task-specific features were also performed on the RadCloud platform. The feature selection methods included the variance threshold (variance threshold=0.8), SelectKBest, and least absolute shrinkage and selection operator (LASSO) methods. LASSO regression is an improved linear regression method that introduces the L1 regularization penalty term to automatically screen key features and prevent model overfitting while fitting data. The core idea is to optimize a loss function that consists of two parts: one is the sum of squared errors in traditional linear regression (which measures the deviation between predicted values and true values), and the other is the penalty term for the sum of absolute values of all regression coefficients. By adjusting the hyperparameter lambda to control the penalty intensity, as the larger the lambda, the stronger the compression of insignificant features in the model, some coefficients will be directly reset to zero, thus achieving feature selection. This method is particularly suitable for high-dimensional data with a much larger number of features than the sample size (such as gene expression or text analysis),

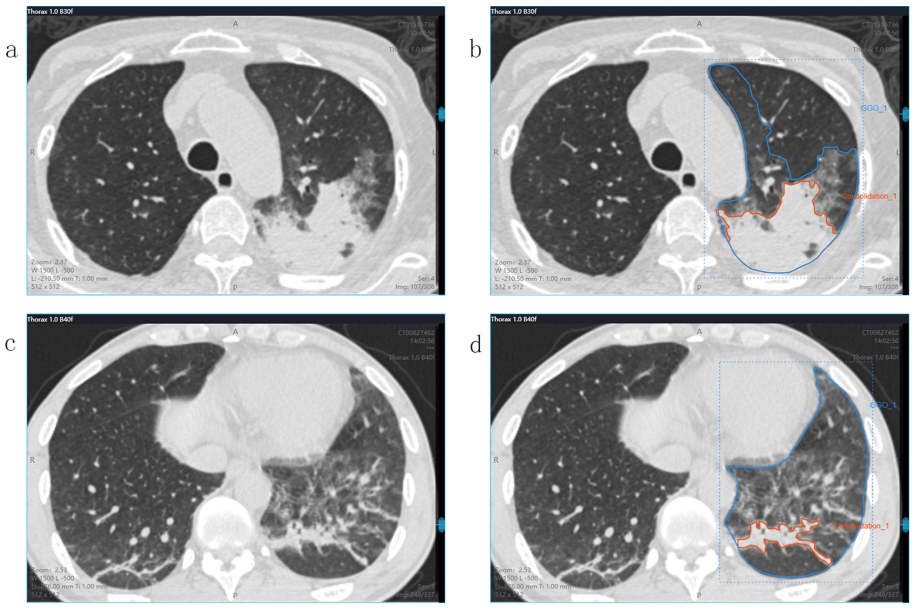

FIGURE 2
CT images and ROI segmentation. Panels **(a, b)** showed a 55-year-old male with IPA, while panels **(c, d)** showed a 36-year-old male with PJP. Both patients presented similar consolidations and surrounding GGO areas on CT images. panels **(b, d)** show the ROI segmentation method. The orange lines include only the consolidation area as the ROI. The blue lines include both the consolidation area and the GGO area as the ROI.

which can improve model interpretability while retaining key variables. In practical applications, the optimal value of λ is usually determined through cross-validation to balance model complexity and prediction accuracy. Based on the variance threshold method, the values of the variance < 0.8 were removed. The SelectKBest method used a p-value to analyze the relationship between the features and classification results, which belong to a single variable feature selection method. Only features with p-values < 0.05 were reserved. The L1 regularizer was used as the cost function in the LASSO model. The error value of the cross-validation was 5, and the maximum number of iterations was 1,000. The radiomics score (radscore) was the sum of the features retained after the LASSO method was multiplied by the corresponding coefficients.

After dimensionality reduction and radiomic features selection, we used six supervised machine learning classifiers for optimal radiomics model construction and selection, including K-nearest neighbors (KNN), support vector machine (SVM), eXtreme Gradient Boosting (XGBoost), random forest (RF), logistic regression (LR), and decision tree (DT). A validation method was used to improve the effectiveness of the model.

Statistical analysis

The area under the curve (AUC) and receiver operating characteristic (ROC) curve were used to estimate the predictive performance, and the sensitivity, specificity, precision, and F1-score [F1-score = precision × recall × 2/(precision + recall)] were calculated using the platform mentioned above to evaluate the performance of the classifier used in this research. Statistical analyses with clinical characteristics were conducted using SPSS 25.0. The data were expressed as median and interquartile range or mean ± SD. The t-test was applied for normally distributed data, whereas the rank-sum test was used for non-normally distributed data. Statistical significance was set at $P < 0.05$.

Results

Patient characteristics

This study included 97 patients, of whom 51 had IPA and 46 had PJP. There were no significant differences in sex between the IPA and PJP groups. The patients with PJP were significantly younger than those with IPA (Table 1).

Radiomics features and model development

Stable features with an ICC > 0.75 were retained and normalized for subsequent analysis. The AUC of the XGBoost classifier with an ROI that included the consolidation area and surrounding GGO area was 0.808, which was better than that of the classifiers with an ROI only including the consolidation area. Using the variance threshold method, 420 features were selected from 1,409 features (Figure 3a), and 26 features were screened out using the selected K best method (Figure 3b). Finally, nine optimal features were selected using the LASSO method (Figures 3c–e). The radiomic features retained after dimension reduction using the LASSO method are listed in Table 2. In the consolidation area with the surrounding GGO area.

The radscore in the IPA group was 0.964 ± 0.446, whereas that in the PJP group was 1.386 ± 0.524, and the difference between the two groups was statistically significant (P<0.001). ROC curve and AUC were applied to compare the predictive performance between the radscore and machine learning classifiers.

The prediction performance using the consolidation+GGO area as the ROI for each classifier in the validation cohort is presented in Table 3. The prediction performance of the validation cohort using only the consolidation area as the ROI is presented in Table 4. The XGBoost model had an AUC of 0.808 in the validation cohort and performed better than other classifiers trained using the consolidation+GGO area as the ROI and showed better prediction efficacy compared with that of the classifiers trained using only the consolidation area as the ROI. The ROC curve of the validation cohort in the XGBoost classifier using the consolidation +GGO area as the ROI is presented in Figure 4. The radscore prediction model had an AUC of 0.643 in the validation cohort (Figure 5), indicating that machine learning classifiers had better prediction efficiency than the radscore.

Discussion

In this study, we used six supervised learning classifiers to establish a radiomics prediction model for differentiating PJP from IPA, and evaluated its predictive performance. The XGBoost classifier trained with the consolidation area and the surrounding GGO area as the ROI had the highest AUC in the validation cohort. This is the first study to demonstrate that such a radiomics model can effectively assist in the differential diagnosis between PJP and IPA.

TABLE 1 Patient characteristics.

Case Profile	*Pneumocystis jirovecii* pneumonia	Invasive pulmonary aspergillosis	Statistics value	P
Number of cases	46	51	–	–
Sex (male/female)	30/16	27/24	χ^2=1.504	0.220
Age	53 (37.25)	62 (19)	Z=-3.379	0.001

Values are presented as median and interquartile range.

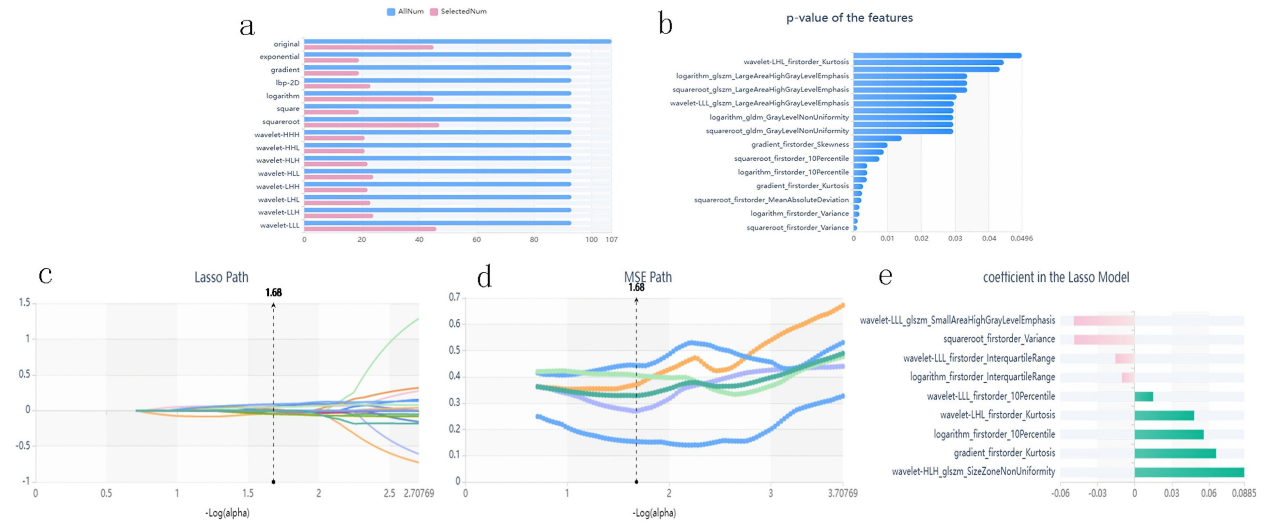

FIGURE 3
Panel **(a)** shows the variance threshold method on radiomics feature selection. The blue bars show all the radiomics features extracted in CT images, while the pink bars represent the features reserved after variance threshold selection. Panel **(b)** shows the SelectKBest method results for further selecting radiomics features. Only features with p-values smaller than 0.05 were reserved. Panels **(c–e)** are the LASSO path, the Mean Squared Error (MSE) path, and the finally screened features with their coefficients in the LASSO model for feature selection, respectively.

TABLE 2 Radiomics features selected with the region of interest (ROI) including the consolidation and ground-glass opacity (GGO) areas.

Radiomics feature	Radiomic class	Filter
Variance	firstorder	squareroot
InterquartileRange	firstorder	logarithm
Kurtosis	firstorder	gradient
10Percentile	firstorder	logarithm
10Percentile	firstorder	wavelet-LLL
InterquartileRange	firstorder	wavelet-LLL
SmallAreaHighGrayLevelEmphasis	glszm	wavelet-LLL
SizeZoneNonUniformity	glszm	wavelet-HLH
Kurtosis	firstorder	wavelet-LHL

P. jirovecii and *A. fumigatus* are the most important pathogens in fungal pulmonary infections (Fishman and Rubin, 1998). PJP and IPA mainly affect immunocompromised patients, including those with malignant tumors, organ recipients, and patients with human immunodeficiency virus infection. Patients with pulmonary fungal infections often present with non-specific symptoms, such as cough, fever, pleuritic pain, dyspnea, and/or hemoptysis, which affect diagnostic accuracy and may be obfuscated by other bacterial or viral infections (Azoulay et al., 2020). Common diagnostic methods for PJP and IPA include imaging, histopathology, direct microscopic examination of respiratory specimens, galactomannan tests, BDG tests, polymerase chain reaction, and mNGS. However, BDG is a circulating component of various fungal cell walls, and other fungal infections may be confounding factors in BDG assays (Karageorgopoulos et al., 2013). Microscopic examination is highly dependent on sample quality and the response of PJP cysts or trophozoites to staining methods (Fan et al., 2013). This problem

TABLE 3 Prediction performances of classifiers in the validation cohort with the region of interest (ROI) including the consolidation and ground-glass opacity (GGO) regions.

Classifier	AUC	95% CI	Sensitivity	Specificity	Precision	F1-score
KNN	0.790	0.639 - 0.941	0.860	0.630	0.670	0.750
SVM	0.777	0.619 - 0.935	0.790	0.690	0.690	0.730
XGBoost	0.808	0.655 - 0.961	0.710	0.810	0.770	0.740
RF	0.763	0.606 - 0.920	0.790	0.690	0.690	0.730
LR	0.799	0.671 - 0.927	0.930	0.750	0.760	0.840
DT	0.670	0.497 - 0.843	0.710	0.630	0.620	0.670

KNN, K-nearest neighbors; SVM, support vector machine; XGBoost, eXtreme Gradient Boosting; RF, random forest; LR, logistic regression; DT, decision tree.

TABLE 4 Prediction performance of the classifiers in the validation cohort with an ROI consisting of the consolidation region.

Classifier	AUC	95% CI	Sensitivity	Specificity	Precision	F1-score
KNN	0.723	0.548 - 0.898	0.640	0.630	0.600	0.620
SVM	0.790	0.644 - 0.936	0.790	0.810	0.790	0.790
XGBoost	0.661	0.500 - 0.822	0.640	0.810	0.750	0.690
RF	0.681	0.526 - 0.836	0.570	0.880	0.800	0.670
LR	0.790	0.631 - 0.949	0.640	0.810	0.750	0.690
DT	0.567	0.385 - 0.749	0.570	0.560	0.530	0.550

KNN, K-nearest neighbors; SVM, support vector machine; XGBoost, eXtreme Gradient Boosting; RF, random forest; LR, logistic regression; DT, decision tree.

persists in the microscopic diagnosis of IPA. Polymerase chain reaction-based diagnostic assays have significantly improved diagnostic efficiency; however, commercial kit prices are relatively high (Zhang F. et al., 2021). The final diagnosis requires the direct detection of pathogens from low respiratory secretions or tissues. BALF is the preferred sample for galactomannan testing in IPA diagnosis (Husain and Camargo, 2019). BALF is also considered to be of the highest quality as a respiratory sample for the diagnosis of PJP and thus has become the current gold standard method of detection (Bateman et al., 2020).

NGS has been successfully applied to detect various infectious pathogens, with a high positive rate for PJP compared with traditional methods. Since mNGS can identify all potential pathogenic microorganisms in BALF samples, we chose NGS results using BALF samples to diagnose and differentiate patients with PJP from those with IPA. However, mNGS has some limitations. It is costly, time-consuming, and affects timely diagnosis and drug treatment.

CT plays a key role in the radiological diagnosis and evaluation of disease activity, response to treatment, and related complications in invasive fungal lung infections (Sanguinetti et al., 2019). Although the CT scan pattern is neither specific nor sensitive for invasive pulmonary fungal infections, it is an effective tool for guiding mycological pre-diagnosis and early initiation of treatment (Bruno et al., 2007). Imaging diagnosis of PJP and IPA remains challenging owing to similar findings in GGO and consolidation areas. Fungal infections should be considered in the differential diagnosis because IPA remains one of the most common infectious mimics of PJP (Cereser et al., 2019). In patients without HIV, PJP shows various findings on CT imaging. Typically, GGO first exists at symptom onset and is symmetrical and predominant in the perihilar and apex regions. Mosaic patterns and architectural distortions are aggravated in cases of ineffective therapy with the same distribution as in the acute phase. GGOs can also exhibit an atypical distribution that predominantly exists in the focal extent or lower lobes (Hardak et al., 2010). Consolidations are common and tend to develop rapidly, typically in patients without HIV, and are occasionally diffuse (Tasaka et al., 2010). Nodules, "crazy paving" patterns, pulmonary cysts, and diffuse alveolar damage are other atypical findings of PJP (Cereser et al., 2019). Similarly, imaging manifestations observed in patients with IPA include GGO, consolidation, nodules, halo signs, and masses (Xu et al., 2012).

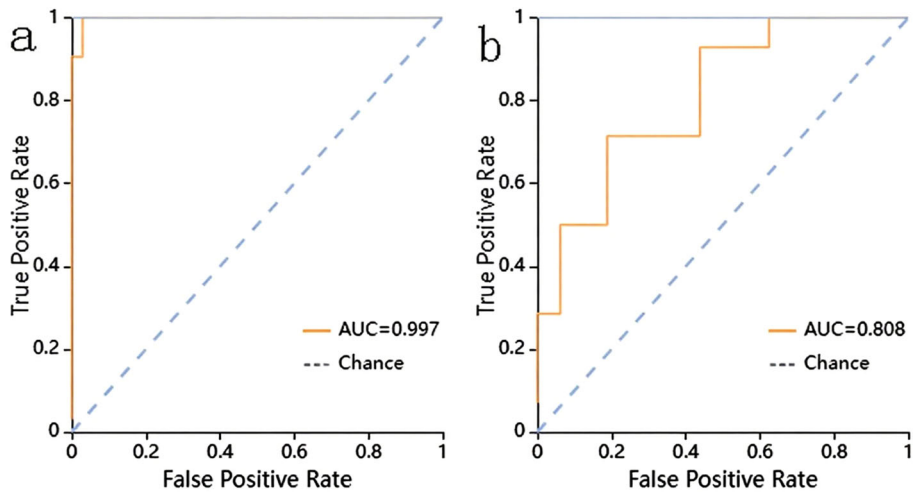

FIGURE 4
The ROC curve of the XGBoost classifier trained with consolidation area and surrounding GGO area. **(a)** showed the ROC curve in training cohort. **(b)** showed the ROC curve in validation cohort.

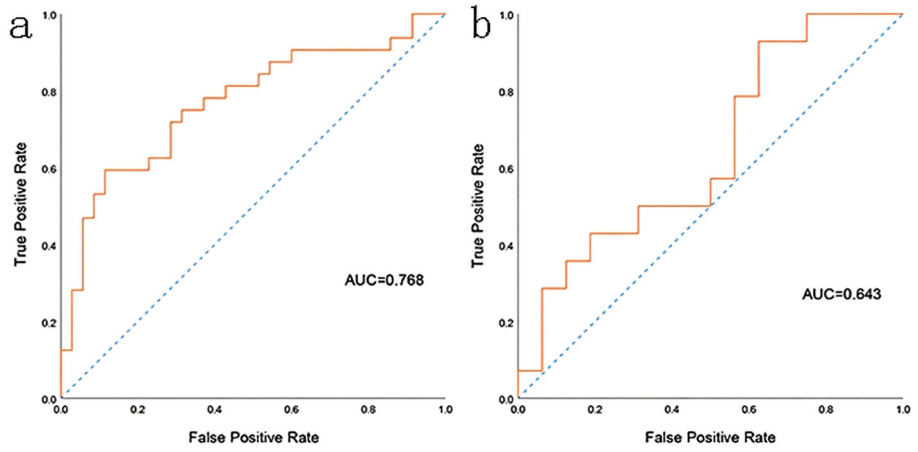

FIGURE 5
The ROC curve of the radscore model. **(a)** showed the ROC curve in training cohort. **(b)** showed the ROC curve in validation cohort.

IPA has vascular infiltrative and airway invasive forms, presenting with different aspects on CT scanning. Typical vascular-invasive CT findings include dense, well-circumscribed lesions >1 cm in size with an early ground-glass attenuation halo (halo sign) (Sanguinetti et al., 2019). The "air crescent sign" is characteristic of a nodular cloudy line permeable crescent that typically appears 1–2 weeks after the onset of IPA (Prasad et al., 2016). Alveolar consolidations or masses, internal low-attenuation or low-density signs, bud patterns, and pleural effusions may also be observed in CT images of the angio-invasive form (Sanguinetti et al., 2019). Airway-infiltrating aspergillosis is characterized by the thickening of the tracheal or bronchial wall and central leaflet nodules that are dendritic, patchy, or predominantly peribronchial consolidation (Franquet et al., 2003). Although the difference between PJP and IPA in CT images is usually non-specific to the human eye, it may present statistically significant radiomic factors.

In our study, radiomics models were effective in differentiating PJP from IPA. Classifiers trained with the ROI comprising both GGO and consolidation areas seem to have better prediction ability than those trained with consolidation areas. The pathophysiological differences between these pathogens may explain the differences in the diagnostic efficacy of the different ROIs. *P. jirovecii* lives almost exclusively in the alveoli, adheres to the surface of the alveolar epithelium of type 1 lung cells, and causes lung damage (Avino et al., 2016). Vascular infiltration in IPA is characterized by hyphae penetrating the vessel wall and the formation of fungal thrombosis, tissue necrosis, and hematogenous dissemination; the halo sign reflects a surrounding hemorrhage of the inflammation site, whereas the air crescent reflects necrosis retraction (Ledoux et al., 2020). Airway-infiltrating aspergillosis is characterized by the destruction of the bronchiolar wall, resulting in the thickening of the trachea or bronchial wall, multiple lobular central nodules, and a bud appearance on CT scans (Franquet et al., 2003).

Radiomics has shown the potential to aid clinical care in disease diagnosis, prognosis prediction, and treatment selection (Gillies et al., 2016). CT-based radiomics is also widely used to detect pneumonia. Gülbay et al (Gülbay et al., 2021) evaluated the discrimination of GGO and consolidation areas between COVID-19 and other atypical pneumonias using radiomic features. They correctly predicted 80% of COVID-19 cases and 81.1% of atypical pneumonia cases. Zhang et al (Zhang M. et al., 2021) constructed a multi-class classification model using radiomics and artificial intelligence for adjunctive empirical antibiotic therapy for bacterial pneumonia in children. In their study, the comprehensive radiomics model using an SVM classifier showed an average AUC of 0.73 in the validation cohort. This is the first innovative study to demonstrate that the radiomics model can effectively differentiate between PJP and IPA. In our study, the radiomics model trained using supervised machine learning classifiers presented good classification efficiency. This may help in early diagnosis, timely initiation of empirical antibiotic use, and personalized precision therapy. This technology has the potential to serve as a foundation for future clinical staging studies, such as assisting in determining disease outcomes through dynamic monitoring of changes in imaging findings. The XGBoost model with the high-precision discrimination framework (AUC=0.808) can provide technical support for subsequent precise classification therapy. The main limitation of this study is the lack of a direct association with clinical staging, which will be emphasized in future work.

In this study, only images of IPA and PJP were collected, the sample size was small, external validation could not be conducted, and other fungal pneumonias were not included in our study; multicenter studies on different kinds of fungal pneumonias should be conducted in the future to take full advantage of radiomics and machine learning. Furthermore, future studies will incorporate clinical severity scoring systems such as APACHE II and SOFA to evaluate the translational potential of our CT-based radiomics model.

By correlating the identified discriminative radiomics signatures (e.g., texture heterogeneity in ground-glass opacities or nodule morphology patterns) with dynamic clinical staging scores, we aim to validate their utility in stratifying disease severity and predicting outcomes in immunocompromised hosts with invasive fungal pneumonias.

Conclusion

The radiomics model shows potential efficacy in differentiating PJP from IPA, which may provide clinicians with early diagnostic evidence for initiating precise antibiotic treatment. The consolidation area with the surrounding GGO area was more suitable for ROI segmentation.

Data availability statement

The original contributions presented in the study are included in the article/supplementary material. Further inquiries can be directed to the corresponding author.

Author contributions

ZP: Resources, Supervision, Writing – review & editing. XG: Data curation, Formal Analysis, Writing – original draft. MH: Writing – review & editing. XD: Writing – review & editing. DW: Writing – review & editing. ZD: Methodology, Writing – review & editing. DY: Methodology, Writing – review & editing. HS: Resources, Writing – review & editing. JT: Resources, Writing – review & editing. YH: Funding acquisition, Investigation, Writing – review & editing, Conceptualization, Project administration, Supervision.

Funding

The author(s) declare that financial support was received for the research and/or publication of this article. This study was supported by grants from the National Natural Science Foundation of China (grant number: 81600092) and Molecular Characterization of Breast Cancer with ESR1 Gene Mutation and Relevance to Treatment (260101120023BL).

Conflict of interest

Author ZD was employed by the company Huiying Medical Technology Co., Ltd.

The remaining authors declare that the research was conducted in the absence of any commercial or financial relationships that could be construed as a potential conflict of interest.

Generative AI statement

The author(s) declare that no Generative AI was used in the creation of this manuscript.

Publisher's note

References

Avino, L. J., Naylor, S. M., and Roecker, A. M. (2016). Pneumocystis jirovecii pneumonia in the non-HIV-infected population. *Ann. Pharmacother.* 50, 673–679. doi: 10.1177/1060028016650107

Azoulay, E., Russell, L., Van de Louw, A., Metaxa, V., Bauer, P., Povoa, P., et al. (2020). Diagnosis of severe respiratory infections in immunocompromised patients. *Intensive Care Med.* 46, 298–314. doi: 10.1007/s00134-019-05906-5

Bateman, M., Oladele, R., and Kolls, J. K. (2020). Diagnosing Pneumocystis jirovecii pneumonia: A review of current methods and novel approaches. *Med. Mycol.* 58, 1015–1028. doi: 10.1093/mmy/myaa024

Bruno, C., Minniti, S., Vassanelli, A., and Pozzi-Mucelli, R. (2007). Comparison of CT features of Aspergillus and bacterial pneumonia in severely neutropenic patients. *J. Thorac. Imaging* 22, 160–165. doi: 10.1097/RTI.0b013e31805f6a42

Cangir, A. K., Orhan, K., Kahya, Y., Uğurum Yücemen, A., Aktürk, İ., Ozakinci, H, et al. (2022). A CT-based radiomic signature for the differentiation of pulmonary hamartomas from carcinoid tumors. *Diagn. (Basel)* 13 (23), 3490. doi: 10.3390/diagnostics12020416

Cereser, L., Dallorto, A., Candoni, A., Volpetti, S., Righi, E., Zuiani, C., et al. (2019). Pneumocystis jirovecii pneumonia at chest High-resolution Computed Tomography (HRCT) in non-HIV immunocompromised patients: Spectrum of findings and mimickers. *Eur. J. Radiol.* 116, 116–127. doi: 10.1016/j.ejrad.2019.04.025

Chen, X., Li, Y., Zhou, Y., Yang, Y., Yang, J., Pang, P., et al. (2022). CT-based radiomics for differentiating intracranial contrast extravasation from intraparenchymal haemorrhage after mechanical thrombectomy. *Eur. Radiol.* 32, 4771–4779. doi: 10.1007/s00330-022-08541-9

Dai, Z., Zhao, H., Cai, S., Lv, Y., and Tong, W. (2013). Invasive pulmonary aspergillosis in non-neutropenic patients with and without underlying disease: a single-centre retrospective analysis of 52 subjects. *Respirology* 18, 323–331. doi: 10.1111/j.1440-1843.2012.02283.x

Dercle, L., McGale, J., Sun, S., Marabelle, A., Yeh, R., Deutsch, E., et al. (2022). Artificial intelligence and radiomics: fundamentals, applications, and challenges in immunotherapy. *J. Immunother. Cancer* 10 (9), e005292. doi: 10.1136/jitc-2022-005292

Fan, L. C., Lu, H. W., Cheng, K. B., Li, H. P., and Xu, J. F. (2013). Evaluation of PCR in bronchoalveolar lavage fluid for diagnosis of Pneumocystis jirovecii pneumonia: a bivariate meta-analysis and systematic review. *PloS One* 8, e73099. doi: 10.1371/journal.pone.0073099

Fishman, J. A., and Rubin, R. H. (1998). Infection in organ-transplant recipients. *N. Engl. J. Med.* 338, 1741–1751. doi: 10.1056/NEJM199806113382407

Franquet, T., Müller, N. L., Giménez, A., Martínez, S., Madrid, M., and Domingo, P. (2003). Infectious pulmonary nodules in immunocompromised patients: usefulness of computed tomography in predicting their etiology. *J. Comput. Assist. Tomogr.* 27, 461–468. doi: 10.1097/00004728-200307000-00001

Gillies, R. J., Kinahan, P. E., and Hricak, H. (2016). Radiomics: images are more than pictures, they are data. *Radiology* 278, 563–577. doi: 10.1148/radiol.2015151169

Gülbay, M., Özbay, B. O., Mendi, B. A. R., Başţuğ, A., and Bodur, H. (2021). A CT radiomics analysis of COVID-19-related ground-glass opacities and consolidation: Is it valuable in a differential diagnosis with other atypical pneumonias? *PloS One* 16, e0246582. doi: 10.1371/journal.pone.0246582

Hardak, E., Brook, O., and Yigla, M. (2010). Radiological features of Pneumocystis jirovecii Pneumonia in immunocompromised patients with and without AIDS. *Lung* 188, 159–163. doi: 10.1007/s00408-009-9214-y

Husain, S., and Camargo, J. F. (2019). Invasive Aspergillosis in solid-organ transplant recipients: Guidelines from the American Society of Transplantation Infectious Diseases Community of Practice. *Clin. Transplant.* 33, e13544. doi: 10.1111/ctr.13544

Jiang, Y. W., Xu, X. J., Wang, R., and Chen, C. M. (2022). Radiomics analysis based on lumbar spine CT to detect osteoporosis. *Eur. Radiol.* 32, 8019–8026. doi: 10.1007/s00330-022-08805-4

Karageorgopoulos, D. E., Qu, J. M., Korbila, I. P., Zhu, Y. G., Vasileiou, V. A., and Falagas, M. E. (2013). Accuracy of β-D-glucan for the diagnosis of Pneumocystis jirovecii pneumonia: a meta-analysis. *Clin. Microbiol. Infect.* 19, 39–49. doi: 10.1111/j.1469-0691.2011.03760.x

Kuhlman, J. E., Fishman, E. K., Burch, P. A., Karp, J. E., Zerhouni, E. A., and Siegelman, S. S. (1988). CT of invasive pulmonary aspergillosis. *AJR Am. J. Roentgenol.* 150, 1015–1020. doi: 10.2214/ajr.150.5.1015

Ledoux, M. P., Guffroy, B., Nivoix, Y., Simand, C., and Herbrecht, R. (2020). Invasive pulmonary aspergillosis. *Semin. Respir. Crit. Care Med.* 41, 80–98. doi: 10.1055/s-0039-3401990

Limkin, E. J., Sun, R., Dercle, L., Zacharaki, E. I., Robert, C., Reuzé, S., et al. (2017). Promises and challenges for the implementation of computational medical imaging (radiomics) in oncology. *Ann. Oncol.* 28, 1191–1206. doi: 10.1093/annonc/mdx034

Prasad, A., Agarwal, K., Deepak, D., and Atwal, S. S. (2016). Pulmonary Aspergillosis: What CT can Offer Before it is too Late! *J. Clin. Diagn. Res.* 10, Te01–Te05. doi: 10.7860/JCDR/2016/17141.7684

Roux, A., Canet, E., Valade, S., Gangneux-Robert, F., Hamane, S., Lafabrie, A., et al. (2014). Pneumocystis jirovecii pneumonia in patients with or without AIDS, France. *Emerg. Infect. Dis.* 20, 1490–1497. doi: 10.3201/eid2009.131668

Sanguinetti, M., Posteraro, B., Beigelman-Aubry, C., Lamoth, F., Dunet, V., Slavin, M., et al. (2019). Diagnosis and treatment of invasive fungal infections: looking ahead. *J. Antimicrob. Chemother.* 74, ii27–ii37. doi: 10.1093/jac/dkz041

Schweer, K. E., Jakob, B., Liss, B., Christ, H., Fischer, G., Vehreschild, M., et al. (2016). Domestic mould exposure and invasive aspergillosis-air sampling of Aspergillus spp. spores in homes of hematological patients, a pilot study. *Med. Mycol.* 54, 576–583. doi: 10.1093/mmy/myw007

Shur, J. D., Doran, S. J., Kumar, S., Ap Dafydd, D., Downey, K., O'Connor, J. P. B., et al. (2021). Radiomics in oncology: A practical guide. *Radiographics* 41, 1717–1732. doi: 10.1148/rg.2021210037

Tasaka, S., Tokuda, H., Sakai, F., Fujii, T., Tateda, K., Johkoh, T., et al. (2010). Comparison of clinical and radiological features of pneumocystis pneumonia between Malignancy cases and acquired immunodeficiency syndrome cases: a multicenter study. *Intern. Med.* 49, 273–281. doi: 10.2169/internalmedicine.49.2871

Wang, D., Zhao, J., Zhang, R., Yan, Q., Zhou, L., Han, X., et al. (2022). The value of CT radiomic in differentiating mycoplasma pneumoniae pneumonia from streptococcus pneumoniae pneumonia with similar consolidation in children under 5 years. *Front. Pediatr.* 10, 953399. doi: 10.3389/fped.2022.953399

Xu, S., Qiu, L., Liu, W., and Feng, Y. (2012). Initial computed tomography findings of invasive pulmonary aspergillosis in non-hematological patients. *Chin. Med. J. (Engl)* 125, 2979–2985.

Yayuan, G., Fengyan, Z., Ran, Z., Ying, C., Yuwei, X., Fang, W., et al. (2021). RadCloud—An Artificial Intelligence-Based Research Platform Integrating Machine Learning-Based Radiomics, Deep Learning, and Data Management. *J. Artif. Intell. Med. Sci.* 2, 97–102. doi: 10.2991/jaims.d.210617.001

Zhang, F., Chen, J., Huang, H., Deng, X., Zhang, W., Zeng, M., et al. (2021). Application of metagenomic next-generation sequencing in the diagnosis and treatment guidance of Pneumocystis jirovecii pneumonia in renal transplant recipients. *Eur. J. Clin. Microbiol. Infect. Dis.* 40, 1933–1942. doi: 10.1007/s10096-021-04254-x

Zhang, M., Yu, S., Yin, X., Zeng, X., Liu, X., Shen, Z., et al. (2021). An AI-based auxiliary empirical antibiotic therapy model for children with bacterial pneumonia using low-dose chest CT images. *Jpn. J. Radiol.* 39, 973–983. doi: 10.1007/s11604-021-01136-2

Zhao, X., Liang, P., Yong, L., Jia, Y., and Gao, J. (2022). Radiomics study for differentiating focal hepatic lesions based on unenhanced CT images. *Front. Oncol.* 12, 650797. doi: 10.3389/fonc.2022.650797

Zheng, Y., Zhou, D., Liu, H., and Wen, M. (2022). CT-based radiomics analysis of different machine learning models for differentiating benign and Malignant parotid tumors. *Eur. Radiol.* 32, 6953–6964. doi: 10.1007/s00330-022-08830-3

Frontiers in
Cellular and Infection Microbiology

Investigates how microorganisms interact with their hosts

Explores bacteria, fungi, parasites, viruses, endosymbionts, prions and all microbial pathogens as well as the microbiota and its effect on health and disease in various hosts.

Discover the latest Research Topics

See more →

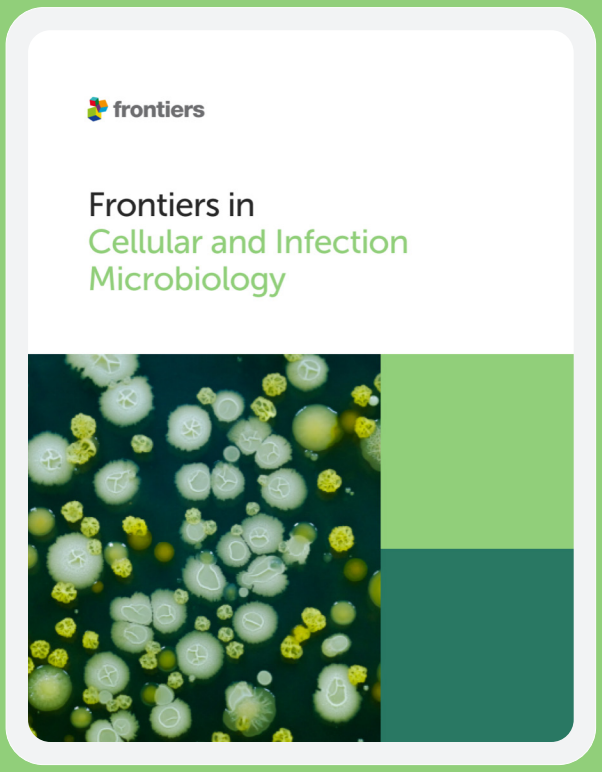

Frontiers

Avenue du Tribunal-Fédéral 34
1005 Lausanne, Switzerland
frontiersin.org

Contact us

+41 (0)21 510 17 00
frontiersin.org/about/contact